Hydrologie et modélisation hydrologique des tourbières acides du Massif Central (France)

Arnaud Duranel

▶ **To cite this version:**

Arnaud Duranel. Hydrologie et modélisation hydrologique des tourbières acides du Massif Central (France). Géographie. Université de Lyon, 2016. Français. NNT : 2016LYSES012 . tel-01560566

HAL Id: tel-01560566

https://theses.hal.science/tel-01560566

Submitted on 11 Jul 2017

HAL is a multi-disciplinary open access archive for the deposit and dissemination of scientific research documents, whether they are published or not. The documents may come from teaching and research institutions in France or abroad, or from public or private research centers.

L'archive ouverte pluridisciplinaire **HAL**, est destinée au dépôt et à la diffusion de documents scientifiques de niveau recherche, publiés ou non, émanant des établissements d'enseignement et de recherche français ou étrangers, des laboratoires publics ou privés.

N°d'ordre NNT : xxx

THESE de DOCTORAT DE L'UNIVERSITE DE LYON
opérée au sein de
l'Université Jean Monnet

Ecole Doctorale N° 483
Sciences Sociales

Spécialité de doctorat : Géographie

Soutenue publiquement le 23/03/2016, par :
Arnaud DURANEL

Hydrologie et modélisation hydrologique des tourbières acides du Massif Central (France)

Devant le jury composé de :

Hervé PIÉGAY, Directeur de Recherche au CNRS, UMR CNRS 5600 EVS, Université de Lyon, Université Jean Moulin, Président

Luc AQUILINA, Professeur, Géosciences Rennes UMR CNRS 6118, Université de Rennes 1, Rapporteur

André-Jean FRANCEZ, Maître de Conférences-HDR, UMR ECOBIO 6553 – IFR CAREN, Université de Rennes 1, Rapporteur

Fatima LAGGOUN-DÉFARGE, Directrice de Recherche au CNRS, Observatoire des Sciences de l'Univers en région Centre, Université d'Orléans, Examinatrice

Didier GRAILLOT, Directeur de Recherche, UMR 5600 CNRS, École Nationale des Mines de Saint-Étienne, Examinateur

Robert WYNS, Géologue, Bureau de Recherches Géologiques et Minières, Orléans, Examinateur

Hervé CUBIZOLLE, Professeur, UMR CNRS 5600 EVS, Université de Lyon, Université Jean Monnet, Directeur de thèse

EVS-ISTHME UMR 5600 CNRS Environnement, Ville, Société

THÈSE DE DOCTORAT DE L'UNIVERSITE DE LYON

opérée au sein de

l'Université Jean Monnet

Spécialité de doctorat : Géographie physique

Soutenue publiquement le 23 mars 2016 par

Arnaud DURANEL

HYDROLOGIE ET MODÉLISATION HYDROLOGIQUE DES TOURBIÈRES ACIDES DU MASSIF CENTRAL (FRANCE)

Sous la direction de:

Prof. Hervé CUBIZOLLE (EVS-ISTHME UMR 5600 CNRS, UJM, France)

Dr Julian R. THOMPSON (Department of Geography, University College London, UK)

Dr Helene BURNINGHAM (Department of Geography, University College London, UK)

Avertissement

Ce document correspond à un travail de thèse de doctorat préparé en co-direction à l'University College London (UCL, Royaume-Uni) et à l'Université Jean Monnet de St-Etienne (France), et soutenue avec succès à UCL le 7 septembre 2015 pour l'obtention du titre de Doctor in Philosophy (PhD) sous le titre « Hydrology and hydrological modelling of acidic mires in central France ». Le présent document, soutenu à St-Etienne pour l'obtention simultanée du titre de Docteur de l'Université de Saint-Etienne, reprend à l'identique le corps du document soutenu à UCL, à l'exception de la page de garde, des remerciements (en partie traduits en français), et des résumés généraux et de chaque chapitre en français qui y ont été ajoutés pour répondre aux exigences de l'UJM.

Résumé

L'objet de la présente thèse est de caractériser, quantifier et modéliser les flux d'eau au sein de la Réserve Naturelle Nationale de la Tourbière des Dauges, située en Limousin (Massif Central, France) et qui inclue une tourbière acide de fond de vallon et son bassin versant. Un ensemble de techniques, incluant la description de coupes superficielles existantes, la réinterprétation de sondages géologiques profonds, la tomographie de résistivité électrique et une modélisation de la distribution spatiale des formations affleurantes, ont été utilisées pour caractériser la nature et la géométrie des formations d'altération du granite. Les dépôts alluviaux et tourbeux ont été caractérisés et cartographiés par sondage à la tarière et à la tige filetée, et leur conductivité hydraulique estimée par choc hydraulique. Les précipitations, les paramètres météorologiques nécessaires au calcul de l'évapotranspiration potentielle, les débits et niveaux dans les ruisseaux, et les niveaux piézométriques dans la tourbe et les formations minérales sous-jacentes ont été mesurés en continu pendant trois ans. Le modèle hydrologique distribué à base physique MIKE SHE / MIKE 11 a été utilisé pour modéliser les écoulements et les niveaux piézométriques au sein de la tourbière et de son bassin versant avec un pas de temps quotidien et une résolution spatiale de 10m. Il est montré que les apports souterrains issus de la zone fissurée du granite et suintant au travers du dépôt tourbeux constituent une part quantitativement importante et fonctionnellement essentielle de la balance hydrique de la zone humide. Ces suintements sont les plus importants en périphérie de la tourbière. Ils maintiennent la nappe en surface ou proche de celle-ci dans la zone humide pendant toute l'année à l'exception de la période estivale. La présence d'une nappe affleurante entraîne une évacuation rapide vers les cours d'eau des apports par ruissellement ou par précipitation directe du fait de la saturation des histosols. Toutefois, il est montré que le fonctionnement hydrologique à l'échelle locale peut s'éloigner de ce schéma général du fait d'une grande hétérogénéité du taux d'humification et de la conductivité hydraulique de la tourbe, de la présence de dépôts alluviaux très perméables sous ou au sein du dépôt tourbeux et de perturbations anthropiques passées. Une fois calibré, le modèle hydrologique, qui représente la zone fissurée du socle granitique comme un milieu poreux équivalent, donne des résultats satisfaisants à très bons selon les indicateurs de performance utilisés : il est capable de reproduire les débits dans les cours d'eau au niveau des quatre stations de jaugeage disponibles, et le niveau de la nappe dans la plupart des piézomètres installés. A l'échelle du bassin versant étudié, le niveau moyen de la nappe simulé par le modèle montre une très bonne concordance avec la distribution observée des végétations de zone

humide, cartographiée de manière indépendante. Les analyses de sensibilité ont montré que la porosité efficace et la conductivité hydraulique horizontale de la zone fissurée du granite sont les paramètres auxquels les débits et les niveaux de nappe (y compris dans la tourbe) simulés par le modèle sont les plus sensibles, ce qui démontre l'importance d'une meilleure caractérisation des formations d'altération du granite dans tout le bassin versant pour la compréhension et la modélisation du fonctionnement hydrologique de ce type de zone humide. Le modèle a été utilisé pour simuler l'impact potentiel d'un changement d'occupation des sols au sein du bassin versant sur la balance hydrique et les niveaux de nappe dans la zone humide, ainsi que sur les débits dans les cours d'eau. Le modèle suggère que le remplacement des végétations actuellement présentes sur le bassin versant par des plantations de conifères conduirait à une réduction substantielle des apports de surface et souterrains à la tourbière, et à un abaissement conséquent des niveaux de nappe dans les histosols en période estivale et en périphérie de la tourbière.

Abstract

This thesis identifies, quantifies and models water fluxes within the Dauges National Nature Reserve, an acidic valley mire in the French Massif Central. A range of techniques were used to investigate the nature and geometry of granite weathering formations and of peat deposits. Rainfall, reference evapotranspiration, stream discharge, stream stage, groundwater table depths and piezometric heads were monitored over a three-year period. The distributed, physics-based hydrological model MIKE SHE / MIKE 11 was used to model water flow within the mire and its catchment. It was shown that the mire is mostly fed by groundwater flowing within the densely fissured granite zone and upwelling through the peat deposits. Upwelling to the peat layer and seepage to overland flow were highest along the mire boundaries. However hydrological functioning differs from this general conceptual model in some locations due to the high variability of the peat hydraulic characteristics, the presence of highly permeable alluvial deposits or past human interference including drainage. The equivalent porous medium approach used to model groundwater flow within the fissured granite zone gave satisfactory results: the model was able to reproduce discharge at several locations within the high-relief catchment and groundwater table depth in most monitoring points. Sensitivity analyses showed that the specific yield and horizontal hydraulic conductivity of the fissured zone are the parameters to which simulated stream discharge and groundwater table depth, including in peat, are most sensitive. The model was forced with new vegetation parameters to assess the potential impacts of changes in catchment landuse on the mire hydrological conditions. Replacement of the broadleaf woodlands that currently cover most of the catchment with conifer plantations would lead to a substantial reduction in surface and groundwater inflows to the mire and to a substantial drop in summer groundwater table depths, particularly along the mire margins.

Table of contents

Avertissement 3
Résumé....5
Abstract....7
Table of contents....9
List of figures....15
List of tables....25
Remerciements....29
Copyright permissions....33
Acronyms and abbreviations....35
Chapter 1. Hydrology and hydrological modelling of mires....37
1.1. Introduction....37
1.2. Peat, peatlands and mires....37
1.2.1. Definitions....37
1.2.2. Peatland distribution....39
1.2.3. Mire classification....40
1.2.4. Vegetation and environmental gradients in mires....43
1.2.5. Values and environmental services....46
1.2.6. Threats to mires....50
1.3. Peatland hydrology....53
1.3.1. Water and water flow in peat soils....53
1.3.2. Mire water balance....60
1.4. Peatland hydrological modelling....65
1.4.1. Hydrological modelling....65
1.4.2. Use of hydrological modelling in peatland research and conservation....70
Résumé du chapitre 1 (introduction générale)....81
Chapter 2. Mires of the Massif Central and the Dauges catchment....83
2.1. Introduction....83
2.2. Peatlands of the French Massif Central....83
2.2.1. Physical context....83
2.2.2. Statutory designations....84
2.2.3. Changes in landuse in the Massif Central over the last century....86
2.3. Review of available research on peatland hydrology within the Massif Central....87

2.4. Thesis aims 88
2.5. Research objectives 88
2.6. Research site: the Dauges National Nature Reserve 89
2.6.1. Location and general context 89
2.6.2. Geology 93
2.6.3. Landuse 95
2.6.4. Rationale for the choice of the Dauges catchment as a research site 96
2.7. Research design and thesis outline 97
Résumé du chapitre 2 100
Chapter 3. Geological model of the Dauges catchment 101
3.1. Introduction 101
3.2. Surface topography 101
3.2.1. Methods 101
3.2.2. Results 104
3.3. Development of a 3D model of granite weathering formations 107
3.3.1. Current knowledge on granite weathering and peri-glacial formations within the research site 107
3.3.2. Methods 108
3.3.3. Results and discussion 116
3.3.4. Conclusion on granite weathering formations and periglacial formations within the Dauges catchment 140
3.4. Development of a 3D hydrogeological model of peat and alluvial deposit 143
3.4.1. Methods 143
3.4.2. Results and discussion 146
3.5. Hydraulic conductivity of peat and alluvial sediments 154
3.5.1. Methods 154
3.5.2. Results and discussion 157
3.6. Pedological survey of mineral soils 164
3.7. Conclusion 165
Résumé du chapitre 3 168
Chapter 4. Hydrology: data acquisition and qualitative analysis 171
4.1. Introduction 171
4.2. Stream stage and discharge monitoring 171
4.2.1. Methods 171
4.2.2. Results and discussion 175
4.3. Piezometry 185

4.3.1. Methods 185
4.3.2. Results and discussion 190
4.4. Conclusion: conceptual hydrological and hydrogeological model 214
Résumé du chapitre 4 216
Chapter 5. MIKE SHE / MIKE 11 model development 219
5.1. Introduction 219
5.2. Model objectives and choice of modelling environment 219
5.3. The MIKE SHE/MIKE 11 modelling environment 220
5.3.1. General description 220
5.3.2. Use of MIKE SHE in wetland hydrological modelling 227
5.4. Model design and initial parametrisation 233
5.4.1. Precipitation 233
5.4.2. Evapotranspiration and unsaturated flow 233
5.4.3. Land use 239
5.4.4. Hydrographic network and hydrodynamic model 252
5.4.5. Overland flow 255
5.4.6. Saturated flow 255
5.4.7. Summary of initial parameters 258
5.4.8. Model grid size 259
5.5. Conclusion 264
Résumé du chapitre 5 266
Chapter 6. Model calibration, validation & sensitivity analysis 267
6.1. Introduction 267
6.2. Model calibration and validation 267
6.2.1. Calibration and validation against observed time-series 267
6.2.2. Validation of the calibrated model against wetland vegetation distribution 284
6.3. Model sensitivity 287
6.3.1. Sensitivity of the initial model to varying depth and shape of the fissured zone 287
6.3.2. Systematic sensitivity analysis of the calibrated model 291
6.3.3. Sensitivity of the calibrated model to model resolution 296
6.3.4. Impact of spatial variation in potential evapotranspiration and peat characteristics 301
6.3.5. Sensitivity to the length of the warm-up period and the issue of the overland flow component convergence 306
6.4. Model performance and sensitivity: general discussion and recommendations 309
6.4.1. The issue of microtopography 309

6.4.2. Channel flow 310
6.4.3. Parametrisation of the unsaturated and saturated peat 311
6.4.4. Parametrisation of the unsaturated zone on mineral soils 312
6.4.5. Parametrisation of the granite fissured zone 313
6.5. Conclusion 315
Résumé du chapitre 6 317
Chapter 7. Simulated water balance and hydrological fluxes between the mire and its catchment 319
7.1. Introduction 319
7.2. Spatial characterisation of the mire hydrology 319
7.2.1. Methods 319
7.2.2. Results and discussion 320
7.3. Water balance 326
7.3.1. Methods 326
7.3.2. Results and discussion 328
7.4. Conclusion 338
Résumé du chapitre 7 339
Chapter 8. Impacts of catchment landuse on wetland hydrology 341
8.1. Introduction 341
8.2. Impacts of catchment landuse on the hydrology of mires 341
8.3. Methods 343
8.4. Results and discussion 345
8.5. Conclusion 369
Résumé du chapitre 8 372
Chapter 9. Hydrology and hydrological modelling of acidic mires in the French Massif Central: conclusion and recommendations 375
9.1. Concluding review 375
9.1.1. Development of a three-dimensional geological model of the mire and its catchment 375
9.1.2. Hydrometeorological monitoring 377
9.1.3. Conceptual hydrological model 378
9.1.4. Numerical hydrological model 379
9.1.5. Sensitivity analyses 380
9.1.6. Simulated water balance and hydrological fluxes 381
9.1.7. Hydrological response to changes in catchment landuse 382
9.2. Recommendations for further research 383

9.2.1. Improving the hydrological understanding and modelling of the Dauges site 383
9.2.2. Validating research findings using other methodological approaches 391
9.2.3. Broadening research questions: the impact of climate change 393
9.3. Recommendations for conservation management 396
9.3.1. Management of minerotrophic mires in basement regions 396
9.3.2. Management of the Dauges National Nature Reserve and Special Area of Conservation 398
9.4. Conclusion 400
Résumé du chapitre 9 (conclusion) 401
References 403
Appendix A. Mire classification 433
A.1. Hydrogeomorphic classification 433
A.1. Hydrogenetic classification 434
A.2. Ontogenetic classification 439
A.3. Classification based on wetland mechanisms 439
A.4. The issue of scale 442
Appendix B. Von Post humification index 443
Appendix C. Recent advances in hydrogeology of hard-rock regions 445
C.1. The stratiform conceptual model of hard-rock aquifers 445
C.2. Mapping the depth of weathering profiles 451
C.3. Modelling groundwater flow in weathered hardrocks 454
Appendix D. Description of pedological pits 457
Appendix E. Meteorology: data acquisition and reconstruction of missing and historical time-series 465
E.1. Introduction 465
E.2. Methods 465
E.2.1. Météo-France permanent meteorological stations 465
E.2.2. On site 466
E.2.3. Time-series reconstruction 470
E.3. Results 471
E.3.1. Solar radiation 471
E.3.2. Temperature 474
E.3.3. Relative humidity 484
E.3.4. Precipitation 494
E.3.5. Wind speed 499
E.3.6. Reference evapotranspiration 501

E.3.7. In-filled meteorological data 506

E.3.8. Representativeness of the model calibration and validation period in terms of climate 507

E.4. Conclusion 510

Appendix F. Characteristics of dipwells and piezometers installed at the Dauges site 511

Appendix G. Published values of evapotranspiration and unsaturated flow parameters 513

Appendix H. Differential impacts of open habitats, broadleaf forests and coniferous forests on water yield 527

List of figures

Figure 1-1. Relationship between mire, suo, wetland and peatland (Joosten 2004). 39

Figure 1-2. Global distribution of mires (from Lappalainen 1996). 40

Figure 1-3. Water retention curves for Sphagnum (a) and reed (b) peats by degree of decomposition (Brandyk et al. 2002)..... 55

Figure 1-4. Relationship between saturated hydraulic conductivity and (a) bulk density or (b) volume of solid matter (from Brandyk et al. 2002). 56

Figure 1-5. Peat saturated hydraulic conductivity as a function of botanical composition and von Post's humification index (from Eggelsmann et al. 1993). 56

Figure 1-6. Impacts of water table drawdown on peat physical properties and peatland hydrology (from Whittington & Price 2006). 60

Figure 1-7. Average contribution of precipitation, surface water and groundwater to the maintenance of summer water levels in English and Welsh mires as a function of (left) identified wetland water supply mechanism and (right) plant community (from Wheeler et al. 2009). 62

Figure 1-8. Classification of hydrological models (modified from Thompson, unpublished; Singh 1988; and Jajarmizad et al. 2012). 66

Figure 1-9. Workflow in hydrological modelling (modified from Refsgaard 1997). 70

Figure 1-10. Performance of the model developed by Lewis et al. (2013) with regard to groundwater table depth (left: calibration, right: validation)..... 72

Figure 1-11. Impact of afforestation (including drainage) on simulated groundwater table depth in the blanket bog modelled by Lewis et al. (2013). 72

Figure 1-12. Performance of the model developed by Fournier (2008) and Levison et al. (2014) with regard to groundwater table depth. 73

Figure 1-13. Exfiltration and throughflow models tested by van Loon et al. (2009). 74

Figure 1-14. Correspondance between trophic status estimated from indicator plant species (a) and fraction of exfiltrated groundwater (FEG) in the root zone according to the throughflow model (b) and exfiltration model (c) of van Loon et al. (2009). 75

Figure 1-15. The esker-peatland system investigated by Rossi et al. (2012, 2014)..... 76

Figure 1-16. Measured (crosses) vs. simulated (crosses and contour lines) groundwater heads in the upper bedrock aquifer below the Selisoo bog according to Marandi et al. (2013).... 77

Figure 1-17. Performance of the model developed by Armandine Les Landes et al. (2014) with regard to groundwater table levels (left) and wetland spatial distribution (right)..... 78

Figure 2-1. Distribution of mires in Metropolitan France. 85

Figure 2-2. Distribution of peatlands within the Massif Central relative to bedrock lithology... 85

Figure 2-3. Proportion of heathland (purple scale) and forest (green scale) in total landcover in Limousin..... 86

Figure 2-4. Location of the Dauges research catchment and wetland within France (top left), Limousin (top right), and the Monts d'Ambazac massif (bottom right and left). 91

Figure 2-5. Three-dimensional view of the Dauges catchment. 92

Figure 2-6. View of the Dauges wetland from its north-east boundary (January 2011). 92

Figure 2-7. Gaussen-Bagnouls ombrothermic diagram of the St-Léger-Mon met station (1998-2010). 93

Figure 2-8. Plan projection of uranium mining galleries within the Dauges catchment. 94

Figure 2-9. Faults and veins as mapped by GOGEMA. 95

Figure 2-10. Landcover within the Dauges catchment. 96

Figure 3-1. Distribution density of differences in elevation between the BD topo DEM (after bilinear interpolation) and the DGPS survey points. 103

Figure 3-2. Density plot of differences between the DEM (after bilinear interpolation) and DGPS survey points 104

Figure 3-3. Topographic data used to build the catchment-wide DEM. 105

Figure 3-4. Digital Elevation Model of the Dauges wetland. 106

Figure 3-5. Location of sections through weathering formations. 109

Figure 3-6. Location of boreholes drilled by CEA 110

Figure 3-7. Arrangement of electrodes for a 2D electrical resistivity survey using a Wenner array (reproduced from Loke 2000). 111

Figure 3-8. Location of ERT transects. 113

Figure 3-9. Section 1 - close-up view of the upslope side of the quarry. 116

Figure 3-10. Section 2 - Panoramic view of the complete quarry face. 117

Figure 3-11. Section 2 - close-up view of the middle of the quarry face. 117

Figure 3-12. Section 2 - close-up view of the downslope side of the quarry. 118

Figure 3-13. Sections described by Valadas (1998). 118

Figure 3-14. Weathering grades and core recovery percentage in the CEA boreholes 120

Figure 3-15. Electrical resistivities of the main granite weathering formation according to the literature. 121

Figure 3-16. ERT profile 1 (29/10/2012): from top to bottom, measured and calculated apparent resistivity pseudosections, L1-norm inverse model resistivity section. 123

Figure 3-17. ERT profile 1 (29/10/2012): L1-norm inverse model resistivity section with topography. 124

Figure 3-18. ERT profile 2 (30/10/2012): from top to bottom, measured and calculated apparent resistivity pseudosections, L1-norm inverse model resistivity section. 126

Figure 3-19. ERT profile 2 (30/10/2012): L1-norm inverse model resistivity section with topography 127

Figure 3-20. ERT profile 3 (03/11/2012): from top to bottom, measured and calculated apparent resistivity pseudosections, L1-norm inverse model resistivity section. 129

Figure 3-21. ERT profile 3 (03/11/2012): L1-norm inverse model resistivity section with topography (combined protocols). 130

Figure 3-22. ERT profile 4 (04/11/2012): from top to bottom, measured and calculated apparent resistivity pseudosections, L1-norm inverse model resistivity section..... 133

Figure 3-23. ERT profile 4 (04/11/2012): L1-norm inverse model resistivity section with topography..... 134

Figure 3-24. Resistivity as a function of porosity according to Archie's law, for a groundwater electrical conductivity of 27.8 µS.cm^{-1}, with a=1.4 and m=1.58..... 135

Figure 3-25. Using slope to map outcropping formations 138

Figure 3-26. Kernel density estimation of slope distribution in arable land vs. in all dry land. 140

Figure 3-27. Kernel density estimation of slope distribution at mapped rock outcrops vs. in the entire area..... 140

Figure 3-28. Nature of the material on which the rod survey stopped. 147

Figure 3-29. Peat depth at the Dauges site..... 148

Figure 3-30. Thickness of easily-penetrable mineral deposits underlying peat at the Dauges site. 149

Figure 3-31. Altitude (mNGF69) of the base of peat (top) and mineral (bottom) deposits at the Dauges site..... 150

Figure 3-32. Stratigraphic profiles..... 151

Figure 3-33. Acrotelm depth (a) and topographic indices used to model it: terrain slope (b), DInf contributing area (c) and slope over Dinf contributing area ratio (d). 153

Figure 3-34. Box- and scatter-plots of acrotelm depth against potential explanatory variables. 154

Figure 3-35. Location of slug tests. 155

Figure 3-36. Recovery curves following slug tests in peat using temporary piezometers with a 10cm intake..... 158

Figure 3-37. Hvorslev model residuals (temporary piezometers in peat)..... 159

Figure 3-38. Recovery curves following slug tests in permanent piezometers..... 160

Figure 3-39. Hvorslev model residuals (permanent piezometers)..... 161

Figure 3-40. Boxplot of hydraulic conductivities measured in peat using temporary piezometers, according to depth..... 163

Figure 3-41. Location of pedological pits..... 164

Figure 4-1. Automatic gauging stations and manual stageboards at the Dauges site. 172

Figure 4-2. V-notch weir and float-operated stage logger in its stilling well at Rocher..... 173

Figure 4-3. Gauging station at the catchment outlet, with the pressure logger in its stilling well.. 174

Figure 4-4. Logger drift at the D78 gauging station. 176

Figure 4-5. Stream stage at the D78 gauging station. 177

Figure 4-6. Scatterplot of stage records at Pont-de-Pierre vs. D78..... 177

Figure 4-7. D78 stage-discharge scatterplot. 178

Figure 4-8. Logger drift at the Pont-de-Pierre gauging station. 179

Figure 4-9. Stream stage at the Pont-de-Pierre gauging station. 179

Figure 4-10. Power (left) and polynomial (right) stage-discharge curves at the Pont-de-Pierre gauging station. 180

Figure 4-11. Stage-area-mean velocity plots at the Pont-de-Pierre gauging station. 181

Figure 4-12. Comparison of stage-discharge curves established with different methods at the Pont-de-Pierre gauging station. 182

Figure 4-13. Daily mean discharge at the Pont-de-Pierre gauging station. 183

Figure 4-14. Daily mean discharge at the upstream gauging stations. 184

Figure 4-15. Manual stage records. 185

Figure 4-16. Location of piezometer clusters. 186

Figure 4-17. Dipwell and piezometer before installation in the ground. 187

Figure 4-18. Movements of selected shallow piezometers relative to an arbitrary datum. 190

Figure 4-19. Boxplots of water table height manual reading errors, as estimated by the difference between readings made with the manual dipper and with a tape measure. The right boxplot shows the estimated errors of manual readings used to calibrate logger data. 192

Figure 4-20. Difference between manually- and logger-recorded water table heights before correction for logger drift. 193

Figure 4-21. Difference between manually- and logger-recorded water table heights before correction for logger drift, conditional on logger. 195

Figure 4-22. Logger data before and after correction for logger drift. 196

Figure 4-23. Time series of piezometric heads in clusters 3-6. 197

Figure 4-24. Time series of piezometric heads in clusters 7-10. 198

Figure 4-25. Time series of piezometric heads in clusters 11-14. 199

Figure 4-26. Time series of piezometric heads in clusters 15-18. 200

Figure 4-27. Time series of piezometric heads in clusters 19-22. 201

Figure 4-28. Time series of piezometric heads in clusters 23-26. 202

Figure 4-29. Time-series of water table depth in pre-existing piezometers. 203

Figure 4-30. Kernel density estimation of water table depth distribution in the peat layer. 204

Figure 4-31. Depth exceedence frequency curves of the water table in the peat layer. 205

Figure 4-32. Principal component analysis plots of groundwater table depth records (left: manually-recorded, right: logger-recorded). 206

Figure 4-33. Map of dipwell scores on PCA first component. 207

Figure 4-34. Piezometric head and stream stage along a transect SB1-D15, downstream of Puy Rond. 209

Figure 4-35. Location of dipwells relative to topographic indices: a) DInf catchment area, b) DInf slope over catchment area ratio. 211

Figure 4-36. Piezometric heads in cluster 8 and stream stages at stageboard SB3. 212

Figure 5-1. Hydrological processes simulated by MIKE SHE (from Graham & Butts 2005). 221

Figure 5-2. Numeric engines available in MIKE SHE for each hydrological process (from Anonymous 2009b). 221

Figure 5-3. Allowable water content in the upper layer of the two-layer unsaturated zone model, as a function of water table depth (from Anonymous 2009c). 223

Figure 5-4. MIKE 11 branches and MIKE SHE river links (from Anonymous 2009c). 226

Figure 5-5. Linkage between MIKE SHE links and MIKE 11 cross-sections (from Anonymous 2009c). 226

Figure 5-6. Observed and simulated groundwater table depth in the North Kent marshes (from Thompson et al. 2004). 227

Figure 5-7. Observed and simulated groundwater table depth (top) and stream stage (bottom) in Bear Creek Meadow (modified from Hammersmark et al. 2008). 228

Figure 5-8. Observed and simulated discharge in the Paya Indah wetlands (Rahim et al. 2012). 229

Figure 5-9. Observed and simulated groundwater table level in the Paya Indah wetlands (Rahim et al. 2009). 229

Figure 5-10. Performance of the Lanoraie steady-state MIKE SHE model with regard to groundwater head (Bourgault et al. 2014). 230

Figure 5-11. Nested models used by Johansen et al. (2014) to model the Lindenborg fen. 231

Figure 5-12. Observed and simulated groundwater heads in the Lindenborg fen (Johansen et al. 2014). 232

Figure 5-13. Generalised crop coefficient curve (Allen & Pereira 2009) 234

Figure 5-14. Idealised crop coefficient curve (Allen et al. 1998) 236

Figure 5-15. Examples of LAI seasonnal changes in acidic mires. 242

Figure 5-16. Leaf area indices used in the model as a function of vegetation class and day of year. 242

Figure 5-17. Crop coefficients used in the model as a function of vegetation class and day of year. 246

Figure 5-18. Simulated intercepted rainfall fraction in a month as a function of maximum storage capacity (1998-2013). 248

Figure 5-19. Ratio of evaporation from interception to maximum potential evapotranspiration as a function of maximum storage capacity (1998-2013). 248

Figure 5-20. Maximum interception storage capacities used in the model as a function of vegetation class and day of year. 250

Figure 5-21. Simulated fraction of intercepted rainfall in a month as a function of vegetation class (1998-2013). 251

Figure 5-22. MIKE 11 hydrographic network. 253

Figure 5-23. MIKE 11 cross-sections. 254

Figure 5-24. Distribution of peat deposits deeper/shallower than the 0.5m minimum depth of the upper computational layer. 257

Figure 5-25. Spatial distribution of mean aggregated elevations according to model resolution. 260

Figure 5-26. Effect of model resolution and aggregation method on the catchment hypsometric curve (top), elevation density distribution (middle) and slope density distribution (bottom). 262

Figure 5-27. Distribution of vegetation classes according to model resolution. 263

Figure 5-28. Relative frequency of vegetation classes according to model resolution. 263

Figure 5-29. Effect of the model grid size on the representation of the hydraulic network by the MIKE SHE pre-processor. 264

Figure 6-1. Observed and simulated stream discharge (uncalibrated model). 270

Figure 6-2. Observed and simulated groundwater table depth (uncalibrated model). 271

Figure 6-3. Observed and simulated stream discharge (calibrated model). 275

Figure 6-4. Observed and simulated stream stage (calibrated model). 276

Figure 6-5. Model performance with regard to groundwater table depth (calibrated model). 277

Figure 6-6. Spatial distribution of shallow groundwater tables (2011-2013 mean higher than -0.286m below ground level) and of wetland vegetation. 286

Figure 6-7. Topographic position index (scaled to 0-1 range). 289

Figure 6-8. Standardised elevation relative to the modelled palaeosurface elevation. 289

Figure 6-9. Systematic sensitivity analysis with respect to groundwater table depth. 294

Figure 6-10. Systematic sensitivity analysis with respect to discharge at Rocher, Marzet and Girolles. 295

Figure 6-11. Systematic sensitivity analysis with respect to discharge at Pont-de-Pierre. 295

Figure 6-12. Nash-Sutcliffe efficiency for simulated discharge, groundwater table depth and piezometric head as a function of model grid size. 297

Figure 6-13. Percent bias in simulated discharge as a function of model grid size. 298

Figure 6-14. Effect of model resolution on simulated groundwater table depth. 299

Figure 6-15. Effect of local peat specific yield, peat available water capacity and wetland crop coefficient on simulated groundwater table depth. 303

Figure 6-16. Effect of the simulation period on simulated discharge at Marzet and Pont-de-Pierre. 306

Figure 6-17. Simulated discharge at Marzet with a simulation period from 01/08/1998 to 31/12/2013. 307

Figure 6-18. Overland flow component accumulated error (2011-2013) as a function of the total length of the simulation period. 307

Figure 6-19. Mean simulated overland depth (2011-2013) as a function of the total length of the simulation period. 308

Figure 7-1. Simulated mean groundwater table depth, upward groundwater flow from lower to upper computational layers and seepage from saturated zone to overland flow (01/01/2011-31/12/2013). 321

Figure 7-2. Simulated mean upward groundwater flow from lower to upper computational layers (01/01/2011-31/12/2013). 323

Figure 7-3. Simulated mean seepage from saturated zone to overland flow (01/01/2011-31/12/2013). 323

Figure 7-4. Simulated monthly mean groundwater table depth (01/01/2011-31/12/2013). .. 324

Figure 7-5. Simulated monthly mean vertical groundwater flow between computational layers (01/01/2011-31/12/2013). 325

Figure 7-6. Simulated monthly mean seepage from saturated zone to overland flow (01/01/2011-31/12/2013). 326

Figure 7-7. Water balance sub-catchments. 327

Figure 7-8. Simulated water balance of the mire area upstream of Pont-de-Pierre from 01/01/2011 to 31/12/2013 (m^3). 329

Figure 7-9. Simulated monthly water balance of the mire upstream of Pont-de-Pierre. 331

Figure 7-10. Simulated monthly water balance of the mire interception and overland flow components. 332

Figure 7-11. Simulated monthly water balance of the mire unsaturated zone component..... 333

Figure 7-12. Simulated monthly water balance of the mire saturated zone component (upper computational layer only). 334

Figure 7-13. Relative importance of individual evapotranspiration components in simulated monthly actual evapotranspiration (mire upstream of Pont-de-Pierre, 01/01/2011-31/12/2013). 335

Figure 7-14. Relative importance of individual components in simulated monthly inflow to the mire (upstream of Pont-de-Pierre, 01/01/2011-31/12/2013). 335

Figure 7-15. Relative importance of individual components in simulated monthly inflow to the mire saturated zone (upstream of Pont-de-Pierre, 01/01/2011-31/12/2013). 336

Figure 8-1. Distribution of vegetation classes in the catchment landuse scenarios. 344

Figure 8-2. Simulated impacts of catchment landuse on the catchment monthly water balance (absolute changes relative to baseline, 01/01/2011-31/12/2013)..... 346

Figure 8-3. Simulated impacts of catchment landuse on the mire monthly water balance (absolute changes relative to baseline, 01/01/2011-31/12/2013)..... 348

Figure 8-4. Impacts of catchment landuse on monthly water balance errors (01/01/2011-31/12/2013). 350

Figure 8-5. Simulated impacts of catchment landuse on evapotranspiration components within the catchment (01/01/2011-31/12/2013). 351

Figure 8-6. Impacts of catchment landuse on simulated daily discharge at the four discharge monitoring stations (01/01/2011-31/12/2013)..... 357

Figure 8-7. Impacts of catchment landuse on simulated flow exceedence frequency curves at the four discharge monitoring stations (01/01/2011-31/12/2013). 358

Figure 8-8. Impacts of catchment landuse on simulated groundwater table depth in a selection of dipwells within the mire (01/01/2011-31/12/2013). 360

Figure 8-9. Impacts of catchment landuse on simulated groundwater table depth exceedence frequency curves in a selection of dipwells within the mire (01/01/2011-31/12/2013). 361

Figure 8-10. Spatial distribution of change in simulated monthly mean groundwater table depth under the conifer scenario, relative to the baseline (01/01/2011-31/12/2013)..... 363

Figure 8-11. Spatial distribution of change in simulated monthly mean groundwater table depth within the mire under the conifer scenario, relative to the baseline (01/01/2011-31/12/2013). 364

Figure 8-12. Spatial distribution of change in simulated monthly mean groundwater table depth under the grassland scenario, relative to the baseline (01/01/2011-31/12/2013)..... 367

Figure 8-13. Spatial distribution of change in simulated monthly mean groundwater table depth within the mire under the grassland scenario, relative to the baseline (01/01/2011-31/12/2013). 368

Figure 9-1. Mean anomaly in reference evapotranspiration (FAO Penman-Monteith) simulated by the SCAMPEI and SCRATCH08 GCM downscaling experiments for the Dauges area. 394

Figure 9-2. Mean anomaly in monthly precipitation simulated by the SCAMPEI and SCRATCH08 GCM downscaling experiments for the Dauges area..... 394

Figure 9-3. Comparison of reference evapotranspiration and precipitation observed at the Dauges site with those simulated by the SCAMPEI and SCRATCH08 downscaling experiments for the nearest grid cell..... 395

Figure A-1. Cross-sections and plan views of key hydrogeomorphic mire types (from Charman 2002). 433

Figure A-2. Sub-types of horizontal mires (from Schumann & Joosten 2008) 435

Figure A-3. Percolation mire (from Schumann & Joosten 2008)..... 436

Figure A-4. Surface flow mires (from Schumann & Joosten 2008). 437

Figure A-5. Acrotelm mire (from Schumann & Joosten 2008). 437

Figure A-6. Gilvear's & McInnes' (1994) wetland classification scheme (from Gilvear & Bradley 2009). 440

Figure C-1. Classical conceptual hydrogeological model of hard-rock aquifers (translated from Lachassagne et al. 2009). 445

Figure C-2. Conceptual hydrogeological model of stratiform hard-rock aquifers (from Wyns et al. 2004). 448

Figure C-3. Age of weathering formations in Limousin (translated from Mauroux et al. 2009). 451

Figure C-4. Formation of the present-day landscape from the infra-Cretaceous planation surface (from Lachassagne et al. 2001b). 452

Figure C-5. Reconstitution of palaeosurfaces (from Lachassagne et al. 2001b). 452

Figure E-1. Influence of computation method on daily temperature and relative humidity extremes. 469

Figure E-2. Theoretical clear-sky and measured daily global radiations at the Dauges site. 471

Figure E-3. Daily global and reflected radiations and their ratio at the Dauges site, inferred presence of snow on the ground. 472

Figure E-4. Double mass curve of global shortwave radiation at the Dauges site and at the two nearest Météo-France stations. 473

Figure E-5. Scatterplots of global shortwave radiation at the Dauges site and at the two nearest Météo-France stations. 474

Figure E-6. Observed vs. predicted daily global shortwave radiation at the Dauges site. 474

Figure E-7. Scatterplot of air temperatures measured with the Hobo and Enerco loggers at the Dauges site. 475

Figure E-8. Scatterplots of temperature extremes recorded by the Enerco and Hobo loggers at the Dauges site. 476

Figure E-9. Daily temperature extremes at the Dauges site. 476

Figure E-10. Scatterplots of daily maximum temperatures at the Dauges site against records at nearby Météo-France stations. 477

Figure E-11. Scatterplots of daily minimum temperatures at the Dauges site against records at nearby Météo-France stations. 477

Figure E-12. Scatterplots of daily temperature extremes at the bottom of the wetland and at mid-slope (Les Ribières) at the Dauges site. 478

Figure E-13. Temperatures measured at the bottom of the wetland and in the upper part of the catchment (Les Ribières) at the Dauges site. 478

Figure E-14. Scatterplots of daily temperature extremes at mid-slope (Les Ribières) and at St-Léger-Mon. 479

Figure E-15. Scatterplots of the anomaly in daily minimum temperature at the Dauges site against other meteorological variables. 480

Figure E-16. Correlation matrix of potential variables to be included in a model of daily minimum temperatures at the Dauges site. 481

Figure E-17. Observed vs. predicted daily minimum temperatures at the Dauges site. 483

Figure E-18. Observed vs. predicted daily maximum temperatures at the Dauges site. 484

Figure E-19. Uncorrected hourly relative humidity measured by the Enerco and Hobo loggers at the Dauges site. 485

Figure E-20. Uncorrected and corrected relative humidity data from the Enerco logger using two different methods. 487

Figure E-21. Scatterplot of corrected Enerco-recorded vs. Hobo-recorded hourly relative humidity at the Dauges site. 488

Figure E-22. Scatterplots of relative humidity daily extremes recorded by the Enerco and Hobo loggers at the Dauges site. 488

Figure E-23. Daily minimum and maximum relative humidity at the Dauges site. 489

Figure E-24. Scatterplots of daily minimum relative humidity at the Dauges site and at nearby Météo-France stations. 489

Figure E-25. Scatterplots of daily maximum relative humidity at the Dauges site and at nearby Météo-France stations. 490

Figure E-26. Scatterplots of daily temperature extremes at the bottom of the wetland and at mid-slope (Les Ribières) at the Dauges site. 491

Figure E-27. Scatterplots of daily relative humidity extremes at les Ribières and at nearby Météo-France stations. 491

Figure E-28. Predicted vs. observed daily minimum relative humidity at the Dauges site. 493

Figure E-29. Predicted vs. observed daily maximum relative humidity at the Dauges site. 494

Figure E-30. Scatterplots of hourly and daily precipitation recorded by the Enerco and PM3030 raing gauges at the Dauges site. 495

Figure E-31. Double mass curves (left) and cumulative curves (right) of precipitation records at the Dauges site and at nearby Météo-France stations. 495

Figure E-32. Impact of snow fall events on the difference between precipitation records at the Dauges site and at the Saint-Léger-la-Montagne station. 496

Figure E-33. Daily precipitation at the Dauges site. 497

Figure E-34. Scatterplots of precipitation records at the Dauges site against records at nearby Météo-France stations. 497

Figure E-35. Scatterplot of precipitation at the two Météo-France rain gauges in Saint-Léger-la-Montagne. 498

Figure E-36. Observed vs. predicted daily precipitation at the Dauges site. 499

Figure E-37. Daily mean wind speed at the Dauges site. 500

Figure E-38. Scatterplots of daily mean wind speed records at the Dauges site against those at nearby Météo-France stations. 500

Figure E-39. Predicted vs. observed daily mean wind speed at the Dauges site. 501

Figure E-40. Reference evapotranspiration at the Dauges site computed using different methods. 502

Figure E-41. Scatterplot matrix of reference evapotranspiration at the Dauges site computed using different methods. 503

Figure E-42. Scatterplot matrix of different potential evapotranspiration estimations using temperature records from the wetland and from the nearby Météo-France station at Saint-Léger-la-Montagne. 504

Figure E-43. Scatterplots of reference evapotranspiration derived from observed vs. modelled meteorological time-series at the Dauges site. 506

Figure E-44. Scatterplots of reference evapotranspiration derived from observed meteorological data at the Dauges site vs. at Limoges-Bellegarde. 506

Figure E-45. Observed and in-filled meteorological time-series at the Dauges site. 508

Figure E-46. Standardised Precipitation-Evapotranspiration Index (1998-2013). 509

Figure H-1. Maximum change in annual flow following deforestation or afforestation in 137 paired-catchment experiments (from Andréassian 2004). 527

List of tables

Table 1-1. Correspondance between humification classes and humification indicators (Szajdak et al. 2011). 54

Table 1-2. Bulk density, total porosity and specific yield measured in northern Minnesota bogs (Boelter 1968). 54

Table 1-3. Percent of runoff collected in automated throughflow troughs from peat layers in an undisturbed blanket bog hillslope, UK (Holden 2006). 64

Table 2-1. Total area and frequency of vegetation classes within the Dauges catchment. 95

Table 3-1. Position of the survey benchmark. 102

Table 3-2. Characteristics of ERT transects completed at the Dauges site. 113

Table 3-3. Water electrical conductivity in the main stream at the Dauges site. 135

Table 3-4. Hydraulic conductivities ($m.s^{-1}$) measured at different depths in peat using temporary piezometers. 163

Table 3-5. Hydraulic conductivities ($m.s^{-1}$) measured in peat and underlying mineral formations using permanent dipwells and piezometers. 163

Table 4-1. Amplitude of piezometer movements. 191

Table 5-1. Unsaturated zone parameters. 238

Table 5-2. Mean bud break and leaf colouring day-of-year and date estimated for deciduous broadleaved species at the Dauges site based on figures from Lebourgeois et al. (2010). 240

Table 5-3. Mean tree height in the Plateaux Limousins eco-region according to IFN data. 244

Table 5-4. Simulated bulk interception ratio as a function of maximum storage capacity (1998-2013). 249

Table 5-5. Simulated fraction of intercepted rainfall (1998-2013). 251

Table 5-6. Vegetation properties used in the Dauges model. 252

Table 5-7. Summary of initial parameter values used in the model. 259

Table 6-1. Calibrated parameters. 274

Table 6-2. Confusion matrix (% of the total number of pixels). 285

Table 6-3. Nash-Sutcliffe Efficiency before calibration as a function of the shape and depth of the fissured zone 291

Table 6-4. Parameters included in the systematic sensitivity analysis. 293

Table 6-5. Effect of unsaturated peat specific yield, unsaturated peat available water capacity and wetland crop coefficient during the vegetation season on the Nash-Sutcliffe Efficiency for individual dipwells. 302

Table 7-1. Simulated water balances of the mire, of its catchment and of both areas combined from 01/01/2011 to 31/12/2013. 330

Table 8-1. Frequency of vegetation classes within the wetland, catchment and combined water balance computation areas (baseline). 344

Table 8-2. Simulated impacts of catchment landuse on catchment and mire overall water balances (01/01/2011-31/12/2013). 345

Table 8-3. Change (and percent change in brackets) in simulated stream flow quantiles and mean flow ($l.s^{-1}$) under conifer and grassland catchment landuse scenarios relative to the baseline (01/01/2011-31/12/2013). 358

Table 8-4. Impacts of catchment landuse on the number of days per year with a simulated groundwater table depth deeper than 0, -0.1 and -0.2m below ground in a selection of dipwells within the mire (01/01/2011-31/12/2013). 362

Table A-1. Hydrogenetic mire types (modified from Joosten & Clarke 2002). 438

Table A-2. Descriptors of the wetland framework (Wheeler et al. 2009). 441

Table A-3. Wetland Water Supply Mechanisms (WETMECs, Wheeler et al. 2009; Whiteman et al. 2009). 442

Table B-1. Von Post humification index (adapted from Soil Classification Working Group 1998; Quinty & Rochefort 2003; Parent & Caron 2008) 443

Table C-1. Variation of hydraulic conductivity with depth in a leucogranite in St-Sylvestre (Bertrand & Durand 1983). 449

Table C-2. Conceptual models of flow in fractured/fissured media (modified from Singhal & Gupta 2010). 454

Table D-1. Position of pedological pits 457

Table E-1. Météo-France permanent meteorological stations close to the Dauges site. 465

Table E-2. Availability of meteorological data at Météo-France stations close to the Dauges site. 466

Table E-3. Definition of meteorological variables provided by Météo-France 466

Table E-4. 24-hour periods used by Meteo-France to aggregate meteorological variables. 466

Table E-5. Definition of variables measured at the Dauges site 467

Table E-6. Coefficients of the minimal model for global radiation at the Dauges site. 474

Table E-7. Coefficients of the minimal model for daily minimum temperature at the Dauges site. 482

Table E-8. Coefficients of the minimal model for daily maximum temperature at the Dauges site. 483

Table E-9. Correlation of corrected humidity data at the Dauges site with control datasets. .. 487

Table E-10. RMSE of corrected relative humidity data at the Dauges site with control datasets. 487

Table E-11. Coefficients of the minimal model for daily minimum relative humidity at the Dauges site. 492

Table E-12. Coefficients of the minimal model for daily maximum relative humidity at the Dauges site. 493

Table E-13. Coefficients of the minimal model for daily precipitation at the Dauges site. 498

Table E-14. Coefficients of the minimal model for daily mean wind speed at the Dauges site. 501

Table E-15. Mean annual precipitation and reference evapotranspiration at the Dauges site. 507

Table F-1. Characteristics of dipwells and piezometers installed at the Dauges site. 511

Table G-1. Literature review of crop coefficients relevant to the Dauges site. 514

Table G-2. Literature review of leaf area index (LAI) values used in hydrological modelling or measured in contexts similar to the Dauges site. 517

Table G-3. Literature review of rooting depth values used in hydrological modelling or measured in contexts similar to the Dauges site. 519

Table G-4. Literature review of mean leaf resistance (r_l) values used in hydrological modelling or measured in contexts similar to the Dauges site. 520

Table G-5. Literature review of bulk interception ratios measured in contexts similar to the Dauges site. 522

Table G-6. Literature review of maximum and specific storage capacities measured in contexts similar to the Dauges site. 524

Remerciements

I am particularly indebted to Dr Julian Thompson, my primary supervisor at UCL, for giving me the opportunity to undertake the research project I had long dreamed of. His encouragements after each of our meetings, his extraordinarily patient help with the intricacies of MIKE SHE and his meticulous editing of my approximate Frenglish have been invaluable.

I am grateful to Dr Helene Burningham, my secondary supervisor at UCL, for her help with image processing, GIS and DGPS; and always pertinent advice during our meetings.

Le travail de terrain effectué pendant cette thèse n'aurait été ni financièrement ni techniquement possible sans l'aide de mon directeur de thèse à l'Université Jean Monnet de Saint-Etienne, le Professeur Hervé Cubizolle, directeur du laboratoire EVS-ISTHME UMR5600 CNRS, et cette thèse aurait été entièrement différente sans son implication. Son enthousiasme pour mon projet, sa connaissance du financement de la recherche en France, son soutien inconditionnel et son amitié ont été précieux.

Je suis également très reconnaissant aux multiples personnes qui m'ont aidé pendant ce projet :

Mes vieux (et pas si vieux) collègues du Conservatoire des Espaces Naturels du Limousin et de la Réserve Naturelle Nationale de la Tourbière des Dauges : Philippe Durepaire, Karim Guerba, Murielle Lancroz, Anaïs Lebrun, Véronique Lucain, pour avoir réalisé une bonne partie des relevés manuels hydrologiques et météorologiques décrits dans cette thèse, pour s'être pliés avec bonne volonté à mes demandes répétées pour toujours plus de données et toujours plus de précision dans leur collecte, et pour leur accueil. Ce fut un grand plaisir que de passer ces nombreuses semaines de terrain à leurs côtés. Erwan Hennequin, Guy Labidoire, et à nouveau P. Durepaire, M. Lancroz et A. Lebrun, pour m'avoir aidé à porter ces lourdes batteries au plomb et ces cables électriques dans la tourbière inondée lors des relevés de tomographie de résistivité électrique. Je suis certain que peu de personnes ont eut cette expérience, et tout aussi certain que ceux qui l'ont vécue savent les sacrifices que vous avez consentis pour la Science! Véronique Daviaud et Céline Gombert, pour leur aide avec les prélèvements de tourbe et l'expérimentation de la méthode du PVC respectivement. A nouveau G. Labidoire, mon coupeur de bambou préféré! Et enfin Fred Yvonne, Maïwenn Lefrançois, Cécilia Ferté et Pierre Seliquer.

Dr Robert Wyns (Bureau de Recherches Géologiques et Minières), pour l'intérêt qu'il a bien voulu porter à mon travail, sa disponibilité et ses précieux conseils sur les formations d'altération du granite. Cette thèse aurait omis de nombreux points cruciaux sans son aide. Dr Stéphane Garambois, Isabelle Douste-Bacqué, Julien Turpin (Institut des Sciences de la Terre, Grenoble), pour m'avoir permis d'utiliser leur matériel de tomographie et pour leur aide avec l'interprétation des données.

The many members of staff of the UCL Department of Geography that have provided scientific advice or technical help: Prof John French, Dr Mat Disney, Dr Vivienne Jones, Prof Anson Mackay, Prof Neil Rose, Prof Richard Taylor, Dr Handong Yang, Dr Gavin Simpson, Dr Simon Turner, Ajay Chauhan, Catherine D'Alton, Susan Hennessy, Janet Hope, Miles Irving, Tom Knight, Nick Mann, Ian Patmore, Kevin Roe, Tula Maxted, Dr Suse Keay, Maria Rodriguez. And also Amanda Green, Hannah Clilverd, Andrew House, Mohammed Rahman, Luca Marazzi, Luke Mitchell, Miriam Fernandez-Nunez, Charlie Stratford and Lizzie Gardner, some of my fellow PhD students, for mutual (or not!) help and always interesting discussions.

Rashed Khandker (UCL Bartlett), Liz Jones (UCL CEGE), Dr Katherine Holt, Dr Tom Varley (UCL Chemistry), Stuart Laidlaw (UCL Archaeology), for help with scanners, DGPS, IR spectrometers and cameras respectively.

Alain Chomiack (DREAL Limousin), pour son aide avec l'installation des deux enregistreurs à pression à l'aval de la tourbière. Bruno Gratia (Ecole Forestière de Meymac), pour la réalisation des fosses pédologiques. Colin Roberts, Charlie Stratford, Dr James Sorensen, Prof Mike Acreman (Centre for Ecology & Hydrology), for their help at Boxford and with questions relative to hydrological monitoring. Corinne Bauvet, Grégory Agnello (Evinerude), Dr Pierre Goubet (cabinet Sphagnum), Vincent Hugonnot (Conservatoire Botanique National du Massif Central), pour l'identification d'échantillons de bryophytes et lichens. Audrey Gibeaux (AREVA), pour m'avoir permis d'accéder aux archives d'AREVA. Gwen Hitchcock (Wildlife Trust for Bedfordshire, Cambridgeshire & Northamptonshire), Lisa Lane (Berkshire, Buckinghamshire and Oxfordshire Wildlife Trust), for granting access to the nature reserves they manage. Nicolas Saelen (Précis-Mécanique), pour ses conseils sur le matériel de suivi météorologique. Les membres du laboratoire EVS-ISTHME UMR 5600 CNRS, UJM, en particulier le Professeur Bernard Etlicher, pour la journée qu'il a très aimablement consacrée à m'expliquer sur le terrain les formations et processus péri-glaciaires, et pour la relecture qu'il a faite de certains chapitres de cette thèse ; mais aussi Dr Pierre-Olivier Mazagol, Renaud Mayoud, Dr Jérôme Porteret, Carole Bessenay,

Catherine Guillot, Dr Céline Sacca et Axel Mure. Dr Véronique Lavastre (Département de Géologie, UJM), pour ses conseils et son aide concernant l'analyse des sol. Cédric Tavaud (SYMILAV), pour l'intérêt qu'il a porté à mon travail, et le temps et les efforts qu'il a bien voulu y consacrer lors relevés de tomographie à Gourgon ; ainsi que Xavier de Villele, pour avoir mis à ma disposition le matériel du syndicat et un peu du temps de son personnel. Annick Auffray (Météo-France), pour m'avoir fourni de nombreuses données météorologiques. Dr Gilles Thébaud (Herbiers Universitaires de Clermont-Ferrand), pour ses conseils sur l'identification et la cartographie des communautés végétales tourbeuses. Dr Vincent Gaertner, Dr Kristell Michel, Dr Marie-Laure Trémélo (UMR 5600 EVS), pour m'avoir permis d'utiliser le matériel de l'UMR. Vincent Magnet, Cathy Mignon-Linet (Parc Naturel Régional de Millevaches en Limousin), pour leur aide avec la demande de subvention initiale. Dr Jean-Claude Linet, pour son accueil. Tu restes dans nos pensées. Prof Frank Chambers (University of Gloucestershire), for his enthusiasm for the PhD project I submitted to him. Sorry for choosing UCL after all! Ivan and Jacqueline Wright, for their help with microscope calibration. James Giles (Natural England), for allowing access to Thursley Common NNR. Dr Stephan Hennekens (Alterra), for graciously allowing me to use TurboVeg and for his help with the software.

Armelle Denis, Renaud Colin et Benoit Rossignol (Etablissement Public Loire), pour leur aide avec les demandes de subvention , et pour m'avoir invité à présenter mon travail à Bruxelles, Limoges et Clermont-Ferrand. Samuel André, pour m'avoir permis d'obtenir un financement de l'Agence de l'Eau Loire Bretagne.

Les personnes ayant participé à la réunion d'octobre 2009 à St-Gence, France: Dr L. Chabrol (Conservatoire Botanique National du Massif Central), E. Hennequin, P. Durepaire, P. Seliquer, M. Bonhomme et K. Guerbaa (Conservatoire des Espaces Naturels du Limousin), V. Magnet (Parc Naturel Régional de Millevaches en Limousin), Prof M. Botineau (Laboratoire de Botanique et Cryptogamie de la Faculté de Pharmacie de Limoges & Conseil Scientifique Régional de Protection de la Nature), Prof B. Valadas et Prof P. Allée (GéoLab, Universités de Limoges-Clermont), Dr R. Nicolau (Ecole Nationale Supérieure d'Ingénieurs de Limoges), Dr Yoann Brizard (Syndicat d'Aménagement du Bassin de la Vienne Moyenne), Samuel André (Agence de l'Eau Loire Bretagne). L'intérêt marqué dont ils ont fait preuve pour mon projet ainsi que le rappel à la réalité qu'ils m'ont gentiment proposé ont été grandement appréciés.

Gaëlle, Geneviève et Alain (Auberge de St-Martin-des-Olmes). Votre Hotel de Jeunesse est un vrai joyau, ce fut un grand plaisir que d'y passer ces quelques semaines!

Yvan et Elodie, Fred, Arnaud, Michel et Sylvie, Guy et Noëlle, pour leur écoute et pour m'avoir permis de souffler un peu en leur inestimable compagnie.

Jacques et Yvonne, pour leur soutien continu. Marie-Claude, pour avoir suppléé à mes obligations paternelles en de si nombreuses occasions et avec tant de bonne volonté lorsque je désertais la maison familiale pour aller égoistement me "promener" dans les tourbières du Massif Central.

Vincent et Simon, mes bonhommes, pour être venus à ma rescousse tant de fois en demandant "Daddy, can I watch pirates / dinosaurs / Peppa Pig / des chevaliers / castles / des camions de pompier / bin lorries / des requins / whales / un lion / planes… on your computer?" quand vous réalisiez qu'un script sur R commençait à me désespérer.

Sandrine, ce travail n'existerait tout simplement pas sans le soutien inconditionnel, la patience, la compréhension, les encouragements et l'amour dont tu as fait preuve tout au long de celui-ci. De tout coeur, merci.

Ce travail a bénéficié du soutien financier des organisations suivantes : Natural Environment Research Council studentship (UK), Fond Européen de Développement Régional (EU), Agence de l'Eau Loire Bretagne (F), Conservatoire des Espaces Naturels du Limousin (F), EVS-ISTHME UMR5600 CNRS Université Jean Monnet Lyon-St-Etienne (F). Les financements obtenus auprès des institutions européennes et françaises l'ont été dans le cadre du Plan Loire Grandeur Nature, géré par l'Etablissement Public Loire (http://www.plan-loire.fr), grâce à une collaboration entre le Département de Géographie d'UCL et le laboratoire EVS-ISTHME UMR5600 CNRS Université Jean Monnet Lyon-St-Etienne.

Copyright permissions

I am grateful to the following people and organisations for granting permission to reproduce copyright material: Bureau de Recherches Géologiques et Minières (Figure C-3), DHI (Figures 5-2 to 5-5), Elsevier (Figures 1-13, 1-14, 1-17, 5-6, 5-15 and H-1), Geological Society of Malaysia (Figure 5-9), International Association of Hydrological Sciences (Figure C-1), International Peatland Society (Figure 1-2), IWA Publishing (Figure 5-10), John Wiley and Sons (Figures 1-5, 1-6, 1-10, 1-11, 1-12, 5-7, 5-8, 5-11, 5-12, 5-15, 5-15, A-1, A-6, C-4 and C-5), Prof. Dr. Dr. h.c. Hans Joosten & International Mire Conservation Group (Figures 1-1 and A-2 to A-5), Dr M.H. Loke – Geotomosoft Solutions (Figure 3-7), Springer (Figures 1-15, 1-16 and 5-13), Taylor and Francis Group LLC Books (Figures 1-3, 1-4 and 5-1).

Acronyms and abbreviations

3D	three-dimensional
APPB	arrêté préfectoral de protection de biotope
asl	above sea level
AWC	available water capacity
bdin	boundary inflow
bdout	boundary outflow
BRGM	Bureau de Recherches Géologiques et Minières
cal. BP	calibrated radiocarbon years before the present
CEA	Commissariat à l'Energie Atomique
CEN	Conservatoire des Espaces Naturels
COGEMA	Compagnie Générale des Matières Atomiques
DEM	digital elevation model
df	degree of freedom
DGPS	differential global positioning system
DOC	dissolved organic carbon
err	error
ERT	electrical resistivity tomography
Eto	reference evapotranspiration
EU	European Union
evap	evaporation
FAO	Food and Agriculture Organisation
FFM	daily mean wind speed
GAM	generalised additive model
GCM	global climate model
GIS	geographic information system
GLO	daily global shortwave radiation
GLS	generalised least square
GNSS	global navigation satellite system
GPS	global positioning system
GWT	groundwater table
IGN	Institut Géographique National
infilt	infiltration
int	interception
Kc	crop coefficient
L2E	Lambert II étendu
LAI	leaf area index
LM	linear model
MAE	mean absolute error
ME	mean error
MY	million years
neg	negative
NGF	nivellement général de la France
NNR	national nature reserve
NSE	Nash-Sutcliffe efficiency
NTF	nouvelle triangulation de la France
NVC	national vegetation classification
OL	overland
OLS	ordinary least square
PBIAS	percent bias
PCA	principal component analysis
percol	percolation
pos	positive
RGF	réseau géodésique français
riv	river
RMSE	root mean square error
RR	precipitation
RSR	RMSE-observations standard deviation ratio
RTK	real-time kinematic
SAC	special area of conservation
SD	standard deviation
SEV	sum exceedence value
SHE	système hydrologique européen
sto	storage
Sy	specific yield
SZ	saturated zone
T	transpiration
TM	daily mean temperature
TN	daily minimum temperature
TPI	topographic position index
transp	transpiration
TX	daily maximum temperature
UN	daily minimum relative humidity
UTC	coordinated universal time
UX	daily maximum relative humidity
UZ	unsaturated zone
VES	vertical electrical sounding
WGS	world geodesic system
WMO	World Meteorological Organisation

Chapter 1. Hydrology and hydrological modelling of mires

1.1. Introduction

This thesis investigates the hydrology of the Dauges National Nature Reserve (NNR), an acidic mire in the Monts d'Ambazac, on the western side of the French Massif Central. The research is based on a combination of hydrological and hydrogeological surveys, monitoring and modelling using MIKE SHE / MIKE 11, a distributed physically-based hydrological/hydraulic model. The Massif Central is one of the areas with the highest density of mires in Metropolitan France. As a consequence of the high value of these environments for nature conservation, and also of the many environmental services they provide, a large number are protected under both the national and European legislation. The current chapter provides an introduction to the thesis by reviewing relevant scientific literature on mires, mire hydrology and mire hydrological modelling. Specific details of the mires in the Massif Central are presented in Chapter 2 before the mire of the Dauges NNR and its catchment are introduced and the aims and objectives of the research undertaken in this site are presented.

1.2. Peat, peatlands and mires

1.2.1. Definitions

According to the International Mire Conservation Group (Joosten & Clarke 2002; Schumann & Joosten 2008), peat is a sedentarily accumulated material consisting of at least 30% (dry mass) of dead organic material. Peat soils (often called histosols) are generally defined by the presence of a minimum depth of peat (or histic horizon). However the thresholds in both organic content used to define peat and peat depth used to define histosols vary widely in the wetland and soil sciences literature (Chesworth 2008). For instance, the minimum organic content defining peat varies from 20% to 80% (Rydin & Jeglum 2006). The FAO defines a histic horizon as having at least 20-30% organic content, being saturated with water for at least 30 days in most years (unless artificially drained), and having a thickness of at least 10cm. The French *Référentiel Pédologique* (Baize & Girard 2009) uses thresholds of 50% of organic matter and 10cm depth. According to Joosten & Clarke (2002), the organic matter threshold of 30% is the most frequently encountered in definitions of peat and organic soil in the international literature and is that adopted by both the International Mire Conservation Group and the International Peat Society. As defined by Joosten & Clarke (2002), peat is an organic material that has formed on the spot

and has not been transported after its formation. This distinguishes it from other organic sediments such as gyttjas (organic sediments formed at the bottom of open water bodies by the deposition of mainly dead plankton mixed with inorganic constituents) or folisols (upland organic soils formed in cool and moist forest ecosystems of boreal regions by the accumulation of forest material, mostly tree leaves, under well drained but highly acidic conditions). Peat derives from the remains of plant and animal constituents that have accumulated over time under anoxic conditions principally caused by an almost constant and complete water-saturation of soils (Rydin & Jeglum 2006).

Peat can therefore only form in wetlands, which were defined by Joosten & Clarke (2002 p. 24) as "area[s] that [are] inundated or saturated by water at a frequency and for a duration sufficient to support a prevalence of vegetation typically adapted for life in saturated soil conditions". As stated by Singh (2010 p. 30), "there is no single, indisputable, ecologically-sound definition for wetlands, primarily because of the diversity of wetlands and because the demarcation between dry and wet environments lies along a continuum". The *International Convention on Wetlands of International Importance, especially as Waterfowl Habitat*, known as the Ramsar Convention from the name of the city in Iran were it was signed in 1971, defines wetlands based more on hydrological terms as "areas of marsh, fen, peatland or water, whether natural or artificial, permanent or temporary, with water that is static or flowing, fresh, brackish or salt, including areas of marine water the depth of which at low tide does not exceed six metres" (Ramsar Convention Secretariat 2013). A number of definitions have also been proposed that include pedological criteria on top of hydrological and botanical criteria. This is the case with the US Fish and Wildlife Service (Cowardin *et al.* 1979) and the French legislation (*Arrêté du 24 juin 2008 précisant les critères de définition et de délimitation des zones humides en application des articles L. 214-7-1 et R. 211-108 du code de l'environnement*) for instance.

The frequency and duration of soil saturation required for peat formation are generally higher than those required for the development of a vegetation adapted to wet conditions, and therefore peat does not form in all wetlands. A wetland with a naturally accumulated peat layer and dominated by vegetation that is currently producing peat is called a mire (Joosten & Clarke 2002). Joosten & Clarke (2002) proposed the use of "suo" (from Finish) to define a wetland with or without a peat layer dominated by vegetation that may produce peat. This terminology is, however, very rarely used in practice. Wetland, suo and mire are increasingly narrow definitions. A mire is by definition a suo, and a suo a wetland, but the opposite is not true (Figure 1-1).

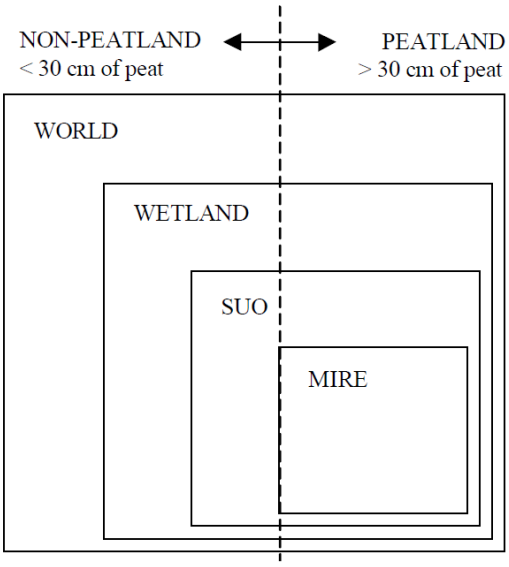

Figure 1-1. Relationship between mire, suo, wetland and peatland (Joosten 2004).

A peatland is an area with a naturally accumulated peat layer at the surface, with or without peat-forming vegetation (Joosten & Clarke 2002). The International Mire Conservation Group has retained a depth threshold of 30cm (Joosten & Clarke 2002; Joosten 2004), but this threshold varies between 20cm and 70cm of peat with country and scientific discipline. By definition, peatlands must have been mires (and wetlands) at some stage in their history for peat to have accumulated, but may have lost their peat-forming vegetation, for instance through vegetation removal for peat mining. They may also have lost all wetland-defining characteristics, for instance through drainage and cultivation.

1.2.2. Peatland distribution

There is no definitive estimate of the area covered by peatlands (Charman 2002; Joosten & Clarke 2002; Rydin & Jeglum 2006; Yu *et al.* 2010). This is, in part, due to the different definitions of peat and peatland used in different countries, but also to technical difficulties in inferring the organic content and depth of peat soils using remote-sensing techniques. Maltby & Immirzi (1993) provided a range of 3.88-4.08x10^6 km^2. Joosten & Clarke (2002) suggested a figure of about 4 x10^6 km^2. The International Mire Conservation Group launched the Global Peatland Database initiative in 2004 to refine these estimates but this is still an on-going project (Joosten 2004). Based on preliminary results, Rydin (2006) estimated the global peatland surface to be 4.16x10^6 km^2, about 3% of the land mass. Peatlands are found in almost every country of the world (Schumann & Joosten 2008), however the overwhelming majority (87% according to Joosten & Clarke 2002) are located under boreal and sub-arctic latitudes (Figure 1-2), where low evapotranspiration rates lead to a positive water balance all year round and the development of

large extents of mires. Most of the other peatlands are located under tropical or subtropical latitudes, particularly in south-east Asian coastal plains and the Amazon Basin, where extremely high rainfall compensate for high evapotranspiration rates. Most tropical peatlands occur within larger forested wetland systems with predominantly mineral soils and are therefore difficult to map precisely (Thompson & Hamilton 1983 in Charman 2002).

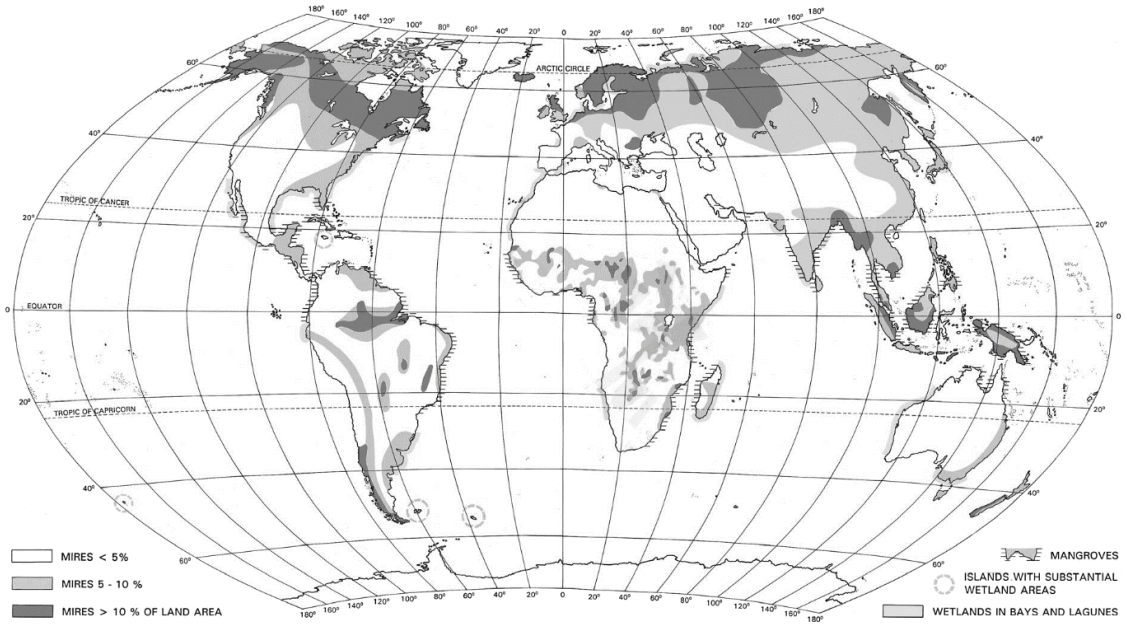

Figure 1-2. Global distribution of mires (from Lappalainen 1996).

1.2.3. Mire classification

Charman (2002 p. 5) stated that "the classification of peatlands is probably one of the most fraught and misunderstood systems of all, […] probably because there are so many criteria that can be used, and almost all of them are continuous rather than discrete variables". Most countries where peatlands cover a substantial area have developed classification systems and few are compatible with each other. Moore (1984) recognised seven main criteria used either individually or in combination to classify peatlands:

- floristics, i.e. based on plant species composition. This is generally favoured in countries where the number and extent of peatlands is small, for instance in France. Plant species are often assumed to be reliable proxies for other factors that are more difficult or time-consuming to measure, such as water chemistry or hydrology.
- vegetation physiognomy, i.e. the structure of the dominant plant species, particularly used in Russian and Scandinavian systems.

- morphology, i.e. the shape of the peatland, sometimes on a variety of scales, from the entire peat mass to micro-topographic features such as pools, hummocks, hollows and lawns. This is generally favoured in large-scale surveys based on aerial photograph interpretation (Ivanov 1981). The development of new methods in GIS-based terrain analysis and high-resolution remote-sensing of ground elevation such as LiDAR have recently led to a renewed interest in morphological characterisation and classification of peatlands (Anderson *et al.* 2010; Richardson *et al.* 2010; Hasan *et al.* 2012; Millard & Richardson 2013; Tang *et al.* 2014).
- hydrology, i.e. the source of water supply and/or the water dynamics within the peatland. More often than not, the hydrology of peatlands is actually inferred from other criteria, in particular floristic and morphological.
- stratigraphy: the characteristics of the peat column based on the examination of peat cores are used to infer the developmental history of the site.
- chemistry of the superficial peat or of the groundwater.
- the peat value for horticultural, energy-production or agricultural uses. These classifications are generally based on peat physical characteristics and its botanical origin.

One of the earliest and most widely used divisions of peatlands is that between bogs and fens. Joosten & Clarke (2002) stated that this division was initially based on the peatland morphology and on the consequent use of the land after peat exploitation. Bogs (*regenmoor* or *hochmoor* in German, *haut-marais* in French) are raised above the surrounding landscape. After peat extraction, carried out under dry conditions after drainage, a mineral subsoil remained. On the contrary, fens (*niedermoor* in German, *bas-marais* in French) are situated in depressions and were exploited by dredging. The result of the exploitation was open water.

This division corresponds to a fundamental distinction in terms of the main source of water. The morphology of fens means that a substantial part of their water input has previously flowed through or on mineral ground: they are minerotrophic peatlands (from Latin *minera* “mine, ore”, and Greek *trophe* "food, nourishment”). Conversely, bogs are peat bodies that are elevated above the surrounding landscape. As such, the unique water and therefore nutrient inputs to the mire upper peat is from precipitation: they are ombrotrophic peatlands (from Greek *ombros* “rain shower” and *trophe* "food, nourishment”). Precipitation water is acidic and poor in dissolved minerals (Vet *et al.* 2014). In contact with the pedosphere and the lithosphere, the chemical composition of water changes. The degree of change is extremely variable depending on the properties of climate, soils, vegetation, land use and bedrock within the catchment and

on the water residence time, influenced by the catchment area and topography and the physical properties of soils and bedrock (Hiscock & Bense 2014). However, in most cases contact with the pedosphere and the lithosphere results in higher contents of dissolved minerals and a higher pH. The chemistry of water inflows, and therefore the proportion of inflow received from precipitation, has profound consequences on the ecology of the mire. It determines a fundamental ecological gradient, or more exactly a series of environmental gradients that more or less tally with each other, that can be identified with almost all the criteria listed above and is therefore common to almost all peatland classification systems: the bog – fen / base-poor – base-rich / acidic - alkaline / precipitation-fed (ombrotrophic) – groundwater-fed or surface water-fed (minerotrophic) / convex – concave morphology / *Sphagnum* – brown mosses gradient (see Section 1.2.4). However this general picture can have some exceptions. Some waters flowing through siliceous sands or granites for instance may have a chemical composition very similar to that of precipitation, and minerotrophic fen vegetation in these environments may resemble that of ombrotrophic bogs (Wheeler & Proctor 2000). Inversely, bogs in coastal areas tend to receive more nutrients from precipitation than their counterparts in continental areas, due to higher precipitation totals and a slightly higher concentration of minerals. Consequently, Bridgham (1996) and Wheeler & Proctor (2000) suggested that the definition of bog should include all acidic, base-poor mires generally dominated by *Sphagnum* mosses, while fen should be only used to refer to neutral to basic, base-rich mires generally dominated by graminoïds and brown mosses.

A distinction has also classically been made between cases where peat started to accumulate in open water systems (terrestrialisation mires, for instance floating mats on lakes) or directly on mineral ground (paludification mires, for instance blanket bogs). Another terminology often used in peatland science is based on the suffix –*genous*, from Greek -*genes* "born of, produced by", and a prefix indicating the main source of water inflow to the peatland. Unfortunately there has been a large amount of confusion on the meaning of both suffixes and prefixes. The suffix –*genous* is generally understood as referring to the current source of water (Joosten & Clarke 2002; Rydin & Jeglum 2006; Wheeler *et al.* 2009), but some researchers have used it to describe the conditions, and in particular the source of water, that initially triggered peat accumulation (Julve 1998; Manneville *et al.* 1999). These are identical in most, but not all, cases. For instance many ombrotrophic raised bogs developed from minerotrophic fens (Hughes 2000; Hughes & Dumayne-Peaty 2002; Hughes & Barber 2003, 2004). There has also been much confusion on the meaning of prefixes. Von Post was the first to use this terminology and defined topogenous

mires as those “developing in terrestrialising lakes or river valleys or at springs”, and soligenous mires as fed by “meteoric water running off from the surrounding terrain” (Von Post & Granlund 1926, in Joosten & Clarke 2002). Accordingly, Joosten & Clarke (2002) defined ombrogenous mires as “stemming solely from precipitation water”, soligenous mires as “stemming from precipitation water and superficial runoff”, and lithogenous mires as “also stemming from deep groundwater”. They also defined thallassogenous mires as fed by seawater. Inversely, Charman (2002) and Rydin (2006) defined topogenous mires as arising from a static groundwater table resulting from a particular topographic position, such as in a basin or a floodplain, soligenous mires as those fed by flowing water, for instance spring or sloping fens, and limnogenous mires as those forming as a result of the influence of a lake or river. Charman (2002) states that in practice limnogenous and topogenous mires can hardly be differentiated, and indeed Rydin (2006) cites floating mats as an example in his description of both limnogenous and topogenous mires. Accordingly, Wheeler *et al.* (2009) only retains the terms soligenous, topogenous and ombrogenous.

A number of mire classifications currently in use are detailed in Appendix A, since, taken together, they provide a good overview of the diversity of mire types, of the varying hydrogeomorphic settings that explain them and of their hydrological functioning.

1.2.4. Vegetation and environmental gradients in mires

In two seminal studies, Wheeler & Shaw (1995) and Wheeler & Proctor (2000) investigated the environmental factors driving vegetation in British fens and mires of north-west Europe respectively. They showed that mire vegetation could be summarised by three principal gradients corresponding to base richness and pH, fertility and water level. These three gradients have also been recognised by many authors (Anderson *et al.* 1995; Asada 2002; Hájek *et al.* 2006; Marini *et al.* 2008; Sottocornola *et al.* 2008), even though their respective importance will strongly depend on the scope of the study, in terms of both spatial scale (Hájková *et al.* 2004) and mire types included, and on the variables used to characterise the physico-chemical conditions. The findings described below refer to temperate and boreal mires of the northern hemisphere only.

Base-richness and pH seem to be the primary environmental gradient explaining vegetation in mires (Wheeler *et al.* 2009). pH in itself has little relevance to plant life but is related to a number of other geo-chemical processes, for instance the concentration in the soil solution of phytotoxic metals such as aluminium, manganese and iron. Wheeler & Proctor (2000) stated that the

distribution of pH values in mires is bimodal, corresponding to pH buffering by humic acids (pH<5.5) and the bicarbonate system (pH>6.0), however this was relativized in the case of Scandinavian mires by Økland *et al.* (2001) who observed a more gradual transition. Mires with low pH are dominated by *Sphagnum* mosses, ericoids and calcifuge sedges, while those with high pH are dominated by "brown" mosses and dicotyledonous herbs. Bryophytes seem particularly responsive to this gradient (Vitt & Chee 1990). Ombrotrophic bogs, only fed by meteoric water, are always acidic, even though bogs located in hyper-oceanic climates may have a higher base content than continental ones. The pH and base content of minerotrophic mires depends on the source of water and the bedrock geology. Base-rich mires may become acidified upon drying, due to the release of oxidised forms of sulphur in sulphur-rich mires (Lucassen *et al.* 2002; Clark *et al.* 2005) or to higher infiltration rates of meteoric water, and this mechanism has in some cases been shown to have triggered the development of raised bogs overlying base-rich fens (Giller & Wheeler 1988).

The second most important environmental gradient is fertility (Wheeler & Shaw 1995; Wheeler & Proctor 2000). Ideally, fertility is measured using phytometric assays, whereby biomass production on peat samples is measured in standardised conditions (Wheeler *et al.* 1992). Fertility depends on the availability of nitrogen, phosphorus and potassium but concentrations in mire water or peat extracts may not always reflect it well (Wheeler *et al.* 1992). The fertility gradient is more evident in base-rich than acidic mires (Peterka *et al.* 2014).

Wheeler & Shaw (1995) reported that the third most important environmental gradient in British fens was related to water table depth. Water levels influence a range of physico-chemical processes, in particular nutrient availability. Flow through the root zone has also been shown to influence vegetation. This is for two reasons: redox potential is generally higher in peat through which there is a substantial flow than in stagnant conditions (Armstrong & Boatman 1967), and increased flow leads to increased nutrient supply, even under ombrotrophic conditions.

Wheeler *et al.* (2009) stated that the fact that pH and fertility appears to be more important than water levels in explaining differences in mire vegetation may seem surprising given the obvious importance of this factor as empirically evidenced by vegetation zonations around open water for instance. They explained this apparent paradox by the fact that a limited number of water table depth records can be poor estimators of soil moisture conditions experienced by plants, due to the larger variability in time than in space of water levels in wetlands, to the sensitivity of some species to extreme values and to differences in soil hydrophysical properties. Asada (2002)

for instance found two distinct floristic gradients in a Japanese mire, one strongly correlated to pH and mean, minimum and maximum groundwater table depth, and the other to the groundwater table depth standard deviation. Wierda *et al.* (1997) have also highlighted the importance of the amplitude of groundwater table depth fluctuations. Some researchers have attempted to devise indicators that would be more representative of aeration and hydric stresses to which plants are exposed when air and water, respectively, rarefy within the root zone. Gowing *et al.* (1998) and Silvertown *et al.* (1999) used sum exceedence values (SEV), corresponding to the period of time during the growing season for which the water level is higher or lower than a specified threshold that may vary according to the physical properties of soils. Bartholomeus (2010) and Bartholomeus *et al.* (2008, 2012) developed a new process-based proxy for oxygen stress and demonstrated that it performed better than SEV or mean spring groundwater level at predicting vegetation characteristics. However such proxies are difficult to calculate as they require high-frequency observed or modelled groundwater table depth data over long periods and detailed data on soil physical characteristics.

Understandably given the costs and technical difficulties associated with long-term hydrological monitoring in remote sites, most researchers have used relatively crude estimators of the hydrological regime (see for instance Kleinebecker 2007; Kleinebecker *et al.* 2007, 2010, who used a single record of groundwater table depth in Patagonian mires). Despite this, a large number of studies carried out at the site or regional scale have shown a clear relationship between plant species distribution and hydrological characteristics in mires, and, for a substantial proportion of them, the predominance of the water regime over other environmental factors to explain vegetation patterns (Glaser *et al.* 1990; Bridgham & Richardson 1993; Jeglum & He 1995; Bragazza & Gerdol 1996, 1999a; b; Bragazza 1997, 1999; Wierda *et al.* 1997; Asada 2002; Miserere *et al.* 2003; Hájková *et al.* 2004; Nekola 2004; Hájková & Hájek 2004; Bragazza *et al.* 2005; Yazaki *et al.* 2006; Sottocornola *et al.* 2008; Pellerin *et al.* 2009; Jeglum 2011; Jabłońska *et al.* 2011; Conradi & Friedmann 2013; Hettenbergerová *et al.* 2013). At the microform scale, the association of *Sphagnum* species for instance with particular water table depths and their arrangement along the hollow-hummock gradient has long been recognised in ombrotrophic mires (Lindsay 1995).

Wheeler *et al.* (2009) suggested that the lower importance of the water regime in large scale studies than in site- or regional-scale investigations may be explained by the fact that the response of plant species to soil moisture may differ across sites or mire types due to modulation by other factors such as competition (Nordbakken 1996), facilitation, concentrations of elements

that become phytotoxic in their reduced form (Fe, Mn, S), and the availability of nutrients. Consequently, the search for an exact relationship between water level and plant species that would be valid across large geographical areas has often proved elusive.

1.2.5. Values and environmental services

Values and functions of peatlands were extensively reviewed by Joosten & Clarke (2002) and Parish *et al.* (2008). Joosten & Clarke (2002) distinguished production functions (peat extraction for instance), carrier functions (often resulting in their destruction, such as their use for waste disposal or water reservoir creation), regulation functions (the chief of which is regulation of the global climate), informational functions (recreation, aesthetic, scientific and spiritual functions; including their invaluable function as environmental archives, Charman 2002), and transformation and option functions (possible future functions). It is beyond the scope of this review to detail them all, and only a few functions particularly important at the global scale (global climate regulation) or within the study area (biodiversity, water quality regulation) are discussed.

1.2.5.1. The role of peatlands in the global climate

Peatland sequester atmospheric carbon through photosynthesis and peat accumulation. Even though they occupy a relatively small proportion of the Earth, the high carbon concentration in peat make peatlands a globally important carbon store, with a major role in the global carbon cycle and climate system. Recent reviews of this role can be found in Frolking *et al.* (2011), Yu *et al.* (2011), Worrall *et al.* (2011) Lindsay (2010), Worrall *et al.* (2010), Parish *et al.* (2008), Strack (2008) and Limpens *et al.* (2008). A slightly older but detailed review can be found in Joosten & Clarke (2002). Peatlands contain approximately 600 gigatons of carbon (Yu *et al.* 2010). For comparison, the atmosphere contains 830 gigatons of carbon. The peatland carbon store is equal to the carbon stock in all terrestrial biomass, twice the carbon stock in the forest biomass, and about a third of all terrestrial carbon, even though peatlands occupy only 3% of the land area. Peatlands are the most efficient carbon store of all terrestrial ecosystems (Parish *et al.* 2008). Long-term carbon accumulation rate in peatlands since the last ice age is approximately 16-88 gigatonnes every thousand years.

Pristine mires are currently weak sinks of atmospheric CO_2, moderate sources of methane and very weak sources of N_2O (Frolking *et al.* 2011). Given that these gases have different atmospheric lifespans and global warming potential, the net radiative forcing of mires depends

on the time horizon chosen. It is positive over timescales shorter than 50-100 years, but negative over longer timescales (i.e. carbon sequestration in peat contributes to cooling the global climate), even though minerotrophic mires are larger sources of CH_4 and smaller CO_2 sinks than ombrotrophic ones and as a consequence have a positive radiative forcing even over long time scales (Joosten & Clarke 2002). However carbon fluxes in peatlands are highly dependent on redox, and therefore hydrological, conditions, which may vary at daily to interannual scales. Consequently, peatlands are a large, potentially vulnerable carbon store that could have a major warming effect on the climate if destabilised (Frolking *et al.* 2011). Anthropogenic perturbations such as drainage, peat extraction or fire lead to a switch in the radiative forcing of peatlands from negative to positive. These perturbations are currently responsible for the release of at least 3,000 million tonnes per year of carbon dioxide, more than 10% of the global anthropogenic emissions (Parish *et al.* 2008). Because of the large emissions from degraded peatland, restoring and rewetting them is one of the most efficient way to reduce anthropogenic carbon emissions (Parish *et al.* 2008).

By changing the energy and water balance of mires, climate change will also impact their carbon balance. The distribution of mires, particularly ombrotrophic ones, is clearly climate-driven, and empirical bioclimatic envelope models predict a substantial reduction in the area suitable for peatland development on the southern edge of their present distribution (Gallego-Sala *et al.* 2010; Clark *et al.* 2010; Gallego-Sala & Prentice 2013; Coll *et al.* 2014). It is therefore likely that they will become net sources of carbon. The evolution of carbon fluxes in boreal peatlands is more uncertain. It has recently been shown that carbon accumulation rates in these have increased during warmer climate intervals since the last ice age, suggesting that pristine peatlands have served as a negative feedback to climate change over the Holocene (Yu *et al.* 2011). However the extent to which this will occur in the future is still unclear. There is also much uncertainty about the future of permafrost in boreal mires. Carbon in permanently frozen peat is relatively inert, so climate change could make very large stores of organic matter available for decomposition if it leads to permafrost melting (Frolking *et al.* 2011). Reviewing the current evidence, and while acknowledging for a large uncertainty, Frolking *et al.* (2011) concluded that peatlands will not become a "carbon bomb" in the 21st century, but rather, will be a relatively small but persistent carbon source that will further impede efforts to maintain emissions below target. The potential impact of climate change on mires is further discussed in Section 1.2.6.2.

1.2.5.2. Peatlands and water quality

Because of their hydrological and biogeochemical characteristics, that differ markedly from other types of soils (Reddy & DeLaune 2004), the presence of wetlands, including peatlands, within a catchment may have substantial impacts on the chemistry of water draining from it (Johnston *et al.* 1990; Fisher & Acreman 2004). This impact is particularly relevant to the Monts d'Ambazac where five reservoirs are the only source of drinking water for the more than 200,000 inhabitants of the nearby city of Limoges and surrounding villages (Anonymous 2014). The Dauges mire investigated in the current study is located just upstream of the largest of these reservoirs.

An increase in dissolved organic carbon (DOC) in stream fed by peatland-dominated catchments has been observed over the last decades, principally caused by current climate change (Freeman *et al.* 2001, 2004). DOC concentrations have for instance doubled since the late 1980s in streams draining blanket bogs in England (Evans *et al.* 2005). Increased DOC concentrations in streams used for water abstraction is an important issue for the water supply industry since DOC gives a brown color to water, may be bound to metallic pollutants, promote bacterial growth and leads to the formation of carcinogenic trihalomethane in the presence of chlorine (Gough *et al.* 2014). DOC dynamics in peatlands are complex, but numerous studies have shown that its formation and release are promoted by lower and more variable groundwater levels (Freeman *et al.* 2001; Clark *et al.* 2005, 2009; Strack *et al.* 2008; Fenner *et al.* 2013). It has been shown that the restoration of wetter conditions in peatlands through drain blocking and revegetation of eroded areas lead to a reduction in DOC (Wallage *et al.* 2006; Höll *et al.* 2009; Armstrong *et al.* 2010; Parry *et al.* 2014) (Wallage *et al.* 2006; Höll *et al.* 2009; Armstrong *et al.* 2010; Parry *et al.* 2014). Consequently, a number of water supply companies now fund peatland restoration in Great-Britain (South West Water 2014).

Because they are characterised by organic soils and reductive conditions, peatlands have been shown to constitute major sinks for almost all metallic and metalloid pollutants, including radionuclides (Sobolewski 1999; Brown *et al.* 2000; Ringqvist *et al.* 2002; Tipping *et al.* 2003; Rothwell & Evans 2004; Rothwell *et al.* 2008; Szkokan-Emilson *et al.* 2013). This environmental service provided by mires is particularly relevant to the research site due to its history of uranium mining, further detailed in Section 2.6.2, and to the high concentration in arsenic in bedrocks and groundwaters in the area (Mauroux *et al.* 2009). Moore (1954, in Owen & Otton 1995), for instance, showed in the laboratory that peat could retain up to 98% of uranium contained in water flowing through it. In Sweden, Lidman *et al.* (2012) have shown that approximately 65-80%

of uranium and 55-65% of thorium entering mires are retained in the peat. Some mires, natural or constructed, have been used to clean effluents from uranium mines (Schöner *et al.* 2009). Mires are also sinks for arsenic (Langner *et al.* 2012). For instance, González A et al. (2006) have measured a reduction in arsenic concentrations in a stream crossing an acidic minerotrophic mire in Switzerland from 400µg.l^{-1} upstream of the mire to less than 2µg.l^{-1} downstream. However sequestered pollutants can be released back in soil solution and watercourses if groundwater levels are lowered or become more variable (Schöner *et al.* 2009), for instance following drainage (Rothwell *et al.* 2009, 2010, 2011) or climate change (Tipping *et al.* 2003; Cortizas *et al.* 2007; Wällstedt *et al.* 2010; Rose *et al.* 2012; Szkokan-Emilson *et al.* 2013).

1.2.5.3. Biodiversity in peatlands

Peatland are extreme environments, being constantly wet, partly anoxic, generally nutrient-poor, often colder than surrounding mineral soils, and, for part of them, among the most acidic environments on Earth (Rydin & Jeglum 2006). Organisms that are adapted to these conditions are generally highly specialised and, for a number of them, cannot grow in other habitats (Parish *et al.* 2008). Bryophyte diversity is particularly high in mires: in Russia and the Baltic States, between 21 and 69% of all moss species and between 37 and 70% of all liverwort species are found in mires (Parish *et al.* 2008).

French mires, particularly ombrotrophic ones, are located at the southern edge of the distribution area of mires in the northern hemisphere (Julve 1996). They are relatively rare and highly original habitats within the country, and, as a consequence, species that live in these habitats are also rare. For instance, montane acidic mires offer suitable habitats to a range of boreal species that would not otherwise occur in France. Mires cover about 0.14% of Metropolitan France only (about 79,000 hectares according to the last available inventory, MEDDE/CGDD/SOeS & Fédération des Conservatoires d'Espaces Naturels 2013), yet 9% of vascular plant species legally protected at the national level, 6% of red list vascular species and 6% of all vascular plant species are only or principally found in mires (Julve 1996). Mires are also a habitat for a large number of other wetland species (Manneville *et al.* 1999). As a consequence, most mire habitats within the EU are now protected under the EU 92/43/EEC Habitats Directive, that requires member states to designate Special Areas of Conservation (SAC) to contribute to the conservation of a list of habitats and species for which the EU has a global responsibility. At the global scale, 35% of Ramsar sites (268 sites covering 27M hectares) are peatlands (Joosten & Clarke 2002).

1.2.6. Threats to mires

1.2.6.1. Past and current threats

Threats to mire conservation were extensively reviewed by Charman (2002) and Parish *et al.* (2008). Up to now, the highest threat has lain in mire water balance perturbations through drainage, associated to anthropogenic perturbations such as agriculture, forestry and peat extraction. Peatlands are currently being destroyed at a rate of 4,000km² a year, and the global volume of peat decreases by 20km^3 a year. Agriculture (including palm oil production, Parish *et al.* 2008), forestry and peat extraction are responsible for 50%, 30% and 10% of these losses respectively (Parish *et al.* 2008).

Forestry exploitation of peatlands mainly occurs through logging of natural forested mires, sometimes accompanied by drainage and fertilisation to improve economic returns particularly in Scandinavia and Canada (Charman 2002). Afforestation of mires has been especially common in bogs of western Europe, but this has now virtually ceased following legal and fiscal changes over the last decades and some afforested peatlands are now being restored (Lunt *et al.* 2010; Cris *et al.* 2011; Parry *et al.* 2014). Forestry, including the conversion to *Acacia sp*. plantations for the pulp and paper industry, is an important threat to the conservation of tropical forested mires (Parish *et al.* 2008).

Global peat production is about 30 million tonnes per year (Parish *et al.* 2008). Peat is extracted for two main purposes: energy production and use as a growing medium or soil conditioner in horticulture and agriculture. Use of peat for energy production is the most common, but due to transport constraints it is local and restricted to countries with a large peat resource and/or limited alternative energy sources. For instance, about 5-7% of primary energy consumption in Finland and Ireland relies on peat. In Ireland, peat-powered plants generate 8.5% of electrical consumption (Paappanen *et al.* 2006). The physico-chemical properties of peat make it the ideal growing media: in Europe, peat-based growing media makes for 95% of the market (Parish *et al.* 2008). Peat extraction generally results in major perturbations to the mire ecosystem, through direct destruction or indirectly by lowering the groundwater table in non-exploited neighbouring areas. There has been numerous attempts at reducing the impact of peat exploitation through the restoration of cut-over peatlands (Boudreau & Rochefort 1999; Cooper *et al.* 2001; Price *et al.* 2002; Gorham & Rochefort 2003; Quinty & Rochefort 2003; Rochefort *et al.* 2003; Cobbaert *et al.* 2004; Chirino *et al.* 2006; Lucchese *et al.* 2010; González & Rochefort 2014) or through *Sphagnum* farming (Gaudig *et al.* 2014; Pouliot *et al.* 2015).

Joosten & Clarke (2002) estimated that anthropogenic disturbance has led to the destruction of almost 25% of mires at the global scale. Losses have been the largest in Europe, where about 52% of mires have been lost, with some countries including Germany and the Netherlands having lost over 90% of their original mire area (Joosten & Clarke 2002). In France, it is estimated that the total mire area has been reduced by approximately 50% since the end of the Second World War, when the first peat resource inventory was published (Manneville *et al.* 1999). At present, mire destruction is progressing at the fastest rate in south-east Asia, where 120,000 km² of mires have been lost since the 1960s. Over 90% of peat swamp forests in this part of the world have been sufficiently degraded to become net sources of carbon (Parish *et al.* 2008).

Air and water pollution are also altering the ecology of mires. Atmospheric nitrogen deposition has for instance been shown to impede *Sphagnum* growth (Gunnarsson & Rydin 2000) and to promote the development of *Molinia caerulea* and *Betula pubescens* in raised bogs (Tomassen *et al.* 2003, 2004), and therefore may amplify the impact of climate change (Section 1.2.6.2).

1.2.6.2. Future threats: climate change

Climate is the over-riding factor explaining mire distribution, development and characteristics at the global scale (Parish *et al.* 2008). This is particularly the case for ombrotrophic mires, in which precipitation is the sole inflow, but is also true, even though to a lesser extent, in minerotrophic mires since climate will have an impact on the catchment water balance and surface and groundwater inflows to the mire (Winter 2000; Drexler *et al.* 2013; Bourgault *et al.* 2014).

Palaeoecological records show that mires have switched suddenly (in a matter of years or decades) between different states many times during the Holocene in response to climate change (Charman *et al.* 2006; Dise 2009). Even within the last 200 years, Hendon & Charman (2004) showed that the vegetation of raised bogs in Northumberland (UK) shifted several times between wet *Sphagnum*-dominated communities and dry monocotyledon-dominated communities principally as a result of climate. Peat accumulation rates have also changed accordingly (Mauquoy *et al.* 2002; Yu *et al.* 2003). It may have stopped entirely in some cases during extremely dry periods but generally resumed once conditions became wetter again (Parish *et al.* 2008). Reviewing the evidence on the impact of past climate change on mires, Parish *et al.* (2008) concluded that even though pristine peatlands have generally been resilient, peatland response to climate change may not occur smoothly and sudden changes may occur when specific climate and/or ecological threshold are reached. However, the actual response will be determined by the peatland type and local setting.

The degree of climate change expected in the next century as a result of anthropogenic carbon emissions is far larger than any changes that have occurred since the end of the last ice age (Maslin 2014), during which most modern mires have developed. Therefore it is difficult to assess the potential impact of future climate change on mires purely on the basis of palaeoecological evidence. Experimental and observational studies investigating this issue were reviewed by Zhaojun *et al.* (2011). Mesocosm studies suggest that, even though *Sphagnum* productivity may at first be enhanced by higher temperatures and increased atmospheric CO_2 concentration, climate change is likely to result in a shift from *Sphagnum*-dominated to graminoïd-dominated (Dieleman *et al.* 2015) and/or shrub-dominated (Weltzin *et al.* 2000, 2003; Walker *et al.* 2006; Dieleman *et al.* 2015) communities in acidic mires, as a consequence of reduced soil waterlogging, bryophyte die-off during drought episodes (Gerdol *et al.* 2008; Bragazza 2008) and increased peat mineralisation and nitrogen and phosphorus availability (Zhaojun *et al.* 2011). Multi-decadal observational studies suggest that this shift in vegetation is already happening in varied locations across the globe (Hendon & Charman 2004; Malmer *et al.* 2005; Czerepko 2008).

The most worrying insight into the future of mires probably comes from empirical bioclimatic envelope or process-based models of the present and future distribution of mires at the continental or global scale. As noted in Section 1.2.5.1, such models suggest a substantial reduction in the area suitable for peatland development, in particular on the southern edge of their present distribution (Gallego-Sala *et al.* 2010; Clark *et al.* 2010; Gallego-Sala & Prentice 2013; Coll *et al.* 2014; Keith *et al.* 2014). As stated by Gallego-Sala & Prentice (2013), the decline in suitable bioclimatic space for mires does not necessarily entail their rapid disappearance, but rather that they will come under substantial hydric stress that will likely trigger important changes in hydrology, vegetation and biogeochemistry, including carbon fluxes.

Integrated hydrological modelling studies have suggested that, in some cases, the impact of climate change on the water balance of groundwater-fed mires can be mitigated by a careful management of groundwater resources, in particular trough the reduction of abstraction (Armandine Les Landes *et al.* 2014). Management of mires themselves may also be required, for instance by reducing the dominance of trees and large graminoïds with high evapotranspiration rates (Worrall *et al.* 2007; Banaszuk & Kamocki 2008).

1.3. Peatland hydrology

As evidenced in previous sections, hydrology is one of the most important factors in explaining the diversity of geomorphological, biogeochemical and ecological processes in mires (Charman 2002; Reddy & DeLaune 2004; Rydin & Jeglum 2006). The long-term maintenance of the many environmental services that mires provide depends on the persistence of their water balance and of a shallow groundwater table. The most important threats that mires face result from a perturbation of their hydrological functioning and include drainage (including as a result of peat extraction), afforestation and climate change. Hydrology is therefore central to peatland science. As such, peatland hydrology is further reviewed in this section. Additional extensive reviews of peatland hydrology can be found in Ingram (1983), Siegel & Glaser (2006), Holden (2006) and Labadz *et al.* (2010), even though the focus of the latter two publications is on British blanket bogs. A wider-scoping review of the hydrology of wetland soils, much of which is applicable to peatlands, can also be found in Richardson *et al.* (2001).

1.3.1. Water and water flow in peat soils

Water flow within peat is strongly influenced by its composition and degree of humification (Boelter 1968; Päivänen 1973; Brandyk *et al.* 2002), and therefore these factors are briefly reviewed in the following section. Subsequent sections review hydrologically-relevant peat properties such as porosity, moisture retention and hydraulic conductivity, the acrotelm/catotelm model and the impact of drying on peat properties and hydrology.

1.3.1.1. Peat composition and humification

The solid phase of peat is made of plant fibres, amorphous humus, inorganic particles and amorphous inorganic substances in the form of carbonates, phosphates and hydroxides (Szajdak *et al.* 2011). The water content at saturation and the proportion of each solid constituent depend on the plant species from which peat originates, the importance of external mineral inputs and the compaction, transformation and decomposition processes the organic matter has been subjected to after its deposition. The physical and chemical properties of peat are often expressed as a function of three main descriptors: its botanical composition, its bulk density and its degree of humification. These three descriptors are not independent of each other. Three basic botanical compositions are generally distinguished: *Sphagnum* peat, sedge & reed peat, and woody peat (Rydin & Jeglum 2006). The degree of decomposition (or humification) should theoretically be assessed by measuring the fibre or humus content by wet sieving (Parent &

Caron 2008), but this is very tedious and in practice the most widely used method to estimate the degree of peat decomposition is the von Post method (von Post 1922): a fresh sample of moist peat is pressed in one hand while the extruded liquid or mud is collected in the other hand, and field observations are matched to one of ten humification scores based on visual and tactile criteria (Table B-1 in Appendix B). Despite its simplicity, the von Post index has been proven to perform well compared to (and sometimes even better than) more complex estimators of peat decomposition (Stanek & Silc 1977; Malterer *et al.* 1992), however it tends to underestimate decomposition when applied to relatively dry peats and is not recommended in this case (Parent & Caron 2008). It is well correlated to peat bulk density (Päivänen 1973; Silc & Stanek 1977). A three-class humification scale (fibric, mesic/hemic, sapric/humic) is also often used, theoretically on the basis of the fibre content, but in practice often based on the von Post index. Table 1-1 gives the definition of the three classes according to Szajdak *et al.* (2011).

Table 1-1. Correspondance between humification classes and humification indicators (Szajdak et al. *2011).*

Humification class	Fibre content	von Post index
Fibric	>40%	1-4
Hemic (=Mesic)	10-40%	5-6
Sapric (=Humic)	<10%	8-10

1.3.1.2. Peat porosity and water retention curve

An important attribute of peat soils is their ability to hold and retain water: saturated peat is in many cases more than 90% water (based on a literature review, Letts *et al.* 2000 found median porosity values of 0.83, 0.88 and 0.93 for sapric, hemic and fibric peat, respectively). This ability is highly variable depending on the peat botanical composition, humification and bulk density. Table 1-2 and Figure 1-3 provide examples of this variability. Poorly decomposed fibric peats have very large pores and saturated water content ranges between 90% and 97%. Total porosity and the number of large pores decrease with increasing humification and bulk density, while the number of small pores increases. However total porosity is still substantially higher in highly decomposed peats (between 80 and 85%) than in mineral soils (Boelter 1968; Päivänen 1973; Brandyk *et al.* 2002).

Table 1-2. Bulk density, total porosity and specific yield measured in northern Minnesota bogs (Boelter 1968).

Organic material	Bulk density (g.cm^{-3})	Total porosity (%)	Specific yield (%)
Fibric	<0.075	>90	>42
Hemic	0.075-0.195	85-90	15-42
Sapric	>0.195	<85	<15

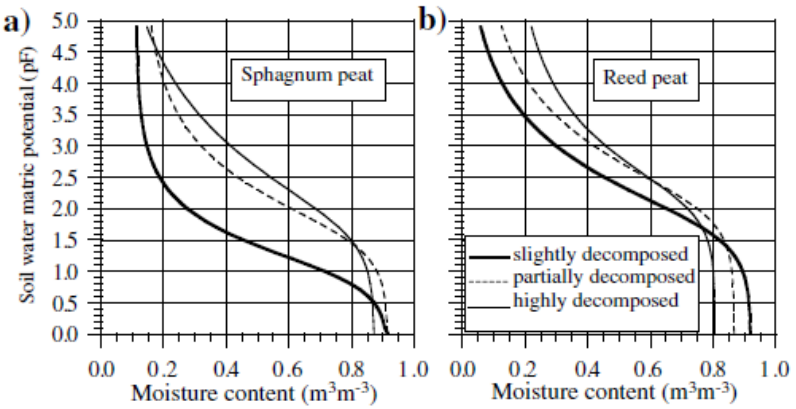

Figure 1-3. Water retention curves for Sphagnum (a) and reed (b) peats by degree of decomposition (Brandyk et al. *2002).*

The range of variation of the peat specific yield is higher than that of total porosity, particularly in *Sphagnum* peats (Figure 1-3). It can exceed 65% in fibric undecomposed *Sphagnum* peats and is about 13% in sapric *Sphagnum* peats (Boelter 1968; Letts *et al.* 2000). Whereas specific yield decreases substantially with increasing humification, the available water capacity and the residual water content (or water content at wilting point) tend to increase with increasing humification (Figure 1-3).

1.3.1.3. Peat hydraulic conductivity

Most researchers who have measured peat hydraulic conductivity have generally used slug tests within piezometers or laboratory methods applied to small peat volumes. The values recorded therefore relate to hydraulic conductivity at the scale of a few tens of centimetres. Using such methods, peat saturated hydraulic conductivity has been found to be very variable, with values ranging from less than 10^{-12}m.s^{-1} (almost impermeable) to more than 10^{-3}m.s^{-1} (highly permeable, Boelter 1968; Ivanov 1981; Letts *et al.* 2000). Hydraulic conductivity is generally negatively correlated to bulk density and to peat humification (Figure 1-4, Figure 1-5), and more so for *Sphagnum* peats than for sedge, reed and wood peats. This large decrease in hydraulic conductivity with peat humification combined with the parallel decrease in specific yield described in Section 1.3.1.1 has important consequences on the eco-hydrological functioning of mires (see Sections 1.3.1.4 and 1.3.2.5). Indeed, peat humification and bulk density tend to increase with depth, leading to the decrease in hydraulic conductivity with depth commonly (but not systematically) observed in peatlands (Päivänen 1973; Ivanov 1981). Päivänen (1973) for instance recorded hydraulic conductivities at a depth of 55cm that were on average 4.5% (1% in *Sphagnum* peats) of those recorded in the upper 15cm.

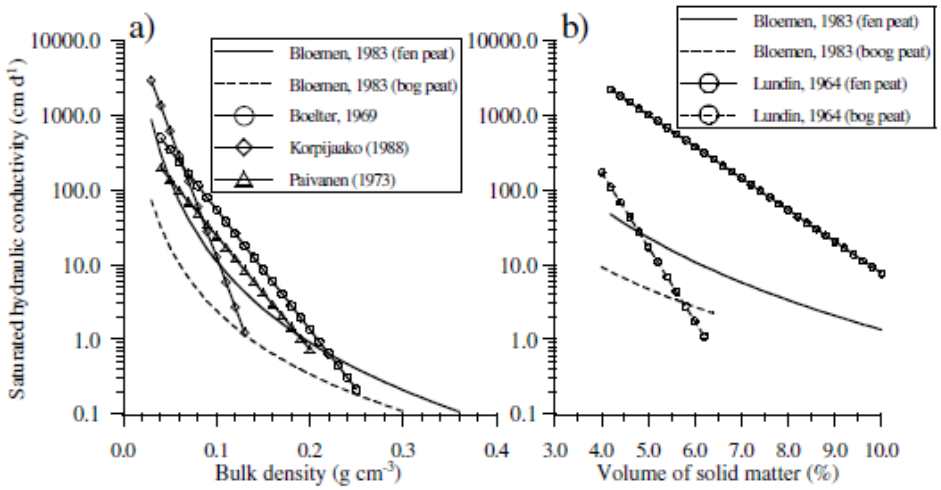

Figure 1-4. Relationship between saturated hydraulic conductivity and (a) bulk density or (b) volume of solid matter (from Brandyk et al. *2002).*

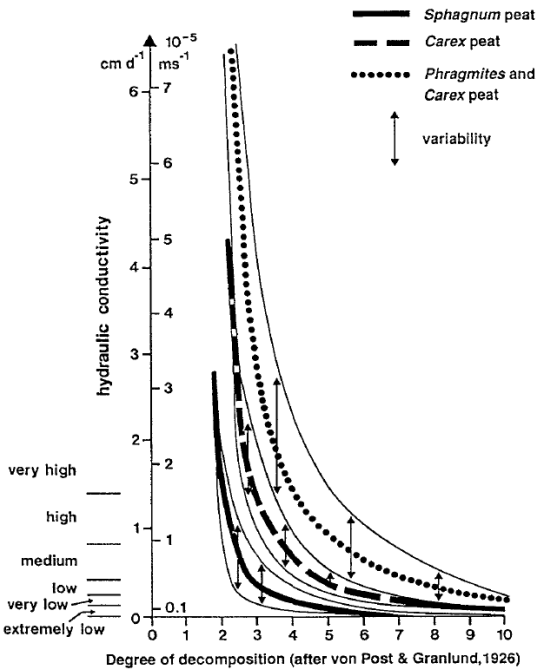

Figure 1-5. Peat saturated hydraulic conductivity as a function of botanical composition and von Post's humification index (from Eggelsmann et al. *1993).*

However the relationship between saturated hydraulic conductivity and bulk density or degree of humification is associated with large errors, and the use of pedotransfer functions based on the latter yields uncertain results (Päivänen 1973; Chason & Siegel 1986).

Based on slug test results, it has been suggested that flow in peat soils may depart from Darcy's law, particularly in humified *Sphagnum* peats (Ingram *et al.* 1974; Rycroft *et al.* 1975; Waine *et al.* 1985): hydraulic conductivity was observed to depend on hydraulic gradient. It was later shown that this apparent departure from Darcy's law could be explained by the effects of matrix

compression and swelling during slug tests which cause variable water storage in peat, and it has been argued that Darcy's law remained an appropriate tool for use in peatland hydrological modelling (Hemond & Goldman 1985; Brown & Ingram 1988). Galvin & Hanrahan (1967) attributed similar laboratory observations to air entrapment, and Baird & Gaffney (1995) to the expansion and contraction of methane bubbles. Ivanov (1953, in Brandyk *et al.* 2002) and Bondarenko *et al.* (1975, in Brandyk *et al.* 2002) found in the laboratory that hydraulic conductivity decreased with time. This was explained by the progressive colmatation of peat pores by gas bubbles and peat particle migration caused by water flow.

Seasonal variation in peat hydraulic conductivity has also been reported. This has been explained by the high compressibility of the peat matrix and the response to seasonal changes in water storage (Oleszczuk et al. 1995, in Brandyk *et al.* 2002) or by the seasonal variations in the production of biogenic gas obstructing peat pores (Beckwith & Baird 2001). Peat saturated hydraulic conductivity is commonly anisotropic due to the horizontal stratification of plant materials such as *Sphagnum* leaves or reed leaves. The ratio between horizontal and vertical hydraulic conductivities is highly variable, but in the order of one or two orders of magnitude (Chason & Siegel 1986). It is generally higher in weakly decomposed peats, and close to unity in strongly decomposed peats (Ostromecki, 1936, in Brandyk *et al.* 2002). The high small-scale variability in peat hydraulic conductivity, both spatially and temporally, results in complex small-scale flow patterns within peatlands that may lead to small-scale variability in peat and groundwater chemistry and in species distribution (Drexler *et al.* 1999; Gilvear & Bradley 2009).

Using laboratory methods, slug tests and steady-state and transient ditch pumping tests, Bromley *et al.* (2004) measured hydraulic conductivity in a large raised bog in Yorkshire, UK, at several spatial scales, from 0.002m^3 (laboratory methods) to 360m^3 (single ditch transient test). They showed that, like in many low permeability materials, the hydraulic conductivity of peat is strongly scale-dependant and varies by up to three orders of magnitude depending on the method used and the scale of investigation. The highest values were obtained at the largest scale and were similar to calibrated values obtained using site-scale hydrological modelling. The authors concluded that site-scale hydrological models should not be parameterised with small-scale measures of hydraulic conductivity. Small-scale techniques only measure the permeability of the peat matrix, and generally fail to account for preferential flow pathways caused by heterogeneities in the peat matrix, macropores or pipes. Even in the absence of substantial anisotropy of the peat matrix itself, the presence of a small layer of poorly decomposed peat within a generally strongly humified peat profile can lead to a very high composite hydraulic

conductivity and the development of a strong lateral preferential flow within that layer (Richardson *et al.* 2001). Layers of wood or reed peat or permeable alluvial or colluvial deposits in minerotrophic mires may also increase the composite hydraulic conductivity of peat when measured at the larger scale. The existence of preferential flow through pipes has long been recognised (Newson 1976; Gilman & Newson 1980; Ingram 1983; Eggelsmann *et al.* 1993),and they can have have a substantial hydrological role. Holden & Burt (2002) for instance found that pipeflow contributed around 10% and at times up to 30% of streamflow volume in a Pennine blanket bog, while Jones (2004) reported contributions in excess of 40% of total stream flow in similar environments.

1.3.1.4. The acrotelm/catotelm model

As stated by Charman (2002), changes in peat structure with depth are obvious to anyone who has dug or cored into a peatland. The peat changes from loose, living vegetation at the surface to brown or black peat much denser in structure at depth. This change is generally not smooth and there is a relatively sharp transition between the upper and lower layers. In pristine mires, hydraulic conductivity and specific yield rapidly decrease with depth, while humification and bulk density increase. This led Ivanov (1953, in Ingram 1978) to conceptualise mires as a two-layer system. The upper layer contains the oscillating water table, has a variable water content, is subject to air entry, is weakly humified and has a high hydraulic conductivity and high specific yield. The lower layer is always saturated, is not periodically exposed to air, is highly humified, and has a negligible hydraulic conductivity and a small specific yield. Ingram (1978) named the upper layer the acrotelm and the lower layer the catotelm, and used the lowest groundwater table depth to define the boundary between them. At its origin, the acrotelm/catotelm concept was therefore hydrologically based and strongly linked to Ingram's (1982) groundwater mound hypothesis. However this definition is highly dependent on the observation period (Morris *et al.* 2011), and other definitions have been proposed. Clymo (1984) defined the acrotelm as the upper, primarily oxic layer where decomposition is relatively quick; and the catotelm as the lower, primarily anoxic layer where decomposition is slow. Van der Schaaf (2002) proposed to define the acrotelm pedologically, as the top layer of a mire from the surface downwards to the level where the von Post humification index first reaches four.

Even though most authors agree on the presence of a highly conductive, weakly decomposed peat layer in pristine mires, the lower layer may in some cases not be as homogeneous and hydrologically inactive as suggested by the acrotelm/catotelm model. Chason & Siegel (1986)

found considerable variations in hydraulic conductivity and little dependence to depth in a raised bog – spring fen complex in Minnesota, USA. Similarly, Holden & Burt (2003) found little dependence of hydraulic conductivity to depth in Pennines blanket peats, except for a high permeability of the top 10cm of the peat profile. The overall permeability of the catotelm peat is also variable: some researchers have concluded that the catotelm was impermeable (van der Schaaf 2002) while others have measured relatively substantial flow through the catotelm (Chason & Siegel 1986). Indeed, the acrotelm/catotelm model may be more applicable in *Sphagnum*-dominated raised bogs that in some fens with a weakly humified catotelm and where the difference in hydraulic conductivity between the upper and lower peat layer may be smaller (Ingram 1983).

1.3.1.5. The impact of drying on peat soil properties

A drop in the groundwater table, following drainage for instance, can result in a lowering of the ground surface through primary compression, shrinkage, secondary compression and finally wastage (Eggelsmann *et al.* 1993). Primary consolidation occurs through loss of buoyancy of the upper aerated peat layer that results in a compression of the underlying waterlogged peat. Water is expelled from the larger peat pores and the porosity decreases through the reduction in pore size. Primary consolidation can result in a subsidence of 1.5m of an initial 10m peat depth over a year if the water table is maintained at 1m below ground surface (Hobbs 1986). It is larger in weakly decomposed peats due to the larger pore size. Inversely, shrinkage is large in highly humified peats due to the smaller size of fibres. Secondary compression occurs through the expulsion of water from peat micropores, and is much slower than primary compression. Finally, wastage results from the oxidation and decay of the aerated peat (Eggelsmann *et al.* 1993; Brandyk *et al.* 2002). A number of changes in peat physical properties occur during drying. These are summarised in Figure 1-6. Two years after an experimental 20cm water drawdown in a Canadian fen, Whittington & Price (2006) recorded surface subsidence of 5-20cm, a decrease in saturated hydraulic conductivity by one to two orders of magnitude, and an increase in bulk density by up to 60%. If the water table drawdown is prolonged, irreversible changes in these physical properties may occur through increased peat decay and humification. Long-term drying and oxidation of superficial peat, for instance following artificial drainage, leads to the formation of moorsh materials: peat takes a grainy structure and becomes hydrophobic and resistant to rewetting, further preventing recovery (Brandyk *et al.* 2002; Ilnicki & Zeitz 2003; Okruszko & Ilnicki 2003; Kalisz *et al.* 2015).

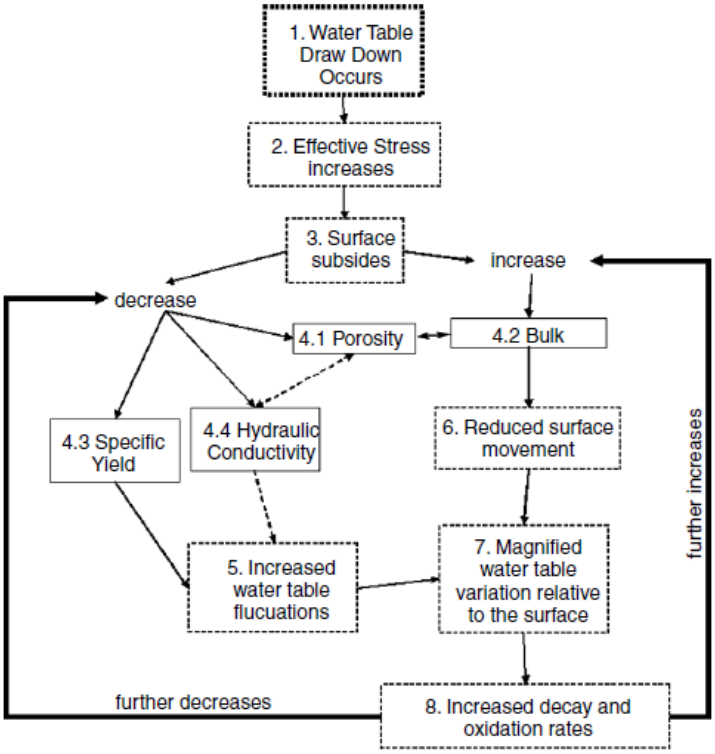

Figure 1-6. Impacts of water table drawdown on peat physical properties and peatland hydrology (from Whittington & Price 2006).

1.3.2. Mire water balance

1.3.2.1. Precipitation inputs

Precipitation is the only water input to ombrotrophic bogs, and therefore they occur only in areas with large and constant effective precipitation. Holden (2006) stated that ombrotrophic mires only exist in areas with over 600mm precipitation per year. Blanket bogs occur where precipitation is over 1500mm. Price (1992a; b) showed that fog deposition accounted for a third of total precipitation inputs in a Newfoundland blanket bog and suggested that this source of water was critical to the development of blanket bogs in this particular area. Minerotrophic mires are additionally sustained by other water sources than precipitation (see Figure 1-7 in Section1.3.2.2), and therefore occur under a larger range of climatic conditions (Joosten & Clarke 2002).

1.3.2.2. Surface and groundwater inflows and outflows

By definition, and as discussed in Section 1.2.3, raised bogs do not receive runoff from surrounding land. They are generally regarded as being disconnected from the regional groundwater by the low permeability catotelm, and vertical flow is generally negligible and

invariably downwards (Ingram 1982; van der Schaaf 2002). However, upward flow from the underlying aquifer has been shown to occur in some raised bogs when precipitation inputs are reduced (Glaser *et al.* 1997). These minerotrophic inputs may in some cases be sufficient to trigger a shift in surface conditions from ombrotrophic to base-rich as evidenced by vegetation and chemistry (Glaser *et al.* 1996). Such processes have been reported in specific hydrogeological settings in North America, but it is unclear whether they occur elsewhere.

Also by definition, minerotrophic mires receive at least part of their water supply from surface runoff or groundwater flow. However the importance and dynamics of these inputs vary widely between mires depending on their topographic and hydrogeological settings. Each minerotrophic mire is almost a unique case and it is beyond the scope of this review to make a detailed account of interactions between minerotrophic mires and their topographic and hydrogeologic catchments. Such an account can be found in Wheeler *et al.* (2009). Wheeler *et al.* (2009) and Whiteman *et al.* (2009) provided a detailed framework to conceptualise these interactions based on the identification of individual wetland water supply mechanisms (see Section A.4 in Appendix A). They estimated semi-quantitatively the contribution of precipitation, surface water and groundwater to the maintenance of summer water levels in the peat layer for each of the wetland vegetation stands they reviewed (over 1500 from over 200 wetland sites in England and Wales). The mean contribution of each water source for each wetland water supply mechanism they identified and each plant community is shown in Figure 1-7, however it should be stressed that, in most cases, this assessment was based on expert opinion, not on a quantitative water balance analysis.

Wheeler *et al.* (2009) and Whiteman *et al.* (2009) insisted on the importance of the uppermost substratum often disregarded by geologists and hydrogeologists either because it is poorly characterised or documented, or deemed unimportant. This top-layer includes materials such as the peat layer, alluvial or lacustrine deposits, marl, tufa, till, head, drift and various induration or seal layers. The physical and spatial characteristics of these layers are often essential in explaining the presence of certain wetland water supply mechanisms and consequently the stand water balance and the presence of specific vegetation units (House *et al.* 2015). Their variability and poor characterisation may in some cases explain the difficulties in modelling flow through specific wetlands.

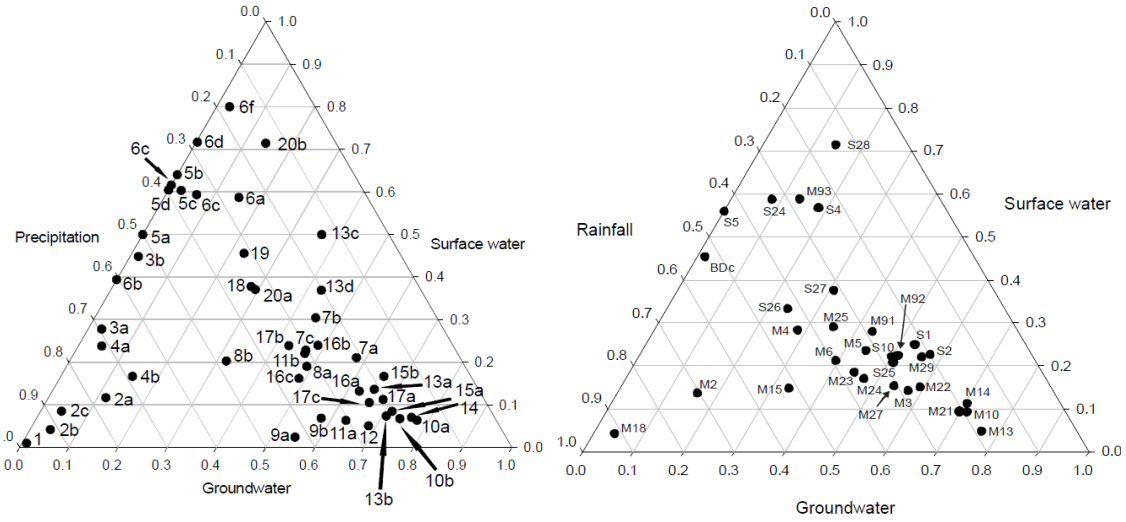

Figure 1-7. Average contribution of precipitation, surface water and groundwater to the maintenance of summer water levels in English and Welsh mires as a function of (left) identified wetland water supply mechanism and (right) plant community (from Wheeler et al. *2009).*

See Table A-3 in Appendix A for wetland water supply mechanisms numbers and names. Codes on the right plot refer to NVC categories (Rodwell 1992, 1998). Letters refer to sub-types of mechanisms not listed in this review, see Wheeler *et al.* (2009) for detail.

1.3.2.3. Storage

Even though water content is between 70% and 95% of the peat volume, the storage capacity of mires is small given the shallowness of the groundwater table (Ingram 1983; Eggelsmann *et al.* 1993; Labadz *et al.* 2010). For instance, Holden (2006) showed that in a blanket bog in Yorkshire, UK, the water table was within 10cm of the surface for 75% of the time over two years. The deepest water table recorded over that period was 25cm. Numerous studies in a large number of sites have shown that shallow groundwater tables are a constant feature of undrained mires (Evans *et al.* 1999; Porteret 2008; Labadz *et al.* 2010). In mires however, the quantification of storage must account for the fact that ground level is not stable but fluctuates seasonally by up to a few decimetres (Eggelsmann *et al.* 1993; Gilman 1994; Camporese *et al.* 2006). Surface level is generally maximum during the wet season and minimum at the end of the dry season, and this phenomenon, known initially in German as *mooratmung* (mire "breathing"), has been explained by both the desaturation and shrinkage of peat and the loss of buoyancy. Gilman (1994), for instance, measured amplitudes of more than 10cm in a Somerset fen, and movements representing between 5% and 12% of the water table movement in a Welsh raised bog. Variations in ground level can account for a large proportion of total changes in water storage: Kellner & Halldin (2002) and Price & Schlotzhauer (1999) calculated that 40% and 70% of storage changes could be attributed to this phenomenon in a Swedish bog and in a partly

restored cutover bog in Canada, respectively. Storage may also occur above ground level, for instance in hollows of the pronounced micro-topography such as *Sphagnum* hummocks and hollows or *Molinia* tussocks that is common to many mires (Carrer *et al.* 2015). Floodplain mires may store very large volumes of water above ground and may play an important role in flood protection (Ouse and Nene washes in England, Marais du Cotentin in France for instance, Purseglove 1988; Baron-Yellès & Goeldner-Gianella 2001).

1.3.2.4. Evapotranspiration

Evapotranspiration in mires was extensively reviewed by Eggelsmann *et al.* (1993) and Gilman (2002). Drexler *et al.* (2004) provides a review of models and micrometeorological methods used to estimate evapotranspiration in wetlands. Holden (2006) noted that evapotranspiration is often the largest component of water loss in mires. Indeed, at equal rates of precipitation and reference evapotranspiration and for similar vegetation physiognomy, actual evapotranspiration is substantially higher in mires than in mineral soils because water supply is rarely limiting due to the large porosity and shallow groundwater table (Eggelsmann *et al.* 1993). Porteret (2008) noted that all twenty studies of evapotranspiration in mires that he reviewed reported higher evapotranspiration rates in mires than on mineral soil.

The ratio between actual (ET) and reference (ET_{ref}) evapotranspiration is often used to compare evapotranspiration between vegetation types while accounting for differences in climate. In the absence of water supply limitation, this ratio gives the crop coefficient (Allen *et al.* 1998). A number of researchers (Schouwenaars 1993; Kim & Verma 1996; Wastiaux 2000) measured ET/ET_{ref} ratios close to unity in acidic fens and bogs, in particular those dominated by *Molinia caerulea*. In a laboratory experiment, Clymo (1973) measured evaporation rates in *Sphagnum cuspidatum*, *S. papillosum* and *S. rubellum* 1.2-1.4 times higher than that from open water, depending on the species and the depth of the water table that varied between 1cm and 10cm below the capitula.

Others have shown that the ET/ET_{ref} ratio from *Sphagnum*-dominated bogs can be substantially lower (around 0.5-0.75, Wastiaux 2000; Kellner 2001a; Lafleur *et al.* 2005), particularly when the capitulum dries out. Contrary to vascular plants, *Sphagnum* mosses are not able to actively draw water from the soil and the supply to the capitulum is through capillary forces only. Furthermore, under dry conditions the larger hyaline cells empty of water and give a whitish colour to the capitulum, lowering the albedo and the evaporative demand. In a degraded bog in the Netherlands, Schouwenaars (1990, 1993, cited by Spieksma *et al.* 1996) showed the actual

evapotranspiration of *Sphagnum spp.* to equal Penman open water reference evaporation when the water table is shallower than 10-15cm below the surface, but to drop substantially below this critical level. Actual evapotranspiration by *Molinia caerulea* was maintained at about the reference evaporation rate for much longer periods under dry conditions. Evapotranspiration from forested mires is generally higher than that from graminoïds or *Sphagnum* mosses (Eggelsmann *et al.* 1993) due to a higher aerodynamic roughness.

1.3.2.5. Runoff and streamflow

Pristine mires, particularly *Sphagnum*-dominated ones, are characterised by the presence of an acrotelm, a highly permeable layer of weakly humified peat overlying the more strongly humified and less permeable catotelm (Section 1.3.1.4). Ingram (1983) cites differences in hydraulic conductivity between upper and lower peat layers in the order of one order of magnitude in some fens but up to eight in raised bogs with a highly humified peat at depth. This strong increase in hydraulic conductivity towards the surface leads to a strong dependence of the transmissivity of the peat profile, and therefore runoff, on the groundwater level. Table 1-3 shows the percentage of runoff collected at different depths in a blanket bog hillslope (Holden 2006).

Table 1-3. Percent of runoff collected in automated throughflow troughs from peat layers in an undisturbed blanket bog hillslope, UK (Holden 2006).

Peat layer (depth, cm)	Percent runoff from hillslope
0-1	74
1-8	21
8-20	5
>20	<0.01

Almost 100% of runoff occurs when the groundwater table is higher than 20cm below ground level. Below that depth, lateral flow is negligible. Evans *et al.* (1999) came to similar conclusions in a blanket bog of northern England. Similarly, Holden (2006) used high-frequency groundwater table depth data to show that, in a blanket bog in Yorkshire, runoff stopped when the groundwater table dropped to more than 8cm below ground. Below this threshold, hydraulic conductivity was too small for a substantial flow to exist, and the groundwater table depth was controlled by evapotranspiration alone. Consequently, catchments that include a large proportion of ombrotrophic mires tend to have very flashy hydrological regimes, with a rapid response to rainfall events and minimal baseflow (Price 1992a; Burt 1995; Evans *et al.* 1999; Holden 2006; Soulsby *et al.* 2006). In the Upper Tees blanket bog catchment in northern England for instance, discharge lower than $0.5 m^3.s^{-1}$ occurred for 75% of the time but made up only 21%

of total discharge. This indicates minimal groundwater flow from the peat, even though high groundwater tables were maintained even during dry periods (Evans *et al.* 1999; Holden 2006).

The widely cited idea that peatlands act as sponges that soak up rainfall and then release it slowly into watercourses has therefore been widely criticised (Burt 1995; Holden 2006; Labadz *et al.* 2010), particularly in the case of ombrotrophic mires. Some types of minerotrophic mires do indeed regulate downstream flow, but in general the reason for this lies in their topographic position and not in the presence of peat. This is the case for instance of floodplain mires that may store large volumes of water above ground level during floods. However, because of the low permeability of peat, headwater peatlands located downstream of otherwise unconfined mineral aquifers constitute aquitards that may in some cases regulate groundwater discharge to streams (Rossi *et al.* 2012, 2014). Unfortunately only a limited number of studies have investigated this issue.

1.4. Peatland hydrological modelling

1.4.1. Hydrological modelling

Hydrological models are simplified representations of all or part of the water cycle. They are developed and used for two primary objectives. The first one is to provide a simplified explanation of a complex system and to understand this system under investigation in a quantitative and systematic manner (Davie 2008). The second objective is to predict the behaviour of the modelled system under a range of conditions that cannot be directly observed, and to use the prediction for decision–making in facility design, resource management or research (Singh 2010).

A number of model types are available to the hydrologists (Figure 1-8), and the choice of the method to be used will depend on the purpose of the study. Physical models reproduce the modelled system at a smaller scale (see for instance Ma *et al.* 2002) or using electrical or hydraulic analogies (Nourani *et al.* 2007, 2014). Conversely, mathematical models use abstract, mathematical function to convert a numerical input to one or several numerical outputs (Klemeš 1986). Nowadays mathematical models are more widely used due to the availability and performance of computers. In the case of deterministic models, a given input can only give one output. Conversely, stochastic models are partly driven by a random process that, for a given input, results in a range of possible outputs (Shaw *et al.* 2010).

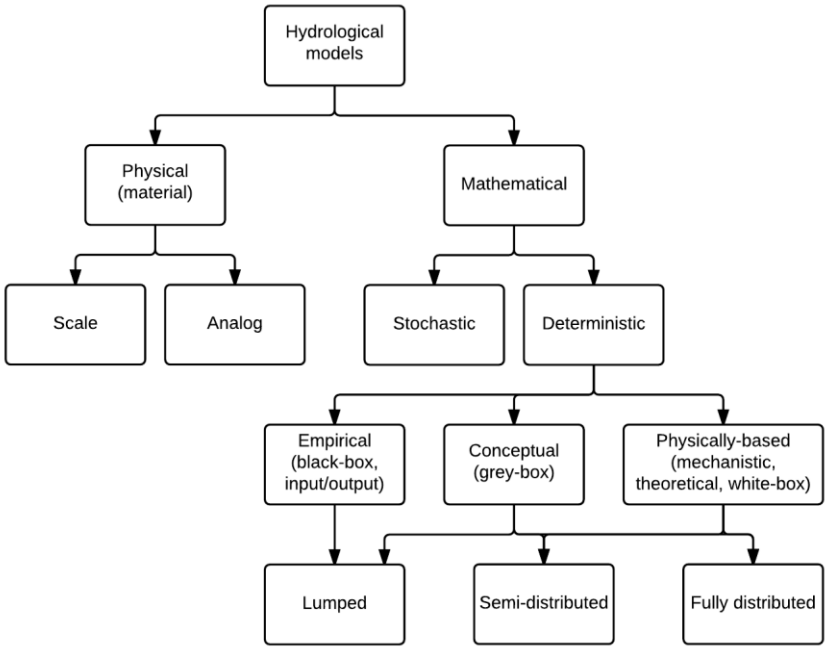

Figure 1-8. Classification of hydrological models (modified from Thompson, unpublished; Singh 1988; and Jajarmizad et al. *2012).*

Empirical (or black-box) models simulate a direct relationship between the input and output using transfer functions established through statistical or machine-learning methods. Parameters have little or no physical significance, and are only valid for the environmental conditions in which they were derived (Davie 2008). Examples of empirical model include those introduced by the Flood Studies Report (Collective 1975; Sutcliffe 1978) and refined in the Flood Estimation Handbook (Bayliss 1999; Faulkner 1999; Houghton-Carr 1999; Robson & Reed 1999a; b; Kjeldsen 2007). In conceptual models, hydrological processes are represented as a series of stores governed by highly simplified equations. Such models are deemed to be conceptually similar to the relevant physical processes (Davie 2008), however, as in empirical models, the model parameters have little or no physical meaning. They cannot be measured in the field and have to be determined through calibration. Examples of conceptual hydrological models include the Stanford Watershed Model, one of the first computer-run hydrological models (Crawford & Linsley 1966); the UK Institute of Hydrology's HYRROM (Eeles *et al.* 1989) and the widely used TOPMODEL (Beven & Kirkby 1979). It should be noted that the term "conceptual model" may lead to confusion as it is not restricted to the above definition. In hydrogeology for instance, a conceptual model is defined as a pictorial or schematic representation of a groundwater flow system that summarizes available geological and hydrogeological information (Anderson & Woessner 1992b; Francés *et al.* 2014). Hence the term "parametric model" is sometimes preferred. Finally, in physically-based models, the relevant hydrological processes are modelled

by a set of physical equations describing real world mass flow and momentum transfer, such as the Darcy equation for saturated flow in porous media, the Richards equation for unsaturated flow or the Saint-Venant equations for channel flow. Each of the physical equations is solved for individual points within a catchment using a grid or mesh pattern (Refsgaard 1997; Graham & Butts 2005). Examples of physically-based models include the 3D groundwater models MODFLOW (McDonald & Harbaugh 2003) and MARTHE (Thiéry 1990).

Hydrological models also differ in the spatial discretisation they use. Lumped model represent the model domain as a single spatial unit, and model parameters are representative of average conditions across the catchment (Davie 2008). Among the examples cited above, the FER/FSH method, the Stanford Watershed Model and HYRROM are lumped models. Semi-distributed models (for instance SWAT) discretise the model domain in a series of sub-catchments or hydrological units of similar hydrological characteristics. Finally, in distributed models (MODFLOW, MARTHE, TOPMODEL for instance), the model domain is discretised into a grid or triangular mesh of relatively small elements. Differential equations are solved using finite difference or finite element methods respectively. In general, spatial discretisation increases from empirical models to conceptual models and to physically-based models: empirical models are generally lumped, conceptual models are generally lumped or semi-distributed and physically-based models are generally semi- or fully-distributed (Rochester 2010). This is a consequence of both the evolution in computing power and of the fact that the physical equations used in physically-based models represent small-scale hydrological processes and require a fine discretisation to be applicable (Graham & Butts 2005). However there are exceptions: TOPMODEL for instance is a fully-distributed conceptual model (Beven & Kirkby 1979).

Several integrated hydrological modelling software suites offer the possibility to use different types of sub-models and cannot be easily classified. This is the case of MIKE SHE for instance, and of the Système Hydrologique Européen SHE (Abbott *et al.* 1986a; b) from which MIKE SHE is developed (Refsgaard *et al.* 2010). MIKE SHE is further detailed in Section 5.3 as this software was used in the current study. SHE was initially fully distributed and physically-based, however lumped or semi-distributed conceptual sub-models were added at a later stage to the modelling environment, in particular to extend its capabilities to larger catchments (Graham & Butts 2005; Refsgaard *et al.* 2010). The semi-distributed Soil and Water Assessment Tool SWAT (Gassman *et al.* 2007), one of the most widely used hydrological models (Refsgaard *et al.* 2010), also combines physically-based and conceptual approaches.

Each type of hydrological model has advantages and limitations. Lumped or semi-distributed conceptual models, for instance, require limited input data and few parameters to be calibrated, and are computationally efficient. However, they often focus on prediction of river discharge at one or a limited number of locations and, since parameters are obtained through calibration and have limited or no physical meaning, they cannot usually be used in ungauged catchments and have little explanatory power. Conversely, distributed physically-based models are able to predict hydrological processes in all spatial discretisation units within the modelled area, and are very useful as research tools to test theories and improve hydrological knowledge. All parameters have a physical meaning and can in principle at least be measured, and, in theory, such models should not require calibration and can be used to make prediction under changing conditions or in ungauged catchments (Davie 2008).

In practice however this is not the case. Indeed, there are important limitations to distributed physically-based models (Beven 1989; Grayson *et al.* 1992; Graham & Butts 2005). They require a deeper understanding of the modelled hydrological system and, due to the large number of parameters and the fine-scale spatial discretisation, their parameterisation requires a very large amount of data. In practice, it is not possible to measure all required parameter values for every single spatial discretisation unit, and some parameters are generally specified for groups of discretisation units. There are also questions about the validity of physics-based governing equations describing small-scale hydrological processes when the grid size is relatively large. This has led Beven (1989) to query whether distributed physically-based models were just lumped or semi-distributed conceptual models with more complex equations. The near-impossibility of obtaining field measurements for all parameters also implies that a large number of parameters must be calibrated, and therefore such models are prone to over-fitting and equifinality issues (Rochester 2010). Finally, physically-based distributed models are very computationally-demanding, which currently limits their application to relatively local applications and short simulation periods. Graham & Butts (2005) stated that these limitations are one of the reasons for the development of modelling suites integrating physically-based and conceptual models such as MIKE SHE, and suggested to use the former for only the processes that are deemed to be important, and simpler, faster, less data-demanding conceptual methods for less important processes.

Anderson & Woessner (1992a) and Refsgaard (1997) proposed a rigorous modelling protocol that should be followed to ensure the validity of the model simulations, particularly in the case of physically-based models (Figure 1-9). The first steps of any hydrological modelling process are

the definition of the model objectives, the conception of a conceptual model of the site hydrology (in the sense of a qualitative, pictorial or schematic representation of the initial understanding of the site hydrological functioning based purely on field data and possibly knowledge of similar sites), and the selection of an appropriate code to fulfil these objectives given the conceptual understanding of the site. Nowadays a large number of hydrological codes and modelling environments are available, and the development of new code is often not required. The next step is the model design and construction, including, if it is physically-based, its parameterisation based on measured or inferred data. It should then be decided how the model performance will be assessed. This can be based on one or several statistics summarising how well the model reproduce observed data (Krause *et al.* 2005; Moriasi *et al.* 2007) but also on expert opinion on the model performance relative to other models in similar conditions (Rochester 2010).

If necessary, the model is calibrated by modifying the value of some parameters to maximise the fit between observed and simulated values. The choice of the parameters to be calibrated may be imposed by the model type, based on data availability or on a sensitivity analysis highlighting the parameters to which the model is most sensitive (Christiaens & Feyen 2002). The results of such an analysis depend on the model parameterisation (Anonymous 2009a), and may therefore need to be repeated several times. Calibration is done by trial and error or by using automated parameter estimation approaches (Madsen 2000, 2003). Model validation is the assessment of the model performance against an independent set of observed data (Anderson & Woessner 1992a). In the case of semi- or fully-distributed models, these data should in theory be totally independent, and therefore recorded at a different location and under different climatic conditions. However this is rarely the case for practical reasons and in most cases available observed time-series are divided in two datasets, with one used for calibration and the other for validation.

After the model has been calibrated and validated, uncertainty analyses should be carried out to provide an uncertainty band around the deterministic output, using the so-called joint stochastic-deterministic modelling approach (Christiaens & Feyen 2002). This involves estimating the error associated to the model inputs and running the model with a sample drawn from the expected input distributions. However this is very rarely done in practice since this approach is computationally demanding and the error distribution of inputs is rarely known. Finally, simulations are used to fulfil the initial objectives.

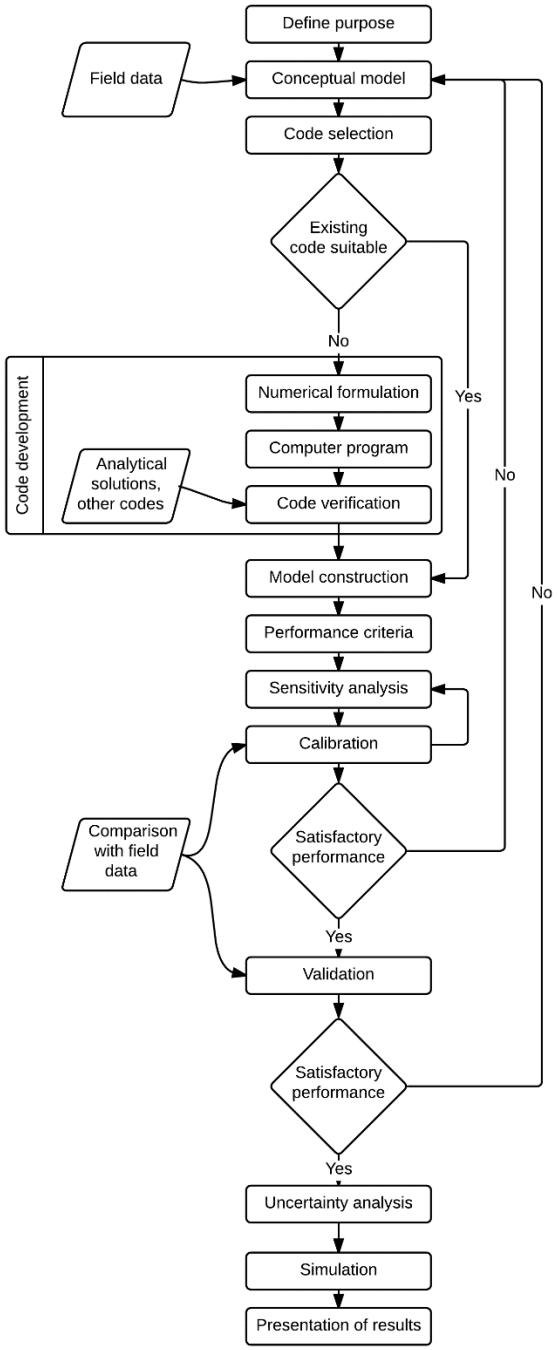

Figure 1-9. Workflow in hydrological modelling (modified from Refsgaard 1997).

1.4.2. Use of hydrological modelling in peatland research and conservation

Hydrological modelling of peatlands has been the focus of a very large number of studies (Bragg *et al.* 1991; Schot & Molenaar 1992; Armstrong 1995; Bradley 1996, 2002; Poiani *et al.* 1996; Brassard *et al.* 2000; Batelaan & Kuntohadi 2002; Beckwith *et al.* 2003; Dekker *et al.* 2005; Lapen *et al.* 2005; Caldwell *et al.* 2007; Schouwenaars & Gosen 2007; Boswell & Olyphant 2007; Chormanski *et al.* 2009; Chormański *et al.* 2009; Grygoruk *et al.* 2011, 2014; Ballard *et al.* 2011;

Binet *et al.* 2013; Dimitrov *et al.* 2014; Haahti *et al.* 2014), and it is beyond the scope of the current work to review them all. Instead this review focusses on a small number of studies that have employed physically-based, distributed models and which are considered relevant to the current study, in terms of the methodology used or hydrogeological context. To provide a benchmark against which to assess the results obtained in the current study, examples of model performance are given when available in the publications cited.

1.4.2.1. Peatlands modelled as independent systems

Bromley & Robinson (1995) used MODFLOW to model groundwater flow in raised bogs. The spatially-distributed model reproduced very closely the analytical solution derived from Ingram's (1982) groundwater mound model for a virtual regularly shaped raised bog. Mismatches between both models were caused by the relatively coarse discretisation of the MODFLOW model. However, unlike Ingram's (1982) model and after calibration, MODFLOW was able to reproduce observed groundwater table depths at Thorne Moors (Yorkshire), an irregularly-shaped bog where conflicts arose between the conservation of bog species and habitats within a NNR and peat extraction on the bog margins outside the NNR. The model was used to predict the potential impact of expanding peat extraction activities on groundwater table depth within the NNR. This was achieved by imposing constant groundwater head boundaries in grid cells corresponding to extraction pits in a range of extraction scenarios.

Lewis *et al.* (2013) used the physically-based distributed hydrological model GEOtop (Rigon *et al.* 2006) to model runoff and groundwater table depth in a 76ha blanket bog in south-west Ireland. The model had an 8m resolution, and simulated the complete hydrological balance over a year with an hourly time-step. It was assumed that flow only occurred within the peat layer. The model was calibrated and validated using observed discharge by changing the saturated hydraulic conductivity. Discharge was reproduced satisfactorily with a Nash-Sutcliffe Efficiency (NSE) of 0.89. Groundwater table depth was slightly overestimated particularly during wet periods (Figure 1-10). The effect of peatland afforestation, including drainage, was investigated by forcing the model with a new drainage network and new leaf area index (LAI), root depth and canopy height. The model suggested a reduction in total annual streamflow by 20% and a groundwater drawdown of 20cm under a semi-mature 15-year-old Sitka spruce plantation.

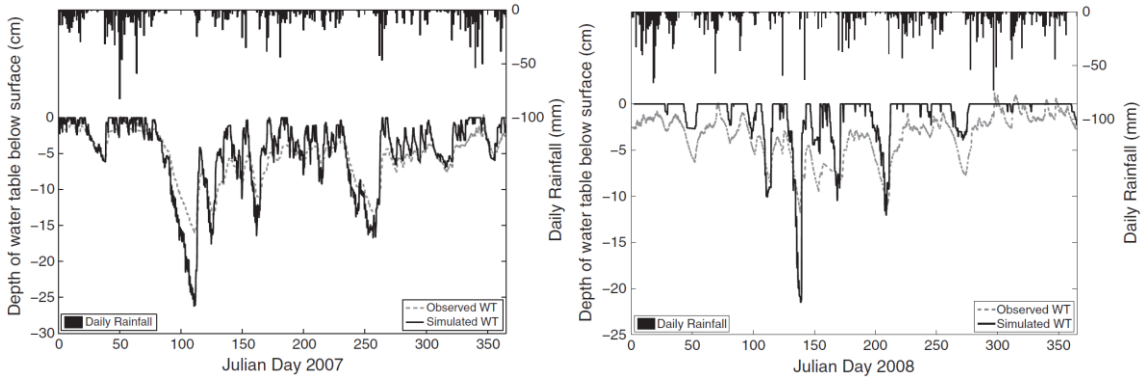

Figure 1-10. Performance of the model developed by Lewis et al. (2013) with regard to groundwater table depth (left: calibration, right: validation).

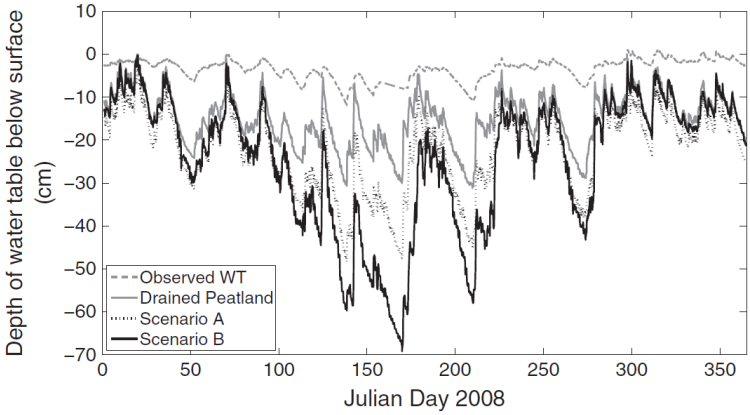

Figure 1-11. Impact of afforestation (including drainage) on simulated groundwater table depth in the blanket bog modelled by Lewis et al. (2013).

Legend: observed WT: observed groundwater table; drained peatland: drainage only; scenario A: drainage & 10year-old Sitka spruce plantation; scenario B: drainage & 15 year-old Sitka spruce plantation.

1.4.2.2. Peatlands modelled as part of a regional groundwater flow system

Reeve *et al.* (2001) used MODFLOW to model 3D steady-state groundwater flow to and from peatlands in northern Minnesota, USA, to validate the hypothesis that the distribution of raised bogs could be explained by regional groundwater discharge through permeable sand deposits. The model, calibrated using observed surface water and groundwater table elevations, suggested that regional groundwater did not discharge where bogs occurred, but rather that groundwater flow within peatlands consisted of local flow systems. This conclusion was however invalidated by a large body of field data, which led Glaser *et al.* (2006) to conclude that, in this case, models are best used as a means not an end, to formulate multiple working hypotheses that can be tested in the field or for interpreting large complex datasets.

Fournier (2008) and Levison *et al.* (2014) also used MODFLOW to simulate a fractured sandstone aquifer and its links with a 51ha peatland in southern Québec, Canada, assuming that the unconfined fractured bedrock aquifer behaves as an equivalent porous medium. Vertical discretisation included 16 layers of increasing thickness. The upper eight layers were thin enough to allow for an accurate representation of the peat stratigraphy. The model covered a 173km² area, and had a resolution of 135m on mineral ground and 67.5 on peat soils. A specified head boundary was used to allow groundwater flow to the regional aquifer. Rivers were represented using MODFLOW's River package and set as constant heads. Groundwater recharge was assumed to represent a constant fraction of net precipitation over each season, and this fraction was calibrated, together with semi-distributed specific yield and hydraulic conductivity values, based on observed groundwater levels and baseflow discharge. Figure 1-12 shows some aspects of the model performance with regard to groundwater head.

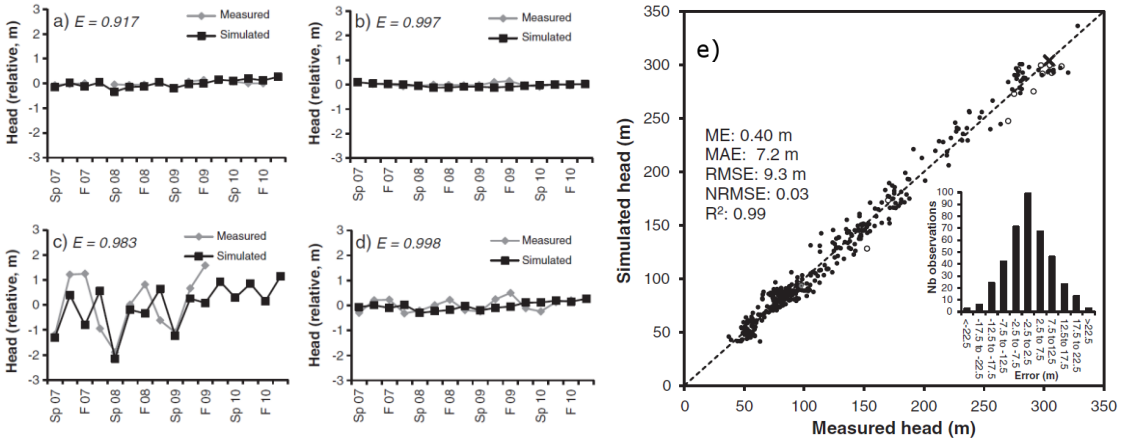

Figure 1-12. Performance of the model developed by Fournier (2008) and Levison et al. (2014) with regard to groundwater table depth.

Observed vs. simulated groundwater heads in selected wells located a) the peatland, b) at the top of the hill, c) mid-slope, d) at the foot of the hill, e) all available wells. Performance statistics are the Nash-Sutcliffe efficiency (E on these figures), mean error (ME), mean absolute error (MAE), root mean square error (RMSE), normalised root mean square error (NRMSE) and coefficient of determination (R^2).

This was judged satisfactory enough to use the model to calculate the peatland water balance and evaluate the potential impact of climate change. The model confirmed that the peatland was fed by the fractured bedrock aquifer all year round. The impact of climate change was evaluated by assuming that the percent anomaly in future groundwater recharge relative to the present calibrated values is the same as that in net precipitation. The model predicted that the highest impact scenario would lead to a complete cessation of groundwater inputs to the peatland in summer, autumn and winter.

Van Loon *et al.* (2009) tested two conflicting hypotheses regarding the distribution of minerotrophic and ombrotrophic vegetation within the Biebrza floodplain, Poland. According to the exfiltration model, groundwater seepage occurs on a regional scale as a result of permanent or periodic (evaporation-driven) upward groundwater flow. Due to the low hydraulic conductivity of superficial peat, there is no redistribution of exfiltrated mineral-rich water at the mire surface and minerotrophic species occur where groundwater discharge exists. The alternative model is the throughflow model, whereby groundwater seepage occurs as edge-focussed discharge along the mire margins, but exfiltrated water is redistributed laterally through a permeable superficial peat layer (Figure 1-13). Both hypothesis were tested by developing two steady-state MODFLOW models that differed only in the conductivity of the first and uppermost computational layer corresponding the root zone. Both models were identical in all other aspects, with a second layer corresponding to the semi-confining poorly permeable deep peat layer, and four other layers corresponding to the underlying glacial till and sand deposits. The model resolution was 50m in both cases, and they both covered an area of about 1600km².

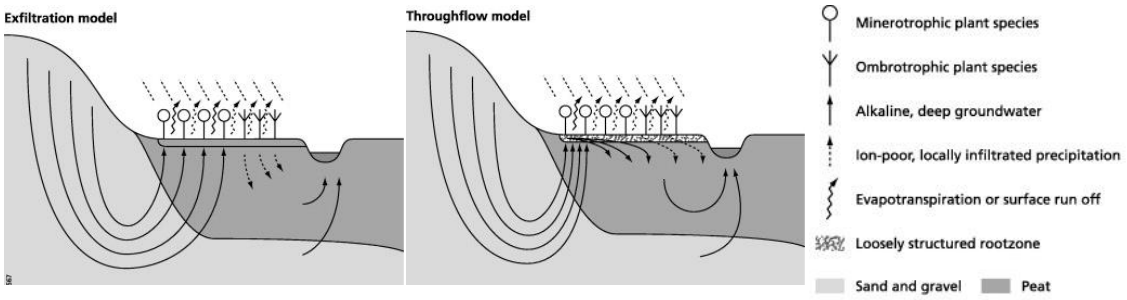

Figure 1-13. Exfiltration and throughflow models tested by van Loon et al. (2009).

The hydraulic conductivity of each layer was calibrated against mean groundwater table depths observed in 52 domestic wells, but the authors did not provide information on the model performance. The fraction of exfiltrated groundwater in the root zone was estimated for each grid cell, and compared to the observed distribution of minerotrophic and ombrotrophic vegetation. The agreement was poor in the case of the exfiltration model and deemed satisfactory in the case of the throughflow model (Figure 1-14), suggesting the upper layer of high permeability, low humification peat is determinant in redistributing groundwater seepage across the mire.

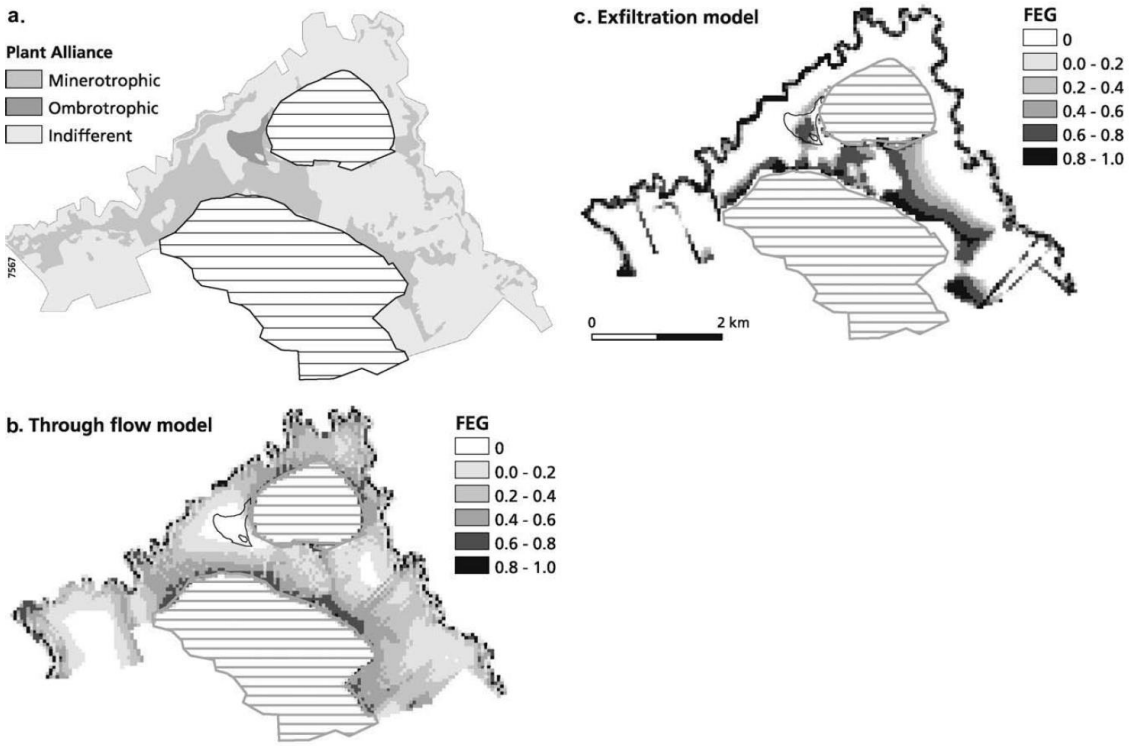

Figure 1-14. Correspondance between trophic status estimated from indicator plant species (a) and fraction of exfiltrated groundwater (FEG) in the root zone according to the throughflow model (b) and exfiltration model (c) of van Loon et al. (2009).

Contrary to many studies investigating the impact on peatlands of changes in the regional aquifer, Rossi *et al.* (2012, 2014) investigated the impact of the drainage of peatlands in northern Finland on an esker aquifer supporting them (Figure 1-15). The steady-state MODFLOW model only included one computational layer representing the esker. Peatlands on the sides of the esker were represented using the MODFLOW drain package by adjusting the drain conductance value based on the physical characteristics of the peat layer. Mean annual aquifer recharge was calculated externally. The esker hydraulic conductivity and the drain conductance within the peatlands were calibrated automatically using the PEST software (Dougherty 2005). Both parameters could vary spatially to match long-term mean groundwater table levels and stream discharge recorded in 25 and 18 observation points distributed across the modelled area. Unfortunately the authors did not provide information on the model performance. Restoration of the peatlands was simulated by varying the drain conductance and bottom level. The model suggested that restoration would raise groundwater levels in the middle of the esker by up to three metres depending on the restoration scenario. Interestingly, this suggests that peatlands, due to their relatively low permeability, may in some conditions regulate discharge from local aquifers and increase groundwater resources.

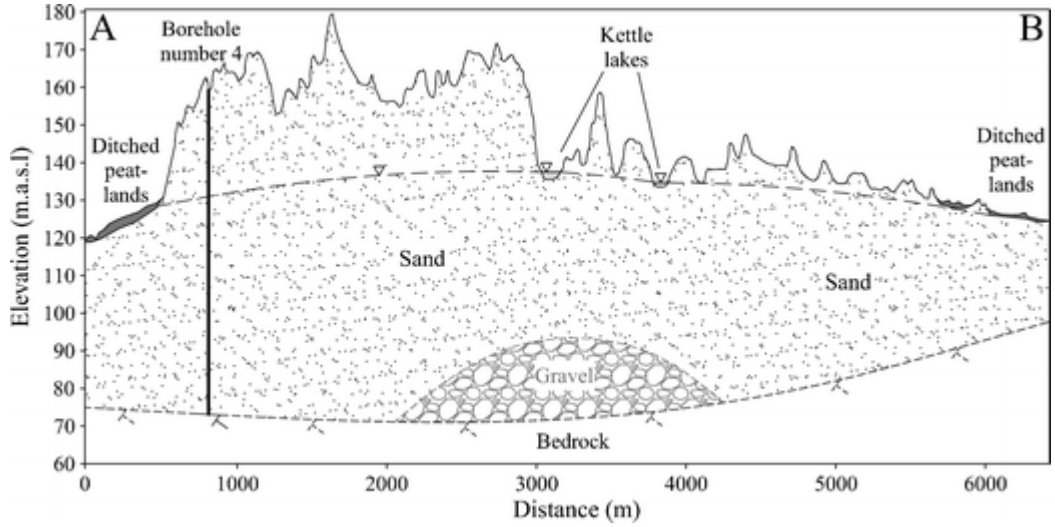

Figure 1-15. The esker-peatland system investigated by Rossi et al. (2012, 2014).

Marandi *et al.* (2013) used MODFLOW to evaluate the impact of underground mining, including mine dewatering, on the water balance of Selisoo bog, a large raised bog in Estonia designated under the EU 92/43/EEC Habitats Directive. The steady-state model covered 430km² with a resolution varying between 30x50m in the centre of the modelled area and 100x120m along its boundaries. It included 11 computational layers, the upper three corresponding to the peat deposits and the rest to the bedrock aquifer and aquitard layers. Constant heads, based on observed piezometric heads in 15 piezometers surrounding the modelled area, were used as boundary conditions. A constant groundwater recharge was specified based on earlier studies. Mine dewatering was modelled by specifying a constant head within the mined area corresponding to the mine floor, 60m below ground. The model was calibrated against average piezometric heads measured in the bedrock surrounding the bog (Figure 1-16). The model was validated against the observed mean monthly volume of water abstracted from the mine. The model under-estimated this volume by 7% only, which was deemed satisfactory. The model showed that the extension of the mine would result in a 2.5m drop in groundwater table depth within the mire.

Armandine Les Landes *et al.* (2014) investigated the impact of both climate change and groundwater abstraction resulting from peat extraction on groundwater flow and groundwater table depth in a regional sandstone and shelly sand aquifer, covering 135km² in Cotentin, France, and in a large peatland located at its northern edge. Peat was represented by the uppermost computational layer of a steady-state MODFLOW model. Recharge to the groundwater was modelled separately using a lumped model, and used as an input to MODFLOW.

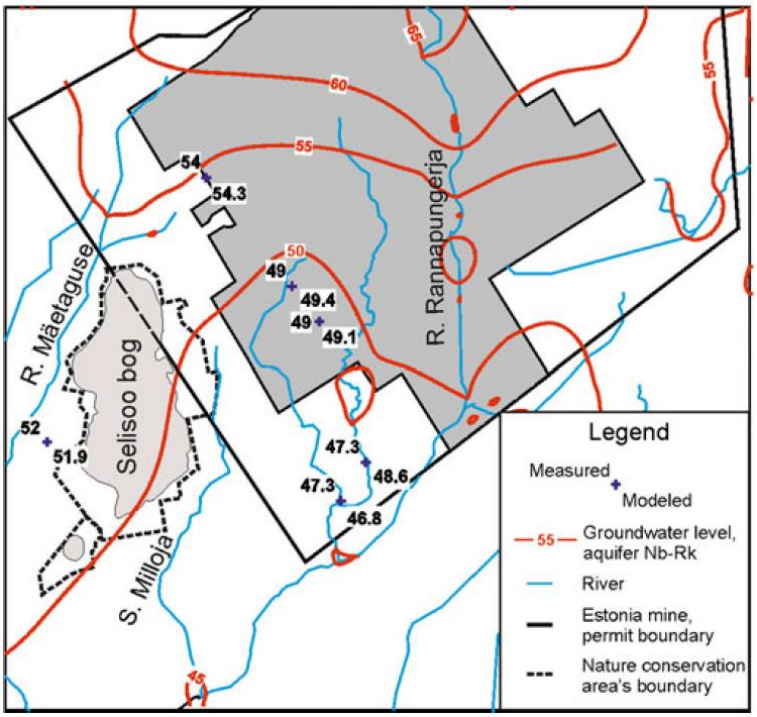

Figure 1-16. Measured (crosses) vs. simulated (crosses and contour lines) groundwater heads in the upper bedrock aquifer below the Selisoo bog according to Marandi et al. (2013).

The impact of peat extraction was modelled using a prescribed head boundary condition corresponding to the artificially lowered groundwater table within the peat cuttings. The MODFLOW model was calibrated automatically based on the spatial distribution of wetlands and on groundwater table depth records from 24 dipwells distributed across the modelled area. This was achieved by adjusting the hydraulic conductivities of the different layers within ranges provided by field measures. The model error was substantial in some locations but it nevertheless reproduced the distribution of wetlands relatively satisfactorily (Figure 1-17). It was used to predict the impact of climate change and groundwater abstraction on the extent of wetlands, assuming that wetlands occurred where the simulated groundwater table depth was less than 0.5m below ground. It was suggested that the impact of climate change may under some scenarios be mitigated by ceasing water pumping within the peat cuttings.

A number of additional studies have used MIKE SHE to model the hydrology of a range of different types of wetland. Since this is the modelling system employed in the current study, these are detailled in Section 5.3.2.

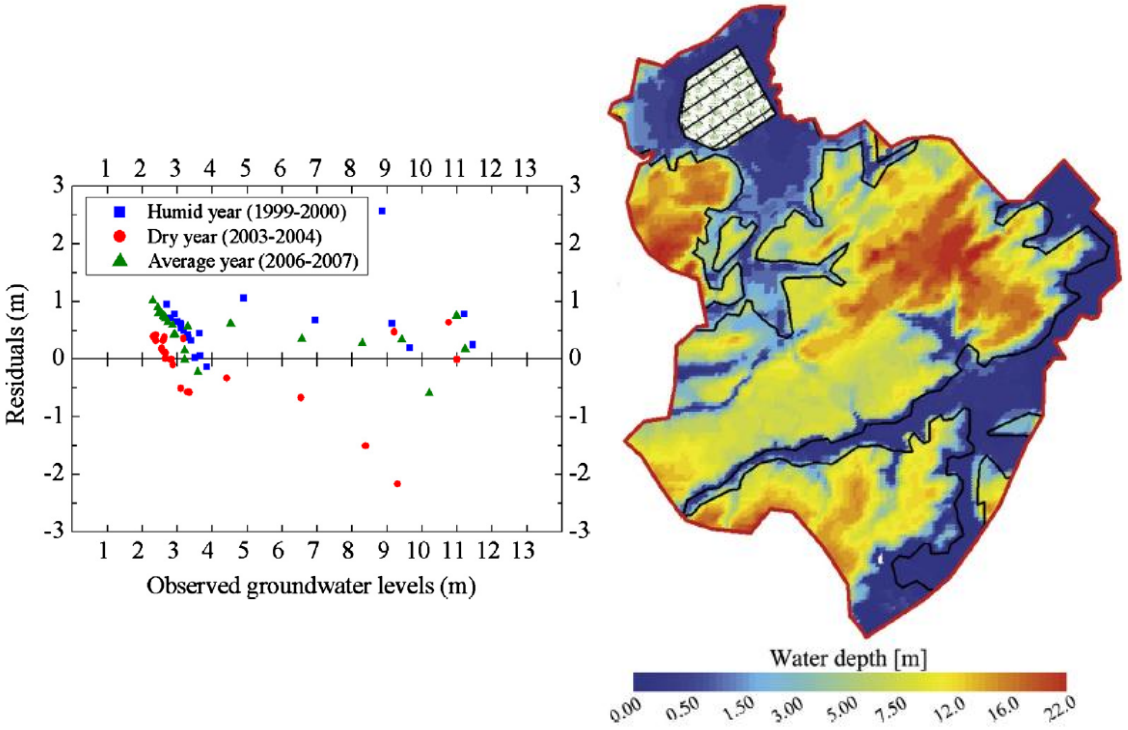

Figure 1-17. Performance of the model developed by Armandine Les Landes et al. (2014) with regard to groundwater table levels (left) and wetland spatial distribution (right).

The left map shows the observed wetland boundaries (black line) and the simulated groundwater table depth (colour gradient). The white polygon at the top of the figure shows the location of the peat cuttings.

1.4.2.3. Persisting issues in peatland hydrological modelling

Although the hydrological modelling studies presented in Sections 1.4.2.1 and 1.4.2.2 show how useful models can be to better understand the hydrological functioning of peatlands and to test management options, there are a number of persisting issues (Whitfield *et al.* 2009). Widely used general hydrological modelling suites such as MODFLOW or MIKE SHE, as well as other less known generalist models such as SIMGRO, were not designed with peatland hydrological modelling in mind, and a number of peatland-specific processes cannot be modelled using these codes (Whitfield *et al.* 2009). This is the case of peat shrinkage and compression that occur on short time scales following a drop in the groundwater table depth (Sections 1.3.1.5 and 1.3.2.3), and directly impact the mire topography and the peat hydraulic conductivity and specific yield (Price & Schlotzhauer 1999). In short-term studies like those described in Sections 1.4.2.1 and 1.4.2.2, these interactions are generally not accounted for. Given the relatively small changes in ground level (a few centimetres to one or two decimetres at most, Gilman 1994; Price & Schlotzhauer 1999) caused by peat shrinkage and compression, the pronounced micro-topography not accounted for in most modelling studies and the difficulties in measuring highly variable peat properties, this simplification is probably not an important source of error. In the

longer term however, interactions between groundwater flow, peat decay and accumulation rates and peat physical properties are much more significant, and their inclusion in models of peatland hydrology and development over scales of tens to tens of thousands of years is fundamental. Querner *et al.* (2012) used an indirect strategy to model both groundwater table depth and peat subsidence in Dutch peat meadows with the physically-based distributed hydrological model MOGROW: subsidence was evaluated a posteriori using an empirical regression model relating annual peat subsidence to the lowest groundwater table depth in summer. There was no direct coupling of the hydrological and peat subsidence models.

A number of models have also been developed that couple hydrology and peat deposition processes (Clymo 1984; Hilbert *et al.* 2000; Gilmer *et al.* 2000; Borren & Bleuten 2006; Ise *et al.* 2008; Frolking *et al.* 2010; Baird *et al.* 2012), but these are not widely available. Furthermore, most of these models are zero- or one-dimensional (Baird *et al.* 2012): this is the case for instance of Clymo's (1984) bog growth model or of Frolking's *et al.* (2010) Holocene peat model. Baird *et al.* (2012) and Morris *et al.* (2012) recently developed Digibog, an integrated model of raised bog development. Based on the assumption that raised bogs are disconnected from the regional groundwater, saturated flow within the bog is modelled using the Dupuit-Forchheimer approximation, and assumed to be horizontal only. Therefore it cannot be used in minerotrophic peatlands. Borren & Bleuten (2006) developed a tri-dimensional peatland development model by integrating MODFLOW within a distributed peat accumulation model. The groundwater table depth modelled by MODFLOW determined peat accumulation, and in turn the thickness of the MODFLOW layers was updated at each time step to reflect peat accumulation. When run from the start of the Holocene to the present day, the model reproduced relatively well the present distribution and thickness of peat in a Siberian watershed, however the data that could be used to validate the model were relatively limited. This model is nevertheless promising since it can be integrated in a larger MODFLOW model of regional flow.

The rapid but gradual transition between the acrotelm, a poorly humified, highly conductive peat layer with a large specific yield at the mire surface, to the more humified, less conductive peat with a smaller specific yield at depth constituting the catotelm is characteristic of mires. Together with the pronounced microtopography, this results in a self-regulation of groundwater table depths within the peatland, resulting in the progressive increase in throughflow and overland runoff when the water table rises (Verry *et al.* 1988; van der Schaaf 2002; Jutras *et al.* 2009). In their Peatland Hydrologic Impact Model, Guertin *et al.* (1987) modelled this behaviour by using two logarithmic functions describing both lateral flow and cumulative water storage as a function

of water table depth, that must be calibrated using observed data. However these processes are difficult to model using classical distributed physically-based hydrological models that impose sharp boundaries between computational layers within the saturated zone, and between the saturated zone and overland flow. Furthermore the depth of the acrotelm is relatively small compared to the other model layers, which in some cases may cause numerical instabilities. The acrotelm is therefore rarely accounted for except in small-scale applications.

Résumé du chapitre 1 (introduction générale)

Une revue de la littérature internationale portant sur les tourbières, leur hydrologie et les méthodes de modélisation hydrologique qui leur ont été appliquées est proposée en introduction de cette thèse. Une tourbière se définit par la présence de tourbe, un sédiment déposé en place composé d'au moins 30% de matière organique. La tourbe dérive de l'accumulation des restes d'organismes vivants, essentiellement végétaux, en conditions anoxiques liées à une saturation quasi-permanente des sols dans certaines zones humides. Les tourbières couvrent environ 3% des terres émergées, principalement dans les zones boréale et subarctique. Elles ont classiquement été divisées entre tourbières hautes (uniquement alimentées par les précipitations directes) et tourbières basses (alimentées au moins en partie par des apports issus d'un bassin versant minéral), toutefois cette distinction hydrogéomorphique ne recoupe pas entièrement les divisions floristiques observées, les tourbières basses acides étant plus proches floristiquement des tourbières hautes que des tourbières basses neutres à alcalines. La richesse en bases et le pH correspondent en effet au principal gradient floristique observé dans les tourbières. Les deux autres gradients principaux correspondent à la fertilité et à l'humidité des sols, elle-même liée à la profondeur de la nappe et conditionnant un grand nombre de processus physico-chimiques tels que les concentrations en composés phytotoxiques ou en nutriments.

Les services environnementaux rendus par les tourbières sont nombreux, l'un des plus importants étant le stockage du carbone : bien qu'occupant une surface restreinte, elles contiennent environ un tiers du carbone stocké dans la biomasse terrestre et les sols à l'échelle mondiale, ce qui en fait l'écosystème terrestre le plus efficace pour la capture et le stockage du carbone. Les tourbières constituent également un piège efficace pour les métaux lourds et métalloïdes d'origine naturelle ou anthropique, et contribuent à l'amélioration de la qualité de l'eau en aval. Toutefois, la perturbation de leur balance hydrique, conduisant à une baisse du niveau de la nappe dans la tourbe ou à une augmentation de sa variabilité, peut entraîner le relargage de ces polluants et du carbone qu'elles ont stockés au cours des siècles passés. Enfin, à l'échelle de la France et de l'Europe, les tourbières constituent des écosystèmes originaux qui contribuent de façon importante par rapport à leur surface à la biodiversité. En conséquence, un grand nombre d'habitats et d'espèces caractéristiques des milieux tourbeux bénéficient d'une protection réglementaire à l'échelle locale, nationale, européenne ou internationale.

A l'échelle mondiale, environ un quart des tourbières ont été détruites par les activités humaines, essentiellement par mise en culture, transformation en forêt commerciale ou extraction de tourbe, souvent associées à un drainage plus ou moins prononcé. Les changements climatiques en cours et à venir, en modifiant la balance hydrique des tourbières, constituent une nouvelle menace dont l'importance reste toutefois difficile à quantifier.

Le fonctionnement hydrologique des tourbières conditionne un grand nombre de processus géomorphologiques, biogéochimiques et écologiques y prenant place, et sa compréhension est donc primordiale pour la mise en place d'une gestion conservatoire appropriée. L'hydrologie des histosols diffère nettement de celle des sols minéraux : la tourbe est un matériau organique, hétérogène, compressible, dont les propriétés physico-chimiques peuvent évoluer relativement rapidement, de manière réversible ou non, en fonction du degré de saturation en eau. La plupart des tourbières peu impactées par les activités humaines présentent une couche superficielle de tourbe peu décomposée, très perméable, donnant progressivement place à une tourbe plus décomposée et moins perméable en profondeur. Ces deux couches fonctionnelles, appelées acrotelme et catotelme, conditionnent l'hydrologie des tourbières et contribuent au maintien d'une nappe relativement stable dans la tourbe.

Ces caractéristiques propres sont difficiles à représenter au moyen des principaux modèles hydrologiques généralistes actuellement disponibles, qui représentent en général le sous-sol en couches superposées aux limites tranchées et aux propriétés hydro-physiques stables dans le temps. Inversement, les quelques outils existants qui permettent de modéliser les propriétés hydrologiques propres des tourbières ne peuvent que rarement être couplés à des modèles plus généralistes permettant de modéliser leur bassin versant. En conséquence, lorsque la tourbière doit être modélisée comme partie intégrante d'un système hydrologique plus large, certaines simplifications sont nécessaires. Malgré ces simplifications, plusieurs études ayant utilisé des modèles physiques distribués tels que MODFLOW ou MIKE SHE ont pu reproduire de manière satisfaisante les flux observés dans un certain nombre de systèmes tourbeux.

Chapter 2. Mires of the Massif Central and the Dauges catchment

2.1. Introduction

This chapter first introduces the peatlands of the French Massif Central and summarises the limited published literature on the hydrology of these particular wetlands. This enables the identification of some major research gaps that are addressed in the thesis. The aims and research objectives of the thesis are detailed, and the Dauges mire and its catchment, which have been selected to implement these objectives, are presented. Finally, the last section presents the research design and outlines the thesis structure.

2.2. Peatlands of the French Massif Central

2.2.1. Physical context

The Massif Central is a range of uplands and small mountains located, as its name suggests, in central France. The Massif Central is a relatively recent geographical denomination: it was first used by the geographer and author of school wall maps Paul Vidal de La Blache in 1903, to name the ensemble of uplands located in central France and traditionally separated in several provinces including Auvergne, Limousin, Ardèche and Cévennes (Faure 2005). Its precise delimitation depends on the criteria used. The primary delineation is based on altitude, and includes all land above 500m asl in central France, with a total area of about 45,000km². The boundaries are sometimes extended to neighbouring lowland areas based on geological, administrative or legal criteria, to cover up to 85,000km². The Massif Central culminates at 1885m asl at Puy de Sancy. The Massif Central includes a variety of geological and geomorphological entities, but is primarily an igneous and metamorphic basement massif formed during the Hercynian orogenesis between 450 and 280 million years ago, dominated by granites and gneisses (Figure 2-2). Its geological and geo-morphological history was reviewed and summarised by Etlicher (2005). The Hercynian relief was reworked during a series of successive peneplanation and tectonic uplift events until the end of the Eocene. A number of rifting and compression phases linked to the opening of the Atlantic ocean and the Pyrenean orogenesis created a series of rift valleys, horsts and grabens that still define the present main regional units and landforms such as the Rhône, Loire and Allier valleys. A strong compression

phase concomitant to the Alps uplifting took place from the Miocene to the Quaternary and resulted in the present relief. Volcanic activity was present from the Eocene to the Quaternary, with the most recent events occurring in 5600 BP in the Chaîne des Puys. This volcanic activity resulted in a large number of volcanic landforms: large stratified cones in Auvergne, Mont Dore and Cantal, major lava fields in Cezallier, Devès, Aubrac and Coiron, and systems of domes, cones, maars and lava flows in Velay, Ardèche and Auvergne (Etlicher 2005). The physical context of the Limousin uplands, located on the north-west boundary of the Massif Central and where the current study was carried out, is further detailed in Section 2.6.

The Massif Central is one of the areas with the highest density of mires in Metropolitan France: a third (about 27,000 hectares) of all mires are found within its boundaries (Figure 2-1). The physical factors explaining the distribution of mires at the scale of the Massif Central have never been formally investigated. The much larger density of mires on the western side of the massif as a whole and on the western sides of the sub-massifs strongly suggests an influence of orographic precipitation, but this is not the only factor as attested by the low frequency of mires on the slopes of the Plomb du Cantal and Puy de Sancy, the highest mountains of the massif culminating at elevations of 1885m asl and 1855m asl respectively. Figure 2-2 suggests that the nature of the underlying bedrock also plays a major role, with most mires occurring in granitic areas. However, it should be noted that the mire distribution data presented in Figure 2-1 and Figure 2-2 have clear methodological limitations since they were derived from an aggregation of a number of inventories with varying methodology, geographical extent, scope, completeness and accuracy (MEDDE/CGDD/SOeS & Fédération des Conservatoires d'Espaces Naturels 2013). Further work is clearly needed to clarify the climatic conditions and hydrogeomorphic settings that promoted peatland development in the Massif Central.

2.2.2. Statutory designations

Mire habitats and species are an important conservation priority within the Massif Central. No less than 79 Special Areas of Conservation have been designated principally or in part for the conservation of mire habitats of European interest under the EU 92/43/EEC Habitats Directive. Two National Nature Reserves have been designated principally for the conservation of mire habitats, including the Dauges NNR where the current study was carried out (see Section 2.6), and another two NNR include mire habitats. Fourteen mire sites are also strictly protected by an *Arrêté Préfectoral de Protection de Biotope* (APPB). An application for Ramsar status has recently

been made for the Millevaches plateau, in Limousin on the north-west side of the Massif Central, where the highest density of mires within the Massif Central is found (Figure 2-2).

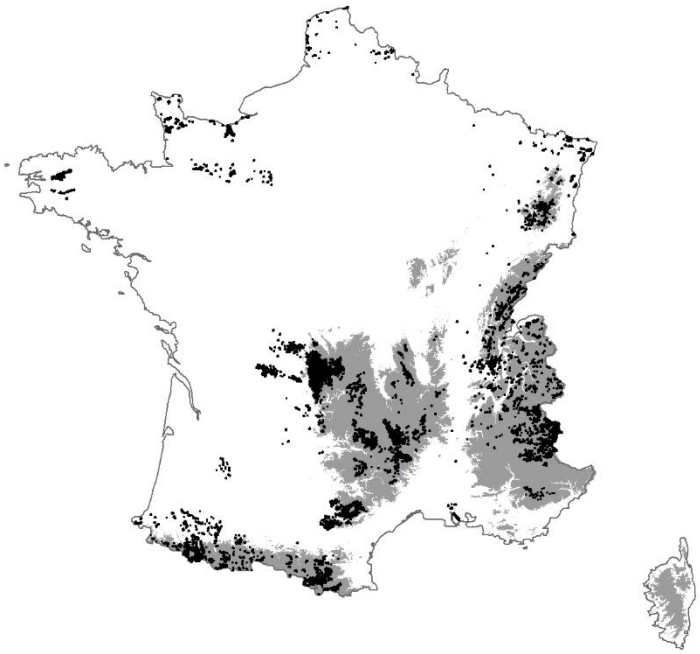

Figure 2-1. Distribution of mires in Metropolitan France.

Mires are shown in black (data: MEDDE/CGDD/SOeS & Fédération des Conservatoires d'Espaces Naturels 2013). Mire boundaries have been widened to increase readability. Areas above 500m NGF69 are shown in grey.

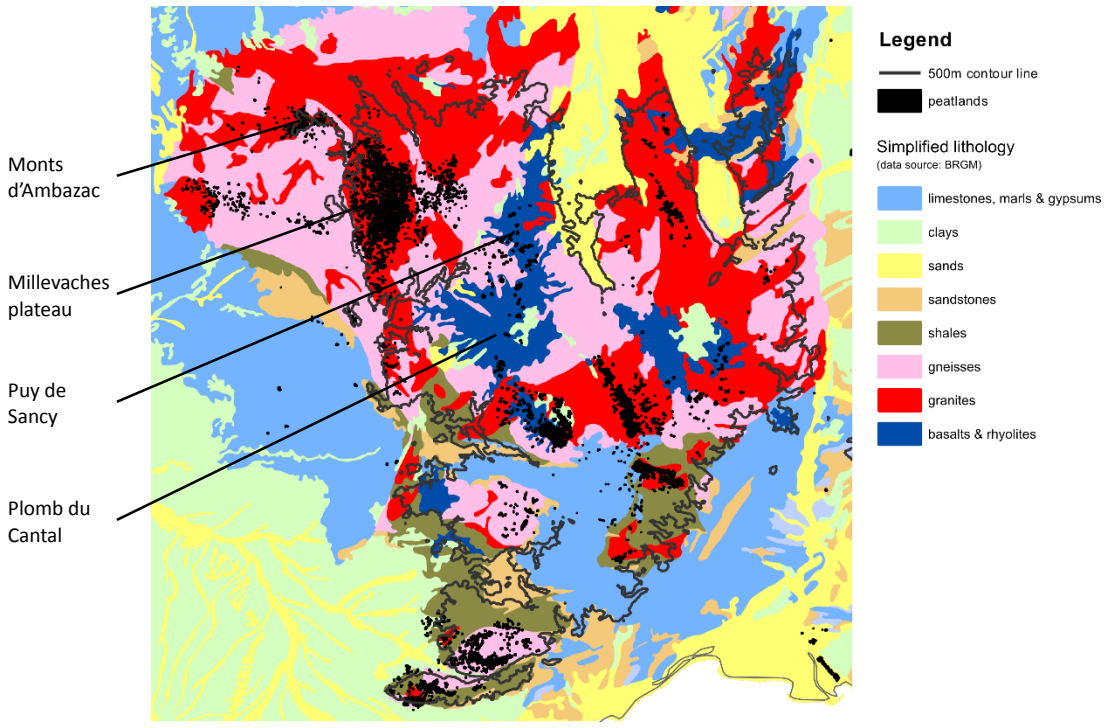

Figure 2-2. Distribution of peatlands within the Massif Central relative to bedrock lithology.

2.2.3. Changes in landuse in the Massif Central over the last century

During the last century or so, many granitic uplands of the Massif Central have witnessed a marked conversion of unimproved grassland and heathland to forest, either through cessation of agricultural activities and uncontrolled afforestation or through planting (Deuffic 2005; Dodane 2009). Figure 2-3 shows changes throughout the 19th and 20th centuries in the proportion of land covered in either heathland or forest in Limousin. The lower left graph shows landcover statistics at the regional scale.

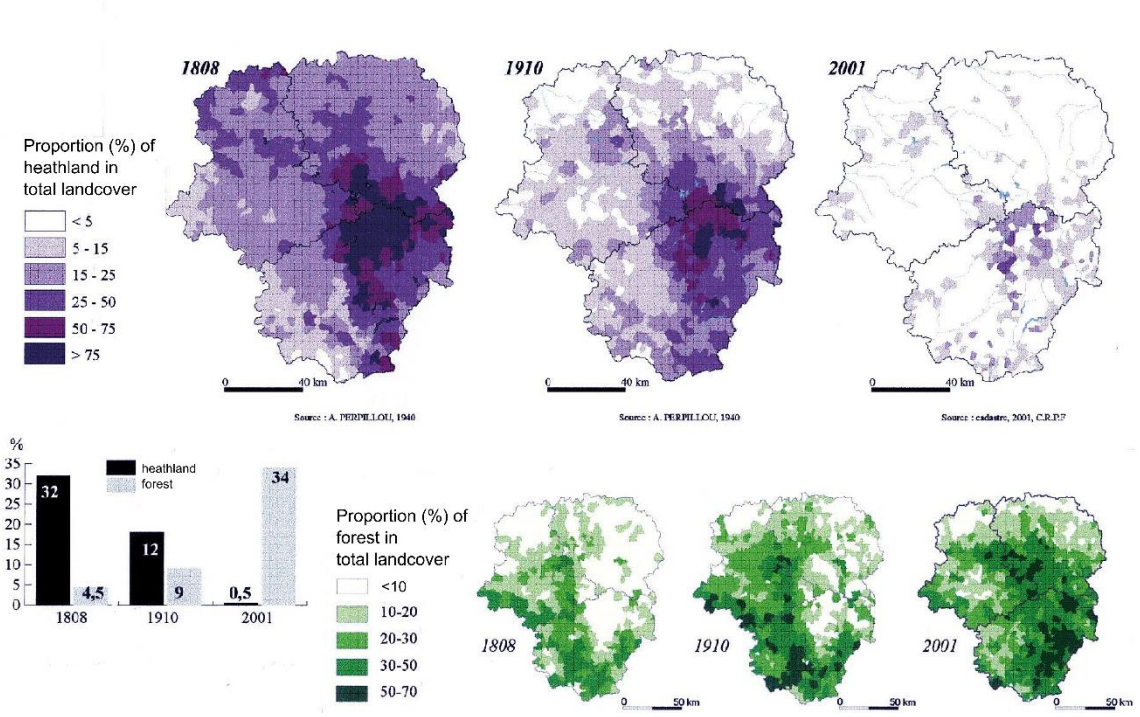

Figure 2-3. Proportion of heathland (purple scale) and forest (green scale) in total landcover in Limousin.

(unpublished data, CEN Limousin & Laboratoire de cartographie, Université de Limoges - Laëtitia Feydel, 2003).

In the early 19th century, heathlands covered a third of the regional area, and more than 75% of the landscape on the uplands of the Millevaches plateau. Forests were found principally on the south-west lowlands. Over the last two centuries, and particularly during the second half of the 20th century, 98% of heathlands have disappeared, converted to improved pasture or arable land in the lowlands, and to forests in the uplands. Woodlands now occupy up to 70% of the area in some upland districts. According to the most recent national forestry statistics (Inventaire Forestier National, http://inventaire-forestier.ign.fr), 56% of forests on the Millevaches plateau are coniferous plantations, but this figure masks large local variations. Scots pines, mainly planted in the early 20th century, cover 11% of forested land; Norway spruce 18% and Douglas fir 21%. The latter species, introduced mainly after major storms in 1982, is now used in the vast

majority of new plantations and replantations. Most mires, and in particular those designated as Special Areas of Conservation under the EU 92/43/EEC Habitats Directive, as NNRs or as ZNIEFF (*Zones Naturelles d'Intérêt Ecologique Floristique ou Faunistique*: sites of special ecological and wildlife interest), are located in these upland areas, yet the impact of the massive catchment afforestation on mire ecology and hydrology has never been assessed in Limousin, in the Massif Central, or indeed anywhere in France. Only a handful of studies have been carried out globally on this issue (Smith & Charman 1988; Helmschrot 2006; Krause *et al.* 2007). Yet, as detailed in Appendix H, the impact of forests on the water cycle is important. Even though mires in Limousin and in the wider Massif Central have relatively rarely been directly afforested, it is possible that the substantial changes in the land cover of their catchment that have occurred in the last 50-100 years have had a major impact on their hydrological condition.

2.3. Review of available research on peatland hydrology within the Massif Central

A number of hydrological studies focussing on runoff and flood generation processes in mountaineous areas were carried out in a paired watershed experiment on granitic bedrock in Lozère (Dupraz *et al.* 1984, 1985; Didon-Lescot 1984; Dejean & Durand 1987; Lelong *et al.* 1987; Durand *et al.* 1992). One of these paired catchments contained a small minerotrophic valley mire so that the impact of this mire on runoff was also investigated. Martin *et al.* (2002) and Martin & Didon-Lescot (2007) compared discharge from the paired catchments and showed that they had similar flood event volumes, but that peak flow was smaller and delayed downstream of the mire. They explained these observations by a higher resistance to overland flow and a higher flood storage capacity within the mire, but did not conclude on whether this higher storage capacity was a consequence of the mire topography or of the presence of peat itself. They also recorded smaller low flows downstream of the mire.

Cognard-Plancq *et al.* (2004) used a lumped rainfall-runoff model to simulate discharge from both catchments and also concluded that peak discharge was reduced and delayed downstream of the mire. Martin *et al.* (2008) investigated the impact of restoration through drain blocking in another mire also located in Lozère that had been drained for 30 years. They found limited effects of drain blocking on groundwater table depth within the mire. The comparison of discharge downstream of the drained mire with a paired catchment without mire suggested larger peak flows and larger low flows downstream of the former.

Brenot *et al.* (2014) and Négrel *et al.* (2010) used chemical and isotopic approaches combined with discharge and piezometric measurements to identify inflows to and outflows from a maar peatland in Velay. They identified at least three different fluxes with distinct chemical and isotopic signatures supplying water to the mire, as well as a strong contamination of the mire by calcium amendments leaching from the mire's farmed catchment. Porteret (2008) investigated the hydrology of four mires of different hydrogeomorphic types in Forez. He highlighted the technical and methodological difficulties associated to the collection of long-term and accurate hydrological time-series in mountainous environments and to the measurement of the impact of mires on downstream flow. He found distinct groundwater table depth patterns between the different hydrogeomorphic types.

As the preceeding paragraphs have demonstrated, there has been very little research on the hydrology of mires within the French Massif Central despite their recognised importance at the European scale for biodiversity conservation and, as demonstrated in Chapter 1, the fundamental importance of hydrology in driving geomorphological, biogeochemical and ecological processes in mires. There has been no attempt at quantifying and modelling water fluxes to, from, and within representative sites. As a consequence, there has been no quantitative analysis of the hydrological impacts of some of the potential threats that these mires face, in particular changes in catchment landuse.

2.4. Thesis aims

In accordance with some of the research needs identified in Section 2.3, the overall aims of this thesis are to identify, quantify and model water fluxes to, from and within an acidic valley mire representative of a large proportion of mires in the Massif Central, in particular of the Limousin uplands, and to assess the potential impacts of catchment afforestation on its hydro-ecological condition.

2.5. Research objectives

To achieve these aims, this thesis has the following objectives:

- to develop a three-dimensional geological model of the mire and its catchment,
- to acquire continuous precipitation and reference evapotranspiration time-series, to be used as model inputs,
- to acquire hydrological time-series, including stream discharge, stream stage, groundwater table depth and piezometric head,

- to acquire a number of additional datasets required for the development of a hydrological model of the site, including landuse maps, topographic data, and stream profile data,
- to develop a conceptual hydrological model of the mire and its catchment based on a qualitative analysis of the data listed above,
- to develop, calibrate and validate a MIKE SHE / MIKE 11 spatially-distributed, physically-based hydrological model of the mire and its catchment, allowing to reproduce discharge to and from the mire as well as groundwater table depth in any point of the mire,
- to undertake sensitivity analyses of the model to identify factors that have the greatest influence on simulated groundwater table depth and discharge and may potentially be the largest sources of error,
- to use the model to establish a detailed water balance of the mire and its catchment, to quantify the respective contribution of precipitation, runoff from surrounding mineral ground and groundwater to the peat water balance and groundwater dynamics within the peat, and to characterise the spatial distribution of water fluxes within the mire and its catchment,
- to use the model to assess the potential impact of catchment afforestation on the mire hydrological conditions.

2.6. Research site: the Dauges National Nature Reserve

2.6.1. Location and general context

The selected research site is located near the small village of Saint-Léger-la-Montagne, in the administrative department of Haute-Vienne and region of Limousin, France (latitude: 46°00'42"N, longitude: 1°25'07"E, Figure 2-4). It lies at the heart of the Monts d'Ambazac, a low altitude mountain range at the north-western limit of the Massif Central. The study area was defined as the topographic catchment of a small permanent stream, the Ruisseau des Dauges, at its intersection with the first road it meets (road D78) where all surface flow is channelled into a concrete culvert by the natural topography, the road embankment and the associated drainage ditches, making this point the ideal location to monitor the catchment's surface outflow. The catchment covers 231.3 hectares. The site has been described as a prime example of etch-basins (*alvéoles* in French) widely found in Hercynian mountains (Valadas 1998): a circus-like valley with a flat bottom, surrounded by gentle hills, and opening into a narrow linear valley that, beyond the research catchment outlet, leads itself to another etch-basin further downstream

(Figure 2-5). The catchment is defined by the hills overlooking the main etch-basin and the narrow corridor downstream of it. Smaller etch-basins occur upstream of the main one at approximately mid-slope. Elevation ranges from 532m above sea level (NGF69) at the catchment outlet to 664m at the top of Puy de la Garde, on the south-eastern boundary. A 30m-high residual hill, Puy Rond, rises dramatically at the centre of the main basin (Figure 2-6).

The catchment boundaries approximately match those of the Dauges National Nature Reserve (*Réserve Naturelle Nationale de la Tourbière des Dauges*), designated in 1998. The NNR is additionally designated as a Special Area of Conservation (FR7401135) under the EU 92/43/EEC Habitats Directive. The main reason for the designation of the site as a NNR and SAC is the presence at the bottom of the basin of a relatively large (for the region and country) extent of acidic mire habitats covering approximately 43 hectares. Wetland habitats cited in the SAC designation procedure include habitats 4010 (Northern Atlantic wet heaths with *Erica tetralix*), 7110 (active raised bogs), 7120 (degraded raised bogs), 7140 (transition mires and quaking bogs), 7150 (depressions on peat substrates), and 91D0 (bog woodland). As detailed in Section 1.2.3, a number of mire classification systems exist that rely on different types of descriptors. These classifications do not overlap entirely. Plants for instance may indicate specific hydrogeomorphic types in some areas but not in others. In France, habitats within candidate SACs have generally been identified using botanical and phyto-sociological criteria only. This explains why "raised bog" habitats were identified on the Dauges wetland even though it is clearly a fen when using hydrogeomorphic criteria.

Other habitats of conservation interest cover a large proportion of the hillslopes, and include Atlantic beech woodlands, dry heathlands and *Nardus stricta* acidic grasslands. The rest of the catchment is covered by oak-beech and chestnut woodlands, a few Douglas fir and Scottish pine plantations, and some permanent or temporary grasslands. There is no arable land. A simplified landuse map is given in Section 2.6.3. The site hosts a range of relatively rare species associated with wetland habitats and acidic mires in particular, such as the orchid *Spiranthes aestivalis*, the fern *Lycopodiella inundata*, the moss *Bruchia vogesiaca*, the dragonfly *Coenagrion mercuriale*, the butterfly *Euphydryas aurinia*, etc. Overall, about 150 species with a legal protection or a conservation concern have been recorded within the NNR (Durepaire & Guerbaa 2008).

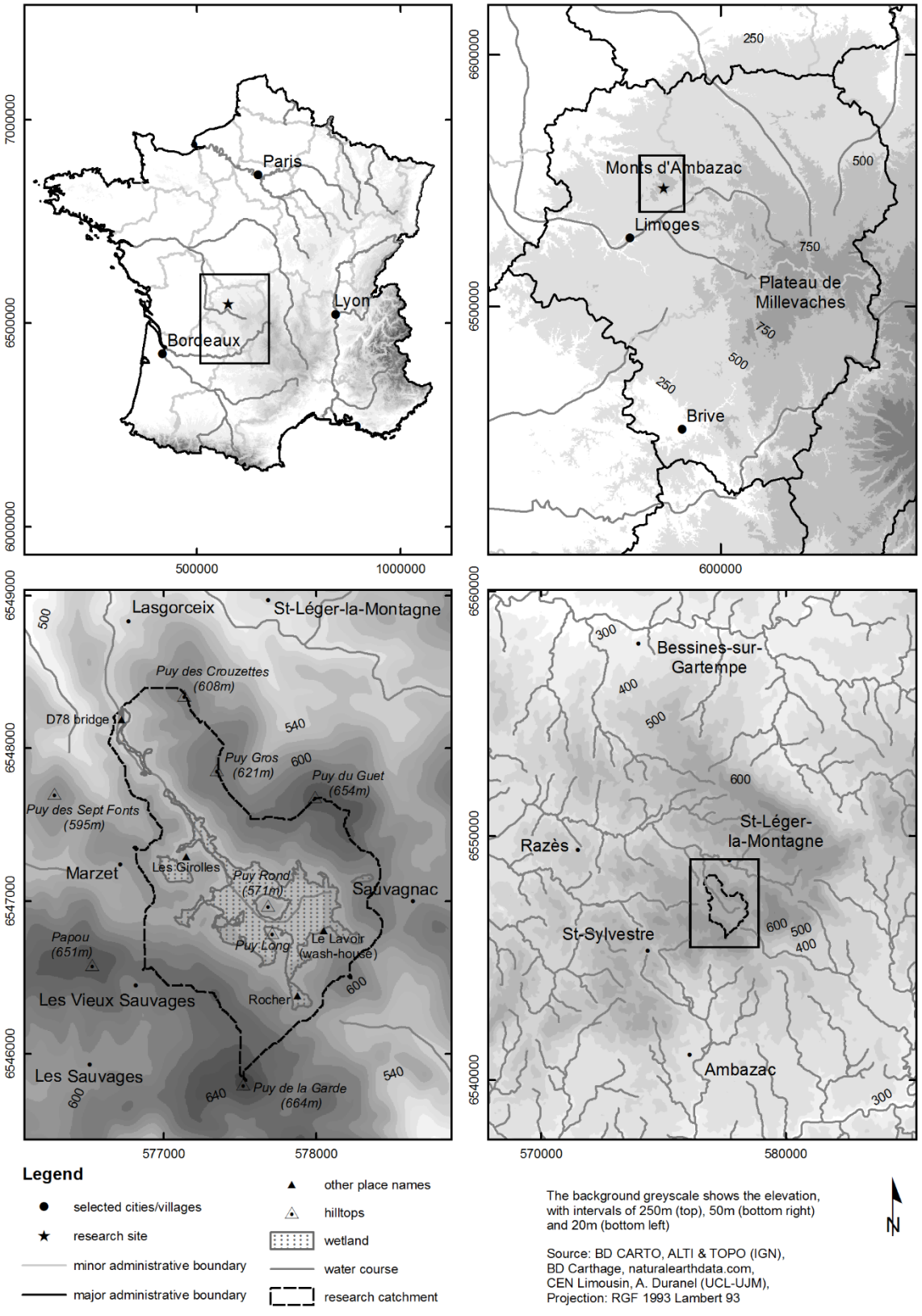

Figure 2-4. Location of the Dauges research catchment and wetland within France (top left), Limousin (top right), and the Monts d'Ambazac massif (bottom right and left).

Figure 2-5. Three-dimensional view of the Dauges catchment.

The green arrow points north. The red line shows the boundaries of the research catchment, the blue line the simplified hydrographic network. Data from BD Ortho IGN 2010, BD Topo IGN, A. Duranel UCL/UJM.

Figure 2-6. View of the Dauges wetland from its north-east boundary (January 2011).

The hill in the middle of the wetland at the centre of the picture is Puy Rond, that at the horizon is the Papou. The edge of the forest in the background marks the boundary between peat and mineral soils. Photo: CEN Limousin.

According to Joly *et al.* (2010), the research catchment lies at the transition between an altered oceanic climate and a mountainous climate. Figure 2-7 shows the ombrothermic diagram of the area, based on climatic normals (1998-2010) provided by Météo-France for the nearest meteorological station recording both precipitation and temperature, located at St-Léger-la-Montagne (St-Léger-Mon, Le Pétalus, 87159002), 4.2 kilometres from the research site at an altitude of 629m. Mean annual precipitation and temperature are 1367.1mm and 10.1°C respectively. Precipitation is well distributed throughout the year. The site climatology is further described using data collected as part of this study in Appendix E.

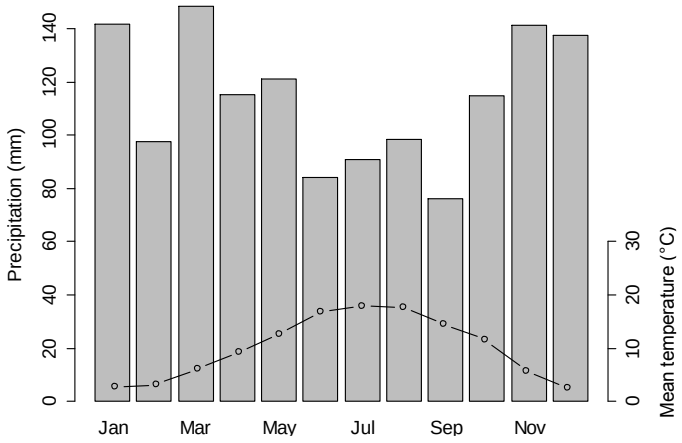

Figure 2-7. Gaussen-Bagnouls ombrothermic diagram of the St-Léger-Mon met station (1998-2010).

2.6.2. Geology

The Dauges catchment is located on the Saint-Sylvestre granitic massif, a two-mica leucogranite of which three types have been recognised from west to east: a calc-alkalic leucogranite with orthoclase and plagioclase, an alkalic granite with perthite and plagioclase, and an alkalic sodic granite with perthite and albite (Dutartre *et al.* 1982). The transition between these different types is gradual. The Dauges catchment lies at the transition between the last two types.

The Saint-Sylvestre leucogranite is a light-colored rock with coarse- to medium-sized equant grains. It is post-tectonic and intruded up through metamorphic formations and other granite types during the Namuro-Westphalian (320 MY). Numerous uranium deposits are found along the faults and intrusions in the granite, and these were mined during the second part of the 20th century by the *Commissariat à l'Energie Atomique* (CEA) and *the Compagnie Générale des Matières Atomiques* (COGEMA), now AREVA, including within the Dauges catchment where large-scale underground mining was in operation until the 1990s (Figure 2-8). The galleries are relatively shallow, their depth reaching 40-50m where they cross the valley at the outlet of the

main basin and as little as 10-15m further downstream. The depth of the gallery located below the main wetland area and Puy Rond is about 100m. The galleries were kept dry by pumping during the mining operations but this ceased when the mine was closed. As a consequence of the mining activity, the geology and the tectonic history of the area are well known. Within the Dauges catchment, the leucogranite is dissected by numerous veins of lamprophyres (called *minettes* in the French mining jargon), particularly downstream of the main wetland area.

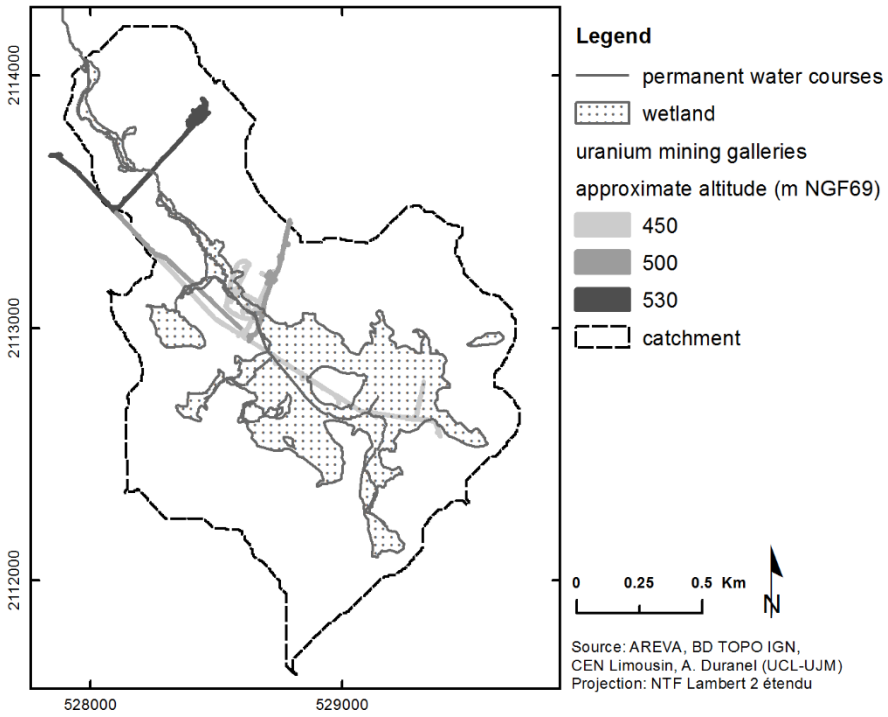

Figure 2-8. Plan projection of uranium mining galleries within the Dauges catchment.

A map of faults and veins in the catchment at the 1/2000 scale was obtained from AREVA (Anonymous 1995), geo-referenced and digitised (Figure 2-9). Unfortunately it does not extend to the southern part of the catchment. Faults oriented NNE-SSW such as the Gorces fault are major faults, with wide damage zones (Anonymous 1995).

A synthesis of the available knowledge on the site geomorphology and on granite weathering and peri-glacial formations is given in Section 3.3.1.

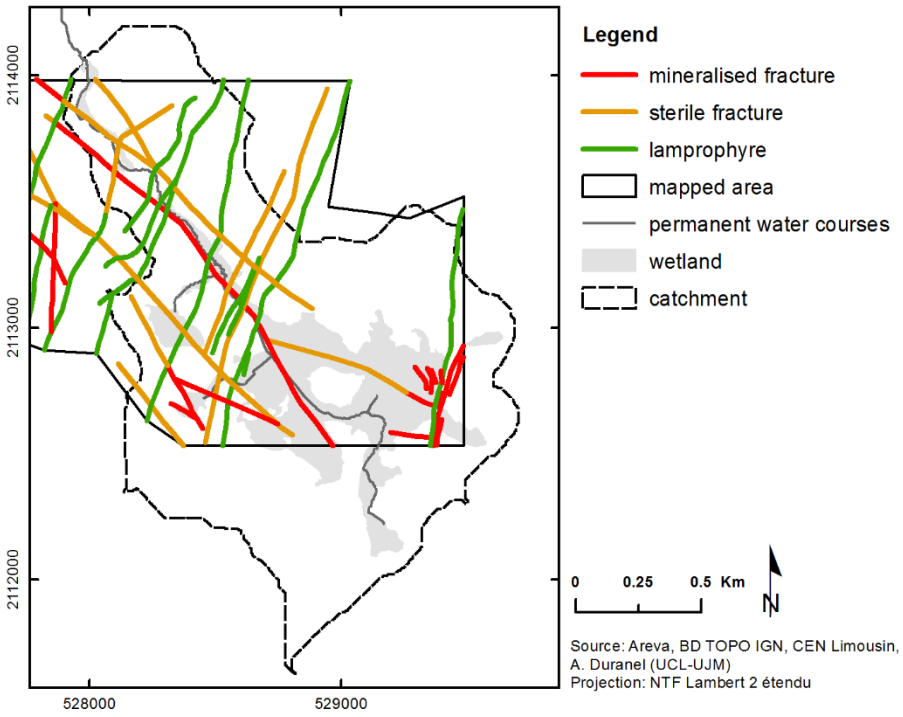

Figure 2-9. Faults and veins as mapped by GOGEMA.

2.6.3. Landuse

A vector vegetation map at the 1:1000 scale of the NNR was obtained from the CEN Limousin (Durepaire & Guerbaa 2008). It follows the CORINE biotopes classification (Bissardon *et al.* 2003), and was derived in 2008 by visual interpretation of ortho-rectified aerial photographs and systematic ground checks. As part of the current study, contours of the main habitat types were validated against the most recent (2010) ortho-rectified aerial photographs available. The map was found to be detailed and accurate enough to be used for hydrological modelling purposes. A few gaps at the margins of the catchment were filled based on the most recent ortho-rectified aerial photographs (Figure 2-10). Table 2-1 gives summary statistics on landcover within the research catchment.

Table 2-1. Total area and frequency of vegetation classes within the Dauges catchment.

Vegetation class	area (hectares)	% total area
broadleaf woodlands	111.9	48.4
coniferous woodlands	18.2	7.9
heaths and shrubs	29.2	12.7
impervious	0.4	0.2
mixed woodlands	6.5	2.8
pastures and meadows	22.4	9.7
wet woodlands	3.8	1.6
wetland	39.0	16.9

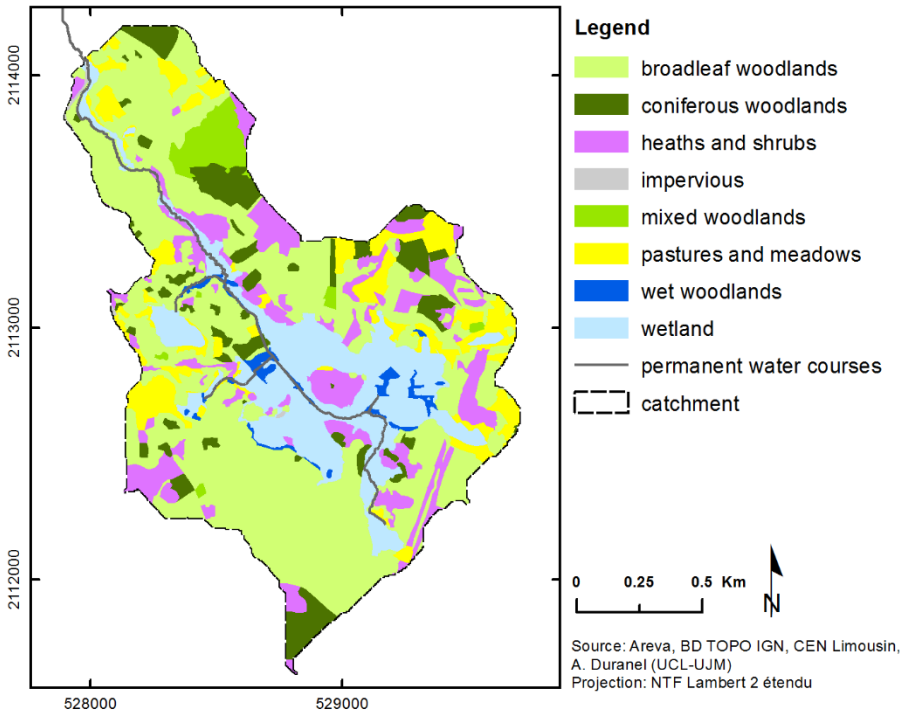

Figure 2-10. Landcover within the Dauges catchment.

2.6.4. Rationale for the choice of the Dauges catchment as a research site

The site is located at the north-western limit of the distribution of acidic mires in Limousin and within the Massif Central, at a slightly lower altitude than the Millevaches plateau where elevations range from about 500m to 977m and where the highest densities of mires within the Massif Central are found. However long-term mean temperature and precipitation are within the range of those recorded on the Millevaches plateau. More importantly, the geology and geomorphology of the site is representative of conditions found across nearly all the uplands of Limousin, and in most of the crystalline Massif Central. The hydrogeomorphic settings of the mire -at the bottom and on the toeslopes of an etch-basin-, its surface topography and the vegetation communities that have been identified within it are very similar to those of most mires of the Limousin uplands and of many mires of other granitic sub-massifs within the Massif Central. Conclusions made on the hydrogeology and hydrology of the site are therefore applicable to these sites, at least qualitatively. The Dauges catchment was selected above other potentially suitable sites because of its designation as a NNR and SAC, and hence the permanent presence of field staff on site, their willingness to collaborate to the monitoring of the site, the landownership structure and NNR regulations allowing full access to the site, and the important added value that such a work would bring when applied to the conservation management of the NNR and SAC.

2.7. Research design and thesis outline

Very few data relating to the Dauges catchment and suitable for hydrological modelling were available at the start of this study. A very large amount of time was therefore devoted to the development of the large database required to develop both the conceptual hydrogeological model and the distributed physically-based hydrological model.

Chapter 3 describes the development of a three-dimensional geological model of the catchment, including granite weathering formations, peat deposits and alluvial deposits. A high-resolution topographic survey was carried out within the mire using differential GPS. Existing topographic maps were digitised and used to model the catchment topography. A number of methods were used to investigate the nature and depth of granite weathering formations, including soils and periglacial formations. Existing deep geological drilling logs were reinterpreted and an electrical resistivity tomography (ERT) survey carried out. Existing outcrops and small-scale quarries were investigated and their stratigraphy described. Finally, the spatial distribution of outcropping formations was investigated and modelled based on available direct or indirect indicators such as slope, landuse and hard-rock outcrops. The development of the 3D model of peat and alluvial deposits was based on manual augering and probing. The hydraulic conductivity of these deposits was measured using slug tests.

The development of the database of precipitation and Penman-Monteith reference evapotranspiration is described in Appendix E, since the discussion of the methods used to develop it is not central to this thesis. Meteorological data were recorded within the site over a three-year period. Due to instrument failures, a large amount of work was devoted to data correction and quality control. Missing and historical time-series were reconstructed using statistical modelling based on data recorded at the closest permanent meteorological stations. The representativeness of the hydrological model calibration and validation period relative to long-term records was assessed.

Chapter 4 describes the acquisition, processing and qualitative analysis of the hydrological time-series. Stream discharge was monitored using V-notch weirs and automatic loggers in three locations upstream of the main wetland extent. In the downstream reaches, stage was monitored at two locations using automatic loggers and discharge calculated after stage-discharge curves had been established. Stream stage was monitored automatically at the two gauging stations located downstream of the wetland, and manually at three further points within

the wetland. A total of 57 dipwells and piezometers were installed to monitor groundwater table depths and piezometric heads in peat, underlying alluvial sediments and mineral soils. Automatic loggers were installed in 16 dipwells or piezometers to provide high-resolution records, while others were monitored on a fortnightly basis on average. Chapter 4 also describes the conceptual hydrogeological model derived from a qualitative analysis of the hydrological and stratigraphical data.

Chapter 5 details the development of a distributed, physically-based hydrological model of the Dauges mire and its catchment using MIKE SHE and MIKE 11. Constraints relative to computation time and consequent methodological choices are explained. A modification of the two-layer evapotranspiration model is proposed to allow a better representation of interception and evapotranspiration processes, that were identified as being particularly important in explaining the difference in water yield between broadleaf woodlands, coniferous woodlands and open habitats. A detailed literature review of plant-specific evapotranspiration parameters for species relevant to the Dauges site was carried out and used to parametrise the evapotranspiration model.

Chapter 6 describes the calibration and validation strategy employed for the model and discusses the model performance. The model was calibrated and validated against observed hydrological time-series, and further validated spatially by comparing simulated mean groundwater table depths and the observed distribution of wetland vegetation. A detailed analysis was carried out to identify the parameters to which the model predictions were most sensitive, to evaluate the potential consequences of the high uncertainty associated to the geometry of granite weathering formations and to evaluate the impact of some design choices such as grid size and warm-up period. The limits of the model and possible improvements are discussed.

In Chapter 7, the calibrated and validated model is used to quantify water fluxes throughout the mire and its catchment under current conditions. A detailed water balance analysis is carried out, and the spatial distribution of groundwater table depth, vertical flow between computational layers and saturated zone seepage to overland flow is analysed. The adequation between results of the MIKE SHE model and the conceptual hydrological model inferred from the qualitative analysis of hydrological and stratigraphical data is discussed.

In Chapter 8, the potential impact of catchment-scale landuse changes on the mire hydrology is evaluated. The impact of catchment landuse on the catchment and mire water balances, on stream discharge and on groundwater table depths is assessed by forcing the MIKE SHE model

with new landuse maps corresponding to a conversion of the catchment, currently dominated by broadleaf woodlands, to coniferous plantations or to grassland respectively.

Chapter 9 summarises and discusses the principal results from the study and provides some recommendations focused on mire conservation management and future research needs.

Résumé du chapitre 2

Le Massif Central est l'une des régions de France métropolitaine où l'on trouve la plus forte densité de tourbières. En reconnaissance de leur valeur patrimoniale et des services écosystémiques qu'elles fournissent, un grand nombre d'entre elles font l'objet d'une protection réglementaire au niveau national ou européen. Malgré cela, et à l'exception de leur phytosociologie et de la chronologie de leur mise en place, les tourbières du Massif Central ont été relativement peu étudiées. Leur fonctionnement hydrologique en particulier est mal compris. Une grande partie des tourbières du Massif Central sont situées sur socle granitique, et le type hydrogéomorphique le plus fréquent dans cette région correspond à des tourbières de fond d'alvéole, suggérant une connectivité hydrologique importante entre ces tourbières et leur bassin versant ; toutefois aucune étude n'a jamais été menée pour quantifier la balance hydrique de ces zones humides. D'autre part, certaines régions du Massif Central, en particulier les hauts-plateaux limousins, ont connu une afforestation massive en quelques décades au cours du vingtième siècle, avec en particulier d'importantes plantations d'essences résineuses, sans que les conséquences sur la ressource en eau de manière générale et sur l'hydrologie des tourbières en particulier aient été étudiées. Il est remarquable que, à l'échelle mondiale, seule une poignée d'études aient été réalisées sur l'impact de l'afforestation des bassins versants sur les zones humides. Les objectifs de cette thèse sont donc de caractériser, quantifier et modéliser les flux d'eau et les niveaux de nappe dans une zone humide représentative des tourbières acides du Massif Central ainsi que dans son bassin versant; et d'évaluer par simulation l'impact de l'afforestation et de l'enrésinement de ce bassin versant sur l'hydrologie de la tourbière.

Le site choisi pour mener à bien cette étude est la Réserve Naturelle de la Tourbière des Dauges, située dans les Monts d'Ambazac en Limousin, sur la bordure nord-ouest du Massif Central. D'une superficie de 231 hectares, le site étudié constitue un exemple type d'alvéole granitique, dans le fond duquel s'est développée une tourbière acide couvrant une quarantaine d'hectares. Une colline résiduelle d'une trentaine de mètres de hauteur, le Puy Rond, se dresse au milieu de celle-ci. Le site présente des végétations tourbeuses et un contexte géologique, géomorphologique et climatique tout à fait similaires à ceux rencontrés dans la plupart des tourbières du Limousin et dans un grand nombre de tourbières du Massif Central. Les sols minéraux sont essentiellement occupés par des boisements semi-naturels feuillus, avec quelques milieux ouverts et plantations de résineux.

Chapter 3. Geological model of the Dauges catchment

3.1. Introduction

The three objectives of this chapter are:

- within the Dauges research site, to characterise and map the 3D distribution of the geological formations that may have a substantial role in the hydrology of the wetland and of its catchment, in particular granite weathering formations (including periglacial deposits), alluvial sediments and peat deposits;
- to contribute to the development of a conceptual model (in the hydrogeological meaning of the term) of water flow within the mire and its catchment;
- to provide the information required for the development of the MIKE SHE geological model.

To fulfill these objectives, granite weathering formations were investigated using a number of complementary approaches, including topographic surveys, an analysis of existing geological drill logs, a survey of existing sections through superficial formations, ERT surveys and a number of GIS-based geomorphological analyses. Peat and alluvial deposits were described using manual augering and probing, and mapped using geostatistics. Their hydraulic conductivity was measured using slug tests.

3.2. Surface topography

3.2.1. Methods

Topographic data from different sources were assembled to produce a DEM with sufficient extent to cover the entire catchment and sufficient accuracy to faithfully model the small-scale topography within the wetland.

3.2.1.1. DGPS surveying

The surface topography of the wetland was surveyed using Real Time Kinematic navigation with a differential GPS system composed of a Leica GPS500 base station and a 1200 rover (2010-11), a Trimble 5800 system (2011) or a Leica 1200 base station and CS15 rover (2012). In February 2011, a permanent survey benchmark was set up in the middle of the site on Puy Rond using a yellow survey marker anchored 50cm deep into the mineral soil. The GPS base station was

installed on top of this benchmark and run for at least four consecutive hours several times over two weeks to work out the precise location of the benchmark. Data were post-processed with the Leica GeoOffice software. The position of the benchmark was first corrected using data broadcast by the French Geographic Institute (IGN) permanent GNSS network (http://rgp.ign.fr/accueil.php#). Data were downloaded from the three closest stations: Montmorillon (MTMN), Masseret (MSRT) and Toulx-Sainte-Croix (BOUS). After post-processing, the coordinates were projected from WGS84 to RGF Lambert 93 and NTF Lambert 2 étendu using the IGN Circé software.

The post-processed position of the top of the metallic centre of the marker is shown in Table 3-1 (all data are given in metres).

Table 3-1. Position of the survey benchmark.

X +/- SD WGS84	Y +/- SD WGS84	Z +/- SD WGS84
4436492.367 +/- 0.002	109936.926 +/- 0.001	4566551.412 +/- 0.002

Easting L93	Northing L93	Easting L2E	Northing L2E	Elevation NGF69
577713.982	6546937.301	528981.616	2112742.076	566.128

The rover data were then corrected to account for the post-processed position of the base station. In surveys carried out after February 2011, the previously determined geographic position of the benchmark was entered directly in the base station prior to the surveys and the rover position acquired directly through RTK. The vertical precision (standard deviation) relative to the position of the base was generally less than a centimetre except in some places where overhanging trees were degrading the signal quality. The absolute vertical and horizontal precision was checked against the nearest local benchmark installed by IGN (http://geodesie.ign.fr/fiches/pdf/X.H.Q3-143_321627.pdf). The result was within the error margin provided by IGN for the coordinates of the benchmark. The other four IGN benchmarks available in the vicinity could not be surveyed due to dense overgrowth or buildings degrading the satellite signal or preventing direct access to the marker.

Two different methods were employed to survey the surface topography of the mire. First, ground elevation was surveyed in about 1800 points distributed according to a 25m resolution grid using the DGPS rover mounted on a pole, concomitant to the survey of peat depth (see Section 3.4). As the micro-topography of the mire can be quite heterogeneous, the measurements were consistently taken from hollows, as opposed to hummocks. Secondly, to

allow for the collection of data at a higher resolution, the DGPS rover was mounted on a backpack and the mire was walked along parallel lines approximately 10m apart. A DGPS measurement was automatically taken every metre along those lines, resulting in about 21000 measures. The actual error of these measures depends on the roughness of the terrain. On the relatively flat surface used for quality-control purposes it was less than 10cm.

3.2.1.2. Analysis of existing topographic data

Outside the wetland and on most of the catchment, existing topographic data were collected from two main sources. High resolution scans of topographic maps at the 1:1000 scale were provided by COGEMA. The maps were drawn in 1993 and included topographic data collected since the 1970's. Mass points were surveyed using traditional levelling techniques with a 10cm precision, and it is understood that contour lines at 1m intervals were derived using stereo-photogrammetry. The maps were geo-referenced in ArcGIS, and a total of 2272 mass points and 310km of contour lines were digitised semi-automatically using the ArcScan extension. Checks carried out using DGPS have shown that the accuracy of mass points is within +/-10cm. On the outer part of the catchment, topographic data were obtained from the IGN BD Alti, a nation-wide DEM with a resolution of 25m. The mean vertical error of this DEM was checked after bilinear interpolation against the DGPS data. Figure 3-1 shows the density distribution of errors. The mean error was 2.079m +/-4.310, and the RMSE 4.785m. Errors as large as +/-20m occurred on steep slopes.

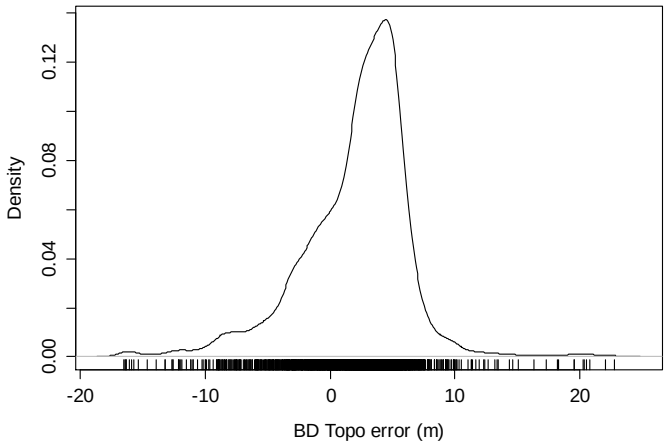

Figure 3-1. Distribution density of differences in elevation between the BD topo DEM (after bilinear interpolation) and the DGPS survey points.

3.2.1.3. DEM interpolation

To build a catchment-wide DEM, data from the different sources were merged, keeping only the most accurate data where these were available, and adding less accurate data elsewhere (Figure 3-3). Because it is one of the few methods able to deal satisfactorily with contour lines (Wilson & Gallant 2000; Hutchinson *et al.* 2011), the ANUDEM algorithm as implemented in ArcGIS was used to interpolate the topographic data to a 5m grid. Breaklines were introduced where the validation procedure of the algorithm indicated high error, generally along steep banks.

3.2.1.4. Catchment delineation

ArcHydro for ArcGIS was used to enforce the actual stream network into the DEM and to delineate the catchment area of several points of interest such as water-level recorders.

3.2.2. Results

Figure 3-4 shows the Digital Elevation Model of the wetland. There was no independent dataset available to test the accuracy of the DEM. After bilinear interpolation, it was checked against the ground elevation data collected using the DGPS rover mounted on a pole, which was the most accurate dataset available. This does not give the actual DEM error since this dataset was used to construct the DEM and did not cover the whole catchment, however it gives an idea of the mean error in the vicinity of the wetland, which was -0.024m +/-0.178. Figure 3-2 shows the density distribution of the DEM error. The RMSE was 0.179m. The largest errors, up to two metres as shown in Figure 3-2, were localised on the steep slopes just above the wetland.

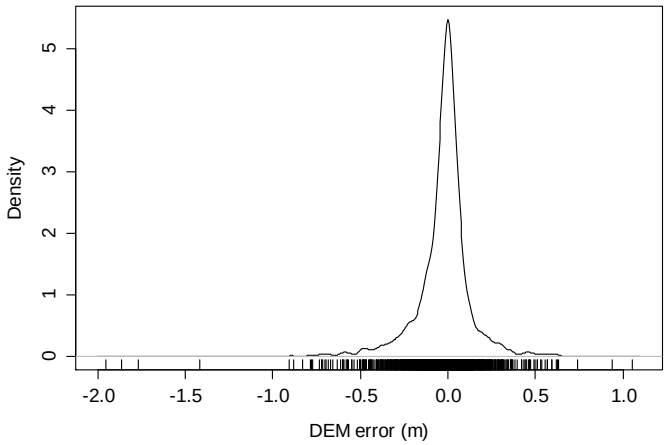

Figure 3-2. Density plot of differences between the DEM (after bilinear interpolation) and DGPS survey points

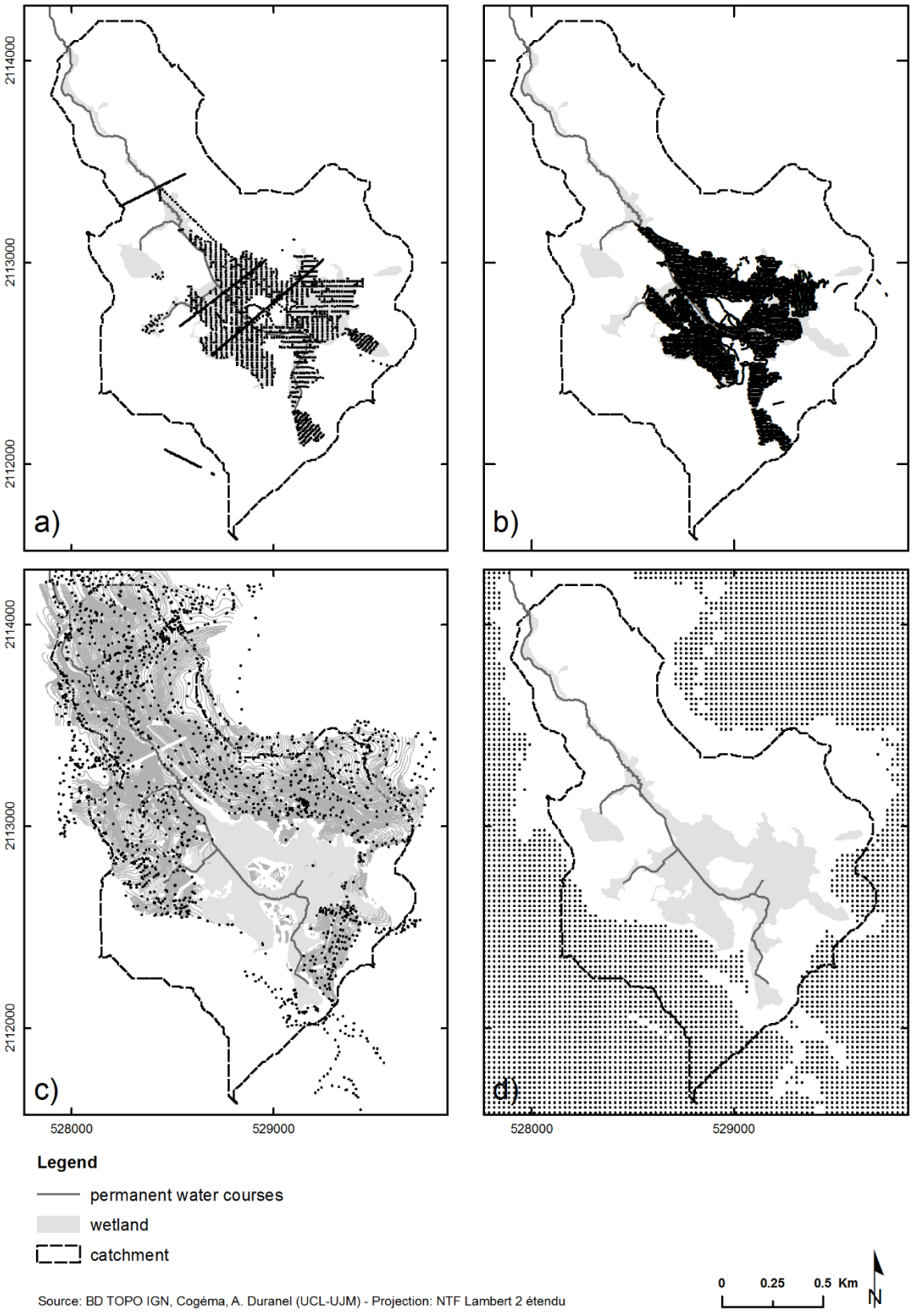

Figure 3-3. Topographic data used to build the catchment-wide DEM

a: pole-mounted DGPS survey, b: backpack-mounted DGPS survey, c: contour lines and mass points digitised from the COGEMA topographic maps, d: BD Alti 25m DEM.

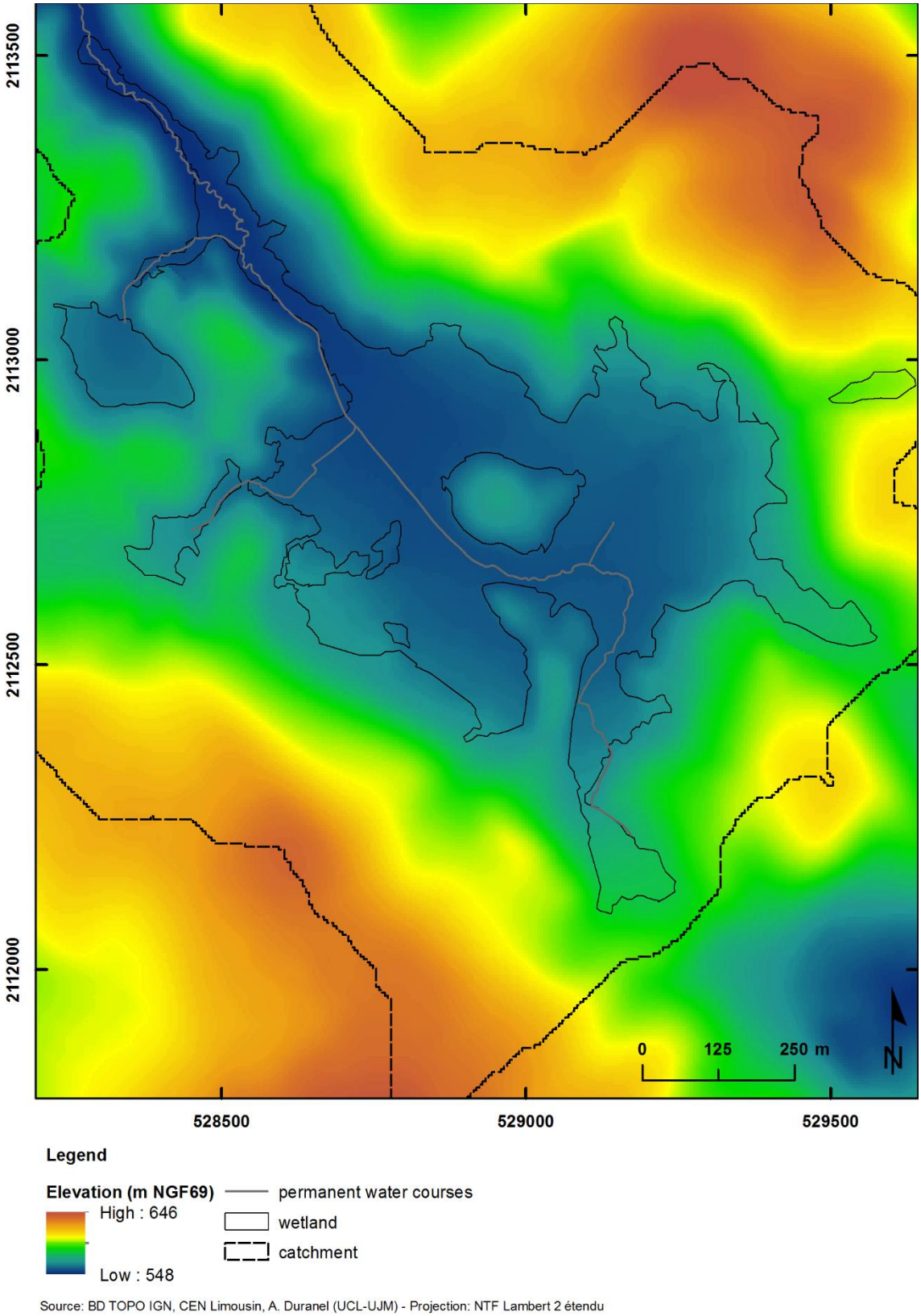

Figure 3-4. Digital Elevation Model of the Dauges wetland.

3.3. Development of a 3D model of granite weathering formations

Recent advances in the hydrogeology of hard-rock regions, and in particular of granitic terrains, are reviewed in Appendix C. The following sections apply concepts and terms defined in Appendix C to the Dauges catchment.

3.3.1. Current knowledge on granite weathering and peri-glacial formations within the research site

Within the Dauges research site as elsewhere in the Monts d'Ambazac, and more generally in Limousin, the fissured granite layer is expected to be relatively deep (Mauroux *et al.* 2009). Tectonic activity posterior to the formation of the weathering profile may complicate the stratiform arrangement of the weathering layers described in Appendix C. The tectonic history of the Monts d'Ambazac is very well known due to its importance for the understanding and mapping of uranium deposits. Gros *et al.* (1983) have shown that the main faults, oriented E-W, NW-SE and NNE-SSW, were formed during the Late Carboniferous and Early Permian, and were remobilised during the Middle Permian. Mesozoic and Cenozoic tectonic activity only resulted in minor remobilisations of these pre-existing faults. The weathering profile, which in the study area is dated from the infra-Cretaceous at most, has therefore not been disturbed by substantial tectonic activity. However, in the Monts d'Ambazac, the stratiform conceptual model is complicated by the fact that the area lies at the boundary between the infra-Cretaceous and the Eocene palaeosurfaces (Mauroux *et al.* 2009). The presence of erosion scarps between the two palaeosurfaces makes it difficult to reconstitute the altitude of the interfaces between weathering layers, as in this context it is possible to find Eocene weathering profiles intertwined with older and higher infra-Cretaceous profiles (Wyns, pers. comm.). Moreover, most infra-Cretaceous saprolites have been largely eroded away, and only a few metres are left in a limited number of place. This was confirmed using airborne spectral radiometry and DEM-derived morphological indices to map the distribution of saprolites (Mauroux *et al.* 2009).

Glaciers that existed in the Massif Central during the Quartenary glaciations never reached the uplands of Limousin. However residual in-situ saprolites were profoundly restructured by cryogenic and ice-related processes, and are overlaid by periglacial deposits on most slopes (Valadas 1984; André *et al.* 2001; Etlicher 2005). The classic sequence of periglacial deposits described in many places in the Massif Central includes from bottom to top the bedded grus and the head. The bedded grus (*arène fauchée* and *arène litée*) results from the in-situ saprolite being

gradually displaced by frost creep. It is recognisable by its laminated structure parallel to the surface slope that results from the repeated seasonal growing and thawing of ice lenses. At the base of the horizon, the residual rocks joints and veins show a gradual inflexion in the direction of the slope, and this part of the horizon has been named the cambered grus (*arène fauchée*). Bedded grus deposits were formed in a cold and relatively humid climate with deeply penetrating frost, and have been attributed to the Middle Devensian. Overlaying the bedded grus is the head, a poorly sorted mix of sandy to clayey matrix and 10-40cm long angular blocks. This formation has been named in different ways by French geomorphologists: *convoi limoneux à blocs, formation à blocs, formation gélifluée à blocs, arènes remaniées à blocs, etc*.). In Limousin, Flageollet (1977) has shown that the matrix is similar to in-situ saprolites in terms of granulometry, with only a slight enrichment in silt (+5% on average). The presence of a silt coating on all faces of the blocks shows a substantial rotational movement during transport. This formation is thought to be the consequence of a dry and cold climate, promoting the gelifraction of hilltop rock outcrops leading to the formation of blocks (Valadas 1984). The enrichment in silts would be related to frost-shattering of plagioclases. Blocks and matrix would have been displaced by gelifluction processes, whereby the presence of a permafrost would have restricted water infiltration and promoted the relatively rapid displacement of the thawed, saturated superficial layer in summer. At higher latitudes in the Massif Central, a compacted fragic horizon is often found, which coincides with the top of the permafrost and has important consequences for present groundwater flow (Etlicher 1986, 2005). However it has never been observed in Limousin (Valadas 1984). The head formation is generally attributed to the late Devensian, even though it may be more ancient in some cases. Both these formations have been recorded from the mid-slopes of the Dauges etch-basin by Valadas (1998).

3.3.2. Methods

3.3.2.1. Introduction

Within the Dauges catchment, the methods developed by the BRGM (Wyns 1998; Durand 2005; Durand *et al.* 2006; Lachassagne *et al.* 2006) and reviewed in Section C.2 of Appendix C were followed to map the interface of the different layers of the weathering profile. Existing information was gathered from the BRGM subsoil database (infoterre.brgm.fr), AREVA archives, geological maps, and published and grey literature. The entire catchment was also prospected along existing paths for outcrops and evidence of the fissured zone / saprolite interface. Unfortunately this interface could only be seen in two outcrops (n°2 and 3 in Figure 3-5), and no

outcrop was found that showed the fissured layer / unweathered bedrock interface. This is in part due to the fact that most of the catchment is heavily wooded, and that most open land is actually located at the bottom of the slopes where the weathered granite has been covered by deep Holocene sediments. Electrical resistivity tomography was therefore used to survey the saprolite and fissured layers along four transects and to complement data from existing geological drilling logs and field prospections. In order to predict the distribution of the outcropping fissured layer and of easily eroded in-situ saprolite and colluvial and alluvial deposits at any point within the catchment, the relationship between surface topography and indirect indicators such as granite outcrops and arable land were investigated. Periglacial deposits were described from existing superficial sections and soils from purpose-dug pedological pits.

3.3.2.2. Description of existing superficial sections

Only four outcrops were found where a deep enough section through weathering formations could be described (Figure 3-5). Two of them (1 and 2 on Figure 3-5) are small-scale grus extraction pits used by local inhabitants. The other two (3 and 4) are near-vertical banks cut through superficial formations when the path along the south-eastern side of the wetland was widened by COGEMA to allow access to a ventilation well. They were first described by Valadas (1998).

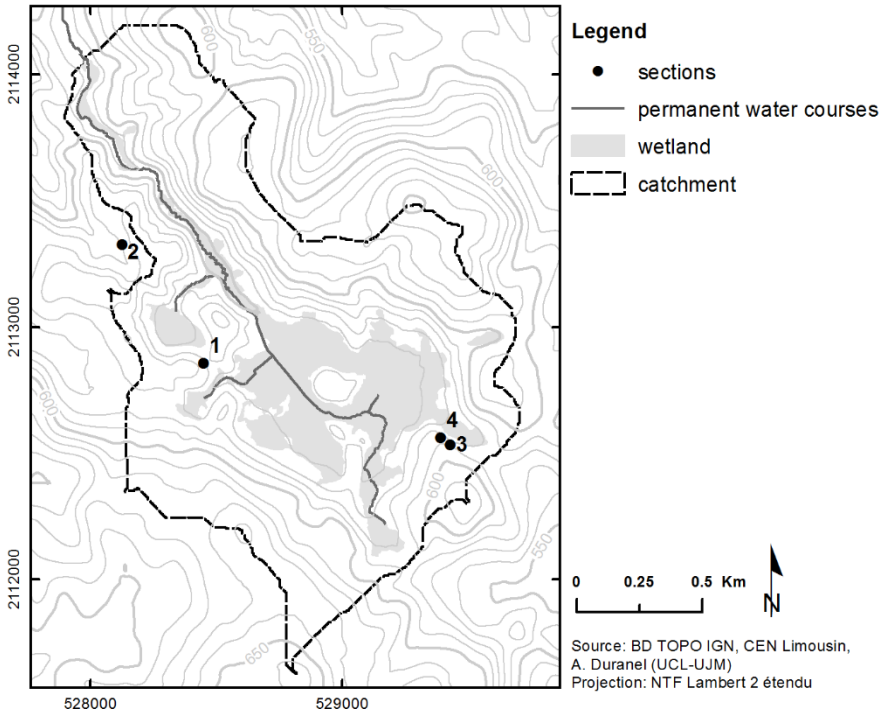

Figure 3-5. Location of sections through weathering formations.

3.3.2.3. Geological boreholes

Raw drilling logs of seven boreholes drilled in 1973 within the Dauges catchment by the CEA were obtained from AREVA (reference Sauvagnac 195.s). At least sixteen other boreholes have been drilled by CEA and AREVA (then COGEMA) within the Dauges catchment, however the drilling logs seem to have been lost (Figure 3-6). The boreholes for which information is available were used to characterise the depth of the granite weathering front. They are all located in the western part of the wetland. These boreholes were drilled for the purpose of uranium exploration and were selectively positioned using radiological surveys along mineralised faults. They are therefore not representative of the entire catchment. Furthermore, the data that can be used to characterise the weathering structures were not collected for that purpose and there is some incertitude on their precise signification: the weathering grade scale that was used did not follow international standards and it is not clear how the core recovery percentage was computed (Anonymous 2013).

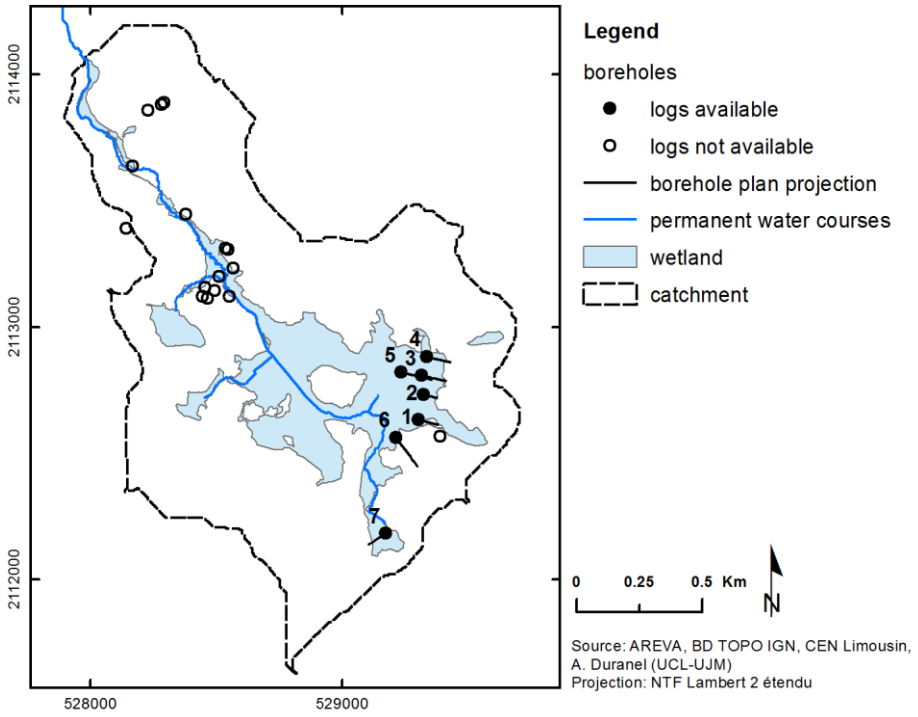

Figure 3-6. Location of boreholes drilled by CEA

3.3.2.4. Electrical Resistivity Tomography

ERT was used to investigate the depth of granite weathering formations in selected locations within the research site. A detailed description of this technique can be found in Loke (2000), of which a short summary is given here. ERT determines the apparent subsurface resistivity

distribution from measurements on the ground surface. The actual resistivity of the subsurface can then be estimated by inverse modelling. The actual resistivity of the subsurface depends on various characteristics of the material investigated, including porosity, degree of water saturation, ionic concentration of the groundwater, clay content, etc. The 2D resistivity images can therefore be used to characterise the nature of the subsurface formations. The measurements are generally made by injecting current into the ground through two electrodes and measuring the voltage difference at two other electrodes. The resistivity measurement depth increases with the distance between electrodes. To produce 2D images, a large number of electrodes are therefore laid at regular intervals along a transect, and measurements are taken from all possible electrode configurations (Figure 3-7). The resolution of the survey is therefore negatively related to the electrode interval, while its maximum depth is positively related to this interval.

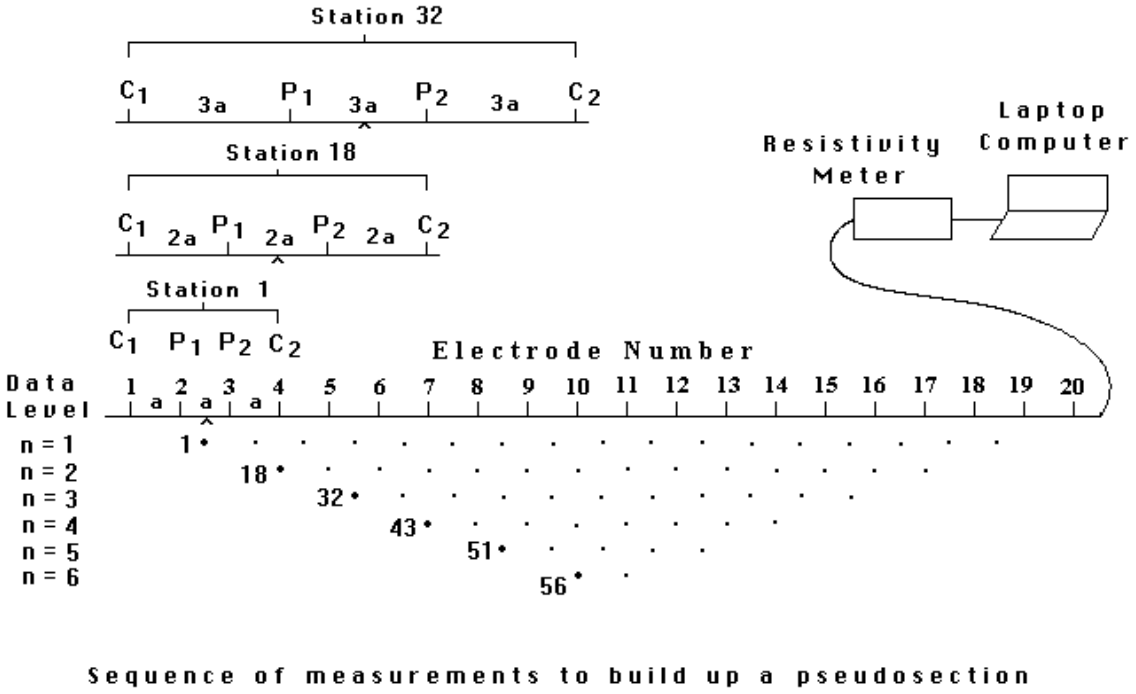

Figure 3-7. Arrangement of electrodes for a 2D electrical resistivity survey using a Wenner array (reproduced from Loke 2000).

Stations 1, 18 and 32 show the disposition of current (C1 and C2) and potential (P1 and P2) electrodes to measure the apparent resisitivity at points 1, 18 and 32 respectively.

Figure 3-7 shows electrodes arranged according to a Wenner array, but the disposition of the four electrodes relative to each other can actually vary, and the resulting arrays differ in their respective patterns of sensitivity and maximum depth of measurement. For instance, the Wenner array has a good vertical sensitivity but a low horizontal sensitivity, and is therefore appropriate when the aim is to map horizontal structures such as the groundwater table,

sediments or weathering horizons. The dipole-dipole array has opposite characteristics, and is therefore more appropriate to survey vertical geological structures such as dykes or faults. The Wenner-Schlumberger has intermediate properties with a reasonably good sensitivity both horizontally and vertically. It is also possible to combine data from two successive surveys with different arrays, resulting in a higher combined sensitivity in both horizontal and vertical directions. The cables can be rolled along to extend the length of the surveyed transect beyond the length of the cables. The data recorded by the field equipment are apparent resistivity values. These are conventionally plotted in a pseudo-section, where each value is plotted at a horizontal location mid-way between the electrodes used to measure it, and at a vertical location that is proportional to the distance between the electrodes. However this pseudo-section does not represent the distribution of the true subsurface resistivity. The latter is estimated by inverse modelling, whereby a computer program searches in an iterative manner for the distribution of true resistivity values that best explains the observed apparent resistivity. There are two optimisation methods, namely the L1 and L2 norm smoothness-constrained optimisation methods. The former (commonly known as the blocky inversion method) gives sharper boundaries and is better adapted when the subsurface geology has also sharp boundaries (ore bodies, igneous intrusions in sedimentary rocks, or groundwater table for instance), whereas the latter is better adapted when the geology varies gradually (for instance in the case of weathering formations). The pseudo-section can also be inverted with both methods, giving the range of possible models that can explain the observed data. Features that are common to both are more likely to be real (Loke 2000).

Four ERT transects were completed at the Dauges site (Figure 3-8), using an ABEM Terrameter LS with 64 electrodes. Electrodes were located 5m apart to give the maximum survey depth, about 50m, achievable with this equipment. This gave a minimum transect length of 315m. Cables and electrodes were rolled along to survey longer transects, up to 875m. Three transects were positioned across the wetland, perpendicular to the main watercourse, to investigate weathering profiles on the lower slopes and underneath the wetland. One transect was carried out at the top of one of the main hills surrounding the wetland. The aim of this transect was to assess saprolite depth in the upper part of the catchment. It was located slightly outside the research catchment because the method requires a linear stretch, at least 315m long, of open land without overhanging trees where the cable can be laid down and the position of each electrode surveyed using DGPS. There was no location meeting these conditions on the hilltops within the catchment. At least one other transect was initially planned along the COGEMA

boreholes across the eastern boundary of the mire, to validate the ERT interpretation using observed geological data. Unfortunately, equipment failure prevented this, and budget constraints did not allow for another field session to be organised. Due to time and equipment limitations and to expectations regarding the underlying geological structures, the ERT protocols that were used differed from one transect to the other (Table 3-2). A Wenner array was used for transect 4 as it is located on relatively flat ground on a hilltop and a horizontal weathering profile was expected. The Wenner array has a better horizontal sensitivity than other protocols (Loke 2000). A Schlumberger array was used for transects 1, 2 and 3 as it offers a good compromise between horizontal and vertical sensitivities and both horizontal and vertical structures were expected on these transects due to the varied topography and the presence of faults.

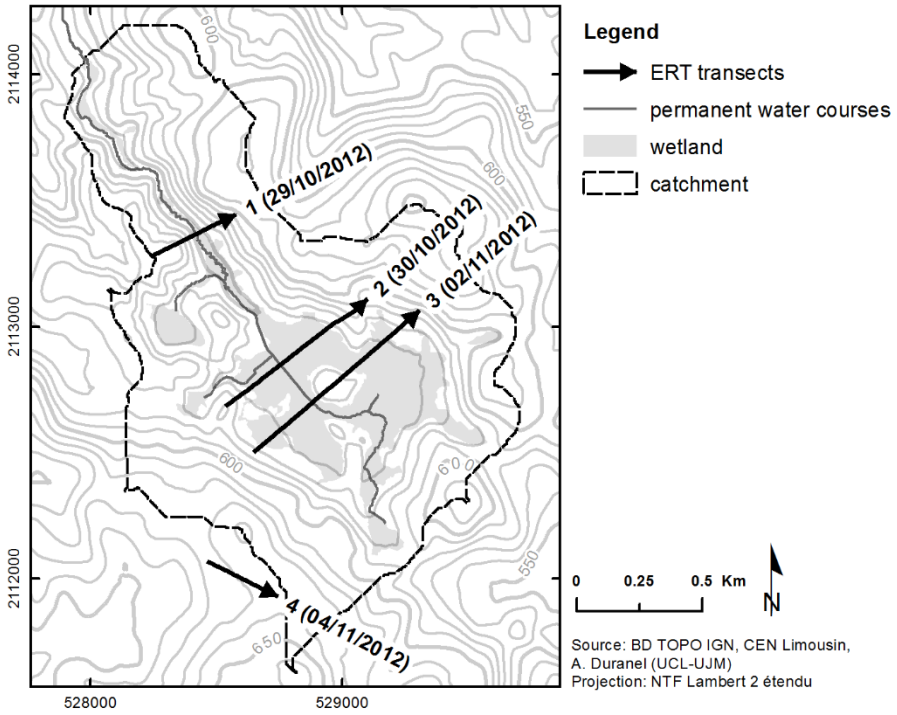

Figure 3-8. Location of ERT transects.

Table 3-2. Characteristics of ERT transects completed at the Dauges site.

ID	Date	Horizontal length (m)	Protocol
1	29/10/2012	380	Schlumberger
2	30/10/2012	707	Schlumberger
3	02/11/2012	868	Schlumberger and Wenner
4	04/11/2012	315	Wenner

As a few problematic negative resistivity measures were encountered along transects 1 and 2, a Wenner array was used on top of the Schlumberger array along transect 3. Both arrays were then combined during the inversion process. The position of each electrode was recorded using a Leica 1200 base station and CS15 rover (see Section 3.2.1). Inversion of the pseudo-sections was

conducted by Dr Stéphane Garambois at the ISTERRE laboratory in Grenoble using the RES2DINV software (Loke 2013) and both the blocky L1 and smooth L2 norms. The former gave the best interpretable results, and only the sections obtained using this method are presented in this chapter. To guide the interpretation of the modelled resistivity sections, Archie's law (Archie 1942) was used to estimate the expected resistivity of a saturated material with a non-conductive matrix as a function of porosity, as follows:

$$R_t = a\phi^{-m} S_w^{-n} R_w \qquad \text{Equation 3.1.}$$

where R_t is the saturated material resistivity, Φ is the porosity, S_w the saturation, R_w the solution resistivity, a the tortuosity factor, m the cementation factor and n the saturation exponent. Coefficients a and m were derived empirically by Archie for a range of rock types. For igneous rocks, Nabighian (1988) gives a=1.4 and m=1.58. Saturation was taken as equal to one, which corresponds to a fully saturated rock. The groundwater electrical resistivity was estimated by measuring water specific conductance (electrical conductivity at 25°C) in the stream at the wetland and catchment outlets in August and October 2011. Groundwater specific conductance records were also obtained from the French national groundwater quality monitoring database ADES (www.ades.eaufrance.fr). A total of 93 measures, taken from 1996 to 2011, were obtained for 14 spring catchments used for drinking water supply, located up to 5km from the site and with similar lithology.

3.3.2.5. Mapping the distribution of saprolite/sediments and fissured granite outcrops using indirect indicators

In the absence of sufficient visible outcrops, the distribution of saprolite and its depth can be measured or estimated using a range of methods such as geological drilling, proton magnetic resonance (Wyns *et al.* 2004), ground penetrating radar (Descloîtres *et al.* 1997; Mahmoudzadeh *et al.* 2012) or electrical resistivity sounding or tomography. However all these methods are time-consuming and expensive, requires highly specialised equipment and skills, and therefore cannot be carried out with a high resolution over large areas. However, the physical characteristics of the different layers of the weathering profile have geomorphological consequences that can be used as indirect indicators to help mapping their distribution at the local scale (Courtois *et al.* 2003). In particular, the fissured layer and the fresh basement are more resistant to erosion and tend to be associated with steeper slopes. Conversely, saprolites, but also colluvia and alluvia, are not mechanically resistant and are easily eroded, leading to gentle slopes. The interface

between saprolite, colluvia and alluvia on one hand and fissured or unweathered granite outcrops on the other hand generally coincides with a break of slope.

Another indirect indicator is landuse, which is strongly influenced by the nature of the outcropping formation. In an actively farmed granitic landscape, the distribution of arable land for instance is driven partly by the presence or absence of soils that are sufficiently deep and boulder-free to be ploughed, and therefore by the presence of saprolite, colluvia or alluvia. Other important factors that modulate this relationship are landownership structure, distance to farm buildings, water table depth, and slope, the effect of the latter variable being difficult if not impossible to distinguish from that of the presence of saprolite, colluvia or alluvia. In the study area, only a minority of the present landscape is still farmed, let alone cultivated. Therefore, the distribution of arable land in the early 19th century, at a time when the extent of arable farming was at its peak in the area, was preferred to modern landuse maps. Landuse in the early 19th century was obtained from the Napoleonic cadastre. The cadastre maps, drawn at the 1/2500 scale, show with outstanding accuracy the boundaries of each land plot, and the associated registry gives the usage made of each plot at the time of the completion of the cadastre, in 1836 in the area. The cadastre maps covering the catchment were obtained from the Haute-Vienne departmental archives, scanned, geo-referenced by matching them with the current cadastre, rectified, and digitised automatically using the ArcScan extension for ArcGIS.

Yet another indirect indicator of outcropping formations is the presence of large granite outcrops, which indicates that erosion has been important enough to remove most or all of the overlying soft material. Larger rock outcrops were mapped in most of the area by COGEMA, as part of topographic mapping of the area at the 1/1000 scale. Outcrops were probably not identified explicitly, but mapped as part of the general topography characterisation. Rock outcrop contours were manually digitised after the map had been geo-referenced. In an attempt to estimate the slope threshold that could be used to distinguish outcropping fissured and unweathered granite on one hand and saprolite, colluvia and alluvia on the other hand, the frequency distribution of slope values at rock outcrops was compared to that in the entire area mapped by COGEMA. Similarly, slope frequency distribution in land that was arable in the 19th century was compared to that in the entire area for which landuse data was available. Plots noted as *pâture* (grazed pasture) or *pré* (mown meadow) were excluded from the analysis since, in the landuse nomenclature used for the Napoleonic cadastre in the area, they correspond to wet land where arable farming is impeded by other factors than the presence or absence of saprolite or sediments. Slope was calculated from the 5m DEM using the Spatial Analyst ArcGIS extension.

3.3.3. Results and discussion

3.3.3.1. Sections showing weathering and periglacial formations

Section 1 (Figure 3-9) is located on a pass position between the Marzet basin and the main Dauges basin (Figure 3-5). The following formations have been recognised from top to bottom: soil (30cm deep on average), bedded grus (approximately 1.5m deep), and in-situ saprolite (at least 1.5m deep). The fissured granite – saprolite is not visible. There is no head, probably because the section is located on a ridge and was subject to erosion rather than deposition.

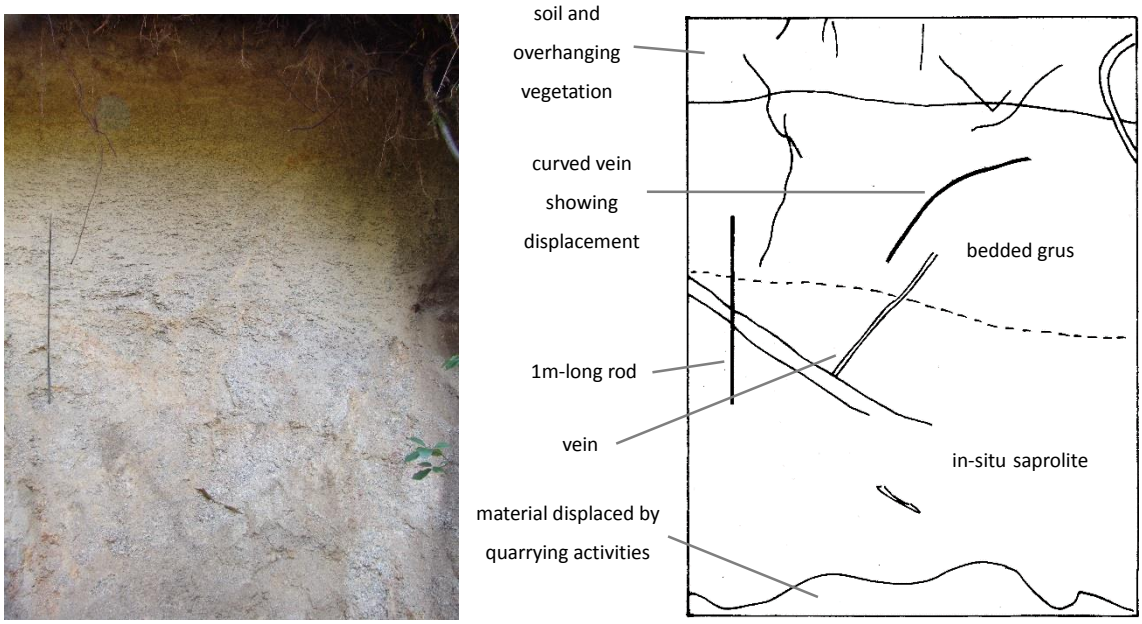

Figure 3-9. Section 1 - close-up view of the upslope side of the quarry.

Section 2 (Figure 3-10) is located just outside the Dauges catchment, in a small quarry dug at midslope within a small thalweg. The quarry face is parallel to the steepest slope direction. On the left (upslope) side of the quarry face, the saprolite layer is very shallow or inexistent, and fissured / fractured granite can be seen just beneath the soil layer. On the left (downslope) side of the quarry, the saprolite thickness reaches 2-3m. Two profiles have been described in more detail, in the centre of the quarry face and on the downslope side. The first profile (Figure 3-11) show the presence of, from top to bottom, the soil layer (30cm deep), head deposits (about 50cm deep), bedded grus (about 1m deep), in-situ saprolite (1-1.5m deep), and granite that is obviously weathered but still resistant to attempts to break it. Head deposits are not present on the second profile (Figure 3-12). The soil, 30 cm deep, directly overlays the 1m-deep bedded saprolite and the in-situ saprolite (at least 1m deep). The fissured granite is not visible but the compactness of the in-situ saprolite suggests that it does not lie far below.

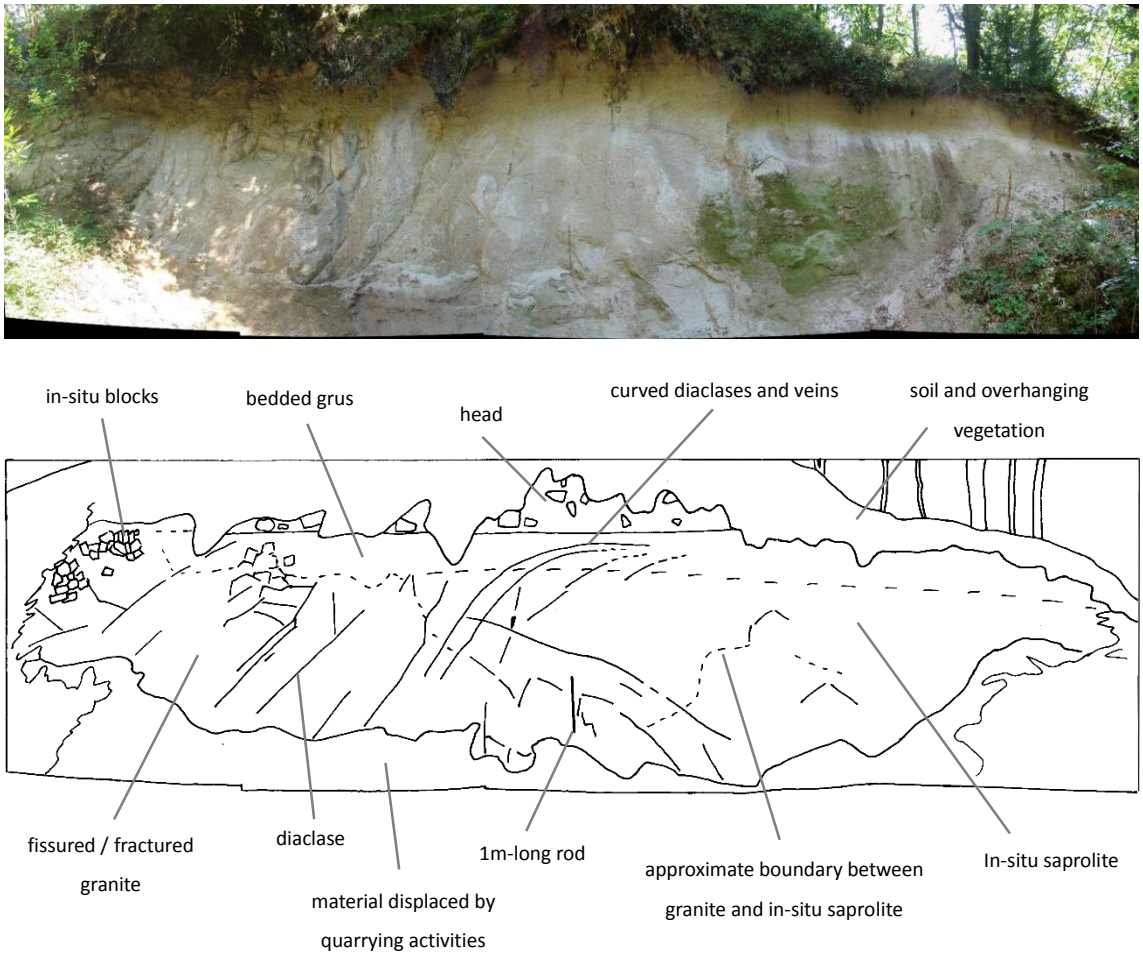

Figure 3-10. Section 2 - Panoramic view of the complete quarry face.

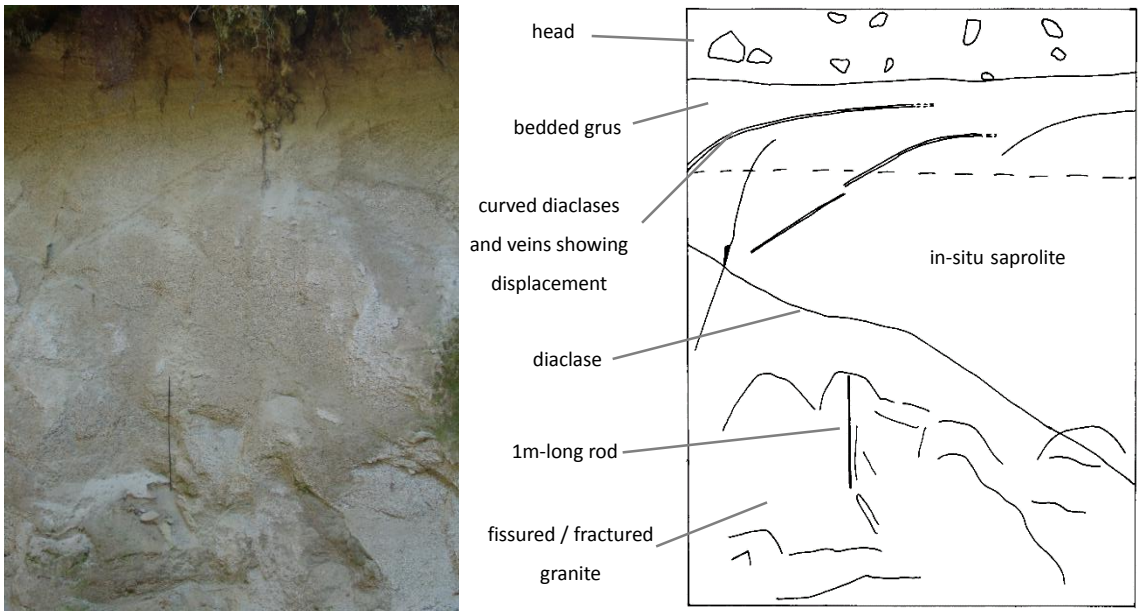

Figure 3-11. Section 2 - close-up view of the middle of the quarry face.

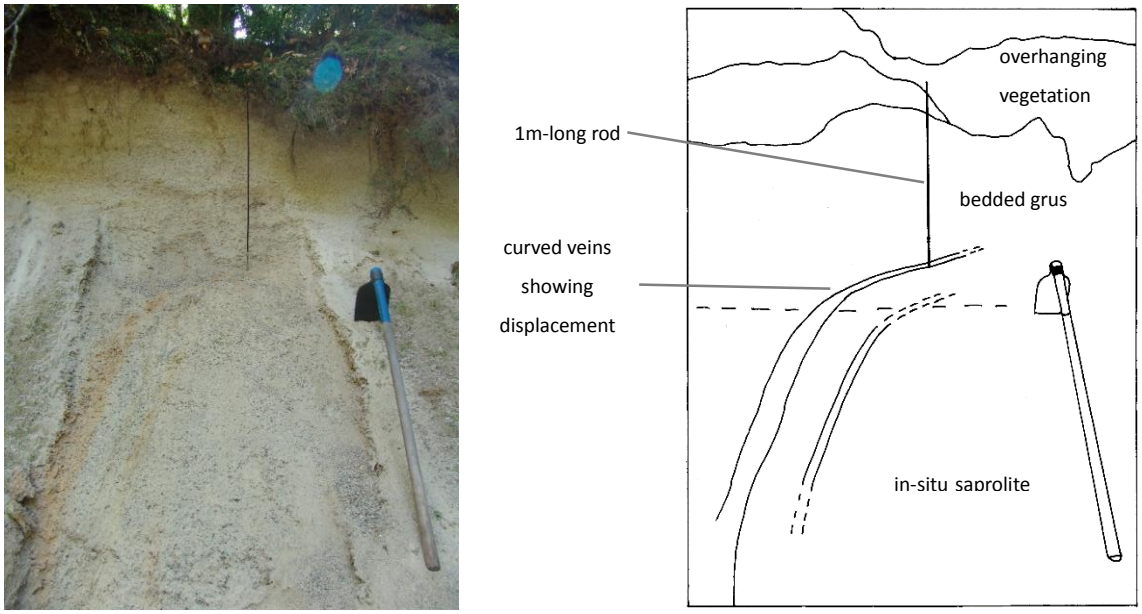

Figure 3-12. Section 2 - close-up view of the downslope side of the quarry.

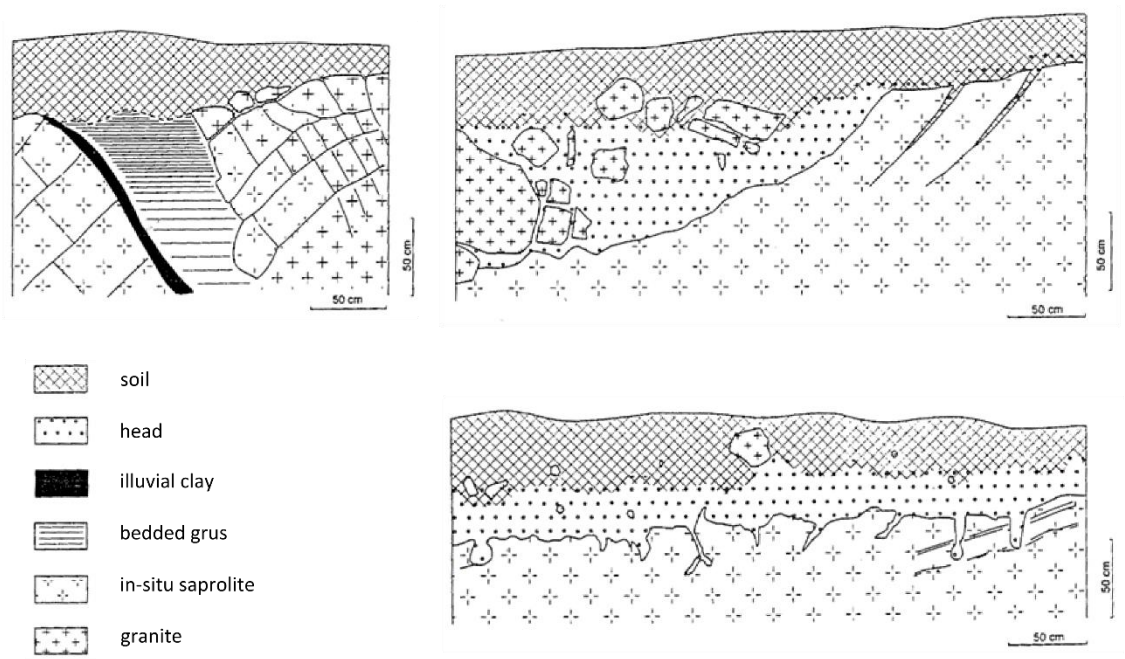

Figure 3-13. Sections described by Valadas (1998).

Figure 3-13 shows sections 3 and 4, that were described by Valadas (1998). Section 3 (corresponding to the drawing on the top left of Figure 3-13) is located on a steep slope through which the path from Sauvagnac to Les Sauvages is cut. The fissured granite is visible just below the soil layer, and the in-situ and bedded saprolite is only found locally in small pockets in the middle part of the profile. Head deposits are not visible. Section 4 (corresponding to both drawings on the right of Figure 3-13) is located a few tens of metres further away, on a more

gently sloping terrain. It is approximately 15m long but quite shallow (about 1.5m deep), and the fissured granite can be seen nowhere. The soil layer is 30-50cm deep, and overlays relatively shallow and discontinuous head deposits, and the in-situ saprolite. Bedded grus is not visible and has probably been eroded away before the formation of head deposits. In all profiles, in-situ and bedded saprolites are quite coarse. No fragic horizon was found. Overall, the analysis of available sections on the hillslopes suggests that the saprolite (in-situ saprolite and bedded grus) is quite variable in depth, from about 3m deep to inexistent. It should be noted that the deepest saprolite layers have been observed in quarries that were opened for their extraction, and probably are in the upper range of depths found in the catchment. Head deposits are very limited in depth and extent.

3.3.3.2. Drillings

The logs of seven geological borehole drillings carried out by CEA were obtained from AREVA and digitised (Figure 3-14). The following interpretation of the logs in terms of weathering formations can be proposed:

- grus, core recovery percentage mostly null, 0-37m thick: this is clearly saprolite, with possibly some colluvium at the top.
- highly weathered, core recovery percentage very low or highly variable, 19-30m thick, reaching a depth of 19-56m: the low core recovery percentage at the top of boreholes 1 and 7 may suggest that this layer corresponds to the laminated layer. However it can also be found below substantial depth of material weathered to a lesser degree (borehole 1) or be associated with a higher core recovery percentage (borehole 5). This suggests that it may correspond to both the laminated and fissured zone.
- weathered, core recovery percentage high but variable, 6-30m thick, reaching a depth of 15-65m: this is clearly the fissured layer
- slightly weathered, high core recovery, 0-90m thick, reaching a depth of 60-140m: it is unclear if this is part of the lower fissured layer or of the bedrock. The second hypothesis would reduce the variability of the depth of the fissured layer – bedrock transition, and would also agree with the results of other drillings along fractures elsewhere in the Ambazac massif (Cottez & Favin 1980).
- mostly unweathered to unweathered, core recovery percentage mostly 100%, rare fractures, 40-140m deep and below: unweathered bedrock.

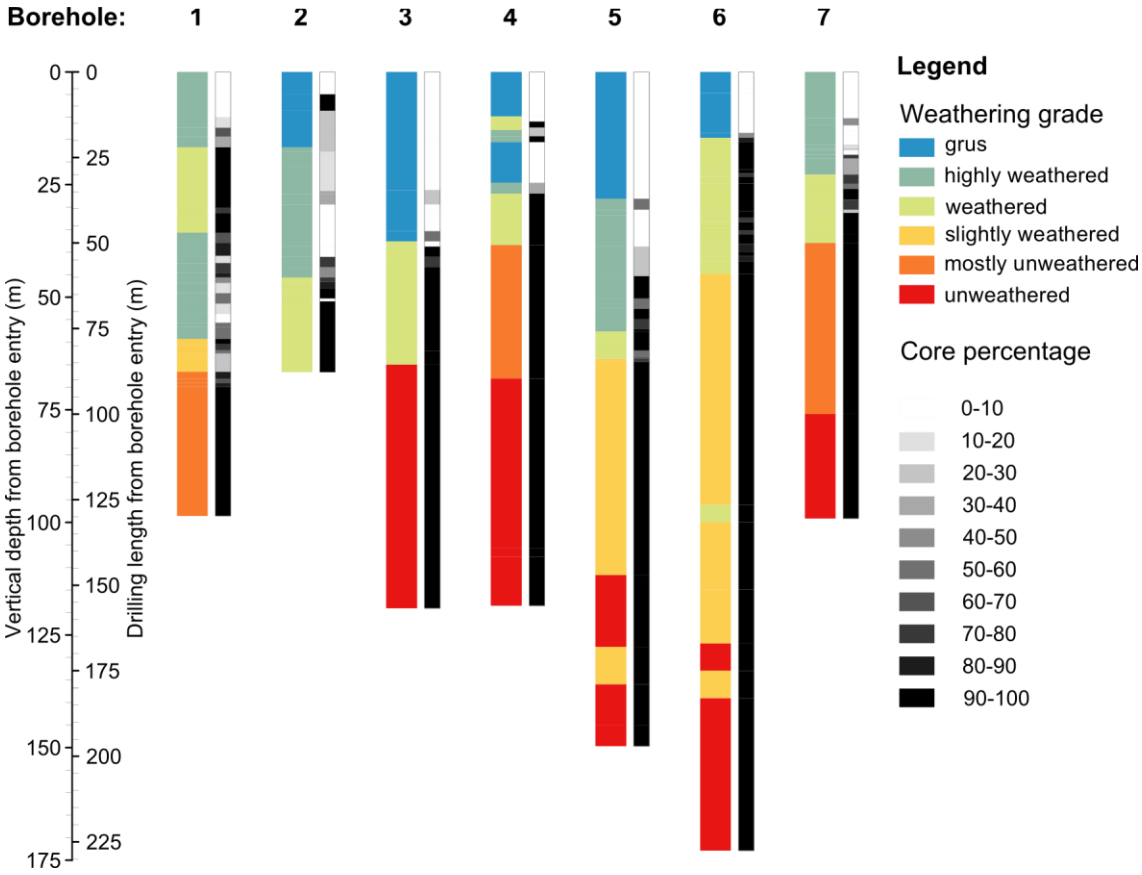

Figure 3-14. Weathering grades and core recovery percentage in the CEA boreholes

The boreholes were drilled with a 49.5° angle relative to the horizontal.

The borehole logs show a large variability in the presence and depth of the different weathering zones, which confirms that the stratiform weathering model might not be applicable at the very local scale due to the deepening of the weathering front along anomalies in the bedrock such as tectonic faults. It should be noted, however, that these boreholes were drilled for the purpose of uranium prospection and purposely cut through mineralised faults located using geophysical and radiometric surveys. Depending on the location of the fault and associated fractures and mineral deposits, such a variability is to be expected. The logs can therefore not be taken as representative of the catchment as a whole, and indeed, they may be at odds with the results of the ERT survey.

3.3.3.3. Electrical resistivity tomography

In order to aid the interpretation of the ERT results, resistivity values encountered in the different weathering zones on granite were compiled from the literature (Figure 3-15). There is a clear gradient of increasing electrical resistivity from the surface to the bedrock, and authors each suggest that it is possible to distinguish between the saprolite, fissured zone and bedrock using

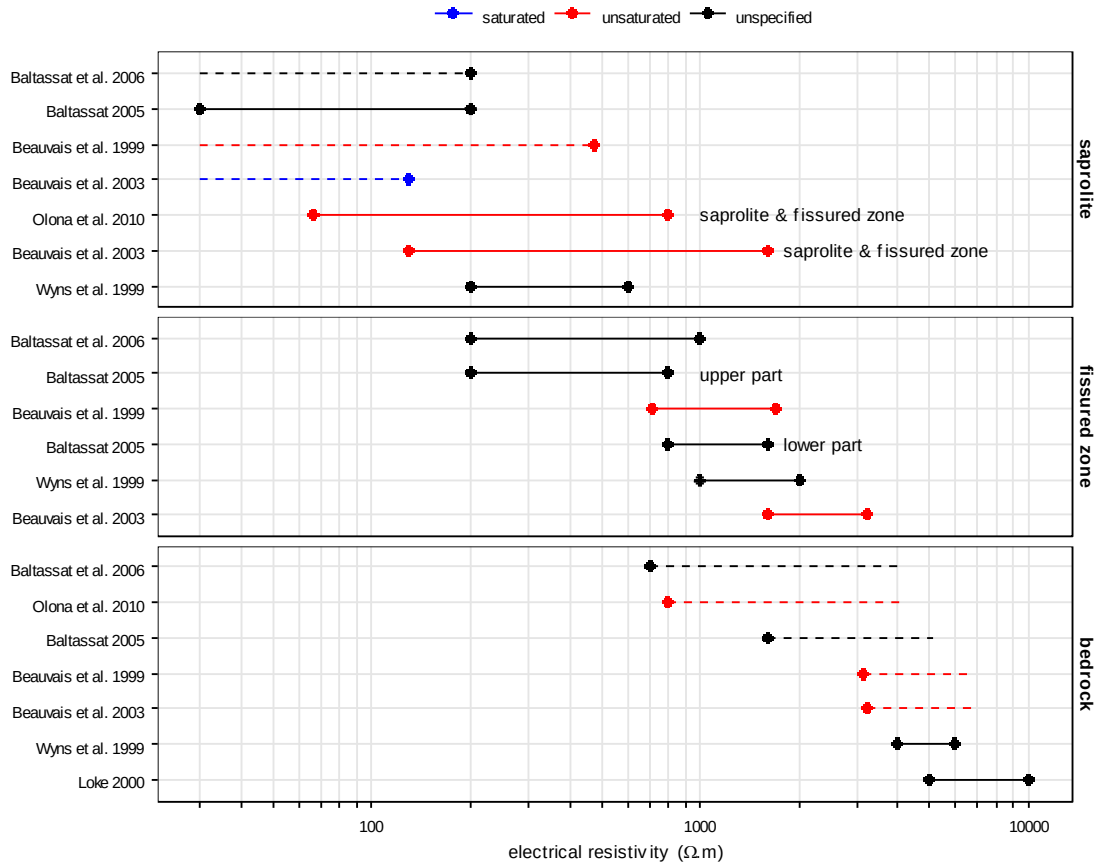

Figure 3-15. Electrical resistivities of the main granite weathering formation according to the literature.

Note the logarithmic scale of the x axis. Dots give the minimum and maximum observed values, and the solid line shows the range of these values. For the saprolite and bedrock, authors often only give the maximum and minimum observed values respectively. These are shown by a single dot together with a dashed line indicating whether the value is the maximum or minimum of the observed range. The methods used are as follows: Baltassat (2005): ERT interpretation in a geologically well-known small catchment in the Vosges massif, France; Baltassat *et al.* (2006): ERT interpretation validated by borehole geological and resistivity logging in India; Beauvais *et al.* (1999): ERT validated with geological logging and cross-borehole resistivity survey, Senegal; Beauvais *et al.* (2003): ERT interpretation, Senegal; Loke (2000): general values; Olona *et al.* (2010): ERT validated with geological logs, Spain; Wyns *et al.* (1999): VES sounding validated by geological logging in Britany, France.

electrical resistivity survey. Overall, values of about 200-400 Ω.m and 2000-3000 Ω.m seem to best discriminate between the three main zones. However the actual thresholds proposed by the literature vary considerably from one study to the other, which suggests that they should be used as a guide only and validated for each study site. This may be due to differences in saturation, as it is not always clear whether the zone for which resistivities are given is fully, partially or not at all below the groundwater table, and water content is given in none but one study. Clay content of the saprolite and fissured zone, which depends on the lithology, as well as the electrical conductivity of the groundwater may also vary from one site to the other and explain the observed differences. These values were used as a help to interpret the ERT transects at the Dauges site.

Profile 1 – 29/10/2012

Profile 1 runs across the steep valley downstream of the wetland outlet, starting on the relatively flat area on top of the hill. A Schlumberger protocol was chosen as both horizontal and vertical structures were expected due to the topography and the presence of a fault at the bottom of the valley. Figure 3-16 and Figure 3-17 show the measured and apparent pseudosections and the modelled section without and with topography. Below the steep slopes, on each side of the valley, the survey shows quite clearly the presence of a deep, resistive (3000-140000 Ω.m) layer. The presence of steep slopes and numerous rock outcrops and large boulders at the surface suggests that this is either fresh or fissured granite. However, the first hypothesis is not compatible with the presence of a more conductive (900-3000 Ω.m) material underneath. The only possible explanation is that the entire profile depth is fissured granite, and that the interface between the resistive and the conductive layer is the water table, which agrees with the fact that its depth decreases relatively regularly as one moves closer to the valley bottom. The presence of air in fissures above the water table dramatically increases the resistivity of the granite. Slightly higher resistivity values (up to 4200 Ω.m) below the inferred water table on the northern side might be explained by heterogeneities in the fissure density, or by errors in modelled resistivity due to sparser data at the margins of the profile. On the flat area on top of the southern hill, a one-block (0-2.8m) deep shallow layer of lower resistivity values (370-600 Ω.m) is visible, that coincides with the presence of a pasture, well above the water table. This is likely to be saprolite. Resistivity values are slightly higher than those given for saprolite in the literature, but given the low vertical resolution of the survey and the small thickness of the layer, the measured resistivities most probably include part of the underlying unsaturated fissured layer. The lower values observed here compared to values interpreted as unsaturated saprolite in transect 2 might be explained by either the presence of a lamprophyre vein in the vicinity and a more clay-rich substrate, or a different proportion of saprolite vs. fissured granite within measured blocks. A conductive (300-700 Ω.m) pocket can be seen underneath the thalweg, located below more resistive material at the surface of the thalweg and extending well below the superficial resistive formation of the valley slopes. Again, the only credible explanation is that this is saturated fissured granite.

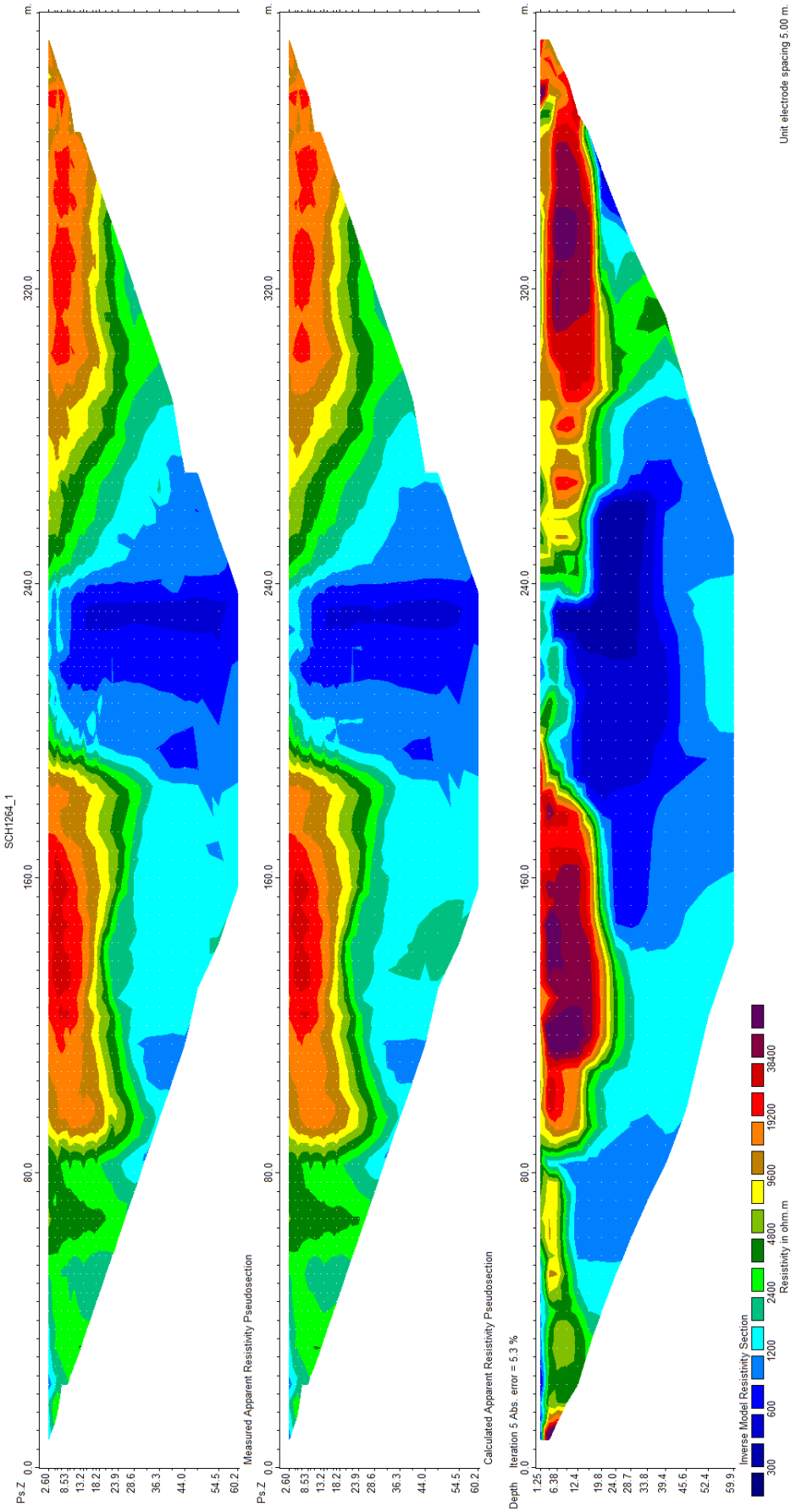

Figure 3-16. ERT profile 1 (29/10/2012): from top to bottom, measured and calculated apparent resistivity pseudosections, L1-norm inverse model resistivity section.

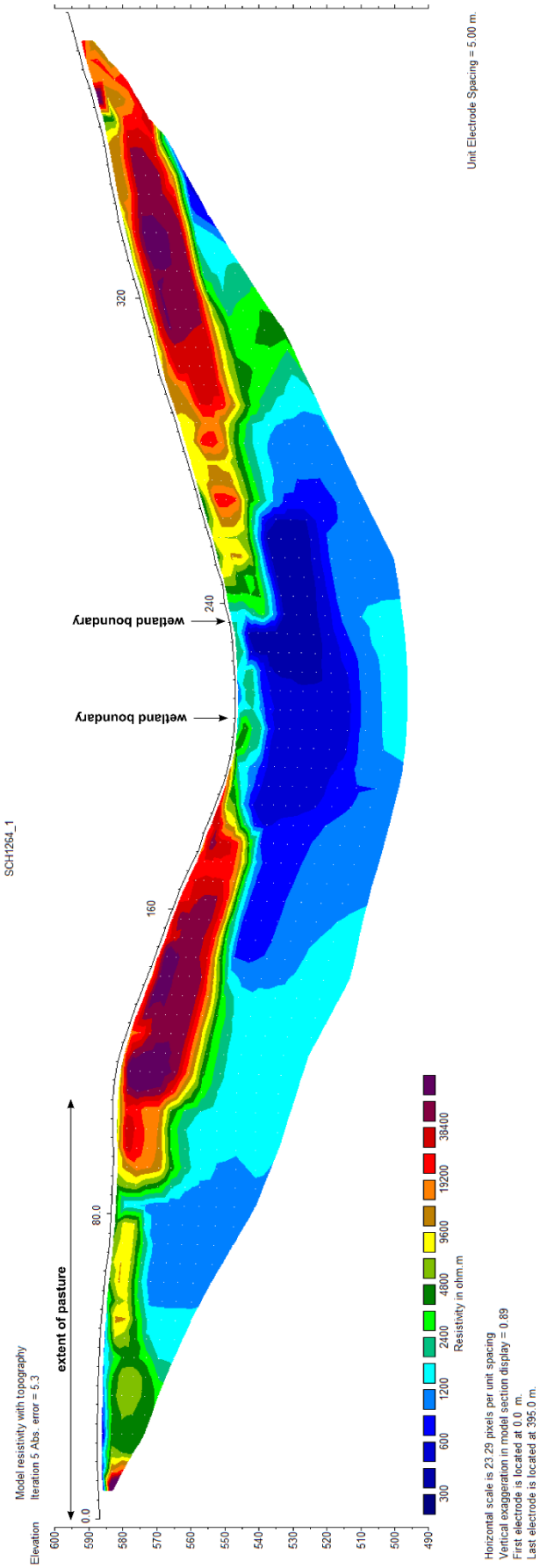

Figure 3-17. ERT profile 1 (29/10/2012): L1-norm inverse model resistivity section with topography.

The vicinity of a fault may have led to accelerated weathering, a larger density of fissures, a larger porosity and possibly a larger amount of clay leading to better courant conduction. The damage zone of the fault seems to be quite large and extends to the surface, however when this densely fissured granite is unsaturated, its resistivity is similar to less densely fissured, unsaturated granite. It is also possible that the decreasing resistivity of the saturated zone from the sides of the transect towards the thalweg reflects an increase in groundwater residence time and electrical conductivity, and therefore the flow of groundwater from the upper part of the catchment to the thalweg. These hypotheses are not exclusive of each other and probably all contribute to the observed pattern. There is no evidence of the presence of substantial amounts of saprolite, colluvium or alluvium at the bottom of the thalweg. A small conductive (520-960 Ω.m) zone can also be seen at the bottom of the northern end of the profile. As a lamprophyre vein mapped by the COGEMA coincides with it, it might be interpreted as either a more densely fissured zone, clay-rich weathered lamprophyre, or both. It is also very possible that this is an artefact caused by the sparser data at the margins of the profile. Finally, it is noticeable that nowhere along the bottom of the profile resistivities that could indicate unweathered granite are to be found. Furthermore, there is no clear increase of the resistivity with depth within the fissured zone, suggesting that fracture density does not substantially decrease with depth within the profile, and therefore that the fissured zone extends beyond the maximum depth (50-60m) reached by the survey.

Profile 2 – 30/10/2012

Profile 2 also runs across the wetland perpendicular to its main axis. It is located downstream of Puy Rond and extends to the lower hillslopes on each side. As for profile 1, a thick, resistive layer (4600-142500 Ω.m) is present on the hillslopes, that overlays more conductive formations. Again, this can be interpreted as unsaturated fissured granite overlaying saturated fissured granite. The resistivity of the formations underneath the water table below the hillslopes is generally in the range of 400-3000 Ω.m, which is similar to values cited in the literature and measured in the same settings on profile 1. A few lower values, as little as 140 Ω.m at the far left end of the profile, were measured, highlighting differences in fracture density and the fact that densely fractured granite can be as electrically conductive as saturated saprolite. This has important implications for the interpretation of the more conductive material that can be found below the valley bottom on this transect and transect 3.

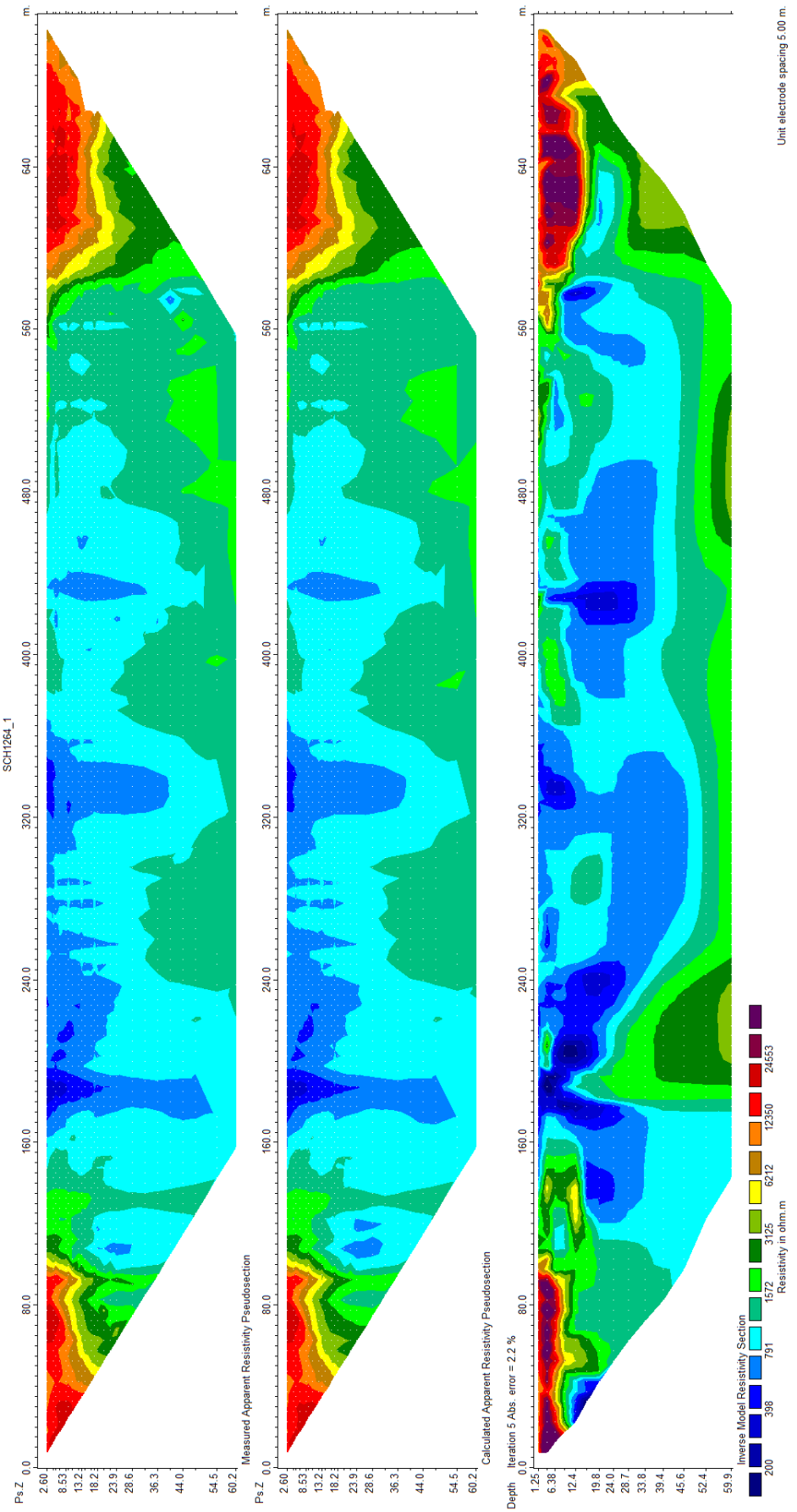

Figure 3-18. ERT profile 2 (30/10/2012): from top to bottom, measured and calculated apparent resistivity pseudosections, L1-norm inverse model resistivity section.

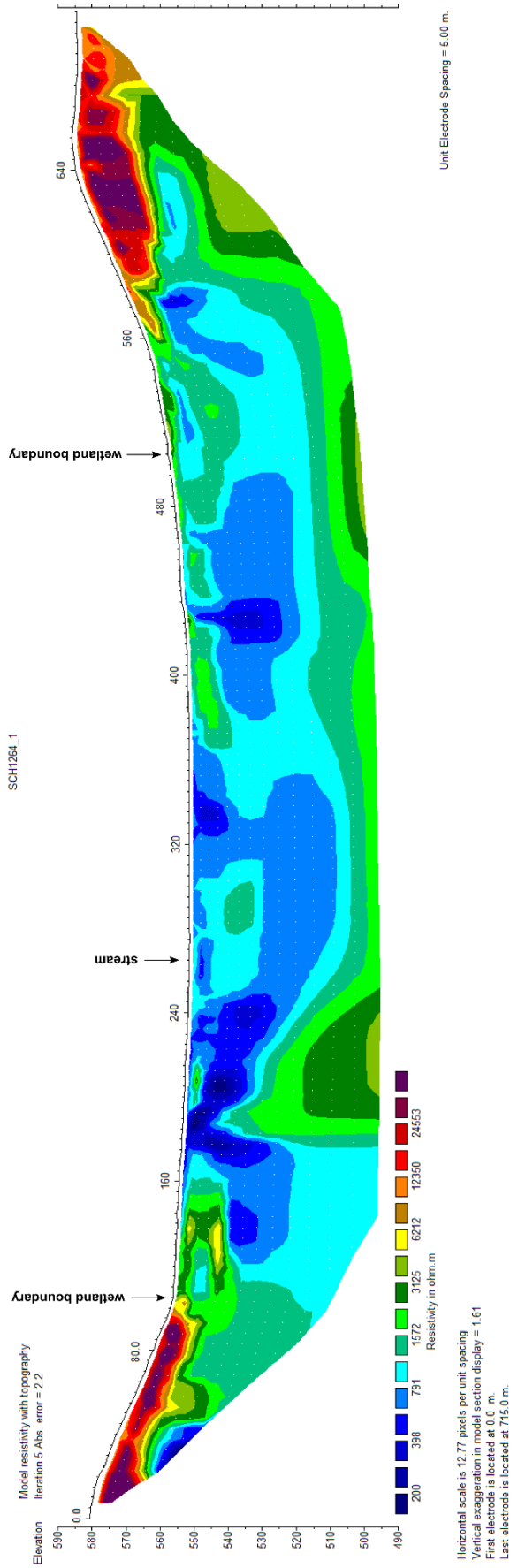

Figure 3-19. ERT profile 2 (30/10/2012): L1-norm inverse model resistivity section with topography

The bulk of this material shows resistivities between 600 and 3000 Ω.m, similar to material interpreted as saturated fissured granite below the hillslopes of transects 1 and 2, and the same interpretation can be made here. Pockets of more conductive material, with resistivities as small as 110 Ω.m, may be found across the profile, however in most cases they are located at depth, below more resistive material. It is therefore unlikely that this material is saprolite, and the lower resistivities are better explained by a higher fracture density within the fissured layer. The superficial conductive pocket located between electrodes 175 and 195 might be an exception, even though, as no fault has been mapped at this location, there would be no straightforward explanation for it. Conversely, superficial pockets of more resistive material between electrodes 100 and 150, with resistivities between 3000 and 6000 Ω.m, can be interpreted as blocks of more massive granite less impacted by weathering. Overall, below the valley bottom, the resistivity increases relatively regularly with depth, as a consequence of the rarefaction of fractures with depth within the fissured zone. Values higher than 3000 Ω.m, which, according to the literature, may be associated to unweathered granite, were measured in some places at the very bottom of the profile, at depths of around 55m below ground level. It is also worth noting that the faults mapped by COGEMA and crossing the transects, including the major Dauges fault, are not visible on the resistivity profile. The only place where the results could suggest a more or less vertical linear conductive structure is below electrodes 175 to 185, and no fault was mapped there. Peat and mineral detritic deposits are also less visible than on profile 3, except maybe on the southern side where a very shallow slightly more conductive layer may be seen.

Profile 3 – 02/11/2012

This profile runs transversally from one side of the mire to the other across Puy Rond, and extends to the lower hillslopes on each side (Figure 3-20, Figure 3-21). Both Wenner and Schlumberger protocols were used and subsequently combined to produce the inverse model section. As in profiles 1 and 2, the two ends of the profile below the hillslopes are characterised by a highly resistive layer overlaying a more conductive material. Again, this can be interpreted as fissured granite from top to bottom, the boundary between resistive and conductive material (at around 3000 Ω.m) corresponding to the water table. Here this boundary is more sinuous and less well characterised than in the other profiles. This may be due to model errors, more likely at the margins of the profile due to scarcer data, as the profile does not extend as far up the hillslopes. Similarly, Puy Rond stands out in the middle of the profile as an electrically resistant mass with resistivities of 3700-62500 Ω.m, lying on a more conductive substrate.

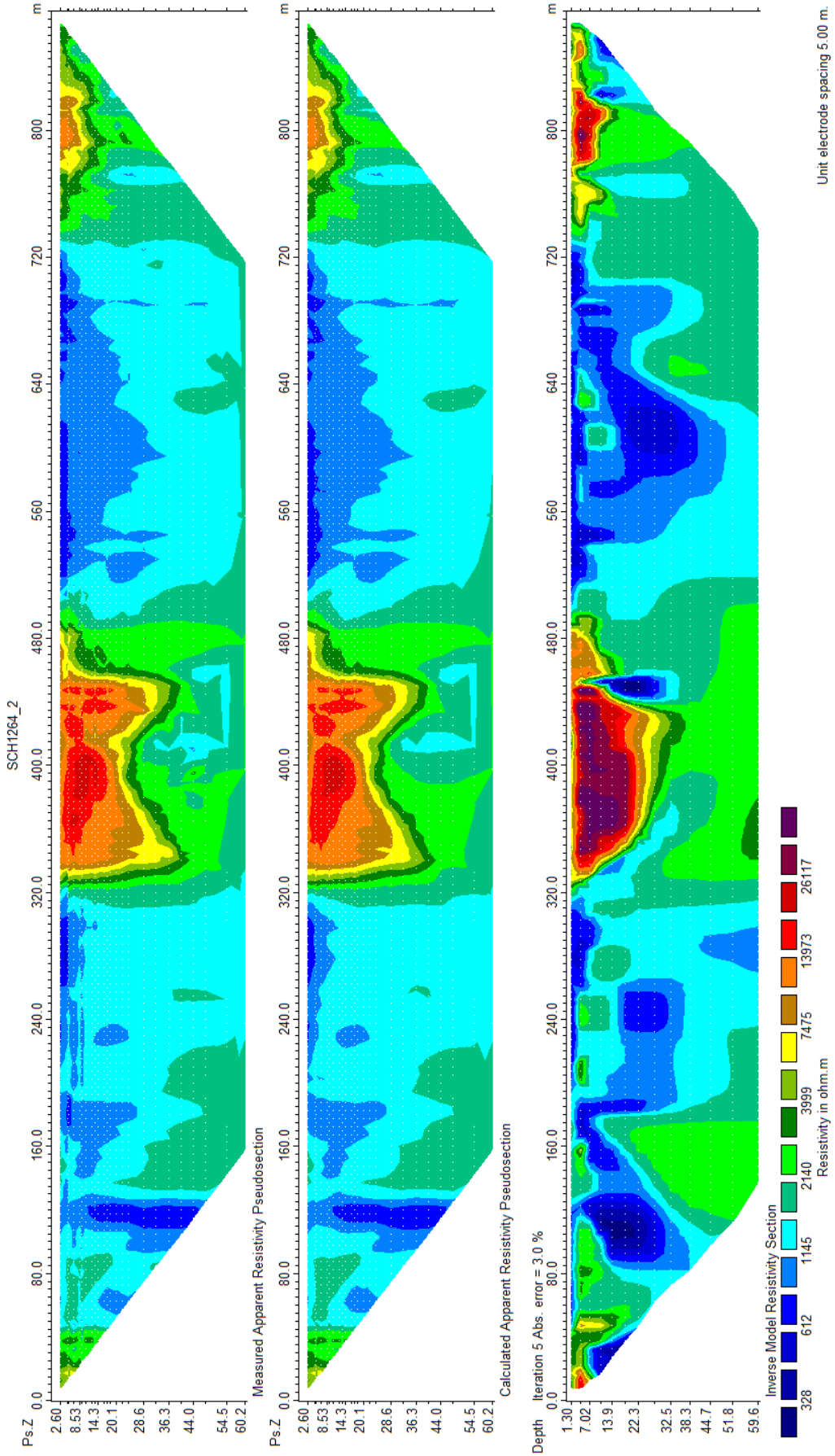

Figure 3-20. ERT profile 3 (03/11/2012): from top to bottom, measured and calculated apparent resistivity pseudosections, L1-norm inverse model resistivity section.

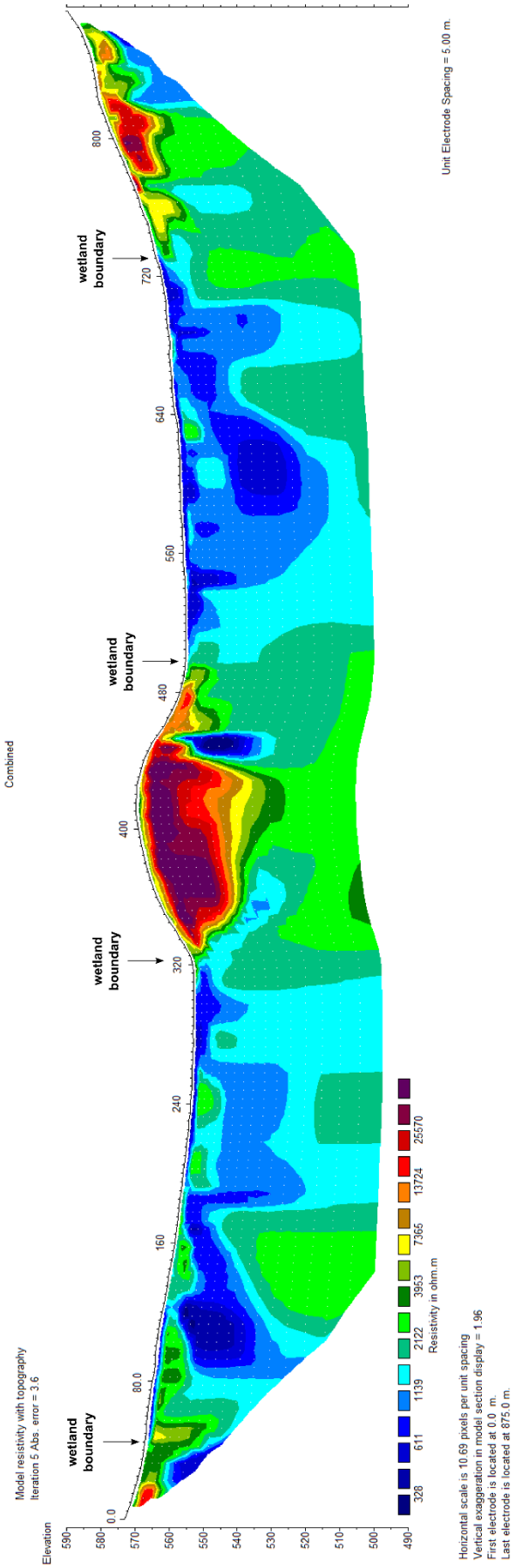

Figure 3-21. ERT profile 3 (03/11/2012): L1-norm inverse model resistivity section with topography (combined protocols).

As for all other profiles, this can be interpreted as unsaturated fissured granite overlaying saturated fissured granite, with resistivities measured below the water table in the range of 1000-2400 Ω.m, similar to values interpreted as saturated fissured granite in profile 1 and 2. In this case however, the upper resistive layer seems to extend below the local water table, suggesting a much lower degree of weathering. This explains why Puy Rond has resisted erosion and stands out as a proper inselberg in the middle of the basin. Lower resistivity values below Puy Rond suggest that the degree of weathering increases again at depth. As in profile 2, most of the subsurface below the wetland shows resistivities between 600 and 3000 Ω.m, comparable to material interpreted as saturated fissured granite on this profile below the hillslopes and on profiles 1 and 2. As on profile 2, material with resistivities lower than 600 Ω.m that could, on this basis only, be interpreted as saturated saprolite according to values found in the literature, are mostly found at depth below more resistive material, which rules out this possibility. In fact, the lowest resistivity of the entire profile (190 Ω.m) was measured below Puy Rond, underneath highly resistive material interpreted as poorly weathered to unweathered granite. The origin of this quite large but well defined highly conductive anomaly 15-30m below the northern slope of Puy Rond is unclear. A now flooded mine gallery was dug below Puy Rond by COGEMA, but more than 200m below ground and slightly more southward. The detailed structural map provided by AREVA does not show any fault or vein coinciding with the anomaly, however some COGEMA working documents (ref *Sauvagnac 195S – Plan d'ensemble*) show that a linear geophysical anomaly had been mapped that passed above it, which may suggest the presence of a fault associated to higher degree of weathering and fracture density.

Overall, there is no evidence for the presence of substantial depths of saprolite. There are small isolated superficial pockets of conductive material with resistivities lower than 600 Ω.m on the northern side of Puy Rond, but these are no more than 4m deep and coincide with relatively thick colluvial or alluvial deposits as evidenced by manual augering and probing. Similarly, low resistivities in the uppermost (circa 1.5-2m deep) block layer (300-800 Ω.m), contrasting quite sharply with more resistive deeper structures immediately underneath particularly on the left side of the profile, correlate very well with the boundaries of the wetland as defined by the vegetation, and the presence of saturated peat and underlying detritic mineral deposits. A more resistive section (1000-3000 Ω.m) at positions 125-190m coincides with shallower, submetric peat depths overlying a hard-rock substrate evidenced by manual probing and coring.

Profile 4 – 04/11/2012

This profile is located just outside the catchment on a relatively flat area along the main ridge that marks the south-western boundary of the catchment (Figure 3-22, Figure 3-23). The profile runs across an artificial pasture and a relatively young plantation woodland. It was set up to assess the saprolite thickness on the gentle slopes of the hilltops surrounding the wetland. A Wenner array was chosen as a layered structure was expected due to the flat topography. The 2D picture does not clearly show such a structure, and, unexpectedly, resistivity decreases with depth. The highest resistivities (3000-74000 Ω.m) are measured in the upper part of the profile. All uppermost block centres have values of more than 1500 Ω.m and all but one of more than 3000 Ω.m. This is way above any value associated to saprolite in previous studies or interpreted as indicative of unsaturated saprolite in profile 1. This suggests that, even though the presence of an artificial pasture on part of the profile argues in favour of the presence of saprolite, its depth is small enough (less than about a metre on the whole length of the profile) to stay undetected using a five metre electrode interval.

Overall, the image obtained for profile 4 as a whole is similar to the one observed below the steep slopes of profile 1, with a highly resistive layer at the top and a more conductive layer at the bottom. Again, the most plausible explanation is that the profile cuts entirely within the fissured zone, and that the top of the more conductive layer corresponds to the water table. Here the threshold between the saturated and unsaturated fissured zones is around 6000-7000 Ω.m, which is substantially higher than the 3000-3500 Ω.m estimated from profile 1 and may be due to differences in weathering and porosity. The boundary interpreted as the water table is not as flat as it ought to be in this location. In particular, the highly resistive layer extends below the hypothesised water table on the right hand side of the profile. The presence of a more massive block of granite may possibly be invoked as an explanation. Similarly, a more resistant area can be noticed below the water table on the left hand side, which may be explained by differences in weathering and fissure density. Conversely, two small conductive zones seem to cut through the upper highly resistive layer up to the surface. Since there was 15mm of rain the night before the survey, one possible explanation is that this is caused by water infiltrating in the fissured granite along a preferential flowpath, due to either the presence of ditches nearby or weathering heterogeneities. The more conductive zone at the right end of the profile may be explained in the same way, but could also be an artefact caused by sparse data at the margin of the profile.

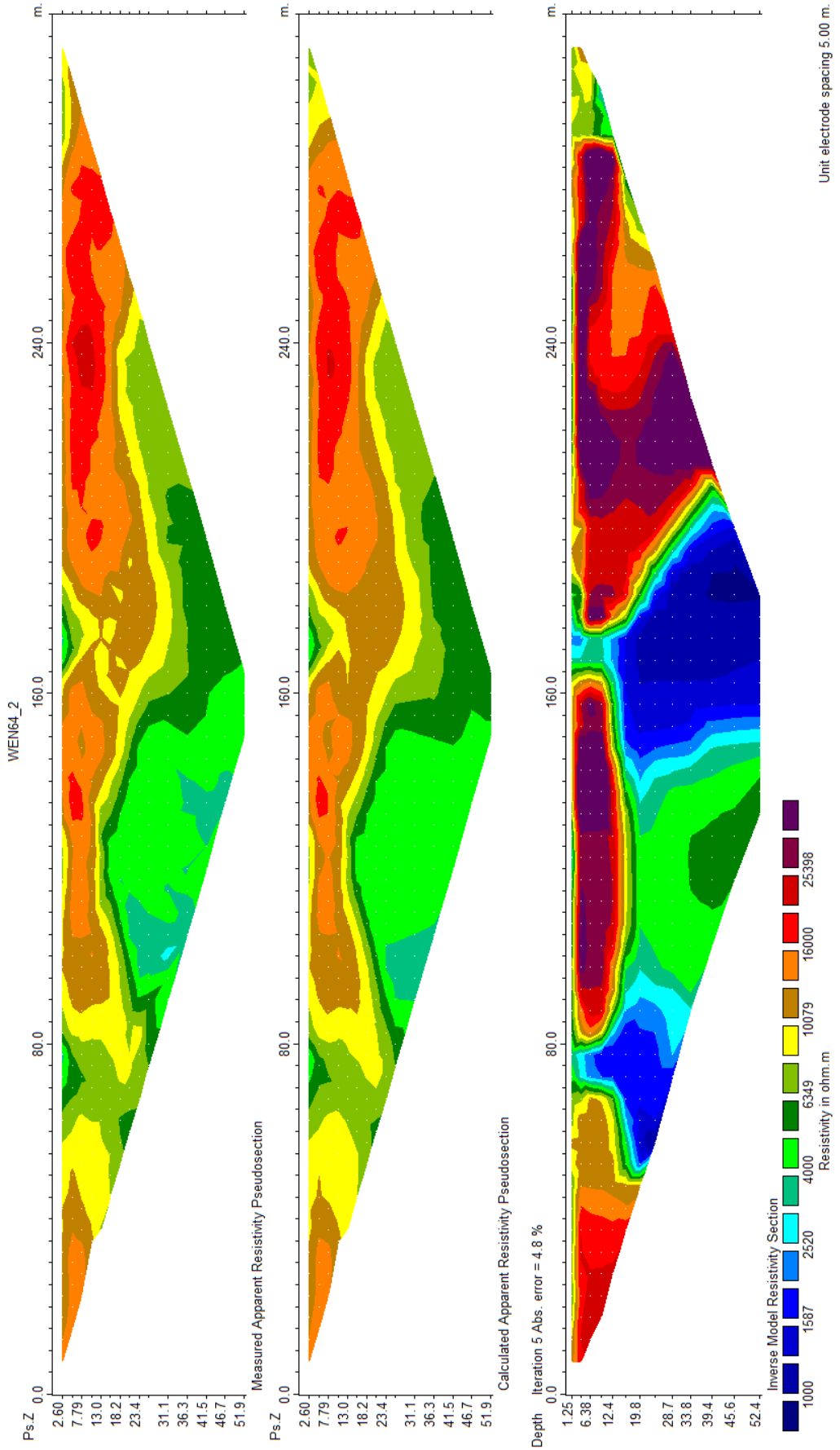

Figure 3-22. ERT profile 4 (04/11/2012): from top to bottom, measured and calculated apparent resistivity pseudosections, L1-norm inverse model resistivity section.

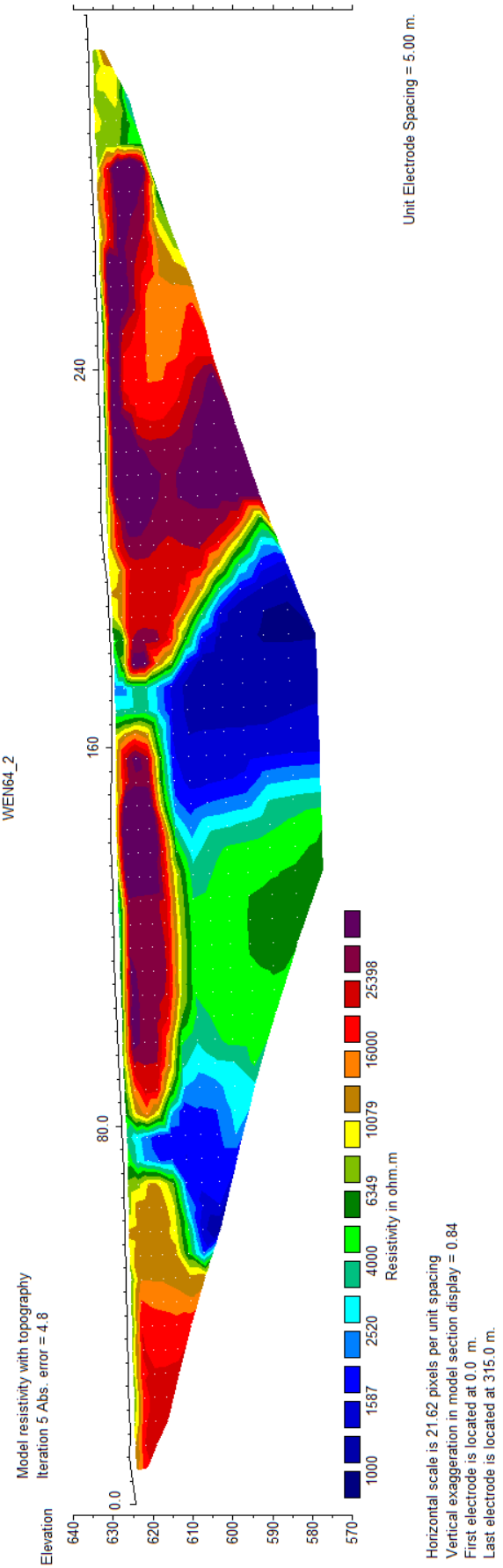

Figure 3-23. ERT profile 4 (04/11/2012): L1-norm inverse model resistivity section with topography.

Estimation of the fissured zone porosity using Archie's law

Water electrical conductivity measured in the stream at the wetland and catchment outlets, at low flow, is given in Table 3-3.

Table 3-3. Water electrical conductivity in the main stream at the Dauges site.

Location	Date	Electrical conductivity at 25°C (µS.cm-1)
Wetland outlet (Pont-de-Pierre)	16/08/2011	36
Wetland outlet (Pont-de-Pierre)	28/08/2011	35
Wetland outlet (Pont-de-Pierre)	28/10/2011	39.6
Catchment outlet (D78)	16/08/2011	33

Conductivity (25°C) data obtained from the ABES database for 14 spring catchments on similar lithology in the vicinity had a mean of 37.2 µS.cm^{-1} (sd: 6.5 µS.cm^{-1}, min: 25 µS.cm^{-1}, max: 66 µS.cm^{-1}, n=93), which is very similar to the values measured at the wetland and catchment outlets. Groundwater conductivity in the site was therefore assumed to be 37 µS.cm^{-1} at 25°C, which is equivalent to 27.8 µS.cm^{-1} at 12.5°C, the temperature measured in the deepest instrumented piezometer and assumed to be representative of groundwater temperature during the ERT measurements. This corresponds to a resistivity of 359.7 Ω.m. Figure 3-24 gives the expected resistivity as a function of porosity of a non-conductive rock fully saturated with a solution of the same conductivity, according to Archie (1942).

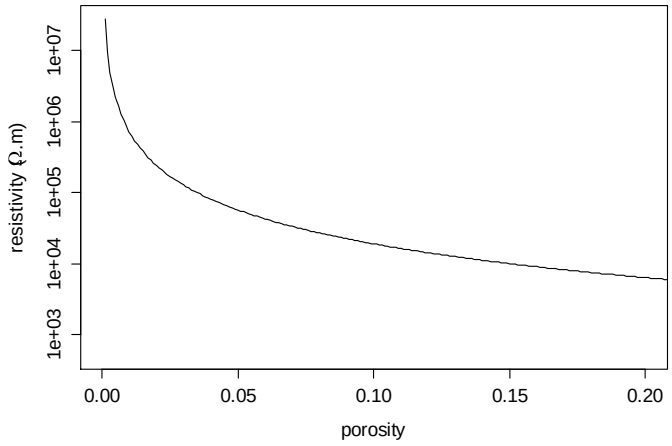

Figure 3-24. Resistivity as a function of porosity according to Archie's law, for a groundwater electrical conductivity of 27.8 µS.cm^{-1}, with a=1.4 and m=1.58.

Porosities deduced from the resistivities measured in the fissured zone using ERT and from the conductivity measured in stream and spring waters are an order of magnitude higher than storage coefficients usually cited in the literature (0.2-5%, Wyns *et al.* 1999, 2004). Resistivities of 600 Ω.m and 3000 Ω.m, which correspond to the range of resistivity values interpreted as corresponding to the fissured zone in this study and in others, would require improbable

porosities of 90% and 32% respectively. The conductivity of the groundwater was estimated from surface and spring waters, yet the former is often higher than the latter due to a higher residence time (Wyns pers. comm.), so it is possible that the estimate of the groundwater conductivity is wrong. However measurements in stream waters were very similar to those obtained from a large number of springs in the area. As these are used for water supply, it is reasonable to assume that they are permanent and therefore groundwater-fed. As most of the saprolite layer has been eroded away in the Monts d'Ambazac, one can assume that these springs tap into the fissured zone aquifer. Measurements in the nearest water supply borehole, located 3km away at La-Jonchère-St-Maurice and tapping 50m deep at the contact between leucogranites and gneisses gave conductivity values of 42-49µS/cm. Measurements in the granitic bedrock 200m below ground in the uranium mine of Fanay-Augères, 4km west of the study site, gave an average value of 77µS/cm. None of these measurements are high enough to give reasonable porosity estimates according to Archie's law. In Archie's law, the tortuosity and cementation factors are empirical factors that should be calibrated for each rock type. It is simply possible that the factors used cannot be applied to the fissured layer, due to physical and chemical differences with fresh granite caused by the weathering process. In particular, the presence in fissures of clay produced during the weathering process may increase the conductivity of the rock.

Conclusions

The following conclusions can be made from the ERT survey:

- On the flat area of the higher hilltops, the combined thickness of the soil and saprolite layer is very small (about a metre or less), sometimes too small to get detected. It is totally undetectable on the steeper hillslopes.
- The presence of conductive material underneath much more resistive material on the hilltops and slopes and below Puy Rond demonstrates that most of the material investigated corresponds to the densely fissured layer of a truncated weathering profile, forming a continuous aquifer. The interface between resistive and conductive material corresponds to the groundwater table. The threshold between the saturated and unsaturated fissured zones seem to be around 3000 Ω.m, however higher resistivity values may be measured below the groundwater table where fissure density is lower than usual. The 3000 Ω.m upper threshold is similar (even though in the upper range) to those cited in the literature for the fissured layer as a whole, which suggests that in all cases these values were measured in the saturated fissured zone even though this is rarely specified. The presence of substantial volumes of air within the unsaturated

fissured layer results in much larger resistivity values, generally higher than those cited in the literature for unweathered granite.

- The absence of an increase in resistivity with depth suggests that the interface between fresh unweathered granite and fissured granite is never reached, except maybe at the very bottom of profile 2 and 3 where values higher than 3000 Ω.m have been observed. The fissured granite layer reaches depths of at least 50-65m, and so does the aquifer.
- Below the wetland, even though no highly resistive material can be observed at the top of the profile due to full saturation up to the surface, there is no indication of the presence of saprolite: resistivity values are only slightly lower than those observed in the saturated fissured layer below the hilltops and slopes, probably as a result of a higher fissure density, clay content and/or groundwater electrical conductivity, and are generally higher than those cited in the literature for saprolite. There are a number of cases where low resistivity values similar to those observed elsewhere in unsaturated and even saturated saprolite were measured, however in nearly all cases these were observed at depth and overlaid by more resistive material, ruling out an interpretation as saprolite.
- Interestingly, these low resistivity values, as low as 110 Ω.m, measured within the saturated fissured layer suggest that when the water table lies above the saprolite-fissured layer interface, it may be difficult or even impossible to map this interface using electrical resistivity methods. As soon as the water table drops below this interface, the contrast between the unsaturated saprolite and unsaturated fissured layer becomes very sharp again, as shown in profile 1.
- Nowhere can any of the faults mapped by COGEMA as crossing the profiles be clearly seen on the ERT profiles. The major Dauges fault is associated with a wide and diffuse lower resistivity zone, suggesting a progressive increase in fracture density around it but this does not extend very deep. There is no evidence for saprolite plunging along faults and veins.

3.3.3.4. Mapping the distribution of granite outcrops using indirect indicators.

Figure 3-25a shows the spatial distribution of slope within the research catchment. It highlights the typical shape of etch-basins in Hercynian landscapes: an almost circular valley with a flat bottom occupied by the wetland, surrounded by a ring of small hills with steep slopes and relatively flat tops, and only opened on its downstream side by a narrow and deep, almost canyon-like, corridor.

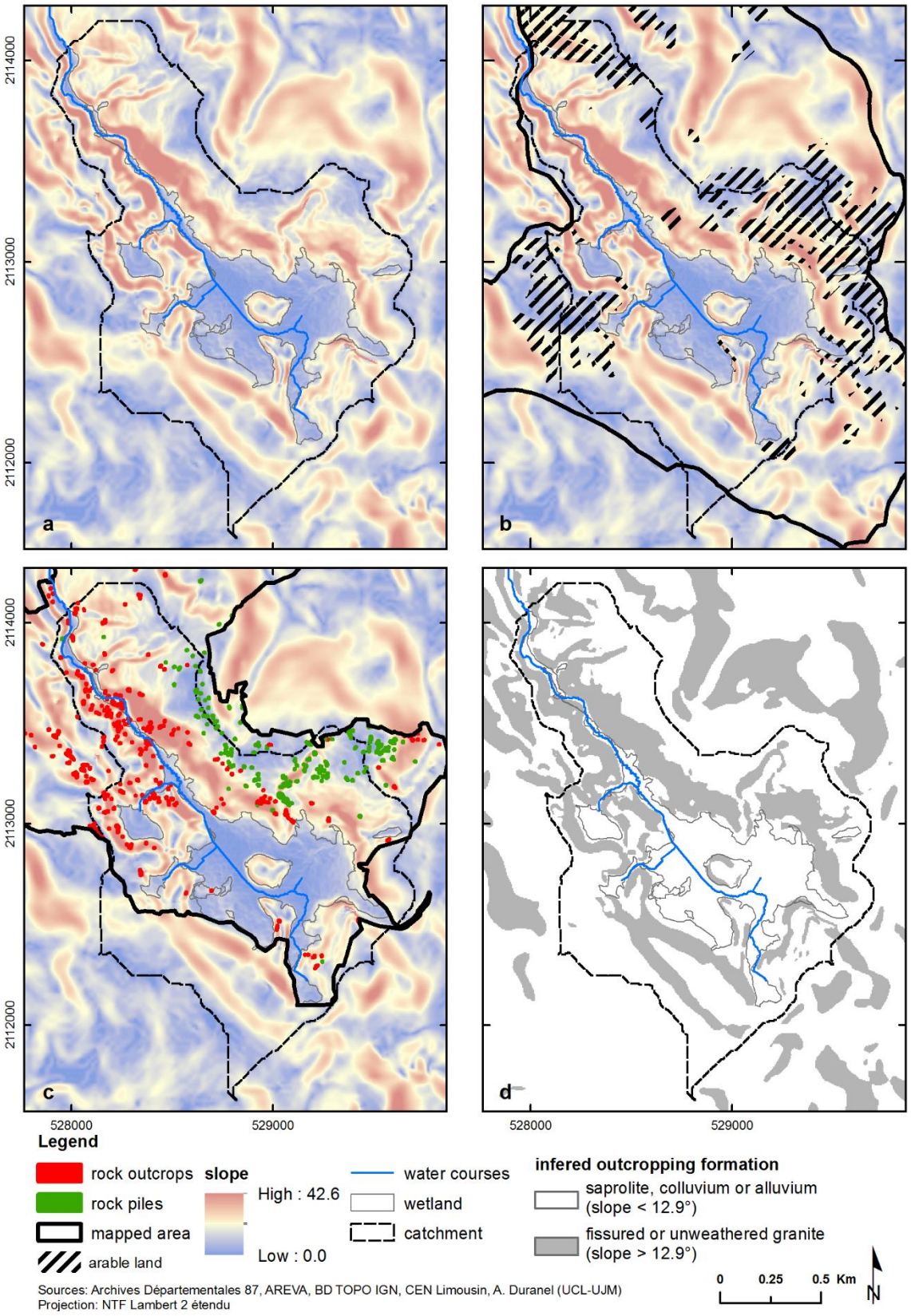

Figure 3-25. Using slope to map outcropping formations

a: terrain slope; b: distribution of arable land in 1836; c: distribution of rock outcrops and piles as mapped by COGEMA; d: distribution of inferred outcropping formations.

A few smaller etch-basins very similar in shape to the main one, as well as elongated intermediary shelves, can be found at approximately mid-slope. Figure 3-25b and Figure 3-26 shows that in some places, land was cultivated on surprisingly steep slopes in the 19th century, even though, overall, arable land tended to be located on the gentler slopes of the hilltops and intermediary shelves closest to the surrounding settlements (villages of Sauvagnac, Marzet and Lagorceix). Arable land was over-represented on slopes smaller than 12.9°, and under-represented above that threshold.

Figure 3-25c shows the distribution of large rock outcrops as mapped by COGEMA. Two types of rock features were distinguished. Unfortunately, no legend was available with the maps, but based on field knowledge it seems clear that a distinction was made between large rock outcrops and boulders on one hand, and man-made piles of smaller rocks on the other hand. The clear association of the latter with arable land, stone-walls and large paths confirms this hypothesis. Only the former type, i.e. large outcrops and boulders, was therefore included in the analysis. Figure 3-27 shows that large outcrops and boulders are over-represented on slopes higher than 12.9°.

The similar slope thresholds obtained using two totally different datasets covering slightly different extents strongly suggest that a strong geo-morphological mechanism drives the distribution of slopes within the study area, and that this mechanism is indeed linked to the difference in resistance to erosion between the more resistant fissured layer or unweathered bedrock, and the more easily eroded saprolite, colluvium and alluvium. A slope higher than 12.9° may be taken as indicative of fissured or unweathered rock outcrops. Figure 3-25d shows the inferred distribution of these areas. An interesting detail is noticeable on the gentler hillslopes along the north-east catchment boundary. In this topographical position, the gentler slopes are most certainly due to the presence of saprolite, yet man-made stone piles are numerous and widespread, and there are occasional large rock outcrops or large boulders. This suggests that the interface between saprolite and fissured layer is quite shallow in this area, in agreement with ERT observations on the other side of the catchment and with field and airborne radiometry observations made by Mauroux *et al.* (2009) at the scale of the Saint-Sylvestre granitic massif.

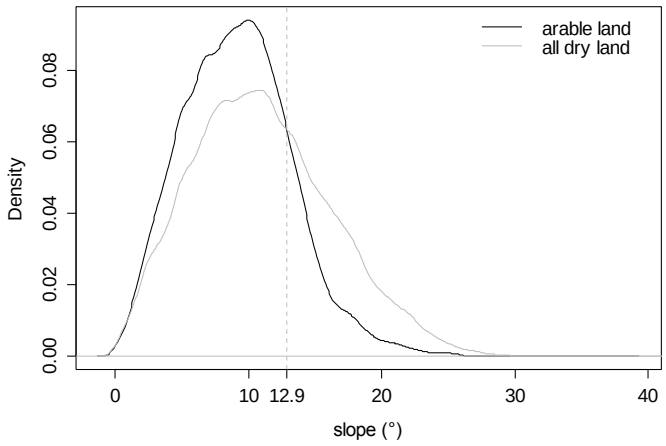

Figure 3-26. Kernel density estimation of slope distribution in arable land vs. in all dry land.

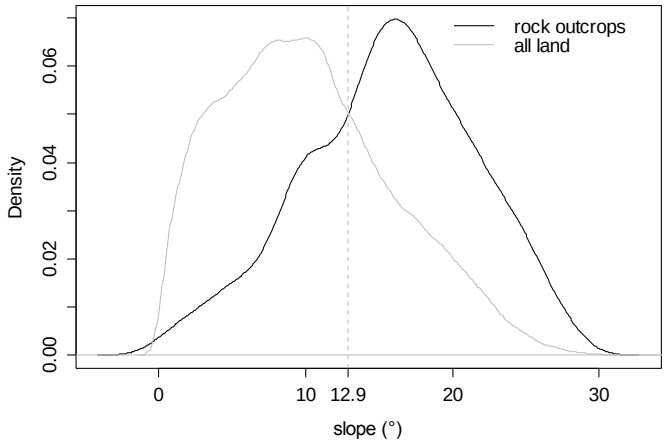

Figure 3-27. Kernel density estimation of slope distribution at mapped rock outcrops vs. in the entire area.

3.3.4. Conclusion on granite weathering formations and periglacial formations within the Dauges catchment

The analysis of sections cutting through periglacial deposits show that they are very patchy. Head is frequently missing and shallow when present. Bedded grus is logically associated to preserved in-situ saprolite (but the opposite is not true), and can reach depths of 1-1.5m. In the Monts d'Ambazac, Flageollet (1977) noted that bedded grus and head matrix are very similar to in-situ saprolite in terms of granulometry. Together with the absence of a fragic horizon, this suggests that, within the Dauges catchment, periglacial deposits can be considered equivalent to in-situ saprolite in terms of their hydrological behaviour. The analysis of the distribution of arable land in the 19th century and of large granite outcrops and boulders suggests that there are indeed two different outcropping materials leading to different slopes, namely fissured or fresh granite on one hand and more easily mobilised material such as in-situ saprolite, colluvium and alluvium on the other hand. The presence of deeper soils and saprolite on the intermediate hilltops and

gentler hillslopes is suggested by their widespread use for arable farming in the early 19th century except on the southern part of the catchment. However the widespread occurrence of large man-made stone piles and occasional large granite outcrops as mapped by COGEMA in the same area suggest that most of the saprolite layer has been eroded, and that arable farming took place on erosion surfaces cut across the lower part of the saprolite layer where boulders of unweathered granite are more frequent. The shallowness or even absence of the saprolite layer on the higher hilltops was confirmed by the ERT survey: even though the presence of an artificial pasture on part of profile 4 along the southern hilltops suggested the presence of at least some loose material, it could not be seen with the electrode interval used, and was therefore less than about a metre deep. The presence of some saprolite was evidenced on an intermediate hilltop on the eastern boundary of the catchment, but again it was less than a couple of metres deep. This is in line with observations made on a limited number of outcrops within the catchment, and with field observations and the interpretation of airborne radiometry data made by Mauroux *et al.* (2009), who showed that most of the saprolite cover in the Monts d'Ambazac had been eroded away.

In their morphotectonic evolution model of the Limousin relief, and of the Monts d'Ambazac in particular, Klein and co-workers (Klein 1978; Desire-Marchand & Klein 1986; Klein *et al.* 1990) interpreted the higher hilltops around the Dauges catchment, with an altitude ranging from 650 to 700m, as residual inselbergs protruding above the remnants of a younger pediplain, the latter corresponding to the plateaux and shelves located at around 600-630m within the catchment. A consequence of this interpretation is that, even on gentle slopes, there would be no substantial depths of saprolite left on the higher hilltops (Puy de Sauvagnac to the east, Puy de la Garde and Papou to the south-west, Puy du Guet to the north-east), whereas remnants of deep weathering mantles could be found in hilltop position at lower altitudes, around Puy des Crouzettes and Puy Gros, around the villages of Sauvagnac and Marzet, on the hill south of the wash house and on the midslope shelf that runs along the southern boundary of the catchment (see Figure 2-4 to locate place names). This agrees quite well with the ERT results that did not detect saprolite on the higher hilltops south of the catchment but did on the smaller and flatter hill north of Marzet. It also agrees relatively well with the current and past distribution of arable land.

The results of the analysis of the distribution of large granite outcrops and boulders suggest that resistant granite is exposed on the steeper slopes. This was confirmed by ERT survey, which systematically showed the presence of a permeable fissured layer, extending beyond depths of at least 50-60m. The bottom of this fissured layer was possibly reached only at the very bottom

of profile 2, downstream of Puy Rond, at depths of at least 55m below surface (corresponding to an altitude of about 500m NGF69), which is consistent with data from the CEA boreholes drilled at the bottom of the main basin that suggested depths of 54m on average (minimum 38m, maximum 65m) and altitudes of 492-513m NGF69 (mean 505m). Since the ERT profiles rarely reach the fissured zone – bedrock interface and all but one of the CEA boreholes have been drilled from a restricted area at the bottom of the basin and from similar altitudes, it is difficult to conclude on the shape of this interface. Borehole 7, located higher up in the small basin at the south-east of the wetland (Rocher) suggests that the depth of the interface is less variable than its altitude, as it is reached 38m below surface but at an altitude of 539m. This would be consistent with a localised deepening of the weathering front in the centre of the catchment that led to subsequent differential erosion and the formation of a topographic basin, but more data would be needed to confirm this.

It is clear though that this thick fissured layer allows the development of a relatively thick aquifer. On all profiles the margins of the wetland matched the point where this aquifer cuts through the ground surface. Puy Rond stands out as a more massive block of granite, with a much lower degree of weathering that the surrounding fissured zone. According to the ERT data, the fissured layer at the bottom of the basin is generally more densely fractured than below Puy Rond and the surrounding hilltops and slopes. This is the result of differential weathering, also at the origin of the basin topography, and caused by differences in tectonic fracture density. Manual augering showed the presence of a saprolite layer below the main extent of the wetland, but the method did not allow to estimate its thickness. The ERT survey suggested that it was nowhere substantial. This is backed by the rod survey data that shows the presence of hard rock at shallow depths directly below organic and inorganic sediments on the south-eastern part of the wetland. It is remarkable that none of the faults and lamprophyre veins mapped by COGEMA could be seen on the ERT profiles. There was no evidence of saprolite, or even highly fissured granite, plunging along the faults. It seems that, at the bottom of the basin and if one neglects the relatively shallow sediment deposits, the top of the fissured layer follows quite closely the ground surface, and is quite flat. Only differences in fracture density could be inferred from the ERT data.

This is at odds with the results from the geological drillings completed along the toeslope further east, that show the presence of a 15-40m deep saprolite layer. This may result from a quite localised deepening of the weathering front along this particular fracture that is not repeated elsewhere, caused by the presence in this area of several faults and lamprophyre vein parallel and close to each other. This could have led to the weathering front deepening and widening to

a larger extent than along other isolated faults and veins. However the saprolite layer cut by borehole n°5 is located some distance away from the nearest fault, and the saprolite layer does not seem to deepen much further as one gets closer to the faults. It is possible that this material has simply not been entirely removed by erosion during the formation of the basin, due its position upstream of Puy Rond. The map of the base of peat and inorganic deposits (Figure 3-31) shows a slightly higher ridge prolonging Puy Rond towards the north-east. As a consequence, sediment fluxes in the last stage of the basin formation followed the course of the current stream, through the bottleneck between Puy Rond and Puy Long. This may have caused a less complete evacuation of in-situ saprolite and colluvia from the eastern part of the basin, particularly at the toeslope. Downstream of Puy Rond and of this bottleneck, where all ERT profiles cutting across the bottom of the basin are located, erosion might have been more complete and nearly reached the top of the fissured layer.

Taken together, the results of the ERT survey and of the rod survey suggest that, below the wetland at least, substantial masses of in-situ saprolite or colluvia do not extend beyond the north-east corner of the wetland where the CEA boreholes were drilled. A fifth ERT profile was planned for across the CEA boreholes as this would have been extremely useful to validate the interpretation of the other ERT profiles and to investigate the actual extent of this saprolite pocket, unfortunately equipment and logistical issues prevented it. It would also be advisable to carry out localised checks of superficial formations along the ERT transects using drilling equipment. In the absence of such cross-validation, the possible discrepancy between the ERT survey and the CEA drilling logs suggests that the interpretation of either surveys should be taken with some caution.

3.4. Development of a 3D hydrogeological model of peat and alluvial deposit

3.4.1. Methods

Data on the stratigraphy of the peat were collected within the Dauges wetland by Laplace-Dolonde *et al.* (2007), who described 93 profiles spread more or less evenly across the wetland. The profiles rarely extended below the first few tens of centimetres of the underlying mineral substrate. Most profiles were located using a portable GPS, with an estimated accuracy of 10-40m, but a few were located using a topographic map and their position accuracy is probably poorer than 50m. Data from this earlier study were collated, checked, harmonised and entered into the site GIS database. A further 23 soil profiles were described as part of the current work

during the installation of the dipwells and piezometers (see Figure 4-16 in Section 4.3.1.1), using a Russian corer in peat and a 50mm Dutch soil auger in mineral materials. Description of the peat included color, type of plant remains when identifiable, humification rate using the von Post index, texture, presence of sand or gravel and an estimation of wetness (Riley & Michaud 1994), all estimated in the field visually and manually. Samples were classified as fibric, hemic or sapric based on the von Post index and the texture of the peat. The granulometric composition of mineral horizons was estimated manually on site. The altitude and location of these soil profiles were surveyed using DGPS with centimetric accuracy.

Peat depth was measured in 794 points across the entire wetland site following a predefined 25m-resolution grid. Peat depth was estimated using a probe made of threaded metal rods. The friction of gravel and sand against the rod threads allowed a clear identification by touch of the transition between peat and underlying mineral horizons. An assessment of the method against the augered profiles showed that it was generally accurate to within 10cm. However, particularly along the margins of the wetland, peat and mineral horizons were sometimes intermixed. In this case it proved difficult to accurately establish the actual depth of the deepest peat layer, and the value obtained may be an underestimation. The depth of the underlying alluvial or colluvial deposits was also roughly estimated by driving the rod as deep as possible. These sediments were often less compacted and had a higher water content than the underlying in-situ formations, and could relatively easily be probed unlike the more compact in-situ saprolite beneath them. The altitude and location of each survey point was determined with centimetric accuracy using DGPS. Peat depth values obtained using probing and augering were aggregated with data from Laplace-Dolonde *et al.* (2007), keeping only points that had been located using GPS.

Peat and underlying mineral sediment depths were interpolated to a 5m-resolution grid using ordinary kriging. To improve the accuracy of peat depth interpolation at the wetland margins, the limits of peat soils were estimated visually based on actual measures, the vegetation map and the DEM. Dummy zero points were added at 25m intervals along and beyond these boundaries. Actual measurement points were scarce downstream of the main wetland outlet at Pont-de-Pierre, and peat depth was therefore roughly estimated for a number of dummy points within the narrow riparian wetland downstream of Pont-de-Pierre and the small basin east of Marzet ("Girolles"). This was based on a small number of measurement points, the vegetation map and topography. The dummy points were added to the rest of the peat depth data for kriging. This was deemed acceptable as peat depths and surfaces downstream of Pont-de-Pierre are very

small compared to the rest of the site, and should not have a major influence on water circulation and on the results of the MIKE SHE model. However the interpolated map of peat depth should not be relied upon for other purposes downstream of Pont-de-Pierre.

In places where data on peat stratigraphy was available, the acrotelm depth was estimated using the pedological definition proposed by van der Schaaf (1999, 2002), as the "top layer […] from the surface downwards to the level where the degree of humification first reaches 4 […] in the von Post classification". This definition is based on the relationship between humification and hydraulic conductivity, with the hydraulic conductivity decreasing rapidly as the von Post index increases to about 4, and decreasing at a much lower rate or being stable beyond that value (Verry *et al.* 2011). Only GPS-located stratigraphical surveys were used, reducing the dataset to 69 points. Scatterplots and regression trees (using the rpart R package, Therneau *et al.* 2014) were used to explore the relationship between acrotelm depth and a number of potential explanatory variables. These included vegetation type, peat depth, slope, contributing area and slope over contributing area ratio. These variables were chosen as they may be related to the volume, velocity and hydrochemistry of water flowing through and above the peat and may have an impact on peat accumulation and humification and therefore on the acrotelm depth.

It has long been recognised that peat properties, in particular hydrologically relevant properties such as humification, bulk density, porosity and hydraulic conductivity, influence and are influenced by the vegetation from which the peat is formed (Rydin & Jeglum 2006). In a valley mire such as the Dauges mire, peat depth and surface slope are also expected to be related to the depth and variability of the water table, with shallower and more stable groundwater tables found in the low-lying centre of the mire where peat is deeper and slope small or null. Furthermore, the amount of runoff flowing through a particular location is in part related to its contributing area (or catchment area), while various indices expressing the ratio between slope and contributing area have repeatedly been shown to be related to the depth of the groundwater table (Beven & Moore 1993; Merot *et al.* 1995, 2003; Rodhe & Seibert 1999; Wilson & Gallant 2000). Slope, contributing area and slope over contributing area ratio have been shown to be related to pedologically-defined acrotelm depth in raised bogs (van der Schaaf 2002).

These variables were computed for the Dauges catchment using DEMs of varying resolutions (5, 10 and 25m) derived from the 5m DEM described in Section 3.2.1.3. The catchment area and slope over catchment area ratio were calculated using the DInf algorithm implemented in the TauDEM extension for ArcGIS (Tarboton 2008), which results in a better estimation of surface

water fluxes than the classical D8 algorithm available in core ArcGIS (Tarboton 1997). The slope over catchment area ratio is the inverse of the widely used topographic wetness index (Beven & Kirkby 1979; Quinn *et al.* 1995; Wilson & Gallant 2000).

3.4.2. Results and discussion

Figure 3-29 shows peat depths interpolated from rod and auger surveys. Data with a sufficient resolution are only available for the main wetland extent upstream of Pont-de-Pierre, including the small perched basins of Marzet and Rocher. Consequently, the following maps and figures do not include the peat deposits downstream of Pont-de-Pierre, which are very limited in extent and depth. The mean peat depth is 0.80±0.49m (based on the kriged data). The maximum depth, 3.45m, was recorded by Laplace-Dolonde *et al.* (2007) just east of Puy Long, but the deepest peat deposits are generally found downstream of Puy Rond. The total peat volume is estimated to be around 293039m^3. Comparison of peat depth and altitude of the base of the peat deposit (Figure 3-31, top) shows that deep peat deposits are predominantly found along palaeo-thalwegs that pre-existed peat inception. These palaeo-thalwegs match quite well the current permanent water courses upstream of Puy Rond and Puy Long, but not downstream where the plan profile of the stream makes it clear that it has been artificially straightened and diverted.

Figure 3-30 shows the estimated thickness of alluvial deposits. Even though it should be interpreted with caution given the caveats of the method used (manual probing), it gives an idea of the depth of easily penetrable sediments. Comparison with the hand auger survey and with rod probing tests carried out close to the piezometer clusters where the stratigraphy is known showed that they correspond to saturated sands and gravels that have been substantially impoverished in silts and clays compared to in-situ saprolite, indicating that they have been displaced by running water. They are located in two main places: at the break of slope along the north-eastern boundary of the wetland, and downstream of Puy Rond where the deposits occurred on a flatter area obstructed by the Pont-de-Pierre bottleneck and are clearly correlated to a deeper palaeo-thalweg that preceded sedimentation (Figure 3-31, bottom). The presence of hard rock at shallow depths just underneath the peat or a shallow layer of sediment is obvious from Figure 3-28 along the south-east and east parts of the wetland.

Figure 3-32 gives a schematic representation of the twenty profiles surveyed by manual augering in peat soils. The stratigraphic survey confirmed the presence of substantial and highly permeable deposits of washed sands and gravels, up to 1.7m thick, along the main watercourse and north-east of Puy Rond.

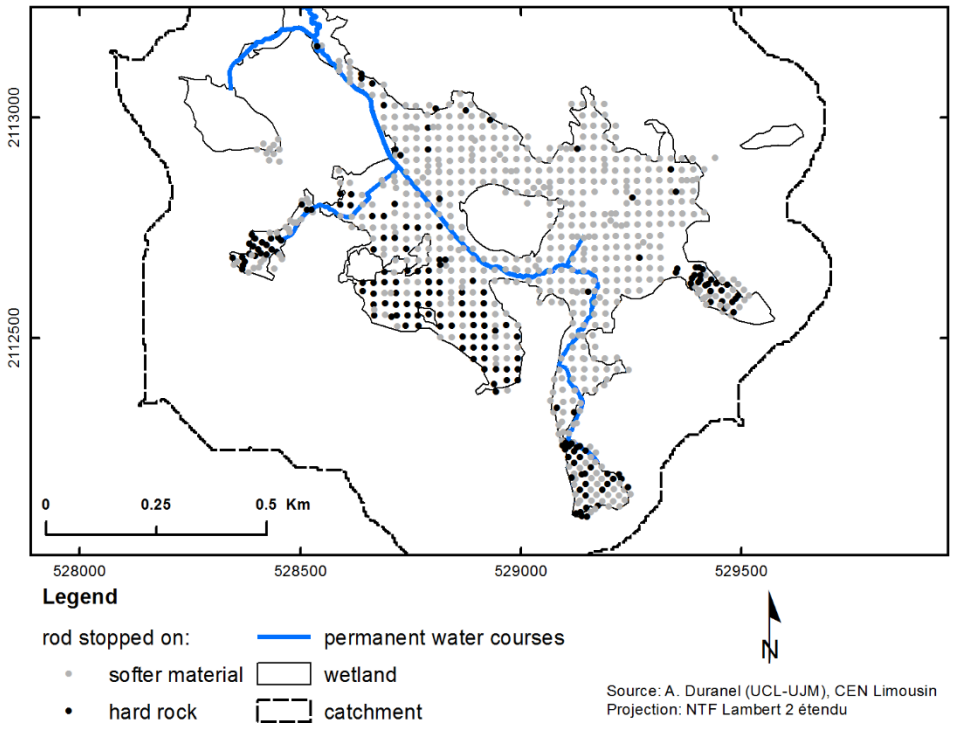

Figure 3-28. Nature of the material on which the rod survey stopped.

Together with data from Laplace-Dolonde *et al.* (2007), it shows that the Dauges mire histosols are highly varied and complex. Colluvial and alluvial mineral deposits are often found between organic horizons, particularly on the margins of the wetland and along the current and pre-engineering courses of the main water course downstream of Puy Rond. The deeper organic horizons are often highly humified, and therefore poorly permeable in theory. The upper peat horizons are also highly variable, and range from dry, highly decomposed peat on the northern and eastern margins of the wetland to nearly intact *Sphagnum* peat on the southern side for instance. Figure 3-33 shows the acrotelm depth as mapped using the pedological definition by van der Schaaf (1999, 2002), as well as the topographical indices derived from the DEM and used to model it. Figure 3-34 shows box- and scatter-plots of acrotelm depth against potential explanatory variables. There seems to be a larger proportion of large acrotelm depths in habitats classed as either *Carex/Eriophorum angustifolium* mire or *Narthecium ossifragum* mire in the low-lying areas west of Puy Long and between Puy Rond and the main wetland outlet at Pont-de-Pierre. No relationship with any of the other potential descriptors could be inferred from the plots. An exploratory regression tree showed the lowest cross-validated error for the size 1 tree (i.e. no effect of any explanatory variable). Small-scale spatial variation in the acrotelm depth is clearly visible in Figure 3-33-a, and suggests that a high-resolution systematic survey would be required to map it with sufficient accuracy.

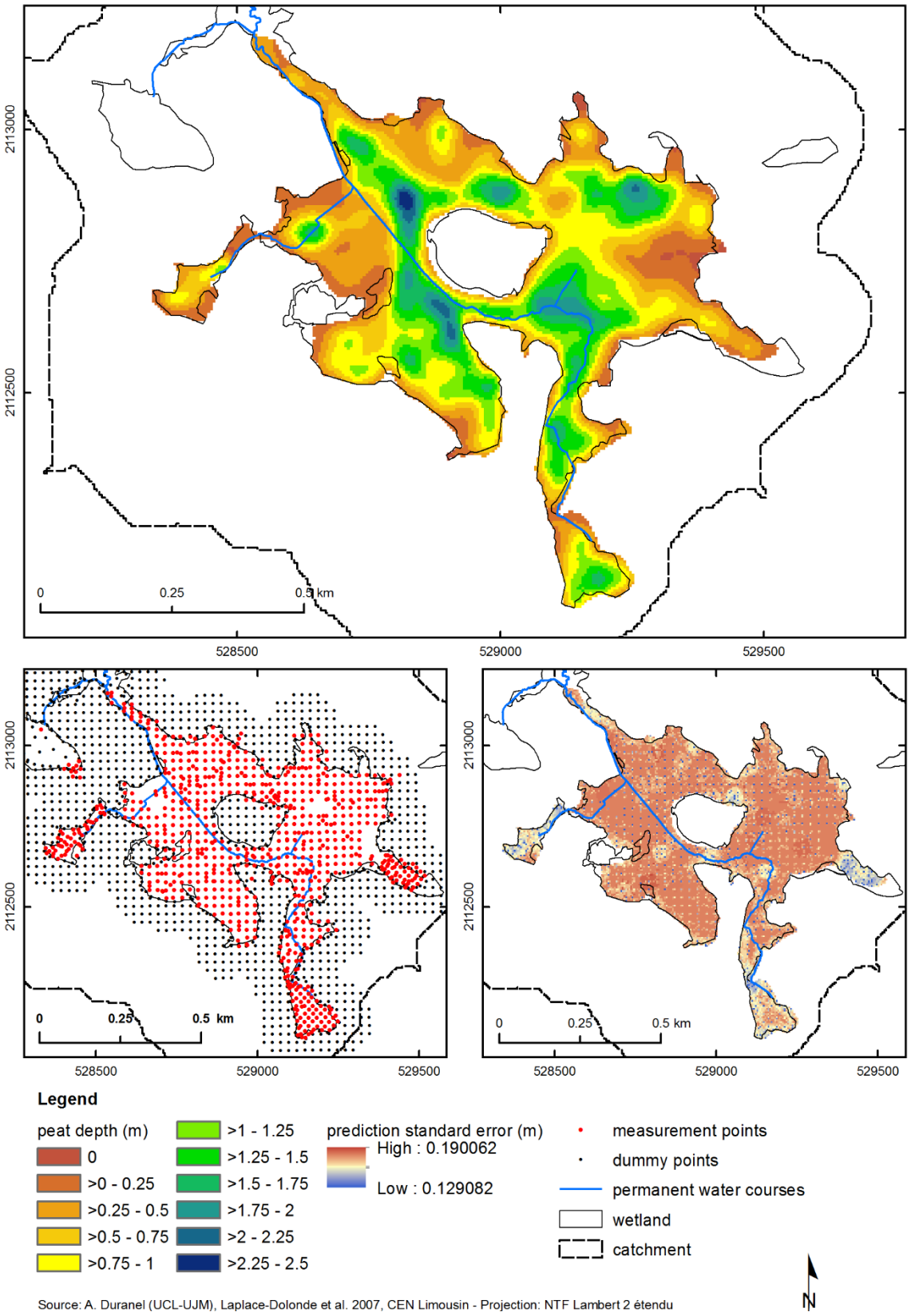

Figure 3-29. Peat depth at the Dauges site.

Top: peat depth kriging prediction; bottom left: measurement and dummy points; bottom right: kriging prediction standard error. Wetland boundaries are based on the vegetation map.

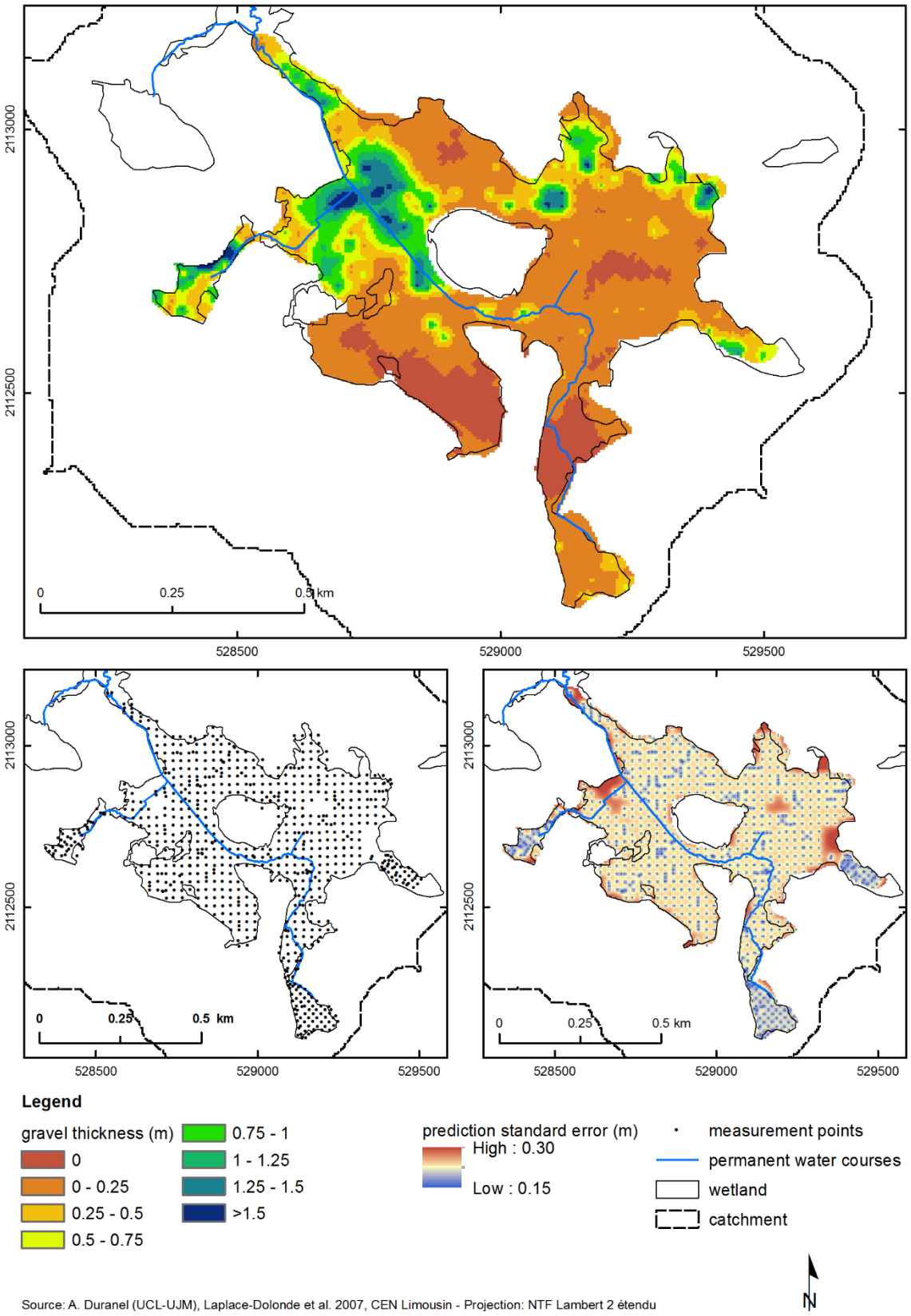

Figure 3-30. Thickness of easily-penetrable mineral deposits underlying peat at the Dauges site.

Top: sediment thickness kriging prediction; bottom left: measurement points; bottom right: kriging prediction standard error. Wetland boundaries are based on the vegetation map.

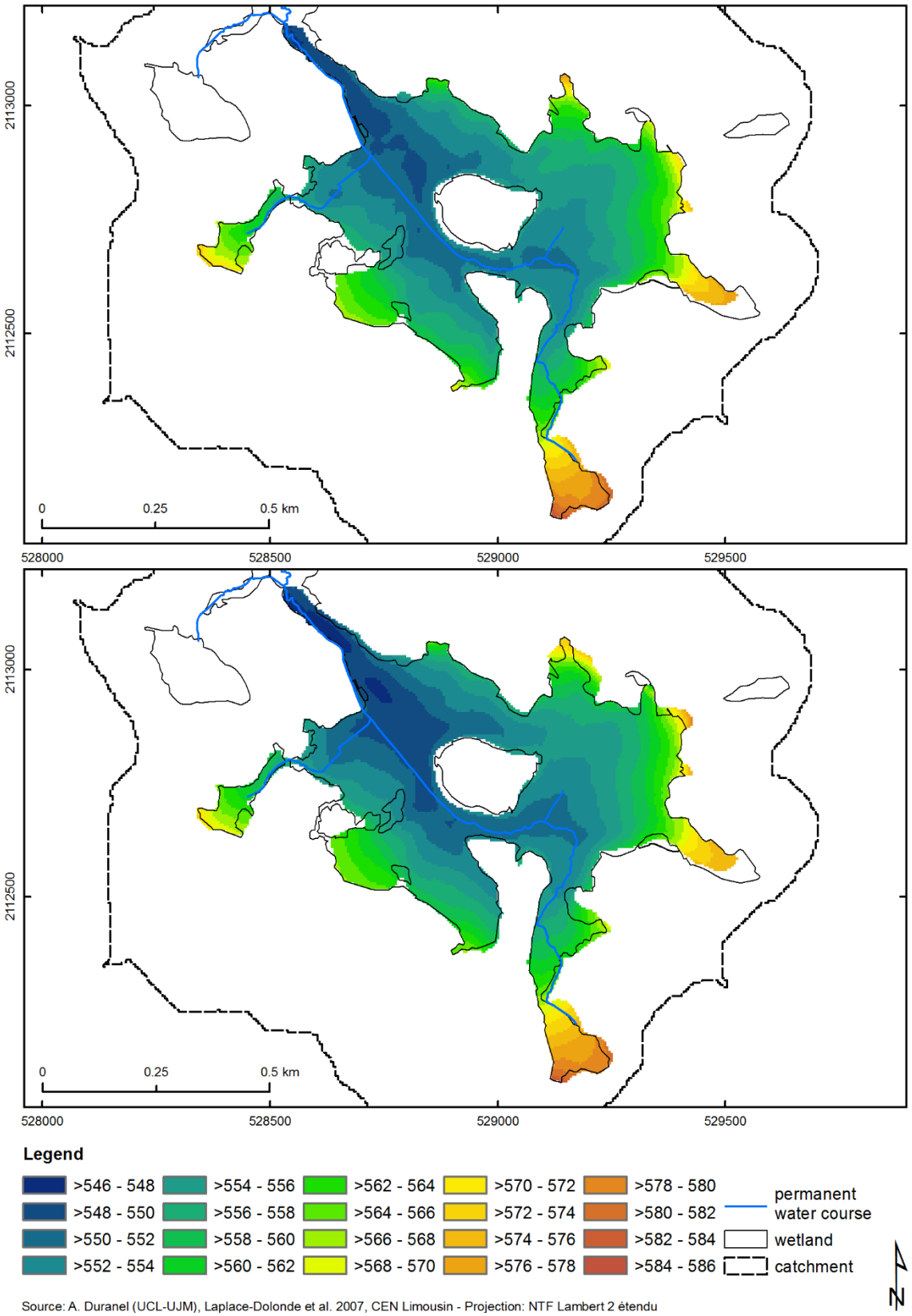

Figure 3-31. Altitude (mNGF69) of the base of peat (top) and mineral (bottom) deposits at the Dauges site.

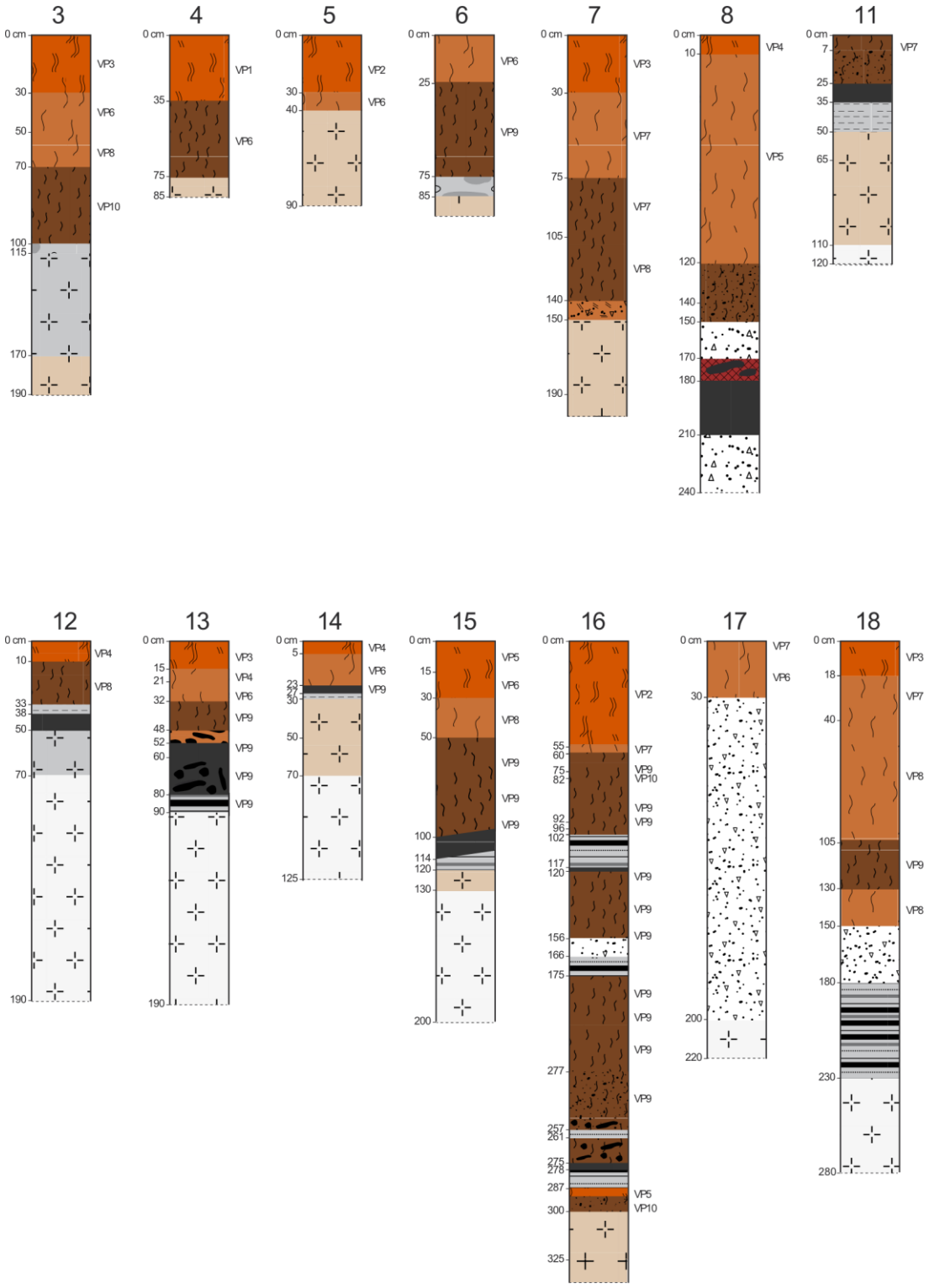

Figure 3-32. Stratigraphic profiles.

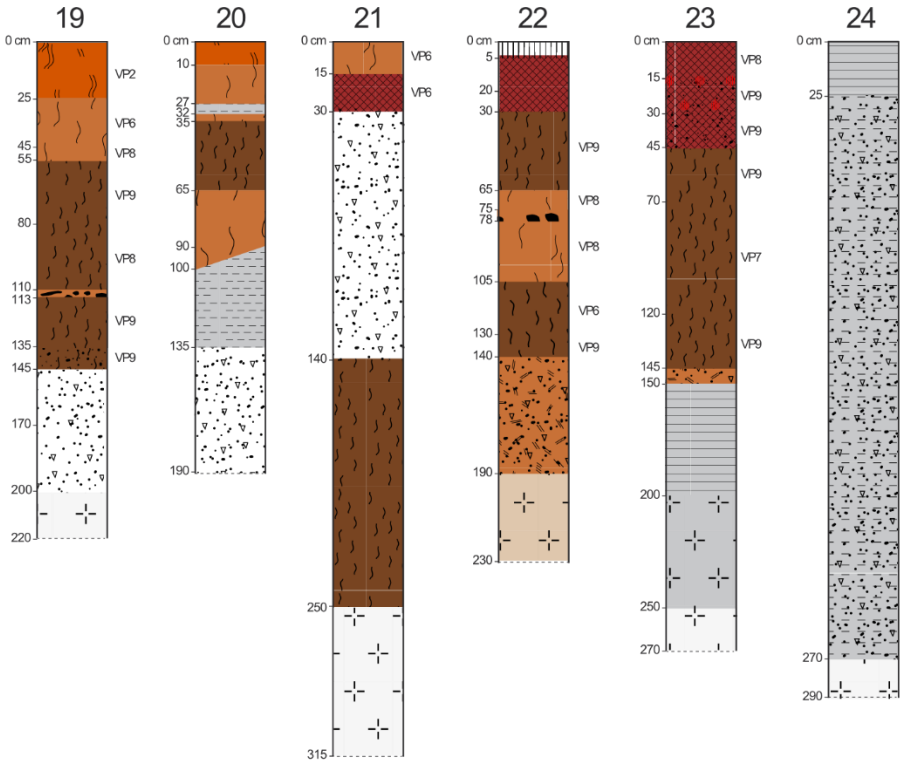

Legend

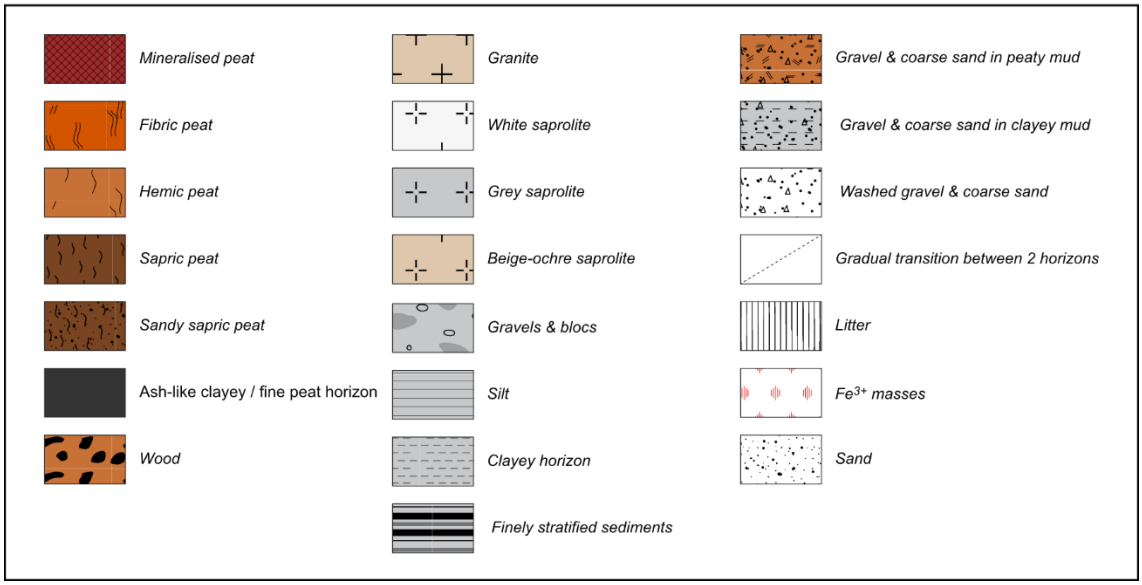

Figure 3-32 (continued). Stratigraphic profiles.

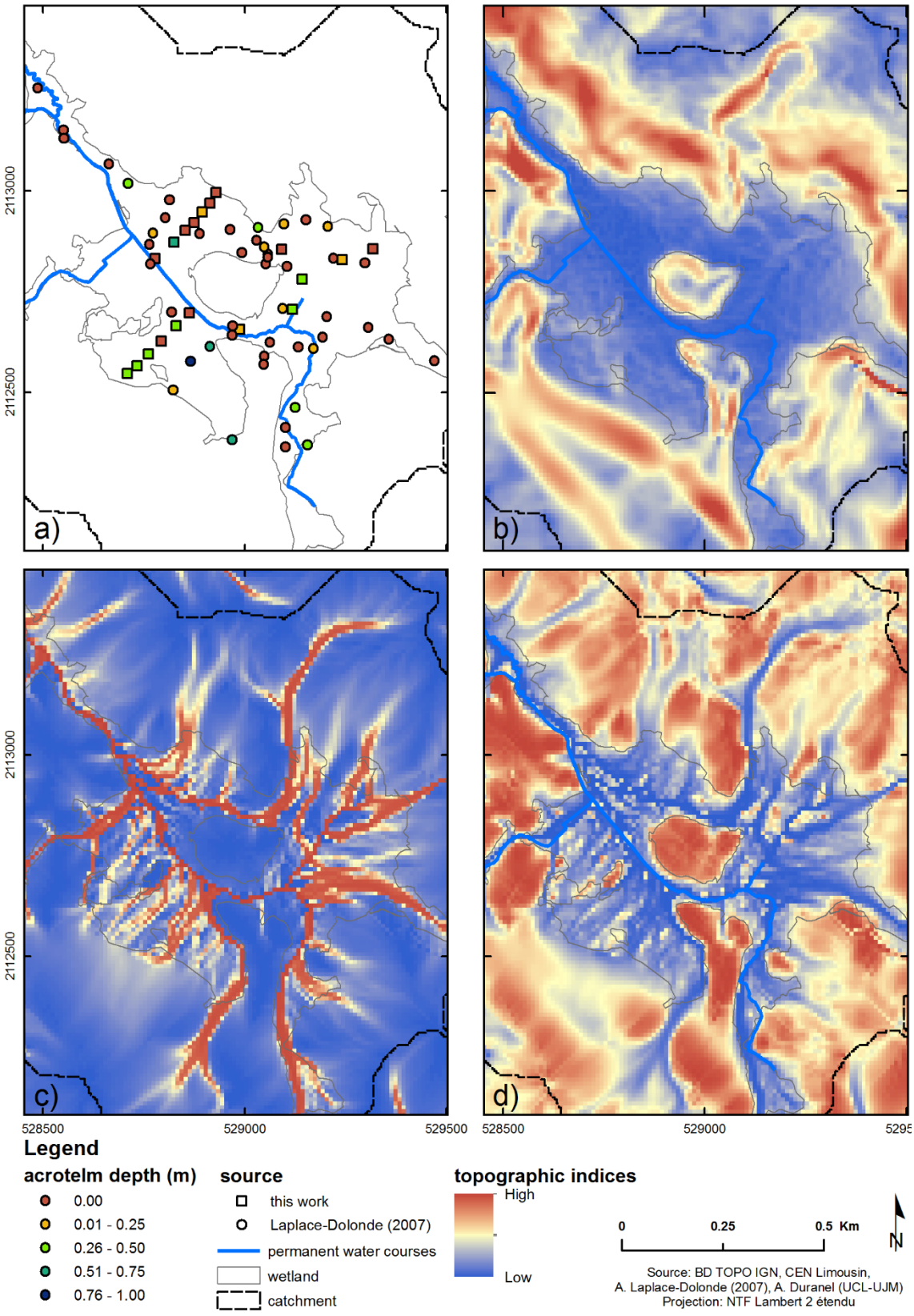

Figure 3-33. Acrotelm depth (a) and topographic indices used to model it: terrain slope (b), DInf contributing area (c) and slope over Dinf contributing area ratio (d).

Only the topographic indices computed using the 10m-resolution DEM are shown.

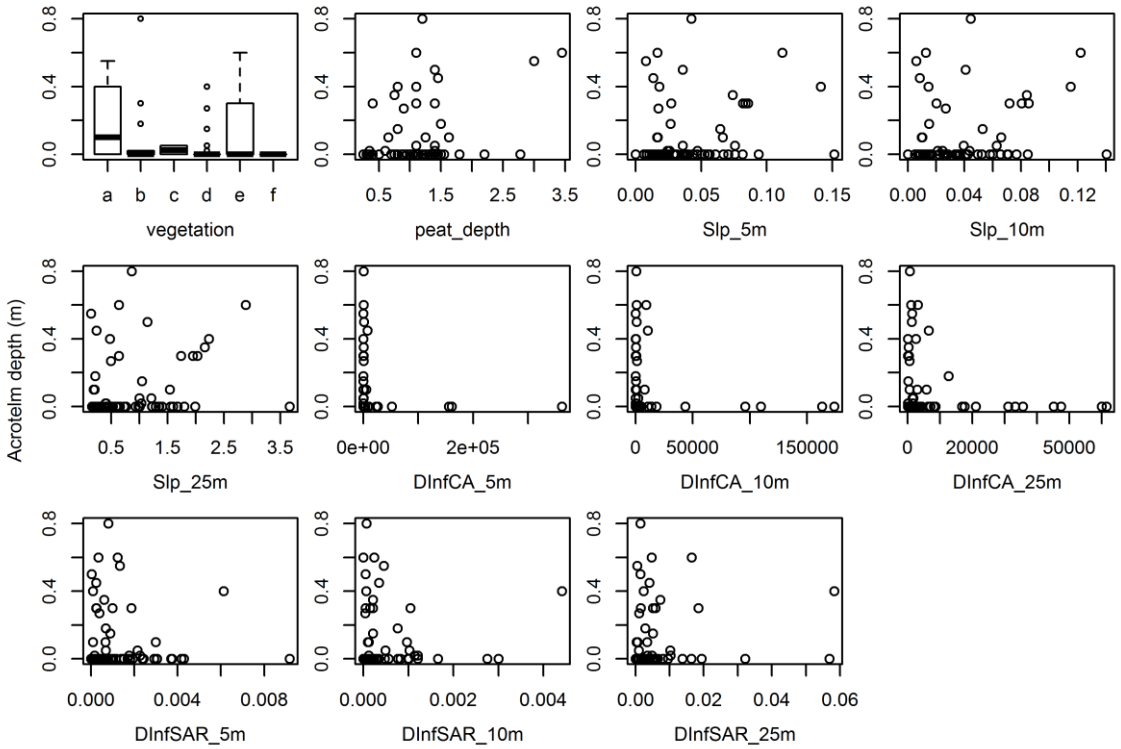

Figure 3-34. Box- and scatter-plots of acrotelm depth against potential explanatory variables.

Vegetation classes: a: *Carex/Eriophorum angustifolium* minerotrophic mire, b: *Calluna vulgaris-Erica tetralix* mire, c: *Nardus stricta – Juncus squarrosus* grassland, d: *Molinia caerulea-Juncus* grassland, e: *Narthecium ossifragum* mire, f: *Molinia caerulea* mire; Slp: slope; DInfCA: DInf contributing area; DInfSlp: slope over Dinf contributing area ratio.

3.5. Hydraulic conductivity of peat and alluvial sediments

3.5.1. Methods

Hydraulic conductivity of the peat and most superficial underlying mineral formations was assessed using slug withdrawal tests following the procedures described in Baird *et al.* (2004). The procedure was carried out in selected existing dipwells and piezometers (see Section 4.3) and in temporary piezometers specifically installed for that purpose in selected places to better characterise expected changes in peat hydraulic conductivity with depth. The locations of the temporary piezometers were subjectively chosen to best represent the expected spatial variability of the peat hydraulic conductivity, based on the stratigraphy of the peat as investigated in Section 3.4 and on the mire vegetation (Figure 3-35). The temporary piezometers were made of PVC tubing, 27 and 32mm internal and external diameter respectively, with a plug at the bottom end. A 10cm-long intake was drilled 10cm above the bottom of the pipe using a 5mm drill bit. The perforated/total area ratio of the intake was about 70%.

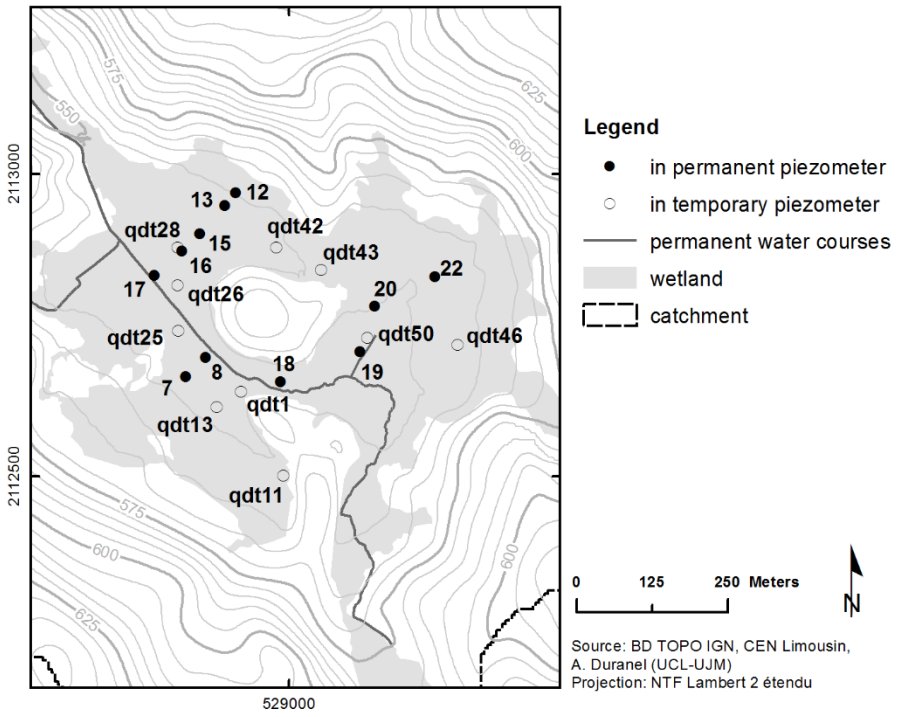

Figure 3-35. Location of slug tests.

Three tube lengths were used to investigate hydraulic conductivity in the acrotelm (intake at 10-20cm below ground), the upper catotelm (60-70cm) and the lower catotelm (140-150cm). The three tubes were installed in a cluster 20-30cm from each other. A screw auger with a 30mm diameter was used to drill a hole into which the piezometer was carefully pushed. In some places, the peat layer was shallower than 160cm, and the deepest piezometer was therefore installed at a shallower depth, making sure the intake was well above the peat/mineral interface. Temporary piezometers were labelled according to the name of the cluster ("qdt" plus a number, for legacy reasons) and the minimum and maximum depth below ground of the intake, in centimetres ("qdt25 10-20" for instance).

After the water table in the piezometer had equilibrated, the piezometer was fully emptied using a manual pump to trigger a strong inflow and remove any material that may have got smeared during the installation of the piezometer and could lower the hydraulic conductivity around the intake. This procedure is known as "development" (Baird *et al.* 2004). An automatic Mini-Diver pressure logger was installed at the bottom of the pipe below the intake, and the water table left to equilibrate again. A manual pump was used to rapidly remove water from the piezometer, and the recovery of the water table was monitored with the automatic logger. Slug withdrawal tests were preferred over slug insertion tests as it has been shown that the former are more reliable and provide results that are more consistent with Darcy's law assumption of a rigid

porous medium (Baird *et al.* 2004). The recovery data were analysed within the framework developed by Kirkham (1946) and Hvorslev (1951), and detailed in Baird *et al.* (2004). In a rigid porous media, the discharge of water into the piezometer after slug withdrawal or insertion is given by:

$$Q = A\frac{dh}{dt} = FKh \qquad \text{Equation 3.2}$$

where *Q* is the discharge, *A* the inside cross-sectional area of the piezometer, *h* the difference in elevation between the water table in the piezometer and the surrounding soil, *t* the time, *K* the hydraulic conductivity of the soil and *F* the shape factor of the piezometer intake, which depends on the intake size and shape and on the flow pattern around it. According to Hvorslev (1951) and subsequent workers (Baird *et al.* 2004), for closed-bottom cylindrical intakes, F can be calculated as:

$$F = \frac{2.4\pi l}{ln(1.2l/d + \sqrt{1 + (1.2l/d)^2})} \qquad \text{Equation 3.3}$$

where *l* is the length of the intake and *d* its external diameter.

Hvorslev (1951) defined the basic hydrostatic time lag *T* as:

$$T = \frac{A}{FK} \qquad \text{Equation 3.4}$$

and showed that the change in normalised head (the head ratio, or difference between heads in the piezometer and in the soil) is given by:

$$\frac{h}{h_0} = e^{-t/T} \qquad \text{Equation 3.5}$$

where *t* is the time since the start of the test, *h* is the head ratio at time *t* and h_0 the head ratio at t_0. *T* can therefore be estimated from the curve of change in head ratio against time, and *K* calculated from *T* using Equation 3.4. Following Baird *et al.* (2004), *T* was estimated numerically by fitting Equation 3.5 to the observed recovery curve using non-linear least-square regression, specifying *T* as the parameter to optimise. The nls() function in R (R Core Team 2014) was used in this order. In some cases, particularly when the peat hydraulic conductivity was very small, the

water table depth in the soil was difficult to measure precisely. This was due to a combination of factors: not enough time had been given for the water table to stabilise after the diver had been inserted in the piezometer, or too large an amount of water was removed from the piezometer and the recovery took too much time to monitor entirely or to minimise the effect of diurnal water table movements. Yet an incorrectly specified soil water table can lead to unrealistic estimates of *T* and *K*. A second model was therefore fitted to the recovery curve, specifying the soil water table as a second parameter to be optimised. *K* was then estimated from *T* using Equation 3.4.

3.5.2. Results and discussion

A total of 25 slug tests were carried out using temporary piezometers inserted at three different depths in peat. Figure 3-36 shows the observed recovery curves with fitted Hvorslev models. When included as a parameter to be optimised, computed groundwater table depth values were within a few millimetres of measured ones, which is well within the accuracy of the manual dipper. As the latter were not available for all tests, hydraulic conductivities were calculated using the former, which resulted in a better fit of the Hvorslev model with the observed recovery curves. Run tests showed that in all slug tests there was a statistically significant departure from the Hvorlsev model. The only exception was the test labelled "qdt25 10-20", which can be explained by the fact that only seven data points were available.

The departure from the Hvorslev model is also obvious from the residuals (Figure 3-37) that are not distributed randomly. Three different patterns can be seen from the residual plots. The first one shows daily cyclicity and is very likely a consequence of the daily groundwater fluctuation caused by evapotranspiration losses. This type of pattern is visible in tests "qdt43 120-130" and "qdt11 140-150" for instance. The second type of pattern shows short peaks, for instance in "qdt43 60-70" or "qdt46 60-70". These coincides with short precipitation events. The third type of pattern is found in nearly all residual plots, sometimes superimposed to other types of residual patterns. It can be seen most clearly in test "qdt13 140-150": the residuals follow an inverted S shape, whereby the Hvorslev model underestimates the recovery curve at first, then overestimates it and finally underestimates it again. The curve shape is broadly similar whatever the duration of the recovery, i.e., residuals are dependent on the h/h_0 ratio but not on time. Apparent departure from Darcy's law in peat has been reported by several researchers (Ingram *et al.* 1974; Rycroft *et al.* 1975; Waine *et al.* 1985; Baird & Gaffney 1994), who also measured larger hydraulic conductivities at the start of slug tests than towards the end.

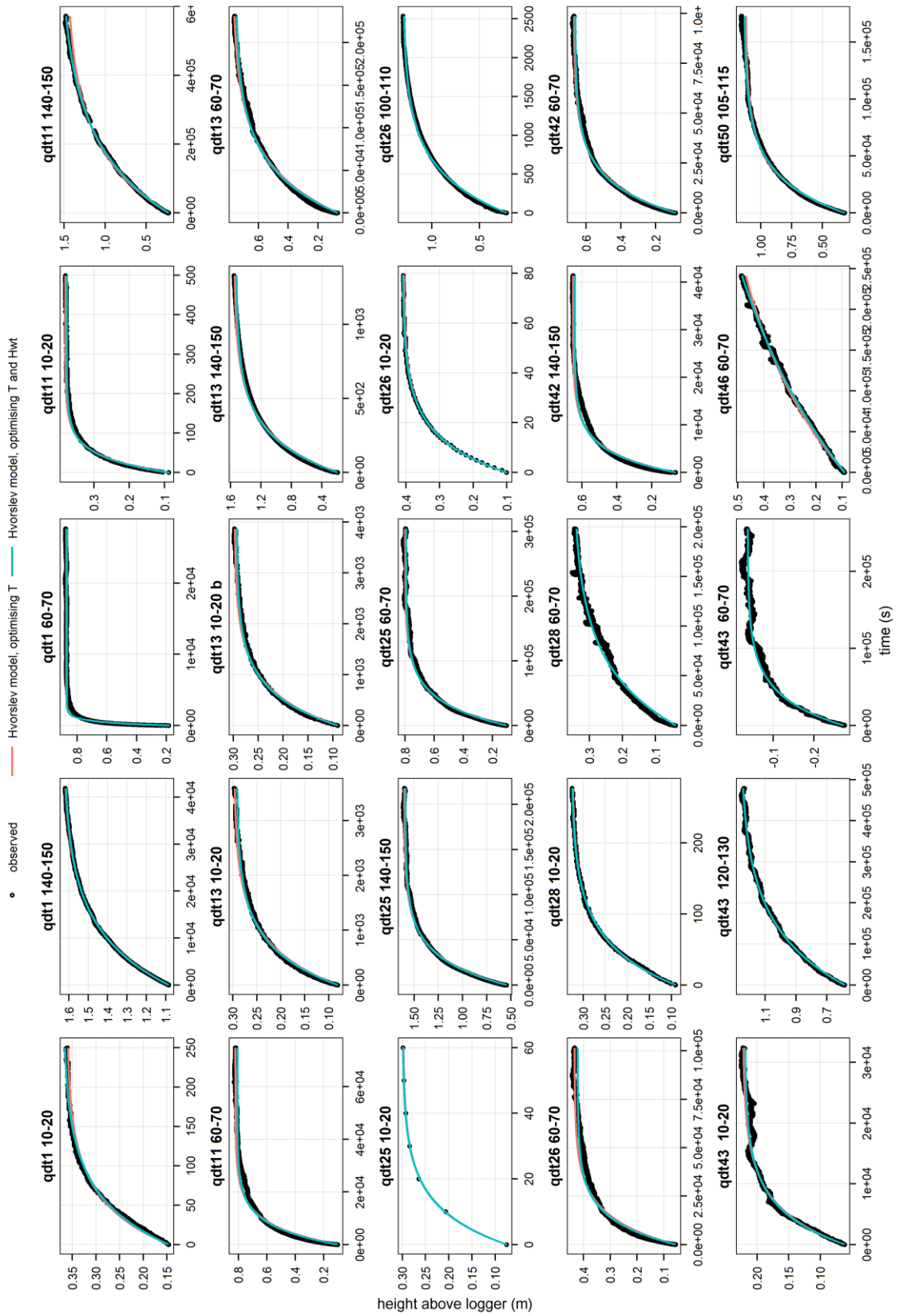

Figure 3-36. Recovery curves following slug tests in peat using temporary piezometers with a 10cm intake.

Tests are labelled according to the cluster name as per Figure 3-35 and to the depth of the piezometer intake during the test, in centimetres. Test "qdt13 10-20" was carried out twice. Note the different x and y scales.

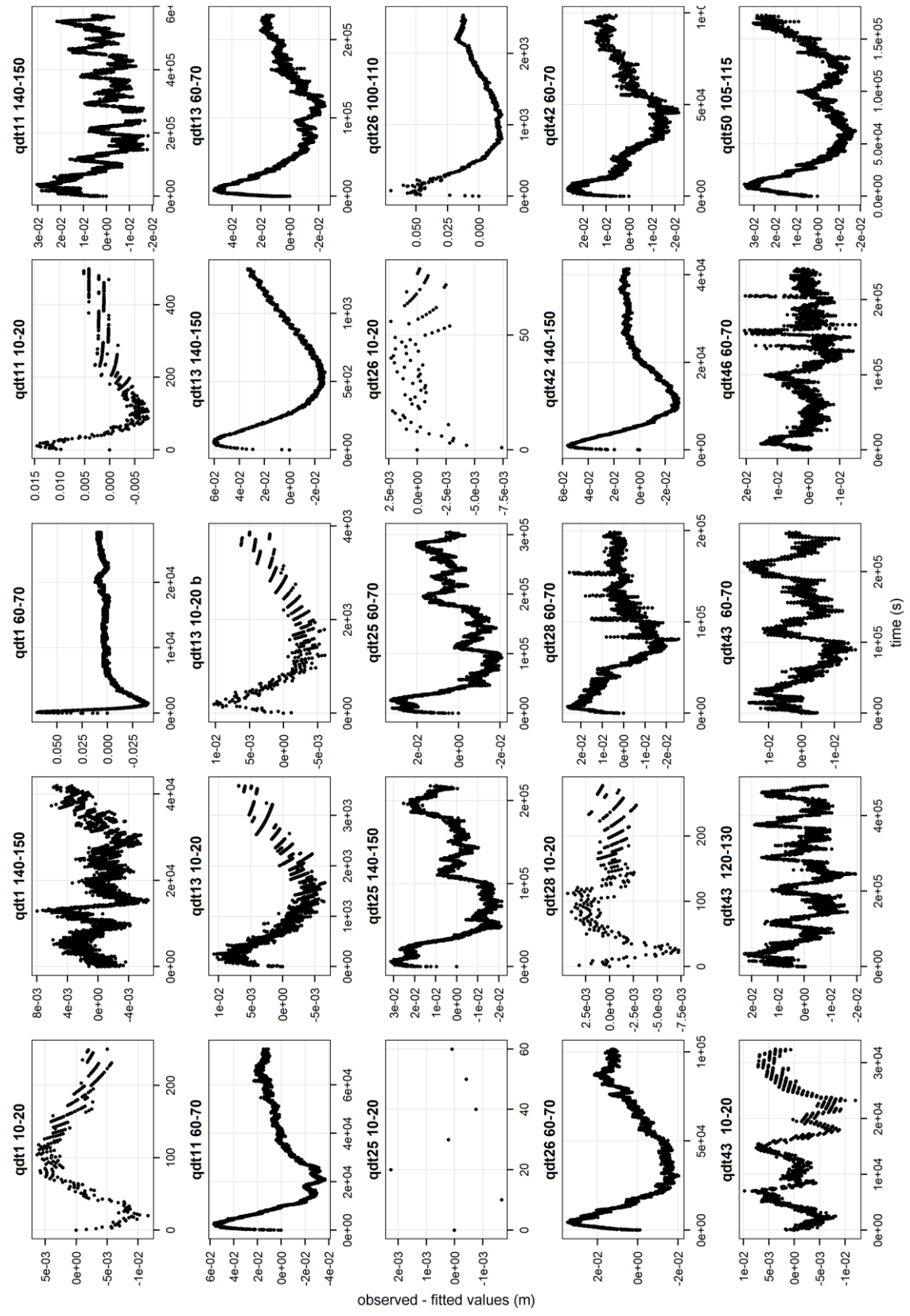

Figure 3-37. Hvorslev model residuals (temporary piezometers in peat).

The residuals shown are those of the Hvorslev model in which both T and Hwt were optimised. Tests are labelled according to the cluster name as per Figure 3-35 and to the depth of the piezometer intake during the test, in centimetres. Test "qdt13 10-20" was carried out twice. Note the different x and y scales.

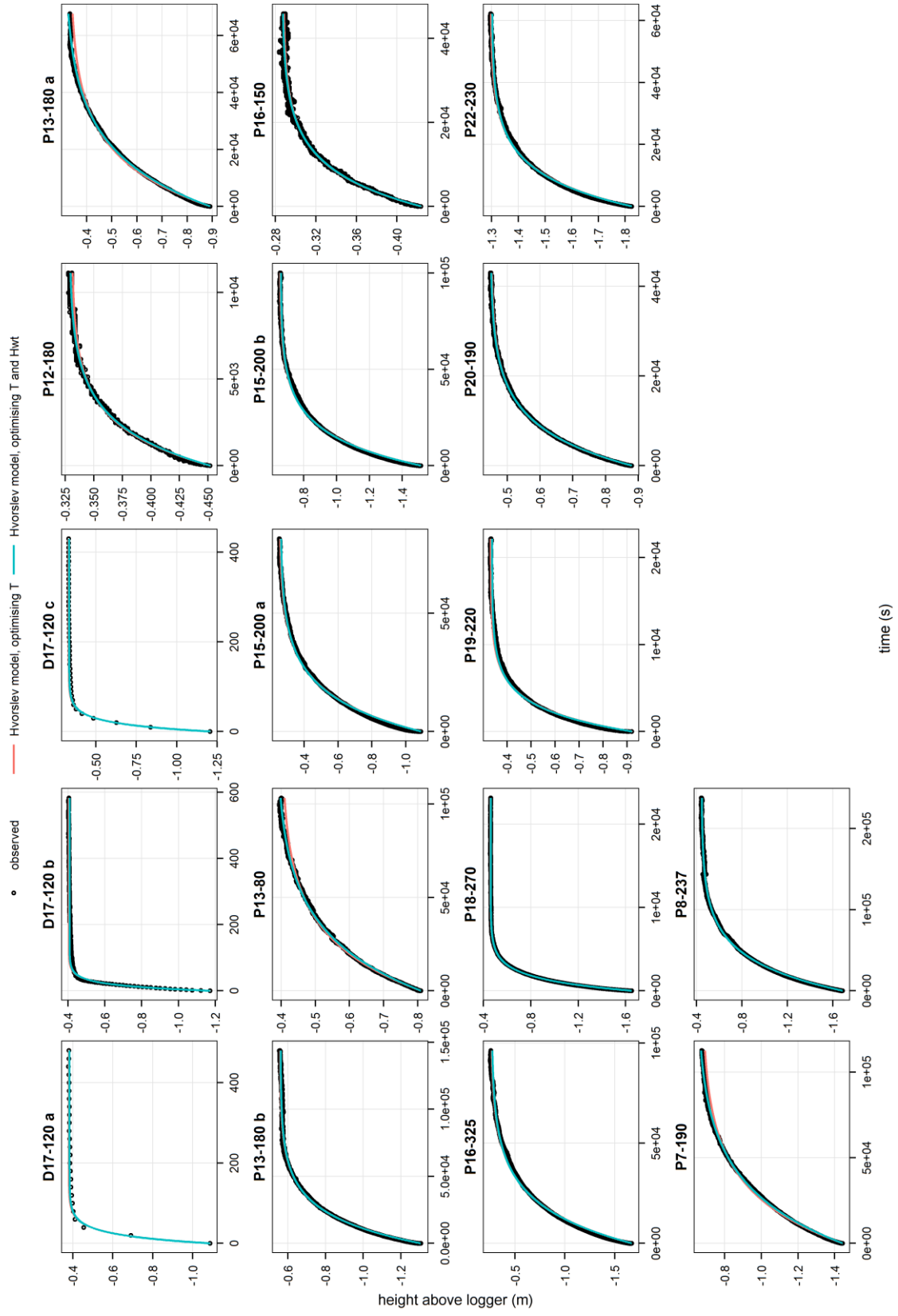

Figure 3-38. Recovery curves following slug tests in permanent piezometers.

Tests are labelled according to the cluster name as per Figure 3-35 and to the depth of the piezometer intake during the test, in centimetres. Test "qdt13 10-20" was carried out twice. Note the different x and y scales.

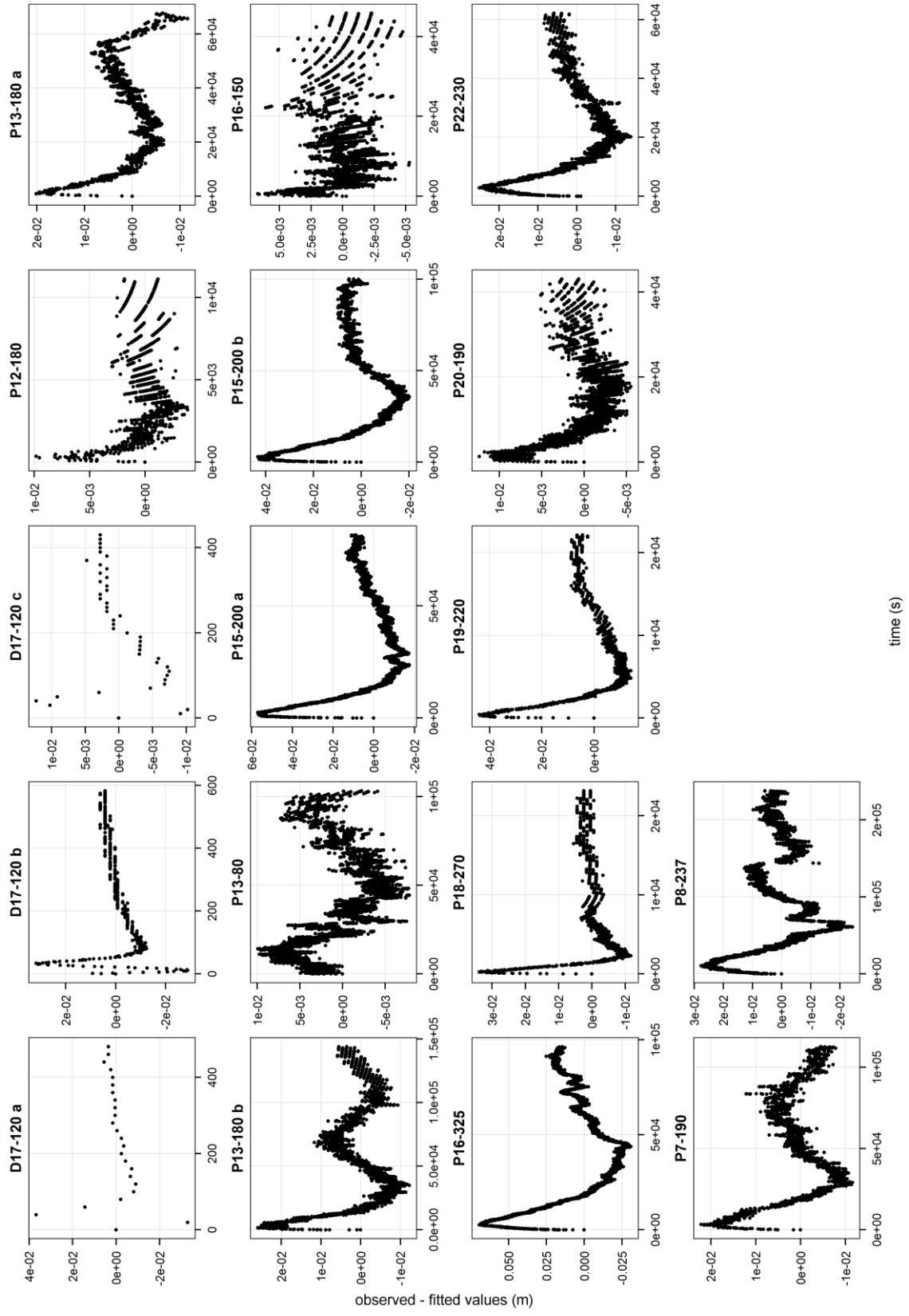

Figure 3-39. Hvorslev model residuals (permanent piezometers).

The residuals shown are those of the Hvorslev model in which both T and Hwt were optimised. Tests are labelled according to the cluster name as per Figure 3-35 and to the depth of the piezometer intake during the test, in centimetres. Test "qdt13 10-20" was carried out twice. Note the different x and y scales.

Galvin & Hanrahan (1967) attributed similar laboratory observations to air entrapment. It was latter shown that apparent departure from Darcy's law could be explained by the effects of matrix compression and swelling which cause variable water storage in peat (Hemond & Goldman 1985; Brown & Ingram 1988). The same explanation may hold for the departure from Hvorslev's theory apparent in Figure 3-37. However, the same residual pattern was found when the Hvorslev model was fitted to recovery curves obtained from permanent piezometers (Figure 3-38 and Figure 3-39), be it in peat or, crucially, in the underlying mineral formations. The maximum departure is similar in peat and mineral formations, in the order of 1-3 centimetres. This observation suggests that either alluvial deposits and in-situ saprolite have the same compressibility as humified peat, which is unlikely, or that the inverted S shape pattern observed in residuals is not caused by a particular physical property of the aquifer matrix, but rather by an equipment or analytical issue. Clearly more work is required to explain these patterns. Nevertheless, the departure from the Hvorslev model is relatively small, and probably negligible when compared to the very large variability of saturated hydraulic conductivity observed in both peat and mineral formations.

Figure 3-40 and Table 3-4 give the saturated hydraulic conductivity values measured in the peat using temporary piezometers. They show quite clearly that hydraulic conductivity in the superficial peat (10-20cm below surface) is 2-3 orders of magnitude higher than at higher depths. The existence of a conductive but shallow surface layer overlaying less permeable peats has long been recognised in many mires (Holden & Burt 2003), and forms the basis of the acrotelm-catotelm model sensu Clymo (1984). The median hydraulic conductivity 10-20cm below the surface is 2.6×10^{-5} m.s^{-1}, but values measured at this depth vary by three orders of magnitude, compatible with values found in the literature (Letts *et al.* 2000) for fibric to hemic peats. This reflects the high spatial variability in the humification rate of surface peat already described in Section 3.4. Such a large spatial variability also exists in ombrotrophic mires such as blanket bogs (Holden & Burt 2003).

The hydraulic conductivity is slightly less variable 60-70cm below ground level. The median value at this depth is 4.3×10^{-8} m.s^{-1}, compatible with values given in the literature for hemic to sapric peats (Letts *et al.* 2000). However the variability in hydraulic conductivity increases again 1.0-1.5m below ground level. In some clusters (qdt26, qdt13), the hydraulic conductivity even increases substantially between 0.6-0.7m and 1.0-1.5m. Again this highlights the large heterogeneity of peat hydraulic properties in acidic fens, where the presence of coarse mineral alluvium within the peat, its varied botanical origin, the spatial and long-term temporal

variability of peat moisture and the subsequent variability in peat humification, as well as localised water flow caused by springs or upwelling below the peat layer lead to a generally more complex stratigraphy than found in raised bogs. The classical model of a regular decrease in hydraulic conductivity with depth caused by an increasing humification of peat often described from raised bogs is therefore not valid in acidic fens.

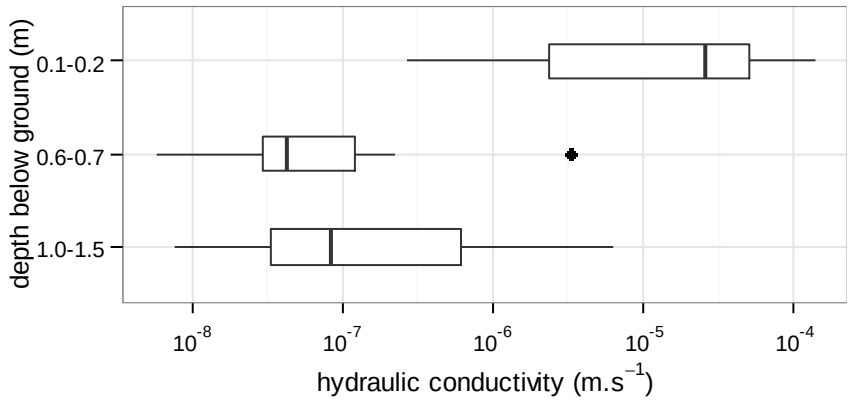

Figure 3-40. Boxplot of hydraulic conductivities measured in peat using temporary piezometers, according to depth.

Table 3-4. Hydraulic conductivities ($m.s^{-1}$) measured at different depths in peat using temporary piezometers.

Location	0.1-0.2m	0.6-0.7m	1.0-1.5m
qdt25	1.39 10^{-04}	4.26 10^{-08}	5.27 10^{-08}
qdt26	1.11 10^{-04}	1.21 10^{-07}	2.88 10^{-06}
qdt11	3.95 10^{-05}	2.21 10^{-07}	7.60 10^{-09}
qdt28	2.60 10^{-05}	2.62 10^{-08}	-
qdt1	2.55 10^{-05}	3.33 10^{-06}	1.37 10^{-07}
qdt13	2.35 10^{-06}	2.92 10^{-08}	6.40 10^{-06}
qdt43	2.67 10^{-07}	4.06 10^{-08}	1.11 10^{-08}
qdt42	-	1.01 10^{-07}	3.67 10^{-07}
qdt46	-	5.76 10^{-09}	-
qdt50	-	-	4.90 10^{-08}

Table 3-5. Hydraulic conductivities ($m.s^{-1}$) measured in peat and underlying mineral formations using permanent dipwells and piezometers.

Piezometer	Top of intake (m below ground)	Bottom of intake (m below ground)	Material	Hydraulic conductivity ($m.s^{-1}$)
D17-120 a	0.2	1.2	gravel	4.75 10^{-05}
D17-120 b	0.2	1.2	gravel	1.57 10^{-05}
D17-120 c	0.1	1.2	gravel	3.18 10^{-05}
P18-270	1.5	2.7	gravel & saprolite	1.90 10^{-07}
P19-220	1.5	2.2	gravel & saprolite	1.31 10^{-07}
P20-190	1.4	1.9	gravel & saprolite	4.11 10^{-08}
P22-230	1.9	2.3	gravel & saprolite	6.98 10^{-08}
P13-80	0.5	0.8	peat	2.60 10^{-08}
P16-150	1.2	1.5	peat	3.59 10^{-08}
P12-180	0.7	1.8	saprolite	2.90 10^{-07}
P13-180 a	1	1.8	saprolite	1.55 10^{-08}
P13-180 b	1	1.8	saprolite	2.16 10^{-08}
P15-200 a	1.3	2	saprolite	2.51 10^{-08}
P15-200 b	1.3	2	saprolite	3.56 10^{-08}

Table 3-5 (continued). Hydraulic conductivities ($m.s^{-1}$) measured in peat and underlying mineral formations using permanent dipwells and piezometers.

Piezometer	Top of intake (m below ground)	Bottom of intake (m below ground)	Material	Hydraulic conductivity ($m.s^{-1}$)
P16-325	3.1	3.25	saprolite	$2.05\ 10^{-08}$
P7-190	1.5	1.9	saprolite	$1.16\ 10^{-08}$
P8-237	2.1	2.37	saprolite	$7.27\ 10^{-09}$

3.6. Pedological survey of mineral soils

Verger (1998) dug and surveyed five pedological pits on Puy Rond and on mineral soils at the periphery of the wetland. A further five pits were dug and described in August 2012 as part of the current study, with the help of Bruno Gratia, teacher in pedology at the Meymac forestry school (Figure 3-41). Taken together, these surveys are thought to be broadly representative of the topographical and vegetation conditions found within the catchment (histosols excluded).

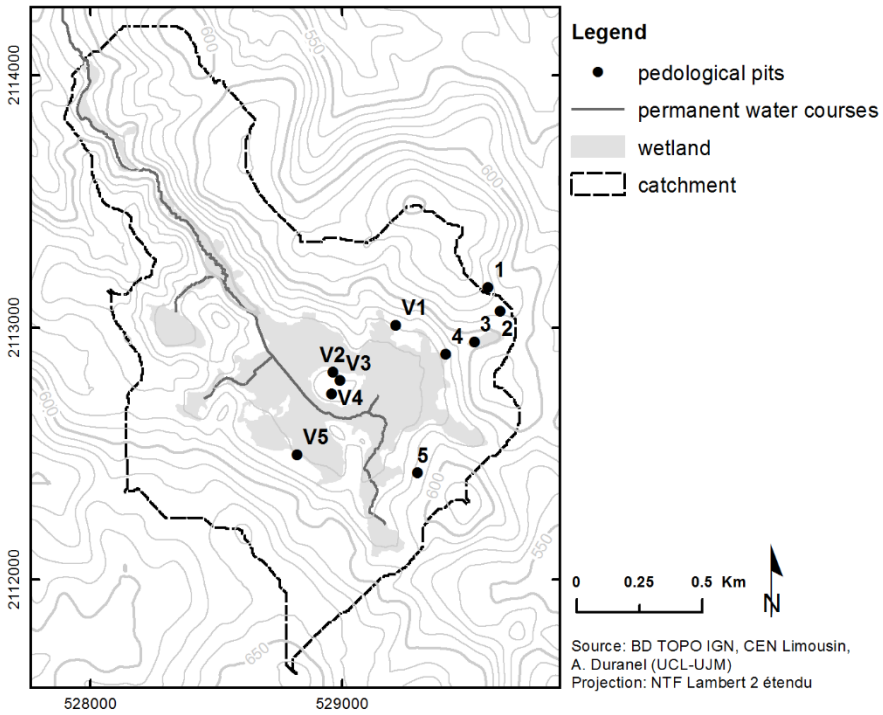

Figure 3-41. Location of pedological pits.

V1-V5: from Verger (1998), 1-5: this study.

The aim of the pedological survey was not to map soils precisely within the entire catchment, but to get a qualitative estimate of average soil characteristics to be used in the MIKE SHE model for the whole catchment, histosols excluded. The description of the pedological pits dug as part of this study is given in Appendix D. Together with soil profiles described by Verger (1998), they show that soils outside the wetland are generally relatively deep (40-70cm), even on hilltops and

relatively steep slopes such as those found on Puy Rond. It should be noted, however, that shallower profiles are regularly encountered on rock outcrops on steep slopes for instance. According to the French pedological classification (Baize & Girard 2009), they mostly belong to acidic *podsosols ocriques, allocrisols* and *brunisols*. Texture is loamy-sandy to sandy-gravelly, and drainage is always good. The clay content is slightly higher in illuvial situation at the bottom of small depressions but even there no sign of reduction could be seen and these topographic conditions are rare outside the wetland boundaries.

3.7. Conclusion

The analysis of sections cutting through periglacial deposits show that they are very patchy. Head is frequently missing and shallow when present. No fragic horizon was found. In the Monts d'Ambazac, Flageollet (1977) noted that bedded grus and head matrix are very similar to in-situ saprolite in terms of granulometry. Together with the absence of a fragic horizon, this suggests that, within the Dauges catchment, periglacial deposits can be considered equivalent to in-situ saprolite in terms of their hydrological behaviour.

Even though the use of hilltops and slopes for arable farming in the early 19th century suggests the presence of at least some loose material, the widespread occurrence of large man-made stone piles and occasional large granite outcrops in land previously ploughed suggests shallow saprolite depths. This was confirmed by ERT that only detected saprolite less than a couple of metres deep on an intermediate hilltop on the western boundary of the catchment. This is in line with field observations and the interpretation of airborne radiometry data made by Mauroux *et al.* (2009), who showed that most of the saprolite cover in the Monts d'Ambazac had been eroded away.

The presence of substantial depths of saprolite underneath the wetland is still uncertain. Seven existing geological drilling logs show the presence of a 15-40m deep saprolite layer north-east of Puy Rond, however the boreholes were all drilled in a restricted area along uranium-rich mineralised faults and may not be representative of the rest of the basin. Nevertheless they show that, for the least, saprolite has not been completely eroded away from the bottom of the basin east of Puy Rond. The ERT did not allow to find any evidence of saprolite at the bottom of the basin downstream of Puy Rond. This may be due to a complete evacuation of saprolite in this area or to similar resistivity values in saturated saprolite and in saturated fissured granite.

Additional ERT profiles along the existing boreholes would allow to calibrate the ERT results but could not be carried out due to equipment failure.

ERT transects show the presence of a densely fissured granite zone at least 50-60m deep in all investigated locations, with some variations in fissure density, seemingly larger underneath topographic lows, in line with the current understanding of differential weathering and erosion processes that lead to the formation of etch-basins in basement regions (Valadas 1984; Lageat *et al.* 2001). Existing geological drilling logs suggest a thickness ranging from 38 to 65m, with an average of 54m. The ERT shows clearly the presence of a relatively thick aquifer circulating in the fissured zone. On all profiles the margins of the wetland match the point where this aquifer cuts through the ground surface, suggesting a determining role of groundwater seepage in the mire water balance and a high degree of hydrological connectivity between the mire and its catchment.

The stratigraphical survey and slug tests in peat confirmed the presence of a poorly decomposed and highly conductive layer overlaying a more decomposed and less permeable layer. Hydraulic conductivities in the first tens of centimetres of the peat column are quite high, with a median value of $2.6x10^{-5}$ $m.s^{-1}$, and 2-3 orders of magnitude lower in the lower peat column, where a median value of $4.3x10^{-8}m.s^{-1}$. This is in line with many studies showing a rapid decrease of hydraulic conductivity with depth in mires (Ingram 1978; Ivanov 1981; van der Schaaf 1999, 2002) and corresponds to the classical acrotelm-catotelm model (in the broad sense, Morris *et al.* 2011) of mire hydrology. However it was shown that peat characteristics are highly variable. For instance, the depth of the poorly humified highly permeable superficial layer ranges from 0 to 60cm and could not be related to a number of potential explanatory variables.

This high spatial variability of peat physical characteristics is common to many mires. Brandyk *et al.* (2002) for instance found a large nugget effect when kriging peat bulk density, saturated moisture content, saturated hydraulic conductivity and van Genuchten's soil moisture retention parameters measured with a one-metre resolution in the Biebrza Basin in Poland, indicating large small-scale spatial variability. Within the Dauges mire, a large number of profiles are complex, for instance showing layers of poorly humified peat located beneath highly humified peat, which suggests substantial changes in surface wetness over time. Furthermore, alluvial deposits are commonly found within peat deposits, particularly along the main stream and downstream of Puy Rond, indicating stream migration. Substantial depths of highly permeable gravel deposits were found downstream of Puy Rond, which most probably increase exchanges between the

stream and the mire in this area. The stratigraphic survey also suggested a hydrological and pedological degradation of superficial peat in the north-eastern part of the peatland, associated to the disparition of peat-forming vegetation.

Résumé du chapitre 3

Ce chapitre a pour objectifs principaux de caractériser et de cartographier les formations géologiques ayant potentiellement un rôle important dans l'hydrologie de la tourbière des Dauges et de son bassin versant, en particulier les formations d'altération du granite (y compris les formations périglaciaires), les alluvions et les dépôts tourbeux ; de contribuer au développement d'un modèle conceptuel hydrogéologique du site ; et de décrire l'acquisition des données additionnelles nécessaires au développement d'un modèle physique distribué MIKE SHE.

Pour remplir ces objectifs, un ensemble de méthodes complémentaires ont été utilisées. Un modèle numérique de terrain à haute résolution a été développé à partir de levés topographiques au GPS différentiel et de données existantes. Les formations d'altération du granite ont été étudiées grâce à la réinterprétation des logs de sept sondages géologiques profonds réalisés par le CEA, la réalisation de quatre transects de résistivité de tomographie électrique, la recherche et l'analyse de coupes superficielles existantes, et une analyse sous SIG de la distribution spatiale d'indicateurs indirects de la nature des formations affleurant en surface. Les dépôts tourbeux et alluvionnaires ont été caractérisés et cartographiés par sondage au carottier russe, à la tarière manuelle et à la tige filetée.

L'analyse des quatre coupes superficielles disponibles montre que les formations périglaciaires sont discontinues. Les arènes remaniées à blocs sont fréquemment absentes, et très peu profondes lorsque présentes. Aucun horizon fragique n'a été mis en évidence. Dans les Monts d'Ambazac, Flageollet (1977) a montré que les arènes fauchées, les arènes litées et la matrice des arènes remaniées à blocs diffèrent très peu des arènes en place en terme de granulométrie. A l'intérieur de la zone d'étude, les formations péri-glaciaires peuvent donc être considérées comme équivalentes aux arènes en place d'un point de vue de leurs caractéristiques hydro-dynamiques.

La présence de terres arables dans la première moitié du 19e siècle sur les pentes et les sommets de certains puys en périphérie du bassin versant, attestée par les registres du cadastre napoléonien, suggère l'existence de matériaux meubles en surface, en particulier d'arènes. Néanmoins, la présence aux mêmes endroits de nombreux empilements de pierres d'origine anthropique et de quelques affleurements granitiques suggère que ces arènes sont peu profondes. Cela est confirmé par la tomographie de résistivité électrique, qui n'a permis de

détecter des arènes épaisses d'un à deux mètres environ que sur un puy d'altitude intermédiaire en périphérie ouest du site. Sur le reste des transects réalisés sur les sommets et pentes entourant l'alvéole principal, l'épaisseur des arènes, si présentes, est inférieure à la résolution verticale de la méthode, soit environ 1m. De même, l'analyse des coupes superficielles existantes a mis en évidence des épaisseurs d'arène de quelques mètres au plus. Ces observations sont en accord avec les investigations de terrain et radiométriques aéroportées décrites par Mauroux et al. (2009), qui ont montré que la plupart des arènes avaient été quasiment entièrement érodées dans les Monts d'Ambazac.

La présence d'épaisseurs substantielles d'arènes sous la zone humide reste incertaine. Les logs des sondages géologiques disponibles indiquent la présence d'arènes épaisses de 15 à 40m sous la partie nord-est de la tourbière. Néanmoins, ces sondages ont tous été réalisés dans une zone restreinte le long de failles minéralisées, dans le cadre d'une recherche de minerai uranifère orientée par des études géophysiques et radiométriques préalables. Ils ne sont donc pas représentatifs de l'ensemble du site. Ils montrent néanmoins que les arènes n'ont pas été entièrement évacuées de la partie située en amont du Puy Rond. A contrario, les trois transects de tomographie de résistivité électrique réalisés en aval du Puy Rond n'ont pas permis de mettre en évidence la présence d'arènes épaisses de plus de 1-2m. Cette observation peut s'expliquer soit par une érosion plus complète des arènes en aval du Puy Rond du fait d'une topographie plus favorable, soit par une équivalence en termes de résistivité électrique des arènes saturées et de la zone fissurée du granite. La réalisation de transects de tomographie de résistivité électrique supplémentaires et de sondages géologiques serait nécessaire pour résoudre cette ambiguïté.

La tomographie de résistivité électrique a permis de montrer que la zone fissurée du granite atteint des profondeurs d'au moins 50-60m sur toutes les zones prospectées, avec toutefois des variations du degré d'altération et de la densité de fissuration, ceux-ci étant plus importants sous les creux topographiques. Ces observations concordent avec les modèles actuels d'altération et d'érosion différentielle ayant conduit à la formation des alvéoles granitiques (Valadas 1984; Lageat et al. 2001). Elles sont aussi compatibles avec les sondages géologiques disponibles, qui indiquent que l'épaisseur de la zone fissurée est comprise entre 38 et 65m, avec une moyenne de 54m. La tomographie de résistivité électrique suggère que la zone fissurée constitue un aquifère continu. Sur tous les transects, les limites de la zone humide correspondent à l'affleurement en surface de la nappe circulant dans la zone fissurée du granite, ce qui suggère

un rôle déterminant des apports souterrains dans la balance hydrique de la zone humide et une forte connectivité hydrologique entre la zone humide et son bassin versant.

L'analyse stratigraphique du dépôt tourbeux et les tests de perméabilité confirment la présence en surface d'une couche de tourbe peu décomposée et très perméable, superposée à une couche plus humifiée et moins perméable. La conductivité hydraulique 10-20cm sous la surface est forte, avec une valeur médiane de 2.6x10-5 m.s-1. Elle est de deux à trois ordres de grandeur plus faible dans la partie inférieure du dépôt tourbeux, où une valeur médiane de 4.3x10-8 m.s-1 a été enregistrée. Ces données concordent avec de nombreuses études montrant une réduction rapide de la conductivité hydraulique avec la profondeur dans les tourbières (Ingram 1978; Ivanov 1981; van der Schaaf 1999, 2002) et avec le modèle classique acrotelme-catotelme (au sens large, Morris et al. 2011). Toutefois, le taux d'humification et la conductivité hydraulique de la tourbe varient très fortement dans l'espace. Par exemple, l'épaisseur de la couche superficielle peu décomposée varie entre 0 et 60cm, et n'a pu être corrélée à aucun des facteurs explicatifs potentiels étudiés. Un nombre important de profils stratigraphiques étudiés sont complexes, et témoignent de la présence de couches de tourbes peu décomposées sous des tourbes plus humifiées. De plus, des dépôts alluviaux de sables et de graviers sont fréquemment présents au sein de ou sous la tourbe, particulièrement aux abords du ruisseau et dans la partie aval de la zone humide. Ces dépôts alluvionnaires, très perméables, favorisent les échanges souterrains entre le ruisseau et la zone humide sur ce secteur. L'analyse stratigraphique indique également une dégradation hydrologique et pédologique de la tourbe en surface dans la partie nord-est de la zone humide, associée à la disparition des espèces turfigènes.

Chapter 4. Hydrology: data acquisition and qualitative analysis

4.1. Introduction

This chapter has two main objectives:

- to describe the acquisition of hydrological time-series required to calibrate and validate the model;
- to develop a conceptual model (in the hydrogeological meaning of the term) of water circulation to, from and within the mire based on a qualitative analysis of hydrological time-series and of the geological model developed in Chapter 3.

River stage and discharge in and out of the mire, groundwater table depths both in and around the mire, and piezometric heads in the peat and underlying superficial mineral formations were monitored for a period of two to three years. Time-series were corrected to account for substantial drift observed in automatic loggers.

Hydrological time-series were analysed using a range of methods including principal component analysis and visual inspection of depth exceedence frequency curves, vertical piezometric gradients at specific locations and horizontal piezometric gradients along transects representative of the hydrological functioning of the wetland.

4.2. Stream stage and discharge monitoring

4.2.1. Methods

Discharge was measured at five locations shown on Figure 4-1. In drains and small streams in the upstream part of the wetland, discharge was measured using V-notch weirs and automatic stage loggers installed at three suitable locations in July and September 2010. A location was deemed suitable if the large-scale and small-scale ground topography was such that all surface flow from the upstream catchment would go through the weir, and if the stream slope was such that water sprung free of the notch whatever the discharge.

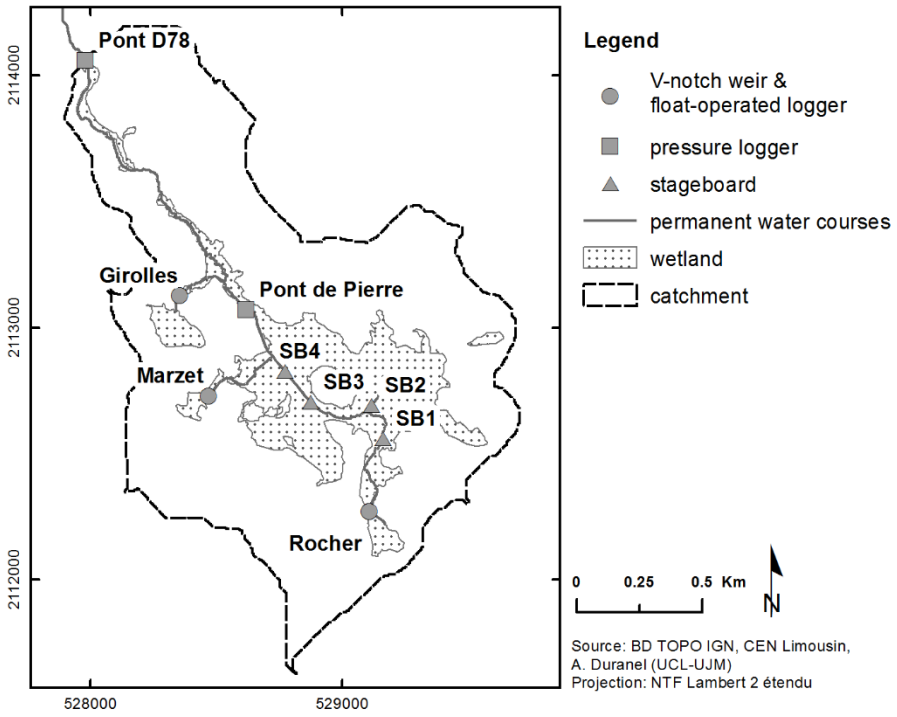

Figure 4-1. Automatic gauging stations and manual stageboards at the Dauges site.

Unfortunately, such locations were rare, and it was for instance not possible to accurately measure surface flow through the north-eastern boundary of the wetland because drain channels in this area are shallow and not well defined. The weirs were hand-made using water-resistant plywood for the body of the weir and 1mm-thick aluminium strips for the sharp edge of the notch (Figure 4-2). The peat on the side of the stream was cut using a hand saw, and the weir was hammered into position. It was levelled as precisely as possible, and its bottom and sides were made watertight using pieces of humified peat and, where necessary, bentonite. Water tightness was checked on a regular basis during the duration of the study. A mm-graduated ruler was installed on the upstream side of the weir as far away as possible of the notch to measure the height of the water above the point of the notch. A float-operated automatic stage logger (Thalimèdes, OTT) was installed in a stilling well upstream of the weir at a distance equal to four times the maximum width of the V-notch (Herschy 2008). Logger data were regularly checked against actual stage, and when instrument drift had occurred, they were post-corrected assuming a linear drift since the last check. Fifteen-minute resolution stage data were converted into discharge using the stage-discharge equation for sharp crested V-notch weirs provided by Dingman (1994, p. 544) :

$$Q = C_w g^{1/2} tan\left(\frac{\theta_w}{2}\right)(Z_w - Z_v)^{5/2} \qquad \text{Equation 4.1}$$

where g is the gravitational acceleration, θ_w is the V-notch angle in degrees, Z_v the elevation of the base of the V-notch, Z_w the elevation of the water surface and C_w a weir coefficient, taken as equal to 0.43. In larger streams the installation of a V-notch weir was not possible for practical and regulatory reasons. It was therefore necessary to establish a stage-discharge relationship by periodically measuring flow for a range of stage values.

Figure 4-2. V-notch weir and float-operated stage logger in its stilling well at Rocher.

Two gauging stations were installed, one at the main outlet of the wetland, and the other at the outlet of the NNR and of the research catchment. The former was installed in December 2010 at a location called Pont-de-Pierre, where the stream is 2m wide and 0.8m deep and has a straight long profile and a relatively constant cross-section due to past channel engineering. The latter was installed in September 2009 at the mouth of a small culvert underneath the D78 main road. The culvert is rectangular in section, 1m wide and approximately 1.5m high (Figure 4-3). Stream stage was monitored every 15 min using Orpheus-Mini loggers (OTT) installed in stilling wells. A stageboard was also installed near each logger to allow for the logger data to be regularly checked against an independent benchmark. Stage loggers at both stations showed a substantial linear drift over time, which was modelled as a linear function of time using ordinary least square regression. Stage records were corrected accordingly. Disharge was periodically measured by the NNR staff using a Nautilus C2000 electromagnetic flowmeter (OTT).

Figure 4-3. Gauging station at the catchment outlet, with the pressure logger in its stilling well..

Unfortunately, after a year of measurements, it was discovered that the flowmeter had been faulty since the start of the monitoring. Consequently, data collected from September 2009 to December 2010 had to be discarded, and discharge measurement could only resume in June 2011. Additional measurements were carried out in 2012 using a FlowMate 2000 electromagnetic flowmeter and in 2011 using salt dilution gauging during low and medium flow events, following the method described in Moore (2004, 2005) and using a CTD diver (Schlumberger Water Services) logging at 1Hz to measure specific conductance. The stage-discharge relationship was modelled using different least-square based statistical techniques. First, a power law was fitted by non-linear least-square regression using the nls() function of R. The equation used took the following shape:

$$Q = C(h + a)^n \qquad \text{Equation 4.2}$$

where Q is the discharge, h the measured stage, C and n constants, and a the datum correction. The datum correction is the inverse of the stage reading when flow is null, and was determined

by looking at stages recorded in early July 2011, when flow stopped for a very short period at the Pont-de-Pierre station. Second, a polynomial (cubic) model was fitted by ordinary least squares using the lm() function of R. It took the following shape:

$$Q = C1(h + a) + C2(h + a)^2 + C3(h + a)^3 \quad \text{Equation 4.3}$$

Terms in the model were tested for significance by comparing nested models with an F-test and removed if not significant. Thirdly, in order to extrapolate the stage-discharge curve beyond the highest measured discharge, the stage-area-velocity method (Herschy 2008) was used. The cross-section of the stream bed was surveyed using differential GPS (see Section 5.3.1.3). At the Pont-de-Pierre station, it was not possible to survey the bed exactly where the logger had been installed due to overhanging trees, and the stream was surveyed a few metres downstream of the logger instead. Since this stretch of the stream had been engineered in the past, cross-sections were similar. The lowest point of the section was assumed to correspond to the zero flow stage, and the empirical stage-wetted area relationship was calculated. The mean velocity was calculated for each discharge measurement by dividing discharge by the corresponding wetted area. A stage-mean velocity relationship was estimated using linear regression. Discharge was then estimated for each observed stage by multiplying the corresponding mean velocity and wetted area. Observed stages and estimated flows at a fifteen-minute resolution were aggregated to daily means using the same aggregation period as the one used for rainfall (from 6:00am on day d, not included, to 6:00am on day d+1, included) following WMO guidelines (see Appendix E).

Within the main wetland, stage was measured manually at four stageboards distributed along the permanent water courses (Figure 4-1) and fixed to 10cm diameter wooden posts hammered in the stream bed. The stageboards were levelled using DGPS or a total electronic station. Measurements were taken approximately every two to three weeks, simultaneously to groundwater table manual measurements in piezometers (Section 4.3).

4.2.2. Results and discussion

4.2.2.1. D78 culvert (catchment outlet)

The Orpheus-Mini logger at the D78 culvert gauging station showed a substantial drift over time (Figure 4-4). The scatter is compatible with the expected accuracy of the manual measurements, obtained from a centimetre-graduated stageboard and within +/-15min of the logging time. Drift

was assumed to be linear, modelled as a function of time using linear regression, and the stage data were corrected accordingly. The linear model predicted a 0.004m difference between logger- and manually-recorded stages when the logger was first set up in September 2009, compatible with the accuracy of manual measurements.

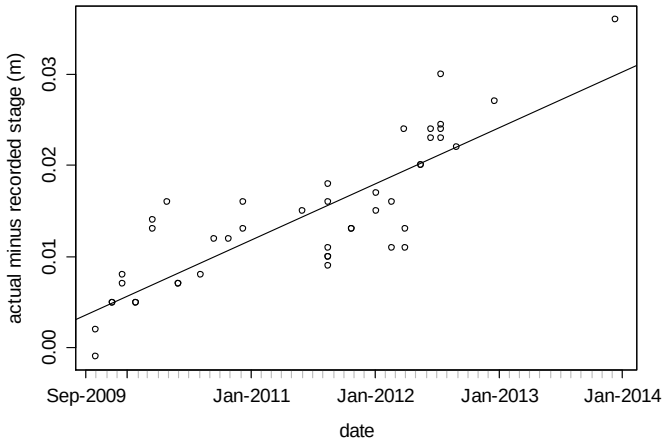

Figure 4-4. Logger drift at the D78 gauging station.

The line shows the fitted linear model.

Figure 4-5 shows the adjusted logger-recorded stage as well as the stage observations undertaken manually at the time of discharge measurements. Figure 4-5 shows two substantial issues. Firstly, zero flows have been measured twice (each time using the Nautilus flowmeter) at relatively high stages, highlighted on the figure by the two horizontal dotted lines. Secondly, there is a clear upward trend in stage records. Unfortunately, due to the flowmeter fault, any change in the stage-discharge relationship that occurred before the spring of 2011 cannot be directly assessed. Correlations with stage further upstream could only be examined after the Pont-de-Pierre logger was set up in December 2010.

Figure 4-6 shows the relationship between stages at both stations as a function of time, symbolised by a colour scale. The scatter shape should not change over time if the stage-discharge relationship remained constant at both stations. This is clearly not the case. There has been a small but distinct change in the relationship between stages at both stations in April or May 2011: the red to orange points form a line slightly below the main scatter of points and parallel to it, suggesting the entire stage-discharge curve was affected. This may have coincided with the brief but large flooding event that occurred on 02/05/2011 and that could have mobilised sediments and changed the channel section a short distance downstream of the D78 logger. Earlier stage records cannot be reliably converted to discharge and should therefore not be relied upon.

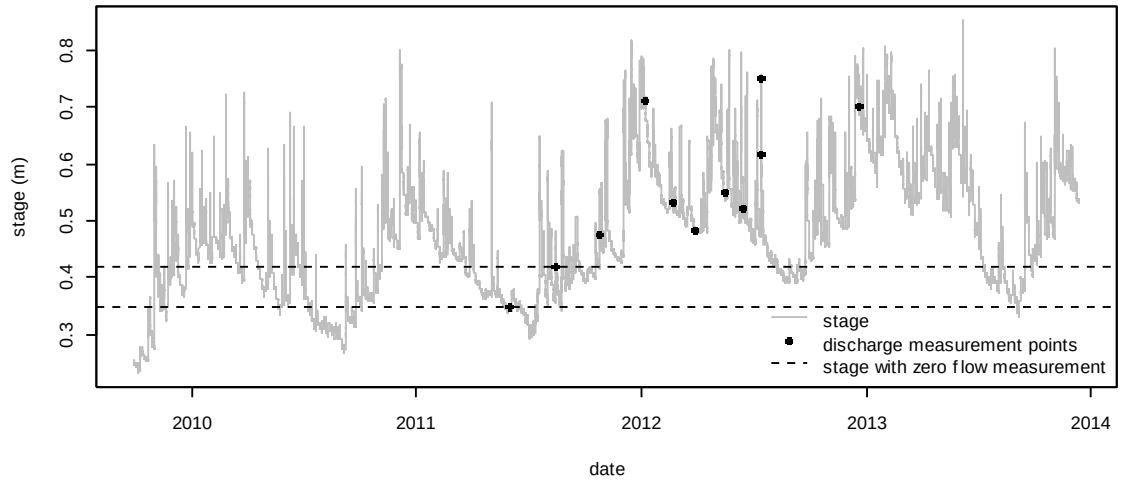

Figure 4-5. Stream stage at the D78 gauging station.

The black dots show the manually-recorded stage at the time of discharge measurements.

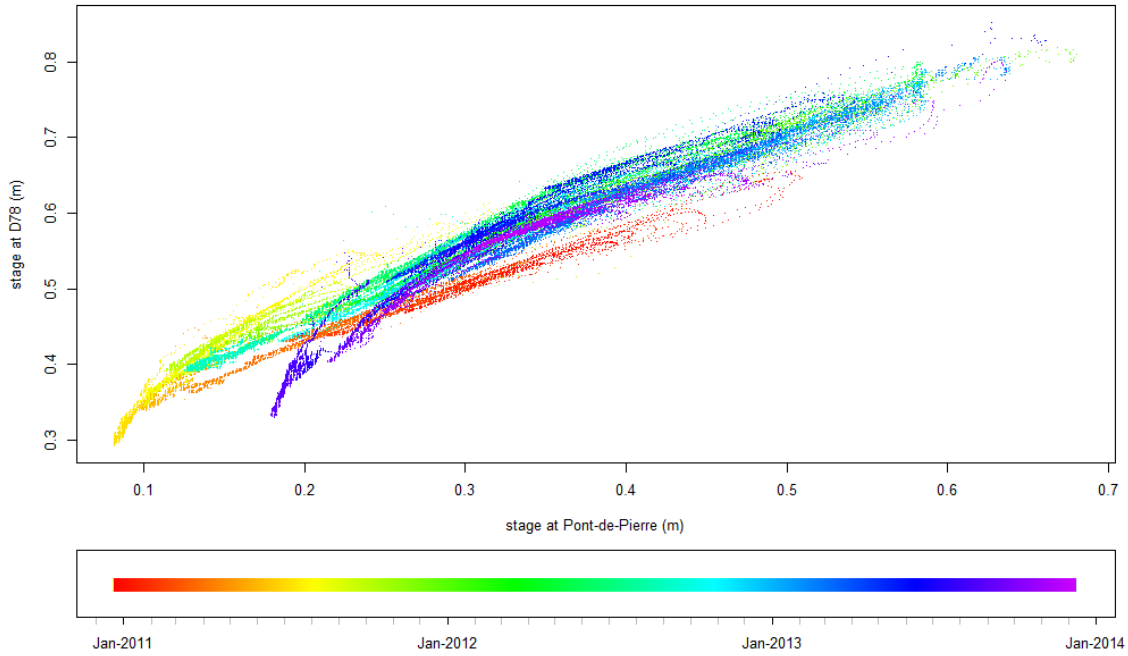

Figure 4-6. Scatterplot of stage records at Pont-de-Pierre vs. D78.

Figure 4-6 also shows that the relationship between stages at both gauging stations changed at low stages (less than 0.5m at D78 and less than 0.25m at Pont-de-Pierre, navy blue to purple points) around June 2013. Stages at the D78 station were indeed slightly lower in summer 2013 summer than in summer 2012, whereas stages at the Pont-de-Pierre station followed the opposite pattern. It is however difficult to pinpoint in which station the stage-discharge relationship actually changed. All float-operated loggers upstream of the wetland stopped working following a large flow event in June 2013 and could not be used for comparison. This issue is further discussed in Section 4.2.2.2. Figure 4-5 shows that, at the D78 station, zero flows

were measured at relatively high stages below which the water level dropped substantially for relatively long periods, even after May 2011. In August 2011, a discharge of 7.3 $l.s^{-1}$ was measured using dilution gauging while the Nautilus flowmeter measured a zero flow. This is due to the fact that, following the apparent change in channel section, water is ponded at low flow, the wet area is quite large and velocities are too small to be measured using the flowmeter. As only one dilution gauging could be undertaken at low flow for logistical reasons, the accuracy of the stage-discharge relationship would therefore be reduced at low stages. Furthermore, Figure 4-7 shows that stage-discharge measurement points are relatively scattered at high stages, above 0.6-0.7m.

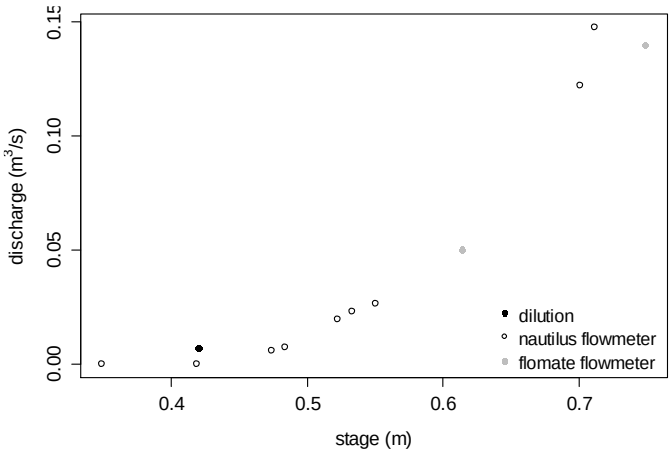

Figure 4-7. D78 stage-discharge scatterplot.

Overall, the estimation of discharge from stage records at the D78 gauging station is fraught with a number of substantial issues, and it was decided not to use these records any further. To improve the accuracy of the records in the future, it would be necessary to remove sediments that have accumulated downstream of the gauging station to lower the downstream topographic controls back to their 2009-2010 original levels and to stabilise the stream profile. Another possibility would be to build a raised flume-like structure at the mouth of the culvert to increase velocity and get rid of the influence of topographic controls downstream.

4.2.2.2. Pont-de-Pierre (main wetland outlet)

The Orpheus-Mini logger showed a substantial drift over time. Drift was apparently linear, and was therefore modelled as a function of time using linear regression. The values predicted by the model were used to correct the stage data. Figure 4-8 shows a scatterplot of "actual" (i.e. manually-recorded using the permanent stageboard) vs. logger-recorded data.

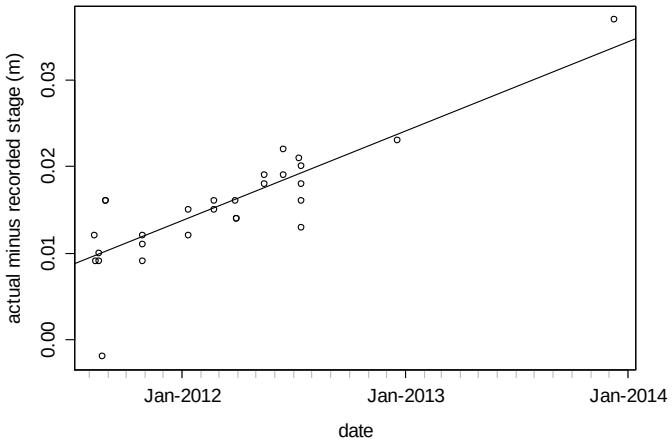

Figure 4-8. Logger drift at the Pont-de-Pierre gauging station.

The line shows the fitted linear model.

The scatter is compatible with the expected accuracy of the manual measurements, obtained from a centimetre-graduated stageboard and within +/-15min of the logging time. The linear model predicted a 0.003m difference between logger- and manually-recorded stages when the logger was first set up in December 2010, compatible with this assessment of measurement accuracy. Figure 4-9 shows corrected stage records and flow measurement points at the Pont-de-Pierre gauging station, at the outlet of the wetland. It shows that the average recorded stage at Pont-de-Pierre has slightly increased over time at low flows. Lower stages during the 2011 summer compared to the 2012 summer can be explained by lower flows during the 2011 drought.

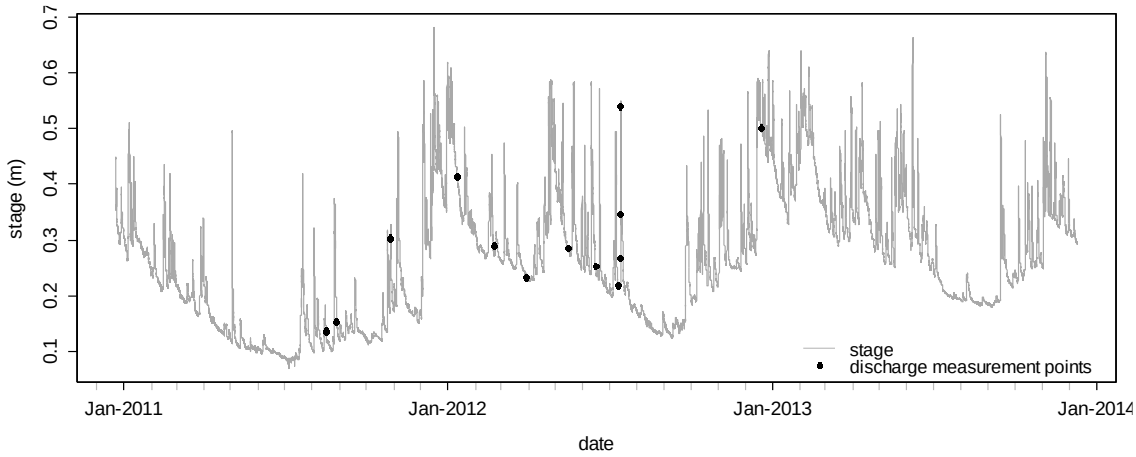

Figure 4-9. Stream stage at the Pont-de-Pierre gauging station.

The black dots show the manually-recorded stage at the time of discharge measurements.

The total rainfall from 01/10/2010 to 30/09/2011 was 989mm, whereas it was more than 1300mm in the previous and following hydrological years, and total potential evapotranspiration was also higher. The stream actually dried out for a few days in summer 2011 while it never did

in 2011. However, the higher stages recorded during summer 2013 cannot unequivocally be explained by higher stream flows, and it may well have been the result of a change in the stage-discharge relationship. This is evidenced by Figure 4-6, that shows that the relationship between stages at the D78 and Pont-de-Pierre stations have changed at low stages around June 2013 (less than 0.5m at D78 and less than 0.25m at Pont-de-Pierre). In the absence of direct flow measurement in 2013, it is difficult to pinpoint at which gauging station this change in stage-discharge relationship occurred. However, even if it occurred at the Pont-de-Pierre station, the effect on flow estimation will be limited to the low stages (less than 0.25m) of the summer 2013, and therefore the potential water balance error will be small.

Issues encountered at both gauging stations highlight the dynamic nature of stage-discharge relationships in small pristine headwater streams. The construction of a more permanent and stable gauging station would be advisable if reliable flow measurements are to be pursued at the Pont-de-Pierre wetland outlet. Figure 4-9 shows that the discharge measurements were relatively well distributed throughout the range of observed stages. The highest recorded stage was 0.680m, whereas the highest stage at a time when a flow measurement was undertaken was 0.538m. The latter stage was only exceeded in 1.8% of the 15min-resolution records. This happened at least once in 57 days out of the 1084 days for which records are available. Several methods were tested to fit a curve to the stage-discharge scatterplot. Figure 4-10 shows stage-discharge scatterplots with the fitted power and polynomial models.

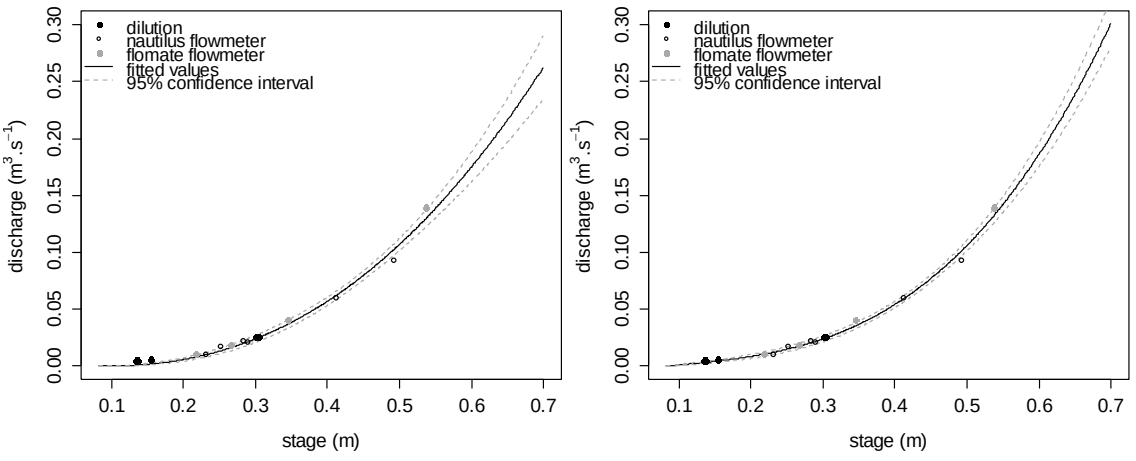

Figure 4-10. Power (left) and polynomial (right) stage-discharge curves at the Pont-de-Pierre gauging station.

The polynomial model fitted the data better than the power model, especially at low flow, with a RMSE of 0.00401 vs. 0.00478 respectively. When extrapolated to stages higher than 0.538m, it predicted larger discharges than the power model. It took the following form:

$$Q = 0.0575(h - 0.082) + 1.1037(h - 0.082)^3 \qquad \text{Equation 4.4}$$

where Q is discharge and h the stage (adj. R^2=0.992, F-statistic: 973.4 on 2 and 14 df, p-value <0.001). The power model took the following form (a determination coefficient cannot be given as it does not make sense for non-linear regression):

$$Q = 0.7713(h - 0.082)^{2.2794} \qquad \text{Equation 4.5}$$

The statistical models were checked against the stage-discharge curve estimated by the stage-area-mean velocity method. Figure 4-11 shows the results obtained for each step of the procedure: topographic survey of the cross-section, linear modelling of the stage – mean velocity curve, calculation of the stage – wet area curve from the topographic section, and calculation of the stage – discharge relationship by multiplying the predicted mean velocity and wet area for each possible stage. If one excludes measurements of discharge made at stages below 0.2m, points on the stage - mean velocity scatterplot were quite well distributed along a straight line, which was modelled as a linear function of stage and used to derive the stage-wetted area curve. Higher mean velocities at stages less than approximately 0.2m are probably due to small-scale differences in the bed topography between the actual section where flow measurements were made and the section that was surveyed using DGPS, the latter being a few metres downstream of the former (the stream could not be surveyed immediately adjacent to the logger due to overhanging trees).

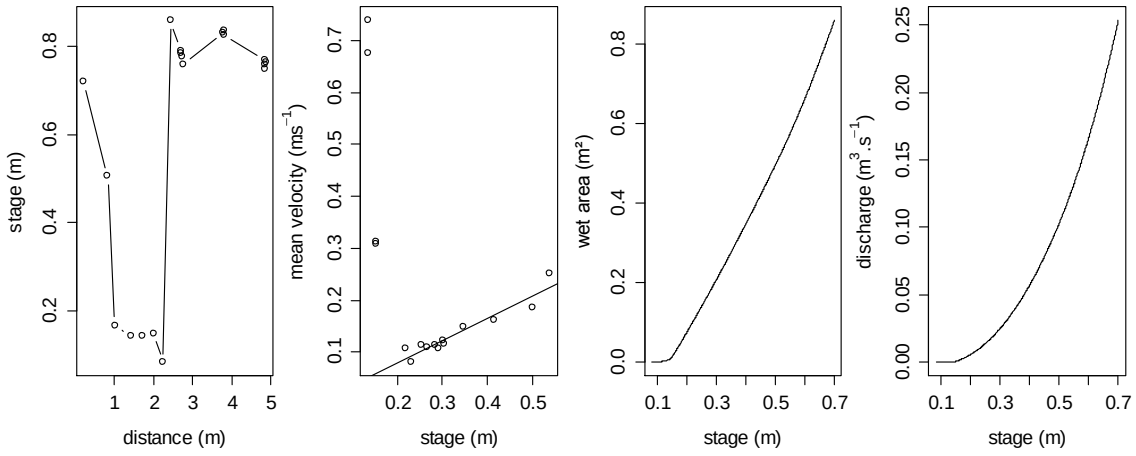

Figure 4-11. Stage-area-mean velocity plots at the Pont-de-Pierre gauging station.

From left to right: stream bed cross-section; mean velocity – stage scatterplot (the line is the linear model fitted to the points, excluding stages <0.2m); wetted area – stage curve; stage-discharge curve.

At higher stages, since the stream was engineered in the past and has a very regular cross-section, the wetted areas of both sections become similar. Discharge estimates made using this method will therefore not be accurate at stages less than about 0.2m.

Figure 4-12 shows the stage-discharge curves obtained using the three different methods. The fitted power curve and the stage-area-velocity curve are almost identical at stages less than 0.538m, and, when extrapolated to stages higher than the highest stage with a flow measurement, also give very similar results. Both under-predict low flows, when stage is below 0.2m approximately and the stage-wetted area relationship changes.

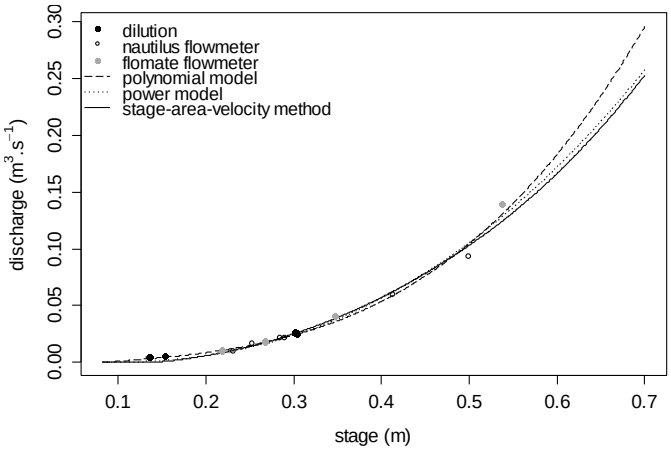

Figure 4-12. Comparison of stage-discharge curves established with different methods at the Pont-de-Pierre gauging station.

The polynomial model has a better fit in the lower part of the stage-discharge scatterplot but largely over-predicts discharge when extrapolated beyond 0.538m. To improve accuracy at both ends of the stage-discharge relationship, the final rating curve at the Pont-de-Pierre gauging station was therefore derived from a combination of both the polynomial model for low stages and the stage-area-mean velocity curve for larger stages, the cut-off point being taken as 0.2695m, where both curves cross each other. Figure 4-13 shows the discharge calculated using the adjusted stage records and the composite rating curve.

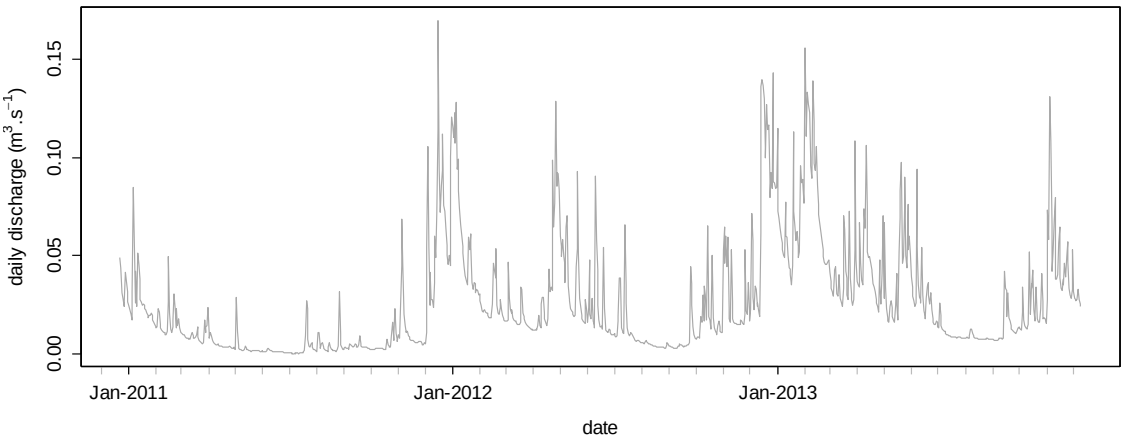

Figure 4-13. Daily mean discharge at the Pont-de-Pierre gauging station.

4.2.2.3. Rocher, Marzet and Girolles

The float-operated stage loggers (Thalimedes, OTT) used in the smaller streams upstream of the wetland proved far less reliable than the pressure loggers (Orpheus-Mini, OTT) used at Pont-de-Pierre and at the D78 culvert. For instance the cable that operates the recording pulley is easily dislodged by sudden large flood events, as happened on 07/06/2013 when all three loggers stopped recording simultaneously. For logistical reasons it was not possible to resume recording and this event therefore signalled the end of stage recording upstream of the wetland. The logger initially installed at Rocher also became faulty in early October 2010 and could only be replaced two months later. A delay in data downloading in late 2012 due to logistical constraints meant that data collected between 16/12/2012 and 17/02/2013 were overwritten when the device memory got full at a later stage.

The temporary weirs proved relatively efficient and robust, however a limited number of issues were encountered. First, a leak developed underneath the weir at Rocher in February 2012 and could only be stopped in March 2012. Second, even though the weir itself had been fenced off at Marzet, cattle trampled the stream downstream of it, which meant that the flow through the notch was not free for approximately a month in summer 2011. Third, debris became trapped in the weir V-notch at Girolles in early summer 2012, meaning that stage got over-estimated for approximately two months. In each case, the start of the problematic period was identified by checking stage time-series against each other, and data collected during these periods were deleted. Figure 4-14 shows the daily mean discharge measured using V-notch weirs in the upper part of the catchment.

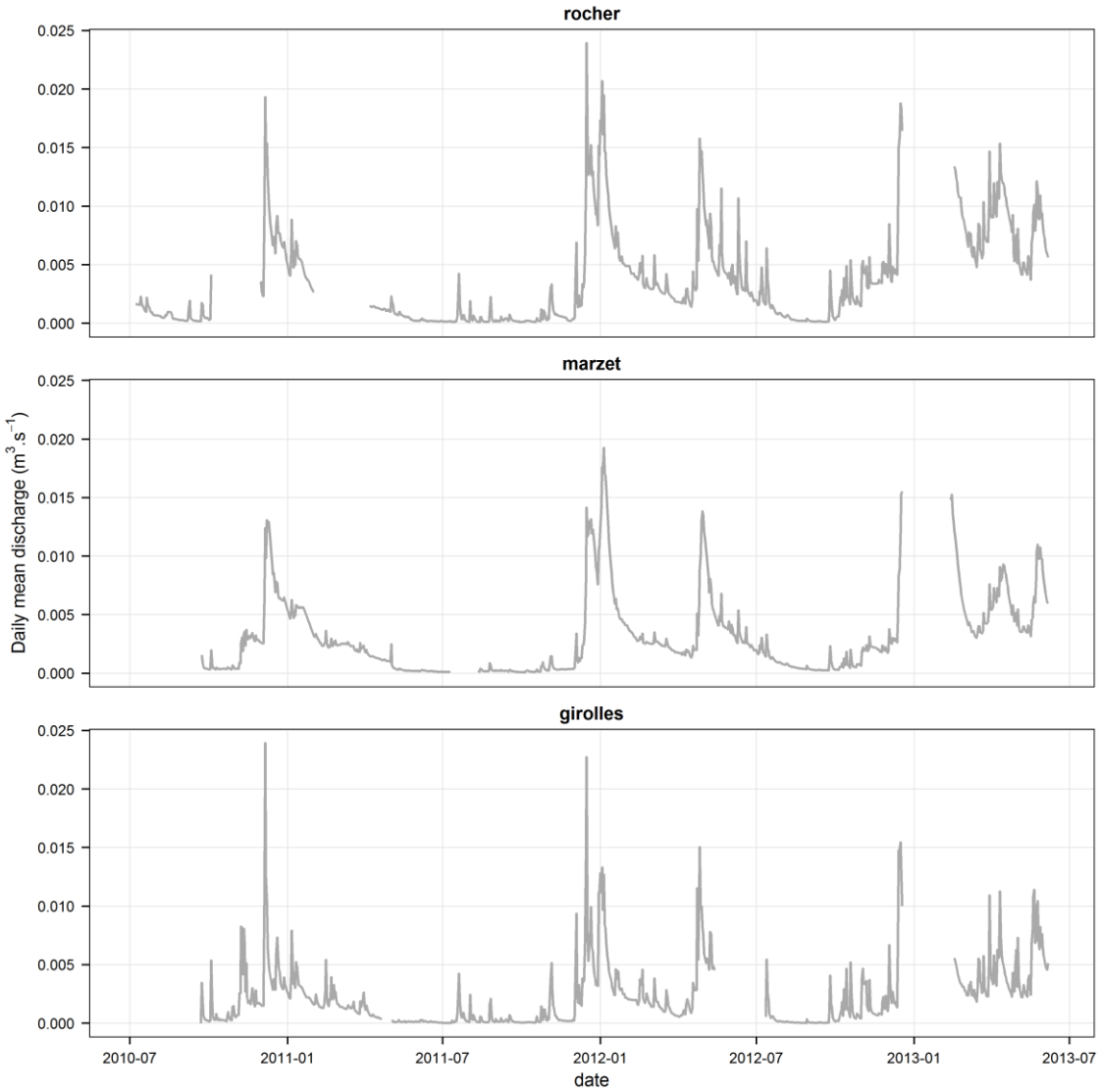

Figure 4-14. Daily mean discharge at the upstream gauging stations.

4.2.2.4. Stageboards

Figure 4-15 shows manually-recorded stage using the 4 stageboards distributed along the permanent watercourses within the main wetland. Together with continuous stage records at the main wetland outlet, at the Pont-de-Pierre station, the manual records suggest that the range of stream water levels increases from upstream to downstream. This may be due to the fact that stream channels are rather ill-defined in the upper part of the wetland, where the flow is often diffuse or subterranean and over-bank exchanges with the wetland dampen peak flows; whereas the channel gets deeper, larger and better defined further downstream, accommodating most of peak flows within its banks.

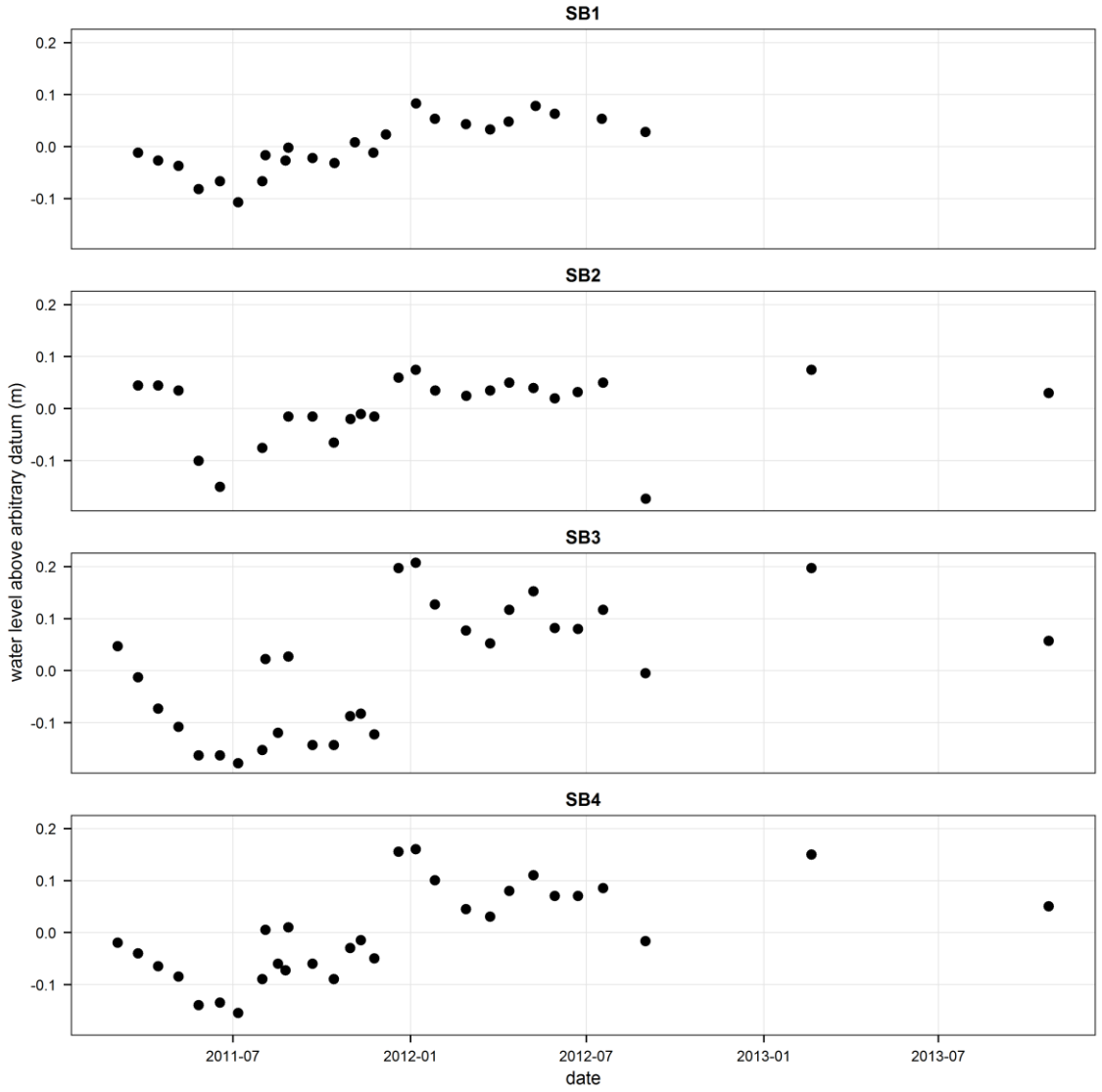

Figure 4-15. Manual stage records.

4.3. Piezometry

4.3.1. Methods

4.3.1.1. Equipment

A total of 57 piezometers and dipwells were installed between December 2010 and April 2011 to monitor the piezometric head in the main peat horizons and in the upper-most part of the underlying mineral formations. Unfortunately due to financial and technical constraints it was not possible to install boreholes in the weathered granite formations in the upper part of the catchment. Within the wetland, dipwells and piezometers were arranged in 21 clusters that were themselves distributed along three transects from the mineral soils at the foot of the valley

slopes just outside the wetland to the lower part of the wetland close to its outlet (Figure 4-16). One transect (clusters 26 to 17) follows the line of lowest slope from the north-eastern footslope, the other two (clusters 3 to 8 and 9 to 17) are perpendicular to it. This design was chosen to minimise the amount of time required to check all piezometers while maximising the diversity of topographical, geological, pedological and ecological contexts for which hydrological information can be obtained within the wetland.

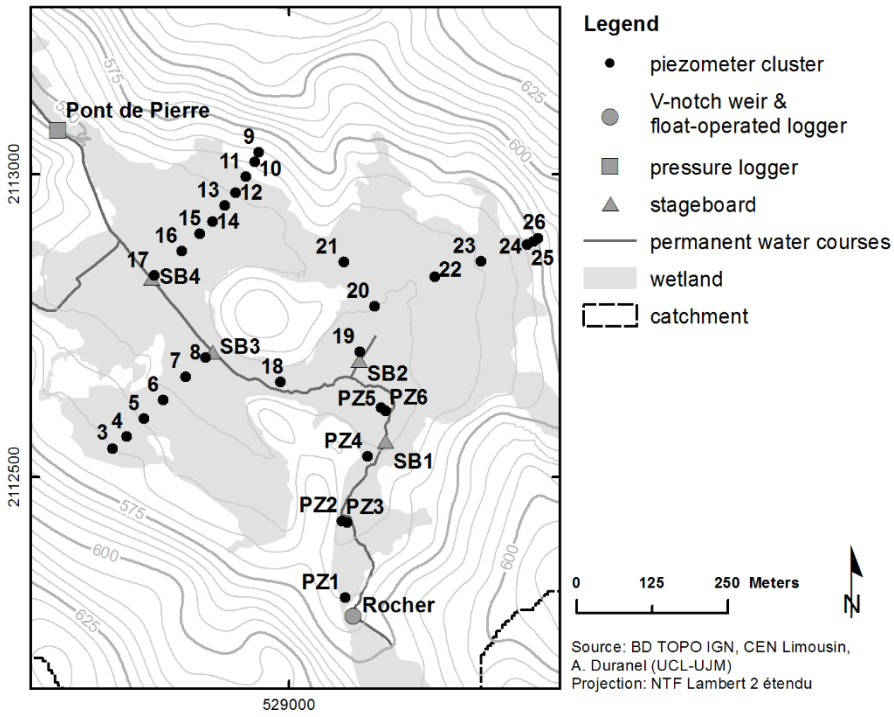

Figure 4-16. Location of piezometer clusters.

Each cluster includes at least one dipwell and between one and three piezometers depending on the depth and variability of the peat column and of the nature of the underlying mineral substrate, which were determined by hand augering. Wherever possible, four tubes were installed: one deep (1.0-1.5m) dipwell, in which an automatic logger could be inserted to measure the water table depth all year round; one shallow dipwell in the peat acrotelm; one deep piezometer in the catotelm; and one piezometer in the underlying mineral substrate. In mineral soils outside the wetland, only one deep dipwell was installed. Table F-1 in Appendix F gives the details of the piezometers and dipwells installed within the site.

All piezometers and dipwells were made of 32mm external diameter (27mm internal diameter) PVC tubes. The diameter was chosen so that it was small enough to make installation easier and the piezometers more reactive to actual changes in the water table in the surrounding soil material, especially in the low-permeability highly humified peat (Holden & Armstrong 2007),

but large enough to accommodate automatic loggers (which are 22mm in diameter). To prevent tubes from silting up, they were screened using a highly permeable geotextile. To install piezometers in the mineral substrate underneath the peat, a 5cm hand auger was used to create a hole with a slightly larger diameter than the tube. To prevent artificial movement of water between the mineral substrate and the upper peat horizons, and to be able to detect a potential vertical piezometric gradient, a bentonite seal was installed at the mineral/peat interface. The space left between the tube and the hole wall was then filled with bentonite pellets.

Figure 4-17. Dipwell and piezometer before installation in the ground.

Left: dipwell (short tube) and piezometer (long tube) with the (black) socket of permeable textile protecting the screened area. Right: close-up view of the bentonite seal. A longitudinally-slotted plastic glass is taped at the desired position along the tube, filled with bentonite pellets, and closed with tape. This allows for the bentonite pellets to be positioned precisely at the desired depth, generally that of the less conductive peat layer just above the mineral/peat interface. After installation of the tube in the ground, bentonite pellets are pushed in the space left between the tube and the hole wall using a stick to extend the seal to the surface.

Dipwells inserted into mineral soils were installed in a similar way, but sand was used to back fill the space left between the tube and the hole, and a bentonite seal installed at ground surface level to prevent surface runoff from flowing directly into the dipwell. Piezometers and dipwells installed in the peat layer were pushed into it after a driving hole of a slightly smaller diameter had been created with a 30mm diameter screw-headed soil auger. Tubes belonging to a same cluster were installed 20-30cm apart. The tubes stuck out of the ground surface by 20-30cm. As the site is cattle-grazed, this design was chosen to minimise disturbance by cattle: the tubes are tall enough for the cattle to see them and to make them difficult to be stamped upon, but short

enough to prevent cattle from rubbing themselves against them. In three years, only one dipwell, installed in mineral soil in a place where cattle frequently rest, was damaged. Data from six pre-existing dipwells were also available (labelled PZ1 to PZ6 in Figure 4-16). These were installed in October 2009 by a specialised contractor. They were made of 50mm PVC tubing drilled all the way up, cut at ground level and topped with a metal cap. Unfortunately, these are deeply anchored into the underlying mineral substrate, which makes the interpretation of the data difficult in case of vertical movement of water from or towards the mineral substrate. A shorter additional dipwell, limited to the peat layer, was therefore installed in October 2011 near each existing dipwell for control purposes.

The water level in all dipwells and piezometers was measured approximately every fortnight from the installation date to the late summer of 2012 using a water level metre (SDEC). Sixteen pressure loggers (SWS Mini-Diver, 0-10m range) were initially installed in a selection of dipwells thought to best represent the range of hydrological conditions that could be found within the wetland (dipwells D3-100, D6-70, D7-130, D8-100, D9-130, D10-120, D11-100, D12-100, D13-100, D15-100, D16-120, D17-120, D18-100, D20-100, D21-140 and D23-130). The position of some pressure loggers was re-evaluated in late October 2011 for three different reasons. Firstly, some loggers (D6-70, D20-100) had become faulty. Secondly, it was realised that the groundwater table in the peat was below the bottom of dipwell D23-130 more than half the time, and the logger was transferred to dipwell D22-130 where manual checks had shown that this was not the case. Thirdly, manual checks had shown that there was a substantial upward hydraulic gradient between the underlying mineral formations and the peat, and it was decided to equip some piezometers inserted in the mineral formations (P7-190, P13-180, P15-200 and P22-230) to investigate the seasonal variation of this gradient in more detail. In clusters 7 and 13, manual checks proved that the groundwater table in the peat did not drop below the bottom of the shallowest dipwell as was initially feared, and the logger was therefore moved from the longest dipwells (D7-130 and D13-100) to the shallowest dipwells (D7-70 and P13-40). This was to ensure that the data were better representative of the groundwater table depth in the peat and not biased by upwelling, particularly in the case of dipwell D13-100 that was inserted in both peat and saprolite due to the shallowness of the peat layer at that location.

Pressure records were compensated for atmospheric pressure and converted to hydraulic head above diver using data from a barometric logger (SWS Baro-Diver). To reduce artefacts caused by the water level loggers and the barometric logger being exposed to different temperatures (Cuevas *et al.* 2010), the latter was suspended at the bottom of a 1m-long dry tube inserted into

the peat at the centre of the mire. The tube was groundwater- and rainfall-proof but in full communication with the atmosphere.

4.3.1.2. Elevation of piezometers

In the field, water level was always recorded relative to the top of the dipwell or piezometer, be it manually or automatically. The elevation of one tube per cluster – generally the deepest dipwell - was surveyed using DGPS, as described in Section 3.2.1. The elevation of other tubes within the same cluster was then surveyed relative to the reference dipwell using a spirit level and a tape measure, allowing for the water level records to be converted to elevation above the reference NGF69 datum. Only then were water levels converted to depth below ground level. Given the very uneven micro-topography and the gradual transition between living vegetation and soil that characterise mires, ground elevation is difficult if not impossible to define precisely in such environments. It can vary by several centimetres from one side of the piezometer to the other, even for small diameter tubes, and can vary rapidly through time depending for instance on *Sphagnum* growth and saturation.

To allow for water table levels expressed as depth below ground to be compared within piezometers belonging to the same cluster, a common ground elevation was defined for all tubes belonging to the same cluster, based on ground elevation around the dipwell surveyed using DGPS. Ground level was defined as the mean of a minimum of three DGPS elevation measures taken within 30 cm of this dipwell and spread around it. Measuring the altitude of the ground was especially challenging for the six dipwells that were installed prior to this study in a part of the wetland dominated by *Molinia caerulea* which forms large tussocks. Consequently, even though the depth of the water below the top of each tube could be measured with an accuracy of a few millimetres, and the water level relative to the NGF69 datum could be calculated with an accuracy of a few centimetres, its position relative to the ground level was much more approximate. Furthermore, the measured ground level might not correspond to the minimum level at which overland flow occurs if the tube is located in a local depression. This explains why, in some dipwells, the mean water table may be constantly a few centimetres above ground level when the mire is fully saturated in winter. The consequences of this issue for hydrological modelling of wetlands are discussed in Section 6.4.1.

As a result of the variation in the amount of water stored in the peat, ground level in mires varies according to seasonal (Gilman 1994) and even diurnal cycles. Consequently, water levels recorded in shallow dipwells that are not inserted in the mineral substrate underneath the peat

layer but anchored onto the peat surface, and that are monitored using the dipwell top as the reference datum, might not truly reflect the actual elevation of the water table relative to a standard datum. Conversely, dipwells that are inserted deep in the peat or in the underlying substrate might give data that are not representative of the water table depth relative to the ground level. To measure peat surface movement and to ensure that data from shallow dipwells could be compared with data from deep piezometers, the vertical movement of four representative shallow dipwells was recorded from December 2011 to September 2012. This was achieved by manually measuring the distance between the top of each dipwell and the top of a long iron rod hammered into the underlying mineral substrate a couple of centimetres away from this dipwell.

4.3.2. Results and discussion

4.3.2.1. Vertical movement of peat surface and piezometers.

A small vertical movement of shallow piezometers was detected, with lower and larger elevations measured during dry and wet periods respectively. This corresponds to the "mire breathing" phenomenon classically described in the literature (Gilman 1994; Camporese *et al.* 2006) and caused by both the desaturation and shrinkage of peat on one hand, and the loss of buoyancy on the other hand. The maximum annual amplitude recorded at the Dauges site was between 3 and 5mm, depending on the dipwells (Figure 4-18, Table 4-1). This is much smaller than values cited in the literature: Gilman (1994), for instance, measured amplitudes of more than 10cm in a Somerset fen.

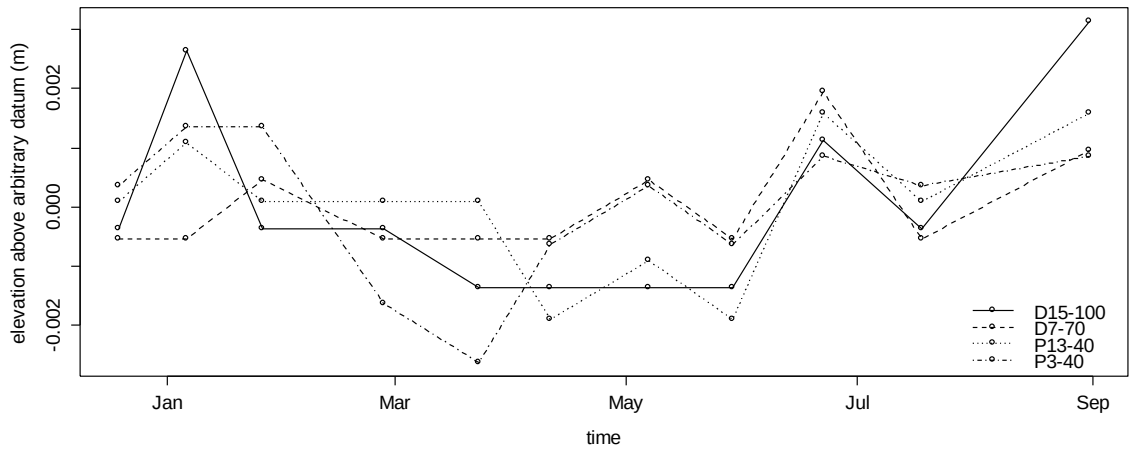

Figure 4-18. Movements of selected shallow piezometers relative to an arbitrary datum.

Table 4-1. Amplitude of piezometer movements.

Piezometer	Movement amplitude (m)
D15-100	0.005
D7-70	0.003
P13-40	0.004
P3-40	0.004

The smaller movements observed at the Dauges site may be explained by a shallower peat layer and a more stable water table compared to the site cited above. Consequently, ground movement is not a substantial issue and it is possible to compare water tables in tubes that are anchored in the underlying mineral substrate and in those that are not. Water tables can be expressed relative to a standard datum, to the top of the tube or to the ground surface.

4.3.2.2. Quality control of piezometric data

The manual dipper used by the NNR staff to manually record water table depth in piezometers proved to be somewhat inadequate to get accurate readings. This was due to two factors. First, the electrical conductivity of the water was on some occasions too low to switch the dipper light on in some piezometers, and staff had to rely on the sound produced by the dipper entering the water to measure its depth. Second, the dipper had a relatively voluminous metal head that displaced 10.6 cubic cm of water before the electrodes contacted the water. In narrow 27mm ID tubes inserted in poorly permeable peat, this can result in a maximum increase in water head of 1.9cm. The actual water head increase caused by the dipper head depends on the permeability of the peat around the top of the water column which makes the head displacement difficult to predict. The error introduced by the dipper was therefore estimated by repeating some measurements using a mm-graduated tape measure. This could only be carried out when the water level in the tube was sufficiently shallow to be clearly visible by eye. The results are given in Figure 4-19 and show that the dipper records a slightly higher water table depth than it actually is (median 0.013m, n=68).

The error in piezometers equipped with loggers was actually smaller (median 0.006m, n=30) and was considered low enough to use the dipper data without further correction to calibrate the loggers. On top of the error associated with manual readings, there were several other sources of error that could not be alleviated when calibrating the loggers. The first one is the accuracy of the logger system itself, with an accuracy given by the manufacturer of ±0.5 cm H_2O for the Mini-Divers and ±0.5 cm H_2O for the Baro-Diver.

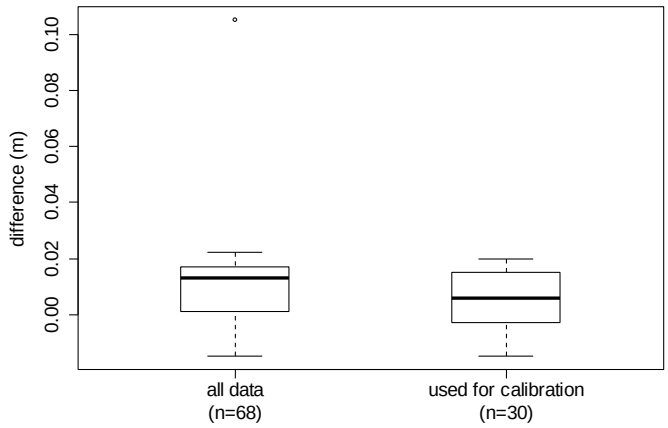

Figure 4-19. Boxplots of water table height manual reading errors, as estimated by the difference between readings made with the manual dipper and with a tape measure. The right boxplot shows the estimated errors of manual readings used to calibrate logger data.

The second one originates from the fact that the system does not allow for a reading to be taken at will while the logger is deployed within a dipwell or a piezometer. Manual readings were therefore very rarely precisely coincident with logger readings, and the logger-recorded water table depth at the time of the manual reading had to be approximated by using the closest logger reading. As much as 15min could therefore separate a manual reading and its corresponding logger reading, which in theory may have introduced some unquantified error if they were taken during periods of rapidly changing water table. In practice, manual checks were rarely carried out during large rainfall events so this source of error is probably negligible.

The larger source of error however originates in the considerable drift that the loggers experienced over the duration of the study. Figure 4-20 shows that there was an increasing difference between water table depths recorded by hand and by automatic loggers until late 2013. The offset seems to have stabilised or even decreased slightly after that date. On average, the logger system drifted by about 10-15cm over the first two years. As this trend is visible in most time series, it is likely that the barometric logger was responsible for most of the observed drift. It was also noticed that retrieving the barodiver from its protective tube to download it sometimes, but not always, resulted in sudden 1-3cm H_2O drops in pressure records, and consequently in equivalent increases in water table depth records. In some cases these changes were temporary and could be corrected, however in a few cases the changes seemed more durable and only gradually returned to normal, in which case the time-series could not be corrected. Individual piezometric loggers also drifted independently of the barometric logger, as shown in Figure 4-21.

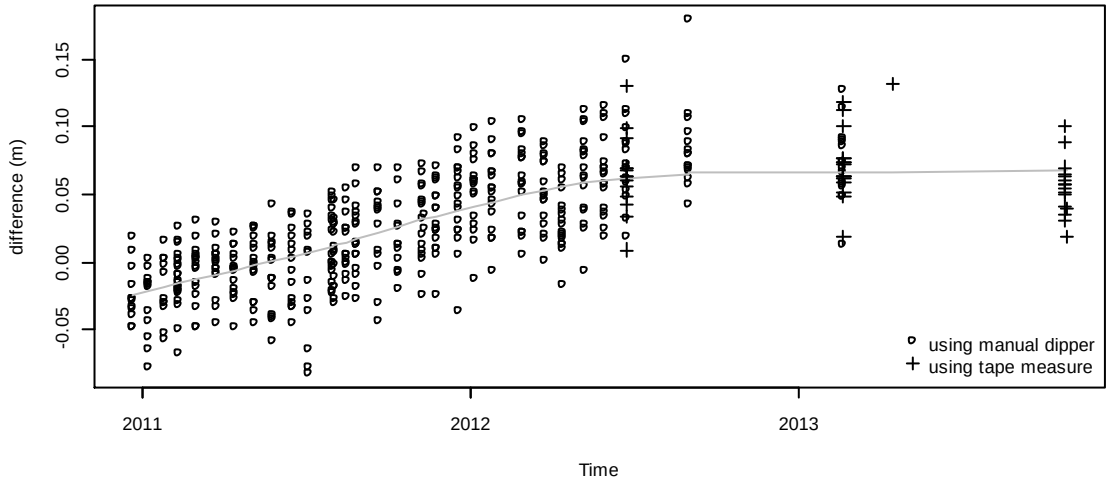

Figure 4-20. Difference between manually- and logger-recorded water table heights before correction for logger drift.

The grey line is a LOWESS smoother with a span of 2/3.

Given the uncertainty associated with control readings, correcting for drift by computing an offset from each manual control reading and for each period preceding that reading was not an option. Instead, a statistical approach was taken. Drift was non-linear for most loggers. An inflexion was noticeable from early 2013 onwards. Some seasonal cyclicity in drift was also noticeable in logger D17-120, and to a lesser extent in loggers D10-120, D3-100 and D8-100; with a larger rate of drift in summer than in winter. This may be related to the impact of temperature on the pressure sensors (Cuevas *et al.* 2010). Drift was therefore modelled as a function of time using Generalised Additive Models. A few loggers (D13-100, D22-130, P7-190) displayed linear drift, and others recorded too short time series (due to logger failure or redeployment) or displayed too much error to fit a GAM or confidently rely on such a model. In these cases (D12-100, D13-100, D14-100, D20-100a, D20-100b, D22-130, D23-130, D6-70, D7-130 and P7-190), drift was modelled as a linear function of time. All time-series were corrected by subtracting the drift modelled using either LM or GAM. Uncorrected and corrected time-series are shown in Figure 4-22. Unfortunately, regular manual checks stopped in late summer 2012, and therefore the uncertainty associated to the drift correction and to the time-series increases substantially after that date, as shown by the larger confidence intervals in Figure 4-21.

4.3.2.3. Piezometric levels.

Figure 4-23, Figure 4-24, Figure 4-25, Figure 4-26, Figure 4-27 and Figure 4-28 show the corrected piezometric heads in all dipwells and piezometers. In these figures, lines and points show data recorded using automatic loggers and manual dips respectively. Ground elevation was taken as

identical within each cluster and piezometric heads can be directly compared between piezometers belonging to the same cluster. Logger-recorded piezometric heads were aggregated to daily means. A number of dipwells and piezometers proved too short to provide continuous water table records, particularly in mineral soils just outside the mire boundary (9, 10, 25 and 26). This was also the case in short dipwells inserted in very shallow peat (clusters 11, 12, 14, 17 and 21), but where these clusters were equipped with a logger it was installed in longer dipwells inserted in both peat and underlying formations. Despite being inserted 130cm deep in peat, dipwell D23-130 proved too short during most of the dry summer of 2011. The logger was therefore moved to cluster 22 in August 2011. P4-60, a piezometer with a 10cm long intake inserted in the lower part of the peat layer, gives records that are difficult to interpret given the piezometric heads recorded in other piezometers belonging to the same cluster. It is possible that the peat around the intake got substantially smeared during its installation and impedes water flow into the piezometer.

The distribution of water table depths recorded in dipwells equipped with loggers and inserted in peat (or in peat and saprolite where the peat layer is very shallow, as is the case in dipwells D11-120, D17-120, D20-100 and D21-140) were summarised visually using both kernel density estimation graphs (Figure 4-30) and depth exceedence frequency curves (Figure 4-31). Both graphs summarise the position of the water table relative to ground level over periods of one year. In density estimation graphs, the area below the curve (more exactly left of the curve in this particular case) is always one, and therefore the density gives an estimation of the proportion of time during which the water table was at a given depth. Depth exceedence frequency curves give the proportion of time during which the water table was above a given depth.

Principal Component Analysis was used to visualise the differences between individual dipwells in terms of water table behaviour (Figure 4-32). On the PCA plots, the distance between dipwells approximates their Euclidian distance in the multidimensional space made of all record dates, and therefore, their similarity in terms of hydrological behaviour. For the manually-recorded dataset, the PCA first axis makes for nearly 90% of the dataset inertia, meaning that the whole dataset can be accurately summarised by a single gradient. This gradient is correlated to all the synthetic descriptors as shown by the grey arrows on the plot ($p<0.001$ in all cases, based on 999 permutations), and separates dipwells in which the water table is deep and has a large inter-seasonal amplitude from those where the water table is shallow and stable throughout the year.

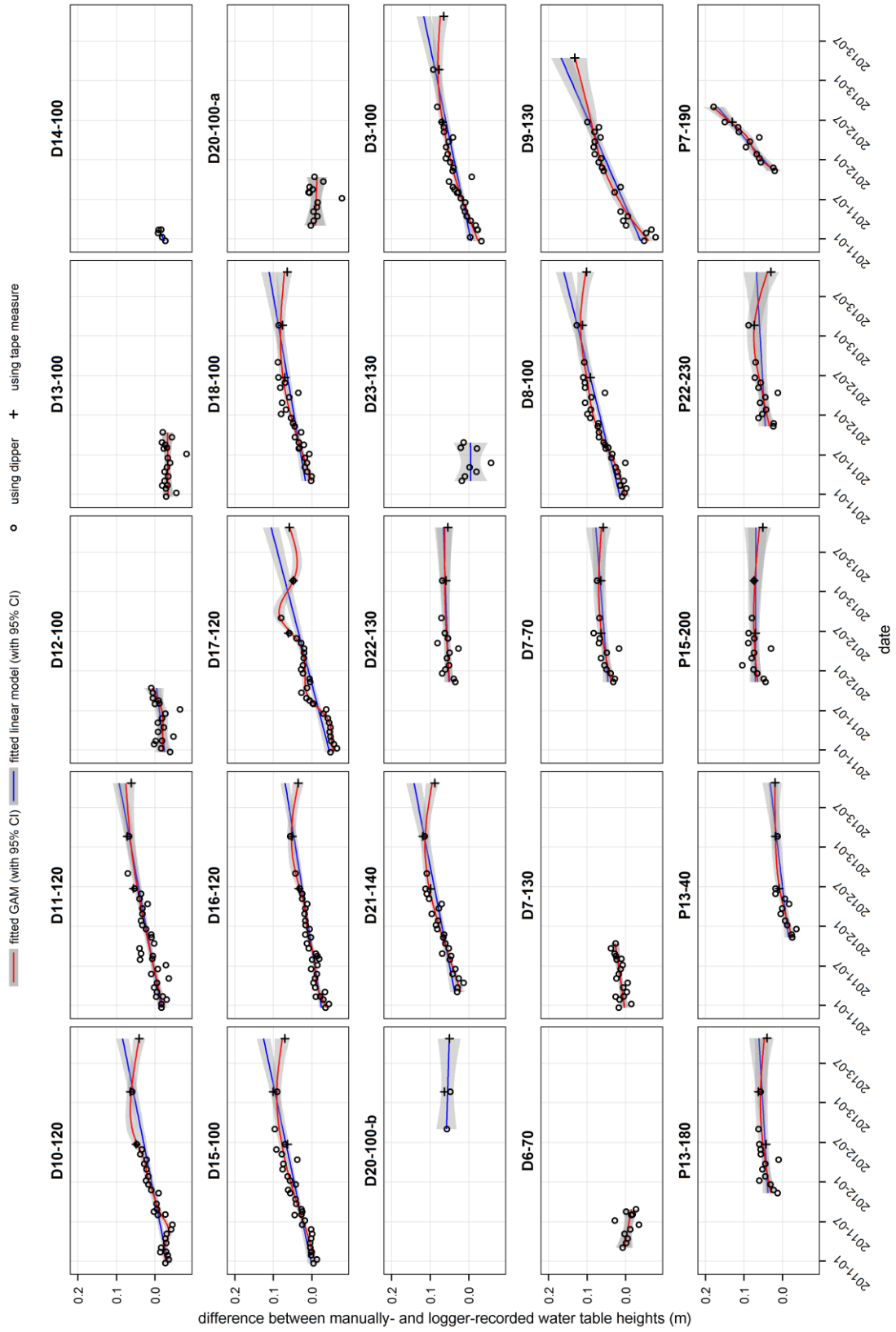

Figure 4-21. Difference between manually- and logger-recorded water table heights before correction for logger drift, conditional on logger.

The blue and red lines show the linear model and generalised additive model fits respectively. The envelopes show the 95% confidence intervals of the models. Two different loggers were used in dipwell D20-100 and a model was therefore fitted to each set of data. For three loggers the number of manually-recorded data was too small to fit a GAM model.

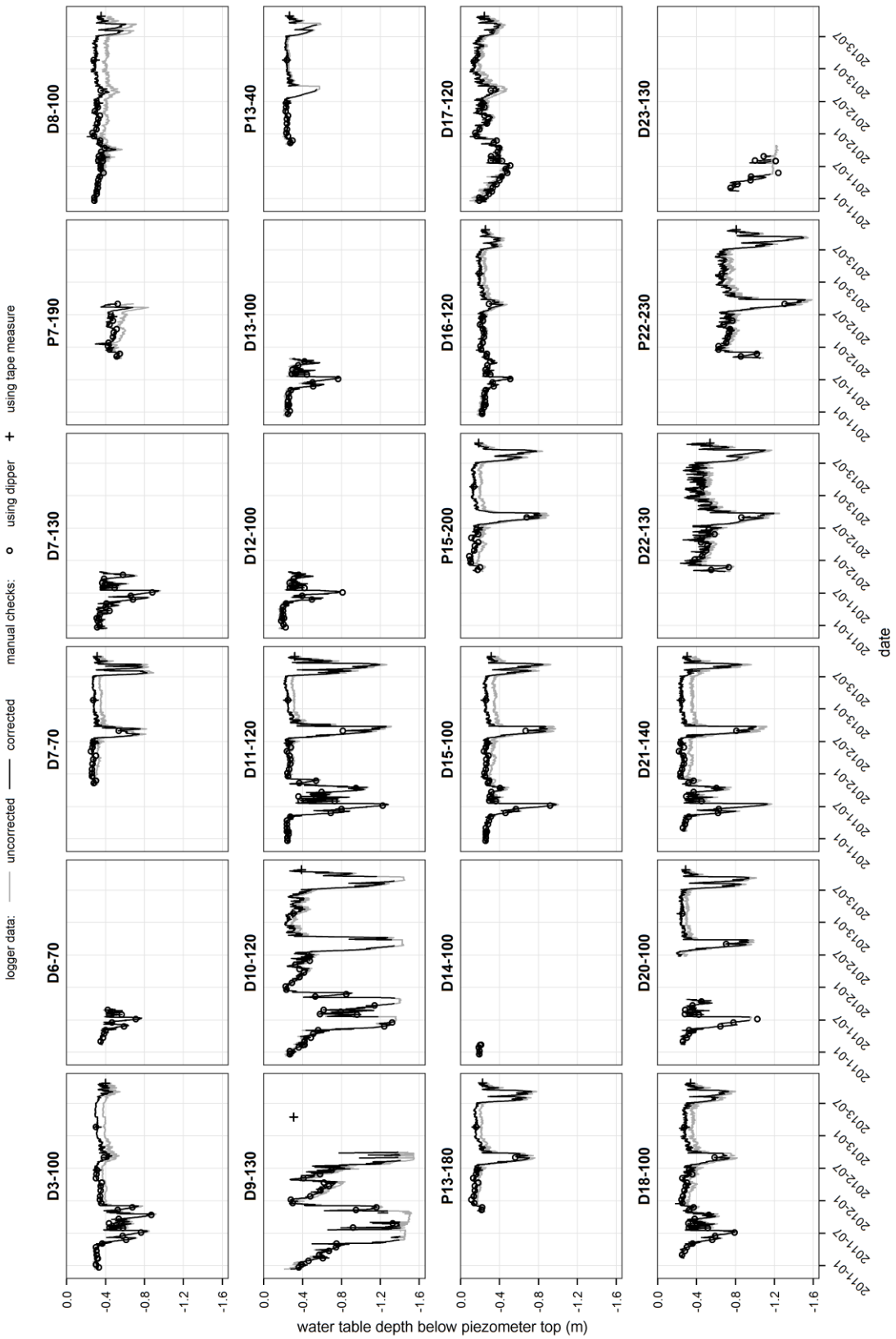

Figure 4-22. Logger data before and after correction for logger drift.

For added clarity of the graph, records were aggregated over a daily period before plotting.

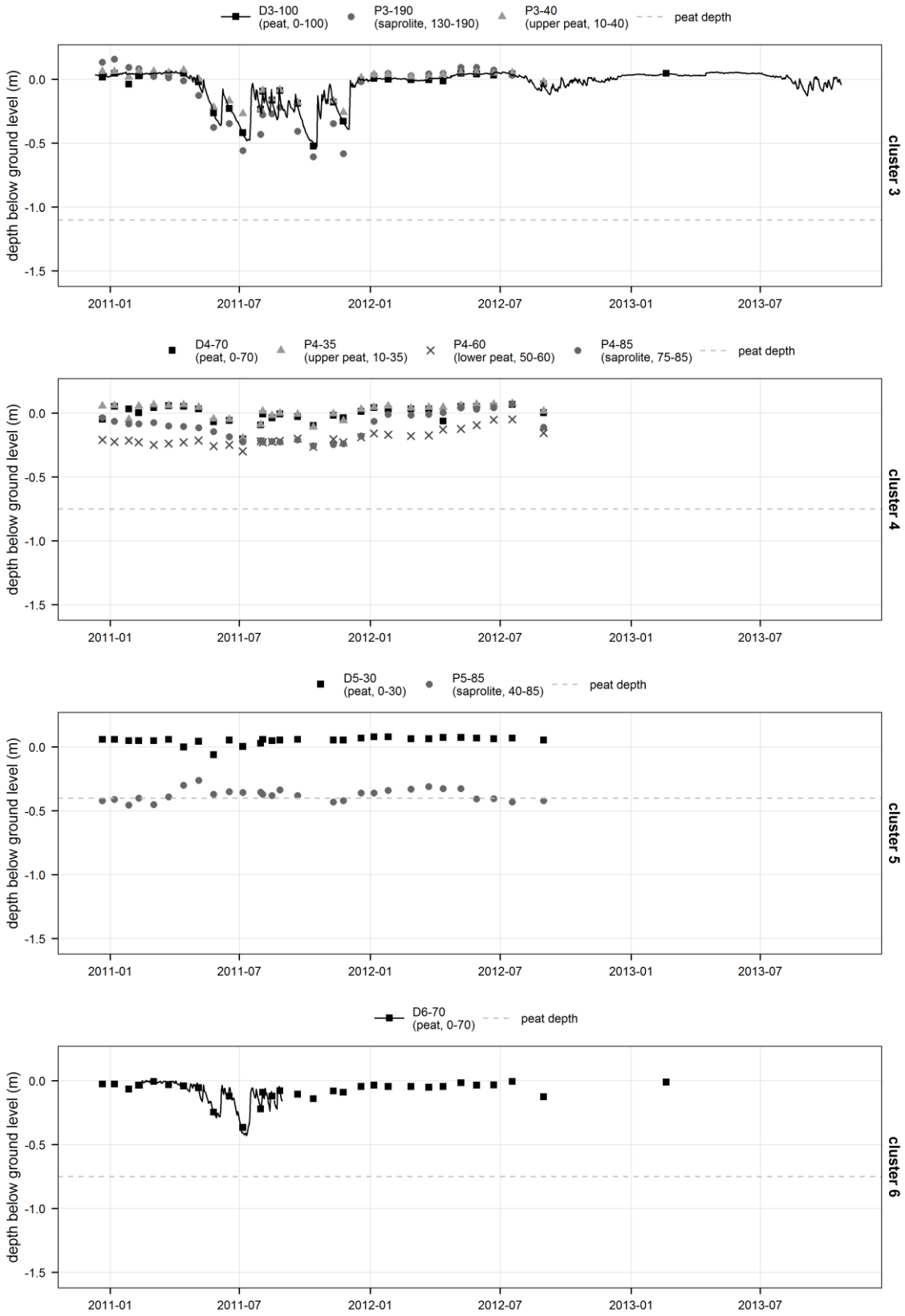

Figure 4-23. Time series of piezometric heads in clusters 3-6.

Numbers between brackets in the legend show the position below ground level of the piezometer intake in cm. The dashed line shows the position of the lower level of the peat layer where present and shallower than 1.5m.

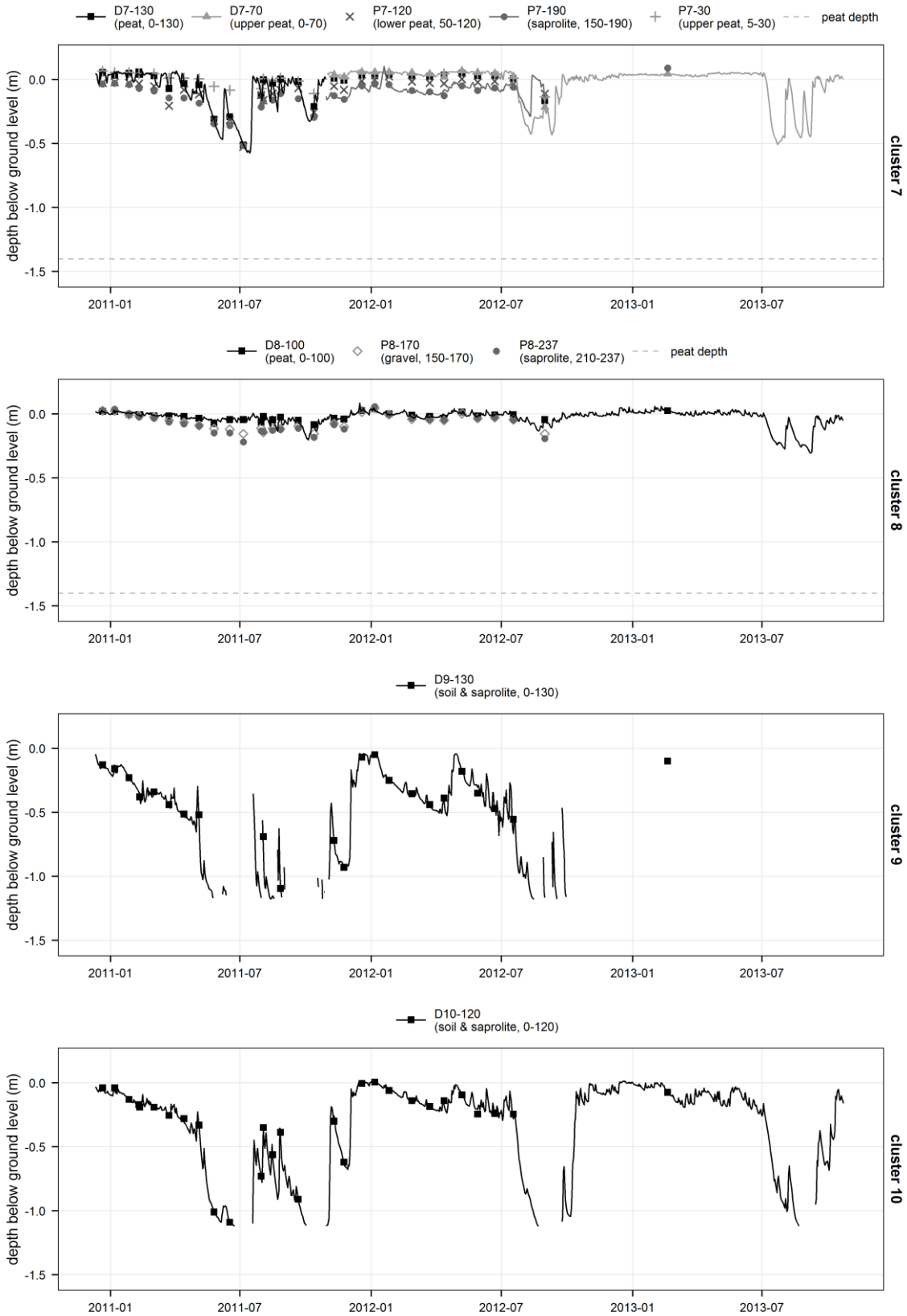

Figure 4-24. Time series of piezometric heads in clusters 7-10.

Numbers between brackets in the legend show the position below ground level of the piezometer intake in cm. The dashed line shows the position of the lower level of the peat layer where present and shallower than 1.5m. Note that loggers in cluster 7 were reshuffled on 30/10/2011.

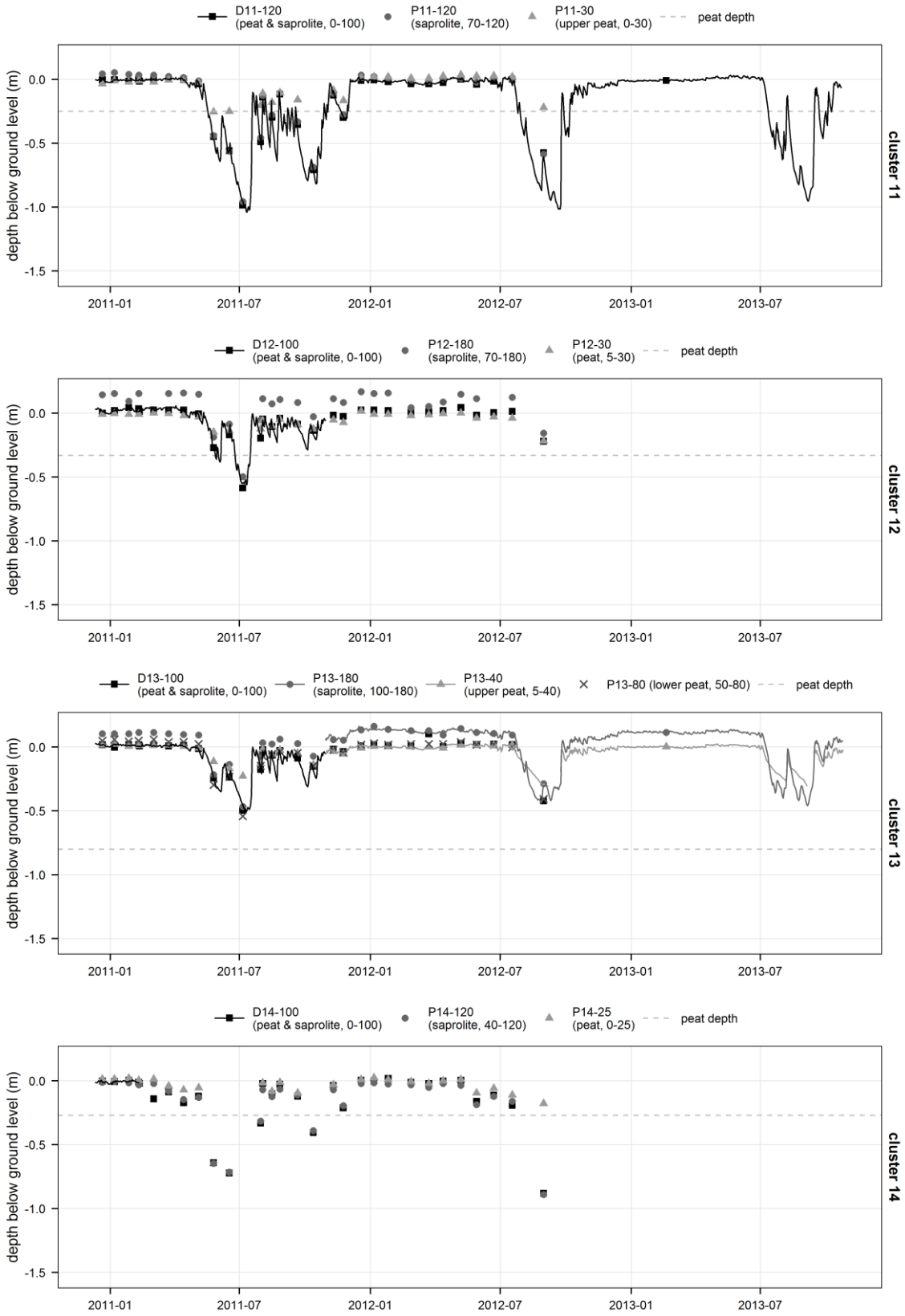

Figure 4-25. Time series of piezometric heads in clusters 11-14.

Numbers between brackets in the legend show the position below ground level of the piezometer intake in cm. The dashed line shows the position of the lower level of the peat layer where present and shallower than 1.5m. Note that loggers in cluster 13 were reshuffled on 30/10/2011.

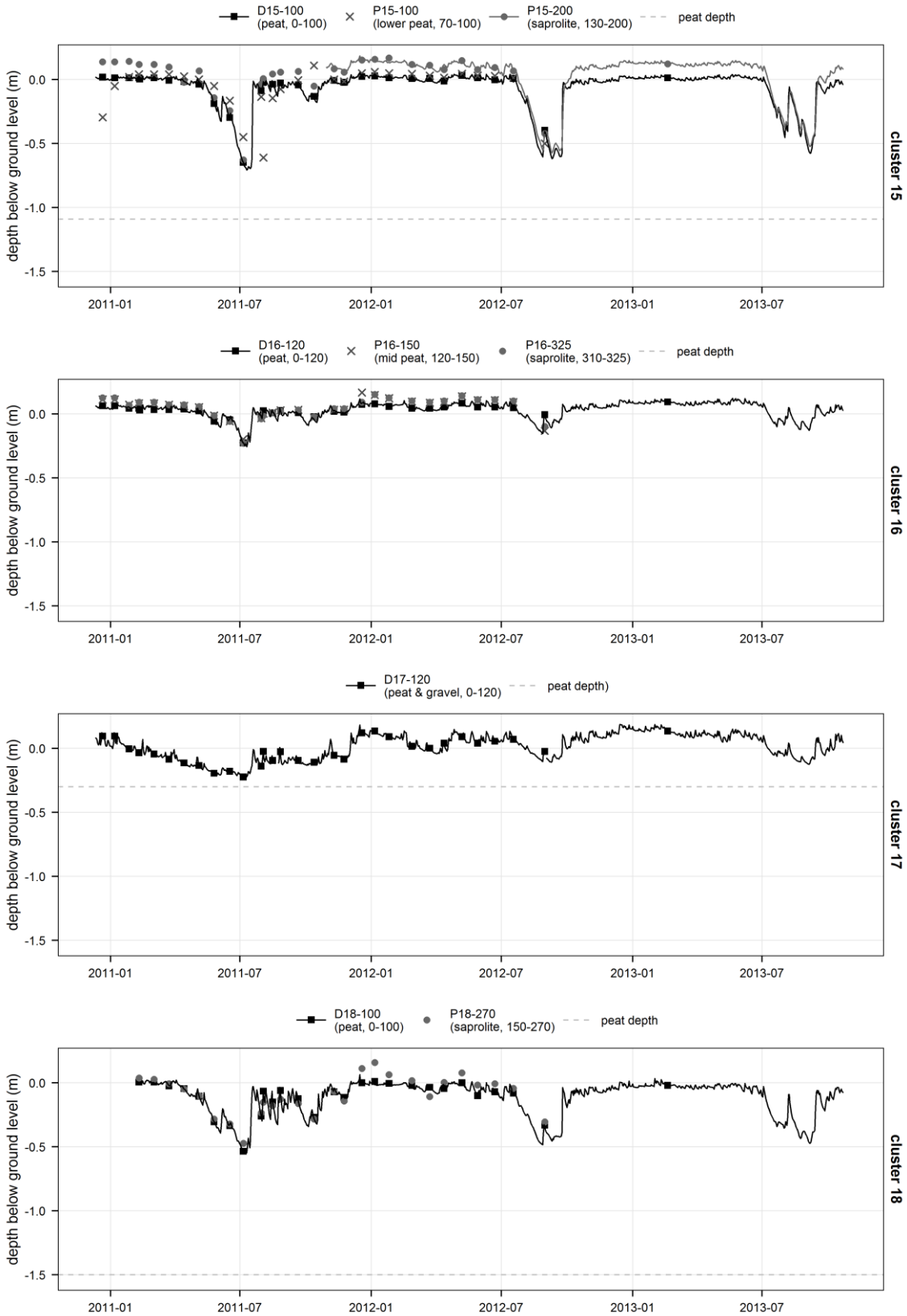

Figure 4-26. Time series of piezometric heads in clusters 15-18.

Numbers between brackets in the legend show the position below ground level of the piezometer intake in cm. The dashed line shows the position of the lower level of the peat layer where present and shallower than 1.5m.

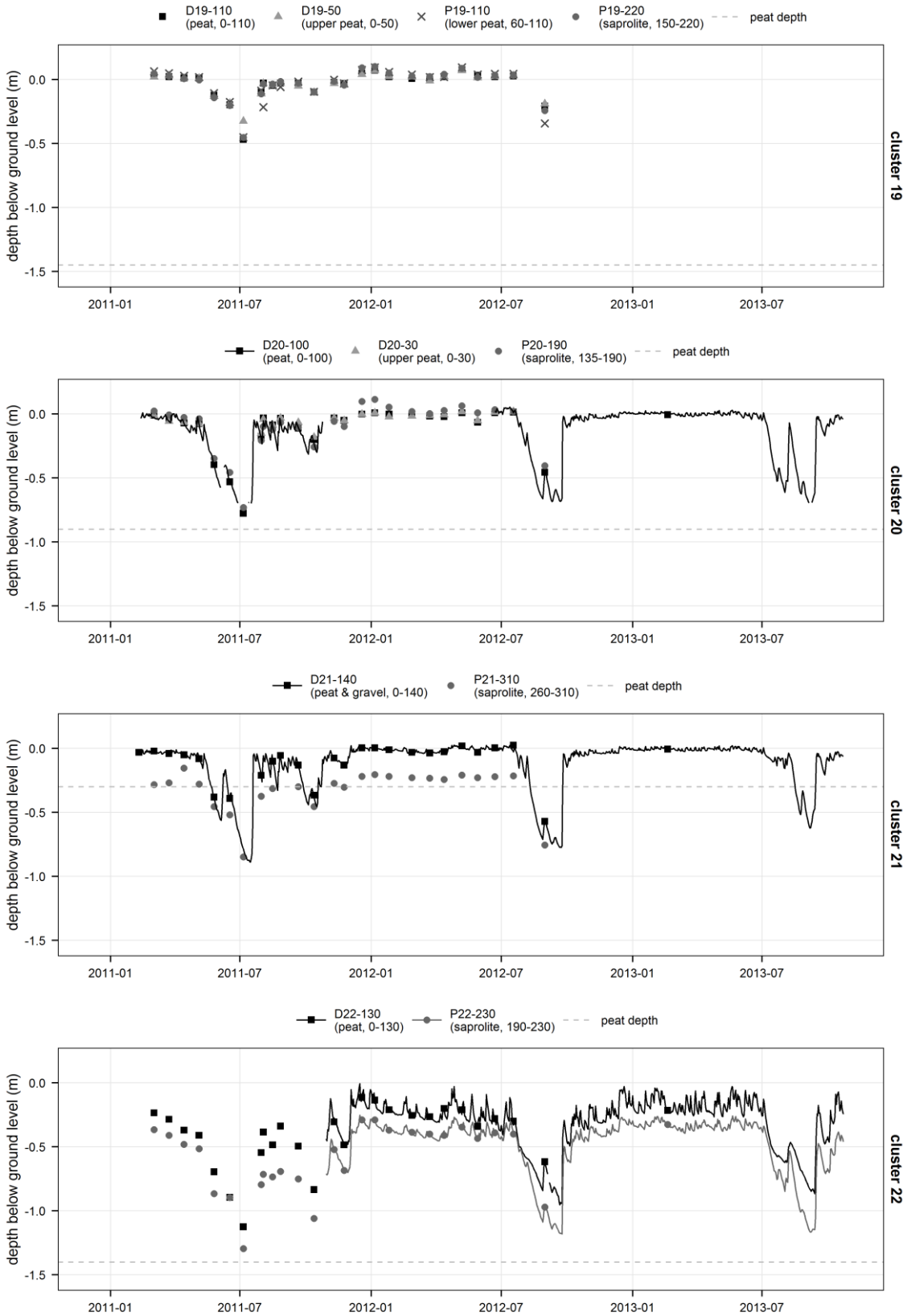

Figure 4-27. Time series of piezometric heads in clusters 19-22.

Numbers between brackets in the legend show the position below ground level of the piezometer intake in cm. The dashed line shows the position of the lower level of the peat layer where present and shallower than 1.5m.

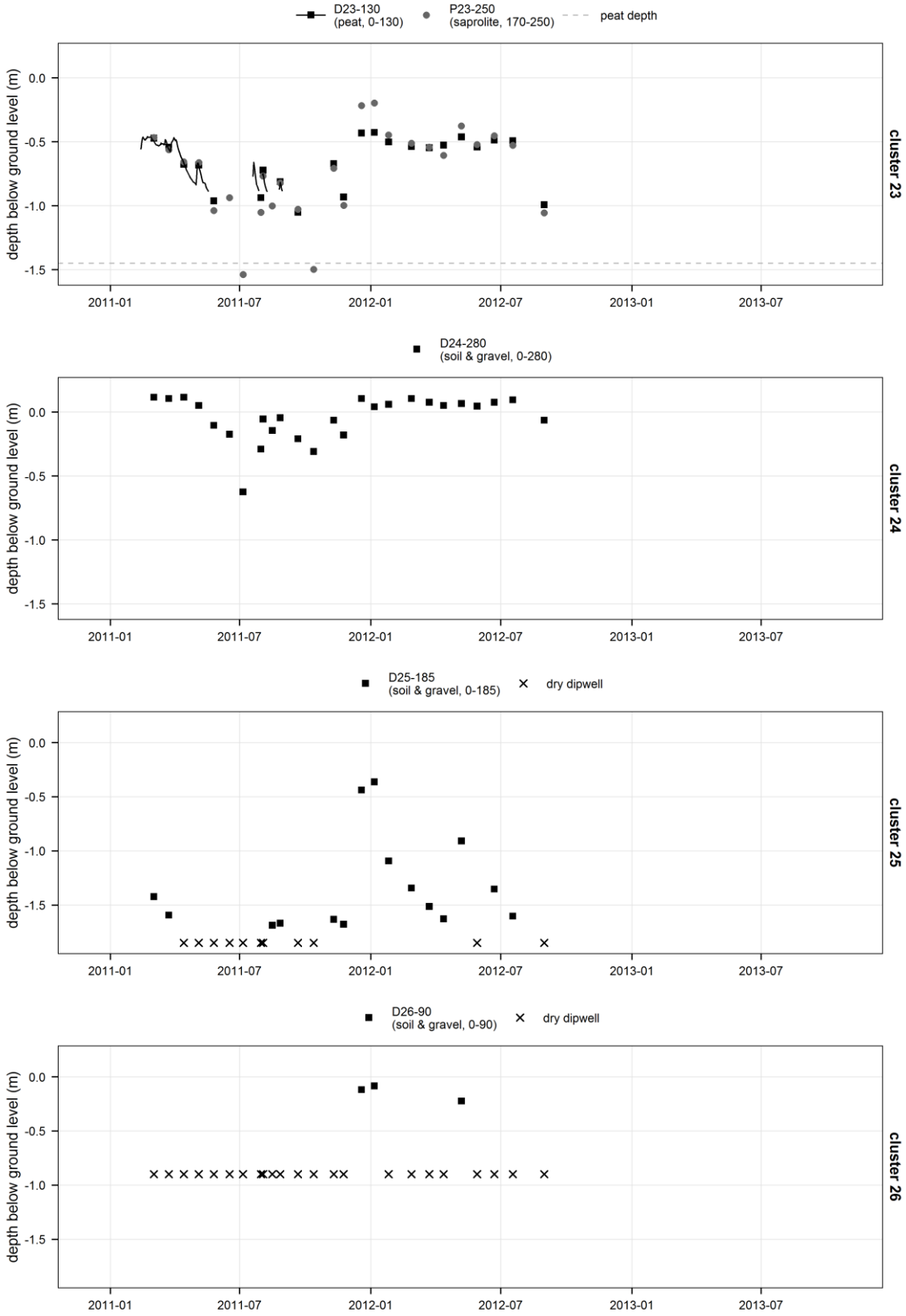

Figure 4-28. Time series of piezometric heads in clusters 23-26.

Numbers between brackets in the legend show the position below ground level of the piezometer intake in cm. The dashed line show the position of the lower level of the peat layer where present and shallower than 1.5m. Note the different y axis scale on the last two plots.

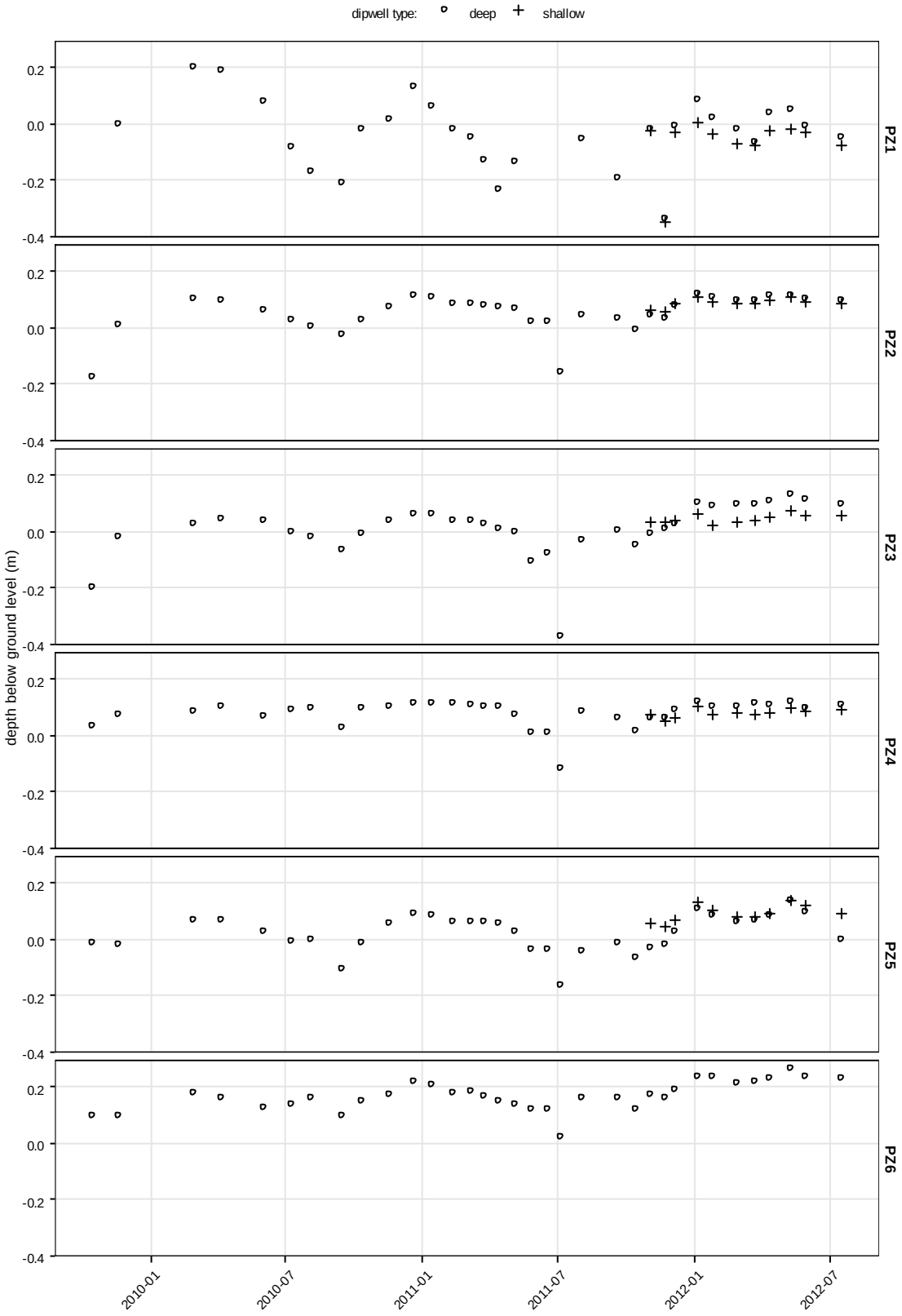

Figure 4-29. Time-series of water table depth in pre-existing piezometers.

Ground elevation was taken as identical within each cluster and water levels can be directly compared between dipwells belonging to the same cluster. Dipwells labelled "deep" are those installed by a contractor prior to this research work. All were more or less deeply anchored into the underlying mineral substrate. "Shallow" dipwells are those installed in the peat layer at a later stage.

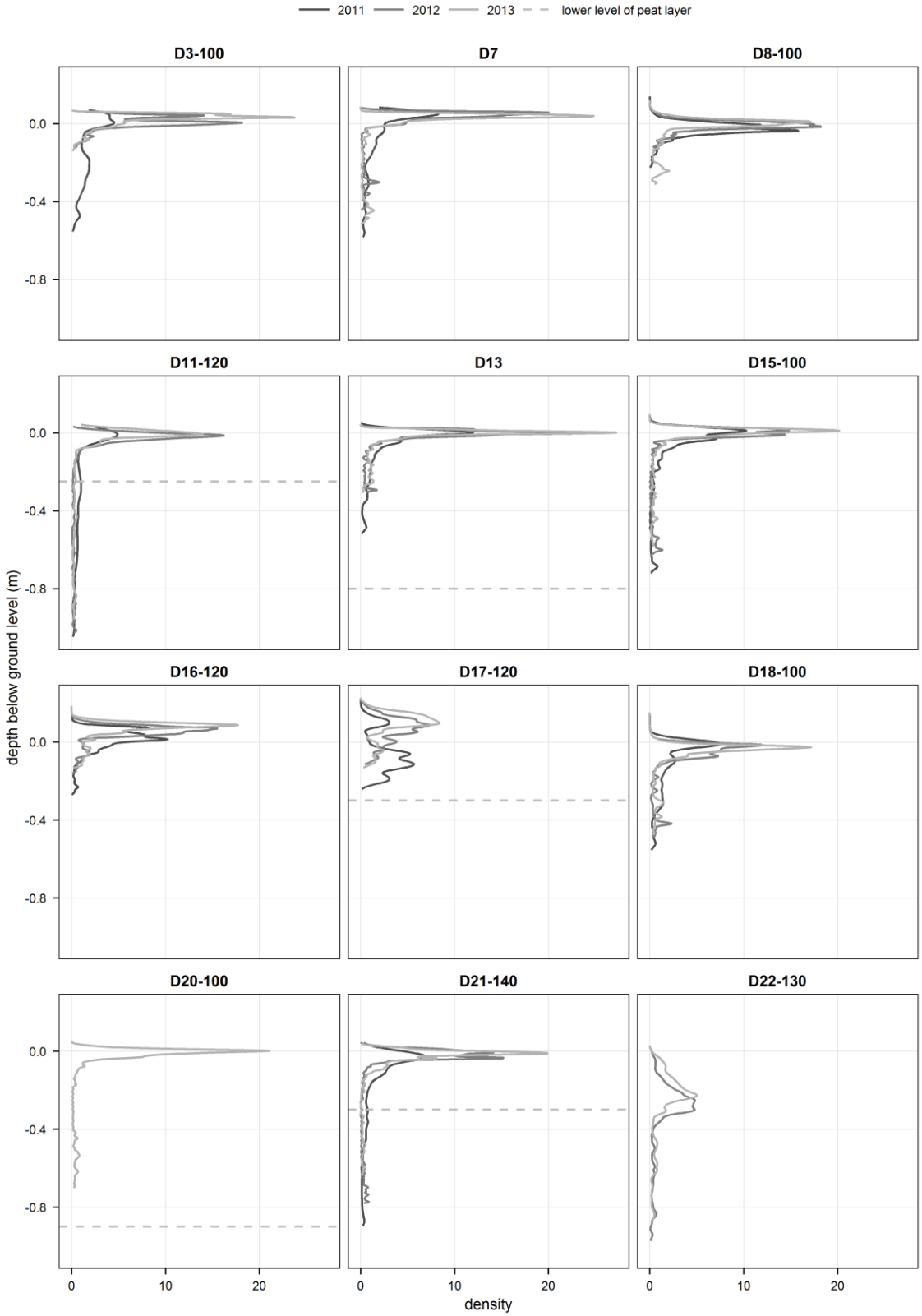

Figure 4-30. Kernel density estimation of water table depth distribution in the peat layer.

2011: from 13/02/2011 to 12/02/2012, 2012: from 01/01/2012 to 31/12/2012, 2013: from 27/10/2012 to 26/10/2013. Piezometers and years with data missing for more than 5% of the corresponding year are not shown. Records from D7-70 and D7-130 on one hand and D13-100 and P13-40 on the other hand were merged to obtain continuous time-series labelled D7 and D13 respectively. Peat depths larger than one metre are not shown.

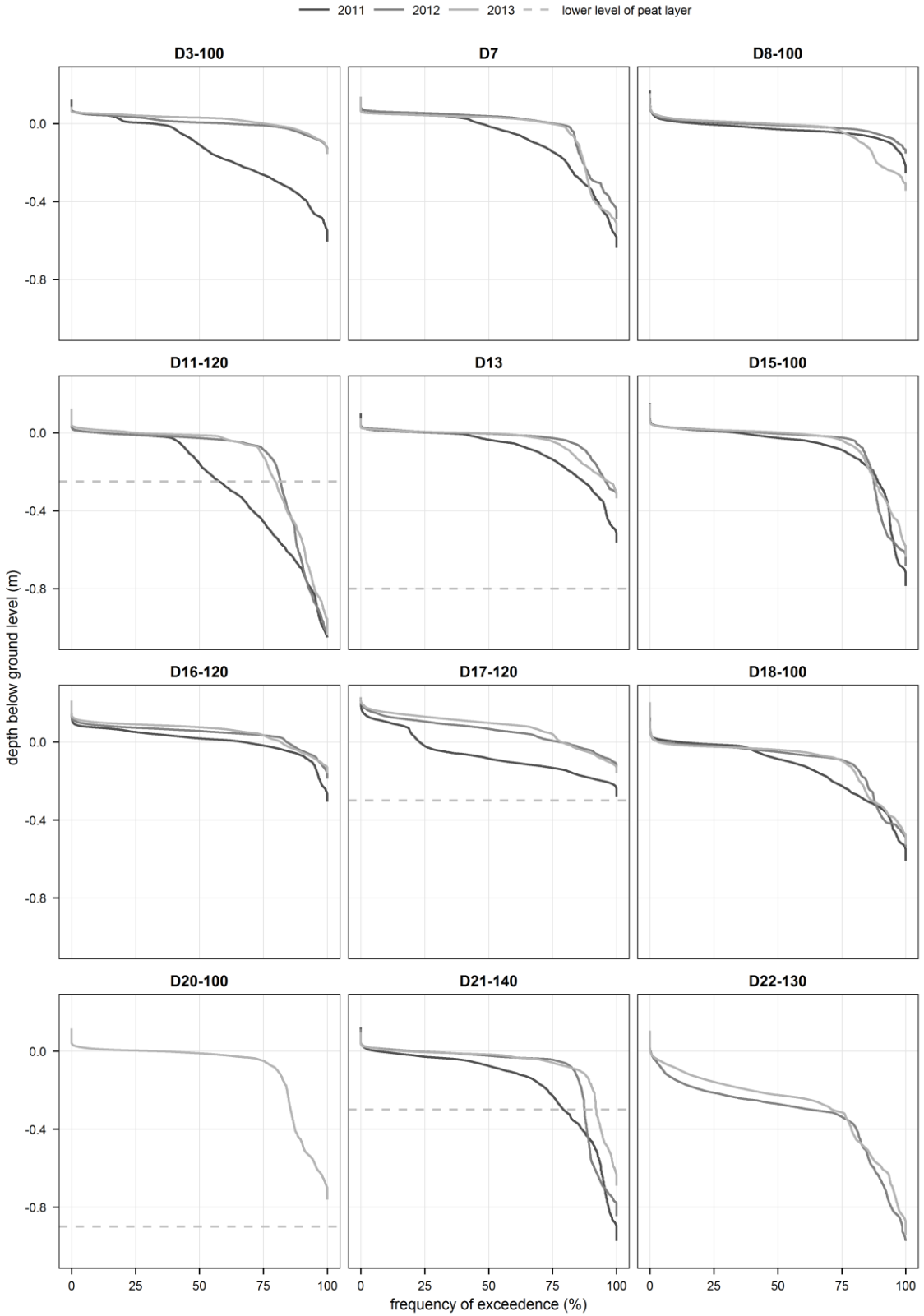

Figure 4-31. Depth exceedence frequency curves of the water table in the peat layer.

2011: from 13/02/2011 to 12/02/2012, 2012: from 01/01/2012 to 31/12/2012, 2013: from 27/10/2012 to 26/10/2013. Piezometers and years with data missing for more than 5% of the corresponding year are not shown. Records from D7-70 and D7-130 on one hand and D13-100 and P13-40 on the other hand were merged to obtain continuous time-series labelled D7 and D13 respectively. Peat depths larger than one metre are not shown.

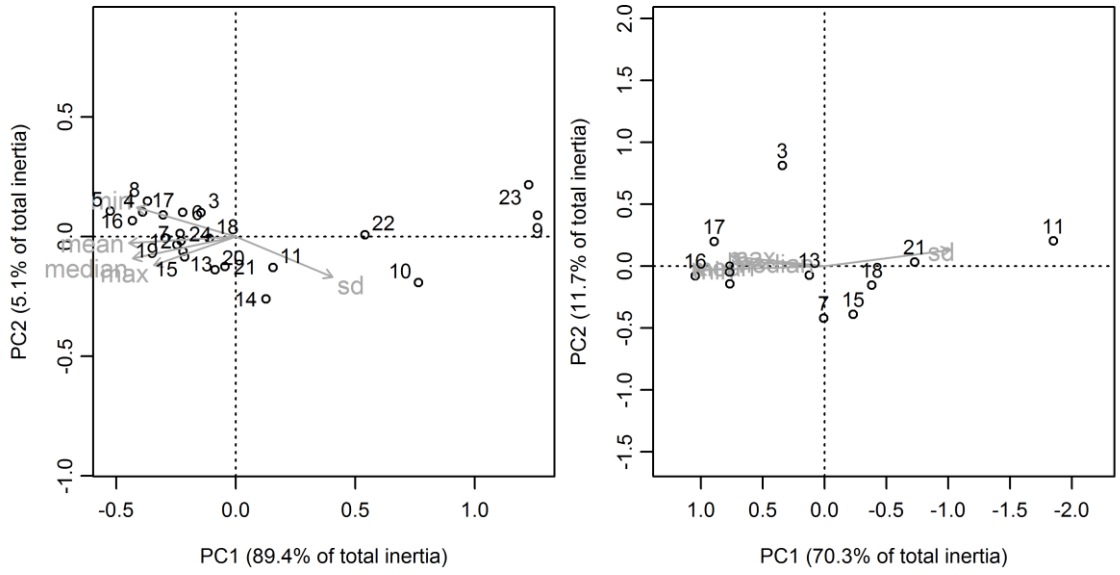

Figure 4-32. Principal component analysis plots of groundwater table depth records (left: manually-recorded, right: logger-recorded).

Distance biplot scaling was used: distances among dipwells in the plots are approximations of their Euclidian distances. Synthetic descriptive variables (minimum, maximum, mean, median and standard deviation of the groundwater table records) were passively projected onto the plots to help interpretation. An orthogonal projection of a given dipwell onto a descriptive variable arrow approximates its position along this variable. The arrow heads point towards large values. Water table depth was expressed as a negative value when below the ground surface, therefore a high value for min, max, mean and median indicates a shallower groundwater table. Number of records included: 26 records x 22 dipwells in the manually-recorded dataset, 956 daily mean records x 10 dipwells in the logger-recorded dataset. As the method requires a complete data matrix, a number of dipwells or record dates could not be included due to a large number of missing data. For manually-recorded time-series with only a few missing values, these were replaced by the maximum dipwell depth (when the dipwell was dry), the value recorded in the corresponding deep piezometer (where both time-series had been shown to be similar) or the mean value (when the water table depth had been shown to be very stable). No missing data imputation was carried out in the logger-recorded dataset.

Overall, this corresponds to a gradient from the upstream margins to the middle and downstream part of the mire on one hand and from mineral to deep peat soils on the other hand, as shown on Figure 4-33. This gradient is very clear along the transect downstream of Puy Rond (dipwells 9 to 17), with the exception of dipwell 14 in which a deeper and more variable water table position was recorded compared to dipwells 12 and 13 further upslope. The mineral vs. peat and mire margin vs. mire centre gradient is not as clear along the eastern transect (dipwells 24 to 18, 8 and 17). Dipwell 24, at the transition between peat and mineral soils, shows a behaviour that is more similar to dipwells installed in the centre of the mire, whereas dipwells 22 and 23 recorded deep and variable water table depths despite being installed in 1.4m-deep peat. The bulk of the dipwells (i.e., others than 9, 10, 11, 22 and 23) are more similar in terms of their hydrological behaviour, and are clustered on one side of the first axis of the PCA plot based on manually-recorded data. The PCA plot based on logger-recorded data (Figure 4-32, right) essentially gives a close-up view of this group of dipwells, since large data gaps prevented dipwells with a deep water table from being included in the analysis.

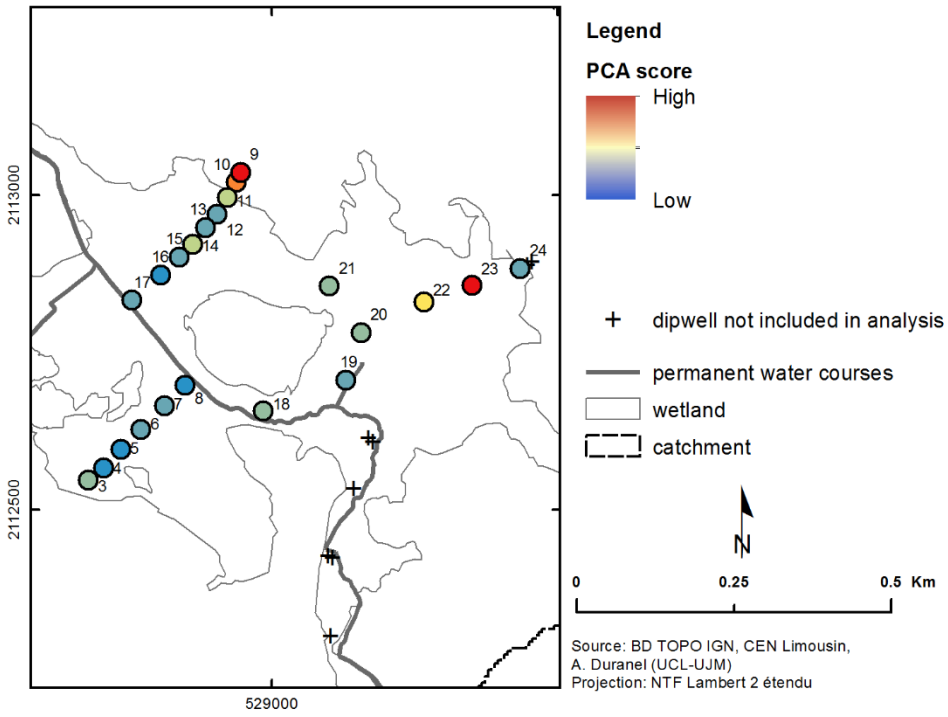

Figure 4-33. Map of dipwell scores on PCA first component.

It gives results very similar to the plot based on manually recorded water table depths, especially along the first axis that, once again, represents the bulk of the dataset inertia (70.3%). This axis is strongly correlated to the mean, minimum and standard deviation of the water table depth ($p<0.001$ based on 999 permutations) but less so to the maximum and median water level, which suggests that the distinction between dipwells is mainly driven by water levels during the dry season. As in the first plot, it separates dipwells with a deeper and more variable water table (11, 21) located on the north-eastern margin of the mire from those with a stable and shallow water table (8, 16, 17) on the low-lying part downstream of Puy Rond. The latter have a very similar behaviour as shown by their proximity on both PCA plots. The second axis of the PCA plot based on logger records accounts for a larger proportion of the total inertia than in the PCA based on manual records (11.7%). It singles out dipwell 3 on the basis of a higher and more stable water table during the 2012 and 2013 dry seasons compared to summer 2011 and to other dipwells (the date with the highest score on axis 2 is 24/09/2012). In other words, relative to its behaviour during the 2012 and 2013 dry seasons, the water table in dipwell 3 was more strongly impacted by the 2011 drought compared to other logger-equipped dipwells included in the analysis. The peculiarities highlighted by both PCA plots can be better understood by looking at piezometric heads and stream stages along the three transects.

Downstream transect (dipwell 9 to stageboard SB4)

In clusters 12, 13 and 15 (Figure 4-25 and Figure 4-26), piezometric heads in mineral formations underneath the peat lie 15-20cm above ground level at all times except in the 2-4 driest months. During this time, the water table in the peat is stable and at surface level. However, in the driest months, piezometric heads in the mineral formations and in the peat drop to similar depths below ground level simultaneously (cluster 12 and 15) or with some delay between the former and the latter (cluster 13). This suggests that the water table in the peat is maintained at a quasi-constant shallow depth by groundwater upwelling from the underlying mineral formations and that water moves relatively freely through the peat layer. Upwelling does occur most of the time around cluster 16 too but to a lower degree possibly due to the flatter topography at the bottom of the mire and the resulting local groundwater stagnation (Richardson *et al.* 2001). Compared to the closest clusters located both upslope and downslope, cluster 14 stands out in two aspects: it recorded a deeper and more variable water table in the peat as highlighted by the PCA on manual records, and there is no evidence of water upwelling. This suggests that water upwelling contributes to maintaining a shallower and more stable water table in the peat around clusters 12 and 13 whereas this phenomenon does not exist in cluster 14. The shallowness of the peat layer around this cluster cannot be invoked to explain this as it is similar to that found around cluster 12. One explanation could be that cluster 14 lies at the downslope end of a small topographic shelf, which may cause a very local groundwater stagnation in the upper part of the soil profile.

Figure 4-34 shows the elevation of piezometric heads in the peat and underlying mineral formations as well as stream stage in the lower part of the transect. Even though one should be careful in interpreting small gradients after September 2012 given the uncertainty in logger drift corrections after that date (see p. 191), Figure 4-34 demonstrates several interesting points. First, water levels in dipwell 17 are almost identical at all times to stream stages at SB4, just 5 metres away. Ground level around dipwell 17 is about 551.8m NGF69, and all records above that altitude correspond to flood levels in the stream with water being out of its banks. Below that altitude, the similarity between stream stage and piezometric records can be explained by the proximity of SB4 and D17 and the presence of thick alluvial deposits of permeable gravels and sands downstream of Puy Rond. The peat layer is only 30cm deep at dipwell 17 (Figure 3-32). As a consequence, there is a direct connection between the stream and dipwell 17 through the alluvial deposits.

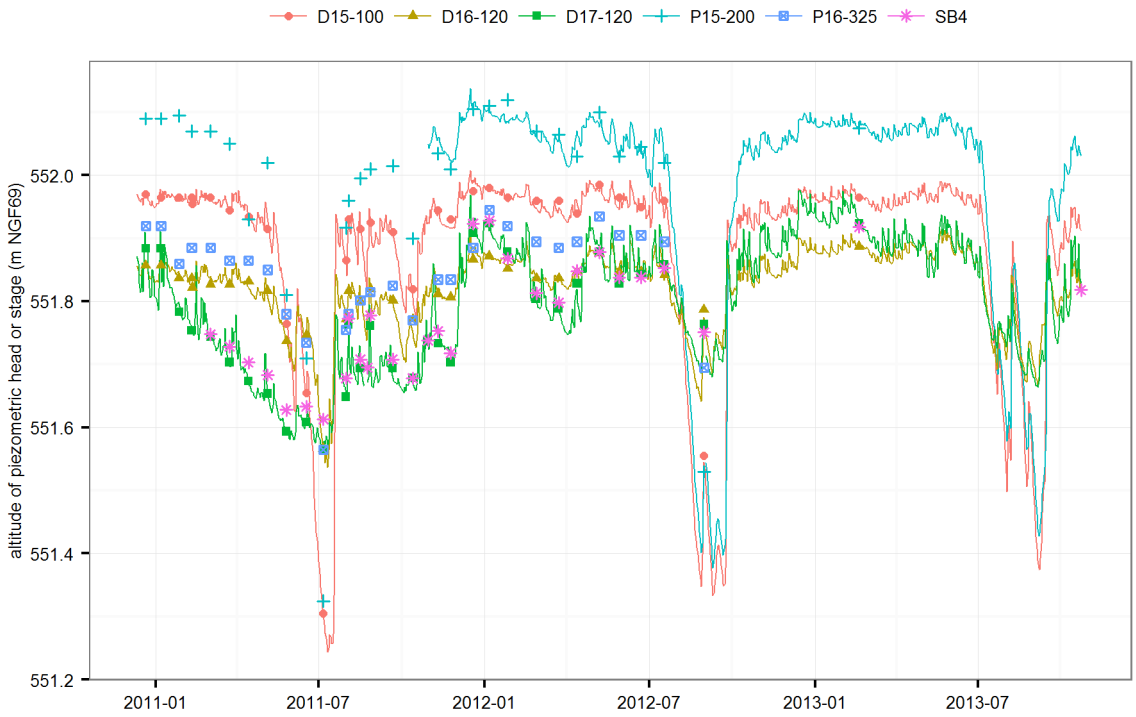

Figure 4-34. Piezometric head and stream stage along a transect SB1-D15, downstream of Puy Rond.

As shown by a water table depth that is generally lower than in dipwell 17 when the stream is above 551.8m NGF69 and obviously flooding, and often substantially and durably so, dipwell 16 does not seem to be under the influence of flood water from the stream even though it lies at the same altitude. This is very evident in January 2012 for instance. This can be explained by the fact that the stream does not run in the lowest-lying part of the mire anymore, but slightly upwards following past engineering works. The shallow thalweg between clusters 17 and 16, relict of the pre-engineering stream course, seems to drain most of the flood water further downstream where it flows into the stream again.

Another interesting point shown by Figure 4-34 is that, during the two or three driest months of the year, flow in both peat and underlying saprolite between clusters 15 and 16 reverts: piezometric heads are higher in cluster 16 than in cluster 15. Contrary to cluster 15, heads in cluster 16 never fall more than a few centimetres below the water table in dipwell 17 and below stream stage at SB4. This suggests that during the dry season, relatively rapid flow does occur from the stream towards cluster 16 through the very fibric upper peat horizon that is 50-60cm deep between dipwell 16 and the stream and through alluvial sands and gravels that are found within the peat in this part of the mire but not further upslope (Figure 3-32). On the contrary, water table depth in dipwell 16 is not correlated to stream stages and levels in dipwell 17 during the wet season as a shallow groundwater table is maintained possibly by some upwelling but

probably more importantly so by downslope surface and sub-surface flow. The maintenance of a relatively shallow water table in late summer in dipwell 16, as opposed to dipwell 15 for instance, can also be explained by a difference in surface peat humification: a 55cm deep layer of poorly humified (von Post index 2) fibric peat was recorded when augering the former, while the von Post humification index was at least 5 right from ground level when augering the latter (Figure 3-32). Peat specific yield in particular is known to be strongly and negatively correlated to peat humification and to the von Post index (Boelter 1964, 1968; Letts *et al.* 2000; Verry *et al.* 2011), and a larger specific yield would result in a lower drop in groundwater table depth for a given change in water storage (Gilman 1994).

Middle transect (3 – SB3)

All clusters along the transect running from the south-western boundary of the wetland to Puy Rond are characterised by relatively shallow and stable water tables in the peat, including during the dry season, as shown in Figure 4-30, Figure 4-32 and Figure 4-33. This is particularly the case in cluster 4, 5 and 8, but less so in cluster 7. The comparison of piezometric heads in the peat and in the underlying mineral formation shows a constant downward vertical flow all year round, except in cluster 3 where there is a slight upward gradient during the wet season and a downward gradient during the driest months. The reason for the absence of upwelling in this part of the mire is uncertain. Manual augering and probing bumped onto hard rock a short distance underneath peat all along the south-west margin of the mire (Figure 3-28, Figure 3-32). One explanation could therefore be that the fissured zone is less densely fissured in this area, preventing or reducing groundwater flow and upwelling. The electric resistivity tomography survey recorded higher resistivity values below the peat in this area than in other locations within the mire (Figure 3-21), which may support this hypothesis even though a large area of low resistivity was found at larger depth. The downward hydraulic gradient observed in cluster 4, 5, 7 and 8 raises the question of the mechanism that maintains a shallow groundwater table in the peat at all times near clusters 4 and 5. A possible explanation is that clusters 4 to 6, and to a lesser extent 3, 7 and 8, are located in a situation of convergent topography that collects local runoff from both the mire on each side of the depression and from the catchment, as shown by a map of topographic indices, in particular of the DInf catchment area (Figure 4-35).

Dipwell D3-100 was singled out by the PCA on logger data because, contrary to other dipwells inserted in peat, it displayed a different behaviour during the summer of 2011 as opposed to 2012 and 2013, with much deeper and variable water tables (Figure 4-23).

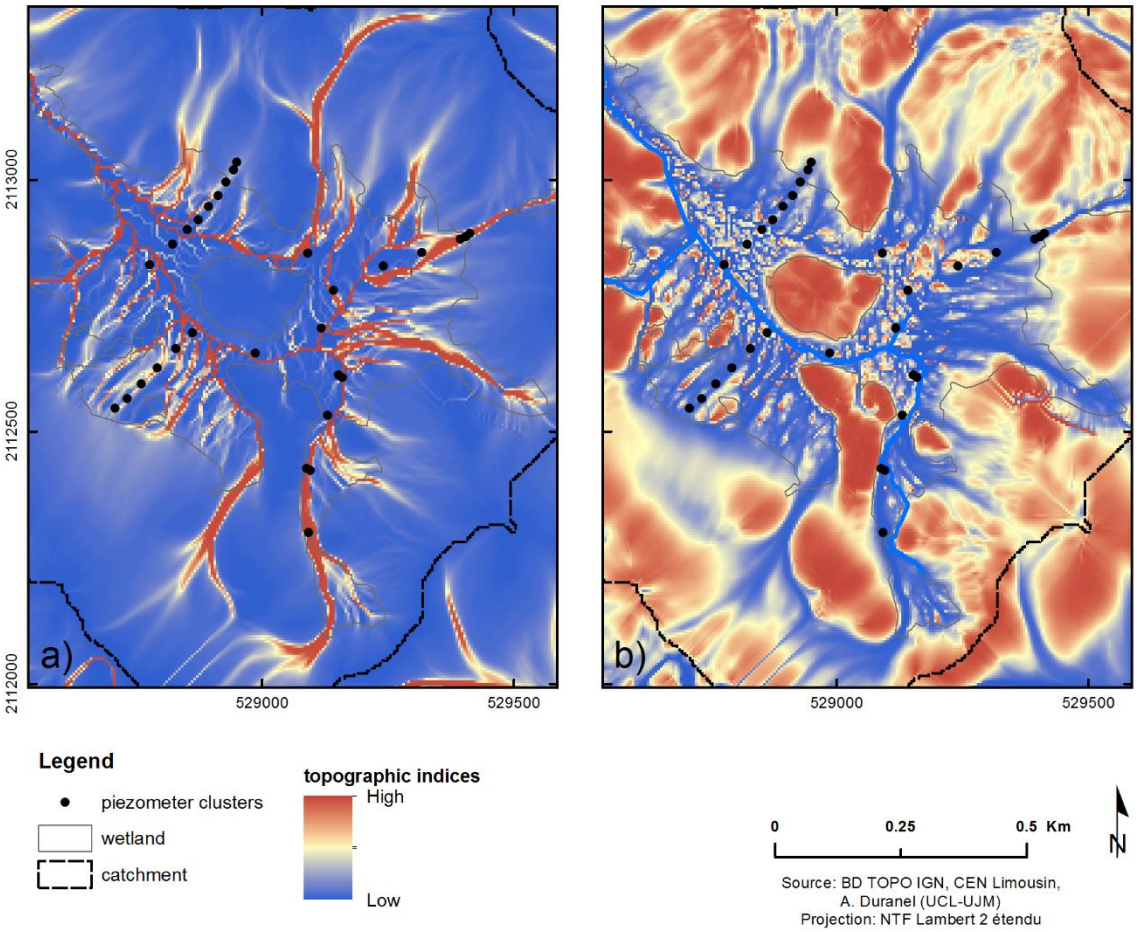

Figure 4-35. Location of dipwells relative to topographic indices: a) DInf catchment area, b) DInf slope over catchment area ratio.

The 2011 summer was very dry (Figure E-46 in Appendix E), however in no other dipwell did the water table in the peat drop to a substantially lower level compared to subsequent summers. In 2011, the gradient between the peat and the underlying saprolite in cluster 3 follows approximately the same pattern as the one described on the other side of the wetland: there is an upward gradient during the wet season, and as soon as the piezometric head in the saprolite falls below ground level, the water table in the peat follows, to reach a maximum depth of 0.5m below ground. Unfortunately only one record of the piezometric head in the saprolite underlying the peat is available in the summer of 2012, however it shows that the head was close to ground surface and did not drop below the piezometric head in the peat as it did in 2011. This strongly suggests that the water table in the peat around cluster 3, at the southern margin of the wetland, is also maintained by water upwelling from the underlying mineral formations.

Figure 4-36 shows piezometric heads and stream stage on the other side of the transect, near Puy Rond. A downward gradient is visible from piezometric heads in the upper part of the peat (D8-100), lower part of the peat (P8-170) and saprolite (P8-237).

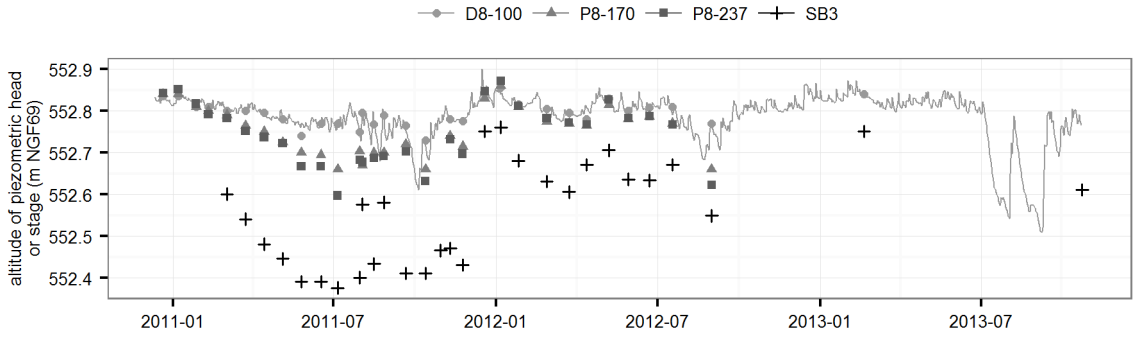

Figure 4-36. Piezometric heads in cluster 8 and stream stages at stageboard SB3.

Except when the stream gets out of its bank and floods dipwell D8-100, which occurs above 552.85m approximately, piezometric heads are always higher than stream stage, showing that water discharges from the peat and underlying mineral formations into the stream.

Upstream transect (D26 – D18)

Dipwells 26 and 24 were inserted in mineral soil. Manual augering stopped when butting against the hard granite at 0.9 and 1.8m deep respectively. Both proved too short to provide meaningful records (Figure 4-28). The PCA on manual records shows that dipwell D24-280, installed just 12m downslope at the transition between peat and mineral soils, has a behaviour that is more similar to dipwells installed in the centre of the mire, with a water table at ground level during the wet season and relatively shallow during the driest months. It is inserted 2.5m deep in loose gravels within a loamy matrix that were interpreted as colluvions, right at a break of slope that, interestingly, approximately matches the 12.9° slope boundary highlighted in Section 3.3.3.4. Above this point, granite is found at shallow depths. The presence of shallow drains dug along the slope break suggests that shallow water tables observed in dipwell 24 occur all along it, whereas water tables in dipwells further down the slope (23 to 20) are deeper and more variable. This is indicative of localised groundwater discharge.

Three non-mutually exclusive mechanisms can be hypothesised regarding the source of this discharge. The first one is a localised discharge from a preferential flow path in the fissured granite, possibly linked to the presence of a series of faults running parallel to the escarpment, but these are mineralised according to COGEMA documents. The second is the formation of springs at the contact between the relatively permeable fissured granite and the less permeable saprolite, substantial thicknesses of which have been found downslope of the escarpment during the CEA drillings. The peat layer does not seem to act as the confining layer here as shown by the absence of significant gradient between piezometric heads in the peat and in the underlying

mineral formation further downstream (cluster 22, Figure 4-28). The third hypothesis is an edge-focused groundwater discharge caused by the slope break, further increased by the large catchment area above cluster 24 as shown on Figure 4-35.

Dipwells 22 and 23 have deep and variable water tables including during the wet season and their behaviour is closer to dipwells 9 and 10 installed in mineral soils beyond the mire boundary. However, they are both inserted in 1.40m-deep peat. The permanent downward hydraulic gradient and therefore the absence of upwelling observed in cluster 22 may in part explain this distinct behaviour, however the main reason probably lies elsewhere since an upward gradient is observed in cluster 23 at least in some part of the year. The piezometer installation logs show that, in both cases, peat in the upper part of the profile (35cm in the first case, 50 in the second) is dry and granular. The peat has a reddish colour and shows traces of iron oxidation (Figure 3-32). These characters have also been observed by Laplace-Dolonde *et al.* (2007) in the vicinity of clusters 22 and 23. The vegetation is dominated by *Nardus stricta*, and no peat-forming species is present. This suggests that the upper peat is currently exposed to aerobic pedogenetic processes that did not exist at the time of its deposition, and therefore that the water table in the peat has been lowered at some point in the past.

One likely explanation is the presence of a drain on each side of dipwells 22 and 23. The drains themselves are only 15-30cm deep on average, however the surface topography shows that the peat has substantially subsided along them, with a difference of up to a metre between the ground surface along the main drain and the top of the residual relief between the two drains, where clusters 22 and 23 are located. It seems that the drains have been maintained over time at a constant depth below the sinking ground surface, progressively increasing water table drawdown and peat degradation. There is also evidence from a local witness of a peat fire in the first half of the 20th century in this part of the mire. The surface topography, which shows a clear subsidence along the drains, suggests that this fire is not the main cause of the pedological and hydrological degradation currently observed, and has at most exacerbated the drainage impact, possibly by propagating preferentially along the drains where the peat was drier.

Data from dipwells 22 and 23 demonstrate that the hydrology of this part of the mire has been profoundly impacted and call for hydrological and ecological restoration measures. They also suggest that, in the long term, the impact of artificial shallow surface drains (locally called *rigoles*) might be more detrimental to the conservation of this type of mire than currently acknowledged by French conservations organisations, especially in places where no groundwater upwelling

contributes to maintaining a shallow water table in the overlying peat. The reasons for the substantial and permanent downward hydraulic gradient observed in clusters 21 and 22 as opposed to clusters 20 and 23 are unclear. The drains around cluster 22 may have resulted in a more pronounced decrease in piezometric head in the underlying formations, and resulted in the area between the drains acting as a constant recharge zone.

4.4. Conclusion: conceptual hydrological and hydrogeological model

Discharge monitoring proved difficult in this headwater catchment: only a limited number of locations were found where a V-notch weir could be installed, and free fall flow through weirs was often impacted by external factors such as cattle trampling or debris accumulating behind weirs. The substantial modification of the stream bed profile prevented an accurate stage-discharge relationship to be established at the catchment outlet. However high-accuracy discharge data could be recorded from the wetland outlet and, most of the time, from the three V-notch weir installed in the upstream part of the mire.

Together with data collected on the nature and distribution of granite weathering formations and peat and alluvial deposits at the bottom of the etch-basin, the qualitative analysis of piezometric records has allowed to build the following conceptual model of the hydrological functioning of the wetland:

- The mire is principally groundwater-fed and has formed where the aquifer flowing within the fissured granite zone intersects the ground surface.
- Despite the moderate permeability of the lower part of the peat deposits, groundwater upwelling maintains shallow water tables in the peat for all but the two or three driest months of the year.
- During this time, precipitation and overland inflow from the catchment probably play a limited role in the water balance of the peat column as saturation excess leads to quick runoff or superficial flow to water courses.
- Excess water from groundwater seepage probably flows rapidly to the low-lying parts of the mire and to water courses through a shallow but highly permeable poorly humified peat layer at the surface. However the depth and therefore hydrological significance of this layer is highly heterogeneous.
- In summer, the reduction or inversion of the vertical hydraulic gradient between the underlying mineral formations and the peat, associated to a higher evapotranspiration, leads to a drop in groundwater table within the peat.

- Groundwater upwelling and seepage may be more important along slope breaks, leading to generally shallower groundwater tables (for instance in clusters 3 and 24) than on gently sloping terrain (clusters 9 to 14).

However this general conceptual model is not valid everywhere across the mire, and many exceptions or variations have been found locally:

- Differences in the underlying substrate, in particular differences in fissure density or the existence of preferential flow pathways within the granite and the presence of substantial depths of saprolite may increase or reduce groundwater inputs. This is possibly the case on the south-west margin of the wetland near clusters 4, 5, 6 and 7, where the vertical hydraulic gradient is directed from the peat to the underlying formations.
- Artificial drainage and possibly peat fire, leading to substantial peat subsidence along drains, have substantially modified the hydrology of the north-east part of the mire, leading to deeper and more variable groundwater table depths and possibly to a reduction in groundwater inputs to the peat.
- The presence of deep and highly-permeable alluvial gravel deposits beneath or within the peat along the stream downstream of Puy Rond leads to a high hydrological connectivity between the stream and the mire in this area. Groundwater flow generally occurs from the mire to the stream, but is reversed in summer when shallow water tables in the mire are maintained by seepage through the stream bed. The flow reversion in summer was paradoxically enhanced when the stream was artificially diverted to slightly higher grounds. In this area, the low topographic gradient in the mire and the low stream profile gradient lead to frequent flooding.

There are still substantial uncertainties regarding this conceptual model, in particular relating to the presence and hydrological role of saprolite beneath the mire. Geological drilling logs showed that there are substantial volumes of saprolite north-east of Puy Rond, but no evidence of substantial saprolite depths downstream of Puy Rond could be found using ERT. Further work, including ERT transects, geological drilling and pumping tests would be required to better characterise the geology of granite weathering formations beneath the mire.

Résumé du chapitre 4

La tourbière des Dauges a fait l'objet d'un suivi hydrologique détaillé pendant trois ans. Les débits ont été mesurés en continu dans les ruisseaux en amont de la tourbière grâce à des seuils à lame mince. Une courbe hauteur-débit a d'autre part été établie en deux points correspondant aux exutoires de la zone humide principale et du bassin versant étudié. La mesure des débits s'est avérée difficile sur ces petits cours d'eau de tête de bassin versant, du fait de modifications fréquentes de leur section suite à la remobilisation de sédiments par les fortes crues et à des dégradations occasionnées par le bétail. Néanmoins des données de qualité ont pu être enregistrées en trois points en amont de la tourbière, ainsi qu'à l'exutoire de la tourbière. Les niveaux dans le ruisseau principal ont également été relevés manuellement à trois emplacements supplémentaires.

Un réseau de 57 piézomètres, groupés en 23 nids, a été installé dans la zone humide et en périphérie immédiate de celle-ci. Les profondeurs de nappe et les niveaux piézométriques à différentes profondeurs dans la tourbe et dans les formations minérales sous-jacentes y ont été relevés manuellement tous les 15 jours environ. Des enregistreurs à pression ont également permis un suivi à haute fréquence dans 16 de ces piézomètres. Les données piézométriques ont été analysées de façon qualitative au moyen d'analyses en composantes principales et de résumés graphiques.

Associées aux données sur la nature et la distribution des formations d'altération du granite et des dépôts tourbeux et alluviaux décrites au chapitre 3, ces analyses ont permis de développer le modèle conceptuel hydrogéologique suivant:

- La tourbière est principalement alimentée par la nappe circulant dans les formations d'altération du granite, en particulier la zone fissurée. Sa présence est essentiellement liée à l'affleurement de cette nappe en surface.
- Malgré la perméabilité modérée de la partie inférieure du dépôt tourbeux, la nappe est maintenue à un niveau proche de la surface par des apports souterrains ascendants issus des formations minérales sous-jacentes, excepté pendant deux à trois mois en période estivale.
- Pendant la majeure partie de l'année, les apports météoriques et par ruissellement jouent donc probablement un rôle négligeable dans le bilan hydrique du dépôt tourbeux, puisque la très faible profondeur de la nappe entraîne leur évacuation

rapide vers les cours d'eau par ruissellement de surface ou par écoulement latéral superficiel.

- L'écoulement latéral à faible profondeur est facilité par la présence d'une couche superficielle de tourbe peu décomposée, peu épaisse mais très perméable : l'acrotelme. Néanmoins, sur le site étudié, l'épaisseur de cette couche et donc son importance hydrologique sont extrêmement variables.
- En été, la diminution des apports souterrains, voire dans certains cas l'inversion du gradient piézométrique, associés à l'augmentation de l'évapotranspiration dans la zone humide se traduisent par une chute du niveau de la nappe dans la tourbe.
- Les gradients piézométriques verticaux observés et les épaisseurs de tourbe plus faibles en périphérie suggèrent que l'exfiltration des eaux circulant dans les formations minérales est plus importante le long des ruptures de pente à la marge de la tourbière qu'au niveau des secteurs à pente plus faible au centre de la tourbière.

Toutefois, ce modèle conceptuel général n'est pas valide uniformément, et de nombreuses exceptions ou variations locales ont été mises en évidence :

- Les apports souterrains semblent variables en fonction de la nature des formations minérales sous-jacentes, et en particulier du degré de fissuration du granite, de la présence d'écoulements préférentiels et de la présence d'épaisseurs substantielles d'arène granitique.
- La création et l'entretien régulier dans le passé de drains à vocation agricole initialement peu profonds, peut-être en association avec des feux de tourbe, ont entraîné un affaissement important de la surface le long de ces drains sur la partie nord-est du site, et ont conduit à une modification substantielle des caractéristiques de la tourbe en surface et du comportement de la nappe sur ce secteur. La nappe y est plus profonde et plus variable que sur le reste du site, et, contrairement à la situation observée sur une grande partie du site, le gradient piézométrique vertical est descendant, montrant l'absence d'exfiltration d'eau souterraine.
- La présence de dépôts alluviaux graveleux sous ou au sein de la tourbe le long du cours d'eau principal dans la partie aval de la tourbière se traduit par une forte connectivité hydrologique entre le ruisseau et la tourbière dans ce secteur. Les échanges souterrains s'y effectuent en général de la tourbière vers le ruisseau, mais s'inversent en été lorsque la nappe dans la tourbe est maintenue à plus faible profondeur que dans le reste du site par des apports issus du ruisseau. Ces apports estivaux ont

paradoxalement été favorisés lorsque le ruisseau fut rectifié et détourné vers un secteur à la topographie légèrement plus élevée.

De nombreuses incertitudes subsistent néanmoins quant à ce modèle conceptuel, en particulier sur la présence et le rôle hydrogéologique d'arène granitique sous la tourbe et les dépôts alluviaux. Les sondages géologiques disponibles montrent la présence d'épaisseurs substantielles d'arènes dans la partie nord-est du site, mais la tomographie de résistivité électrique n'a pas permis de mettre en évidence de telles épaisseurs dans la partie aval du site. Un travail complémentaire associant tomographie, sondages géologiques et tests de débits et de perméabilité serait nécessaire pour mieux caractériser l'hydrogéologie des formations d'altération du granite.

Chapter 5. MIKE SHE / MIKE 11 model development

5.1. Introduction

The modelling phase of the current study aims to answer several applied questions relevant to the development of knowledge on the hydrology of acidic mires in Limousin and to the application of this knowledge to the conservation of these habitats:

- What is the long-term water balance of the wetland? What is the respective importance of inputs from direct precipitation, groundwater and surface runoff from the catchment? Do these inputs vary across the wetland or in time?
- What are the simulated hydrological impacts of substantial landuse changes within the catchment on the wetland? Do these impacts vary in time or space?

These questions will be addressed in Chapters 7 and 8, but, in order for them to be answered as accurately and completely as possible, they imply a specific design and a satisfactory performance of the hydrological model to be developed and open new methodological questions:

- Is it possible to model the hydrology of a groundwater-fed wetland in a basement region and to reproduce small-scale variations in stream discharge and water table depth in peat with a sufficient accuracy for the model to be used for ecological applications in particular?
- What are the parameters to which such a model is most sensitive?

This chapter aims to answer these methodological questions and to describe the model development.

5.2. Model objectives and choice of modelling environment

The research questions defined in Section 5.1 and the site hydrological, geological and topographical characteristics described in Chapters 3 and 4 imply a number of requirements that must be satisfied by the hydrological modelling environment selected for the current study. It must be able to model all relevant water fluxes at both the catchment and wetland scale. At the catchment scale, it must be able to model the impact of landuse on interception, evapotranspiration, groundwater flow and runoff. At the wetland scale, it must be able to reproduce spatially-varying groundwater dynamics on a relatively fine scale relevant to

vegetation ecology, and therefore a number of spatially-distributed hydrological processes: exchanges with the fissured bedrock aquifer, overland inflow and outflow, exchanges with watercourses and with the atmosphere. The MIKE SHE hydrological modelling system coupled to the MIKE 11 1D hydraulic model was chosen as a modelling framework satisfying these criteria (Thompson *et al.* 2004; Graham & Butts 2005; Refsgaard *et al.* 2010).

5.3. The MIKE SHE/MIKE 11 modelling environment

5.3.1. General description

MIKE SHE is a framework for deterministic, distributed physically-based hydrological modelling. It originates from the Système Hydrologique Européen (SHE) developed in the late 1970's and 1980's (Abbott *et al.* 1986a; b). Since the mid 1980s, it has been developed further by DHI Water & Environment (Graham & Butts 2005; Anonymous 2009b; Refsgaard *et al.* 2010) to include pre- and post-processing interfaces and a suite of modules each allowing for the integration of a particular process of the water cycle into an integrated model. Modules include process models for evapotranspiration, overland flow, unsaturated flow, groundwater flow, channel flow and their interactions (Figure 5-1). In the early stages of its development, the SHE was fully physically-based: each hydrological process was modelled by a set of physical equations describing mass flow and momentum transfer, such as the Darcy equation for saturated flow in porous media, or the Richards equation for unsaturated flow. It was also fully distributed: the governing equations were solved using finite-difference approaches based on a gridded spatial discretisation common to all processes (Graham & Butts 2005; Refsgaard *et al.* 2010).

As described in Section 1.4.1, such detailed models have a number of potential limitations (Graham & Butts 2005). MIKE SHE therefore includes a number of simplified process descriptions that, providing assumptions are made, allow for the use of simplified physical equations or even conceptual models based on a distributed, semi-distributed or lumped approach (Graham & Butts 2005; Anonymous 2009b; c). This allows for faster, less data-demanding modelling of processes the importance of which is deemed to be secondary for the hydrology of the modelled site, or for which data is simply not available. Figure 5-2 shows the numerical engines available for each hydrological process. The engines used in the current study are further detailed below.

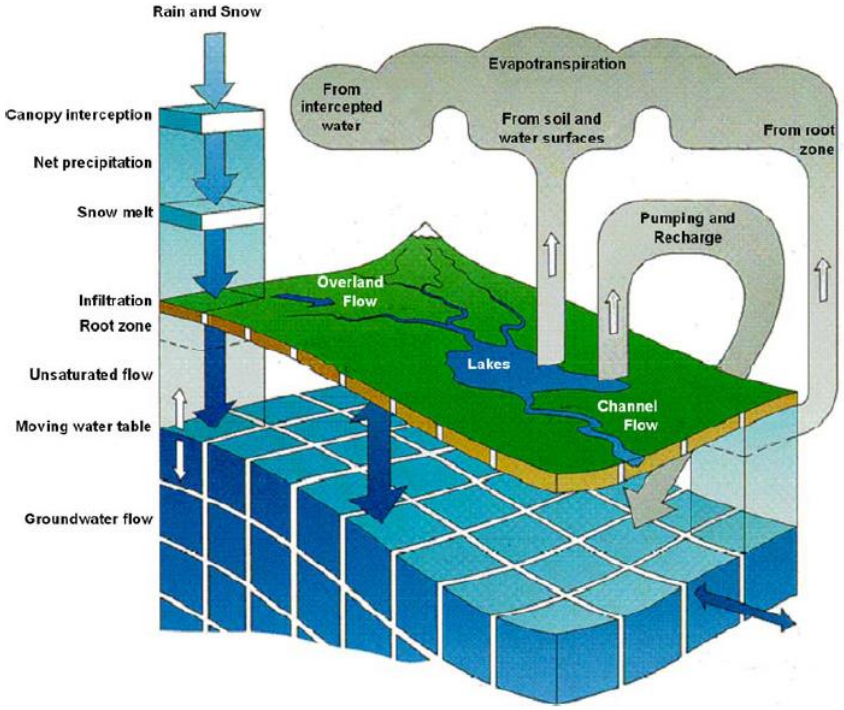

Figure 5-1. Hydrological processes simulated by MIKE SHE (from Graham & Butts 2005).

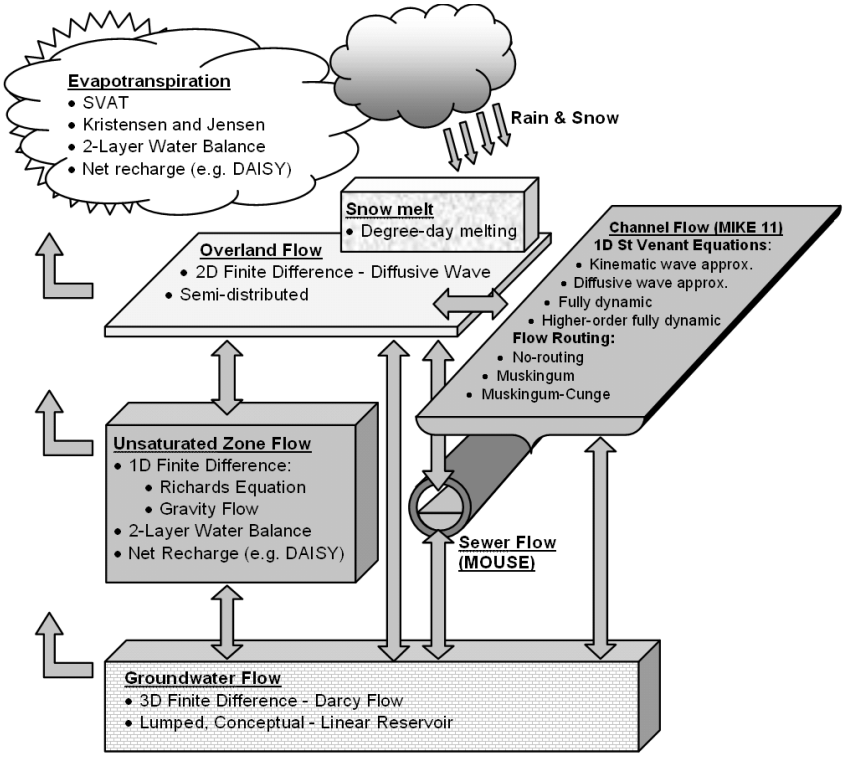

Figure 5-2. Numeric engines available in MIKE SHE for each hydrological process (from Anonymous 2009b).

MIKE SHE and MIKE 11 models can be built and run within MIKE ZERO, the graphical user interface for the DHI MIKE suite of models. The MIKE suite includes AUTOCAL, a generic tool to perform automatic calibration, sensitivity analysis, parameter optimisation and scenario management that interfaces with all MIKE models and can be run within MIKE ZERO (Madsen 2000, 2003; Anonymous 2009a). For institutional reasons this study used the 2009 version of MIKE SHE. Limitations imposed by the 2009 version compared to more recent ones are discussed below when appropriate.

5.3.1.1. Evapotranspiration and flow in the unsaturated zone

In MIKE SHE, evapotranspiration and unsaturated flow processes are modelled in the following order (Anonymous 2009c): rainfall interception and evaporation by the canopy, runoff generation or infiltration to the unsaturated zone, evaporation from ponded water and transpiration by plant roots, and finally percolation to the saturated zone. Two models are available to describe evapotranspiration and vertical flow in the unsaturated zone (lateral flow is assumed to be zero in all cases). The primary one uses the Kristensen and Jensen (1975) formulation to model evapotranspiration and the full Richards (1931) equation for unsaturated flow. This is the most accurate method but it is very computationally intensive, even though computation can be performed only on a representative sample of grid cells and the results extended to the rest of the modelled area. A simplified gravity flow procedure to calculate vertical unsaturated flow is also available when the interest is in groundwater recharge and not in the unsaturated zone dynamics themselves, or when capillary forces can be neglected such as in sandy soils (Graham & Butts 2005). In both cases, a fine description of the hydro-physical characteristics of the unsaturated zone is required. The second evapotranspiration and unsaturated flow model is a simple two-layer model (Yan & Smith 1994), used in the current study and therefore described in more detail. The two-layer model divides the unsaturated zone in an upper root zone where transpiration can occur, and a lower zone where it cannot. The depth of the upper zone is equal to the extinction depth or to the depth of the unsaturated zone when the groundwater table is higher than the extinction depth. The extinction depth is the sum of the thickness of the capillary fringe and of the root depth specified by the user for each landuse class. The lower layer extends from the extinction depth to the top of the saturated zone, and can be null when the latter is higher than the former. Within the upper layer, the water content can vary within an allowable range defined as a function of the user-defined unsaturated zone water content at saturation, field capacity and wilting point (Figure 5-3).

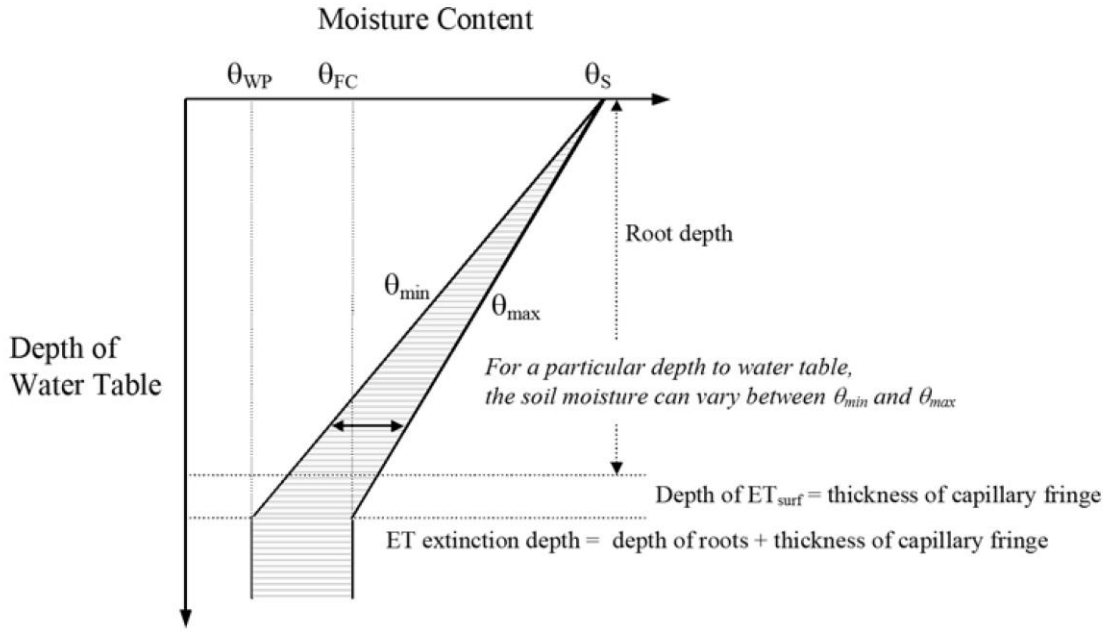

Figure 5-3. Allowable water content in the upper layer of the two-layer unsaturated zone model, as a function of water table depth (from Anonymous 2009c).

The difference between the unsaturated zone water contents at saturation θ_S and at field capacity θ_{FC} gives the specific yield. For consistency between the unsaturated and saturated models, the actual specific yield used for the uppermost saturated zone computational layer is based on this difference, overriding the specific yield obtained from the saturated zone parameters. The difference between the unsaturated zone water contents at field capacity θ_{FC} and at the wilting point θ_{WP} conditions the allowable range of water content in the unsaturated zone.

The 2-layer unsaturated zone model does not account for the relation between unsaturated hydraulic conductivity and soil moisture content, but simply assumes that if water is available within the root zone it is available for evapotranspiration. As a consequence it is particularly efficient in soils with a shallow groundwater such as in wetlands. In drier soils it does not represent the unsaturated flow dynamics accurately, but may still performs reasonably well under most conditions after calibration (Graham & Butts 2005; Anonymous 2009c). Its main advantage is a dramatically reduced computation time compared to the Kristensen and Jensen / Richards model, and a conceptual simplicity that substantially reduces the number of parameters to calibrate when little data is available to fully describe the unsaturated zone.

In both evapotranspiration models, the maximum possible evapotranspiration ET_{max} is defined as a function of the reference evapotranspiration, that must be provided as a time-series by the

user. However the function used differs markedly between the two models, and the consequences of this are further discussed in Section 5.4.2.

In all unsaturated flow models available within MIKE SHE (Richards, gravity flow or two-layer), it is possible to bypass the unsaturated model by routing a fraction of the infiltration directly to the saturated zone. The bypass fraction can be made dependant of the soil moisture conditions. This allows for the representation of fast flow through soil macropores or cracks for instance (Refsgaard *et al.* 2010).

5.3.1.2. Overland flow

MIKE SHE can calculate overland flow using a 2D, finite-difference, diffusive wave approximation of the Saint-Venant equations (Graham & Butts 2005; Anonymous 2009c). Two solution methods are available: a successive over-relaxation numerical solution - used in the current study -, or an explicit numerical solution. The latter is more accurate but requires smaller time steps and longer computation times. It is generally used when flooding from the river network is modelled using overbank spilling. In both case it is possible to specify a uniform or spatially-distributed detention storage depth, i.e. a minimum ponded water depth that has to be reached before overland flow occurs. This can be used to account for water storage in the terrain's micro-topography that cannot be accurately represented by a DEM at the model resolution.

A simplified semi-distributed routing approach based on Manning's equation is also available when spatially-detailed overland flow description is not required, for instance in regional applications.

5.3.1.3. Saturated flow

MIKE SHE offers two approaches to model groundwater flow: a lumped or semi-distributed conceptual linear reservoir approach and a physically-based, fully distributed approach (Graham & Butts 2005; Anonymous 2009c). The former can be used to model groundwater inputs to streams, but not spatially-distributed groundwater table depth, and is therefore particularly of use when modelling large catchments where little hydrogeological information is available and where the focus is on simulating river flow. The latter, used in the current study, uses an iterative implicit finite difference technique to solve the 3-dimensional Darcy equation. The numerical grid is composed of one to several computational layers extending across the model area. The parameters required for the computation of groundwater flow, such as hydraulic conductivity,

specific yield and specific storage, are interpolated to the numerical grid from the user-specified geological model, the geometry of which may or may not correspond to that of the numerical grid. The geological model can include geological layers (extending across the entire modelled area) and geological lenses (that can have a smaller extent and take precedence over geological layers). A no-flow boundary condition is assumed at the bottom of the groundwater model.

5.3.1.4. Channel flow

MIKE SHE uses the MIKE 11 1D hydraulic model to simulate channel flow. Channel flow can either be modelled by solving the 1D Saint-Venant equations or with a more simple kinematic routing method (Havnø *et al.* 1995; Anonymous 2009d). The first method uses an implicit finite difference scheme for the computation of unsteady flow, and is able to accurately model complex 1D flow patterns, including loops, flow control structures and backwater effects. However it generally requires relatively small time-steps (in the order of seconds or minutes). The main advantage of the routing method is that it can be used with much longer time steps, for instance daily, dramatically reducing run times. River stage can be calculated a posteriori based either on user-specified stage-discharge relationships, or on the Manning equation. This method cannot accurately model control structures and backwater effects, so is better suited for fast-flowing upstream reaches.

The MIKE 11 network and cross-sections can take any shape. The coupling between MIKE 11 and MIKE SHE is made using river links, located on the edges of the closest MIKE SHE grid cells (Figure 5-4). At each river link, exchanges between MIKE 11 and MIKE SHE are based on a simplified triangular cross-section, the bottom and bank levels of which are interpolated based on the two closest MIKE 11 sections (Figure 5-5). Exchanges between groundwater and river channel are based on the head difference (Δh in Figure 5-5) and the conductance. The conductance can depend on the conductivity of the aquifer, the river bed or both. Input from overland flow to the river can only occur if overland head is higher than the MIKE SHE link bank.

There are three ways to represent flooding, i.e. flow from the river to the overland flow module. The first one is to neglect it: water can flow to the river but not out. The second one is to use flood codes, whereby floodplains are mapped by the user using grid codes. The river stage calculated by MIKE 11 at each H-point (i.e. MIKE 11 stage computation point, generally coinciding with a cross-section) is then extended to the floodplain, assuming that river and floodplain stages are equal. Water elevation is then interpolated between H-points and mapped onto the floodplain topographic grid with water being removed from MIKE 11.

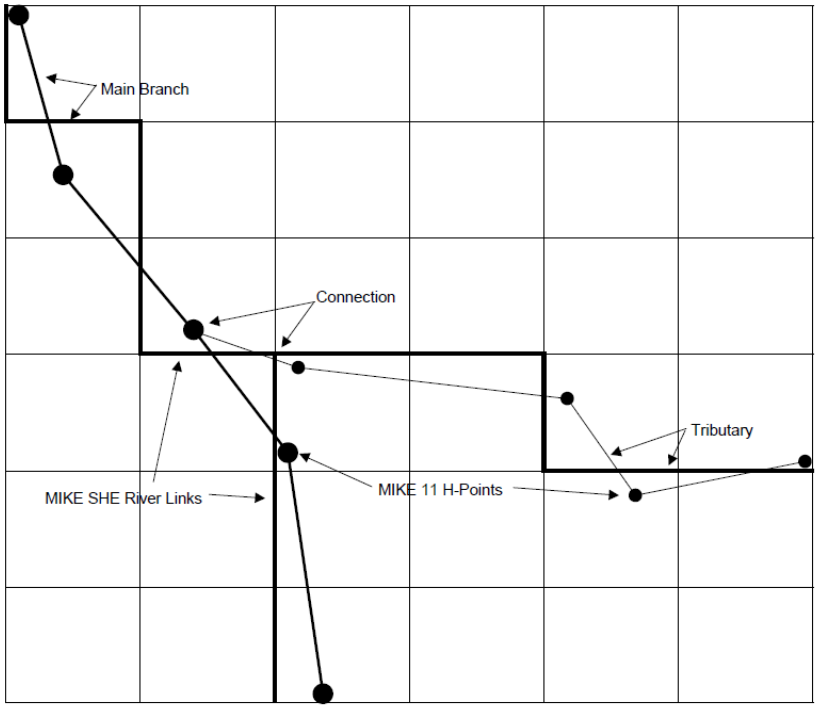

Figure 5-4. MIKE 11 branches and MIKE SHE river links (from Anonymous 2009c).

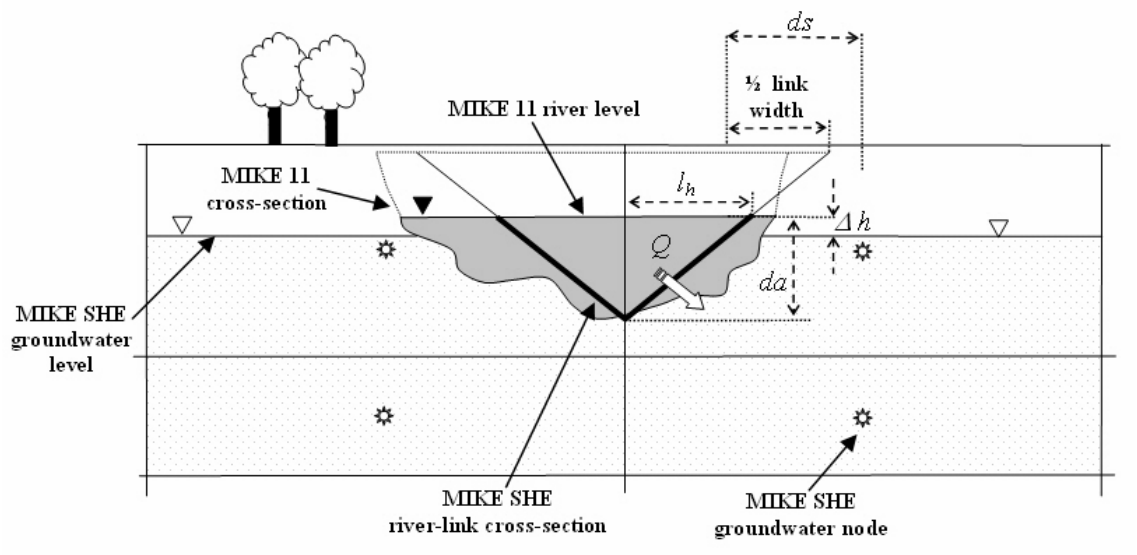

Figure 5-5. Linkage between MIKE SHE links and MIKE 11 cross-sections (from Anonymous 2009c).

The main advantage of flood codes is their computational simplicity, with little impact on run times. However the method is designed as a way to spread water onto the floodplain and to allow for infiltration and evapotranspiration, but not to accurately model 2D overland flow. When overland flow is possible between sections or when the volume of water stored onto the floodplain is large compared to that stored into the river channel, the method leads to numerical instabilities. The third and most accurate solution is to use overbank spilling, whereby the river

bank is modelled as a weir, and floodplain flow is modelled as overland flow. However this is computationally demanding and generally requires long run times.

5.3.2. Use of MIKE SHE in wetland hydrological modelling

The possibilities offered by the MIKE SHE/MIKE 11 modelling framework to develop purpose-built, flexible integrated models that account for all relevant hydrological processes has made it a tool of choice for wetland hydrological modelling. Among the earliest studies that used MIKE SHE to model wetland hydrology are those undertaken by Al-Khudhairy *et al.* (1999), Thompson (2004) and Thompson *et al.* (2004, 2009), the aims of which were to understand and model the hydrology of the North Kent grazing marshes (UK), and to investigate the expected impacts of hydrological management and climate change on the hydrology of this site of high conservation value. In the North Kent marshes, clayey alluvial soils are isolated from the underlying chalk and Tertiary aquifers by a layer of very low permeability London clay. The saturated zone vertical discretisation was therefore limited to a single layer. Flooding was simulated using the flood codes option. The model was highly sensitive to the proportion of bypass flow in the unsaturated zone component, used to reproduce macropore flow through the cracks opened by soil drying. Overall, the model reproduced well both groundwater tables in the alluvium (Figure 5-6) and water levels in ditches.

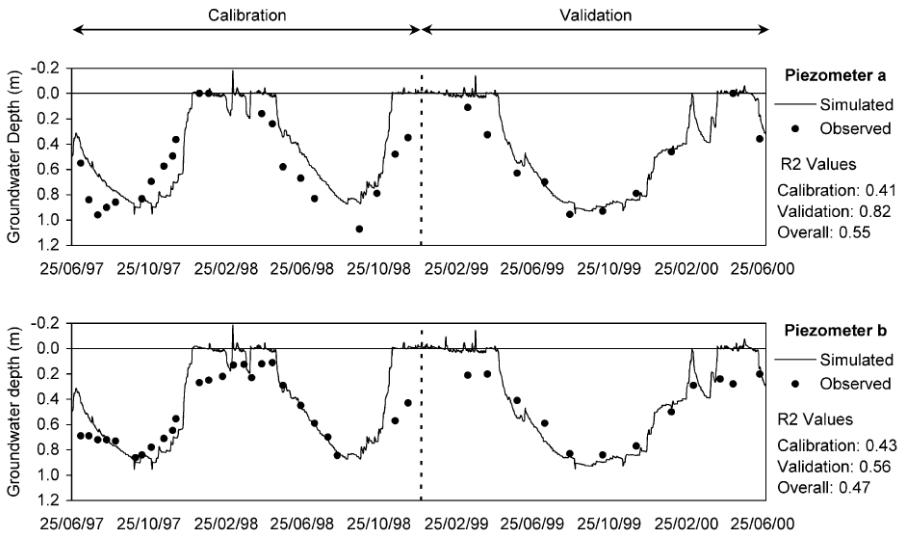

Figure 5-6. Observed and simulated groundwater table depth in the North Kent marshes (from Thompson et al. *2004).*

Lu *et al.* (2006, 2009) used MIKE SHE to model the impact of forest harvesting and climate change in pine flatwoods, a mixture of cypress wetlands and managed pine uplands in Florida, USA. Despite a coarse grid size, the model satisfactorily reproduced observed groundwater tables in

most but not all dipwells. Discrepancies were attributed to the poor representation of the surface micro-topography at the model resolution and to a lack of information on the spatial distribution and hydraulic parameters of soils and geological substrate. Forest harvesting was simulated by reducing the LAI, and climate change by perturbing the meteorological input data by an arbitrary -10% for rainfall and +2°C for temperature.

Hammersmark *et al.* (2008, 2009) used a coupled MIKE SHE / MIKE 11 to investigate the effect of river channel restoration on the hydrology and ecology of Bear Creek Meadow, a riparian meadow in northern California, USA. The model included a three-layer saturated zone, a detailed MIKE 11 network, unsaturated flow based on the Richards equation, and overland flow (diffusive wave approximation). Observed discharge time-series were used as boundary conditions upstream and downstream of the MIKE 11 network. The model was calibrated and validated using punctual observations over a two-year period in 28 shallow dipwells and two river stage monitoring stations. The model performance was excellent, with Nash-Sutcliffe Efficiencies higher than 0.9 for both river stage and groundwater table depth, even though it should be noted that only one groundwater observation per month was available (Figure 5-7). The impact of channel restoration was investigated virtually by modifying the MIKE 11 cross-sections, and it was found to result in a substantial increase in groundwater levels within the riparian meadow.

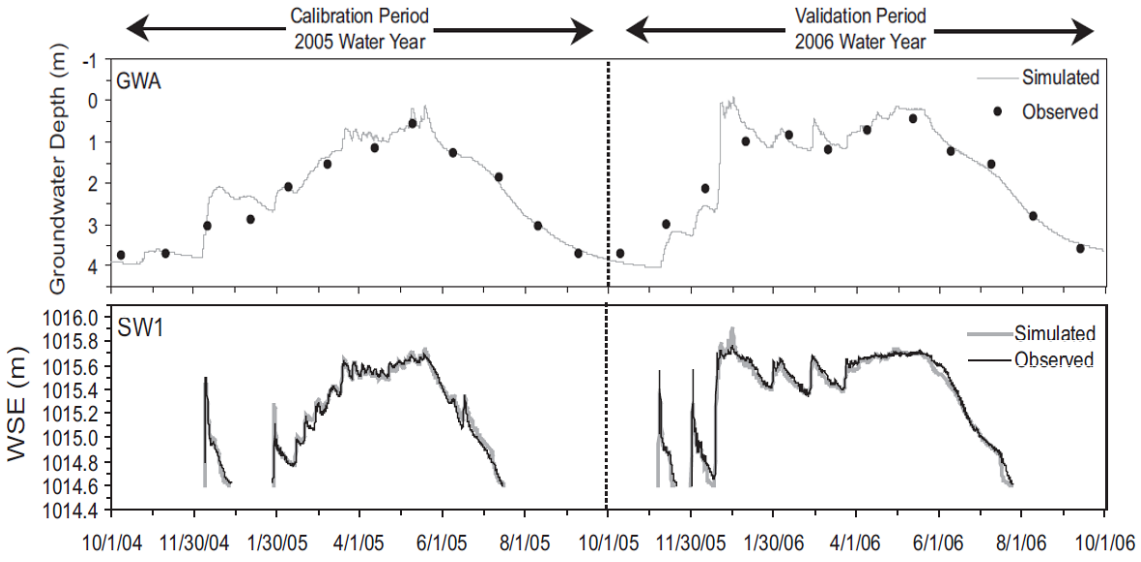

Figure 5-7. Observed and simulated groundwater table depth (top) and stream stage (bottom) in Bear Creek Meadow (modified from Hammersmark et al. *2008).*

Rahim *et al.* (2009, 2012) developed a MIKE SHE / MIKE 11 model of the Paya Indah wetlands, Malaysia, with a groundwater model divided in three layers, the uppermost representing peat. The gravity flow option was used to model unsaturated flow to reduce run times, and

parametrised using the results of hydraulic property tests on 50 randomly sampled soil cores. The model was calibrated and validated using 10 years of data collected at two discharge monitoring stations, two boreholes and two stations monitoring water levels in small lakes within the wetland. Some of the model outputs after calibration are shown in Figure 5-8 and Figure 5-9. The model was used to perform a detailed water balance analysis of the wetland.

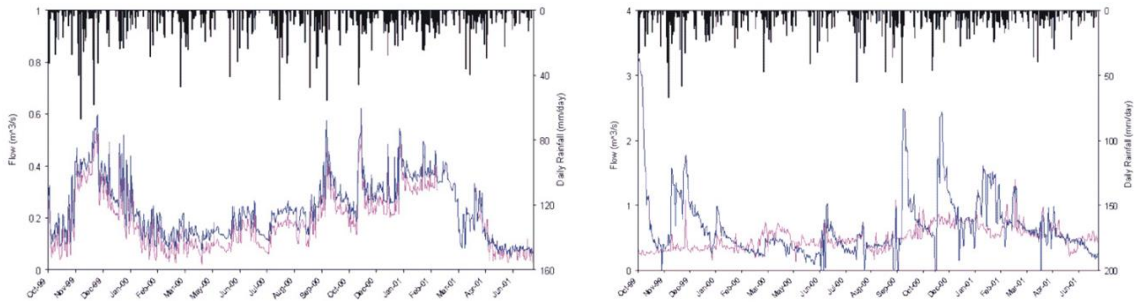

Figure 5-8. Observed and simulated discharge in the Paya Indah wetlands (Rahim et al. *2012).*

Black bars: precipitation; red lines: observed discharge; blue lines: simulated discharge.

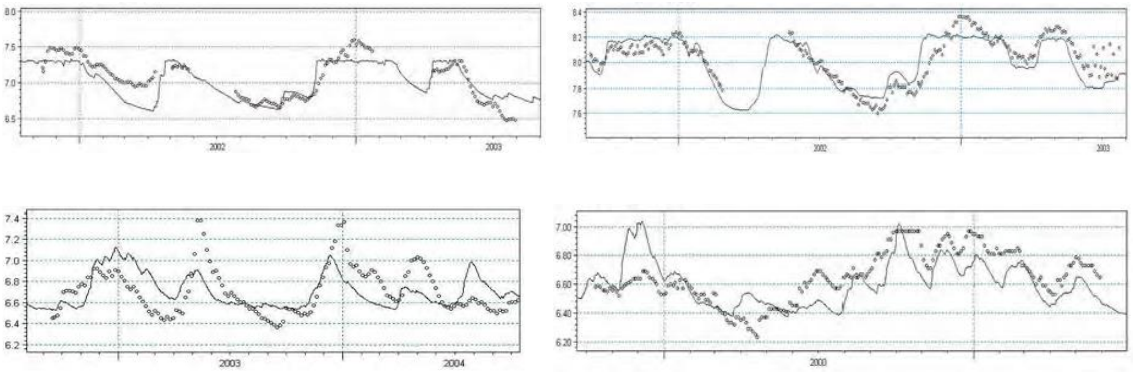

Figure 5-9. Observed and simulated groundwater table level in the Paya Indah wetlands (Rahim et al. *2009).*

Open circles: observed groundwater table levels; lines: simulated groundwater table levels.

Singh (2010) and Singh *et al.* (2010, 2011) modelled the water level regime of Loktak Lake, northeast India. The lake levels themselves were modelled using a relatively simple water balance approach to estimate the lake volume and a volume-level relationship derived from bathymetric surveys. MIKE SHE and MIKE 11 were used to model discharge from the lake catchment. A single-layer saturated zone model was used. Evapotranspiration and unsaturated flow were modelled using the two-layer approach. Despite the scarcity of data, the model goodness-of-fit during validation was judged as excellent. The impact on lake levels of a range of options for barrage operation, water abstraction and climate change were investigated by changing the MIKE SHE inputs or parameters or the water balance terms.

Cook (2012) developed a 400m-resolution MIKE SHE / MIKE 11 surface/subsurface model of the Everglades National Park (Florida, USA), including a large number of control structures. The groundwater model contained two numerical layers corresponding to the distinction between highly permeable superficial oolite and less permeable material underneath. Unsaturated flow was modelled using the Kristensen and Jensen / Richards model and overland flow using the diffusive wave approximation. The model was calibrated and validated using long-term water level and discharge time series, and was found to be most sensitive to the hydraulic conductivity of the saturated zone, the overland Manning's roughness coefficient and the river bed leakage factor.

Bourgault (2013) and Bourgault *et al.* (2014) modelled the Lanoraie peatland complex, part of a 364km² catchment in Québec, Canada. Groundwater was simulated in steady-state, using a 250m resolution grid with rivers represented as head-controlled flux and drains and minor streams as fixed head drains. The saturated zone was discretised horizontally in five computational layers. Evapotranspiration and unsaturated flow were not modelled, but constant groundwater recharge specified as a calibrated model input. The model was calibrated based on groundwater table depth observed in 150 wells and river baseflow calculated from observed discharge. The model performance (Figure 5-10) was considered satisfactory. The model was used to quantify peatland-aquifer-river exchanges at the regional scale, and to assess the impact of climate change on these exchanges.

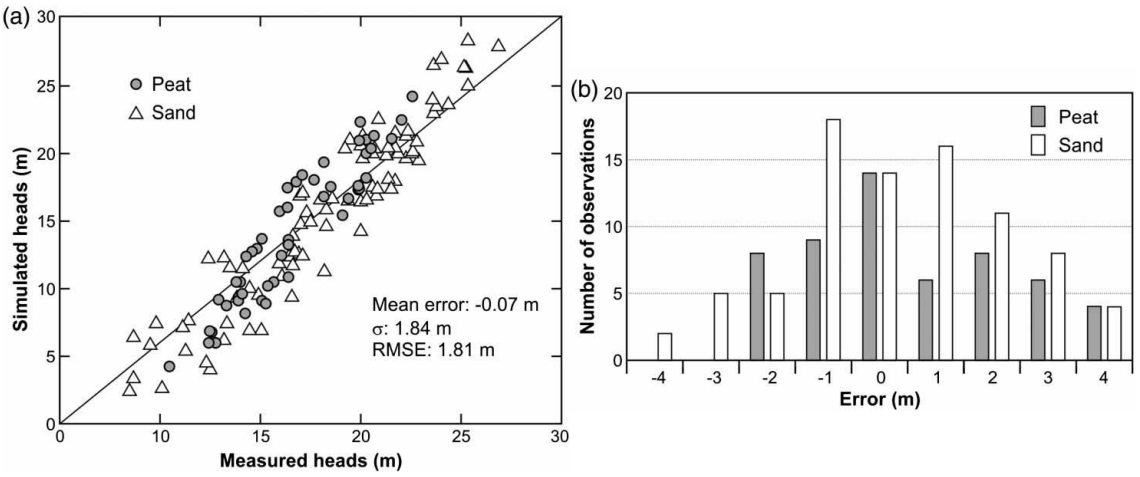

Figure 5-10. Performance of the Lanoraie steady-state MIKE SHE model with regard to groundwater head (Bourgault et al. *2014).*

Johansen *et al.* (2014) modelled the impact of groundwater abstraction on groundwater tables within a groundwater-fed fen in the Lindenborg River valley, Denmark. The unsaturated zone was modelled using the Kristensen and Jensen / Richards model, groundwater flow using the finite difference solver, overland flow using the diffusive wave approximation, and surface flow using a mixture of MIKE 11 channels and subsurface drains included in the groundwater model. The authors used three nested models with decreasing size and increasing resolution (150, 25 and 5m) to model groundwater flow at the regional-, floodplain- and fen-scale respectively (Figure 5-11). The nested models were linked by manually transferring head boundary conditions from larger to smaller models. Overland flow across model boundaries was assumed to be negligible, and there was no river crossing the nested model boundaries. The vertical discretization followed the six geological layers recognised within the modelled area. Localised spring flow caused by preferential flow through fractures in the limestone was an important source of water to the wetland. This was modelled by locally increasing the hydraulic conductivity of the geological model underneath the spring locations. The nested models were calibrated against long-term groundwater table depth observations. The smaller model reproduced relatively well the peat groundwater table dynamics, but generally underestimated its depth by 20-50 centimetres (Figure 5-12). The nested models were used to simulate the impact of groundwater abstraction on the fen hydrology and ecology.

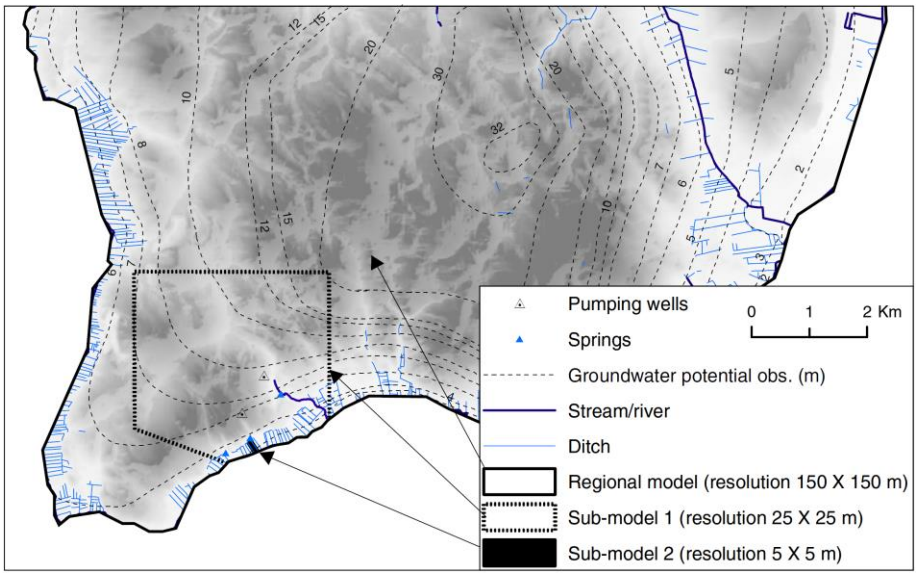

Figure 5-11. Nested models used by Johansen et al. (2014) to model the Lindenborg fen.

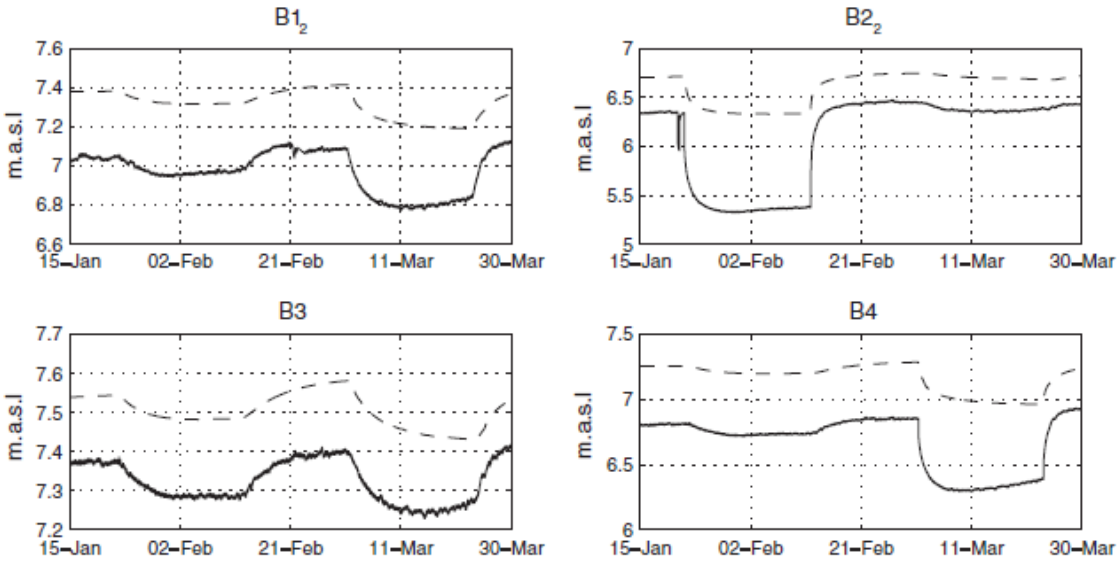

Figure 5-12. Observed and simulated groundwater heads in the Lindenborg fen (Johansen et al. *2014).*

In conclusion, MIKE SHE coupled to MIKE 11 has proved a useful tool to model wetland hydrology in a large number of geographical and environmental contexts. The studies demonstrate the ability of the modelling framework to integrate all relevant hydrological processes. Except when used to model inflow from tributaries to large wetland systems, such as the Loktak lake modelled by Singh (2010) and Singh *et al.* (2010, 2011), the modelled area is generally limited by run times to the small to medium scale, unless nested models are used as in Johansen *et al.* (2014) or a very coarse resolution is used. The latter solution may be acceptable when the terrain is relatively flat as in Cook (2012), but may result in a misrepresentation of overland flow and discrepancies between the MIKE SHE topographic grid and the MIKE 11 network when the topography is more varied, for instance in Lu *et al.* (2006, 2009). Interestingly, in all wetland hydrological modelling studies using MIKE SHE that could be consulted, model components were calibrated in a single step using observed groundwater levels, surface water levels and/or stream discharge only. In particular no example was found of calibration of the evapotranspiration and unsaturated zone sub-model using actual evapotranspiration, canopy interception or soil moisture measurements for instance, even in applications aimed at estimating the impact of landuse or climate change and in which not only the wetland, but also its catchment, were modelled. Such measurements are rarely made in routine but would allow for a better calibration and validation of the model, particularly when the objective is to assess the effect of landuse change or climate change on groundwater or surface water flow.

5.4. Model design and initial parametrisation

5.4.1. Precipitation

Daily precipitation records corrected for missing data, as detailed in Appendix E, were used as inputs to the MIKE SHE model. Precipitation were assumed to be spatially uniform, which is considered a reasonable assumption given the excellent correlation between daily precipitation recorded within the research site and at the St-Léger-Mon met station 4.2km away. In the absence of records on snow depth, snow melt was not simulated and all precipitation were assumed to be liquid. This assumption was made to simplify the model but is considered reasonable on several grounds. First, the number of days with snow on the ground per year is relatively small. Data from Météo-France covering the 1961-1986 period gives a mean of 21 days per year. The number of days with snow on the ground recorded while the albedometer (see Appendix E) was effective at the Dauges site was even lower: 37 days in total over two years. Second, snow melt would only be significant in winter when piezometric monitoring has shown that the wetland is completely saturated and would therefore have no impact on water table depths within the wetland.

5.4.2. Evapotranspiration and unsaturated flow

To model unsaturated flow and actual evapotranspiration, the empirical two-layer model was chosen instead of the Kristensen & Jensen (1975) model for evapotranspiration and the full Richards (1931) equation for unsaturated flow. This choice was made principally for computation time reasons, but was also justified by the lack of detailed data on the unsaturated zone properties, including both soils and the underlying unsaturated fissured granite, and the lack of soil moisture records that could have been used to independently calibrate the unsaturated zone model. The two-layer method requires an estimate of the potential evapotranspiration rate under optimal conditions ET_{pot} for each vegetation class. ET_{pot} is then satisfied in each model time-step by emptying the following reservoirs in turn: snow storage (assumed to be null in this study), interception storage, ponded water, unsaturated zone and saturated zone (provided the water table is above the depth defined by the sum of root depth and capillary fringe thickness). In MIKE SHE, ET_{pot} is obtained by multiplying the reference evapotranspiration ETo (calculated using the FAO Penman-Monteith method in this study, see Appendix E) by a spatially- and time-varying crop coefficient. This is similar to the FAO crop coefficient method (Allen *et al.* 1998), whereby the FAO Penman-Monteith reference evapotranspiration ETo rate is multiplied by a

seasonally- and spatially-varying crop coefficient K_c to adjust it to the characteristics of the actual vegetation. In the FAO method, K_c can be partitioned into different components representing crop transpiration in the absence of water stress (basal crop coefficient K_{cb}), transpiration reduction in the presence of water stress (K_s) and evaporation from wet soil surface and interception storage after rainfall (K_e), see Figure 5-13. Alternatively, a single crop coefficient with averaged soil evaporation effects (K_{cm}) can be used to estimate actual evapotranspiration over longer periods.

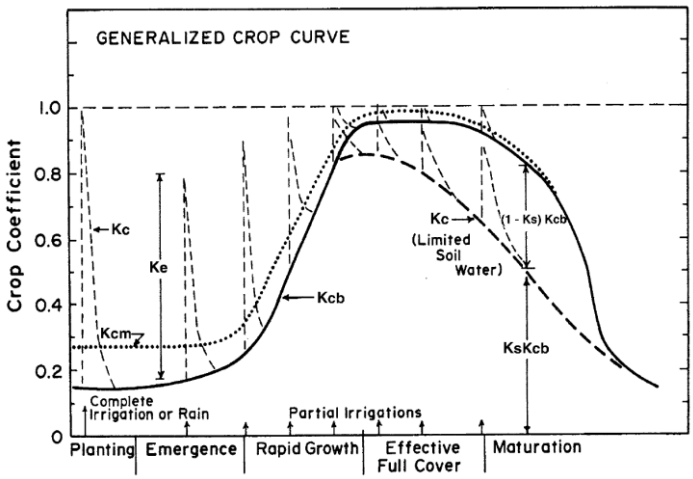

Figure 5-13. Generalised crop coefficient curve (Allen & Pereira 2009)

K_c: crop coefficient (=K_s*K_{cb}+K_e). K_c varies over time due to crop development (included in the basal crop coefficient K_{cb}), evaporation from wet soil surface (K_e) and water stress (K_s) that reduces K_c relative to K_{cb}. K_{cm} is a single crop coefficient with averaged soil evaporation effects. Unlike in this example, Allen *et al.* (1998) make it clear that K_c can be higher than 1, and therefore actual evapotranspiration higher than the reference evapotranspiration ETo.

The crop coefficient method was designed to estimate actual evapotranspiration, reducing it when water stress occurs and increasing it just after rainfall events to account for evaporation from the soil and from interception storage, both of which can be very high (Allen *et al.* 1998). A similar approach is used in a number of eco-hydrological models, such as the widely used SWAT model (Neitsch *et al.* 2005) or the forest eco-hydrology model BILJOU used by French foresters (Granier *et al.* 1999). In these models, evaporation from interception, snow and wet soil can occur up to the energy-constrained upper limit on evapotranspiration (ETo in the case of SWAT), and transpiration up to ETo x K_{cb} (ETo weighted for LAI in the case of SWAT). The total of evaporation and transpiration cannot exceed the energy-constrained limit. Unfortunately in the MIKE SHE two-layer evapotranspiration and unsaturated flow model, evaporation from interception storage, ponded water and wet soil is subtracted from the reference evapotranspiration after it has been corrected by the crop coefficient. In theory, the crop coefficient used in MIKE SHE should therefore be the time-varying FAO dual crop coefficient

($K_c=K_{cb}+K_e$ in Figure 5-13). Unfortunately, the software does not allow for high resolution (daily for instance) crop coefficient time-series to be used. The crop coefficient can only vary seasonally.

This is a drawback as this means evaporation is not modelled independently of transpiration. Adjusting the basal crop coefficient to account for evaporation after rainfall, as recommended by the FAO (Allen *et al.* 1998), would result in an over-estimation of transpiration when the interception storage has been evaporated. Inversely, not adjusting it would result in an under-estimation of the actual evapotranspiration. This is especially the case in wet climates where precipitation events are frequent but small, evaporation from intercepted precipitation, ponded water and wet soil is therefore frequent and important, there is little water stress and transpiration proceeds at the full rate most of the time. Furthermore, and contrary to the Kristensen & Jensen method, the two-layer model does not adjust transpiration for variations in LAI. These two constraints mean that accounting for the absence of transpiration from dead vegetation or for the substantially reduced transpiration rates in deciduous trees during the leafless season while allowing for evaporation from interception storage and ponded water is not straightforward. Setting the crop coefficient to a very low value would reduce not only transpiration, but also the maximum volume of evaporation from interception storage and ponded water, possibly leading to an underestimation of evapotranspiration in winter. On the other hand, maintaining the crop coefficient to a relatively high level would result in transpiration being over-estimated.

In view of these limitations, interception was modelled outside MIKE SHE, using an R script. The same reservoir method was used: precipitation fills an interception storage before flow to the ground can occur. The volume of the interception storage can be adjusted according to vegetation class, LAI and season. Intercepted water can then evaporate provided potential evapotranspiration is large enough. Any intercepted water that is not evaporated is carried over to the next time step. In MIKE SHE, interception storage can be filled and evaporated at every time-step. If the model runs with an adaptive time-step, this means that the total amount of intercepted water can vary independently of rainfall and potential evapotranspiration. Instead, a fixed daily time-step was used to make sure comparisons between model runs were possible.

Assuming that evaporation from ponded water and from wet soil is limited due to the continuous vegetation cover, modelling interception outside MIKE SHE means that potential evaporation and potential transpiration can be modelled independently, similar to the way the FAO dual crop-coefficient proceeds. Transpiration is limited to ETo multiplied by a basal crop coefficient, while

both evaporation from interception and total evapotranspiration are limited to the energy-constrained upper limit on evapotranspiration (cf. below). The crop coefficient in MIKE SHE can then be defined as the basal crop coefficient K_{cb}, that varies seasonally and spatially to model the transpiration characteristics of each vegetation class. K_{cb} has to be simplified into average values for each vegetation development stage. The FAO method allows for such an idealisation of the annual crop coefficient curve into three crop coefficients ($K_{c\ ini}$, $K_{c\ mid}$ and $K_{c\ end}$) each corresponding to a particular vegetation development stage (Figure 5-14).

Crop coefficients have been derived empirically from soil or atmosphere moisture balance experiments for a large number of agricultural crops (Allen *et al.* 1998), but are virtually non-existent for natural and semi-natural vegetation classes. Table G-1 in Appendix G shows a range of values found in the literature for vegetation classes similar to those within the Dauges catchment that could be used to estimate crop coefficients. The values listed in the table are very variable. This might in part be explained by differences between studies in terms of the methods used to measure actual evapotranspiration and to calculate reference evapotranspiration. For instance many older studies used the Penman open water evaporation as the reference, while more recent ones used the FAO Penman-Monteith method.

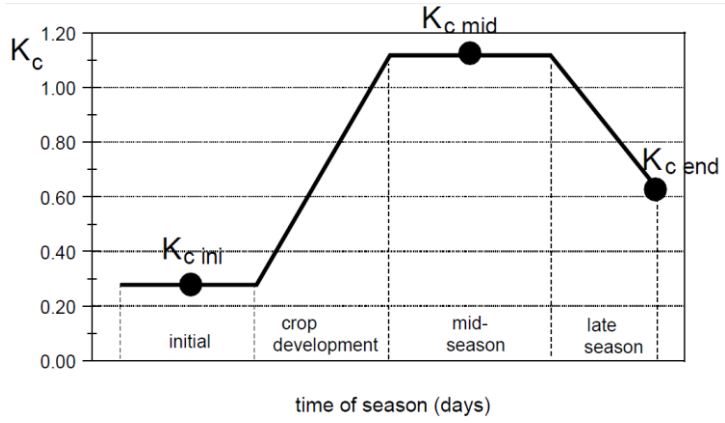

Figure 5-14. Idealised crop coefficient curve (Allen et al. *1998).*

Even though an effort was made to only include coefficients calculated in the absence of water stress, this is not always clearly specified, and some coefficients may have been underestimated as a result of transpiration reduction under these conditions. Conversely, most studies have measured total evapotranspiration, which can increase substantially when the soil and canopy are wet. For natural and semi-natural vegetation for which crop coefficients are not available or reliable, Allen *et al.* (1998) and Allen & Pereira (2009) suggested a procedure to estimate mid-season crop coefficients $K_{c\ mid}$ based on climate, vegetation height, leaf area index or ground

cover, and mean leaf resistance. Section 5.4.3 details how estimates of these parameters relevant to the research site were obtained.

Allen & Pereira (2009) assumed that for expanses of vegetation larger than 500-2000m², an equilibrium boundary layer is established and a maximum upper limit on evapotranspiration ET_{max} exists due to the law of conservation of energy. This energy-constrained limit can be used to estimate the maximum crop coefficient $K_{c\ max}$ following rain and for vegetation having full or nearly full ground cover, so that:

$$K_{c\,max} = max\left(\left\{1.2 + [0.04(u_2 - 2) - 0.004(RH_{min} - 45)]\left(\frac{h}{3}\right)^{0.3}\right\}, \{K_{cb} + 0.05\}\right) \quad \text{Equation 5-1}$$

where u_2 and RH_{min} are the average wind speed and minimum relative humidity at 2m during the particular growth stage, h is the mean vegetation height and K_{cb} is a basal crop coefficient. Equation 5-1 suggests that the energy-constrained maximum evapotranspiration ET_{max} is 1.05-1.30 times the reference evapotranspiration, depending on climate. Equation 5-1 was used in the current study to define the upper limit on both evaporation from interception and total evapotranspiration ET_{max}, as the product of $K_{c\ max}$ and ETo, the daily FAO Penman-Monteith reference evapotranspiration, the computation of which is detailed in Section E.3.6 in Appendix E. In Equation 5-1, *h* was assumed to be that of the FAO reference crop (0.12m), and u_2 and RH_{min} the long-term mean wind speed and minimum relative humidity, giving a maximum evapotranspiration of 1.16 times the Penman-Monteith reference evapotranspiration. The choice of a constant vegetation height is clearly a simplification and may lead to an underestimation of evapotranspiration in forests. However both the method and the calculated ET_{max} value are similar to those used in some forest-focussed eco-hydrology models (Granier *et al.* 1999). The basal crop coefficient K_{cb} is given by:

$$K_{cb} = K_{c\,min} + K_d\left(K_{cb\,full} - K_{c\,min}\right) \quad \text{Equation 5-2}$$

Where $K_{c\ min}$ is the minimum crop coefficient when soil is bare (about 0.15), K_d is a vegetation density coefficient and $K_{cb\ full}$ is the estimated basal crop coefficient during peak plant growth with full ground cover. K_d can be estimated from ground cover or from leaf area index:

$$K_d = 1 - e^{-0.7LAI} \quad \text{Equation 5-3}$$

$K_{cb\ full}$ is estimated as a function of plant height and climate:

$$K_{cb\,full} = F_r \left(min(1.0 + 0.1h, 1.2) + [0.04(u_2 - 2) - 0.004(RH_{min} - 45)] \left(\frac{h}{3}\right)^{0.3} \right) \quad \text{Equation 5-4}$$

The second part (between brackets) of Equation 5-4 is actually the energy-constrained upper limit to evapotranspiration, corrected for the height of the vegetation. The F_r parameter allows for a reduction in the crop coefficient if the vegetation has a higher degree of stomatal control than the reference grass crop. It is given by:

$$F_r \approx \frac{\Delta + \gamma(1 + 0.34u_2)}{\Delta + \gamma\left(1 + 0.34u_2 \frac{r_l}{100}\right)} \quad \text{Equation 5-5}$$

Where r_l is the mean leaf resistance, Δ is the slope of the saturation vapour pressure versus air temperature curve (calculated using the mean temperature over the mid-season development stage, see Equation 13 in Allen *et al.* (1998) for computation details and Section E.3.2 in Appendix E for details on the temperature dataset), and γ is the psychrometric constant (see equation 8 in Allen *et al.* 1998). The data used to calculate crop coefficients for each vegetation class are given in Section 5.4.3.

The other unsaturated zone model parameters were set to different values according to the type of soil, as shown in Table 5-1.

Table 5-1. Unsaturated zone parameters.

Soil type	Water content at saturation	Water content at field capacity	Water content at wilting point	Saturated hydraulic conductivity ($m.s^{-1}$)
Peat	0.88	0.62	0.15	$2x10^{-6}$
Mineral soil	0.3	0.2	0.1	10^{-6}

The parameters for peat soils were based on values given for hemic peat by Letts *et al.* (2000) based on an extensive review of international literature. Schouwenaars *et al.* (2007) describe water retention curves of peat samples taken 5cm below the surface in a Dutch bog with a

vegetation very similar to that of the Dauges site, and their values very closely match those given by Letts *et al.* (2000) for mesic peat. However their research site was a cut-over bog in which the acrotelm had been removed. The parameters for mineral soils were taken from van den Bogaert (2011), who derived soil moisture release curves for soils with similar texture and geological settings in Beaujolais, at the north-east boundary of the Massif Central. The saturated hydraulic conductivity parameter gives the maximum infiltration rate of the soil. Macropore flow is an important component of flow in peat soils. Using a tension infiltrometer, Holden *et al.* (2001) measured a mean percentage macropore flow of 35.9% (+/-19.7, min 1.0, max 79.9) in the upper 20cm of a blanket bog in the Pennines, UK (macropores were defined as pores more than 1 mm in diameter). The macropore contribution was higher under *Sphagnum* cover (mean 51.0%) than under *Calluna* (36.4%) or *Eriophorum* (28.6%). Baird (1997) measured larger macropore contributions, ranging from 51 to 78%, in the surface of sapric fen peat in Somerset, UK, however the site had formerly been drained and cultivated before being restored for nature conservation purposes. In the MIKE SHE unsaturated flow model, the bypass fraction was therefore initially set to 35% of infiltration.

5.4.3. Land use

For the purpose of hydrological modelling, the CORINE biotopes vegetation map described in Section 2.6.3 was aggregated to a smaller number of vegetation classes with distinct interception and evapotranspiration characteristics (see Figure 2-10): needle-leaved evergreen woodlands (mainly Douglas fir plantations, with a few rare Scottish pine plantations); broad-leaved deciduous woodlands (mainly beech and pedunculate oak - beech mature woodlands, with a few chestnut tree woodlands); mixed woodlands; dry heathland, clearings and shrubs; meadows and pastures; wet woodlands; wetland; and impervious areas.

For each of these classes, the maximum (summer) and minimum (winter) leaf area indices, mean leaf resistance, and maximum rooting depth were estimated based on values found in the literature for similar vegetation types and species (see Table G-2, Table G-3 and Table G-4 in Appendix G), and used to estimate crop coefficients. The interception model was also calibrated using data from a literature review of bulk interception ratios and maximum interception storage capacities measured in environments similar to the Dauges site (Table G-5 and Table G-6 in Appendix G).

5.4.3.1. Leaf area index

In the model, maximum LAI for coniferous woodlands was set to 8.5, based on the mean value reported in the literature for *Pseudotsuga menziesii* (mainly from plantations, see Table G-2 in Appendix G). The value used for broadleaf woodlands was a weighted mean of the mean values reported in the literature for *Fagus sylvatica* (6.0), *Quercus robur* (4.8) and *Castanea sativa* (4.9), with weights defined by the area within the catchment in which each of these species is dominant according to the CORINE biotopes map (Section 2.6.3). As noted by Breuer *et al.* (2003), wood parts of deciduous tree species and old leaves of grass species among others still affect precipitation interception during the dormancy stage. As a consequence, in the context of hydrological modelling in which the maximum interception storage is a function of LAI, a LAI greater than zero has to be maintained throughout the year for all vegetation classes but arable crops (see Section 5.4.2), whereas LAI *sensu stricto* only includes actively photosynthesising leaves. This conceptual difference explains the discrepancy between minimum (winter) LAI values in the literature depending on whether they are actual measures or values recommended for hydrological modelling.

Following Granier *et al.* (1999), evergreen needle-leaved species were assumed to keep a constant LAI throughout the year, and LAI in deciduous broad-leaved species was assumed to increase linearly over 30 days starting at bud break from LAImin to LAImax (Bréda 1994). In autumn, LAI was assumed to decrease linearly over 30 days before leaf fall. Bud break is defined as the first date when at least 20% of buds are open on at least 10% of trees. Leaf fall was assumed to be complete 10 days after the leaf colouring date, defined as the date when at least 20% of leaves have changed colour in at least 90% of trees. Mean bud break and leaf colouring dates were estimated from figures in Lebourgeois *et al.* (2010) (Table 5-2), who modelled phenological events as a function of mean climatic variables using data from 51 broadleaved forest stands belonging to the RECOFOR network, a French nationwide long-term forest ecosystem observatory.

Table 5-2. Mean bud break and leaf colouring day-of-year and date estimated for deciduous broadleaved species at the Dauges site based on figures from Lebourgeois et al. (2010).

Species	Mean bud break day-of-year (date)	Mean leaf colouring day-of-year (date)
Beech	115 (25 April)	285 (12 October)
Oak	95 (5 April)	295 (22 October)
Broadleaved	100 (10 April)	290 (17 October)

These estimates were compatible with punctual field observations reported by the NNR staff. No distinction was made between beech and pedunculate oak woodlands, and the dates for broadleaved species as a whole (which in Lebourgeois *et al.* (2010) included *Fagus sylvatica* and *Quercus spp.* only) were used. As is common in hydrological modelling (Thompson *et al.* 2004, 2009; Rochester 2010; Singh 2010), LAImin, LAImax, bud break and leaf fall dates were assumed to be constant from year to year and across the site, even though more complex phenological models could be envisaged to accommodate temporal and spatial variability of vegetation phenology (Jolly *et al.* 2005). Very little information was found on wet woodland properties, however given the small area covered by this vegetation class the impact of this lack of information on the model is assumed to be negligible. The phenology of wet woodland was assumed to be the same as other broadleaved woodlands. Based on informal field observations, the phenology of grasslands was assumed to be similar to that of broadleaf woodlands.

This is clearly not the case in the wetland, where field observations show the vegetation starts to develop in late May, more than a month later than on dry land. Full development is only reached in late June-early July. This matches LAI measurements carried out in similar wetlands in western Europe (Sijtsma & Veldhuizen 1992; Spieksma *et al.* 1997; Nieveen *et al.* 1998; Bortoluzzi *et al.* 2006) (Figure 5-15).

No distinction was made between wetland vegetation communities and they were modelled as an equal mixture of *Sphagnum spp.*, chamaephytes and *Molinia caerulea*. As the vast majority of wetland habitats are relatively closely grazed throughout the growing season, a relatively low value of LAImax was chosen within the range of values reported in the literature. Figure 5-16 shows the LAI values defined using the approach described above for each of the vegetation types used in the model. During transition periods in spring and autumn, crop coefficients, root depths and maximum interception storage capacities are linearly interpolated between their minimum and maximum values following identical phenological curves.

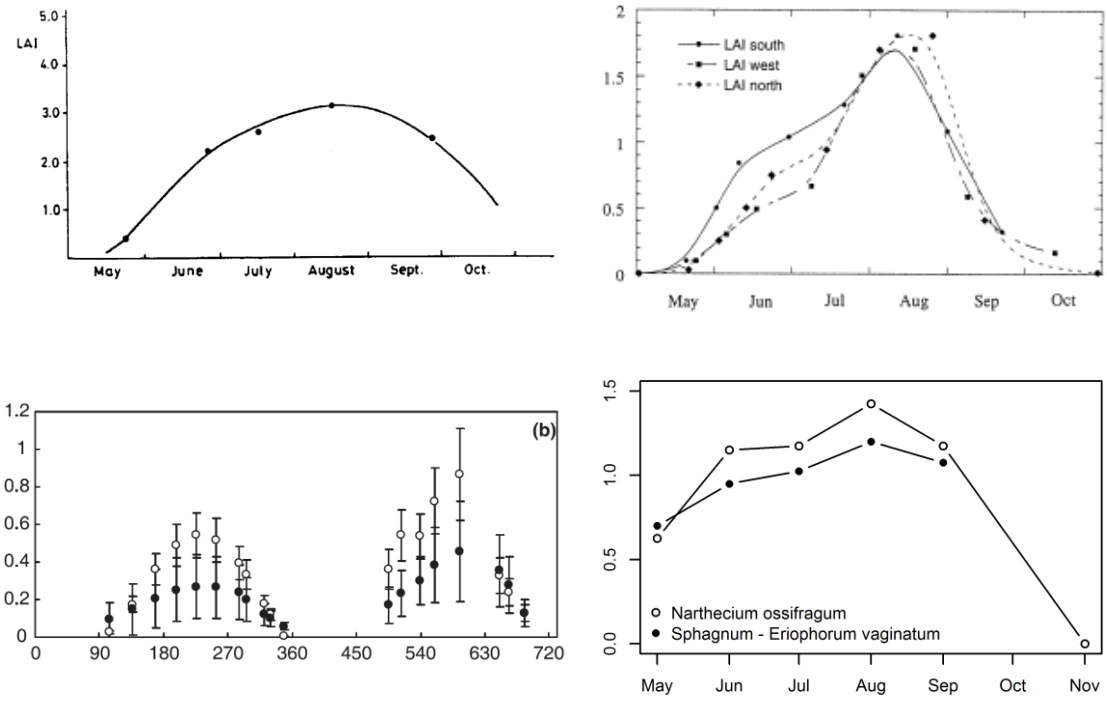

Figure 5-15. Examples of LAI seasonnal changes in acidic mires.

Top-left: *Molinia*-dominated degraded raised bog, Netherlands (Spieksma *et al.* 1997); top-right: *Molinia*-dominated, tussocky raised bog, Netherlands (Nieveen *et al.* 1998); bottom left: *Sphagnum*- (open circles) and *Eriophorum vaginatum*-dominated plots in a raised bog, Jura mountains, France (Bortoluzzi *et al.* 2006); bottom-right: raised bog, Ireland (adapted from Sijtsma & Veldhuizen 1992).

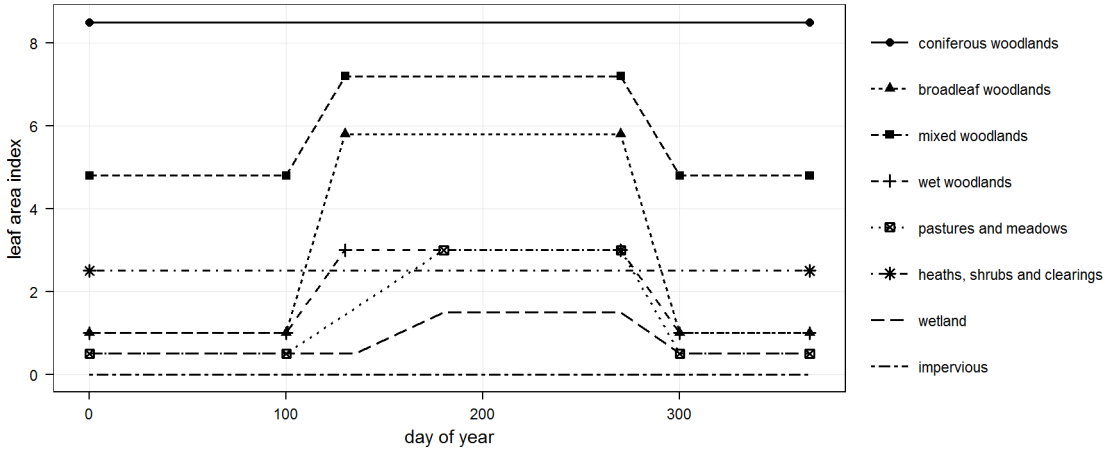

Figure 5-16. Leaf area indices used in the model as a function of vegetation class and day of year.

5.4.3.2. Mean leaf resistance

A single representative leaf resistance value is required to compute the crop resistance factor for natural and semi-natural vegetations (Allen *et al.* 1998; Allen & Pereira 2009). A review of values reported in the literature for species relevant to the Dauges catchment is given in Table G-4 in Appendix G. As shown by this review and as recognised by Breuer *et al.* (2003), leaf resistance

shows a very large variability according to environmental conditions (Jarvis 1976; Whitehead 1998), and this makes the choice of a representative value difficult. In their review of stomatal resistance (a close approximation of leaf resistance), Breuer *et al.* (2003) recorded general values of about 160 $s.m^{-1}$ for herbaceous species (similar to agricultural crops), 250 $s.m^{-1}$ for deciduous forests and 400 $s.m^{-1}$ for coniferous forests. The values found in the literature for Douglas fir (about 400 $s.m^{-1}$) are similar to those identified by Breuer *et al.* (2003) for coniferous trees as a whole. Values reported for the main deciduous tree species found within the research catchment are similar: about 300 $s.m^{-1}$ for oaks, 400 for beech and 500 for chestnut tree. A value of 400 $s.m^{-1}$ was therefore used for deciduous, coniferous and mixed woodlands. Data for tree species found in wet woodlands are rare, but resistance seem to be about 200 $s.m^{-1}$ on average. Values for grassland species (mainly grasses) are very variable. A value of 200 $s.m^{-1}$ was used. The leaf resistances reported in the literature for *Calluna vulgaris* are on average 200 $s.m^{-1}$, which seems quite low when considering the species' leaf architecture, and the low crop coefficients of *Calluna*-dominated heathlands relative to grasslands in the absence of water stress reported by Janssen (1994, in Spieksma *et al.* 1996). The average leaf resistance reported for *Vaccinium myrtillus* is much higher (about 480 $s.m^{-1}$ on average). Duyzer & Bosveld (1988, in Spieksma *et al.* 1996) reported bulk surface resistances of 250-400 $s.m^{-1}$ and 100-400 $s.m^{-1}$ in wet and dry heaths respectively in the Netherlands, suggesting even higher leaf resistances. An intermediate value of 300 $s.m^{-1}$ was used as representative of heathlands. Very little information was found on bog and acidic fen vascular plants, and none on *Molinia caerulea*. Van der Schaaf (1999) and Wastiaux (2000) showed that *Molinia caerulea* has a high evapotranspiration rate compared to chamaephytes. Consequently a value of 100 $s.m^{-1}$, similar to the value used in the FAO Penman-Monteith method for the reference grass, was used.

5.4.3.3. Canopy height

Data collected by the French National Forest Inventory (*Inventaire Forestier National*, http://inventaire-forestier.ign.fr) between 2008 and 2012 were used to estimate the average height of woodlands. As part of the permanent forestry inventory, a number of variables including tree height are regularly measured in a large number of systematically sampled plots across the country. Data were retrieved from woodland plots dominated by *Quercus robur* and/or *Fagus sylvatica* (deciduous woodlands), *Pseudotsuga menziesii* (coniferous woodland) or *Betula spp. and/or Salix spp.* (wet woodland), and located within the same eco-region as the research site (*Plateaux limousins*) to ensure similarity in climatic and edaphic conditions. In the case of wet woodlands, only plots growing on hydromorphic soils were retained, but the

sampling area was extended to the nearby *Plateaux granitiques ouest du Massif central* eco-region to compensate for the small number of records available. An estimate of mature woodland canopy height was estimated for each species by averaging records obtained from large trees (at least 37.5cm in diameter) only, except for *Salix spp*. and *Betula spp*. (Table 5-3).

Table 5-3. Mean tree height in the Plateaux Limousins eco-region according to IFN data.

Vegetation class	Species	Mean +/- SD (m)	Median	Min-Max	Number of trees measured	Number of plots surveyed
Deciduous woodland						
	Quercus robur	21.8 +/-3.7	21.9	9.8-32.9	232	87
	Fagus sylvatica	25.9 +/-4.1	26.4	4.6-35.2	157	46
Coniferous woodland						
	Pseudotsuga menziesii	30.6 +/-4.3	30.5	18.7-42.5	139	24
Wet woodland						
	Betula spp.	12.3 +/-3.4	12.8	4.3-19.2	30	5
	Salix spp.	10.2 +/-2.3	10	5.2-15	19	4

For non-woodland vegetation classes, canopy height was estimated from informal field observations and published values (Rameau *et al.* 1994).

5.4.3.4. Crop coefficients

Water falling on impervious surfaces was assumed to be quickly evacuated as overland flow and not to evaporate (K_c = 0 all year round). Given the very small area occupied by this landuse class, the consequences of this simplification are negligible. The correction of the crop coefficient for LAI advised by Allen & Pereira (2009) as per Equation 5-3 becomes more sensitive to the "bare soil" coefficient with decreasing LAI. A coefficient of 0.15, the upper value recommended by these authors, might not be applicable to wetlands. It probably underestimates evapotranspiration from open water and wet *Sphagnum* mosses that lack stomata and do not actively control water loss (Rydin & Jeglum 2006). Using the coefficient recommended by the FAO for open water (1.05) as the value for $K_{c\ min}$ in Equation 5-2 results in a combined coefficient of 1.0 both in summer and winter.

A number of researchers (Schouwenaars 1993; Kim & Verma 1996; Wastiaux 2000) measured ET/ET_{ref} ratios close to unity in acidic fens and bogs (Table G-1 in Appendix G), in particular in those dominated by *Molinia caerulea*. In a laboratory experiment, Clymo (1973) measured evaporation rates in *Sphagnum cuspidatum*, *S. papillosum* and *S. rubellum* 1.2-1.4 times higher than that from open water, depending on the species and the depth of the water table that varied between 1 and 10cm below the capitula. Others have shown that the ET/ET_{ref} ratio from *Sphagnum*-dominated bogs can be substantially lower (around 0.5-0.75, Wastiaux 2000; Kellner

2001a; Lafleur *et al.* 2005), particularly when the capitulum dries out. In a degraded bog in the Netherlands, Schouwenaars (1990, 1993, cited by Spieksma *et al.* 1996) showed the actual evapotranspiration of *Sphagnum spp.* to equal Penman open water reference evaporation when the water table is shallower than 10-15cm below the surface, but to drop substantially below this critical level. Actual evapotranspiration by *Molinia caerulea* was maintained at about the reference evaporation rate for much longer periods under dry conditions. In the Dauges model, evapotranspiration was therefore assumed to be driven by vascular plants and particularly *Molinia caerulea* when these are dominant in summer, but by *Sphagnum* mosses in winter when *M. caerulea* leaves are senescent and reduced in extent due to late summer and autumn grazing. This was modelled by adopting a crop coefficient of 1 at all times and setting the maximum root depth to 60cm in summer and 15 centimetres in winter.

Since they have the same mean leaf resistance and the effect of height in Equation 5-4 is reduced when higher than 20m, deciduous and coniferous woodlands have very similar crop coefficients in summer (0.79 and 0.78 respectively). This agrees with results from Aussenac & Boulangeat (1980) and Verstraeten *et al.* (2005), who found almost no difference in summer between actual evapotranspiration rates of Douglas fir and of beech in Lorraine (France) and in Belgium respectively. Based on their own data and a literature review, Granier *et al.* (1999) found that, under non-limiting soil water content, the T/ETo ratio in both deciduous and evergreen trees was linearly related to the LAI when LAI was less than 6, but constant above. Stands with a LAI ≥ 6 had relatively similar T/ETo ratios independent of the species (0.65-0.72 for *Pseudotsuga menziesii*, 0.75 for *Fagus sylvatica*, 0.70-0.80 for *Quercus petraea*, 0.70-0.80 for *Picea abies*).

For coniferous woodlands, following Allen *et al.* (1998), Meiresonne *et al.* (2003), Verstraeten *et al.* (2005) and Zhang & Hiscock (2010), the crop coefficient was assumed to be approximately similar in summer and in winter, and $K_{cb\ full}$ was simply adjusted for winter mean wind speed and minimum relative humidity using Equation 5-4. The same reasoning was followed for heathlands dominated by evergreen chamaephytes. During transition periods in spring and autumn, MIKE SHE linearly interpolates crop coefficient values between their winter minimum and summer maximum. For simplicity and comparability, the crop coefficients were calculated using the same definition of winter (days 300 to 100) and summer (days 130 to 270) for all vegetation classes. In MIKE SHE however, the interpolation between summer and winter coefficients follows the LAI curve that differs slightly between wetland, grassland and other vegetation classes (Figure 5-17).

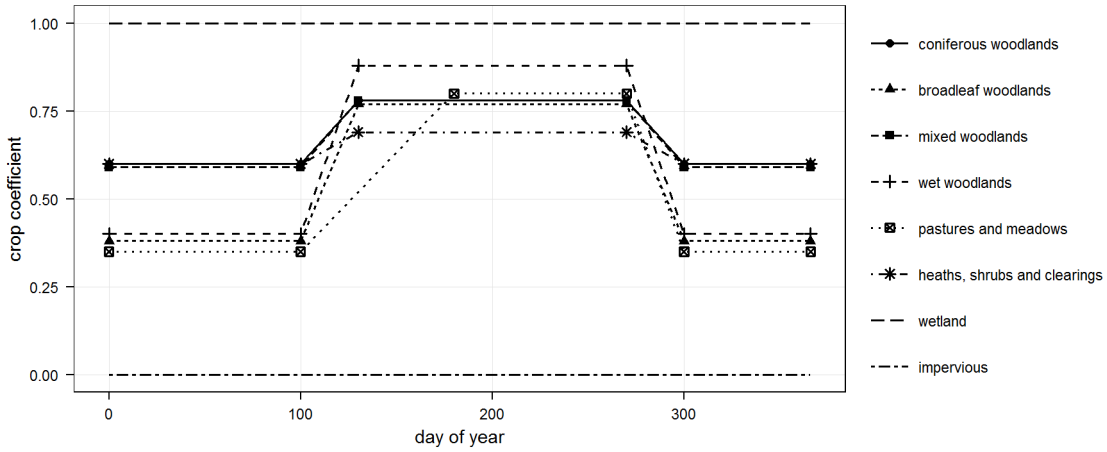

Figure 5-17. Crop coefficients used in the model as a function of vegetation class and day of year.

5.4.3.5. Root depth

In the absence of arable crops within the catchment, root depths were assumed to be constant throughout the year in all vegetation classes, and estimated based on the results of the literature review (Table G-3 in Appendix G): 2m in coniferous, deciduous and mixed woodlands, 1.5m in wet woodlands, 0.6m in heathlands, 0.9m in grasslands and 0m in impervious areas. The only exception was the wetland vegetation class, where root depth was 0.6m in summer and 0.15m in winter, for the reasons explained in Section 5.4.3.4.

5.4.3.6. Interception

Table G-5 in Appendix G shows the results of a literature review of bulk interception ratios in natural vegetation classes and in contexts similar to that found on the research site. Among the wealth of studies on interception in forests, only those in which both stemflow and throughfall were measured have been included, since stemflow can make up a substantial part of net rainfall particularly in deciduous trees. Except for a few high values recorded under *Picea abies* and *Abies grandis*, annual interception ratios are noticeably similar in conifers, seemingly and surprisingly independently of the location. There seems to be no difference between winter and summer, however it should be noted that the studies that differentiated between winter and summer interception were all conducted in Lorraine, France, so this may not apply to other climates. The mean annual ratio for Douglas fir is 0.37. Data on annual interception for beech and oak forests are much more variable, ranging from 0.10 to 0.34. The mean value is 0.21. Interception is higher in summer (0.15-0.36, mean: 0.28) than during the leafless season (0.06-0.25, mean: 0.16). The overwhelming majority of researchers that measured interception in forests did not include interception by the forest understorey and litter. Yet, as shown by Gerrits (2010), this can account

for a very large proportion of total rainfall intercepted by forests, sometimes more than that intercepted by the canopy. This may be an issue when comparing interception fraction between forests and open habitats, in which other methods have been used that do include the effect of dead vegetation. As noted by Breuer *et al.* (2003), surprisingly little information is available on bulk interception ratios in grasslands. The only relevant publication seems to suggest it is of the same order as that observed in heathlands, in the order of 0.11-0.23 (mean: 0.17). No data were found on mires.

Since the bulk interception ratio is dependent on precipitation characteristics, hydrological models often require the maximum interception capacity, defined as the maximum amount of water left at the end of a precipitation event, in the absence of evaporation and after drip has stopped (Breuer *et al.* 2003). Table G-6 in Appendix G gives values found in the literature for this variable. Maximum storage capacity during the leafed season is higher in conifers than in deciduous trees, reflecting a higher LAI but also a different architecture (Breuer *et al.* 2003). It is on average 2.4mm, 1.5mm and 1.3mm in stands dominated by *Pseudotsuga menziesii, Fagus sylvatica* and *Quercus spp*. respectively. It is understandably smaller in deciduous species during the leafless season, about 0.4mm if data are excluded for *Quercus petraea* from Halldin *et al.* (1984), who found much higher values than any other studies both in winter and summer. Data on storage capacity in species of open habitats are scarce, but are quite high relative to LAI: 1.3mm on average during the leafed season, similar to deciduous forests. This had already been noticed by Breuer *et al.* (2003) in a global-scale review. It should be noted that methods used to measure interception in forests and open habitats are not identical, and interception measured in forests does rarely include that of understorey vegetation and litter, while interception in open habitats is often a bulk measure. Consequently, Breuer *et al.* (2003) recommended to add a constant of 2mm to values of forest canopy storage capacity to account for understorey and litter. No published data was found on the storage capacity of open habitats in winter. Data on specific storage capacity (relativized by LAI) are too few and too scattered to be meaningful.

In the absence of observed data allowing for a precise calibration of the interception model, the maximum interception storage capacity for each vegetation class and season was set to a value that resulted in long-term bulk interception ratios similar to those reported in the literature (Table G-5 in Appendix G). As explained above, interception ratios reported in the literature for woodlands do not account for understorey and litter interception, unlike those reported for open habitats. If anything, the approach taken in this study may therefore underestimate the interception ratio in woodlands relative to open habitats. Figure 5-18 shows the impact of a

range of possible values on the proportion of intercepted precipitation per month. This impact is much larger in summer than in winter. Since precipitation is higher in winter, this suggests that interception is constrained by ET_{max}, the energy-constrained upper limit on evapotranspiration described in Section 5.4.2. Figure 5-19 shows that this is indeed the case, with evaporation from interception approaching 100% of ET_{max} in January and December.

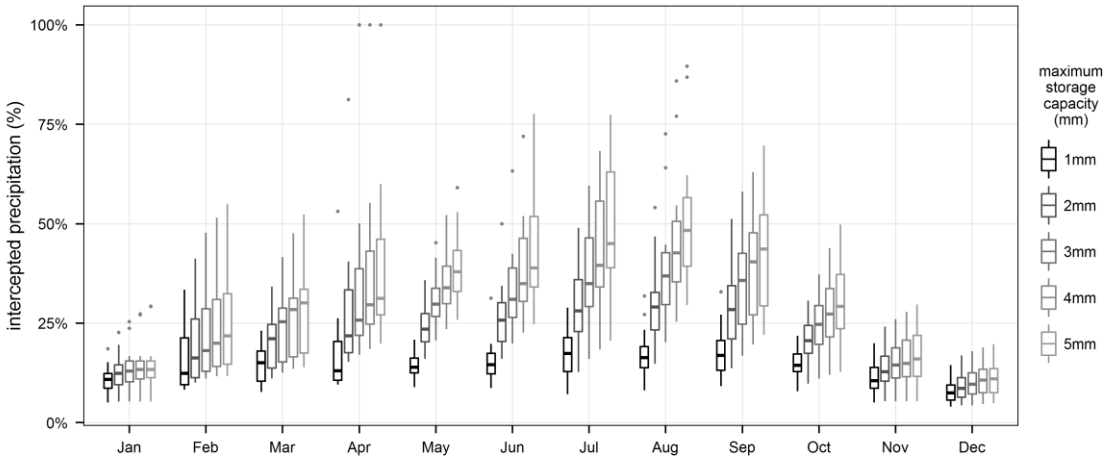

Figure 5-18. Simulated intercepted rainfall fraction in a month as a function of maximum storage capacity (1998-2013).

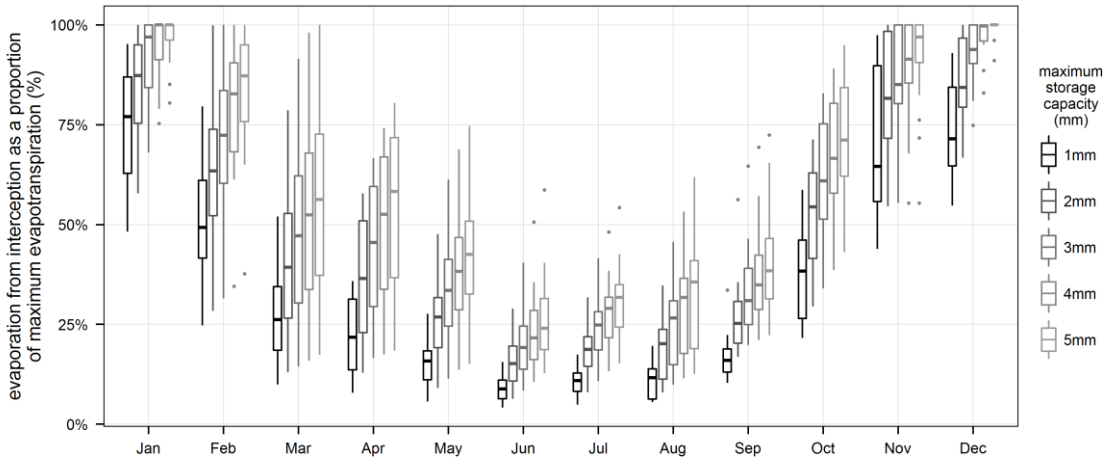

Figure 5-19. Ratio of evaporation from interception to maximum potential evapotranspiration as a function of maximum storage capacity (1998-2013).

Importantly, Figure 5-19 shows that interception is never limited by ET_{max} in summer. This suggests that the main limiting factor is the plant-dependant interception storage capacity, which, if measured on a LAI unit basis, does not vary substantially from one geographical area to another. This validates the approach taken to calibrate the interception model based on bulk interception ratios reported in the literature for other places of relatively similar climate in summer. In winter, evaporation from interception does approach 100% of ET_{max}, and bulk interception ratios measured elsewhere may not be transferable. Table 5-4 gives the seasonal bulk interception

ratios predicted by the interception model for the 1998-2013 period for a range of maximum storage capacity values.

Table 5-4. Simulated bulk interception ratio as a function of maximum storage capacity (1998-2013).

Interception storage capacity	1mm	1.2mm	2mm	2.5mm	3mm	4mm	5mm
Bulk interception ratio in summer (days 130-270)	14.4%	16.6%	24.4%	28.2%	31.4%	36.6%	40.7%
Bulk interception ratio in winter (days 0-100 and 300-366)	10.1%	10.8%	12.8%	13.6%	14.2%	15.3%	16.0%

In summer, maximum storage capacities of 4, 2.5, and 1.2 mm are required to give bulk interception ratios of 37%, 28% and 17%, corresponding to the average values reported in the literature for Douglas fir plantations, oak and beech woodlands and open habitats respectively. These values were therefore used in the model. They are slightly higher than maximum storage capacities reported in the literature (on average 2.4, 1.3-1.5 and 1.3mm respectively for the vegetation classes listed above), but it should be noted that these reported values are instantaneous storage capacities. Particularly in summer, when potential evapotranspiration is non-limiting, the total amount of intercepted rainfall per day may be higher if evaporation from canopy storage occurs during or between rainfall events. In the case of the Dauges model daily maxima of storage capacity are required so the values calculated from bulk interception ratios seem reasonable.

It could also be argued that, in reality and as its name suggests, the maximum interception storage capacity gives the upper limit on interception volume, but throughfall and stemflow do occur before this limit is reached. In a study carried out in Lorraine (France), the daily rainfall was completely intercepted only if it was less than 0.6mm in *Picea abies*, 0.5mm in *Abies grandis*, 0.4 mm in *Pinus sylvestris* and 0.3mm in a *Fagus sylvatica* and *Carpinus betulus* woodland (Aussenac 1968). The proportion of the maximum interception storage capacity that is actually filled is a logarithmic function of the depth of the rainfall event, and is influenced by other factors such as wind speed (Rutter *et al.* 1971, 1975; Rutter & Morton 1977; Calder 1986; Gash *et al.* 1995; Muzylo *et al.* 2009). In MIKE SHE, as in many other hydrological models including SWAT (Neitsch *et al.* 2005), this process is simplified and modelled as an interception reservoir which must be filled before water is allowed to flow to the ground surface. This simplification will have an impact on daily patterns of soil moisture in the wider catchment but is unlikely to have substantial consequences on long-term water flux from and to the wetland.

In winter the proportion of intercepted rainfall simulated for Douglas fir with a maximum storage capacity of 4mm is almost always constrained by the low potential evapotranspiration recorded

at the site and, as a result, half that reported in Lorraine (France), where all the studies that could be found and that investigated winter interception ratios in this species were conducted. As discussed above, this raises the question of setting the maximum interception storage capacity for deciduous trees in winter, since bulk interception ratios recorded in other places where interception is less limited by potential evapotranspiration in winter are not applicable. The literature suggests that it is about a third of that recorded in summer, so a value of 0.8mm was used.

Based on their estimated LAI, wet woodlands were assumed to have half the interception storage capacity of beech and oak woodlands in summer, and the same in winter. Mixed woodlands were assumed to have intermediate capacities between evergreen and deciduous woodlands (3.3mm in summer, 2.3 in winter). Heathlands were assumed to have the same capacity in winter as in summer (1.2mm). No data could be found that could be used to estimate the maximum interception storage capacity of grasslands in winter, so an arbitrary value of 0.4mm, a third of that calculated for the summer period, was used. Since interception is constrained by potential evapotranspiration and makes for a small proportion of precipitation in winter, this uncertainty is unlikely to have significant consequences on the hydrological model outputs. Based on their LAI, wetland habitats were assumed to have half the interception capacity of grasslands in summer and the same in winter. Figure 5-20 summarises the maximum interception storage capacities used in the model for each vegetation class. Figure 5-21 and Table 5-5 show the simulated fraction of intercepted rainfall according to these values (but note that the maximum interception storage capacity of conifers, deciduous woodlands, grasslands and heathlands was actually calculated from some of the values reported in Table 5-5, see above).

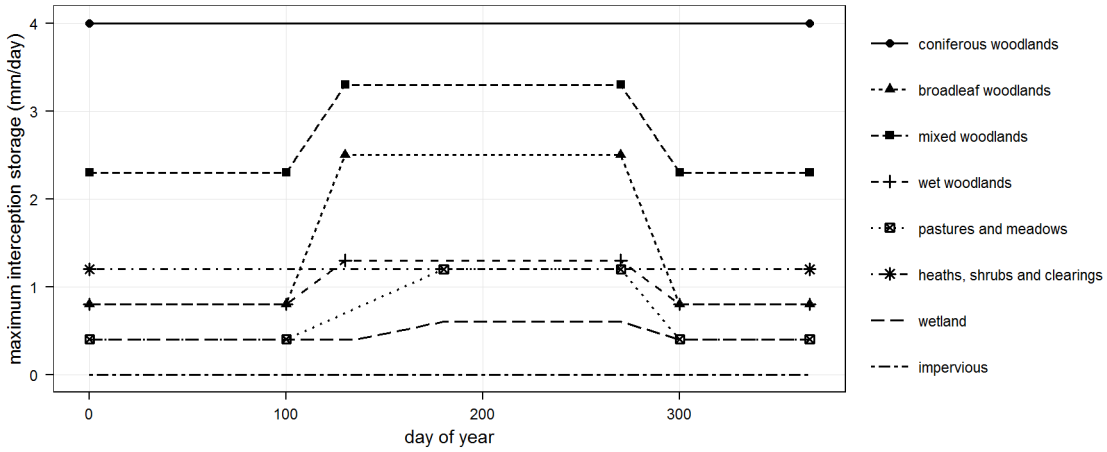

Figure 5-20. Maximum interception storage capacities used in the model as a function of vegetation class and day of year.

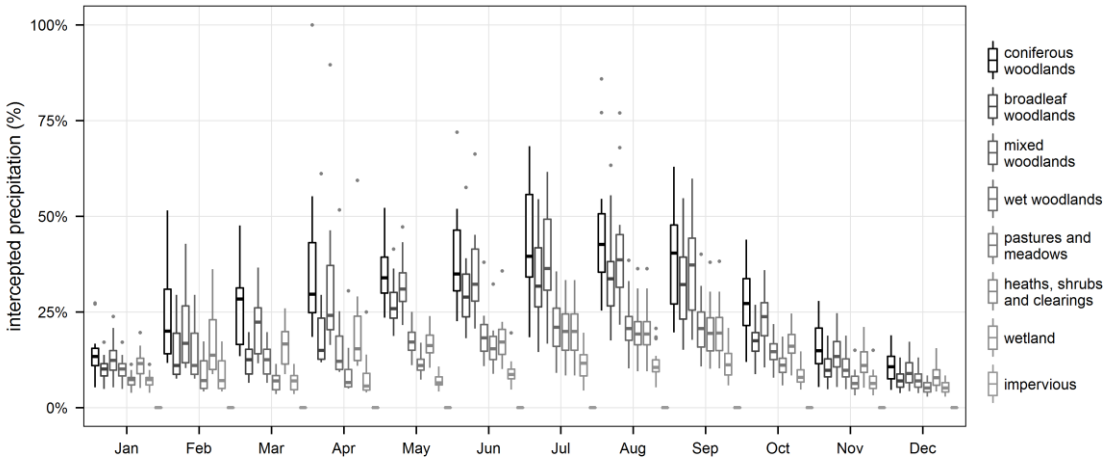

Figure 5-21. Simulated fraction of intercepted rainfall in a month as a function of vegetation class (1998-2013).

Table 5-5. Simulated fraction of intercepted rainfall (1998-2013).

season	conifers	broadleaf	mixed	wet wood	pastures	heath	wetland	impervious
summer (days 130-270)	36.6%	28.2%	33.1%	17.7%	15.5%	16.6%	8.8%	0.0%
winter (days 300-100)	15.3%	9.1%	13.3%	9.1%	5.8%	10.8%	5.8%	0.0%

5.4.3.7. Summary of vegetation properties

Table 5-6 shows the vegetation properties that were used in the MIKE SHE model and in the computation of the crop coefficients and evaporation from interception for each vegetation class. As explained in Sections 5.4.2, 5.4.3.4 and 5.4.3.6, evaporation from interception was modelled outside MIKE SHE for each vegetation class, and the residual potential transpiration (capped to ETo x Kc) used as the reference evapotranspiration in MIKE SHE. Consequently, in MIKE SHE itself, the crop coefficient and the interception capacity were set to 1 and 0 respectively for all vegetation classes. During the transition periods in spring and autumn, root depths, crop coefficients and interception capacities were linearly interpolated between their winter and summer values following the same phenology as LAI (Figure 5-16).

Table 5-6. Vegetation properties used in the Dauges model.

	LAImax	LAImin	summer root depth (m)	winter root depth (m)	summer canopy height (m)	winter canopy height (m)	mean leaf resistance ($s.m^{-1}$)	summer crop coefficient (Kcb full)	winter crop coefficient (Kcb ini)	winter interception capacity (mm)	summer interception capacity (mm)
coniferous woodlands	8.5	8.5	2	2	30	30	400	0.78	0.60	4	4
deciduous woodlands	5.8	1	2	2	24	24	400	0.77	0.38	0.8	2.5
mixed woodlands	7.2	4.8	2	2	27	27	400	0.78	0.59	2.3	3.3
wet woodlands	3	1	1.5	1.5	11	11	200 (400 in winter)	0.88	0.40	0.8	1.3
heath and shrubs	2.5	2.5	0.6	0.6	0.3	0.3	300	0.69	0.60	1.2	1.2
pastures and meadows	3	0.5	0.9	0.9	0.3	0.05	200	0.80	0.35	0.4	1.2
wetland	1.5	0.5	0.6	0.15	0.3	0.2	100	1	1	0.4	0.6
impervious	0	0	0	0	0	0	-	0	0	0	0

5.4.4. Hydrographic network and hydrodynamic model

The path of the watercourses within the catchment was compiled from several sources. Most watercourses were digitised manually from the 0.5m resolution aerial ortho-photograph provided by the IGN (BD Ortho) and taken in 2010. In some of the upstream parts of the wetland, the watercourses are diffuse or run below ground, and the exact course could not be mapped precisely. In this case, the main flowpath was estimated using field knowledge, results from the DGPS topographic survey and peculiarities visible on the aerial picture, such as the presence of darker or greener vegetation. The bank lines shown on the 1/1000 scale COGEMA topographic maps were digitised semi-automatically using the ArcScan extension for ArcGIS. They were then collapsed to derive the centre lines of the watercourses. This dataset proved extremely accurate when checked against the most recent ortho-rectified aerial photograph, except for the shallow agricultural drains that are regularly re-dug in the upper part of the wetland. It was therefore used to map the path of the main watercourses underneath trees where DGPS or aerial photography mapping could not be used, mainly downstream of the Pont-de-Pierre main wetland outlet. Within the wetland, the watercourses were walked and 82 cross-sections surveyed at regular intervals using RTK DGPS. Survey points along cross-sections were subjectively selected, with a particular focus on slope breaks, to obtain the best representation of the cross-section in a minimal number of measures. On average, 10 points were measured along each cross-section.

Stream flow was modelled in MIKE 11 using a simplified hydrographic network including the largest water courses in which flow was observed all year round. A number of smaller drainage ditches were also included if their position meant they had a substantial impact on overland flow by diverting it away from its natural course (Figure 5-22).

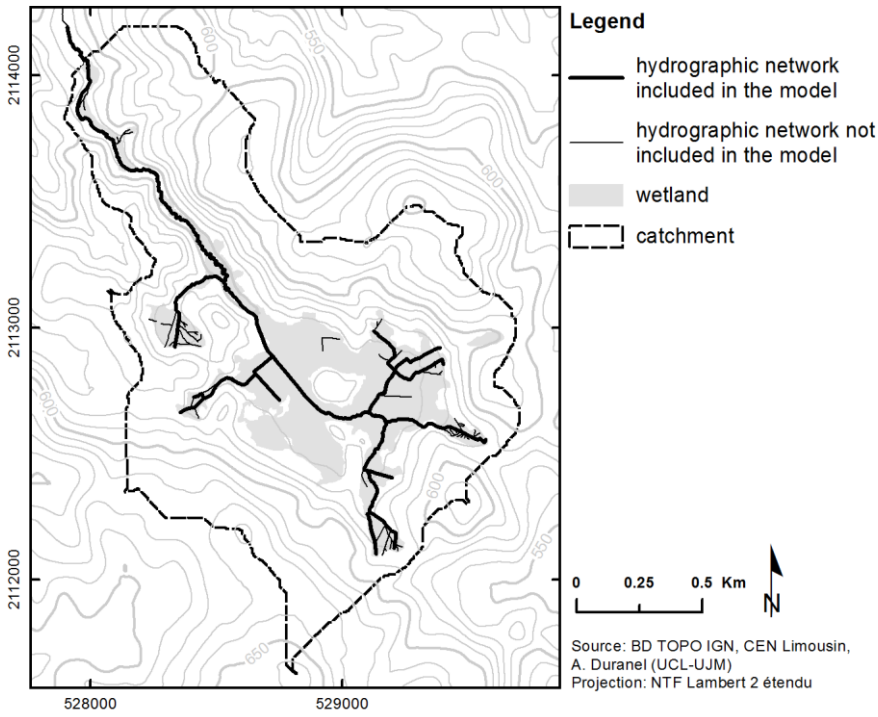

Figure 5-22. MIKE 11 hydrographic network.

The watercourse cross-section profiles are represented in MIKE 11 by a cross-section database, each section being linearly referenced along the relevant stream reach. The cross-section database included the 65 cross-sections surveyed using DGPS along the MIKE 11 reaches. The cross-section stream profile was estimated at a further 123 locations (Figure 5-23). This was based on linear interpolation where surveyed cross-sections were available both upstream and downstream, generally along the largest reaches. Along shallow drainage ditches in the upper part of the wetland, a generic trapezoidal cross-section was used, the width and depth of which was estimated based on aerial photographs, sections surveyed in similar drains and field knowledge.

Observational evidence shows that over-bank spilling does occur relatively frequently along the two main streams within the wetland, and floodplain storage has a substantial effect on discharge downstream of the wetland and on water levels and infiltration to the saturated zone within the wetland.

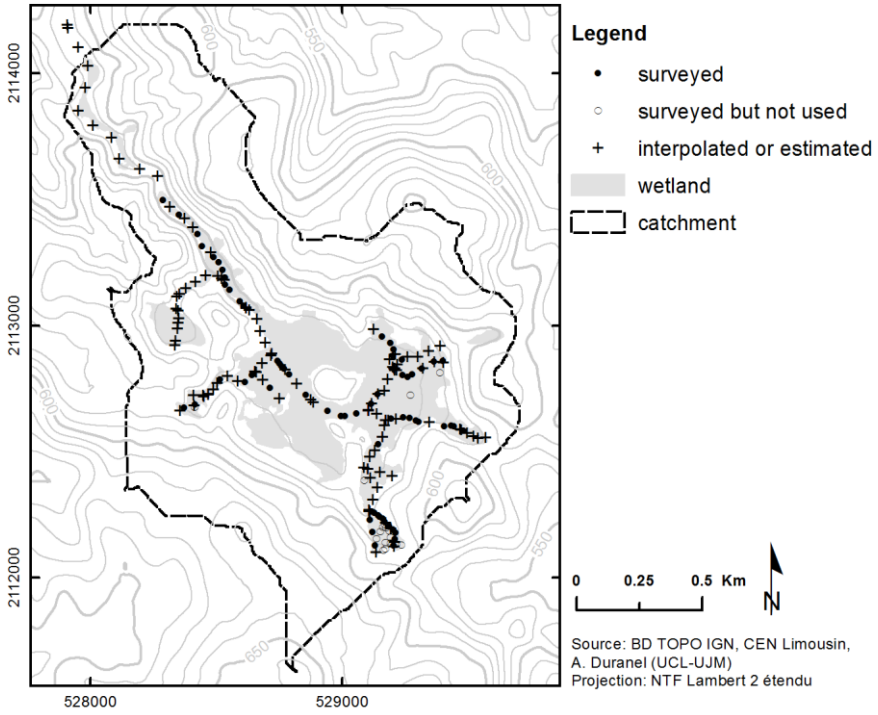

Figure 5-23. MIKE 11 cross-sections.

As seen in Section 4.3.2.3, the presence of very permeable alluvial deposits allows for substantial exchanges between stream water and groundwater along the channel downstream of Puy Rond. This is particularly the case around dipwell D17, in which the water table is closely correlated to stream stage (Section 4.3.2.3). Furthermore, there is observational evidence of widespread backwater effects in water courses flowing through the main wetland area, between stageboards 1 and 2 and the Marzet stream. This is due to the low gradient of the stream bed and to the presence of multiple obstacles to flow such as trees, subsurface pipes, *Sphagnum* mats and *Molinia* tussocks. Precise modelling of stream stage using the Saint-Venant equations would therefore be indicated within the main wetland area at least.

A number of trials showed that a model using this approach was numerically unstable unless a very small time step, in the order of a few seconds, was used. This is due to the steep slopes and high water velocity in the upper part of the catchment that increases the Courant stability criterion, to the small discharge recorded in the site's watercourses (Anonymous 2009d), and probably in part to the small distance between some cross-sections. Such small time steps make a hydrodynamic model based on the Saint-Venant equations impracticable, with run times for the complete coupled MIKE SHE / MIKE 11 model approaching a week for a model with a 10m spatial resolution and a 2-year simulation period, using a 2.53GHz processor. Consequently, stream flow within MIKE 11 was modelled using kinematic routing. This is always numerically

stable and allows for daily time steps. However the method does not account for backwater effects. Water levels are calculated independently at each cross-section using the Manning equation. As a consequence a poor performance with regard to stream stage is expected within the wetland, and flooding cannot be modelled accurately. Flooding was therefore not included in the model, and overland-stream exchanges are one-way only. Exchanges between the saturated zone and the water courses were assumed to be controlled by the conductivity of the saturated zone only. Boundary conditions were specified as discharge boundaries with a constant zero flow at the upstream ends of the network and a fixed water level boundary at the downstream end. The MIKE 11 channel was prolonged 170m beyond the modelled area to limit the influence of this fixed level boundary. Bed resistance was set to a Manning's n value of 0.1, based on the value proposed by Dingman (1994) for very weedy reaches given the small bed section and numerous obstacles to flow.

5.4.5. Overland flow

MIKE SHE uses Manning's M roughness coefficient (the inverse of Manning's n). A uniform value of 10 was used based on values proposed by Dingman for floodplain with medium brush cover (1994 p. 368). This value is similar to calibrated values obtained for heather (16) and grassland (8) by Thompson (2012) for a small catchment in south-west Scotland.

5.4.6. Saturated flow

5.4.6.1. Geological layers and lenses

Saturated flow within the fissured granite was modelled using an equivalent porous medium approach (Section C.3 of Appendix C). The fissured zone was conceptualised as a unique layer of constant depth, set to 55m below ground based on data from the CEA boreholes and the ERT results (Section 3.3), and of homogeneous properties. This is clearly a simplification since both datasets suggest that the thickness of the fissured zone varies across the site, and that the degree of weathering and density of fissure within it vary both horizontally and vertically. However, given the scarcity of geological and geophysical data, it was not possible to map these characteristics with precision, as was for instance done by Lubczynski & Gurwin (2005) or Ahmed & Sreedevi (2008), who benefited from very large geological and geophysical datasets. The sensitivity of the model to the depth, shape and hydraulic properties of the fissured zone was therefore thoroughly tested, and this is further detailed in Sections 6.3.1 and 6.3.2. The unweathered bedrock underneath the fissured zone was assumed to be impermeable, based on

the conceptual hydrogeological model of granitic terrains detailed in Appendix C. Based on literature data (Wyns *et al.* 2004; Dewandel *et al.* 2006), the hydraulic conductivity in the fissured zone was set to 10^{-5} m.s^{-1} horizontally and 10^{-6} m.s^{-1} vertically, specific yield to 1% and specific storage to 10^{-5} m^{-1}.

Surveys of pedological pits and quarry sections showed that soils outside the wetland were 40-70cm deep even on relatively steep slopes (Sections 3.3 and 3.6). These surveys and the review of published data showed that head was very limited in extent and in depth, that soils, periglacial formations and in-situ saprolite were relatively similar in terms of their granulometry, and that no impermeable fragic horizon was present. ERT transects and survey of existing outcrops (Section 3.3) have shown that the saprolite depth is very small or null across most of the catchment. The analysis of the ERT data does not suggest the presence of a substantial saprolite layer at the bottom of the etch-basin, below the peat deposit, even though data from the CEA boreholes do show that such a layer exists in the area north-east of Puy Rond (Section 3.3.3.2). A number of tests were carried out with models differentiating between fissured zone, saprolite and alluvial deposits, however such models proved difficult to calibrate given the multiplication of parameters and the increased computation time. To simplify the model, soils, periglacial formations, alluvial deposits and in-situ saprolite were therefore assumed to have a negligible role in saturated flow within the catchment and were not included in the geological model (but see the description of the unsaturated zone parameters in Section 5.4.2 and of the computational layer set-up in Section 5.4.6.2).

Peat deposits were represented as a single geological lens. No distinction was made between the acrotelm and the catotelm for two reasons. First, the analysis of the depth of the acrotelm and of its correlation with potential descriptors showed that it was spatially highly variable and could not easily be mapped accurately (Section 3.4). Second, its small depth and its patchy distribution do not facilitate its representation as a distinct computational layer in MIKE SHE. Computational layers must extend to the entire modelled area and, in practice, must have a minimum depth to avoid numerical instabilities of the saturated zone component. This minimum depth was found to be around 50cm given the model characteristics, which is too large to represent the acrotelm. The hydraulic conductivity in the peat layer was set to $5\text{x}10^{-8}$ m.s^{-1} in both horizontal and vertical directions based on the slug test results. Specific yield was set to 0.26 based on the general values for hydrological modelling proposed by Letts *et al.* (2000) for hemic peat. Specific storage in peat is one to two orders of magnitude higher than in mineral formations, due to the high elasticity of this material, particularly in weakly humified peat (Reeve

et al. 2006). However, contrary to specific yield, very few values are available in the literature for specific storage. Given the generally high humification indices recorded during the peat stratigraphic survey (Section 3.4) and the very small seasonal changes in ground level suggesting a low compressibility of peat (Section 4.3.2.1) at the Dauges site, a value of 10^{-2} m^{-1} was used, approximately equal to the lower range of values given by Binet *et al.* (2013), who measured specific storage values ranging from 0 to 1.8×10^{-2} m^{-1} in an acidic fen in eastern France. The value used in the current study is similar to that used by Reeve *et al.* (2006) when modelling Canadian mires (10^{-3} to $5x10^{-2}$ m^{-1}).

5.4.6.2. Computational layers

Two saturated zone computational layers were defined. The upper one extended from ground level to the bottom of the peat deposits. However, tests showed that a minimum depth of 0.5m was required to avoid computational instabilities. This meant that in locations with a peat depth smaller than 0.5m, the computational layer hydraulic parameters were obtained by a weighted averaging between the peat and fissured granite characteristics. This was the case in 41% of the total peat area, particularly on the mire margins and along the narrow valley downstream of the main wetland outlet (Figure 5-24). Since computational layers must extend with a non-zero thickness across the entire catchment, a constant depth of 0.5m was used on mineral soils.

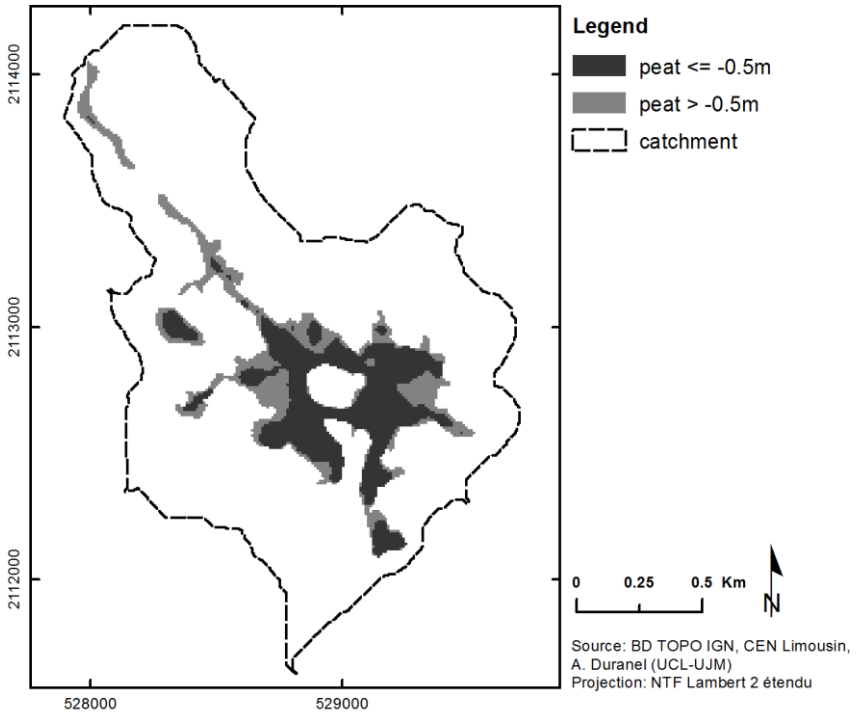

Figure 5-24. Distribution of peat deposits deeper/shallower than the 0.5m minimum depth of the upper computational layer.

In MIKE SHE, the specific yield given to the unsaturated zone automatically overrides any value given to the uppermost saturated zone computational layer. Consequently, the specific yield of the upper 50cm layer on mineral soils was different from that of the lower layer. Since, on mineral soils, the vast majority of the upper layer is located within the unsaturated zone and therefore not active most of the time, this is not a substantial issue (see Figure 7-1 for a map of simulated groundwater table depths validating this affirmation). Specific yield is the only parameter overridden: distinct saturated hydraulic conductivities can for instance be specified for the unsaturated zone and the upper computational layer under saturated conditions. The bottom of the lower layer had a 55m constant depth below ground level.

5.4.6.3. Saturated zone boundary conditions

The saturated zone boundary conditions were defined as follows. It was assumed that no flow existed through the model boundaries located along topographic interfluves, which is believed to be a reasonable assumption given the shallowness of the fissured zone relative to the relief amplitude, the low permeability of the unweathered bedrock, and the expected smaller degree of fissuration and weathering below the hilltops as opposed to the bottom of the etch-basin (Section 3.3.4). Some saturated flow in the fissured layer was allowed along the downstream boundary of the catchment that cuts across the narrow valley by the D78 bridge. Along this stretch, it was assumed that the water table in the fissured zone broadly follows the ground topography: cross-boundary flow is orthogonal to the boundary and parallel to the main axis of the valley, and the cross-boundary head gradient is equal to the ground slope across the boundary, i.e. in a direction perpendicular to the maximum slope. The cross-boundary slope was calculated using a 25m-resolution DEM to smooth the impact of local topography. It was assumed that there was no horizontal saturated flow through the upper computational layer. Since this head-gradient boundary is located at the downstream end of a narrow valley and quite far away from the main wetland and from any data logger used for the model calibration, its influence on the model is most probably negligible.

5.4.7. Summary of initial parameters

Table 5-7 provides the initial parameter values used in the model and the source for those values. The table is divided up into the different parts of the model.

Table 5-7. Summary of initial parameter values used in the model.

Parameter	Initial value	Reference
Channel flow (MIKE 11)		
bed resistance (Manning's n)	0.1	Dingman (1994)
Overland flow		
resistance to overland flow (Manning's M)	10	Dingman (1994)
storage detention	0 mm	
Unsaturated zone		
peat water content at saturation	0.88	Letts *et al.* (2000), this study
peat water content at field capacity	0.62	Letts *et al.* (2000)
peat water content at wilting point	0.15	Letts *et al.* (2000)
peat saturated hydraulic conductivity (UZ)	2e-006 $m.s^{-1}$	Letts *et al.* (2000)
peat bypass max fraction	0.35	Holden *et al.* (2001)
peat water content for reduced bypass flow	same as water content at field capacity	Anonymous (2009c)
peat min. water content for bypass flow	same as water content at wilting point	Anonymous (2009c)
mineral soil water content at saturation	0.33	van den Bogaert (2011)
mineral soil water content at field capacity	0.17	van den Bogaert (2011)
mineral soil water content at wilting point	0.1	van den Bogaert (2011)
mineral soil saturated hydraulic conductivity (UZ)	1e-006 $m.s^{-1}$	Dewandel *et al.* (2006)
mineral soil bypass max fraction	0.2	Legout *et al.* (2009)
mineral soil water content for reduced bypass flow	same as water content at field capacity	Anonymous (2009c)
mineral soil min. water content for bypass flow	same as water content at wilting point	Anonymous (2009c)
ET surface depth	0 m	
Saturated zone		
fissured zone lower level (below ground)	-55 m	this study, Dewandel *et al.* (2006)
fissured zone horizontal hydraulic conductivity	1e-005 $m.s^{-1}$	Dewandel *et al.* (2006)
fissured zone vertical hydraulic conductivity	1e-006 $m.s^{-1}$	Dewandel *et al.* (2006)
fissured zone specific yield	0.01	Wyns *et al.* (2004), Dewandel *et al.* (2006)
fissured zone specific storage	1e-005 m^{-1}	Maréchal *et al.* (2004b)
peat horizontal hydraulic conductivity	5e-008 $m.s^{-1}$	this study, Letts *et al.* (2000)
peat vertical hydraulic conductivity	5e-008 $m.s^{-1}$	this study, Letts *et al.* (2000)
peat specific yield	0.26	Letts *et al.* (2000)
peat specific storage	1e-002 m^{-1}	Reeve *et al.* (2006)

The scientific e notation is used for readability purposes (1e-8 = $1x10^{-8}$).

5.4.8. Model grid size

In distributed hydrological modelling, the choice of the model grid size is always a trade-off between a faithful representation of the catchment spatially-distributed characteristics and the model run time (Refsgaard *et al.* 2010; Thompson *et al.* 2013, 2014a; b). The choice of grid sizes is generally the largest that does not result in a substantial alteration of the modelled hydrological processes compared to a fine resolution. In particular, the grid size of the DEM used to represent the surface topography may have profound impacts on the hydrogeomorphic parameters that are derived from it, such as surface flow paths, slope and specific catchment area. To inform the choice of the grid size, its impact on the representation of surface topography and vegetation classes was investigated by aggregating the relevant data to six grid sizes: 5, 10, 20, 25, 30 and 50m. Two methods of DEM downsampling were tested: a mean aggregation based on the 5m DEM described in Section 3.2, and a direct interpolation to the required grid size of the raw topographic point and contour data also described in Section 3.2, using the ANUDEM algorithm with the same parameters as those used to interpolate the 5m DEM. The resulting

DEMs were compared visually (Figure 5-25) and by plotting their hypsometric curves and their elevation and slope density distribution curves (Figure 5-26). Figure 5-25 shows that large spurious sinks appear in the DEM when it is aggregated to a 50m grid size using a mean function. This is because the valley downstream of the main wetland is too narrow to be adequately represented at this resolution. Such sinks do not seem to exist at higher resolutions. Directly interpolating the raw topographic data to the required grid size using the ANUDEM algorithm did not solve this issue.

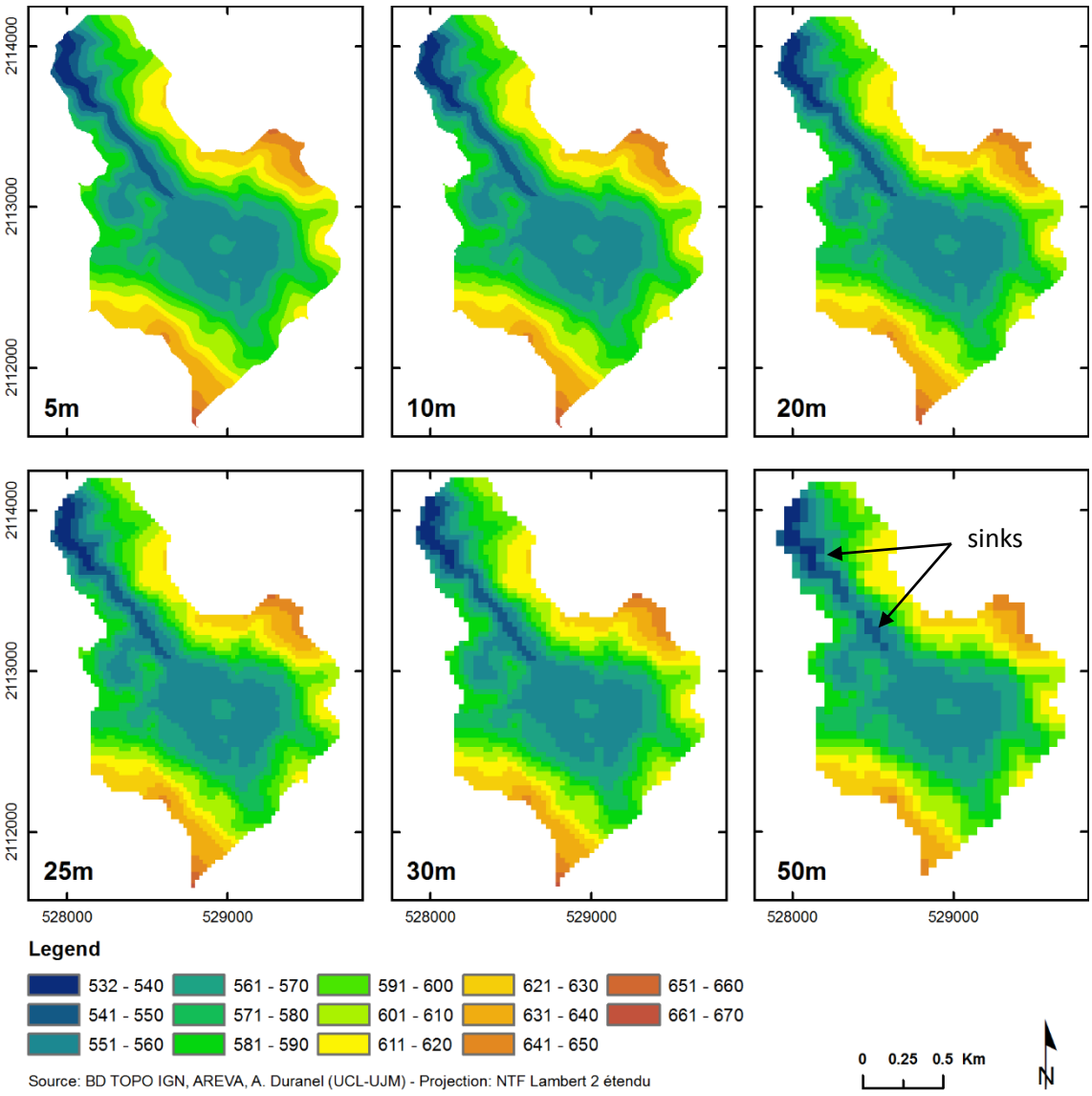

Figure 5-25. Spatial distribution of mean aggregated elevations according to model resolution.

Figure 5-26 shows that neither the grid size nor the aggregation method have a substantial influence on the catchment hypsometric curve, with the exception of the smallest and largest values that are smoothed out. The density distribution curves are more effective at highlighting differences in elevation distributions and show that aggregation results in a smoother

distribution of elevations. Compared to the direct ANUDEM interpolation, aggregating using a mean function results in a higher degree of smoothing for the most common elevation values but a lower degree for the other values. Aggregation has a strong effect on slopes by reducing the frequency of steep slopes while increasing that of low and intermediate slopes. This effect is stronger when directly interpolating to the required grid size than when aggregating the high-resolution DEM using a mean function. Consequently, the latter method was used to derive the grid used for hydrological modelling. In both cases however, there seems to be a quality threshold between 30 and 50m.

To test the effect of the model resolution on the model inputs, the relative frequencies of vegetation classes at a range of grid resolutions were compared. Vegetation classes were available as vectorised data (see Figure 2-10, Section 2.6.3) and therefore required conversion to gridded format. The MIKE SHE pre-processor can implement this operation directly, however it uses a centre cell attribution rule which, in the case of coarse grid sizes and high-resolution vector data, can result in a substantial misrepresentation of vegetation classes at both the local and catchment scale. The vectorised vegetation map was therefore converted to gridded data in ArcGIS using a maximum area attribution rule before being imported into MIKE SHE.

Figure 5-27 and Figure 5-28 show that the spatial and frequency distributions of vegetation classes do not vary substantially with increasing grid size up to 30m. However the relative contribution of vegetation classes that are found in small and fragmented patches such as heathlands, wet woodlands, coniferous woodlands and impervious surfaces decreases markedly when the grid size increases from 30 to 50m. This quality threshold also occurs when modelling the river network (Figure 5-29), with a clear degradation of the network representation between resolutions of 30 and 50m. The MIKE SHE pre-processor does not find a solution when a 25m resolution is used.

The model was therefore run at three different resolutions (5, 10 and 30m) and the impact of resolution on run times and model performance was assessed. Overall, run times required by the 5m-resolution model proved incompatible with multiple runs necessary to calibrate it: a four-year long simulation took at least 7.5 hours with an Intel Core i5-540 2.53GHz processor (parallelisation was only introduced in the 2011 release of MIKE SHE, so only one core could be used in the current study). The 30m model required much shorter simulation times (about 8 minutes for a four-year long simulation), but proved too coarse to accurately model both stream flow and groundwater table depth (see Section 6.3.3 for more detail). However it proved very

useful to explore the model behaviour and to perform sensitivity analyses and an initial calibration, the results of which were transferred to the 10m model and further refined. The final model resolution was therefore 10m, with run times in the order of 70 minutes for a four-year long simulation.

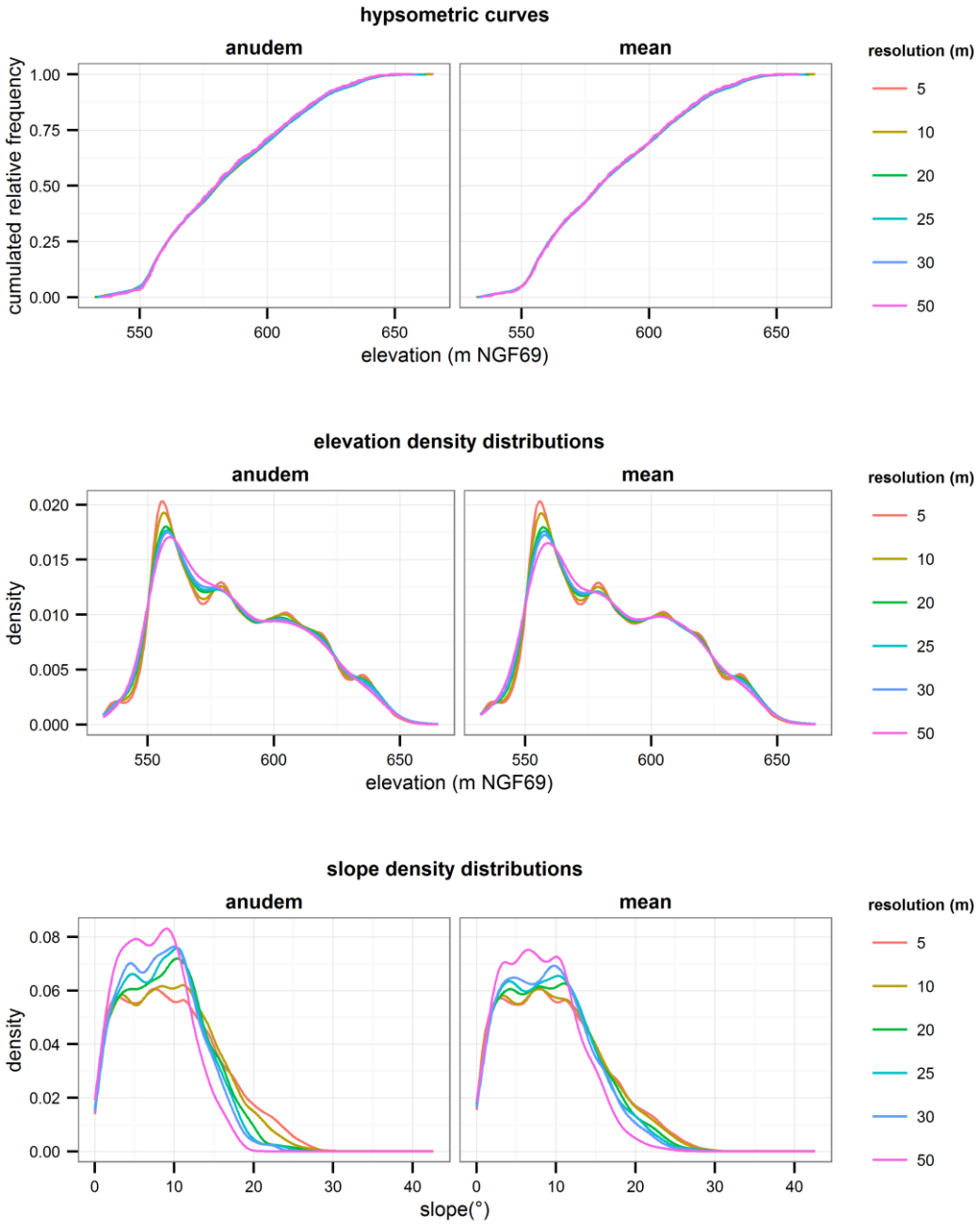

Figure 5-26. Effect of model resolution and aggregation method on the catchment hypsometric curve (top), elevation density distribution (middle) and slope density distribution (bottom).

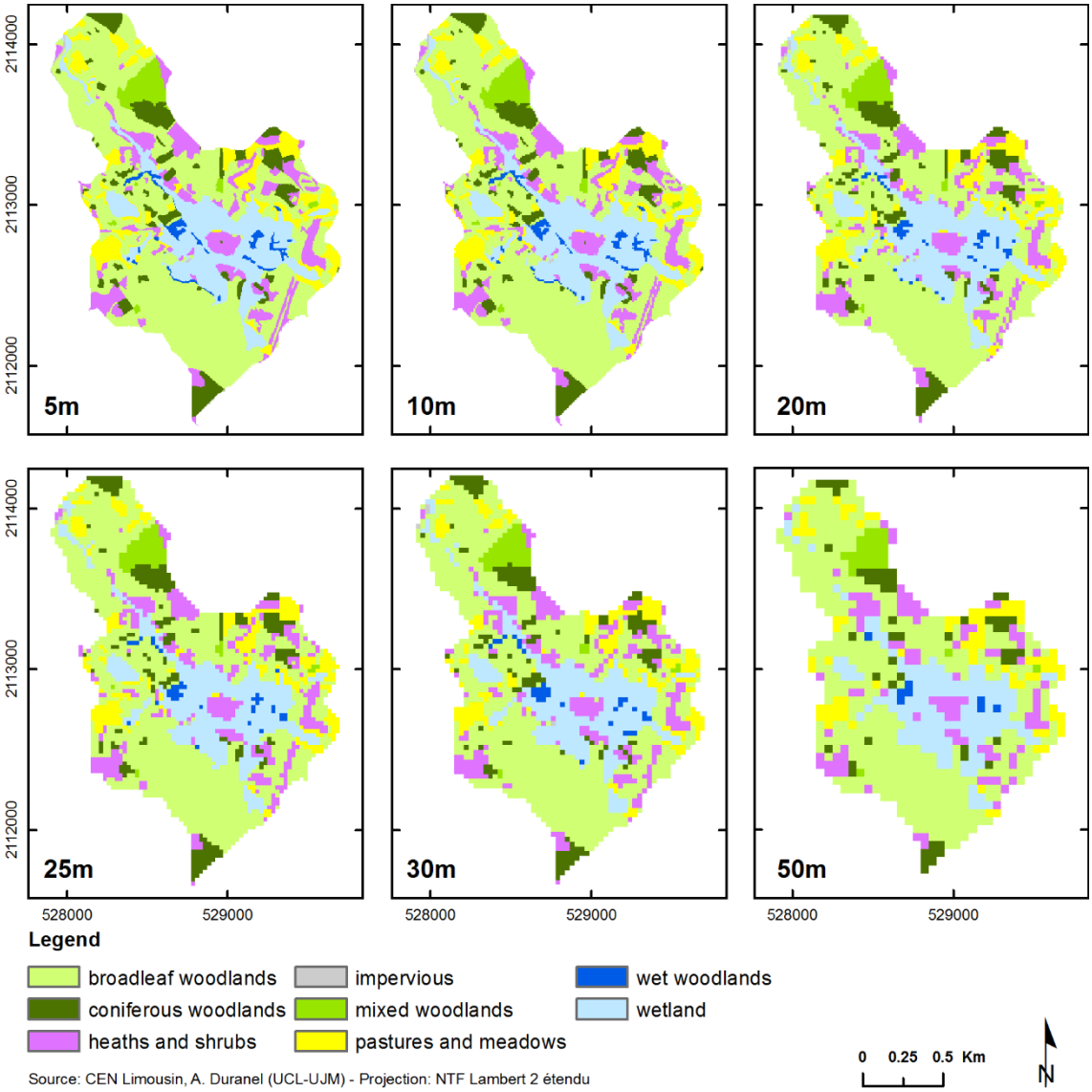

Figure 5-27. Distribution of vegetation classes according to model resolution.

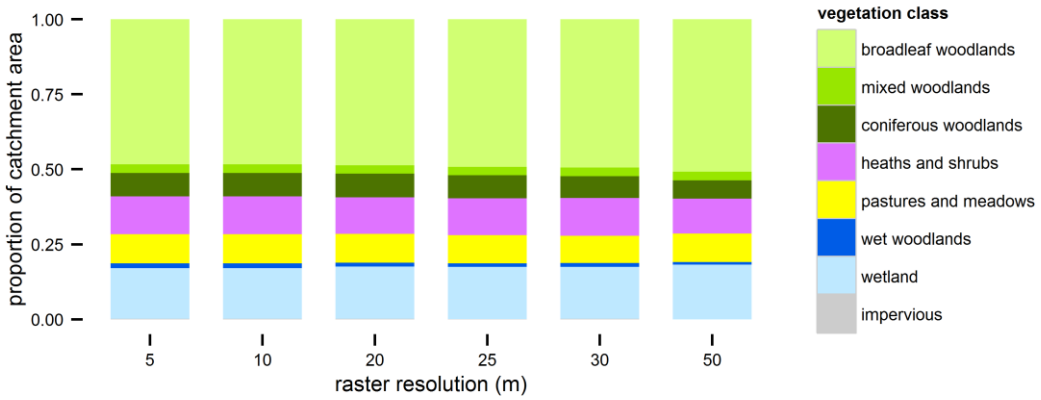

Figure 5-28. Relative frequency of vegetation classes according to model resolution.

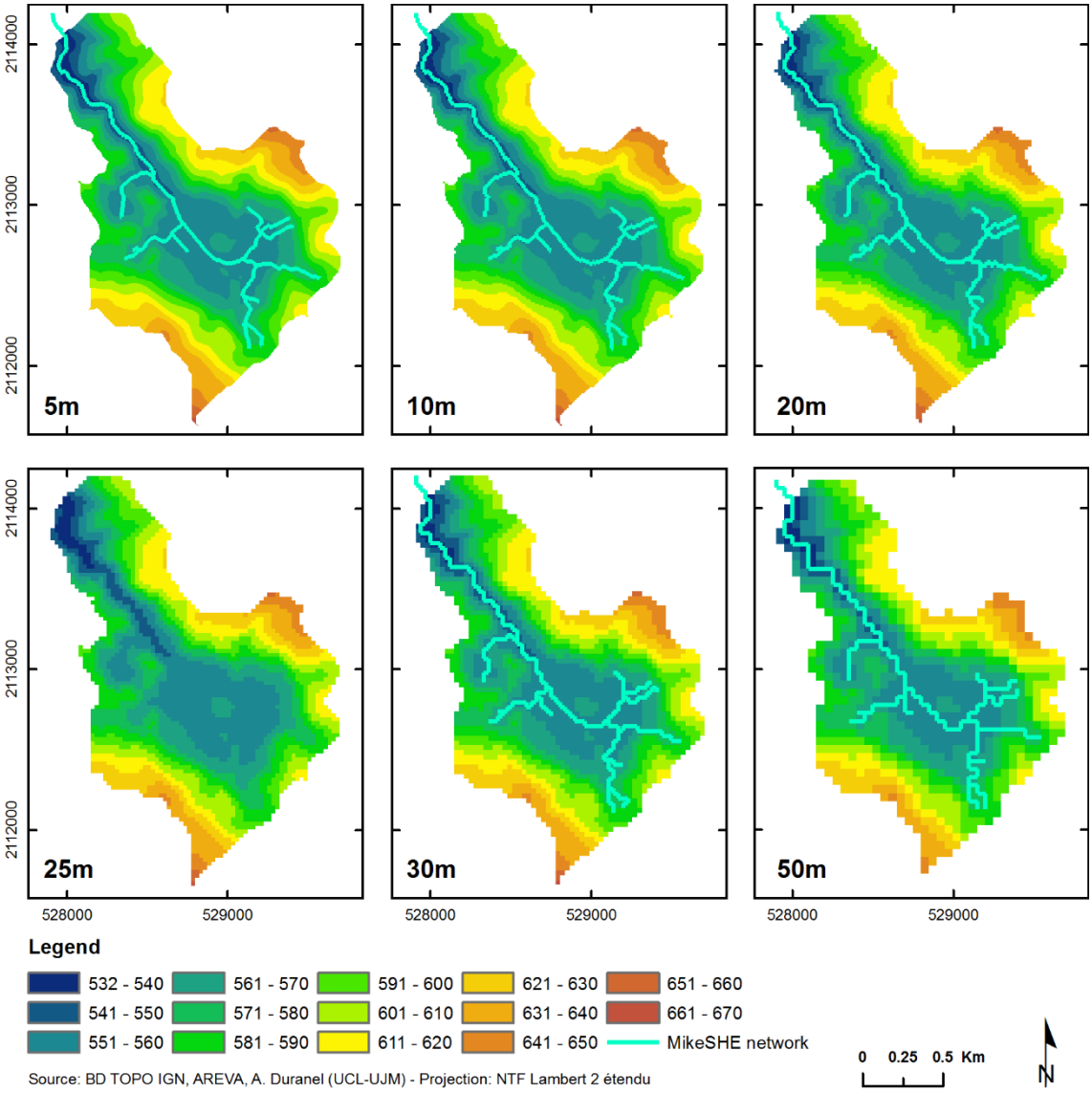

Figure 5-29. Effect of the model grid size on the representation of the hydraulic network by the MIKE SHE pre-processor.

5.5. Conclusion

A MIKE SHE / MIKE 11 hydrological model of the Dauges mire and catchment was developed. In this high-relief environment, a 10m resolution was found to be the best compromise between an adequate representation of the mire and stream topography and computational demand. However the use of the Saint-Venant equations to model channel flow required very small time-steps and proved impossible to implement within the available computational capacity. Kinematic routing was used instead. Consequently exchanges between overland and channel flow engines were assumed to be unidirectional, i.e. over-bank flooding cannot occur. This limitation is further discussed in Chapter 6.

In the absence of detailed data on the hydrological characteristics of unsaturated mineral soils, the two-layer evapotranspiration and unsaturated zone method was used. The method was adapted to allow for a better representation of interception and evapotranspiration processes especially in woodlands, based on formulations proposed by Allen *et al.* (1998) and Allen & Pereira (2009). A thorough literature review was carried out to parametrise the evapotranspiration and unsaturated flow model. After numerous tests, a simple representation of the geology was adopted, consisting in two layers representing peat deposits and the fissured granite zone. The uppermost computational layer followed the bottom of peat deposits within the mire, and, for numerical stability purposes, was set to a uniform 0.5m depth on mineral ground. The bottom computational layer was set to a constant 55m depth below ground.

Résumé du chapitre 5

Un modèle hydrologique en régime transitoire MIKE SHE / MIKE 11 (intégré distribué à base physique) de la tourbière des Dauges et de son bassin versant avec un pas de temps quotidien a été développé. Une résolution spatiale de 10m s'est avérée être le meilleur compromis entre une représentation adéquate de la topographie accidentée de ce site de moyenne montagne et les capacités de calcul disponibles. Le ruissellement de surface est modélisé par une approximation 2D en éléments finis des équations de Saint-Venant. Les débits et hauteurs dans le réseau hydrographique sont simulés avec le modèle unidimensionnel MIKE 11. L'utilisation des équations de Saint-Venant pour modéliser les écoulements dans les cours d'eau s'est avérée nécessiter un pas de temps très court, incompatible avec les capacités de calcul disponibles et la nécessité de limiter les temps d'exécution à quelques heures pour permettre une calibration fine du modèle. En conséquence, une représentation simplifiée par routage cinématique a été utilisée, les hauteurs d'eau étant calculées a posteriori sur la base de la formule de Manning.

En l'absence de données détaillées permettant de caractériser finement la zone non-saturée sur le bassin versant, un modèle simplifié à deux couches a été utilisé pour modéliser les processus d'évapotranspiration et d'écoulement vadose. Cette méthode a été adaptée pour permettre une meilleure représentation des phénomènes d'évapotranspiration, en suivant les propositions d'Allen et al. (1998) et d'Allen & Pereira (2009). Une revue détaillée de la littérature internationale a été réalisée pour paramétrer le modèle d'évapotranspiration et permettre l'évaluation de l'impact des changements d'occupation des sols dans le bassin versant sur le bilan hydrique de la zone humide.

Après de nombreux tests, une représentation simplifiée de la zone saturée a été adoptée. Elle consiste en deux couches de calcul, la plus profonde représentant la zone fissurée du granite et la plus superficielle les dépôts tourbeux dans la zone humide et les sols minéraux sur le bassin versant. Les écoulements en zone saturée sont calculés en résolvant la loi de Darcy en trois dimensions grâce à une approche itérative basée sur les différences finies. La partie fissurée du socle granitique est donc modélisée comme un milieu poreux équivalent. Ses propriétés hydro-physiques sont considérées comme homogènes sur l'ensemble du bassin versant du fait des difficultés méthodologiques et logistiques inhérentes à leur caractérisation, une limitation commune aux études portant sur les aquifères de socle.

Chapter 6. Model calibration, validation & sensitivity analysis

6.1. Introduction

This chapter describes the model calibration and validation procedure and results, and details the sensitivity analyses that were carried out. As shown in Figure 1-9, the design and calibration of a model is generally an iterative empirical process. Sensitivity analyses are only valid locally for a specified set of parameter values, and should be repeated during the design and calibration phase if they are used to guide the choice of parameters to be calibrated. As a consequence there is no easy or logical way to organise this chapter. It was chosen to present first the calibration and validation procedures, including the performance of both the initial uncalibrated model and the final calibrated model; then to detail the sensitivity analyses carried out using both the uncalibrated and calibrated models; and finally to discuss the model performance and potential improvements to the model.

The model was calibrated and validated against observed stream stage, stream discharge and groundwater table depth time-series, and further validated by comparing the simulated mean groundwater table depth and the observed distribution of wetland vegetation across the entire catchment. The sensitivity of the model to a number of factors was investigated, including the depth and shape of the fissured zone layer, all uniformly spatially-distributed model parameters, model grid size and length of the warm-up period. The impact of spatial heterogeneity of peat physical characteristics such as specific yield and available water capacity on the model performance was investigated by calibrating these parameters against individual dipwells in turn and comparing the calibrated values.

6.2. Model calibration and validation

6.2.1. Calibration and validation against observed time-series

6.2.1.1. Hydrometric and piezometric time-series

The performance of the inititial uncalibrated model was assessed over the 01/01/2011-31/12/2013 period. The model was then calibrated over the 01/01/2011-30/06/2012 period, and validated over the 01/07/2012-31/12/2013 period. In both cases the model performance was assessed against observed groundwater table depth, stream discharge and stream stage

data described in Chapter 4. All observation points were used except clusters PZ1 to PZ6 that had been installed before the current study was initiated and that were shown to provide unreliable estimates of groundwater table depths due to the way they had been constructed (Chapter 4). Logger- and hand-recorded groundwater table depth time-series recorded in the same dipwell were merged. Given the relatively unequal microtopography within the mire and the 10m resolution of the model, the actual ground elevation at the location of dipwells and piezometers unavoidably differs from the altitude of the closest DEM cell centre: the mean absolute error was 0.372+/-0.197m. Given the small amplitude of observed groundwater table depths, this makes it problematic to express the groundwater table position relative to a common absolute datum (here NGF69). As a consequence, groundwater table elevations were converted to depth below ground. However, due to the way stream stage was measured (Section 4.2) and for consistency with the MIKE 11 hydraulic model, stages were expressed relative to the absolute NGF69 datum. This difference of datum between dipwells and stageboards may lead to a misrepresentation of head gradients for dipwells that are close to stageboards (clusters 7, 8 and 19), however the datum error was small (0.003, 0.089 and 0.150m respectively) and therefore assumed to be negligible.

6.2.1.2. Model performance evaluation

The model performance was principally evaluated using two statistics recommended by Moriasi *et al.* (2007): the Nash-Sutcliffe Efficiency (NSE) and the percent bias (PBIAS). The NSE is calculated as follows:

$$NSE = 1 - \frac{\sum_{i=1}^{n}\left(Y_i^{obs} - Y_i^{sim}\right)^2}{\sum_{i=1}^{n}\left(Y_i^{obs} - \overline{Y^{obs}}\right)^2} \qquad \text{Equation 6-1}$$

where Y_i^{obs} and Y_i^{sim} are the *i*th observed and simulated values respectively, $\overline{Y^{obs}}$ is the mean observed value and n is the number of observations. The NSE indicates how well a scatterplot of observed vs. simulated values fits the 1:1 line. It ranges from 1 (perfect fit) to -∞. Values less than or equal to 0 indicates that the mean observed value is a better predictor than the simulated values. The NSE includes a scaling/normalisation factor, and can therefore be compared between model outputs with different units or magnitudes. It is one of the criteria recommended by the American Society of Civil Engineers (The ASCE task committee on definition of criteria for evaluation of watershed models of the watershed management committee, Irrigation and Drainage Division 1993), and has become one of the most widely used criteria for

performance evaluation of hydrological models (Moriasi *et al.* 2007). However it cannot be used to assess whether the model under- or over-estimates the observed data. This is the reason why the percent bias (PBIAS), a measure of under- or over-estimation, was used in conjunction with the NSE. The percent bias is calculated as follows:

$$PBIAS = \frac{\sum_{i=1}^{n}\left(Y_i^{obs} - Y_i^{sim}\right) * 100}{\sum_{i=1}^{n} Y_i^{obs}} \qquad \text{Equation 6-2}$$

PBIAS is not appropriate for piezometric heads expressed as elevations above a common datum (the NGF69 datum in the current study), since its value will strongly decrease with altitude independently of the model performance. To a much lesser extent, the same issue also exists in the case of phreatic levels expressed as depth below ground or discharge: PBIAS will decrease when the observed water table average depth increases, independently of model performance, and should therefore not be used to compare the model performance between different measurement points. However it can still be useful when comparing the performance of different models in the same location.

Moriasi *et al.* (2007) also recommended the use of the ratio of the root mean square error to the standard deviation of the observed data (RSR), calculated as follows:

$$RSR = \frac{\sqrt{\sum_{i=1}^{n}\left(Y_i^{obs} - Y_i^{sim}\right)^2}}{\sqrt{\sum_{i=1}^{n}\left(Y_i^{obs} - \overline{Y^{obs}}\right)^2}} \qquad \text{Equation 6-3}$$

A RSR of 0 indicates perfect fit, and increases with model error. As shown by Equation 6-1 and Equation 6-3, the RSR and NSE are related to each other and in practice give similar performance rankings. The RSR is therefore provided for reference in the performance plots shown in Sections 6.2.1.3 and 6.2.1.5 but will not be further discussed. Moriasi *et al.* (2007) provided performance ratings for these statistics in the context of surface runoff modelling: a model is regarded as satisfactory if NSE>0.5, RSR≤0.7 and -25%≤PBIAS≤+25%, good if NSE>0.65, RSR≤0.6 and -15%≤PBIAS≤+15%, and very good if NSE>0.75, RSR≤0.5 and -10%≤PBIAS≤+10%. A number of other performance measures are also provided for reference in the performance plots shown in Sections 6.2.1.3 and 6.2.1.5: the mean error (ME), the mean absolute error (MAE), the root mean square error (RMSE) and Pearson's correlation coefficient (r).

6.2.1.3. Performance of the initial uncalibrated model

The performance of the initial model parameterised using data from the literature was very poor. Figure 6-1 and Figure 6-2 show the results obtained for a small number of discharge and groundwater table depth monitoring points. These were selected a posteriori as representative examples of the types of discrepancies encountered between observed time-series and those simulated by the uncalibrated model, and include the Pont-de-Pierre gauging station downstream of the main wetland, one upstream gauging station, two dipwells located on the mire margins (D3 and D9) and two dipwells located at the centre of the wetland (D7 and D18). On the right plot of the figures, the dashed line is the identity line and the continuous line the OLS regression line.

Simulated discharge at the Pont-de-Pierre wetland outlet was 70% higher than observed, and too large during both base flow and peak flow periods. It was strongly underestimated by 20 to 55% in the upper reaches at Rocher, Marzet and Girolles, where base flow and peak flow were under- and over-estimated respectively. Groundwater table depth was up to 10m lower than observed on the wetland margins and almost constantly at ground level in its centre.

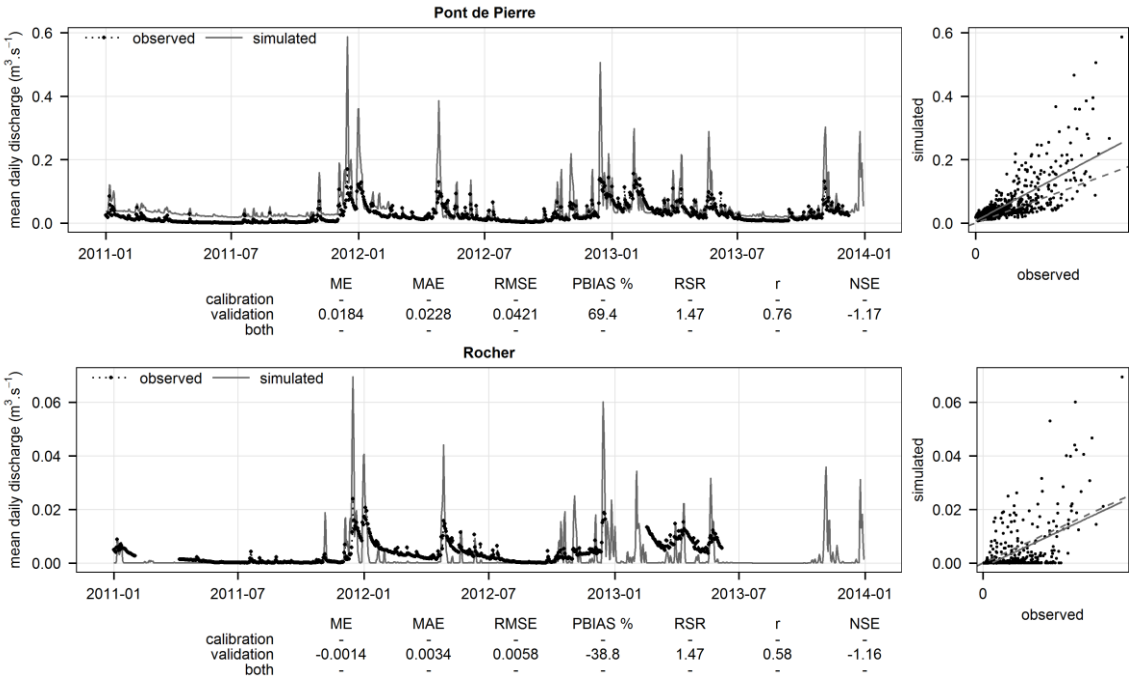

Figure 6-1. Observed and simulated stream discharge (uncalibrated model).

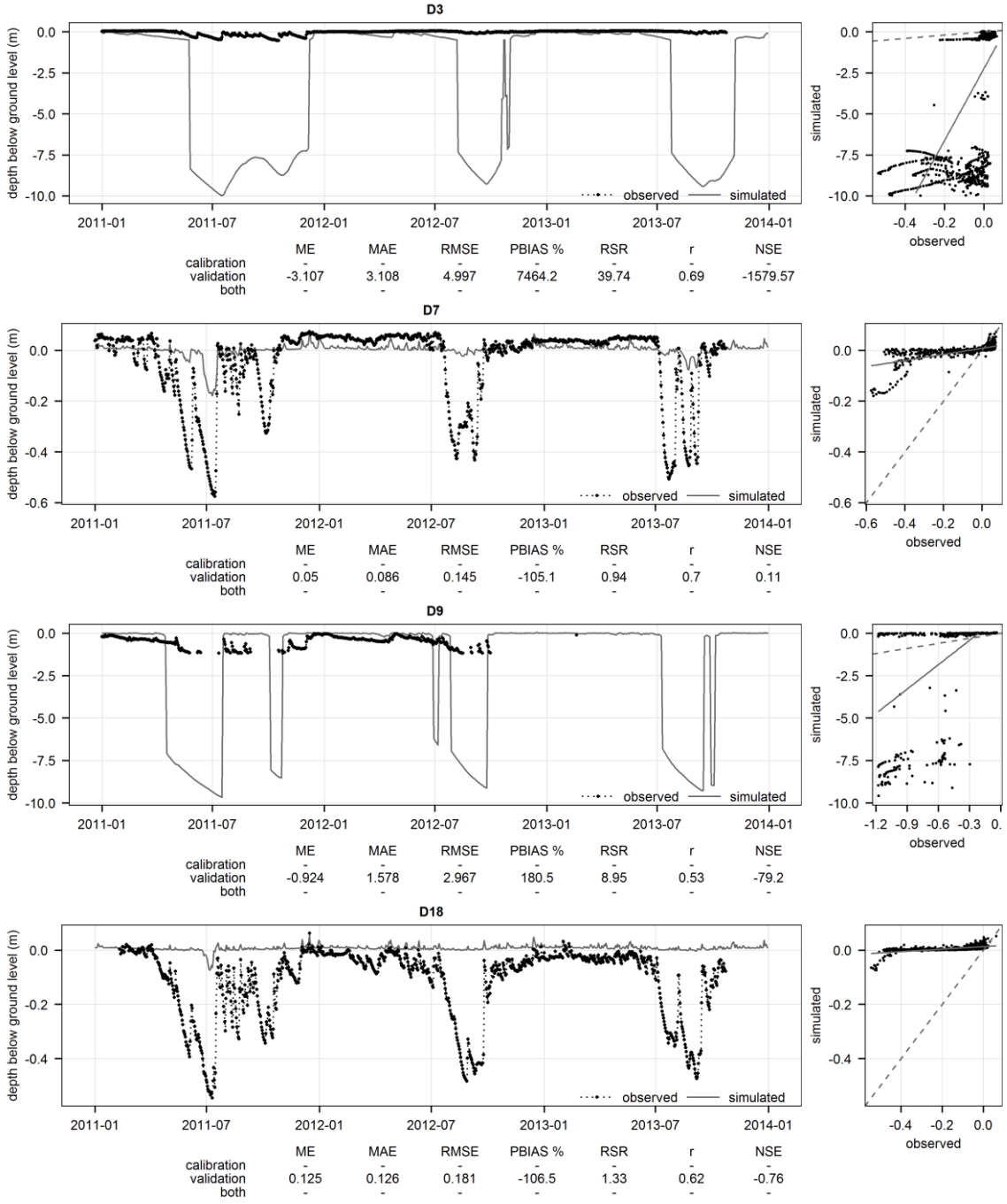

Figure 6-2. Observed and simulated groundwater table depth (uncalibrated model).

6.2.1.4. Calibration strategy

Initially, a sensitivity analysis was performed using AUTOCAL, a generic tool to perform automatic calibration, sensitivity analysis, parameter optimisation and scenario management (Madsen 2000, 2003; Anonymous 2009a). Systematic sensitivity analyses carried out as part of this work and their implementation in AUTOCAL are further detailed in Section 6.3.2. The parameters to which the model outputs were most sensitive were then calibrated automatically using AUTOCAL. In auto-calibration mode, AUTOCAL searches for the best set of parameters that minimise a user-

specified objective function summarising the model performance in one single measure. In AUTOCAL, the objective function is built from basic performance statistics calculated from observed and simulated time-series at each observation point. Available basic statistics are the average error, the root mean square error (RMSE), the standard deviation of residuals, the error of the maximum value and the error of the minimum value. Other widely used (and generally better performing) performance statistics such as those described in Section 6.2.1.2 could not be used as they are not available in AUTOCAL. The basic statistics corresponding to similar variables (groundwater table depths or stream discharge for instance) are aggregated into an aggregated objective function using a weighted sum, sum of absolute values or sum of squares, the weights being specified by the user. A unique model performance measure is then calculated using a weighted sum of the aggregated objectives functions, a weighted sum of aggregated objective functions transformed to a common distance scale or a weighted sum of aggregated objective functions transformed to a common probability scale. For further details of the transformations see the AUTOCAL user guide (Anonymous 2009a). The latter two transformations can be used to compensate for differences in the magnitudes of the different aggregated objective functions so that, if all weights are equal, they all have approximately the same influence on the overall performance measure. The shuffled complex evolution optimisation algorithm was used in the current study, details of which can be found in Madsen (2000, 2003). The algorithm searches for the set of parameters that minimise the overall performance measure within user-specified ranges of possible values. In the current study and given the large uncertainty on parameters estimated from the literature, the range of possible values for each parameter was taken as quite large, based on all possible values obtained from the literature review. The RMSE was used as the basic statistics as it gives an overall performance measure that includes both bias and dynamical correspondence (Anonymous 2009a). Equal weight was given to all measurement points within the two aggregated objective functions corresponding to discharge and groundwater table depth. The aggregated objective functions were transformed to a common distance scale and given equal weights in the overall performance measure.

The automatic calibration proved extremely time-consuming, even with a 30m-resolution model, and the best models still had very poor performances. This was due to a series of issues. For instance, the autocalibration procedure seems to often converge towards a local optimum but to fail to find the global optimum when the number of parameters to optimise is relatively large and their interactions are highly non-linear. The autocalibration results are also very sensitive to

the choice of the performance measure, yet the measures that can be used are relatively limited. Finally, AUTOCAL does not allow for an autocalibration run that crashed to be run again from the last successful model run, imposing substantial run time constraints because of frequent AUTOCAL failures. As a consequence, and similarly to Johansen *et al.* (2014) who encountered the same issues when modelling groundwater-fed fens using MIKE SHE, a manual calibration approach was preferred to automatic calibration. It was based on a combination of systematic tests to investigate the full potential range of some parameters and subjective tests guided by an increasingly detailed understanding of the model behaviour. The calibration was broadly carried out from the top to the bottom of the catchment. First, the parameters driving rainfall infiltration and runoff on mineral soil (unsaturated zone hydraulic conductivity, saturated zone hydraulic conductivity, overland flow Manning's M and detention storage) were calibrated to reproduce the low flow/peak flow discharge patterns recorded at the gauging stations upstream of the mire. Second, the saturated fissured zone specific yield and hydraulic conductivity were calibrated to improve performance for discharge and groundwater table depth in mineral soil. Third, hydraulic conductivity, specific yield, available water capacity and detention storage on peat soils were calibrated to improve performance for groundwater table depth in peat soils. This also required a fine tuning of the fissured zone specific yield and horizontal hydraulic conductivity. Fourth, the unsaturated zone parameters on mineral soil were calibrated to improve the percent bias of discharge. Fifth, the MIKE 11 stream Manning n was calibrated to improve performance for stream discharge and stage. Systematic tests were constantly carried out to test the sensitivity of the model to parameters calibrated in previous steps under the new set of parameter values. Even though the model was very sensitive to the depth of the fissured zone, this parameter was not calibrated to avoid equifinality issues, as preliminary tests suggested broadly similar performances could be obtained with different combinations of depth, specific yield and hydraulic conductivity values for the fissured zone. Since the depth of the fissured zone was the only parameter for which data were available thanks to the ERT survey (Section 3.3), this parameter was kept fixed. During calibration, the 30m-resolution model was used to speed up systematic investigations, and the 10m model when the range of possible values for the set of parameters under investigation had been narrowed down. The model design and validation phase proved complex and very time-consuming, and almost a year of work was devoted to the development and calibration of a model with both an acceptable prediction performance and an acceptable run time. Several hundreds of model designs and parametrisations were tested during this time.

6.2.1.5. Results

Table 6-1 gives the parameter values used in the calibrated model, as well as the range of values used for the systematic sensitivity analysis (Section 6.3.2). These values are discussed in Section 6.4. Figure 6-3, Figure 6-4 and Figure 6-5 summarise the model performance with regard to stream discharge, stream stage and groundwater table depth respectively. All available evaluation points are shown, except for clusters PZ1 to PZ6 for the reasons explained in Section 6.2.1.1 (maps showing the location of these evaluation points can be found in Figure 4-1 and Figure 4-16). On these figures, the vertical dashed line on the left plot shows the limit between calibration (pre 30/06/2012) and validation (post 01/07/2012). On the right plot, the dashed line is the identity line and the continuous line the OLS regression line.

Table 6-1. Calibrated parameters.

Parameter	Calibrated value	Range used in sensitivity analyses
Channel flow (MIKE 11)		
bed resistance (Manning's n)	0.5	0.025-0.5
Overland flow		
resistance (Manning's M)	10	5-50
storage detention (mm)	1 on mineral ground, 3 on peat soils	0-20 (manually tested)
Unsaturated zone		
peat water content at saturation	0.8	0.01-0.95
peat water content at field capacity	0.75	see peat specific yield
peat water content at wilting point	0.7	see peat available water capacity
peat specific yield (UZ)	0.05	0.01-0.99
peat available water capacity	0.05	0.01-0.99
peat saturated hydraulic conductivity (UZ)	2e-6 $m.s^{-1}$	1e-10 – 5e-4 $m.s^{-1}$
peat bypass max fraction	0	0-1
peat water content for reduced bypass flow	0	cannot be tested with max fraction = 0
peat min. water content for bypass flow	0	cannot be tested with max fraction = 0
mineral soil water content at saturation	0.8	0.01-0.95
mineral soil water content at field capacity	0.7	see mineral specific yield
mineral soil water content at wilting point	0.01	see mineral available water capacity
mineral soil specific yield (UZ)	0.1	0.01-0.99
mineral soil available water capacity	0.69	0.01-0.99
mineral soil saturated hydraulic conductivity (UZ)	1e-4 $m.s^{-1}$	1e-8 – 5e-4 $m.s^{-1}$
mineral soil bypass max fraction	0	0-1
mineral soil water content for reduced bypass flow	0	cannot be tested with max fraction = 0
mineral soil min. water content for bypass flow	0	cannot be tested with max fraction = 0
ET surface depth	0 m	not tested.
Saturated zone		
fissured zone lower level (below ground)	-55 m	-100 - -5
fissured zone horizontal hydraulic conductivity	7.5e-7 $m.s^{-1}$	1e-7 – 5e-4 $m.s^{-1}$
fissured zone vertical hydraulic conductivity	5e-5 $m.s^{-1}$	1e-7 – 5e-4 $m.s^{-1}$
fissured zone specific yield	0.015	0.001-0.1
fissured zone specific storage	1e-5 m^{-1}	1e-7 – 1e-4 m^{-1}
peat horizontal hydraulic conductivity	5e-8 $m.s^{-1}$	1e-8 – 5e-4 $m.s^{-1}$
peat vertical hydraulic conductivity	5e-8 $m.s^{-1}$	1e-8 – 5e-4 $m.s^{-1}$
peat specific yield	equal to peat specific yield (UZ)	equal to peat specific yield (UZ)
peat specific storage	0.01 m^{-1}	0.001-0.05 m^{-1}

The scientific e notation is used for readability purposes (1e-x = $1x10^{-x}$).

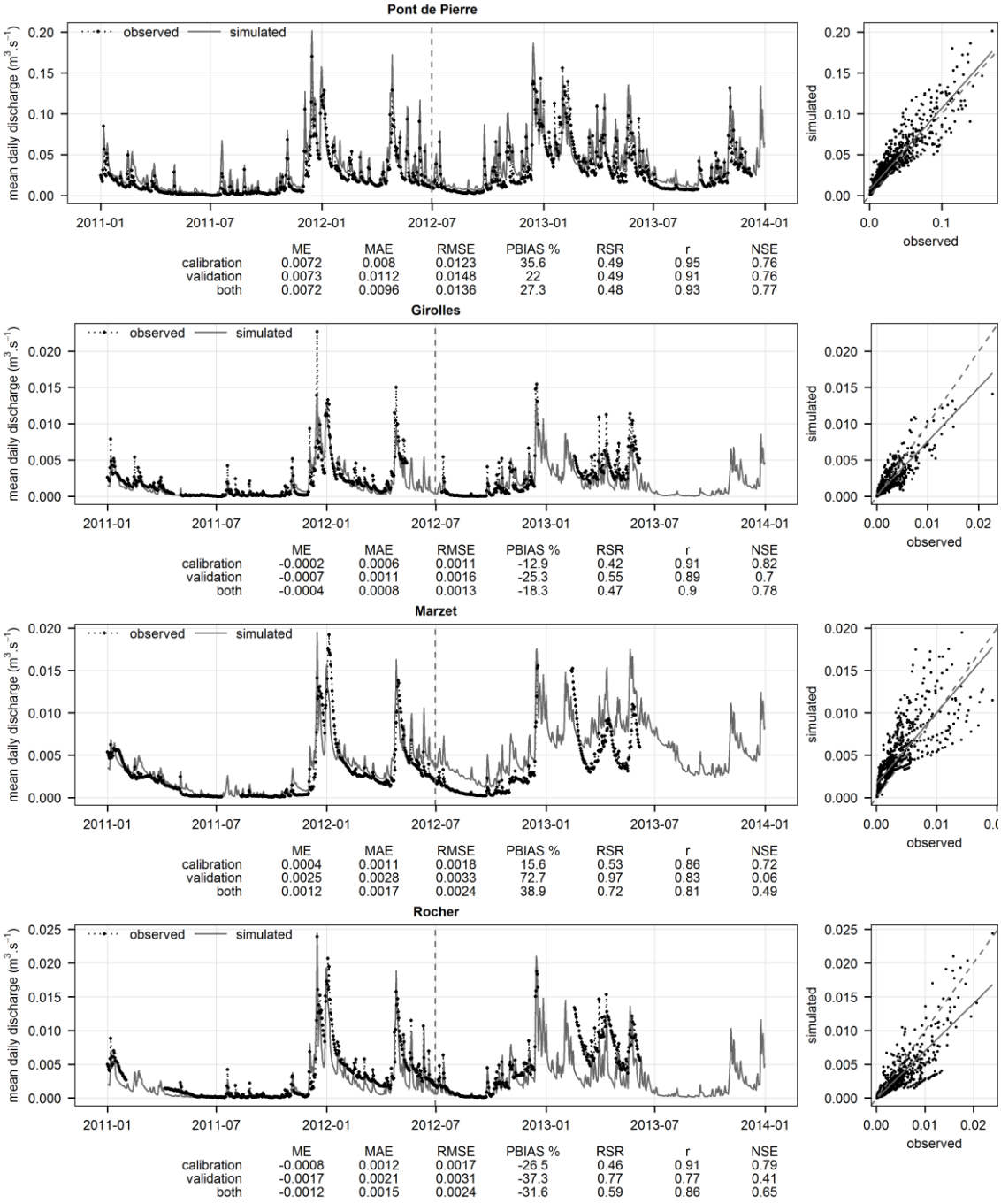

Figure 6-3. Observed and simulated stream discharge (calibrated model).

See Figure 4-1 p. 172 for the location of stream discharge evaluation points.

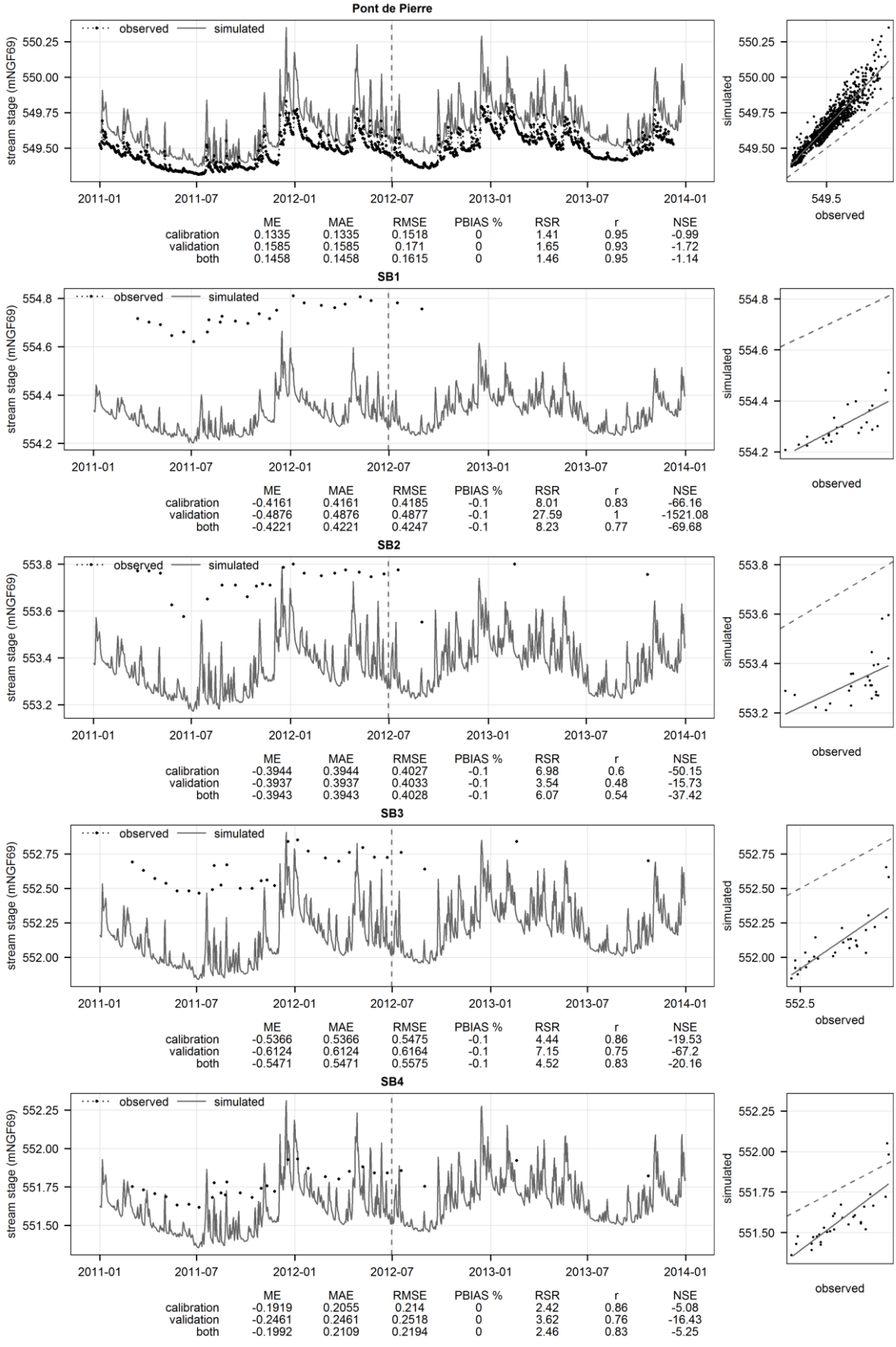

Figure 6-4. Observed and simulated stream stage (calibrated model).

See Figure 4-1 p. 172 for the location of stream stage evaluation points.

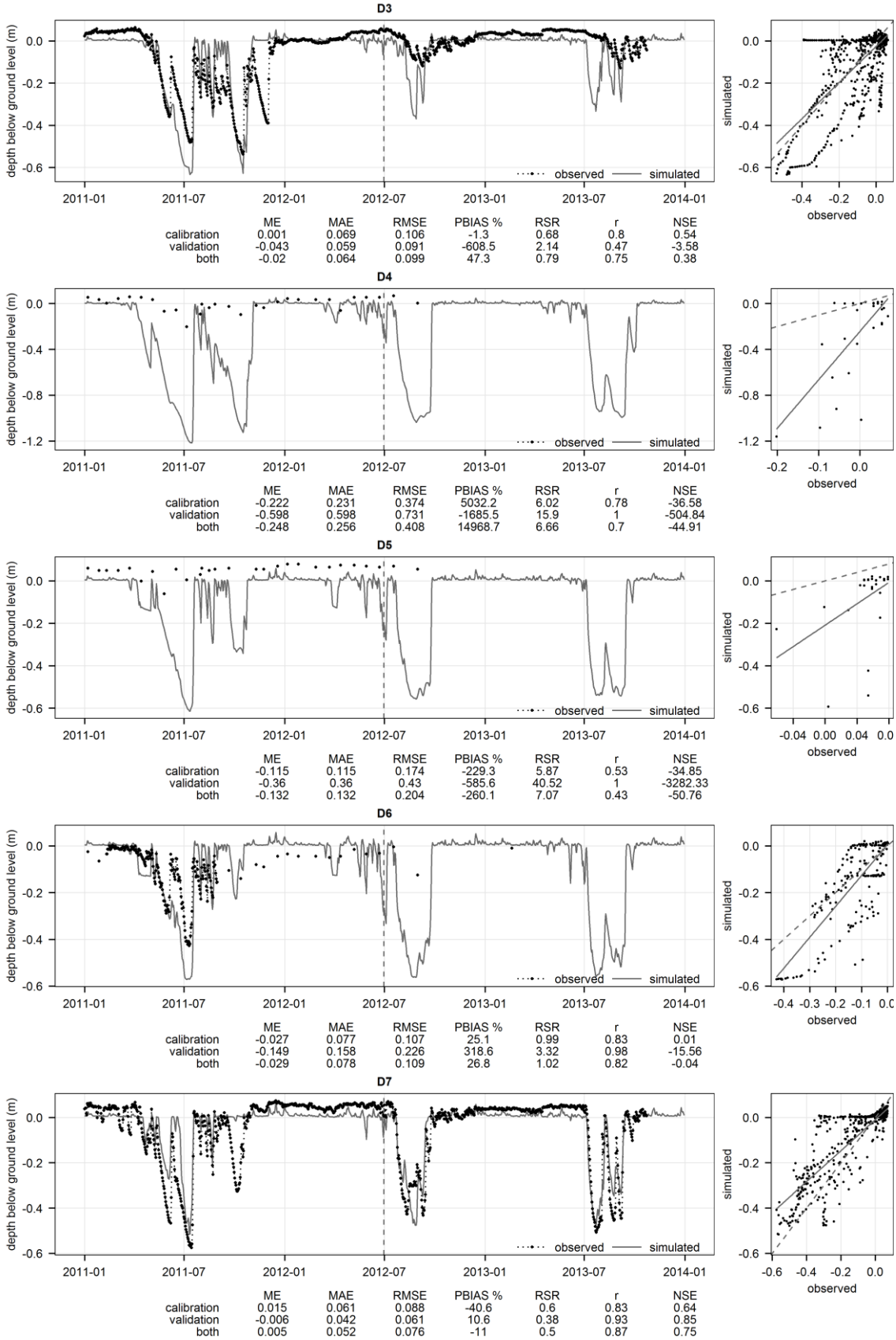

Figure 6-5. Model performance with regard to groundwater table depth (calibrated model).

See Figure 4-16 p. 186 for the location of groundwater table depth evaluation points.

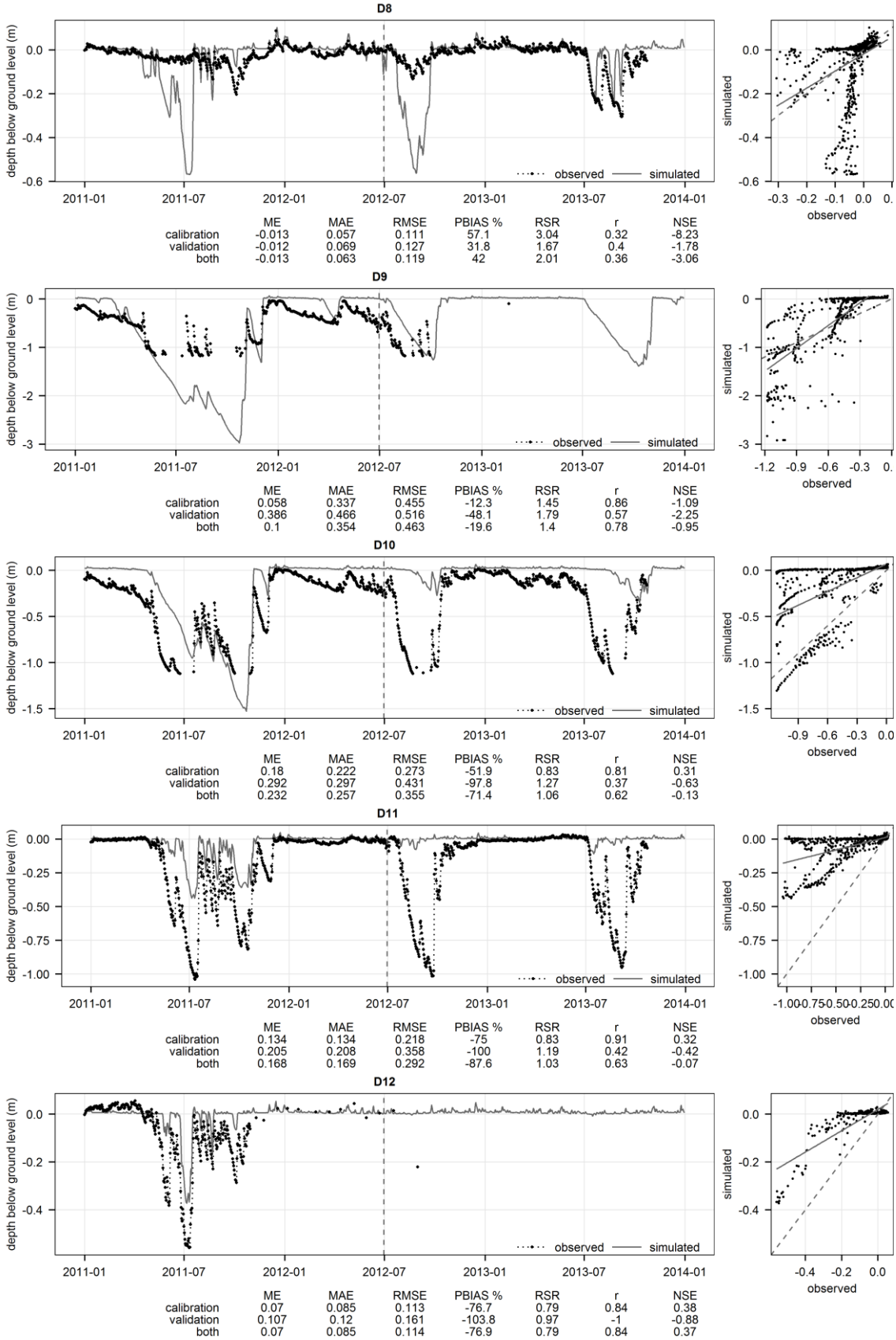

Figure 6-5 (continued). Model performance with regard to groundwater table depth (calibrated model).

See Figure 4-16 p. 186 for the location of groundwater table depth evaluation points.

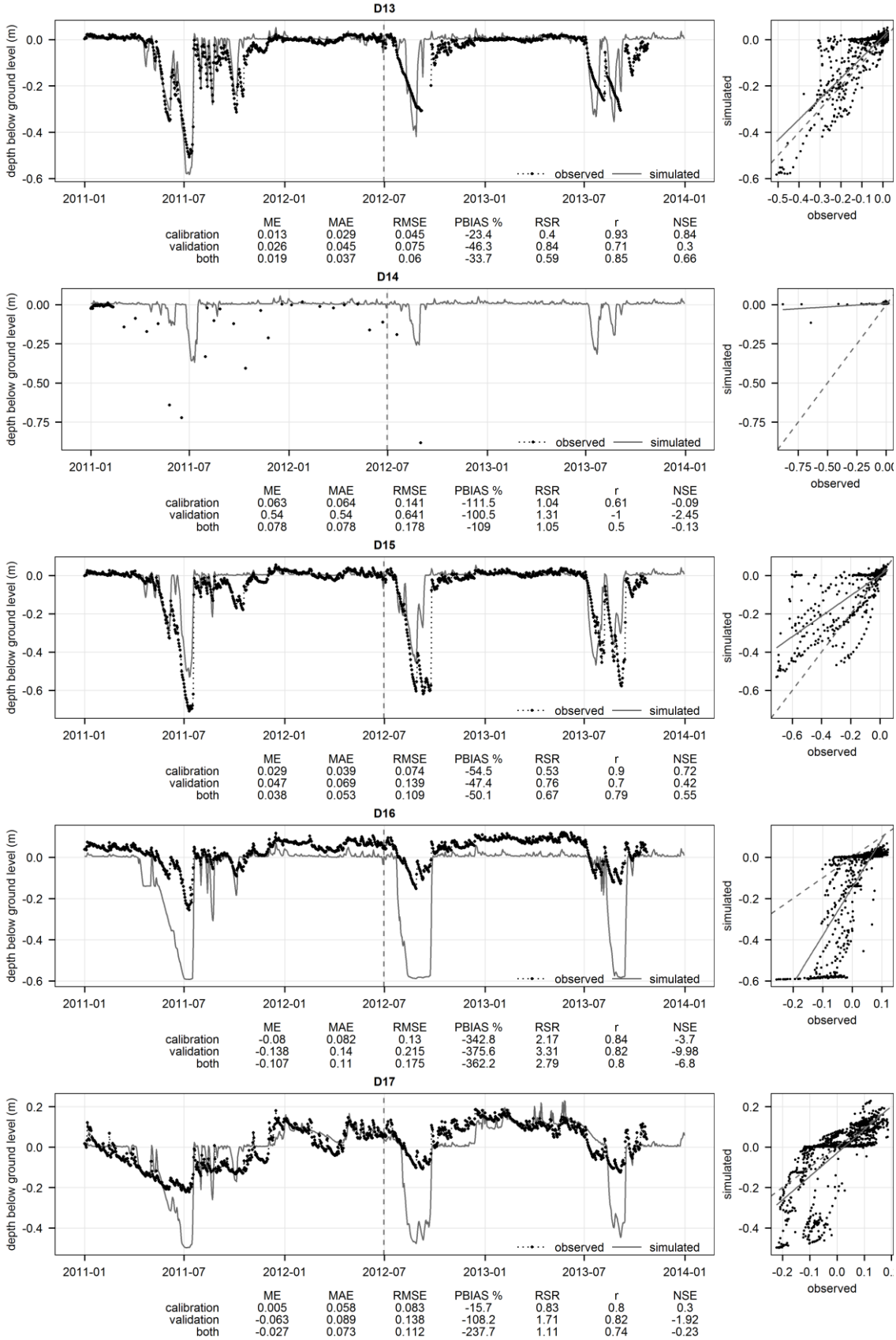

Figure 6-5 (continued). Model performance with regard to groundwater table depth (calibrated model).

See Figure 4-16 p. 186 for the location of groundwater table depth evaluation points.

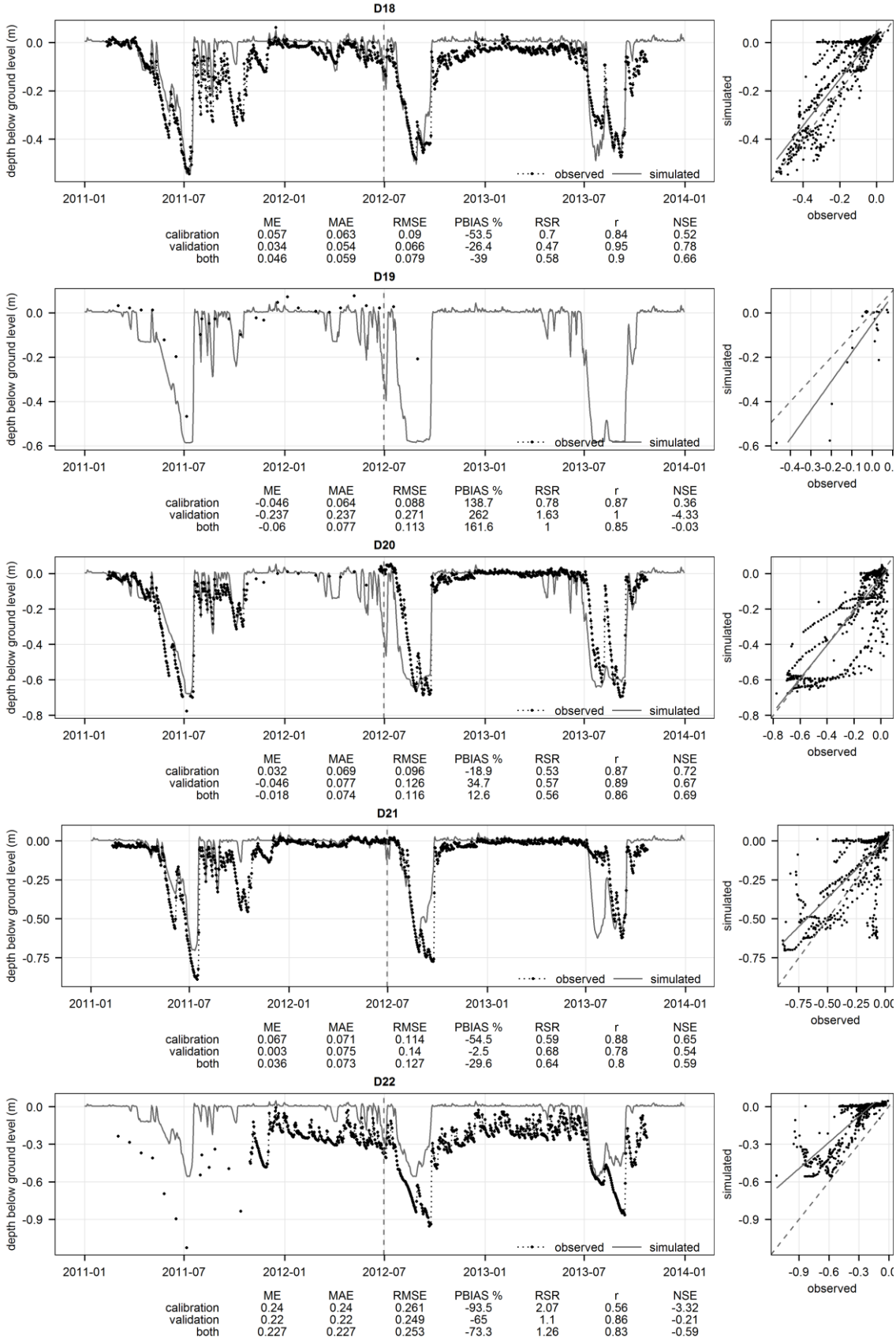

Figure 6-5 (continued). Model performance with regard to groundwater table depth (calibrated model).

See Figure 4-16 p. 186 for the location of groundwater table depth evaluation points.

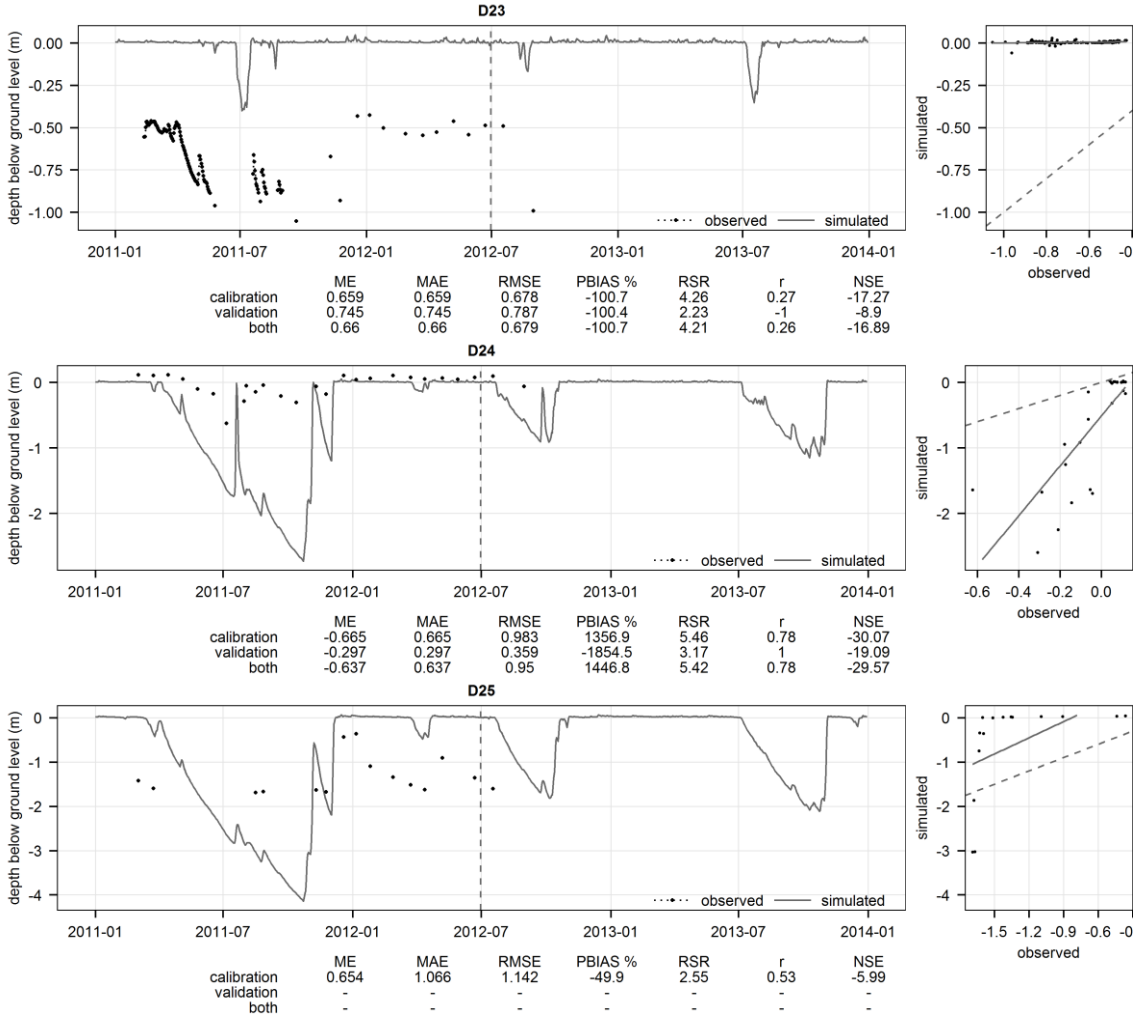

Figure 6-5 (continued). Model performance with regard to groundwater table depth (calibrated model).

See Figure 4-16 p. 186 for the location of groundwater table depth evaluation points.

According to model performance guidelines commonly accepted in the hydrological modelling literature (Moriasi *et al.* 2007), the model performance with regard to discharge can be regarded as satisfactory (NSE=0.65 over the calibration and validation period at Rocher) to good (NSE>0.75, PBIAS<= about 25% and RSR<0.70 at Pont-de-Pierre and Girolles). At Marzet, the model performs well during the calibration period but less so during the validation period. This may be caused by problems of numerical convergence encountered by the overland flow component that could not be solved, and that seem to be particularly important in an area located just upstream of the Marzet gauging station. This issue is further discussed in Section 6.3.5. During the calibration work, it became apparent that much higher performances could be obtained with regard to discharge but at the detriment of model performance with regard to groundwater table depth. This is an example of the trade-offs encountered in multi-objective calibration, defining a Pareto

front along which a balanced solution has to be selected, and explaining the lower overall performance generally achieved by multi-objectives hydrological models (Madsen 2000, 2003).

The model performance with regard to stream stage is generally poor. Calibration tests have shown that the assumptions imposed by the use of kinematic routing were valid for large linear stretches of the main stream with a relatively high slope, for instance around the Pont-de-Pierre gauging station, where a Manning's roughness value of 0.12 gives satisfactory NSE and PBIAS values of 0.71 and 0 respectively. However these assumptions are clearly not valid within the wetland itself, where it has not been possible to efficiently model stream stages as attested by performances at stageboards SB1 to SB4 where water levels are consistently underestimated. This is caused by the small stream slope within the wetland that promotes backwater effects, and by obstacles that could not easily be captured during the stream section survey: roots, tussocks, areas of diffuse flow and subterranean pipes through which part of the stream flows. The former issue could be accounted for by using a fully dynamic hydraulic model solving the Saint-Venant equations, however this would impose very large computational constraints on the study. This is further discussed in Section 6.4.2.

The model performance with regard to groundwater table depth is variable. It should be assessed relative to the site's topography: the altitude range from the bottom of the wetland to the top of the hills surrounding it and delineating the model boundaries is 110m. It is therefore clearly good to very good for a large number of dipwells such as D7, D13, D15, D18, D20 and D21, for which RMSE of around 10cm or less and NSE values between 0.55 and 0.75 are achieved. In these dipwells, the seasonal patterns are well reproduced. This is the case for instance in dipwell D7, at the centre of the mire, where the surface saturation in winter, the drop in groundwater table depth in late spring or early summer and the rapid fluctutations caused by summer precipitation events are well modelled. The difference between observed and simulated levels in winter (about 5cm) when the groundwater table is at ground level should not be attributed to model errors but rather to the difficulty in defining ground level for observed data in mire environments. This is further discussed in Section 6.4.1. In dipwells where the model performs well, small residual discrepancies between observed and simulated groundwater levels can easily be explained by errors in observed data or by the heterogeneity of the peat and vegetation characteristics. This is further tested and discussed in Section 6.3.4.

The model performance is less good, but still satisfactory, in some dipwells which are installed close to the mire boundary or within the mineral soils just outside it, such as D3, D9 and D10. In

D3 for instance, the much shallower groundwater table levels observed in 2012 and 2013 compared to 2011 are not very well reproduced. Inversely in D10, simulated levels are too shallow during the summers of 2012 and 2013. Dipwells D3, D9 and D10, together with D24 and D25, are located where discrepancies between the actual ground elevation of the observation point and that interpolated at the closest DEM grid cell centre are the largest, due to the larger slope. Of all available groundwater observation points, it is in these locations that the approximations caused by the model discretisation are the largest, which probably explains part of the larger discrepancies between observed and simulated data. During the manual calibration, it became evident that these dipwells were more sensitive than those located at the centre of the mire to the parameterisation of the fissured zone, and that, while it was possible to improve the model fit for dipwells on one side of the mire, this improvement was balanced by a deterioration in dipwells located on the other sides. This may be explained by the fact that the fissured zone is modelled as a homogeneous layer for the reasons explained in Section 5.4.6.1, whereas the punctual field observations detailed in Chapter 3 have shown that this is clearly a simplification. This issue may also explain the poor performance achieved in some dipwells located on the southern side of the wetland (D4 and D5), where observed groundwater table levels are close to the surface all year round, whereas simulated levels follow the same seasonal patterns as those observed and simulated in other dipwells. As detailed in Chapter 3 (Figure 3-28), the stratigraphic and rod surveys have shown that this area is characterised by the shallowness or absence of saprolite, and the presence of hard rock close to or immediately underneath the peat. It may correspond to an area of more resistant, less densely fissured granite that impedes water flow through the fissured zone, leads to higher discharge upslope of it and maintains a higher groundwater table in the peat. Another explanation may be that those dipwells are located within an area where surface and subsurface flow converges due to the micro-topography, and that this micro-topography could not be captured by the 10m model resolution. However the analysis of the model sensitivity to its resolution, described in Section 6.3.3, shows no performance improvement with regard to these dipwells when the resolution is increased to 5m.

The poor model performance with regard to groundwater table levels in dipwell D17, and possibly in dipwells D16 and D8, is a consequence of the poor performance with regard to stream stages within the wetland, and of the absence of representation within the model of the permeable alluvial deposits that are found underneath the shallow peat layer along the stream downstream of Puy Rond (Section 3.4). The quantitative analysis of piezometric and surface

water level time-series described in Section 4.3.2.3 has highlighted the rapid exchanges occurring between the stream and the wetland through alluvial gravel deposits in which dipwell D17 is located. This cannot be accurately reproduced until stream stages are correctly modelled. However, as shown by the good performances obtained in dipwell D18 and D19, the impact of the poor simulation of stream stage does not extend beyond the area where substantial alluvial deposits occur and promote exchanges between the stream and the saturated zone.

The poor performance of the model in reproducing water levels in dipwells D22 and D23 may be explained by the alteration of the peat characteristics described in Section 3.4.2 and caused by artificial drainage and possibly past peat fire. The stratigraphic survey highlighted the presence of dry and strongly oxidised peat that can be related to grainy moorsh soils forming in drained peatlands. In these soils the composite hydraulic conductivity is strongly increased due to the presence of cracks and large macropores, whereas both the total porosity and available water capacity are reduced, accentuating water table fluctuations (Zeitz & Velty 2002; Ilnicki & Zeitz 2003). In the absence of a high-resolution map of the peat characteristics, the specificity of this area could not be accounted for in the model. Nevertheless, the model results suggest that groundwater table levels should be higher and more stable had the area similar pedological characteristics to the rest of the mire, and confirm the detrimental impact of past human activities on the mire hydrology.

6.2.2. Validation of the calibrated model against wetland vegetation distribution

6.2.2.1. Methods

The ability of the calibrated model to predict realistic groundwater tables across the entire catchment was investigated by validating a raster map of mean groundwater tables simulated across the site for the 2011-13 period against the observed wetland boundaries, mapped using mainly botanical criteria (see Section 2.6.3 and Figure 2-10). The wetland boundaries included wet woodlands. Both raster maps had the same 10m resolution than the MIKE SHE model. The groundwater table depth threshold best discriminating between wetland and other plant communities was found by optimising a Cohen's kappa agreement function between simulated and observed wetland boundaries. Cohen's kappa is a measure of agreement between model predictions and observations for categorical variables, widely used in remote sensing and geographical information sciences (Congalton 1991). It is calculated as:

$$\kappa = \frac{N\sum_{i=1}^{r} x_{ii} - \sum_{i=1}^{r}(x_{i+}x_{+i})}{N^2 - \sum_{i=1}^{r}(x_{i+}x_{+i})}$$ Equation 6-4

where *N* is the total number of map pixels, *r* is the number of rows and columns in the square confusion matrix (two in this case, corresponding to the presence/absence of observed/predicted wetland vegetation), x_{ii} is the number of pixels in row *i* and column *i* of the matrix (i.e. for which observations and predictions are in agreement), x_{+i} is the total for row *i*, and x_{i+} the total for column *i*. The optimisation was carried out using the optimise() function in R, that was designed for use with unimodal continuous functions and uses a combination of golden section search and successive parabolic interpolation (Brent 2013).

6.2.2.2. Results and discussion

The mean groundwater table best discriminating between wetland and non-wetland plant communities was found to be 0.286m below ground level, and gave a kappa of 0.77. Figure 6-6 shows the predicted vs. observed extents of wetland vegetation, and Table 6-2 gives the corresponding confusion matrix, in percentage of the total number of map pixels.

Table 6-2. Confusion matrix (% of the total number of pixels).

		observed (vegetation map)	
		non-wetland	wetland
predicted (mean GWT>-0.286m below ground)	non-wetland	76.0%	3.4%
	wetland	4.1%	16.5%

Some false positives (pixels wrongly predicted to bear wetland vegetation) may in part be due to errors in the wetland vegetation map itself, for instance along the narrow valley north-east of the catchment (noted (a) on Figure 6-6), where difficult access and tree cover may have hindered mapping efforts (Section 2.6.3). Others are probably caused by errors in the 10m DEM, particularly along the south-east wetland boundary (noted (f) on Figure 6-6), where only low resolution topographic data extracted from the BD Topo were available (see Section 3.2). Finally, the isolated shallow groundwater patch close to the eastern catchment boundary (noted (c) on Figure 6-6) coincides with large errors produced by the MIKE SHE overland flow component, that are further discussed in Section 6.3.5.

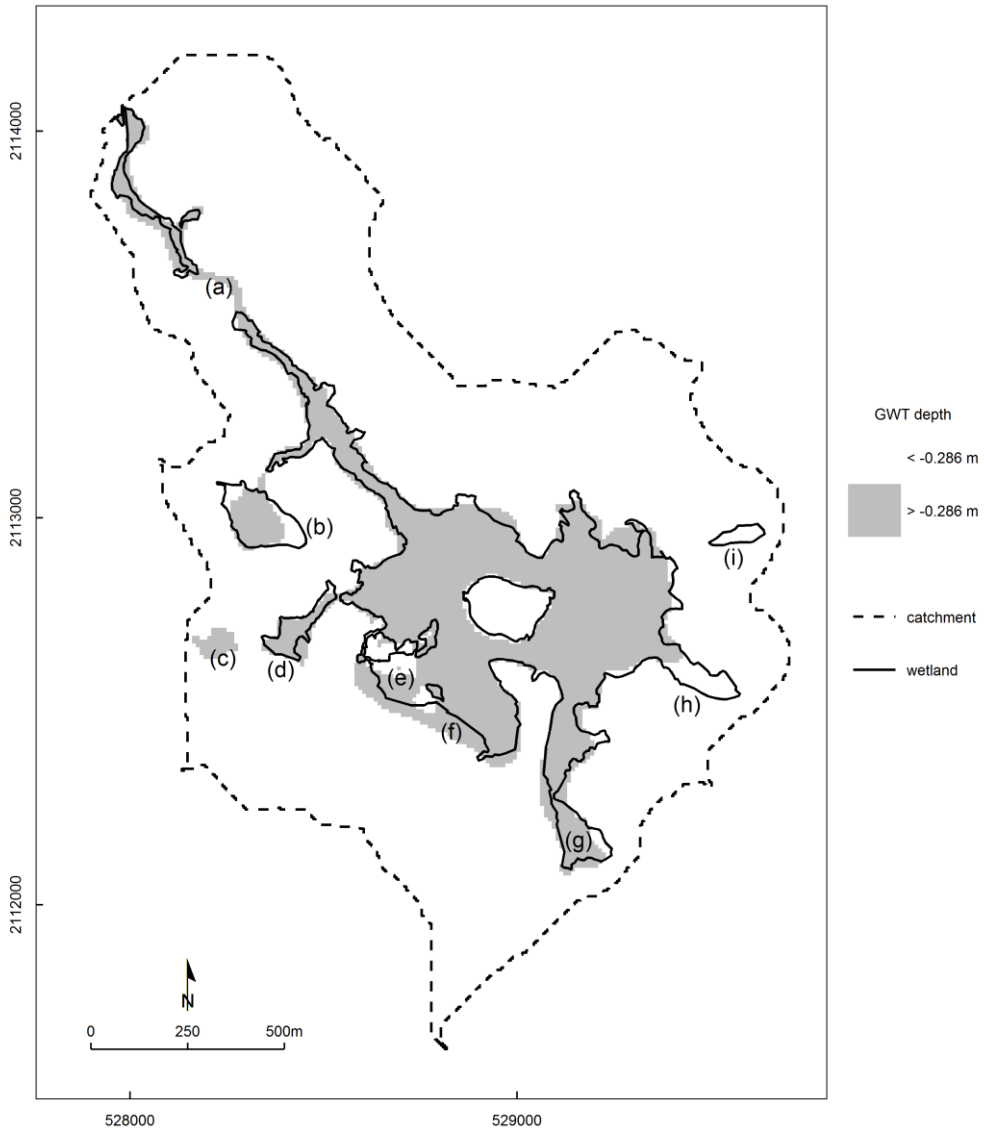

Figure 6-6. Spatial distribution of shallow groundwater tables (2011-2013 mean higher than -0.286m below ground level) and of wetland vegetation.

(a), (b), (c), (d), (e), (f), (g), (h) and (i): refer to text.

False negative (pixels wrongly predicted not to bear wetland vegetation) may have several causes. The small isolated wetland patch close to the north-east model boundary (noted (i) on Figure 6-6) is possibly a result of an error in the vegetation map. It was mapped as a *Molinia*-dominated acidic grassland, but the pit dug in this area during the pedological survey (Section 3.6) showed that no peat was present.

This explanation may also hold for false negatives on the wetland margins in locations (b) and (h), where manual probing demonstrated the absence of peat (Figure 3-29). False negatives in location (e) clearly correspond to model errors as demonstrated by the comparison of observed

and simulated groundwater table depths in dipwells D4 and D5 (Figure 6-5). The possible reasons for these errors are detailed in Section 6.2.1.5.

Despite these limited discrepancies, the spatial agreement between observed wetland vegetation and model grid cells with a mean simulated groundwater table depth higher than -0.286m is generally very good: 92.5% of pixels were correctly classified. This is particularly noticeable along the narrow valley downstream of the main wetland extent and in the small sub-basins upstream of the main wetland extent, in locations noted (d) and (g) on Figure 6-6. These small basins are located 10-30m above the main wetland extent, which suggests that the model does also perform well in the upper part of the catchment. The good prediction of wetland boundaries across the entire modelled area, even in locations where no record of groundwater table depth was available, shows that, even though the hydraulic properties of the fissured zone might slightly vary locally, they are homogeneous enough to be modelled with a satisfactory performance using an equivalent porous medium with homogenous properties at a relatively fine scale.

6.3. Model sensitivity

6.3.1. Sensitivity of the initial model to varying depth and shape of the fissured zone

6.3.1.1. Rationale

Results of the initial sensitivity analysis and of the initial calibration indicated that the depth of the fissured zone in the catchment is of fundamental importance in explaining both river discharge and piezometric heads in the wetland. In the initial model, the fissured zone had been assumed to have a constant depth (55m) below the surface, based on the results of the electrical resistivity tomography survey and on the few geological drilling logs available (Section 3.3). However, the initial model parameterised using data obtained from the literature, in particular for the fissured zone specific yield and hydraulic conductivity, clearly resulted in large discrepancies between obverved and simulated water levels (Section 6.2.1.3). The values obtained by calibration (Table 6-1) differed markedly from these initial values (Table 5-7). Even though the model was relatively insensitive to the vertical hydraulic conductivity (Section 6.3.2), the value obtained by calibration for this parameter was substantially larger than for the vertical hydraulic conductivity. This is in contradiction with the literature and the expected preferential direction of fissures within the fissured zone. One possible explanation could be that the depth of the fissured zone has been wrongly specified. A series of simulations was therefore carried

out to investigate whether satisfactory model performance could be obtained by varying the depth and shape of the fissured layer while keeping the fissured zone specific yield and hydraulic conductivity within the values most commonly cited in the literature (horizontal hydraulic conductivity $1x10^{-5}$ $m.s^{-1}$, vertical hydraulic conductivity $1x10^{-6}$ $m.s^{-1}$, specific yield 0.01, Wyns *et al.* 2004; Dewandel *et al.* 2006).

6.3.1.2. Methods

In Hercynian hardrock landscapes, the local topography derives in part from etching processes, whereby petrographic and structural weaknesses result in localised deepening of the weathering front below the planation surface and the subsequent carving of the landscape by differential erosion when the base level is lowered (Valadas 1984, 1998; Lageat *et al.* 2001; Appendix C). A consequence of this is that, at the local scale, the current topography may give an indication of the thickness of the weathered bedrock that has not been evacuated by erosion, and in particular of the fissured zone. The ERT profiles presented in Section 3.3.3.3 certainly support this assumption: the lowest electrical resistivity values (in saturated conditions) were measured in topographic depressions, while higher values were measured below positive topographic anomalies such as Puy Rond (Figure 3-21). This was interpreted as indicative of fissure density in the fissured zone.

The topographic position index (TPI) as implemented in SAGA GIS was used as an indicator of the rock resistance and relative depth of the fissured zone. The TPI, initially proposed by Guisan *et al.* (1999), compares the position of each DEM cell to the mean elevation of a specified neighbourhood around that cell. A 1.5km-diameter window was used, which corresponds to the size of the etch-basin and to the grain of the local landscape. Figure 6-7 shows the standardised TPI, with high values corresponding to hilltops and ridges, and low values to the deeper valleys and basins. Another index estimating the current ground level elevation relative to the palaeosurface elevation (Figure 6-8), modelled as a second-order polynomial trend of topography using a 4x4km DEM centred onto the site, gave very similar results to the TPI, so only the later was used. The TPI was scaled to match a set of pre-defined ranges (10-30m, 10-60m, 10-90m, 30-60m, 30-90m and 60-90m) corresponding to the thickness of the fissured zone underneath hilltops and valleys respectively. In the first case for instance, the thickness of the fissured zone was set to 10m in places with a TPI equal to 1 (hilltops) and to 30m in places with a TPI equal to 0 (valley bottoms).

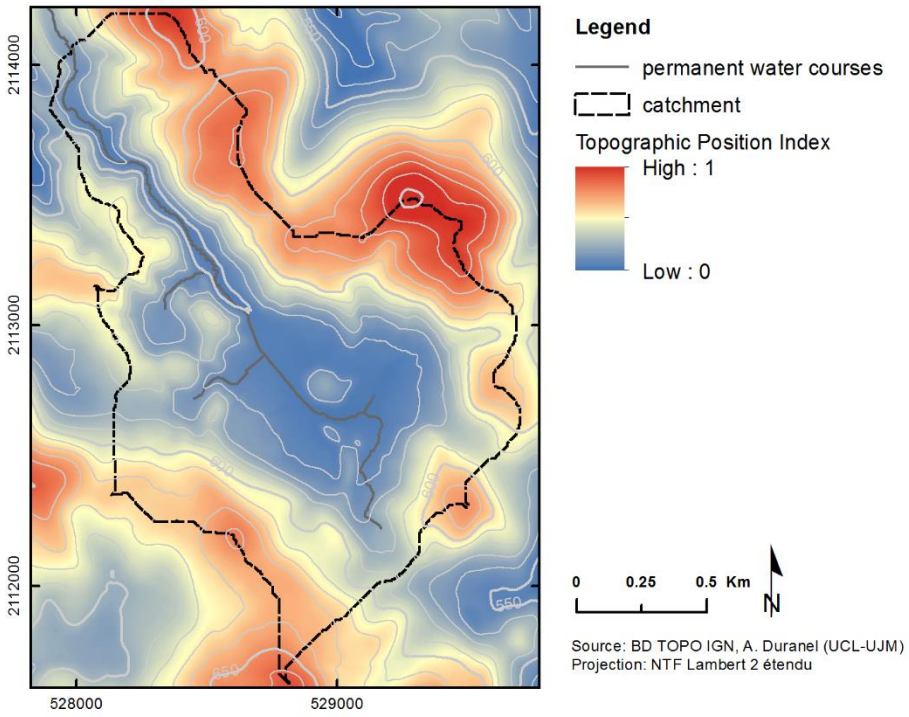

Figure 6-7. Topographic position index (scaled to 0-1 range).

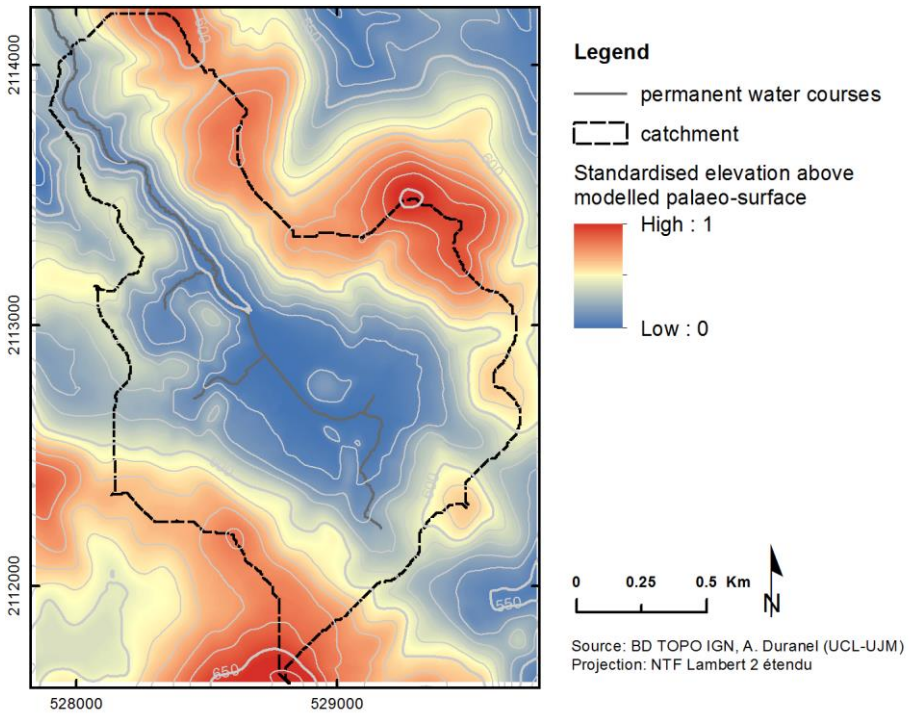

Figure 6-8. Standardised elevation relative to the modelled palaeosurface elevation.

Uniform fissured zone thicknesses of 10, 25, 55, 75 and 100m, independent of the TPI, were also tested. For practical reasons and given the small thickness of the peat layer relative to those tested for the fissured layer, the former was neglected in all above cases: the specified fissured zone thickness was assumed to equal its depth below ground and simply subtracted from the

ground surface elevation to compute the elevation of the bottom of the fissured zone when building the MIKE SHE geological model. A fissured zone with a constant thickness of 5m was also tested, but in this case the peat depth was too large relative to the fissured zone thickness to be neglected. The elevation of the bottom of the fissured zone layer was therefore computed by subtracting its fixed thickness from a map of the elevation of the bottom of the peat layer on peat soils and of the ground surface elevation on mineral soils. This was required to make sure that the thickness of the fissured zone was effectively constant across the entire catchment, including below the mire. Finally, the last scenario used a fissured zone layer with a bottom level set at a fixed elevation. This scenario corresponds to the hypothesis that the depth of the fissured zone is constant relative to the planation surface at both the regional and local scales (Appendix C). The bottom of the fissured zone was set to 500m NGF69. The fissured zone was therefore approximately 50m deep at the lowest point within the main basin, and 150-160m deep below the surrounding hilltops. The performance of the different models over the period 01/01/2011-31/12/2013 was compared using the Nash-Sutcliffe Efficiency (NSE) statistic, for the reasons detailed in Section 6.2.1.2.

6.3.1.3. Results and discussion.

Table 6-3 shows the NSE as a function of the fissured zone shape and depth for all discharge and groundwater table depth monitoring points, except dipwell D26 from which only three records could be obtained and dipwells pre-existing the current study due to methodological issues (Section 4.3). For each time-series the best and second-best models are highlighted in dark and pale grey respectively. In 15 out of 25 dipwells, the best fit between observed and simulated groundwater table depth is obtained with a fixed 5m fissured zone thickness. In the case of discharge, the best fit is also obtained with a fixed 5m fissured zone thickness at Girolles, a 10m fixed thickness at Pont-de-Pierre and Rocher, and a thickness that varies from 5 to 20m as a function of the topographic position at Marzet. However in all cases and whatever the measure, the NSE achieved is much lower than that achieved by the calibrated model detailed in Section 6.2. This is particularly the case for dipwells located near the wetland margins, either in peat or in mineral soils, where the groundwater table depth has been shown to be more variable and more dependent on inputs from the wider catchment (Section 4.3.2.3). This suggests that the poor performance of the initial model is not caused by a misspecification of the depth or shape of the fissured zone, but indeed by hydraulic characteristics of the fissured zone, in particular its horizontal hydraulic conductivity, that differ from those cited in the literature. This is further discussed in Section 6.4.5.

Table 6-3. Nash-Sutcliffe Efficiency before calibration as a function of the shape and depth of the fissured zone

location	5	10	25	55	75	100	5to10	5to20	10to30	10to60	10to90	30to60	30to90	60to90	alt500
pdp	-0.48	-0.24	-0.76	-1.41	-1.54	-1.54	-0.25	-0.34	-0.64	-1.07	-1.19	-1.28	-1.43	-1.56	-1.77
rocher	-0.26	0.08	-0.49	-0.99	-1.28	-1.6	0.01	0.04	-0.3	-0.73	-0.94	-0.87	-1.08	-1.29	-1.64
girolles	0.7	0.47	0.4	0.44	0.45	0.51	0.5	0.47	0.25	0.54	0.42	0.5	0.48	0.46	0.43
marzet	-5.22	-2.3	-1.51	-2.62	-3.17	-3.67	-3.59	-0.76	-1.25	-2.06	-2.49	-2.34	-2.78	-3.18	-3.67
D3	-72.32	-455.9	-1228	-1393	-1345	-1489	-384.4	-1008	-1311	-1384	-1233	-1379	-1262	-1304	-1481
D4	-447.8	-2113	-5662	-7065	-6892	-8707	-1874	-4549	-5980	-6572	-6160	-6887	-6551	-6552	-7784
D5	-705.7	-2737	-6829	-9036	-9700	-1.5e+4	-2456	-5803	-7118	-7992	-7875	-8642	-8715	-9953	-1.1e+4
D6	-7.95	-39.66	-57.98	-57.71	-80.35	-219.5	-35.63	-69.92	-60.93	-56.05	-62.89	-57.02	-72.25	-91.06	-118.7
D7	0.12	0.05	-0	-0.01	0.05	0.44	0.06	0.1	0.01	0.01	0.06	-0	0.08	0.12	0.09
D8	-1.88	-0.56	-0.66	-0.63	-0.52	-0.52	-0.62	-0.56	-0.67	-0.66	-0.57	-0.64	-0.53	-0.47	-0.53
D9	-34.6	-160.7	-169	-65.13	-57.35	-52.53	-160.4	-233.1	-184.3	-82.19	-55.7	-67.46	-54.26	-52.48	-68.43
D10	-22.88	-84.06	-92.63	-38.14	-33.94	-38.71	-85.51	-122.4	-98.96	-42.5	-34.02	-39.26	-31.81	-31.68	-47.71
D11	-16.1	-43.86	-57.53	-38.53	-40.76	-74.08	-44.59	-64.08	-60.25	-35.89	-28.75	-36.21	-32.12	-38.96	-65.62
D12	-12.92	-50.28	-60.48	-32.42	-44.33	-151	-48.96	-73.33	-62.66	-29.3	-23.64	-28.75	-27.92	-41.42	-99.64
D13	-2.81	-10.76	-7.69	-0.44	-0.94	-40.67	-10.49	-13.24	-6.71	-0.07	0.2	-0.12	0.05	-0.68	-13.4
D14	-0.06	-0.03	-0.19	-0.21	-0.18	0.02	-0.06	-0.09	-0.19	-0.21	-0.19	-0.21	-0.18	-0.17	-0.16
D15	0.45	0.24	-0.12	-0.13	-0.1	0.28	0.26	0.02	-0.12	-0.13	-0.11	-0.13	-0.1	-0.09	-0.1
D16	-1.56	0.25	0.08	0.07	-0.3	0.22	0.16	0.43	0.2	-0.53	-0.01	-0.62	0.04	-1.92	0.22
D17	0.4	0.32	-6.06	-11.35	-10.3	-7.9	0.36	-1.76	-8.44	-20.11	-11.06	-15.9	-11.39	-11.24	-22.33
D18	0.51	-0.14	-0.76	-0.74	-0.68	-0.3	-0.06	-0.73	-0.77	-0.73	-0.68	-0.73	-0.68	-0.66	-0.69
D19	0.63	0.65	0.1	0.01	0.08	0.63	0.67	0.26	0.03	0.03	0.12	0.02	0.14	0.2	0.2
D20	0.26	0.46	-0.52	-0.56	-0.22	-1.79	0.48	-0.27	-0.52	-0.46	-0.34	-0.5	-0.27	-0.11	-0.21
D21	0.6	0.47	0.25	-1.31	-4.88	-32.9	0.49	0.43	0.09	-0.97	-1.99	-1.15	-2.99	-5.71	-15.41
D22	-3.13	-4.13	-4.19	-2.69	-4	-36.98	-4.06	-4.29	-4.15	-3.56	-2.55	-3.06	-2.63	-4.08	-11.68
D23	-8.03	-12.09	-22.48	-81.62	-145.5	-231.7	-11.26	-15.77	-24.69	-58.91	-88.32	-71.88	-106.9	-160	-241.8
D24	-76.34	-366.9	-1583	-1648	-1653	-2021	-336.7	-1027	-1660	-1892	-1524	-1823	-1606	-1706	-1828
D25	-5.08	-11.17	-68.49	-9.06	-9.19	-9.22	-11.5	-63.91	-76.27	-8.83	-9.16	-9.01	-9.18	-9.19	-9.2
D26	-9.05	-8.06	-5.96	-6.52	-6.53	-6.64	-8.61	-4.64	-5.92	-6.46	-6.54	-6.52	-6.65	-6.6	-6.65

Column 2: fissured zone with a 5m fixed depth below ground or below the bottom of the peat layer where present; columns 3-6: fissured zone with a fixed depth below ground (10, 25, 55, 75 and 100m); columns 7-14: fissured zone with a depth below ground that varies according to the Topographic Position Index (ranging from 5 to 10, 5 to 20, 10 to 30, 10 to 60, 10 to 90, 30 to 60, 30 to 90 and 60 to 90 m); column 15: fissured zone with a 500mNGF69 fixed altitude. The dark and pale grey shadings indicate the best and second-best models for each time-series.

6.3.2. Systematic sensitivity analysis of the calibrated model

6.3.2.1. Method

The sensitivity of the calibrated model was evaluated by assessing the rate of change in model performance when a single parameter is perturbed by a small proportion (Rochester 2010). In MIKE Zero, this is carried out using AUTOCAL. As detailed in Section 6.2.1.4, the performance measures that can be used in AUTOCAL are limited to five basic statistics: average error, RMSE, standard deviation of residuals, error of the maximum value and error of the minimum value (Anonymous 2009a). Here the RMSE was used as it gives an overall performance measure that includes both bias and dynamical correspondence (Anonymous 2009a). The sensitivity of the model to a parameter *i* is defined as:

$$S_i = \frac{\partial F}{\partial \theta_i}(\theta_{i,upper} - \theta_{i,lower}) \qquad \text{Equation 6-5}$$

where *F* is the output measure (here the RMSE), θ_i is the model parameter investigated, and $\theta_{i,upper}$ and $\theta_{i,lower}$ are the user-specified upper and lower limits of the parameter. The scaling by

the parameter range allows for the comparison of local sensitivity coefficients between parameters of different scales of magnitude. The sensitivity is evaluated locally around a specified set of parameters ($\theta_1, \theta_2, \ldots, \theta_n$), only one of which ($\theta_i$) is perturbed. The perturbation fraction can defined as a fixed proportion of the parameter or of the parameter range. The latter was used in this study to avoid issues caused by the different parameters scales. Table 6-1 shows the parameter ranges used for the sensitivity analysis. A perturbation fraction of 5% of the range was used. In AUTOCAL, sensitivity coefficients are calculated using a finite difference approximation. Three methods are available:

- the forward difference approximation:

$$S_i = \frac{F(\theta_1, \theta_2, \ldots, \theta_i + \Delta\theta_i, \ldots, \theta_n) - F(\theta_1, \theta_2, \ldots, \theta_n)}{\Delta\theta_i}(\theta_{i,upper} - \theta_{i,lower}) \quad \text{Equation 6-6}$$

- the backward difference approximation:

$$S_i = \frac{F(\theta_1, \theta_2, \ldots, \theta_n) - F(\theta_1, \theta_2, \ldots, \theta_i - \Delta\theta_i, \ldots, \theta_n)}{\Delta\theta_i}(\theta_{i,upper} - \theta_{i,lower}) \quad \text{Equation 6-7}$$

- the central difference approximation:

$$S_i = \frac{F(\theta_1, \theta_2, \ldots, \theta_i + \Delta\theta_i, \ldots, \theta_n) - F(\theta_1, \theta_2, \ldots, \theta_i - \Delta\theta_i, \ldots, \theta_n)}{2\Delta\theta_i}(\theta_{i,upper} - \theta_{i,lower}) \quad \text{Equation 6-8}$$

In some cases, the perturbed parameter falls beyond the range specified by the user, or even beyond the range of physically possible values. For instance, a backward difference approximation cannot be calculated when the proportion of bypass flow is set to zero in the initial model. Either backward or forward approximations or both were used when appropriate to cover the range of parameters used in the model.

The sensitivity of the model is evaluated individually at each location where observed and simulated values are available. A sensitivity coefficient of 0 indicates that the model results are independent of the parameter evaluated, and the sensitivity of the model to a parameter increases with the absolute value of its sensitivity coefficient. In AUTOCAL, an aggregated sensitivity coefficient for all or a selection of locations is calculated by summing up individual sensitivity coefficients. Since individual sensitivity coefficients can be negative or positive, it may be argued that this aggregated coefficient underestimates the model overall sensitivity if the

perturbation results in large rates of change but with opposite directions in different locations. Instead, the aggregated sensitivity coefficient was computed as the mean of absolute individual sensitivity coefficients. This prevents large but opposite effects from cancelling each other out, and allows for the comparison of groups of output measures with different sizes.

The AUTOCAL software does not easily allow for testing some parameters when these are defined as spatially-varying using gridded data. This was the case of the overland flow component's Manning's M in this study for instance. Similarly, time-varying parameters such as those included in the MIKE SHE vegetation file are difficult to include in a systematic sensitivity analysis. Consequently, the parameters included in the analysis are those that relate to the saturated zone, the unsaturated zone, overland flow and stream flow only. In the unsaturated zone model, the maximum bypass fraction was set to zero. As a consequence, the parameters regulating the bypass fraction under reduced soil moisture conditions were rendered meaningless and not included in the sensitivity analysis.

Table 6-4. Parameters included in the systematic sensitivity analysis.

Code	Parameter
Channel flow	
stream_Manning_n	bed resistance (Manning's n)
Overland flow	
OL_ManningM	resistance to overland flow (Manning's M)
Unsaturated zone	
UZpeatThetaS	peat water content at saturation
UZpeatSy	peat specific yield
UZpeatAWC	peat available water capacity
UZpeatKint	peat saturated hydraulic conductivity (UZ)
UZpeatBYP	peat bypass maximum fraction
UZminThetaS	mineral soil water content at saturation
UZminSy	mineral soil specific yield
UZminAWC	mineral soil available water capacity
UZminKint	mineral soil saturated hydraulic conductivity (UZ)
UZminBYP	mineral soil bypass max fraction
Saturated zone	
FZ_LL	fissured zone lower level (below ground)
FZ_Kh	fissured zone horizontal hydraulic conductivity
FZ_Kv	fissured zone vertical hydraulic conductivity
FZ_Sy	fissured zone specific yield
FZ_Ss	fissured zone specific storage
peatKh	peat horizontal hydraulic conductivity
peatKv	peat vertical hydraulic conductivity
peatSy	peat specific yield
peatSs	peat specific storage

6.3.2.2. Results

Figure 6-9, Figure 6-10 and Figure 6-11 give the mean absolute scaled sensitivity coefficient for each model parameter that was tested with respect to, respectively, groundwater table depth; discharge at the gauging stations located at Rocher, Marzet and Girolles upstream of the mire; and discharge at the gauging station located at Pont-de-Pierre downstream of the main mire extent. The latter two figures were separated because parameters to which the simulated discharge was sensitive differed between gauging stations located upstream and downstream of the main mire extent. In Figure 6-9, the sensitivity coefficient is given for all dipwells taken

together, dipwells located on mineral soils and dipwells located on peat soils. A distinction is also made between forward and backward evaluation directions. Parameters are arranged in order of increasing sensitivity from bottom to top. Figure 6-9 shows very clearly that the parameters to which simulated groundwater tables, in both peat and mineral soils, are most sensitive are all related to the characteristics of the fissured zone in the saturated flow component of the model: horizontal hydraulic conductivity, specific yield and depth below ground level. Peat characteristics are less important, with non-negligible sensitivity coefficients for peat specific yield, specific storage, vertical saturated hydraulic conductivity and available water capacity.

With respect to discharge in the upstream part of the wetland at Rocher, Marzet and Girolles, the model is sensitive to a relatively similar set of parameters (Figure 6-10): principally horizontal hydraulic conductivity, specific yield and depth of the fissured zone, and to a lower degree, vertical hydraulic conductivity and specific storage of the peat layer. The characteristics of the unsaturated zone on minerals soils (specific yield and available water capacity) are also important. With respect to discharge at Pont-de-Pierre however, the model is equally sensitive to parameters related to the peat layer and to those related to the fissured zone (Figure 6-11). Unlike any other simulated time-series, discharge at Pont-de-Pierre is also sensitive to stream Manning's n.

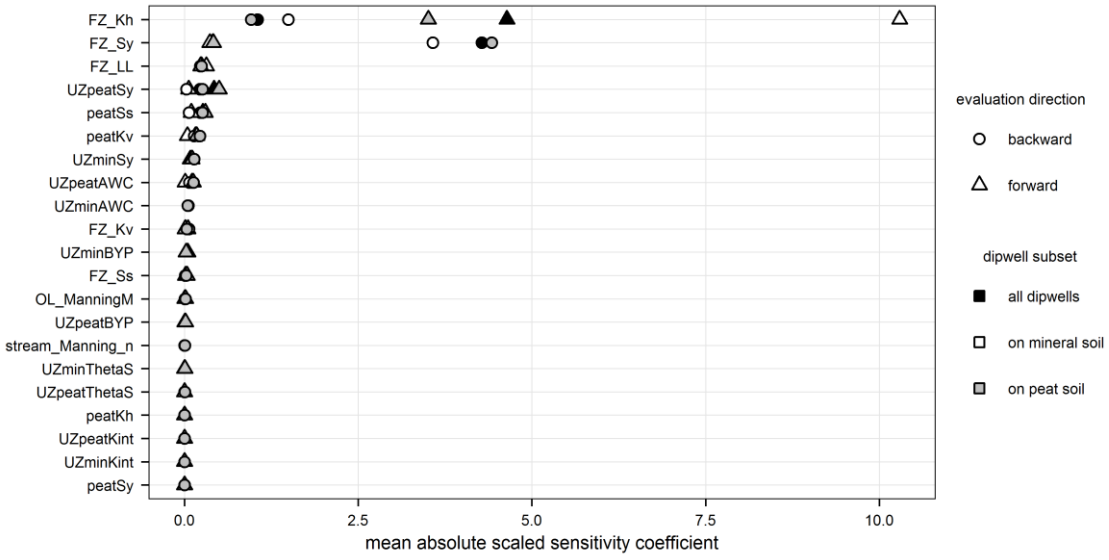

Figure 6-9. Systematic sensitivity analysis with respect to groundwater table depth..

Parameters are coded as follows: FZ: fissured zone (saturated zone); UZpeat & UZmin: unsaturated zone on peat and mineral soils respectively; peat: saturated zone on peat soils; Kh & Kv: horizontal and vertical hydraulic conductivities in the saturated zone; Sy: specific yield (in the unsaturated zone, equal to the difference between water contents at saturation and at field capacity); Ss: specific storage (saturated zone); AWC: available water capacity in the unsaturated zone, equal to the difference between water contents at field capacity and at wilting point; BYP: maximum bypass fraction (unsaturated zone); ThetaS: porosity (unsaturated zone); Kint: saturated hydraulic conductivity (unsaturated zone); OL_ManningM: overland Manning's M (overland flow); stream_Manning_n: stream Manning's n (stream flow).

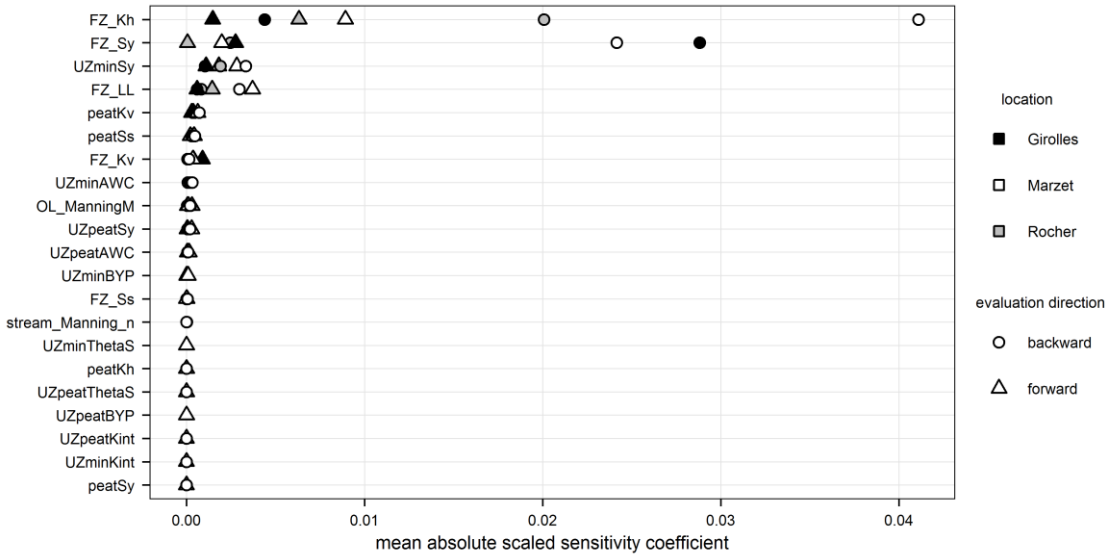

Figure 6-10. Systematic sensitivity analysis with respect to discharge at Rocher, Marzet and Girolles.

See Figure 6-9 for signification of parameter codes.

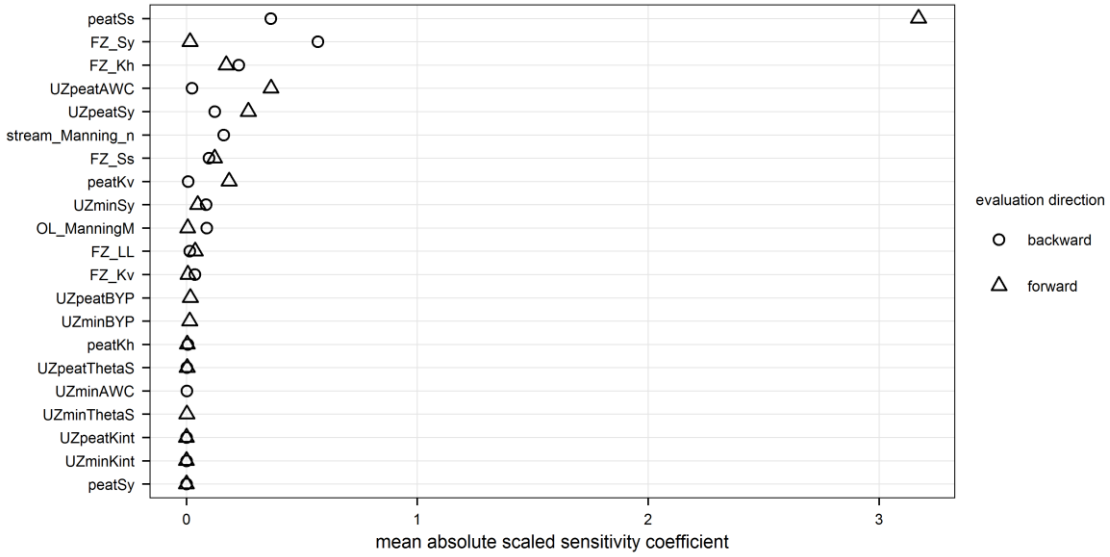

Figure 6-11. Systematic sensitivity analysis with respect to discharge at Pont-de-Pierre.

See Figure 6-9 for signification of parameter codes.

With respect to all simulated time-series, the model shows very little sensitivity to the fissured zone vertical hydraulic conductivity, to the bypass fraction, saturated hydraulic conductivity and porosity in the unsaturated zone in both peat and mineral soils, and to the peat horizontal hydraulic conductivity. As calculated in the current study, the sensitivity of a parameter has only a local validity for the specified location in parameter space. If the model is highly non-linear in its parameter-output interaction, a parameter that is insensitive for a certain parameter set may be highly sensitive for another parameter set (Anonymous 2009a). This is exemplified by the very low or null sensitivity of the model outputs to hydraulic conductivity in the unsaturated zone. It

results from the relatively high values used for both peat and mineral soils in the model, meaning that infiltration is not restricted by the hydraulic conductivity specified for the unsaturated zone even after perturbation. Manual calibration has shown that such values are necessary to achieve a good performance with respect to discharge, and that substantially lower values (below the perturbed value used for the sensitivity analysis) would result in unrealistically high peak flows. The absence of sensitivity to the peat specific yield specified for the saturated zone is a consequence of MIKE SHE overriding the specific yield value specified by the user for the uppermost computational layer, and replacing it with the value calculated from the unsaturated zone parameters for consistency purposes. Since the lower level of the upper computational layer follows the bottom of the peat layer, the specific yield specified for the saturated peat is never applied.

6.3.3. Sensitivity of the calibrated model to model resolution

6.3.3.1. Method

The model was run at three different resolutions (5, 10 and 30m, see Section 5.4.8) with all other parameters set to the calibrated values listed in Table 6-1. The sensitivity of the model performance to its resolution was assessed over the period 01/01/2011-31/12/2013 by comparing the resulting NSE with regard to discharge, groundwater table depth and piezometric head in the mineral formations underlying the mire, and the percent bias with regard to discharge, for the reasons detailed in Section 6.2.1.2.

6.3.3.2. Results

Figure 6-12 shows NSE for each measure point for the different model grid sizes. The model resolution has a substantial impact on model performance, but the strength and direction of this impact varies according to measure location and type. With regard to discharge, model performance increases noticeably with model resolution (i.e. with decreasing grid size) at the Pont-de-Pierre wetland outlet and at Rocher. It is relatively stable at Girolles, possibly due to the relatively high performance obtained even at low resolution. However, at Marzet, the model performance rapidly decreases with increasing model resolution. One likely explanation lies in overland flow model convergence issues observed upstream of Marzet, that may increase with model resolution simply because the number of computations, and therefore the accumulated error, increases. These issues are further detailed and discussed in Section 6.3.5.

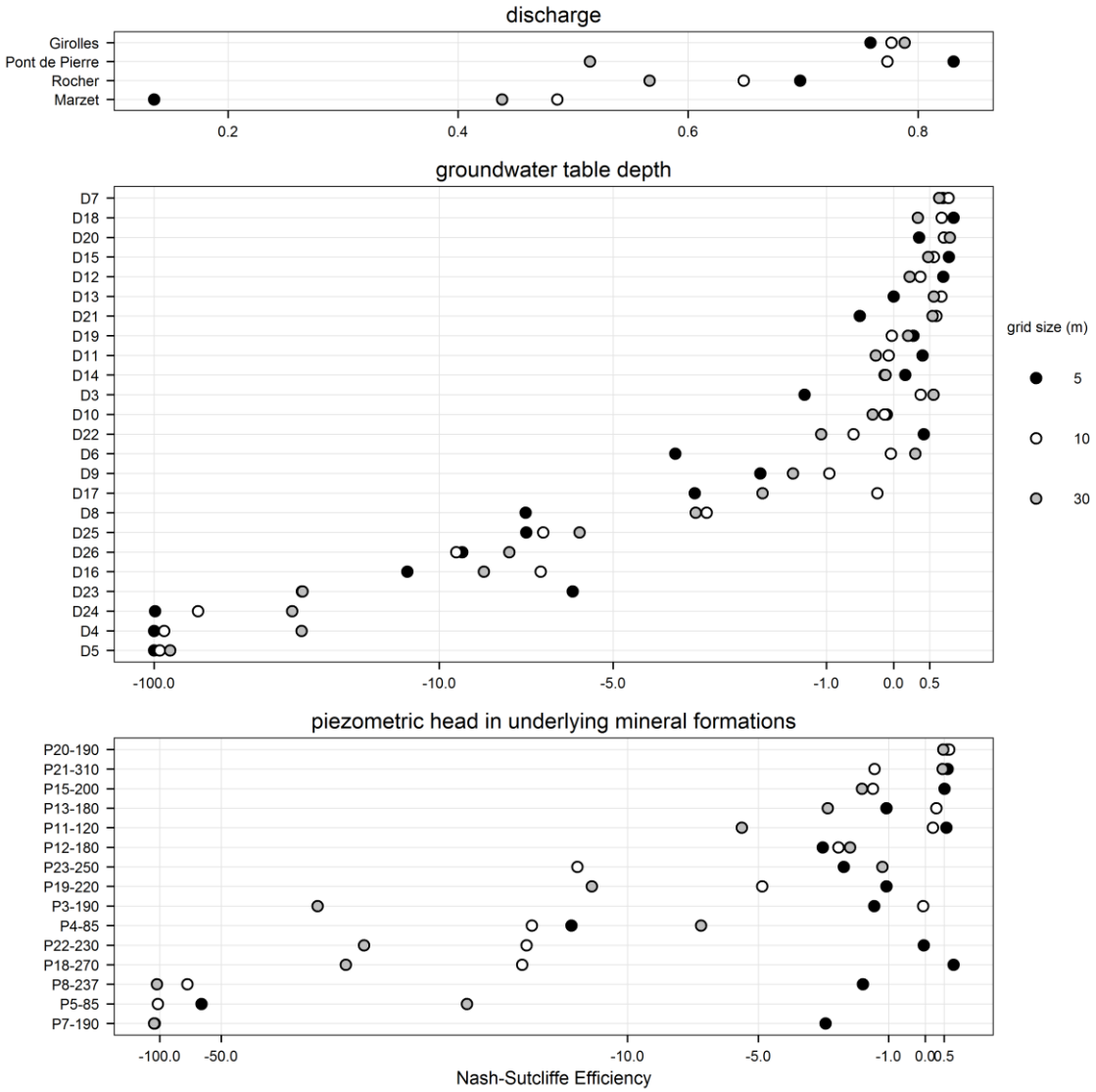

Figure 6-12. Nash-Sutcliffe efficiency for simulated discharge, groundwater table depth and piezometric head as a function of model grid size.

Note the inversed exponential scale for the x axis, used to improve clarity of the two lower plots.

Figure 6-13, that shows the percent bias of simulated discharge, seems to confirm this: percent bias improves with increasing model resolution at Rocher and Pont-de-Pierre, but strongly deteriorates at Marzet, where the 5m resolution model overestimates flow by 77% whereas the 30m resolution model underestimates it by only 5%. The effect of model resolution on model performance with regard to groundwater table depth is also noticeable but very variable (Figure 6-12). The performance of the 5m resolution model seems generally lower than that of the 10m or 30m model, even though there are many exceptions such as in dipwells D11, D22 or D23. There seems to be no correlation between the impact of model resolution and the location of dipwells within the wetland.

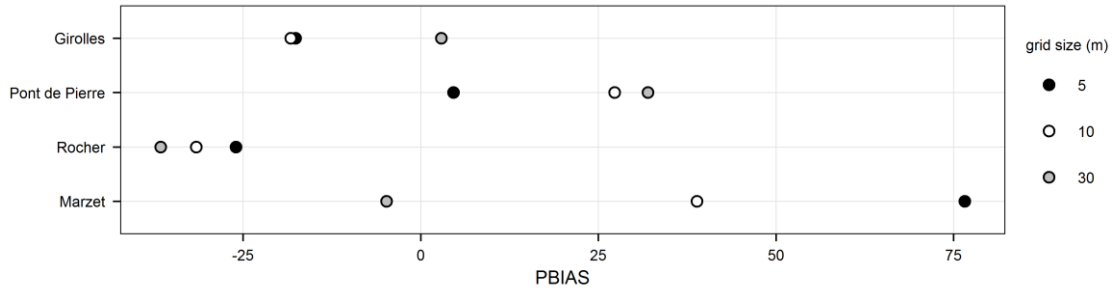

Figure 6-13. Percent bias in simulated discharge as a function of model grid size.

Figure 6-14 shows a few examples of simulated groundwater table depth time series as a function of model resolution, selected to be representative of the range of model responses to grid size. It shows that, in general, simulated groundwater tables become deeper and more variable when the model resolution increases. The reason for this is not clearly understood. The only exceptions are dipwells D7 and D19, in which the model grid size has little influence on simulated groundwater table depths. Depending on whether the water table depth is under- or over-estimated by the 10m-resolution model, increasing the model resolution may either result in an improvement (dipwells D11, D12, D14 and D18) or a degradation (all other dipwells but D7 and D19) of the performance for the relevant measure point. The difference in simulated groundwater table depths is generally larger between the 5m- and 10m-resolution models than between the 10m- and 30m-resolution model (dipwells D3, D5, D6, D11, D12, D13, D14, D15, D20, D21, D22, D23, D24, D25), but again there are exceptions (D9, D10, D26). Again the reason for this is not clearly understood.

The water table depth time-series simulated for dipwell D18 shown in Figure 6-14 illustrate another issue caused by the coarser model resolution: some riparian cells get wrongly flooded during the largest peak flows. This is due to two factors. The first one is the increase in simulated discharge at (and presumably upstream of) Pont-de-Pierre, as shown by a larger percent bias (Figure 6-13), which results in higher simulated stream levels. The second one lies in topographic discrepancies between the MIKE 11 water levels and bank elevations and the MIKE SHE cells located along water courses. Due to DEM aggregation, the cell containing dipwell D18 is 10cm lower in the 30m model than in the 5m or 10m models. The impact of model resolution on model performance seems to be less random with regard to piezometric heads in the mineral formations underlying the peat layer (Figure 6-12): even though there are exceptions, model performance increases with model resolution. The improvement is particularly important when the resolution increases from 10 to 5m. In MIKE SHE and unlike groundwater table levels, piezometric heads at depth cannot be specified as depth below ground, which means that

vertical piezometric head gradients may be misrepresented when the DEM error is large. This error decreases with increasing model resolution, which may explain part of the observed improvement in model performance.

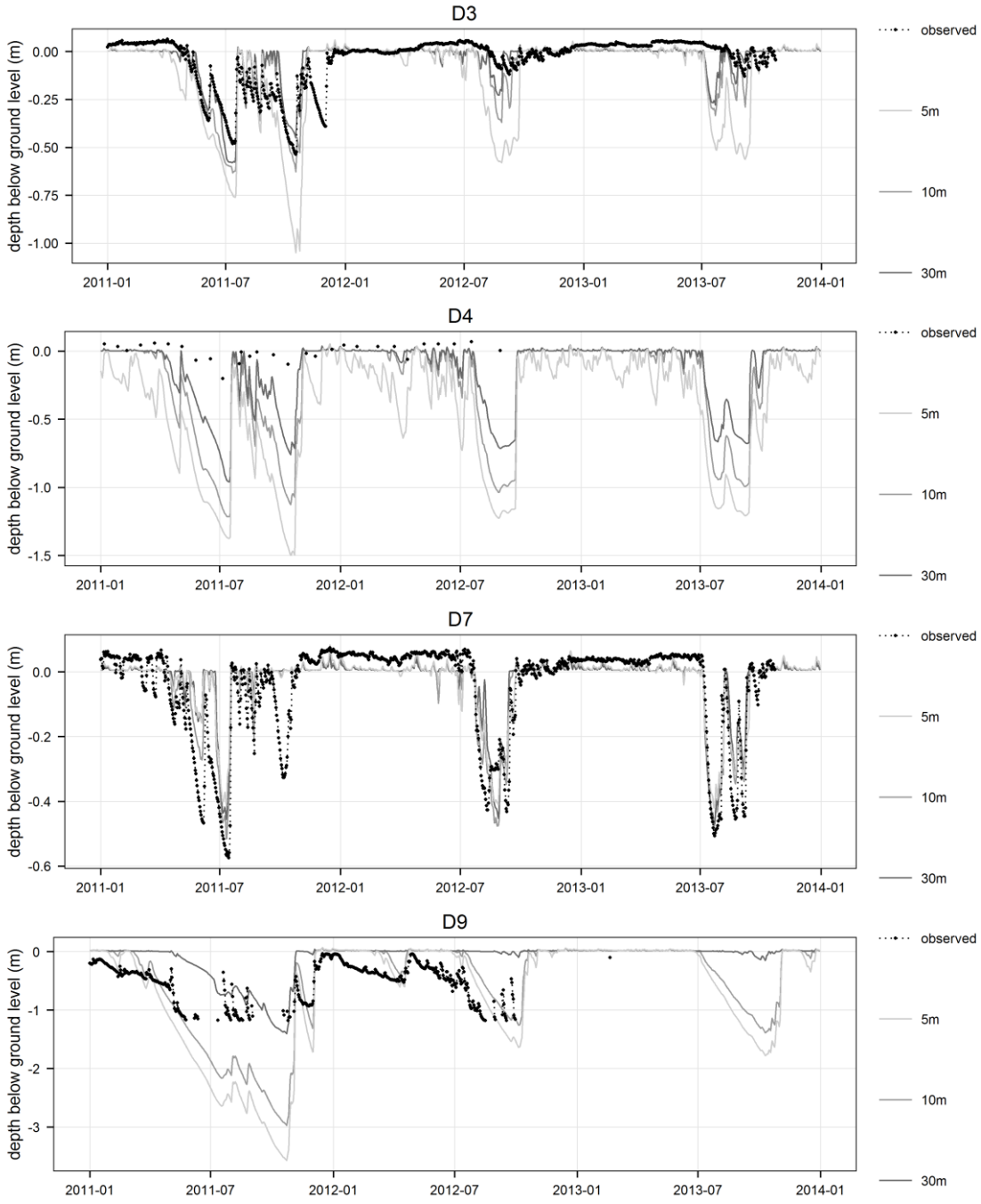

Figure 6-14. Effect of model resolution on simulated groundwater table depth.

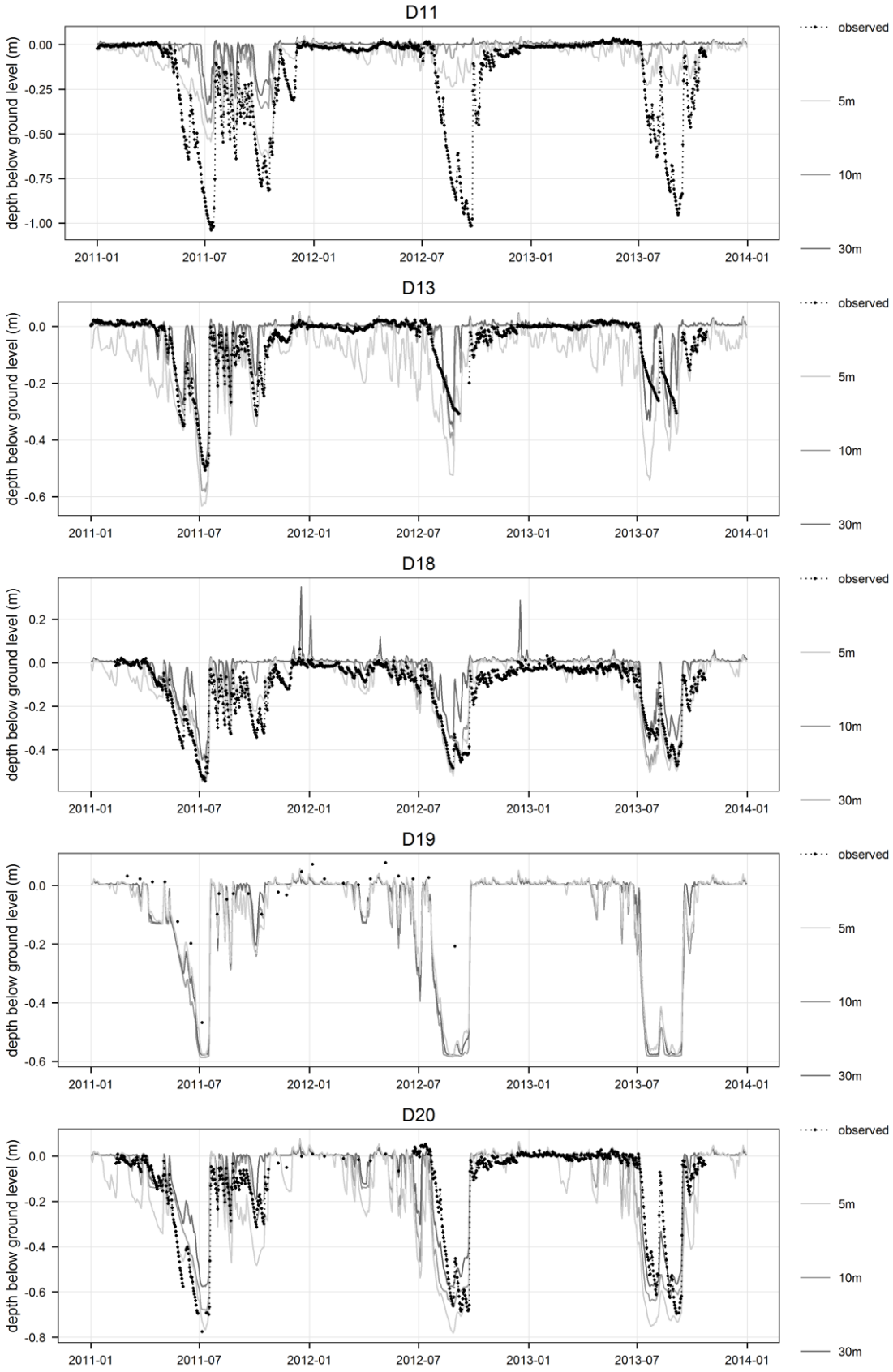

Figure 6-14 (continued). Effect of model resolution on simulated groundwater table depth.

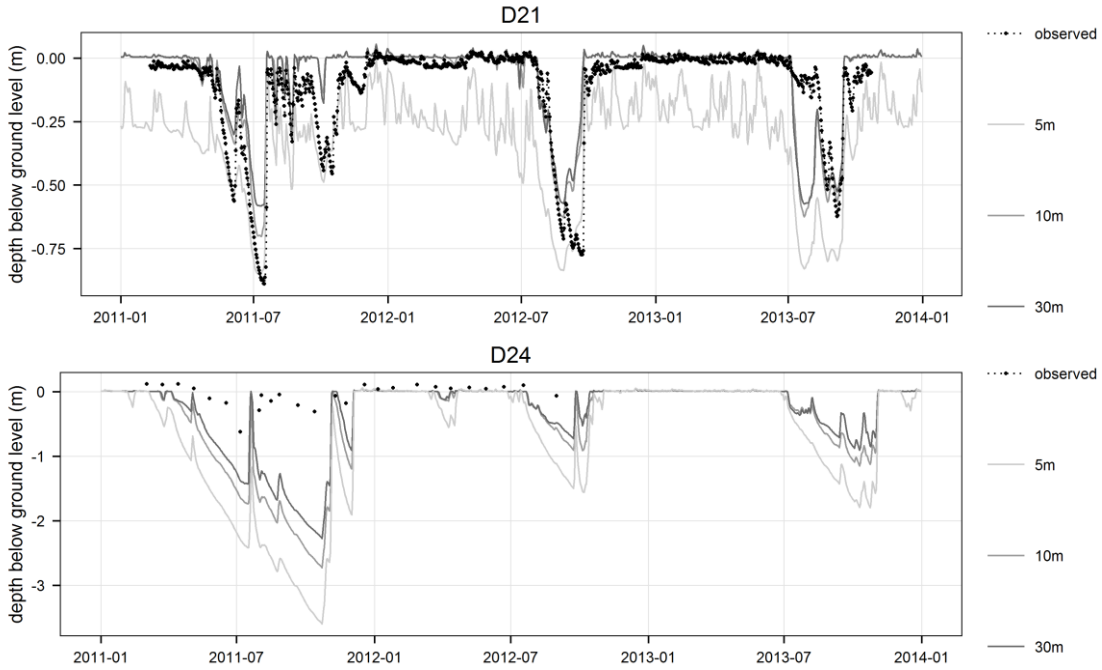

Figure 6-14 (continued). Effect of model resolution on simulated groundwater table depth.

6.3.4. Impact of spatial variation in potential evapotranspiration and peat characteristics

6.3.4.1. Methods

The impact of the heterogeneity of peat and mire vegetation characteristics on model performance with regard to groundwater table depth in peat soils was investigated by repeating the manual calibration of the 10m-resolution model presented in Section 6.2.1.5, this time focussing not on the overall multi-objective performance but on local model performance at a single target dipwell at a time. Dipwells in which the observed groundwater table depth was poorly reproduced by the multi-objective calibrated model for reasons not related to peat characteristics (D4, D5, D8, D16, D17, D22 and D23), as detailed in Section 6.2.1.5, and dipwells not located in peat soils were excluded from the analysis. The parameters investigated included the peat specific yield and available water capacity and/or the wetland crop coefficient during the vegetation season. All other parameters were kept to constant values obtained from the multi-objective calibration and listed in Table 6-1. As for the global calibration detailed in Section 6.2.1.4, a combination of systematic runs and subjective tests guided by an increasing understanding of the model behaviour with respect to the individual target dipwell was used. The model with the best local performance was selected for each target dipwell based on the NSE, for the reasons detailed in Section 6.2.1.2. The performance was evaluated for the 01/01/2011-30/06/2012 period only to reduce run times, in line with the period used for the multi-objective calibration.

6.3.4.2. Results and discussion

Table 6-5 gives the NSE obtained for each dipwell and for each combination of peat specific yield (Sy), peat available water capacity (AWC) and wetland crop coefficient (Kc) tested. For each dipwell, the best and second-best local models are highlighted in dark and pale grey respectively. The best global model (i.e. with the largest mean NSE) is run 197, in bold.

Table 6-5. Effect of unsaturated peat specific yield, unsaturated peat available water capacity and wetland crop coefficient during the vegetation season on the Nash-Sutcliffe Efficiency for individual dipwells.

run	Sy	AWC	Kc	D3	D6	D7	D11	D12	D13	D14	D15	D18	D19	D20	D21	mean NSE
183	0.05	0.15	1	0.41	0.08	0.64	0.24	0.26	0.81	-0.1	0.71	0.53	0.45	0.77	0.72	0.46
194	0.05	0.15	1	0.41	0.07	0.65	0.24	0.26	0.81	-0.1	0.72	0.53	0.48	0.77	0.73	0.46
195	0.15	0.15	1	0.5	0.35	0.48	0.09	0.06	0.74	-0.14	0.6	0.39	0.4	0.64	0.62	0.39
196	0.26	0.15	1	0.45	0.48	0.33	0.02	-0.08	0.64	-0.17	0.48	0.29	0.39	0.55	0.52	0.33
197	**0.05**	**0.05**	**1**	**0.46**	**0.05**	**0.69**	**0.28**	**0.38**	**0.77**	**-0.06**	**0.78**	**0.59**	**0.31**	**0.72**	**0.72**	**0.47**
198	0.05	0.01	1	0.48	0.15	0.65	0.28	0.41	0.71	-0.04	0.73	0.57	0.22	0.81	0.67	0.47
199	0.26	0.01	1	0.36	0.42	0.36	0.03	-0.09	0.69	-0.17	0.5	0.33	0.47	0.66	0.57	0.34
200	0.18	0.01	1	0.39	0.24	0.47	0.08	0.04	0.76	-0.16	0.63	0.42	0.51	0.71	0.62	0.39
201	0.13	0.01	1	0.41	0.09	0.58	0.13	0.15	0.78	-0.15	0.7	0.49	0.51	0.74	0.65	0.42
202	0.02	0.05	1	0.31	0.21	0.62	0.34	0.45	0.67	-0.07	0.74	0.58	0.06	0.51	0.7	0.43
203	0.05	0.05	1.2	0.42	-0.24	0.77	0.4	0.6	0.7	0	0.86	0.67	0.05	0.65	0.78	0.47
204	0.05	0.05	1.4	0.26	-0.5	0.78	0.5	0.71	0.52	0.09	0.83	0.74	-0.51	0.32	0.76	0.38
205	0.05	0.01	1.4	0.39	-0.47	0.71	0.48	0.7	0.37	0.11	0.75	0.73	-0.84	0.11	0.64	0.31
206	0.02	0.05	1.4	-0.05	-0.44	0.57	0.5	0.63	0.21	0.03	0.66	0.71	-0.85	0.01	0.59	0.21

Figure 6-15 shows groundwater table depths simulated by the best global model (run 197) and by the best local model highlighted in Table 6-5, as well as observed records. Both Table 6-5 and Figure 6-15 show that the model performance with regard to groundwater table depths could be substantially improved by allowing for a small number of parameters related to the peat physical characteristics and to the ratio between the actual evapotranspiration and the reference evapotranspiration to vary spatially. In dipwells D7, D12 and D18 for instance, the drop in groundwater table depth observed in late September and early October 2011 is underestimated by the model with the best multi-objective performance. Increasing the crop coefficient during the vegetation season and therefore the evapotranspiration rate leads to a better performance locally. In D6, the observed groundwater table depth during the 2011 drought is over-estimated by the multi-objective model, but the performance can be improved locally by increasing the specific yield and the available water capacity. Stratigraphic surveys detailed in Section 3.4.2 have shown the large variability of the von Post's humification index across the mire. Both

specific yield and available water capacity of peat are strongly correlated to its humification rate and, like the humification rate, are known to vary substantially with both depth and location (Boelter 1964, 1968; Weiss *et al.* 1998; Letts *et al.* 2000; Schouwenaars & Gosen 2007; Verry *et al.* 2011). Similarly, evapotranspiration studies carried out in mires have found very variable ratios between actual and reference evapotranspiration rates, ranging from 0.2 to 1.4 (see Table G-1 in Appendix G and Section 5.4.3.4 for a review). In the absence of high-resolution data on both peat characteristics and actual evapotranspiration data within the mire, they were assumed to be homogeneous throughout the mire, which is clearly not the case. At least in dipwells for which the model performance is satisfactory, a large proportion of the residual error in simulated groundwater tables can safely be attributed to small-scale variations of these parameters.

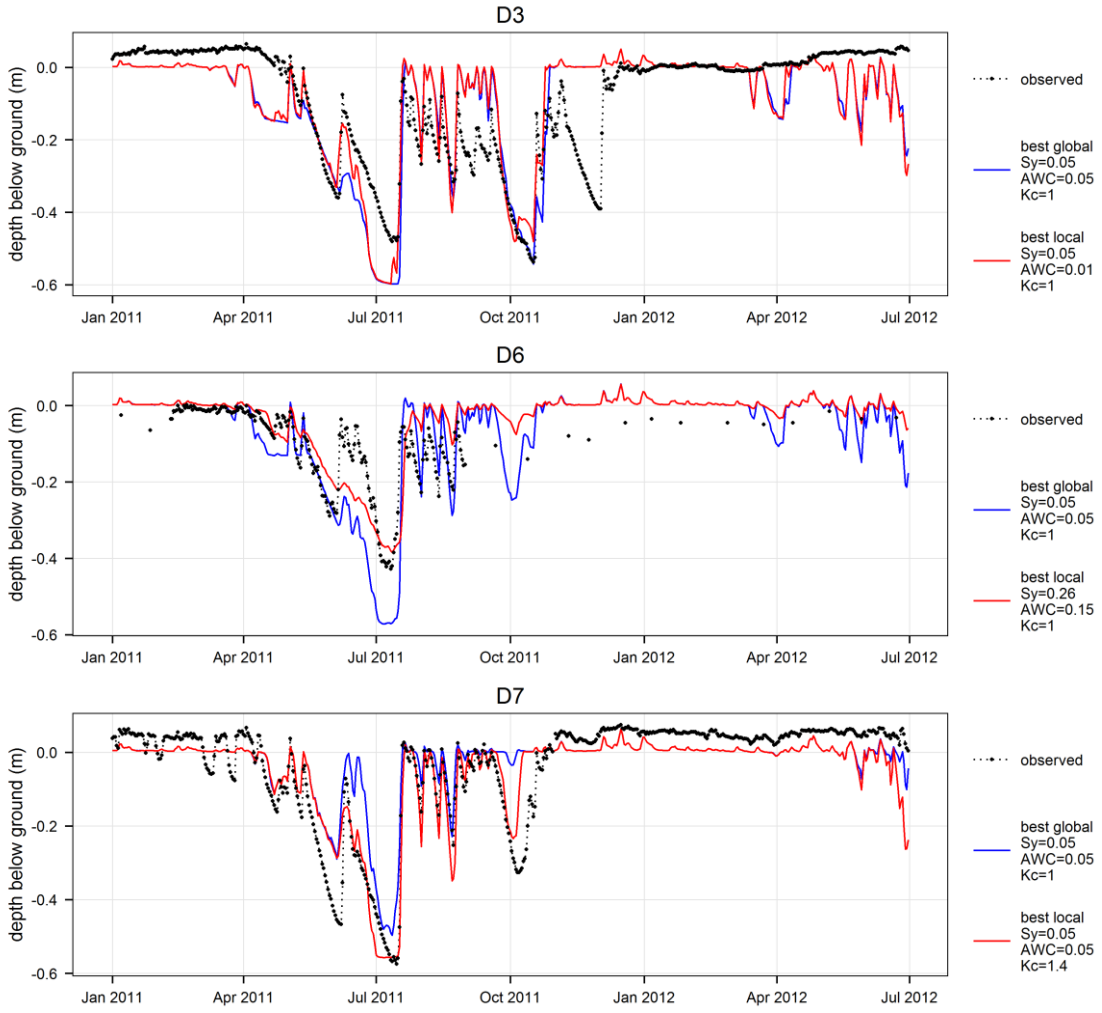

Figure 6-15. Effect of local peat specific yield, peat available water capacity and wetland crop coefficient on simulated groundwater table depth.

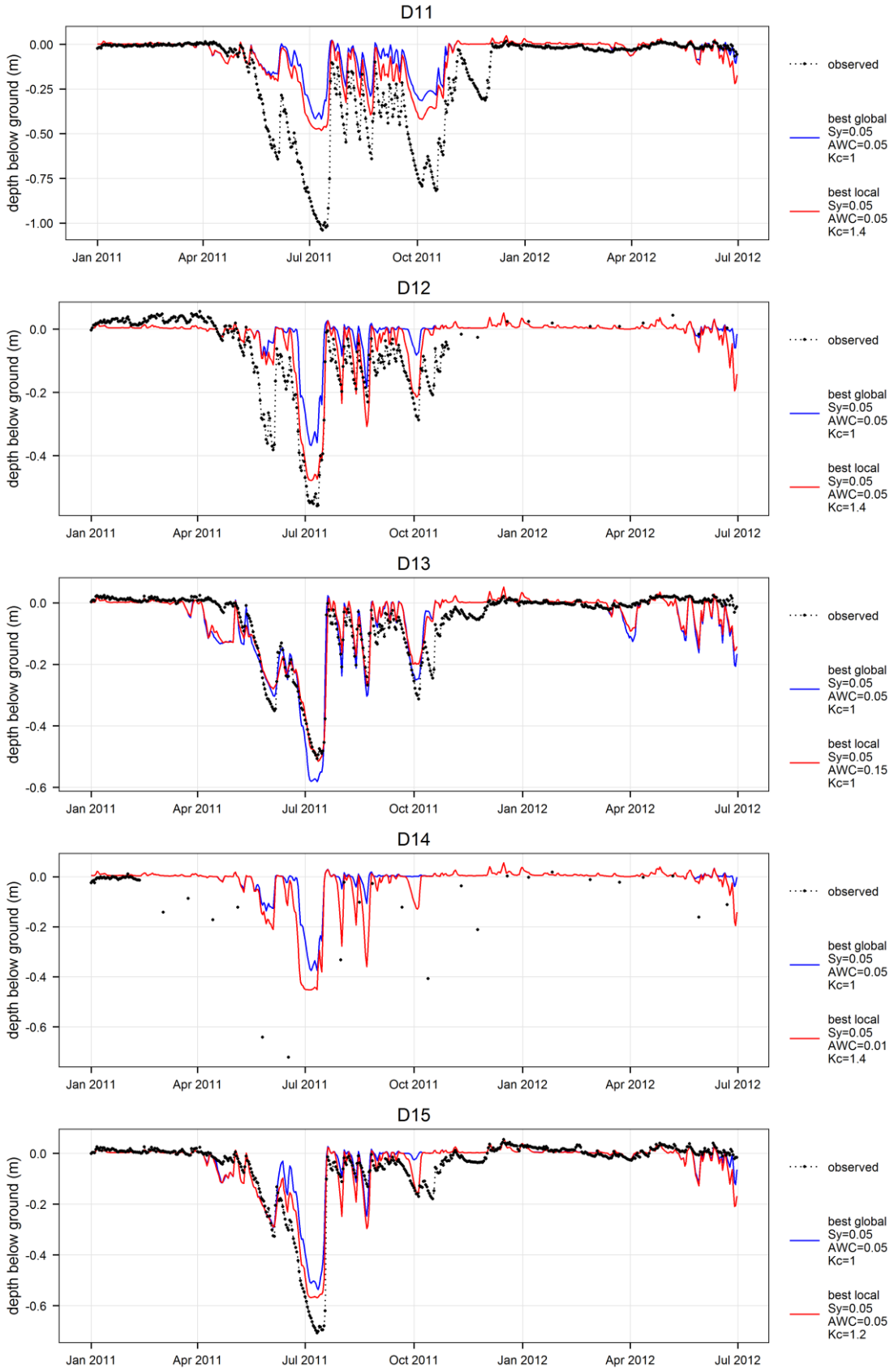

Figure 6-15 (continued). Effect of local peat specific yield, peat available water capacity and wetland crop coefficient on simulated groundwater table depth.

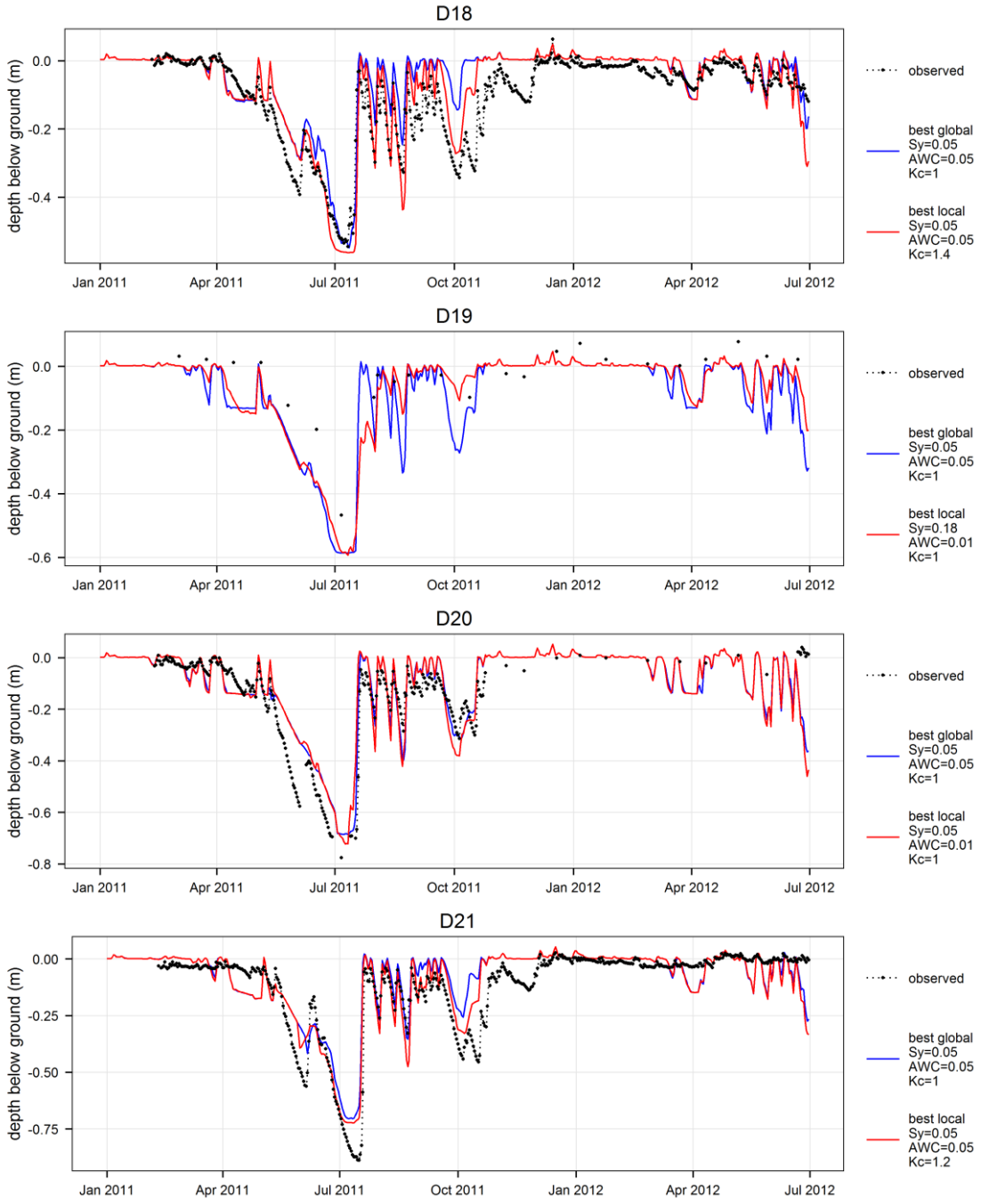

Figure 6-15 (continued). Effect of local peat specific yield, peat available water capacity and wetland crop coefficient on simulated groundwater table depth.

Unfortunately, as shown by the absence of correlation between the acrotelm depth and a range of potential predictors evidenced in Section 3.4.2, mapping these parameters with a sufficient enough resolution to further improve the model performance would require a very large amount of field and laboratory work. This would be beyond the logistical capacity of most studies.

6.3.5. Sensitivity to the length of the warm-up period and the issue of the overland flow component convergence

The length of the warm-up period required to stabilise the model from the arbitrary groundwater table starting depth was assessed by progressively increasing it and visually assessing the simulated time-series for long-term upward or downward trends that would indicate a continuing adjustment of the model. It was found that the model was relatively reactive and that a six-month warm-up period was sufficient. This was increased to two years (2009-2010) as a conservative measure. However, after the model had been calibrated and while running a long-term water balance analysis over the 2000-2013 period, it was realised that there was a substantial difference in terms of simulated discharge for the period 2011-2013 between a model run over the 2009-2013 period and a model run over the 1998-2013 period. This was only the case at Marzet and to a lesser extent at Pont-de-Pierre (Figure 6-16). Discharge in other gauging stations and groundwater table depth in all dipwells did not vary substantially with the length of the simulation period, which suggests that the issue is not caused by an insufficient length of the warm-up period. Figure 6-17 shows the simulated discharge at Marzet when the model is run from 1998 to 2013, including a two-year warm-up period removed from the model output. Again, no long-term trend can be seen. However, very large peaks are visible that suggest computational artefacts.

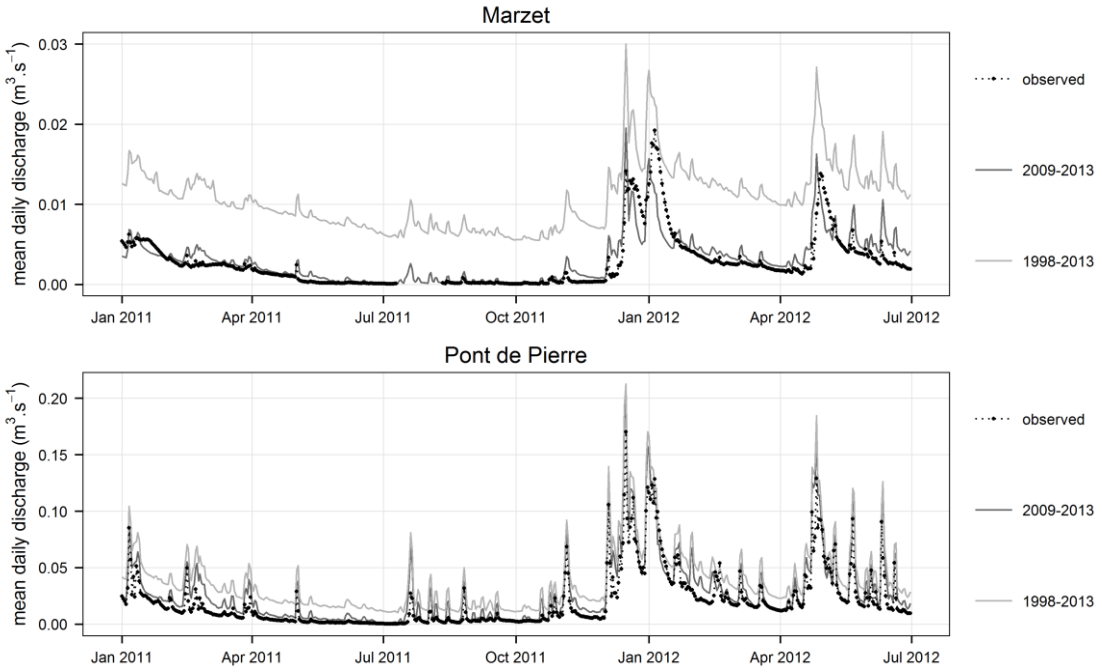

Figure 6-16. Effect of the simulation period on simulated discharge at Marzet and Pont-de-Pierre.

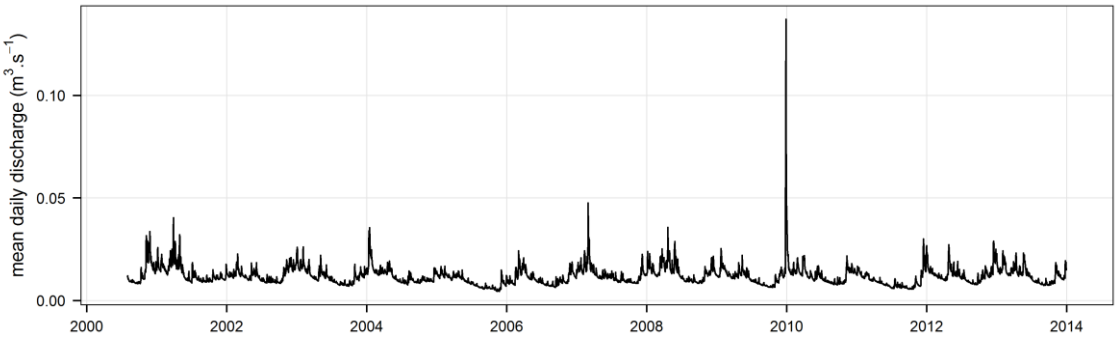

Figure 6-17. Simulated discharge at Marzet with a simulation period from 01/08/1998 to 31/12/2013.

Figure 6-18 shows that the spatial distribution of overland flow component errors is not homogeneous: errors are larger within the wetland, where the topography is flat and forms a large number of DEM "sinks", i.e. isolated or small groups of model grid cells forming a generally small depression a few decimetres deep. Such a depression also exists on mineral soil upstream of Marzet, close to the western catchment boundary, and Figure 6-18 shows that the error associated to this depression is larger when the simulation period is longer (see location labelled (a) on Figure 6-18 and Figure 6-19). Figure 6-19 shows that this error is associated to a very large depth of overland water that largely exceeds the depth of the topographic depression.

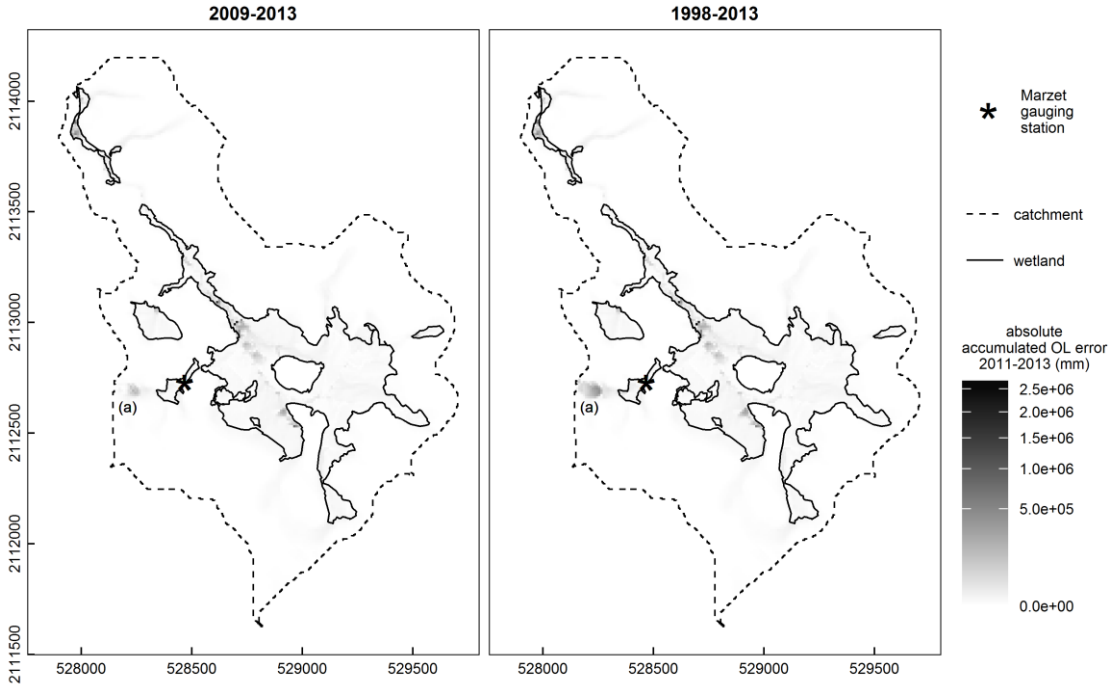

Figure 6-18. Overland flow component accumulated error (2011-2013) as a function of the total length of the simulation period.

(a): see text.

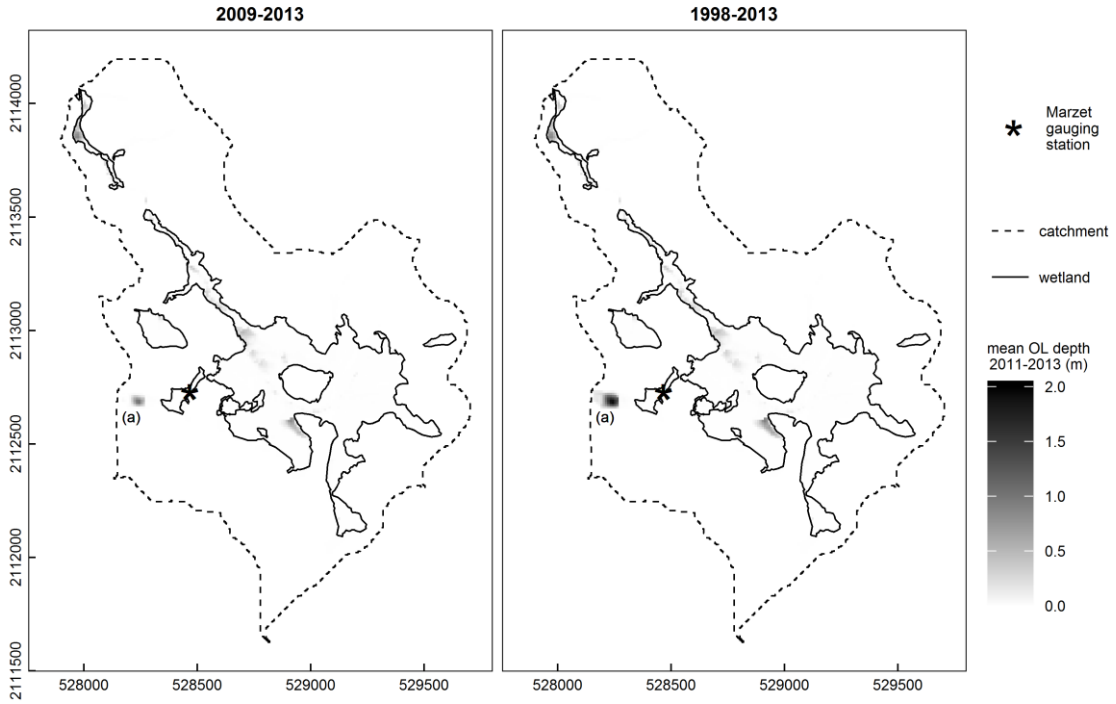

Figure 6-19. Mean simulated overland depth (2011-2013) as a function of the total length of the simulation period.

(a): see text.

The depth of overland water increases with the length of the simulation period. This error of the overland flow component explains the sensitivity of the model, and particularly of the simulated discharge at Marzet, to the length of the simulation period. Attempts were made to reduce this error by filling the sinks of the grid, by reducing the length of the model time-step or by increasing the maximum number of iterations of the overland flow component, all without success. In some cases, reducing the length of the model time-step actually increased the accumulated error of the overland flow component. This issue is one of the main drawbacks of the current model as it makes it unreliable for simulation periods that differ from the one used to calibrate and validate it, in particular for the assessment of the potential impact of climate change on the mire hydrology if long time-series obtained from downscaled regional models with daily time-step are used.

6.4. Model performance and sensitivity: general discussion and recommendations

6.4.1. The issue of microtopography

Mires are characterised by a frequently chaotic micro-topography, caused by peat accumulation and plant growth rates that vary at a very small scale. Purple-moor grass (*Molinia caerulea*) for instance can form tussocks that are up to 50cm high in some mires in Limousin. The definition of ground level is therefore a substantial methodological issue in mire hydrology (Whitfield *et al.* 2009), as this definition will have a profound impact on all quantities defined relative to ground level such as groundwater table depth or flood depth. Yet this definition is very rarely specified in most hydrological studies of mires. Van der Schaaf (2002) defined the surface level as "the average bottom level of the hollows within a radius of 1m around a measuring point". In the current study the surface level was taken as the mean of a minimum of three DGPS elevation measures taken within 30 cm of the dipwell and spread around it. In some dipwells, this definition clearly does not match the level at which overland flow starts to occur. This is the case for instance in dipwells D3-100, D7-130, D7-70 and D12-100, where, except during the two or three driest months of the year, observed groundwater levels are constantly three to six centimetres above "ground level" when there is clearly no substantial and permanent overland flow occurring (Figure 6-5). This issue clearly affects the model performance statistics negatively and substantially, but is difficult to resolve. In the case of the Dauges mire, one option would be to define the ground level based not on inaccurate topographic data, but on the average groundwater table elevation in winter assuming that there is constant seepage and that this elevation corresponds to the interface between saturated flow and overland flow. However this would not be applicable to areas affected by flooding nor to dipwells where groundwater table depths are manually recorded and the amount of data is too limited to make such an estimation. Another option would be to adjust the overland detention storage depth, which in MIKE SHE can be used to model surface storage in small topographic depressions that must be filled in before overland flow can occur. However, such a detention storage depth would have to be spatially-varying and calibrated individually for each dipwell, which would make impossible the evaluation of the model performance across the rest of the mire. Furthermore this would increase the amount of water infiltrating to the unsaturated zone when the watertable drops below ground level, which might not correspond to reality.

The micro-topography also has a demonstrable effect on the amount of water that infiltrates into the peat when the groundwater table depth drops below ground level. During the calibration phase, it was found that the storage detention parameter had to be specified separately for mineral and peat soils (Table 6-1). The former had a substantial impact on the infiltration to the saturated fissured granite and on the ratio between peak and base flows in the upstream reaches, while the latter had an impact on the groundwater table depth in peat. Detention storage had to be increased slightly on peat soils to reduce small scale high-frequency variations in early summer, some of which are still noticeable during the spring of 2012 in dipwell D20 for instance (Figure 6-3). This increase in detention storage required within the wetland to improve the model performance can easily be explained by the lower slopes and much more pronounced micro-topography on peat than on mineral soils, and the substantial volume of water that is stored within this micro-topography and that increases and prolongs rainfall and runoff retention and infiltration to the peat layer, particularly when the acrotelm is shallow or non-existent and the saturated hydraulic conductivity of the superficial peat is low.

6.4.2. Channel flow

During the calibration phase, the bed resistance had to be increased substantially (Table 6-1) and beyond tabulated values given in the flow modelling literature (Dingman 1994) to improve the performance of the model with regard to discharge at the Pont-de-Pierre wetland outlet. This reflects the inadequacy of kinematic routing to model discharge and stage within the wetland itself, where the low slope gradient and the presence of numerous obstacles make the flow sluggish and create constant backwater effects. As a consequence, flooding and exchanges through highly permeable alluvial gravel deposits below the peat cannot be accurately modelled using kinematic routing, as evidenced by the poor model performance in dipwells D8 and D17, even when these permeable sediments are modelled specifically by adding a computational layer to the model. A fully dynamic hydraulic model solving the Saint-Venant equations would ideally have been employed, and several attempts were made at developing such a model. However a fully dynamic hydraulic model requires much smaller time steps than kinematic routing. As a result, it imposes very large computational constraints on the overall model, as detailed in Section 5.4.4. Several potential solutions could be explored. A MIKE SHE model with a coarser resolution could be used to reduce the computational burden, but this would not affect the MIKE 11 run time, and the varied topography of the site would create substantial mismatches between the topographic grid and both the real ground surface elevation and the MIKE SHE river link bank elevations. It was also shown in Section 6.3.3 that a lower resolution would result in a

lower model performance with regard to discharge. The small time steps required by the fully dynamic hydraulic model may also result from the small distance between some cross-sections, because the stability conditions of the MIKE 11 model depend mainly on the ratio between the time step and the computational grid spacing, which cannot be larger than the distance between cross-sections. As a consequence the computational time increases by a factor of four every time the distance between cross-sections is divided by two (Anonymous 2009d). However reducing the number of cross-sections will again result in discrepancies between the topographic grid and river links in some cases. Finally, another option would be to use two nested models: one with a 10m resolution and kinematic routing covering the catchment, and one with a 10m or higher resolution covering the mire and its immediate surroundings where channel flow would be modelled using the Saint-Venant equations. This is similar to the solution used by Johansen *et al.* (2014) to model the hydrology of a groundwater-fed fen in Denmark. Unfortunately, MIKE SHE version 2009 does not allow for time-varying overland flow boundaries to be transferred from one model to another. Johansen *et al.* (2014) assumed no overland flow across the boundaries of the nested model. On the Dauges site however, this assumption does not hold, as shown by the importance of overland flow inputs to the water balance of the mire further detailed in Chapter 7, and the nested model solution could not be employed in the current study. The ability to specify time-varying overland flow boundaries has been incorporated within MIKE SHE version 2011 and later, so the nested model solution could be investigated in future work.

6.4.3. Parametrisation of the unsaturated and saturated peat

During the calibration phase, the peat specific yield and available water capacity had to be reduced substantially to 5% to reproduce the groundwater table dynamics. These values are lower than those cited in the literature even for sapric peat (Letts *et al.* 2000 for instance give a mean value of 0.13 for the specific yield and 0.49 for the available water capacity of sapric peat). It is well known however that peat physical properties are highly variable (Boelter 1964, 1968; Gobat *et al.* 1986; Gobat 1990; Grosvernier *et al.* 1999; Brandyk *et al.* 2002), and the lower specific yield suggested by the model calibration at the Dauges site may result from a higher humification rate caused by drier climatic conditions encountered in central France than in more northern and western parts of Europe where mires are more common and to which most of the available literature refers. The measure of the actual specific yield from peat cores would allow the validation of the value obtained through model calibration. The model was not sensitive to the bypass fraction and for simplification purposes this parameter and those related to it were set to zero. Groundwater table depths on peat soils and discharge at the Pont-de-Pierre wetland

outlet were moderately sensitive to the saturated peat hydraulic conductivity. The calibrated value was found to be almost identical to the median value obtained from slug tests in the catotelm ($5x10^{-8}$ vs. $4.3x10^{-8}$ $m.s^{-1}$, see Section 3.5.2), implying a low to moderate permeability of the peat deposits, compatible with the high humification rate of the catotelm suggested by the calibrated specific yield value and peat stratigraphic surveys. Slightly higher values (up to $2x10^{-6}$ $m.s^{-1}$) gave a relatively similar global performance of the model, but with a shift along the Pareto front towards a better performance for discharge at the wetland outlet and a lower performance for some dipwells. In particular, higher hydraulic conductivities led to slightly deeper groundwater table depths at the wetland margins and shallower groundwater table depths at its centre. This suggests that the peat layer acts as an aquitard leading to the semi-confinement of the aquifer located in the underlying mineral formations, and to higher piezometric heads along the mire margins. This process may have constituted a positive feedback to the mire lateral expansion on steeper slopes and may have consequences on downstream discharge dynamics that should be further investigated.

6.4.4. Parametrisation of the unsaturated zone on mineral soils

The calibrated value of specific yield on mineral soils was found to be 0.1, relatively similar to the 0.16 initial value based on van den Bogaert (2011). However the available water capacity had to be substantially adjusted to improve the model performance, in particular to reduce the percent bias of simulated discharge. The calibrated value was 0.69, which is impossible in mineral soils where the total porosity varies between 0.3 and 0.55 depending on the soil texture (Dingman 1994). This suggests that the current two-layer model does not adequately represent unsaturated flow dynamics on mineral soils where the groundwater table depth is generally below the root zone. This issue is further discussed in Section 8.4. The two-layer unsaturated flow and evapotranspiration model should ideally be replaced by the Kristensen & Jensen evapotranspiration model associated to the gravity or Richards unsaturated flow model detailed in Section 5.3.1.1. However this would require substantial additional data on the hydro-physical characteristics of soils and additional computational capabilities since the Richards unsaturated flow model in particular is much more computationally demanding. The measurement of actual evapotranspiration of deciduous woodlands and of soil moisture content in representative locations would allow to further validate the evapotranspiration and unsaturated zone model. In the meantime however, the model validation against discharge suggests that the two-layer model, even though with an unrealistic available water capacity value, performs reasonably well at the catchment scale. As on peat soils, the model was not sensitive to the bypass fraction on

mineral soils, and a value of zero was also used for simplification purposes. This value is compatible with those cited in the literature for sandy soils where macropore flow is generally small to inexistent (Dingman 1994).

Even though the systematic sensitivity analysis suggests that the calibrated model is not sensitive to the saturated hydraulic conductivity of the unsaturated zone in mineral soils (Figure 6-9, Figure 6-10, Figure 6-11), this was actually not the case of the uncalibrated model. The sensitivity analysis is only valid locally for a given position in the parameter space, and therefore the sensitivity of some parameters may depend on their actual value and on the value of other parameters. The saturated hydraulic conductivity of the unsaturated zone defines the infiltration capacity of soils. During the manual calibration, it became clear that the ratio between peak flow and base flow was very sensitive to this value, and that a larger value was required to reproduce the observed discharge dynamics. The calibrated value was $1x10^{-4}m.s^{-1}$, compatible with large infiltration capacities of sandy soils.

6.4.5. Parametrisation of the granite fissured zone

The satisfactory to good overall performance of the calibrated model with regard to groundwater table depths and discharge shows that saturated flow within the fissured granite can be reasonably well modelled using an equivalent porous medium approach. This conclusion is further strengthened by the 20m altitudinal difference between the discharge monitoring stations and the very good correspondence between the simulated mean groundwater table and the observed distribution of wetland vegetation across the entire modelled area, including in places without discharge or groundwater table depth observations. However, even if the approach taken is satisfactory at the catchment scale, poor performance in some locations such as D4 and D5, an apparent trade-off between performance at dipwells D3, D9, D10, D24 and D25 located on three opposite margins of the wetland, and the detailed analysis of the ERT results and geological drilling logs suggest that, at the local scale, the representation of the fissured zone as an homogenous entity is an over-simplification. This is particularly the case for its hydraulic conductivity. The model was moderately sensitive to the vertical saturated hydraulic conductivity of the fissured zone. The calibrated value was $5x10^{-5}$ $m.s^{-1}$ but values between $1x10^{-5}$ to $1x10^{-4}$ $m.s^{-1}$ gave similar results. The model was however highly sensitive to the horizontal hydraulic conductivity in the saturated fissured zone: this was the most important parameter controlling both discharge in the upper reaches and groundwater table in mineral and peat soils, and the third most important parameter explaining discharge at the Pont-de-Pierre wetland outlet. The

calibrated value was $7.5x10^{-7}$ $m.s^{-1}$. The hydraulic conductivity values suggested by the model calibration substantially differ from those cited in the literature, both in terms of magnitude and, more surprisingly, in terms of anisotropy direction. Dewandel *et al.* (2006) and Wyns *et al.* (2004) gave generic values of $1x10^{-6}$ $m.s^{-1}$ vertically and $1x10^{-5}$ $m.s^{-1}$ horizontally. The anisotropy corresponds to the preferential direction of fissures in weathered granite (Maréchal *et al.* 2003b, 2004b). Yet the sensitivity of the model to these parameters, in particular to the horizontal hydraulic conductivity, suggests that the values obtained through calibration can be regarded with confidence. There may be several explanations to this apparent contradiction between the model results and the literature. First, despite the use of ERT and the availability of some deep geological drilling logs, the knowledge of the shape and depth of the fissured zone is still very limited, and it may have been misrepresented in the model, requiring an adjustment of the horizontal hydraulic conductivity to maintain a reasonable aquifer transmissivity. However different fissured zone shapes and depths were tested as described in Section 6.3.1, and none of these were compatible with the hydraulic conductivity values cited in the literature. The most likely explanation is that fissured granite is more heterogeneous that can be accounted for by a single spatially homogeneous layer. Ahmed & Sreedevi (2008) also used an equivalent porous medium approach to model aquifer flow in a 53 km² granitic catchment in India using MARTHE, a transient groundwater model using finite differences with a rectangular grid. They conceptualised the aquifer in a two-layer system, the superficial one corresponding to the saprolite and the deeper one to the fissured zone. A very large database on the geometry and hydraulic characteristics of both layers was assembled, based on 25 drilling logs and vertical electric sounding surveys, the depth of 900 wells within the watershed, and 34 and 25 pumping and slug tests in the saprolite and fissured layer respectively. Despite this detailed knowledge of the site geology, they found that they could not reproduce the observed piezometric data without introducing linear vertical barriers that they related to observed or assumed dykes and quartz reefs. The calibrated hydraulic conductivities in the fissured zone were very variable (from $1x10^{-7}$ to $3x10^{-5}$ $m.s^{-1}$), due to the heterogeneity in rock weathering. At the Dauges site, the ERT survey has highlighted large variations in the electrical resistivity of the saturated fissured zone that can be related to variations in granite weathering, porosity and clay content (Section 3.3). In particular, electrical resistivity is lower and the inferred degree of weathering higher at the bottom of the etch-basin, which would agree with the current understanding of weathering and etching processes in granite landscapes (Appendix C). A homogeneous fissured layer is therefore clearly an over-simplification, and the relatively low calibrated horizontal hydraulic conductivity very likely results from the existence within 55m below ground of unidentified zones with a low

fissure density and a low horizontal permeability, in particular below the topographic highs, or of mineralised faults and lamprophyre veins impeding flow across them. As stated by Singhal & Gupta (2010), ”the task of modeling groundwater flow and solute transport in [fractured rock systems] appears to be largely hampered by limitations in site characterization, i.e. due to difficulties in collecting the necessary data to adequately describe the hydrogeological properties of the fractured system”. A more detailed and comprehensive hydrogeological survey involving ERT, geological drilling and borehole pump tests would be required to improve the geological model. The model validation would also be more thorough if the groundwater table depth was monitored in a few deep boreholes located in the upper part of the catchment and not in shallow dipwells located at the bottom of the etch-basin only.

6.5. Conclusion

The initial uncalibrated model parameterised using data from the literature review had a very poor performance. Extensive testing showed that the performance could not be improved to a satisfactory level by changing the depth or shape of the fissured granite zone, suggesting the characteristics of the fissured zone differed markedly from those cited in the literature.

After calibration, the model performance was found to be satisfactory to good for all discharge time-series. It was satisfactory to very good for a large number of groundwater table time-series. Small discrepancies could be explained by small-scale variation in peat physical properties. The simulated mean groundwater table showed a close agreement with the observed spatial distribution of wetland vegetation. This good performance with regard to multiple indicators confirms the validity of the conceptual model described in Chapter 4, in particular with regard to the hydrological connectivity between the fissured zone aquifer and the mire.

However the model failed to reproduce groundwater dynamics observed in some dipwells, particularly on the south-west margin of the mire. This may be caused by local differences in fissure density in the fissured zone and small-scale topographic features leading to overland flow convergence not captured by the model resolution.

Stage could not be accurately modelled within the mire using kinematic routing as this method ignores backwater effects. As a consequence, groundwater levels along to the stream downstream of Puy Rond could not be accurately modelled due to the high dependence between stream stage and groundwater table in this area. The Saint-Venant equations should be used to model stream flow and stream stage within the mire, but this solution could not be

implemented due to the limited computational capacity available. Indeed it required much longer run times that were not compatible with the large number of runs necessary to calibrate the model. This issue could probably be resolved using better computing resources or, if using newer versions of MIKE SHE, nested models. In the latter case, kinematic routing could be used at the catchment scale, and the Saint-Venant equations in a smaller area corresponding to the mire upstream of Pont-de-Pierre.

Overall, even though the performance of the model was generally satisfactory for hydrological applications, errors were still too large for modelled groundwater table time-series to be used for ecological applications, since mire plant species and in particular bryophytes do react to groundwater table changes in the order of a few centimetres, an order of magnitude smaller than the model error (Gignac & Vitt 1990; Gignac *et al.* 1991; Gignac 1992, 1994). Achieving such an accuracy would probably not be possible at the scale of the wetland even with substantial additional data and computing capacity due to small-scale variations in the mire topography and peat properties.

Stream discharge and groundwater table depth, including in peat, were most sensitive to the horizontal hydraulic conductivity and specific yield of the fissured granite zone, highlighting the importance of understanding water fluxes within the mire catchment, and in particular within the granite weathering formations, to improve hydrological predictions within the mire. The calibrated horizontal hydraulic conductivity in the fissured zone differed markedly from values cited in the literature (Wyns *et al.* 2004; Dewandel *et al.* 2006). This may reflect the heterogeneity of the fissured zone and calls for more detailed investigations of its hydraulic properties.

Calibrated specific yield and available water capacity for both peat and mineral soils also differed markedly from data commonly cited in the literature. In particular, the available water capacity for mineral soils had to be increased beyond the range of realistic values to improve the model performance with regard to stream discharge at the wetland outlet. This confirms that the two-layer model does not perform well when the groundwater table is relatively deep, or suggests that the actual evapotranspiration was under-estimated. Since the Richards model would require much higher computational capacity, the performance of the gravity model could be investigated. The measurement of soil depth and water retention curves in a number of representative locations would allow a better parametrisation of the unsaturated model, and the acquisition of soil moisture time-series an independent calibration.

Résumé du chapitre 6

Le modèle MIKE SHE / MIKE 11 initial, paramétré principalement sur la base des données issues de la littérature internationale pour des environnements similaires à ceux rencontrés au sein du bassin versant des Dauges, s'est avéré être très peu performant. Une expérimentation systématique a montré que les performances du modèle ne pouvaient pas être améliorées de façon satisfaisante en modifiant la topographie du plancher du modèle géologique, correspondant à l'interface entre le granite fissuré et le granite sain. Ces résultats suggèrent que les caractéristiques hydro-physiques de la zone fissurée, en particulier sa conductivité hydraulique globale, diffèrent significativement des valeurs généralement indiquées dans la littérature.

La performance du modèle a pu être considérablement améliorée par calibration. Elle est considérée comme satisfaisante à très bonne pour les débits au niveau des quatre stations de jaugeage disponibles. Elle est considérée comme satisfaisante à très bonne pour les profondeurs de nappe dans un grand nombre de piézomètres. Pour ces derniers, l'erreur résiduelle peut s'expliquer en partie par la difficulté à définir le niveau du sol lors du nivellement des piézomètres dans ce milieu à la microtopographie accidentée. Des tests de sensibilité ont montré que l'erreur résiduelle peut également s'expliquer en partie par les variations locales des propriétés de la tourbe et de la végétation. La profondeur moyenne interannuelle de la nappe simulée par le modèle montre une bonne correspondance avec les limites de la zone humide cartographiée sur la base de la végétation. Cette bonne performance du modèle au regard de multiple indicateurs confirme la validité du modèle hydrogéologique conceptuel décrit dans le chapitre 4, en particulier en ce qui concerne l'importance fonctionnelle des apports souterrains issus de la zone fissurée du granite dans le bilan hydrique de la zone humide.

Toutefois, la performance du modèle reste insatisfaisante pour certains piézomètres, notamment en bordure sud-ouest du site. Il est possible que cela résulte de variations locales dans le degré de fissuration du granite ou de chenaux préférentiels de ruissellement de surface non capturés par le modèle numérique de terrain à la résolution utilisée. Du fait de l'utilisation de la méthode de routage cinématique, les niveaux d'eau dans les ruisseaux n'ont pas pu être modélisés de façon satisfaisante à l'intérieur de la tourbière elle-même, où les pentes sont faibles et les obstacles à l'écoulement nombreux. En conséquence, les niveaux de la nappe à proximité du ruisseau dans la partie aval de la tourbière n'ont pas pu être reproduit de façon satisfaisante, étant donnée la forte dépendance existant entre les niveaux dans le ruisseau et

ceux dans les dépôts alluviaux et tourbeux sur ce secteur. L'utilisation des équations de Saint-Venant serait nécessaire pour améliorer la performance du modèle MIKE 11, mais elle nécessite un pas de temps très court et n'a donc pas pu être implémentée avec les moyens de calcul disponibles.

La conductivité hydraulique horizontale et la porosité efficace de la zone fissurée du granite sont les paramètres auxquels les débits dans les ruisseaux et les profondeurs de nappe (y compris dans la tourbe) simulés sont les plus sensibles, ce qui démontre l'importance d'une bonne compréhension de l'hydrogéologie des formations d'altération du granite dans l'ensemble du bassin versant pour améliorer les prédictions hydrologiques dans ce type de zone humide. Les valeurs de conductivité hydraulique obtenues par calibration diffèrent significativement des valeurs génériques proposées dans la littérature (Wyns et al. 2004; Dewandel et al. 2006). Il est possible que cela reflète l'hétérogénéité de la zone fissurée, et la présence de barrières moins perméables (Ahmed et al. 2008).

Les valeurs de coefficient de drainage et de réserve utile obtenues par calibration diffèrent également de manière significative des valeurs habituellement citées dans la littérature pour des sols équivalents. En particulier, la réserve utile obtenue par calibration pour les sols minéraux est physiquement improbable, ce qui suggère que le modèle tel qu'implémenté dans cette étude ne reproduit pas de manière satisfaisante les processus d'évapotranspiration et d'écoulement vadose. Les raisons en sont détaillées dans le chapitre 8. L'utilisation de l'un des deux autres modèles disponibles dans MIKE SHE pourrait être envisagée, mais requerrait une plus grande capacité de calcul et une meilleure connaissance des propriétés des sols en particulier sur le bassin versant. La cartographie de leur profondeur et de leurs courbes de rétention hydrique permettrait de mieux paramétrer le modèle. L'acquisition de séries temporelles d'humidité des sols permettrait une calibration du modèle d'évapotranspiration et d'écoulement vadose indépendamment des autres modules de MIKE SHE.

Chapter 7. Simulated water balance and hydrological fluxes between the mire and its catchment

7.1. Introduction

The objective of this chapter is to use the MIKE SHE / MIKE 11 model of the Dauges catchment, the development, calibration and validation of which are detailed in Chapters 5 and 6, to assess the hydrological functioning and water balance of the Dauges mire. The following questions, particularly relevant to the ecology and conservation of the site's protected plant communities (Sections 1.2.4 and 2.6.1), but also to its role in metalloid and radio-nuclide pollutant sequestration (Section 1.2.5.2), are investigated:

- What are the main water fluxes to and out of the mire? Do they vary in time and space?
- What is the role of groundwater upwelling from the underlying mineral formations through the peat layer, compared to precipitation and surface runoff from the catchment, in maintaining the shallow groundwater table within the mire? Does the water within the saturated peat layer mainly originate from groundwater upwelling?

These questions are answered by investigating the spatial distribution of simulated hydrological characteristics and by undertaking water balance analyses of the catchment and the mire, both over the whole simulation period and at a monthly time step.

7.2. Spatial characterisation of the mire hydrology

7.2.1. Methods

The spatial distribution of the mean groundwater table depth, the mean seepage from the saturated zone to the overland flow component and the mean upward groundwater flow from lower to upper computational layers was extracted from the MIKE SHE gridded outputs over three years, from 01/01/2011 to 31/12/2013. The latter measure was used to characterise the volume of water upwelling from the underlying mineral substrate to the overlying peat layer. MIKE SHE requires that computational layers extend across the entire catchment. Furthermore, they must not be too shallow to avoid numerical instability issues (Section 5.4.6.2). In this study the upper layer was given a depth equal to that of the peat layer where larger than 0.5m, and 0.5m elsewhere, including on mineral soils. Consequently, part of the groundwater flow

calculated between the two computational layers within the mire does not occur precisely between mineral and peat formations but within the lower mineral layer and the upper computational layer that includes both mineral and peat formations. This is the case in 41% of the total area occupied by peat soils, and in 34% of the area occupied by peat soils upstream of Pont-de-Pierre (Figure 5-24). However the similarity between maps of mean upward groundwater flow from lower to upper computational layers and of seepage from saturated zone to overland suggests that upward groundwater flow from lower to upper computational layers can be used as a good approximation of groundwater upwelling from mineral formations to the peat layer even when the latter is shallower than 0.5m.

7.2.2. Results and discussion

Figure 7-1 shows the spatial distribution of the mean simulated groundwater table depth, upward groundwater flow from lower to upper computational layers and seepage from the saturated zone to the overland flow component, from 01/01/2011 to 31/12/2013, overlaid with the wetland boundaries (note that the latter do not exactly match peat soil boundaries, see Section 2.6.3 and Section 3.4). The figures show that upward flow from lower to upper computational layers and seepage from the saturated zone to the overland flow component are very similar, which is to be expected where the groundwater table depth is at ground level as is the case most of the time within the wetland. At such times any additional input of water to the ground surface will lead to runoff. The wetland boundaries are closely associated with shallow groundwater table depths, as already shown in Section 6.2.2, but also to water upwelling from the underlying mineral substrate. Groundwater upwelling and seepage are highest along or immediately upstream of the wetland boundary. This is a clear example of edge-focused discharge (Richardson *et al.* 2001), whereby groundwater discharge at the ground surface is enhanced where there is a break in the slope of the surface topography and, consequently, of the water table gradient. The lower topographic slope gradient within the wetland itself leads to a rapid decrease in the vertical hydraulic gradient towards the centre of the wetland. It is therefore clear that accurate modelling of groundwater discharge close to the wetland boundaries requires an accurate representation of the topographic surface in and around this area. As explained in Section 3.2, this is not the case along the south-west boundary of the mire, where only low-resolution and low-accuracy topographic data were available.

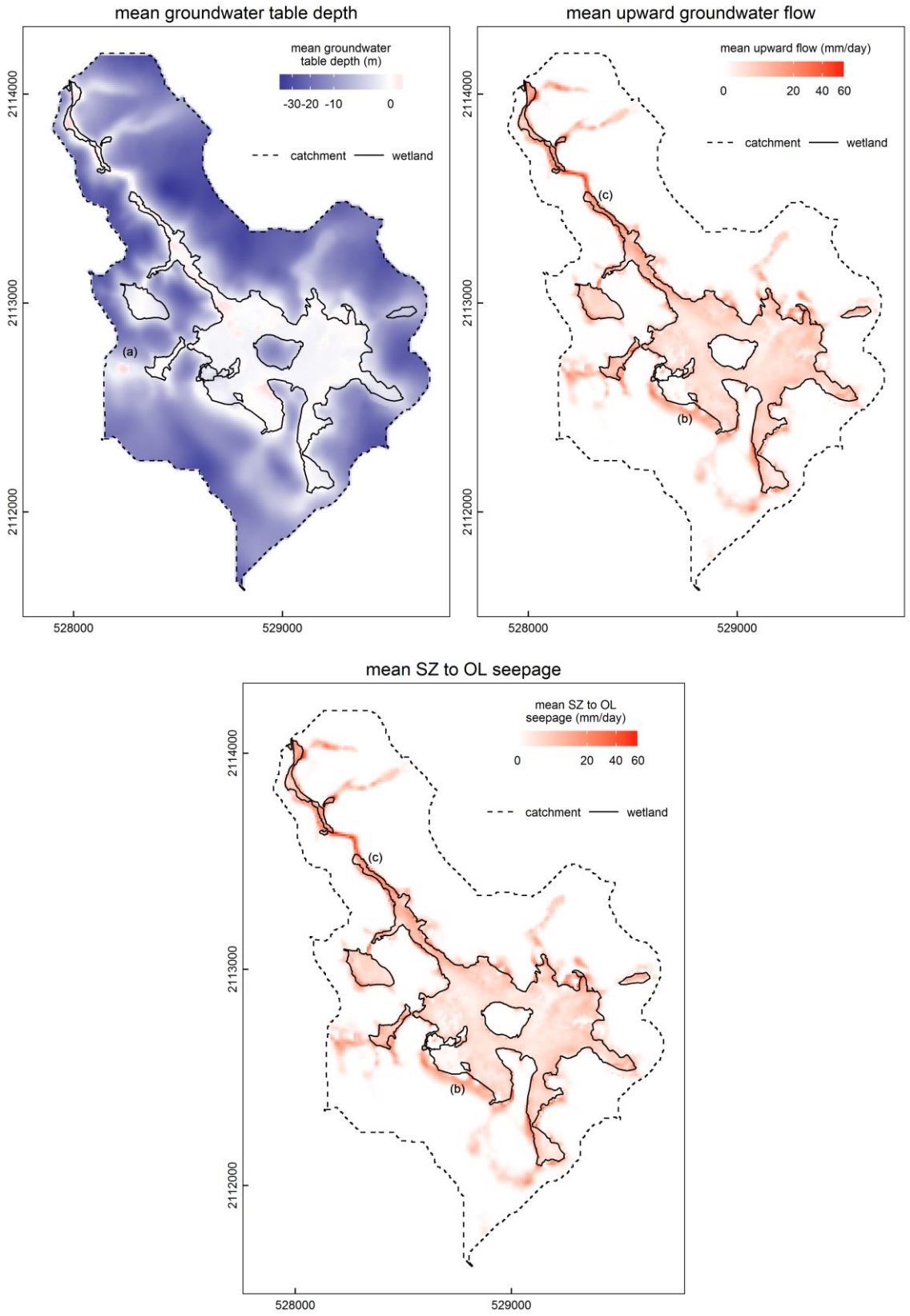

Figure 7-1. Simulated mean groundwater table depth, upward groundwater flow from lower to upper computational layers and seepage from saturated zone to overland flow (01/01/2011-31/12/2013).

Note the square-root transformation of the colour scale used to improve readability. (a), (b), (c): see text.

The model results along this boundary (labelled (b) on Figure 7-1) should therefore be viewed with some caution. Indeed all three datasets on Figure 7-1 show some discrepancies in this area with the wetland boundary, even though close examination of the aerial photograph suggests that the large seepage area predicted by the model just outside the wetland may correspond to a distinct woodland community not identified on the vegetation map. The larger rates of upwelling and seepage seem to occur along the narrow valley located between the main wetland outlet at Pont-de-Pierre and the model outlet at the D78 bridge (labelled (c) on Figure 7-1). The positive groundwater table depth at location (a) on Figure 7-1 is a consequence of the absence of convergence of the overland flow component described in Section 6.3.5.

According to Darcy's law and for a constant head gradient and hydraulic conductivity, the actual volume of groundwater upwelling to the surface within the mire is expected to be an inverse function of the depth of the low-permeability peat deposits. Figure 7-2 and Figure 7-3 suggest that both seepage from the saturated zone to overland flow and groundwater upwelling are indeed partly related to peat depth, and generally lower where peat is deeper, for instance downstream of Puy Rond, in and around area labelled (d). The larger peat depths towards the centre of the mire will therefore further exacerbate the concentration of groundwater discharge to the edge of the wetland. However Figure 7-1, Figure 7-2 and Figure 7-3 also clearly show that the relation between peat depth and groundwater upwelling is relatively weak, and that groundwater upwellling does occur throughout the wetland, albeit at a lower rate than along its boundaries and with local variations probably caused by small-scale variations in surface topography. With respect to the wetland water balance and given the size of the wetland, direct groundwater upwelling through the peat may be as significant as inputs from upwelling and runoff occurring along the wetland boundaries (see Section 7.3).

Figure 7-4, Figure 7-5 and Figure 7-6 show the spatial distribution of the mean groundwater table depth, the mean upward groundwater flow from lower to upper computational layers and the mean seepage rate from saturated zone to overland as a function of the month of the year. There is no unusual pattern in the spatio-temporal distribution of the groundwater table depth: it oscillates between a minimum in October and a maximum in December. The latter date reflects the two wettest months recorded over the three-year study, in December 2011 and December 2012, and the associated high groundwater recharge. Both groundwater upwelling and seepage from saturated zone to overland are also highest in December. They are lowest in late summer, in August or September, depending on whether peat soils only or both peat and mineral soils along the mire margins are considered.

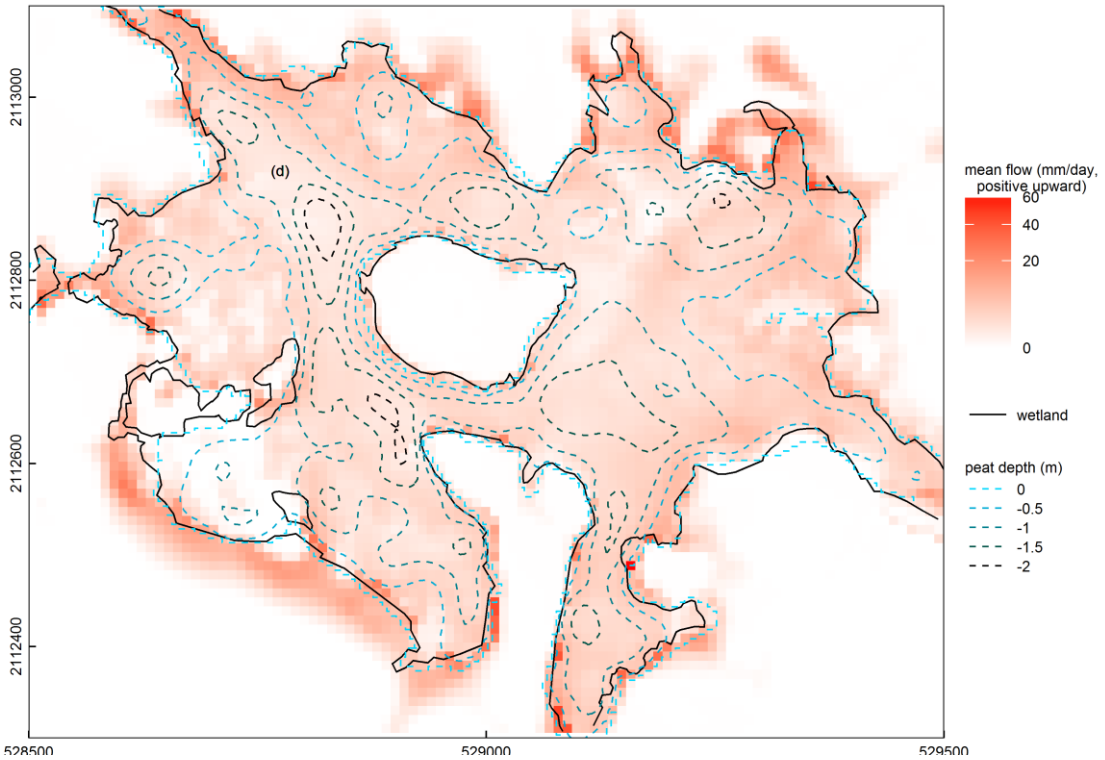

Figure 7-2. Simulated mean upward groundwater flow from lower to upper computational layers (01/01/2011-31/12/2013).

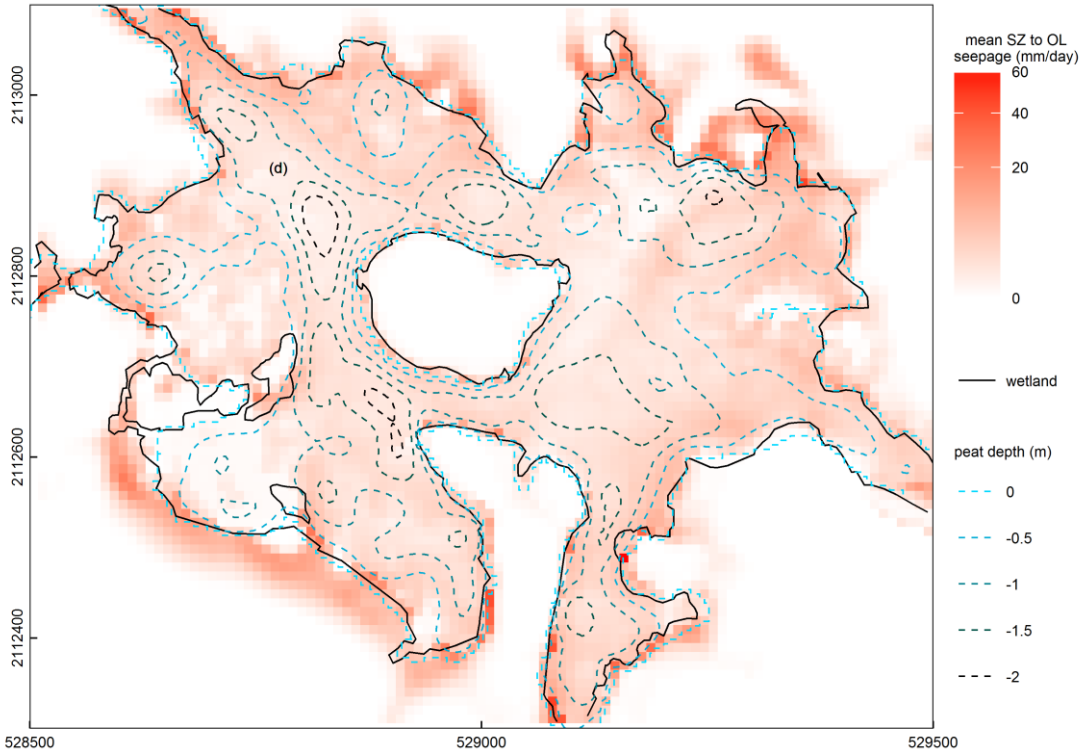

Figure 7-3. Simulated mean seepage from saturated zone to overland flow (01/01/2011-31/12/2013).

Figure 7-5 and Figure 7-6 show that the area where groundwater upwelling and seepage occur reaches its maximum in winter, when it extends largely to mineral soils surrounding the wetland and to thalwegs and slope breaks in the upper part of the catchment. This area progressively shrinks to reach its minimum in September. The almost perfect agreement between areas where upwelling and seepage occur in August and September and the observed wetland boundaries (based on the vegetation map, see Section 2.6.3) is clearly noticeable.

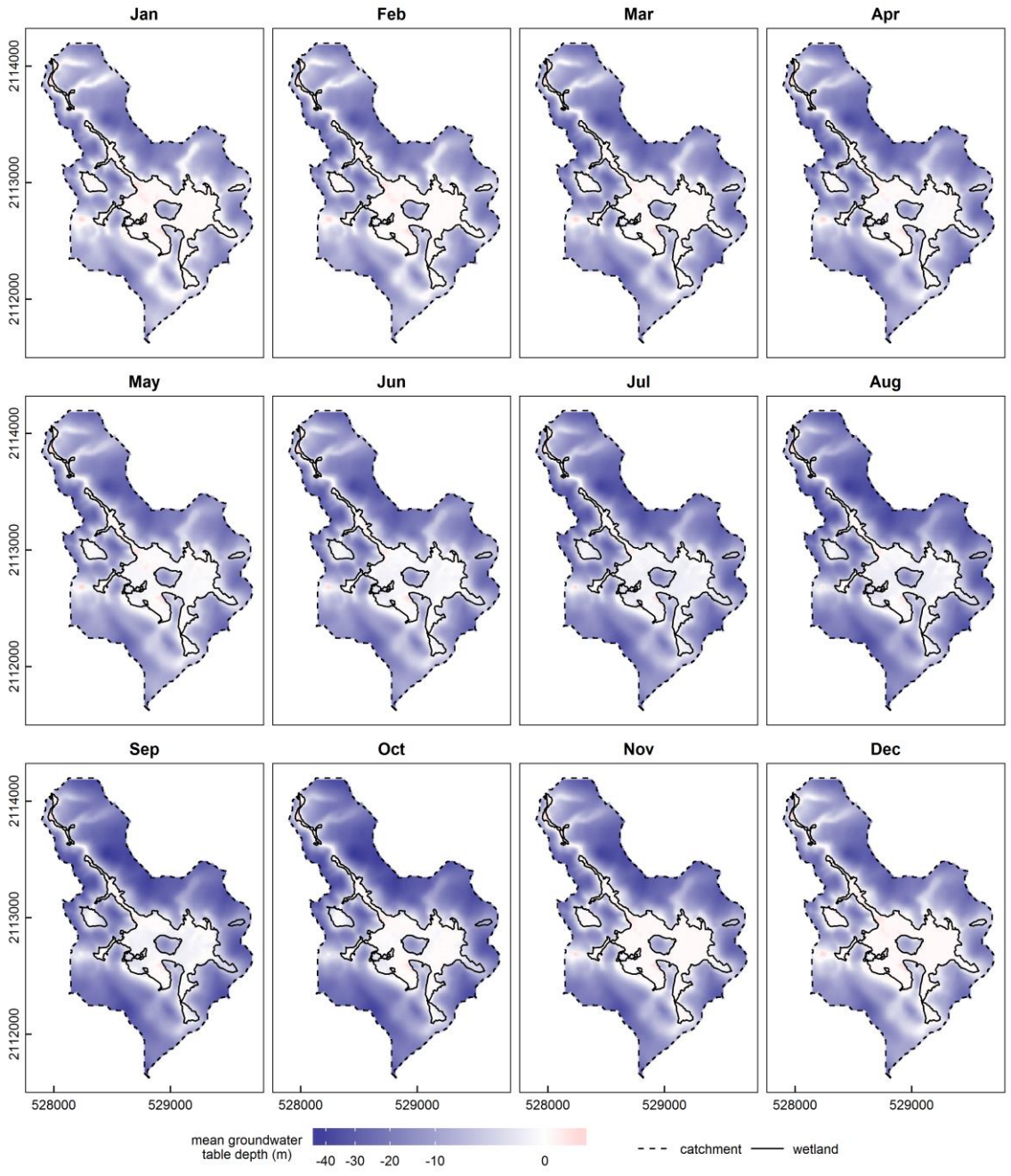

Figure 7-4. Simulated monthly mean groundwater table depth (01/01/2011-31/12/2013).

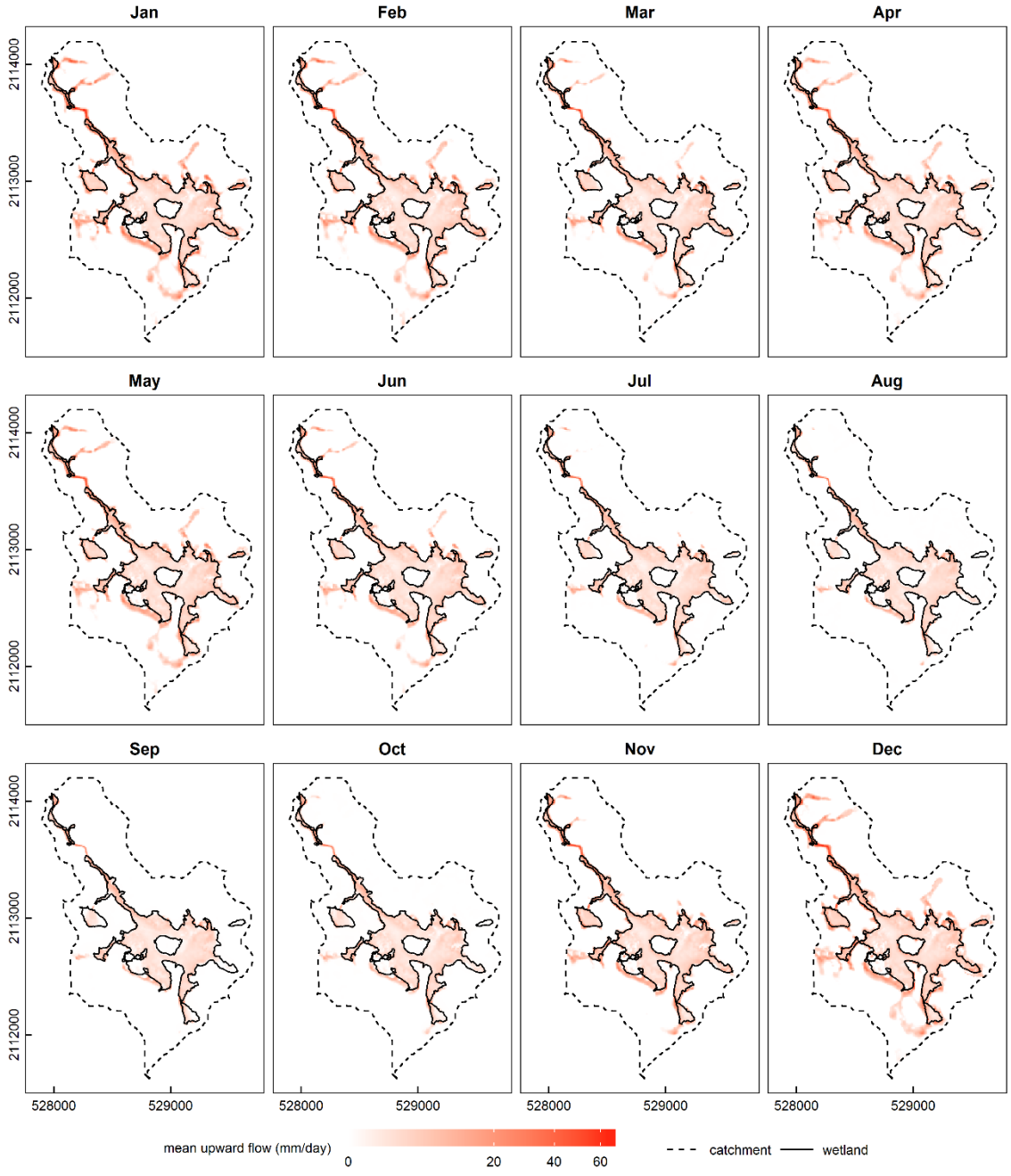

Figure 7-5. Simulated monthly mean vertical groundwater flow between computational layers (01/01/2011-31/12/2013).

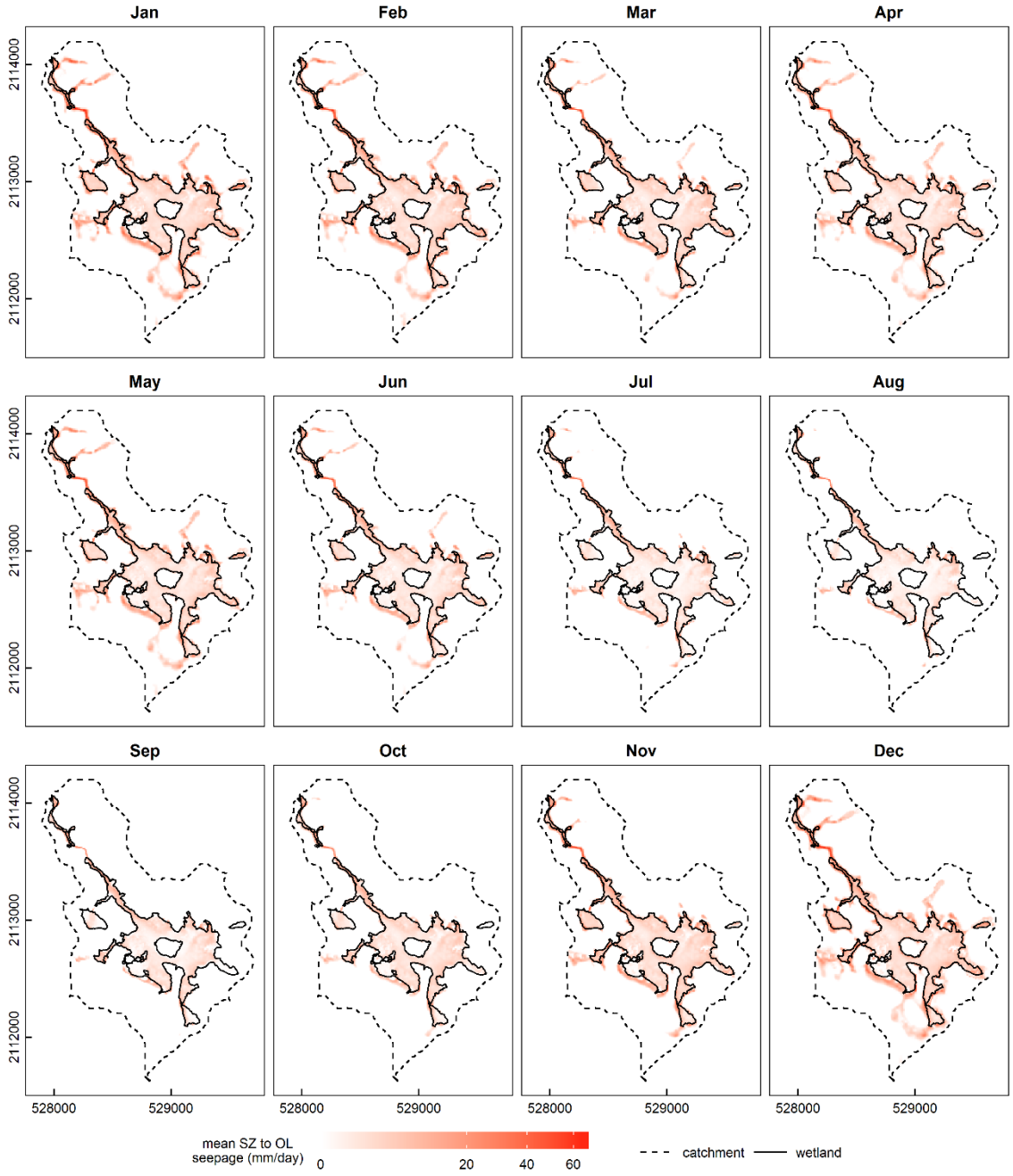

Figure 7-6. Simulated monthly mean seepage from saturated zone to overland flow (01/01/2011-31/12/2013).

7.3. Water balance

7.3.1. Methods

The MIKE SHE water balance tool was used to derive the simulated water balance of the mire and its catchment from 01/01/2011 to 31/12/2013. Both an overall and monthly water balances were calculated. Since interception and evaporation from interception were calculated outside

MIKE SHE, these items were added a posteriori to the water balance calculated by MIKE SHE. To reduce potential error resulting from uncertainties over peat depth downstream of Pont-de-Pierre (Section 3.4) and boundary conditions at the downstream end of the model area, and since the focus is on the main wetland area, water balance computations were restricted to the area upstream of Pont-de-Pierre. The mire water balance includes all peat soils, while the catchment water balance covers areas with mineral soils (Figure 7-7). These two areas cover 36.85ha and 124.95ha respectively. The MIKE SHE water balance tool does not allow for a water balance to be calculated along lines, for instance along the line separating the areas upstream and downstream of Pont-de-Pierre. As a consequence, the mineral soils water balance outflow includes flow across both the mineral-peat boundary and the Pont-de-Pierre watershed boundary on mineral soils. Similarly, it is not possible to make a distinction between flow across the mineral-peat boundary upstream of the mire and across the downstream mire boundary. A combined water balance, covering both peat and mineral soils upstream of Pont-de-Pierre, was therefore computed to provide an estimate of exchanges across the downstream boundary of the entire Pont-de-Pierre watershed. The following abbreviations are used when referring to water balance items in Chapters 7 and 8: OL (overland), UZ (unsaturated zone), SZ (saturated zone), riv (river), RR (precipitation), int (interception), evap (evaporation), transp (transpiration), infilt (infiltration), percol (percolation), bdin/bdout (boundary inflow/outflow), sto (storage), err (error), pos (positive), neg (negative).

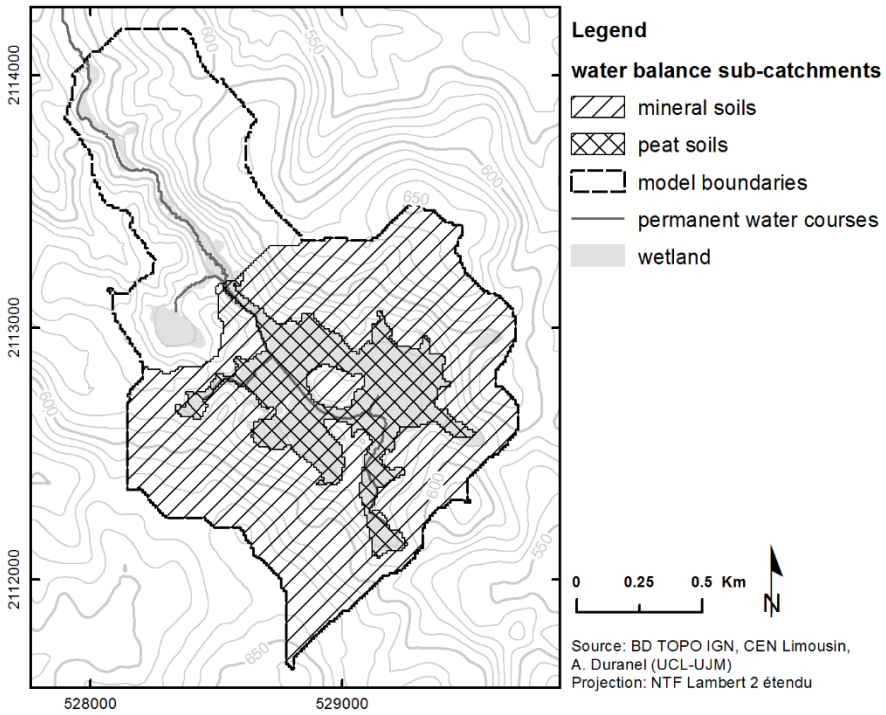

Figure 7-7. Water balance sub-catchments.

7.3.2. Results and discussion

Figure 7-8 shows the simulated overall water balance in cubic metres of the mire extent upstream of Pont-de-Pierre from 01/01/2011 to 31/12/2013. Figure 7-9 shows the monthly water balance of the mire in mm, further detailed in Figure 7-10, Figure 7-11 and Figure 7-12 that give the detailed monthly water balances of the overland, unsaturated zone and upper saturated zone components for the same area and period. Since the focus is on the water balance of the mire, which includes the peat layer and the ground surface and vegetation above it, the lower computational layer, representing the underlying mineral formations, was excluded from the water balances shown in Figure 7-9, Figure 7-10, Figure 7-11 and Figure 7-12. The latter four figures follow the convention used in MIKE SHE: inputs are always negative, outputs always positive, change in storage is positive when storage increases (and vice versa), and the water balance error is the sum of all inputs and outputs. This convention cannot be followed in Figure 7-8 since an input for a given model component can be an output for another. Instead the flow direction is given by an arrow.

Table 7-1 gives the overall water balance of the mire upstream of Pont-de-Pierre, of its catchment and of both areas combined in both mm and cubic metres. Except for boundary flows, the combined water balance in cubic metres is equal to the sum of the mire and catchment water balances, plus or minus a small error caused by the fact that MIKE SHE expresses the water balance in mm and not cubic metres, leading to rounding errors when the water balance is scaled up to the entire area.

The water balance computation provides a large amount of information on the hydrology of the mire and its catchment. The evapotranspiration expressed in mm is higher in the wetland than in the catchment, and is almost equal to the Penman-Monteith reference evapotranspiration. As described in Section 5.4.3.4, a higher crop coefficient was used for the mire (1 all year round) than for broadleaf woodlands (0.38 in winter, 0.77 in summer), however Table 7-1 shows that the main reason for the larger evapotranspiration is the presence of a very shallow groundwater table and the common occurrence of ponded water within the mire, with evaporation from ponded water accounting for 54% of the total evapotranspiration in the mire but only 3% in the wider catchment. Within the mire, evaporation from ponded water is the main evapotranspiration component except during the driest month of the year (June 2011, August 2012 and July 2013) when transpiration from the unsaturated and saturated zones becomes similar or slightly larger, and in December and January when reference evapotranspiration is very

small and is principally fulfilled by evaporation from interception since this reservoir is the first from which evapotranspiration is drawn by the model (Figure 7-13).

The three main sources of water to the mire are precipitation, overland boundary flow (i.e. runoff from the mire catchment) and groundwater upwelling from the underlying mineral formation (calculated as the upward flow from the lower computational layer representing the underlying mineral formations to the upper layer representing the peat deposits). Over the three-year simulation, precipitation contributed 1.4M m^3 and upwelling through the peat from the underlying mineral formations 1.2M m^3. Inputs from overland flow are substantially higher at 2M m^3. However, as previously discussed and shown in Figure 7-1 and Figure 7-3, a large proportion of overland flow inputs actually results from edge-focused groundwater seepage just upstream of the mire boundaries and therefore just upstream of the boundary used for the computation of the water balance.

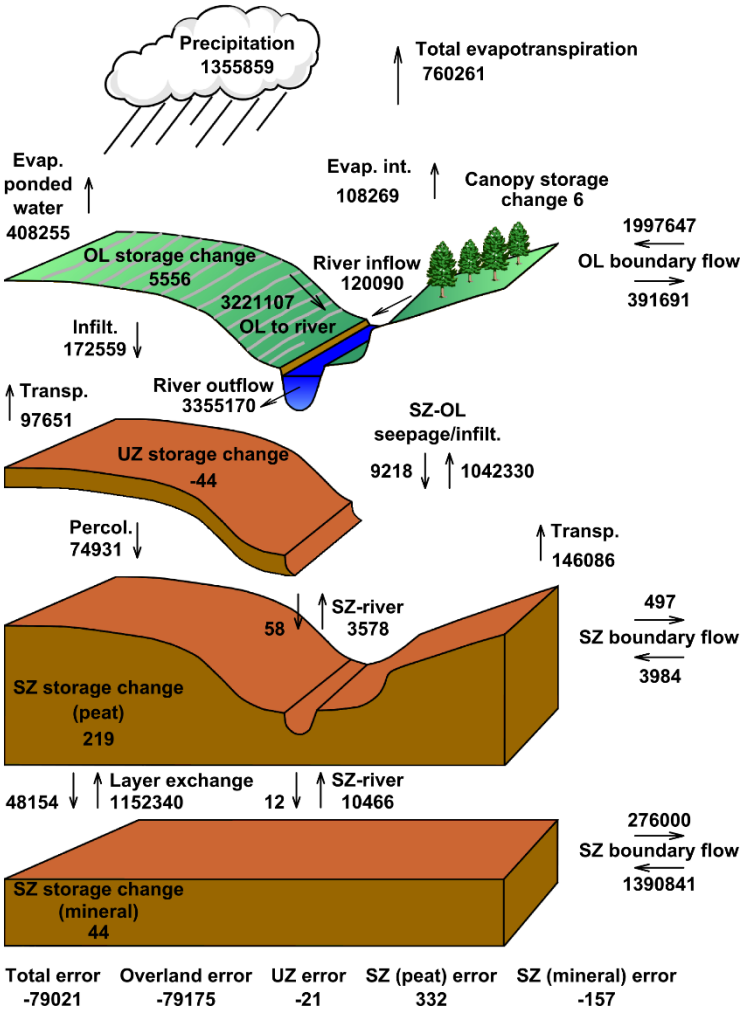

Figure 7-8. Simulated water balance of the mire area upstream of Pont-de-Pierre from 01/01/2011 to 31/12/2013 (m^3).

Table 7-1. Simulated water balances of the mire, of its catchment and of both areas combined from 01/01/2011 to 31/12/2013.

	mm			m^3		
	wetland	catchment	combined	wetland	catchment	combined
Precipitation	3679	3679	3679	1355859	4597410	5953269
Penman-Monteith ETo	2088	2088	2088	-	-	-
Actual evapotranspiration	2063	1611	1713	760261	2012893	2773151
incl. from interception	294	585	518	108269	730609	838878
incl. from ponded water	1108	44	286	408255	54870	463124
incl. from UZ	265	957	799	97651	1195677	1293327
incl. from SZ	396	25	110	146086	31737	177822
OL boundary inflow	5421	302	5	1997647	377604	8202
OL boundary outflow	1063	1594	10	391691	1991877	16519
OL to river	8741	87	2058	3221107	108115	3329222
Infiltration from OL to UZ	468	2837	2297	172559	3544334	3716899
Infiltration from OL to SZ	25	18	20	9218	22922	32140
Seepage from SZ to OL	2829	966	1390	1042330	1206612	2248941
Percolation from UZ to SZ	203	1894	1509	74931	2366791	2441721
SZ boundary inflow	3785	275	55	1394825	343924	89570
to upper layer (peat)	11	-	-	3984	-	-
to lower layer (mineral)	3774	-	-	1390841	-	-
SZ boundary outflow	750	1179	62	276497	1472824	100141
from upper layer (peat)	1	-	-	497	-	-
from lower layer (mineral)	749	-	-	276000	-	-
Upper to lower SZ layer	131	-	-	48154	-	-
Lower to upper SZ layer	3127	-	-	1152340	-	-
SZ to river exchange	38	10	16	14044	12057	26101
upper SZ layer (peat) to river	10	-	-	3578	-	-
lower SZ layer (mineral) to river	28	-	-	10466	-	-
River to SZ exchange	0	0	0	70	82	153
river to upper SZ layer (peat)	0	-	-	58	-	-
river to lower SZ layer (mineral)	0	-	-	12	-	-
Change in interception storage	0	0	0	6	236	242
Change in OL storage	15	1	4	5556	1430	6987
Change in UZ storage	0	-2	-2	-44	-2988	-3033
Change in SZ storage	1	25	19	263	30936	31202
upper layer (peat)	1	-	-	219	-	-
lower layer (mineral)	0	-	-	44	-	-
Total error	-214	246	142	-79021	308360	229338
incl. overland error	-215	218	120	-79175	272767	193597
incl. UZ error	0	12	9	-21	15146	15116
incl. SZ error	1	16	13	175	20447	20625
incl. upper layer (peat)	1	-	-	332	-	-
incl. lower layer (mineral)	0	-	-	-157	-	-

Even though areas where seepage occurs are much smaller in extent on mineral soils than on peat soils, flow rates are larger on the former due to higher hydraulic conductivities and higher hydraulic gradients at slope breaks (Richardson *et al.* 2001). Overall, the total volume of seepage on mineral soils along the wetland margins is slightly larger than that within the wetland itself (1.2M vs. 1.0M m^3 over three years). Figure 7-9 shows that overland boundary inflow to the mire approximately follows the same temporal pattern as precipitation, with larger quantities of runoff flowing into the mire during the wetter months. During the drier months, evaporation from interception and infiltration across the mire catchment are larger, and therefore overland boundary inputs to the mire are smaller and less correlated to precipitation. As a consequence overland flow inputs make for a smaller proportion of the total inflow to the mire (Figure 7-14).

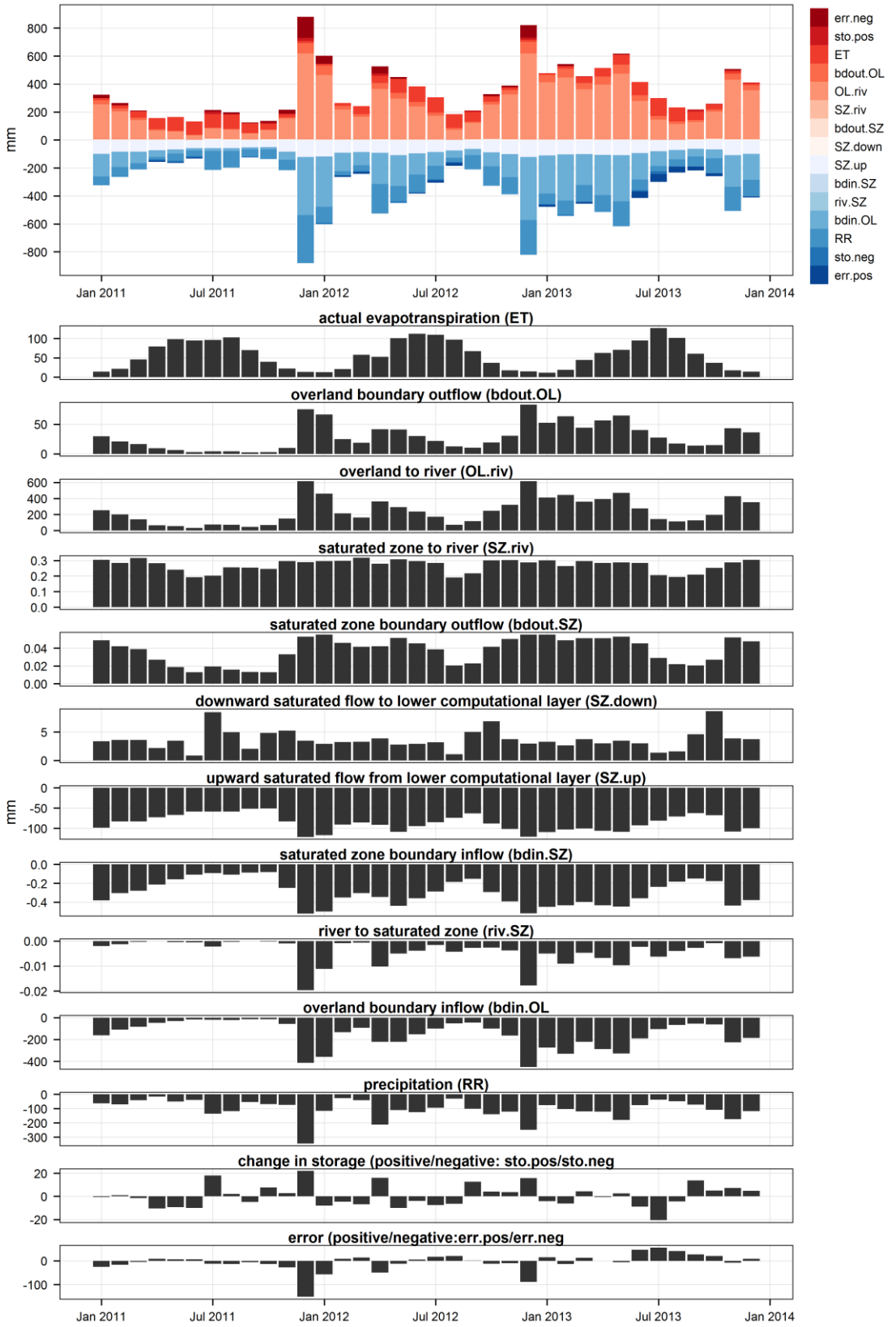

Figure 7-9. Simulated monthly water balance of the mire upstream of Pont-de-Pierre.

Top: combined water balance (common y axis scale), others: individual components (variable y axis scale). See titles of bottom plots for the explanation of component codes used in top plot.

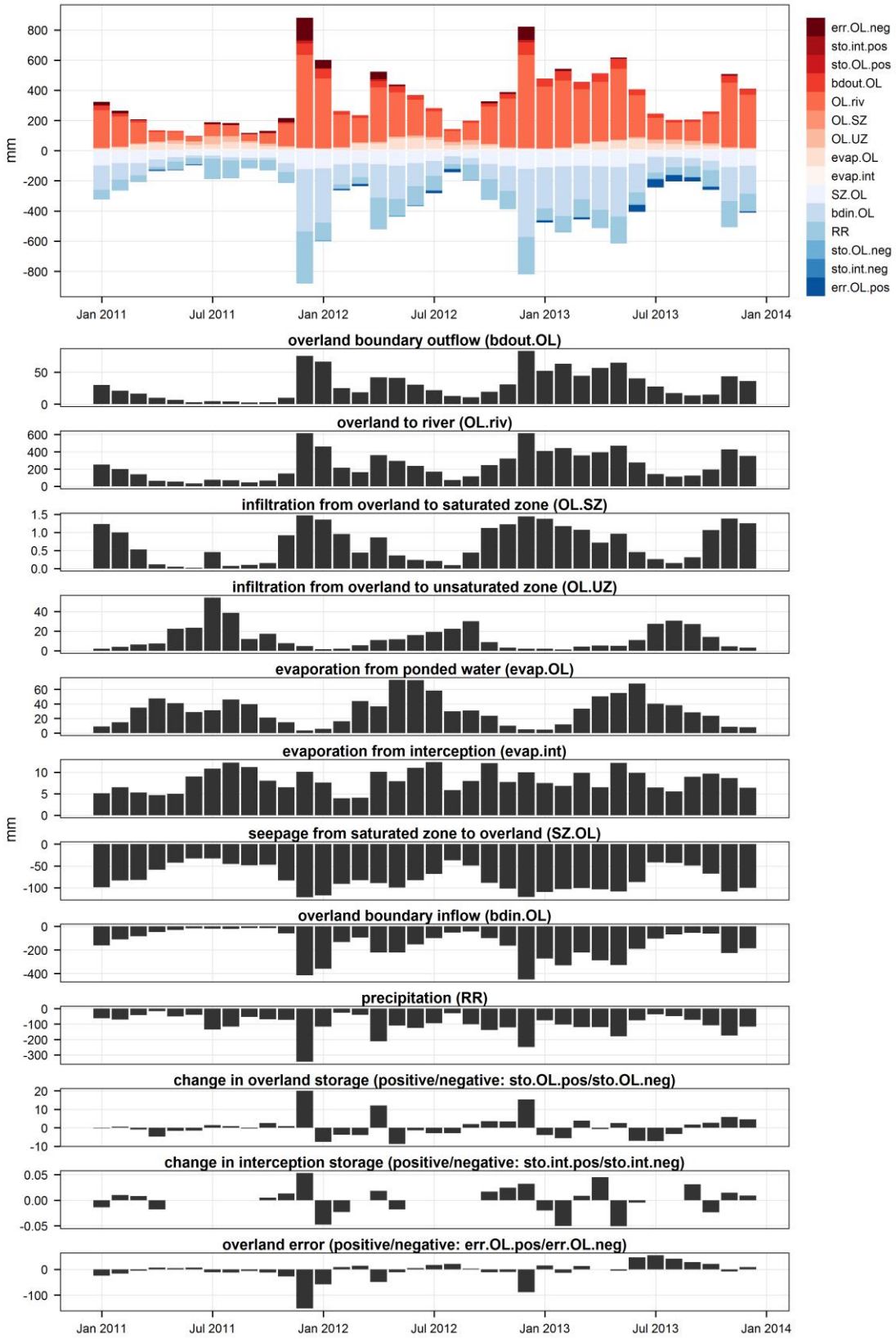

Figure 7-10. Simulated monthly water balance of the mire interception and overland flow components.

Top: combined water balance (common y axis scale), others: individual components (variable y axis scale). See titles of bottom plots for the explanation of component codes used in top plot.

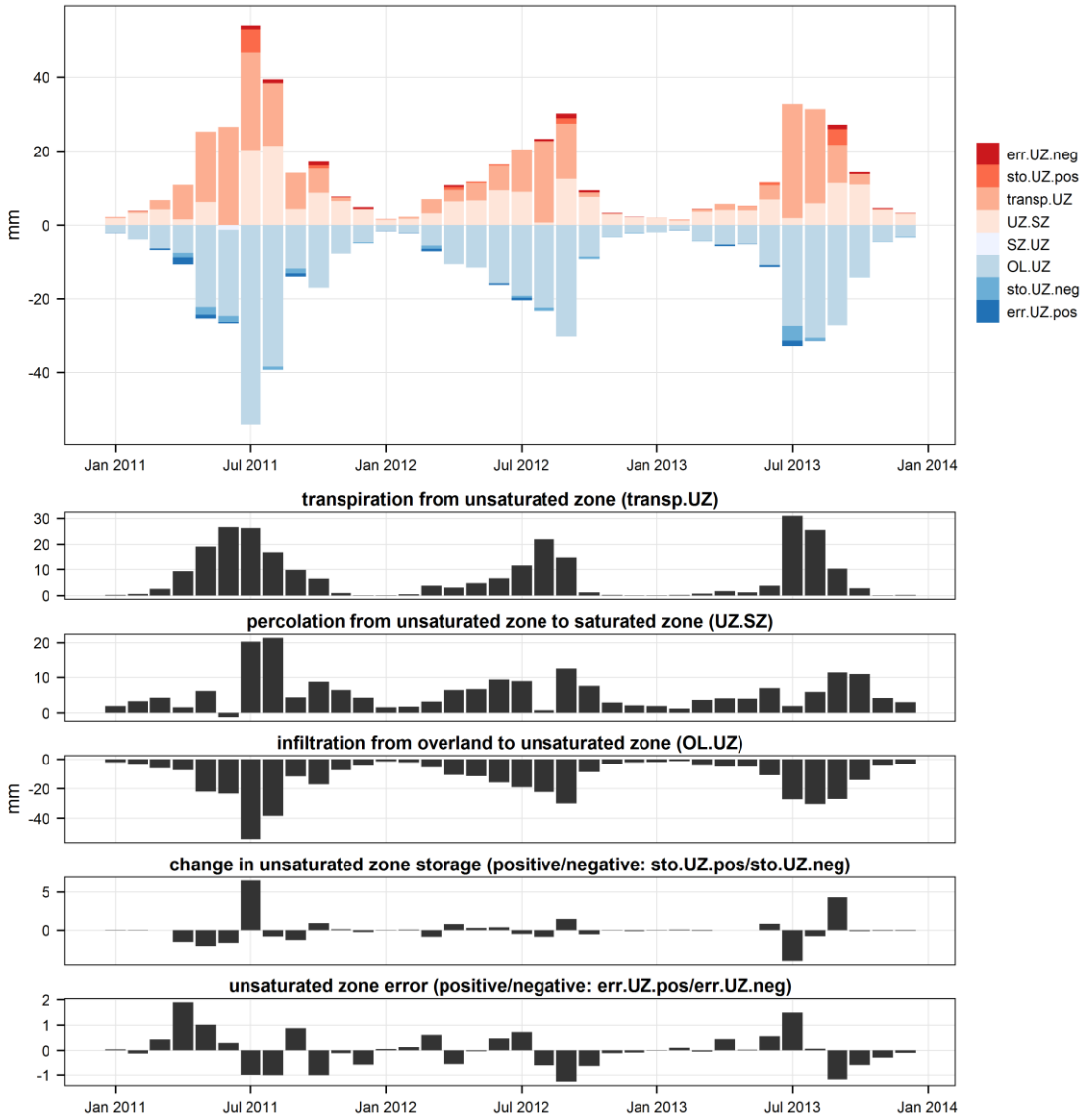

Figure 7-11. Simulated monthly water balance of the mire unsaturated zone component.

Top: combined water balance (common y axis scale), others: individual components (variable y axis scale). See titles of bottom plots for the explanation of component codes used in top plot.

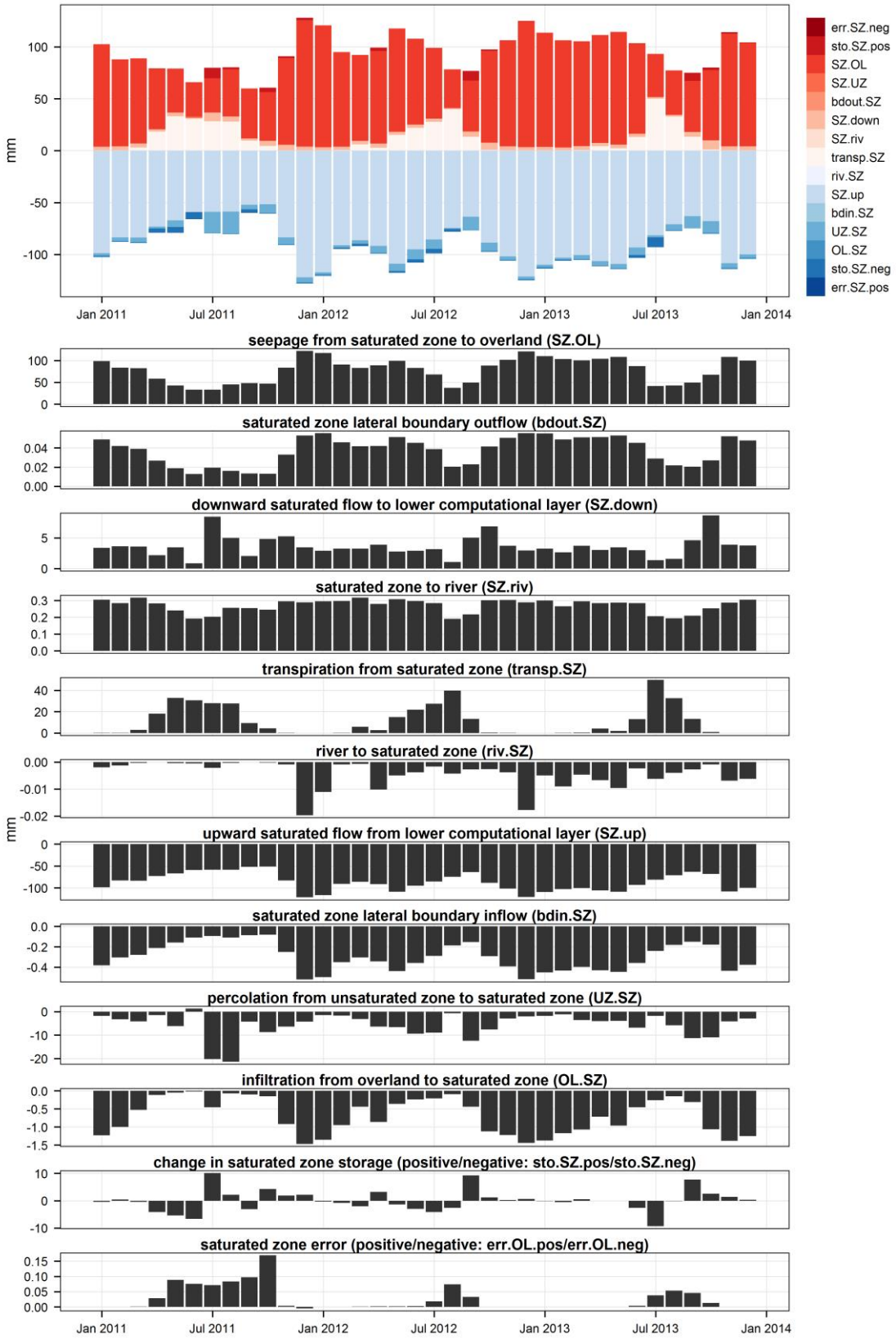

Figure 7-12. Simulated monthly water balance of the mire saturated zone component (upper computational layer only).

Top: combined water balance (common y axis scale), others: individual components (variable y axis scale). See titles of bottom plots for the explanation of component codes used in top plot.

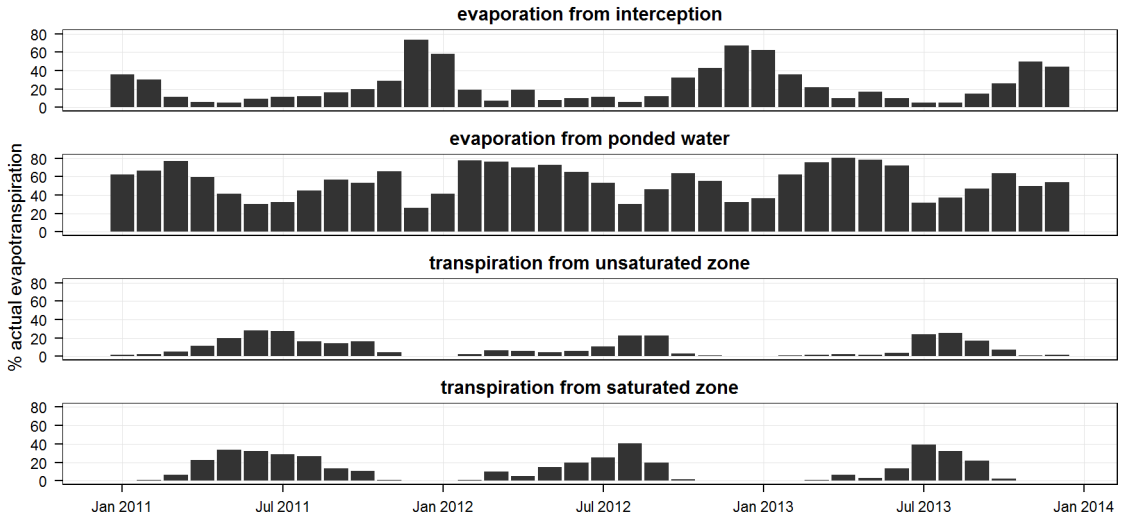

Figure 7-13. Relative importance of individual evapotranspiration components in simulated monthly actual evapotranspiration (mire upstream of Pont-de-Pierre, 01/01/2011-31/12/2013).

Upwelling inputs to the mire are highest in December and January, then decline gradually over time to reach their lowest value in September (Figure 7-9). This pattern is relatively constant in all three years of the simulation. Nevertheless, upwelling inputs are less variable over time than inputs from precipitation and overland boundary flow, and therefore generally make for a larger proportion of the overall inputs in summer (Figure 7-14). Lateral groundwater inputs and inputs from the river to the peat saturated zone are negligible when compared to other inputs: they contribute less than 0.1% of total inputs at all times. However, with regard to inputs from the river, it should be noted that the model does not allow for over-bank flooding (Sections 5.4.4 and 6.4.2) and for saturated flow through the highly permeable gravel deposits found along the stream downstream of Puy Rond (Sections 5.4.6.1 and 6.4.2). Inputs from the river to the mire are therefore probably underestimated downstream of Puy Rond.

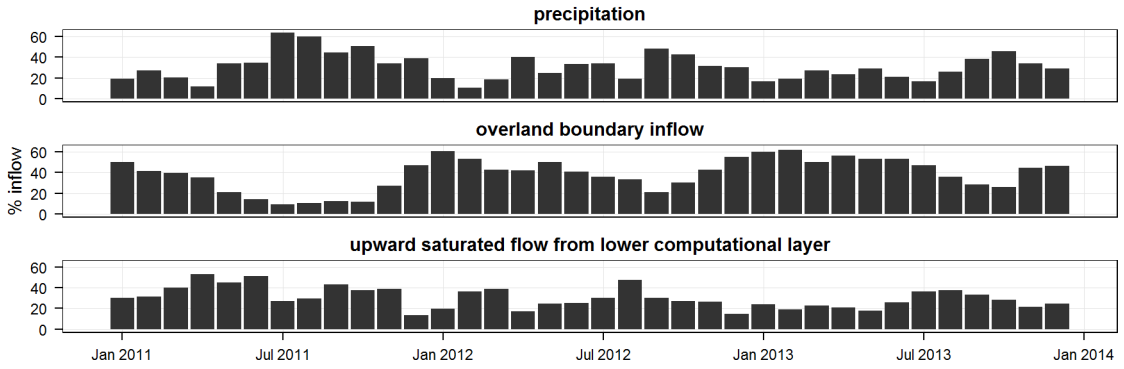

Figure 7-14. Relative importance of individual components in simulated monthly inflow to the mire (upstream of Pont-de-Pierre, 01/01/2011-31/12/2013).

Both the saturated zone lateral boundary inflow and inflow from the river made for less than 0.1% of the total inflow at all times and are therefore not included in the plot.

Figure 7-8 shows that percolation from the unsaturated zone or infiltration from overland makes for only 6.8% of total inputs to the saturated peat. This demonstrates a very small contribution of infiltration, be it from precipitation or overland flow originating from within the mire or from the catchment, to the saturated zone and therefore to the groundwater table dynamics. Precipitation and runoff inputs to the mire occur most frequently during wet periods in winter (Figure 7-9), when the groundwater table is already at, or very close to, ground level and saturation excess overland flow occurs ensuring a quick transfer of excess water to the drainage network. Figure 7-12 and Figure 7-15 show that groundwater upwelling makes for an overwhelming proportion (on average 92%) of inputs to the mire saturated zone at all times. Percolation from the unsaturated zone is largest during the driest months when the water table drops below ground level and the proportion of the mire where an unsaturated zone exists increases. However even during the 2011 drought it did not make for more than a quarter of all inputs to the saturated peat. One important consequence of these model results is that the water contained within the saturated peat overwhelmingly originates from the aquifer contained within the underlying mineral substrate. This suggests that, despite most of the vegetation having been identified and mapped by ecologists as characteristic of "raised bogs" (Durepaire & Guerbaa 2008), the mire is clearly not ombrotrophic, i.e. is not fed principally by precipitation.

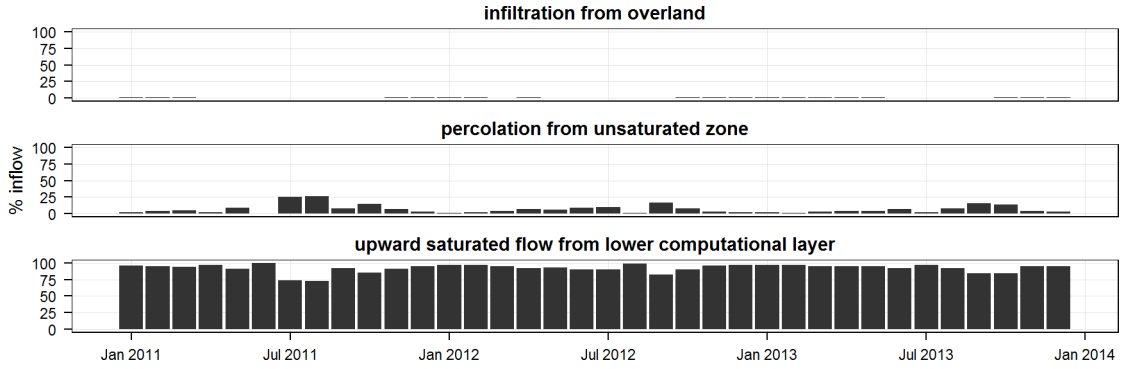

Figure 7-15. Relative importance of individual components in simulated monthly inflow to the mire saturated zone (upstream of Pont-de-Pierre, 01/01/2011-31/12/2013).

Both the saturated zone lateral boundary inflow and inflow from the river made for less than 0.5% of the total inflow at all times and are therefore not included in the plot.

The overwhelming majority (98%) of water inputs to the area upstream of Pont-de-Pierre is from precipitation (about 6M m^3 from 01/01/2011 to 31/12/2013). The rest is made of minor overland and groundwater inflows at the north-western boundary of this area (zero flow was assumed along the model boundaries, see Section 5.4.6.3). Of these inputs, 44.4% were evaporated, 53.7% drained as river flow, 1.6% left the catchment as groundwater flow and 0.3% as overland flow (Table 7-1). Assuming that the relative importance of precipitation, runoff from mineral soil and

groundwater seepage in the overland component water balance within the mire reflects their relative contributions to overland inputs to water courses, 23% of stream discharge at Pont-de-Pierre is water originating from the underlying mineral formations that had seeped through the peat layer. Excluding transpiration, 46% of water that flowed out of the saturated zone through seepage to overland flow, direct seepage to watercourses and groundwater flow out of the area upstream of Pont-de-Pierre did so through the peat layer. Ninety-six percent of stream discharge at Pont-de-Pierre flowed at some point through the mire, either as overland flow or saturated flow. These figures highlight the importance of the mire as an interface between mineral substrate and watercourses, and suggest that physical and geo-chemical processes occurring within the mire such as sediment deposition, metallic pollutant sequestration or release of dissolved organic carbon, as described in Section 1.2.5.2, may have a substantial impact on stream water chemistry.

The water balance computation has a few limitations. First, the model computation approximations led to an accumulated computation error representing 1.7%, 5.8% and 3.8% of the total inputs when the water balance is computed over the mire extent, the catchment extent or the combined mire and catchment extents respectively. These relatively small figures hide larger errors at smaller time steps that cancel each other out. Within the mire for instance, the error in the monthly water balance reaches 25.1% and 21.7% of inputs in July and August 2013 respectively. In absolute terms, the largest error (152mm) occurs in December 2011, at a time when total inputs to the mire also reach their maximum over the three-year simulation. In all cases the water balance error is almost entirely caused by the overland flow component of the model (Table 7-1). The issue caused by the lack of convergence of this model component should therefore be adressed if the water balance error is to be reduced further.

Second, the model design choices that had to be made with regard to channel flow modelling meant that overbank flooding was not accounted for (Sections 5.4.4 and 6.4.2). The contribution of flood water to the water balance of the mire is therefore underestimated, particularly in the area downstream of Puy Rond frequently subject to overbank spilling. Further upstream the extent of flooding is relatively narrow along the main stream and this model limitation has a limited impact on the water balance. The model does not account for the presence of highly permeable alluvial deposits downstream of Puy Rond, which probably leads to a further underestimation of the flow existing between the stream and the saturated zone in this area.

7.4. Conclusion

The results of the calibrated and validated MIKE SHE / MIKE 11 model of the Dauges catchment confirmed the validity of the general conceptual hydrological model of the mire and its catchment presented in Chapter 4. The mire is located where water from the fissured zone aquifer seeps to the ground surface, leading to a shallow and stable groundwater table. The water balance analysis shows that water within the peat layer overwhelmingly originates from groundwater upwelling. Precipitation and runoff inputs to the mire are similar or slightly higher in volume, but occur principally when peat soils are already saturated at or close to the surface by water upwelling from the underlying mineral formations. Inflows from precipitation and runoff are therefore quickly evacuated to streams as saturation excess runoff, and do not substantially contribute to the water balance of the peat layer itself. The model predicts that upwelling occurs throughout the mire. This does not reflect local particularities highlighted by piezometric monitoring and presumably caused by local heterogeneities in the hydraulic properties of the underlying fissured zone. These heterogeneities are not accounted for by the homogeneous geological model which is necessitated by the absence of the high-resolution hydrogeological information which would be required to represent such variations (Section 3.3). Simulated upwelling and seepage are larger along the mire boundaries due to the break in topographic and hydraulic gradient slope (Richardson *et al.* 2001), and smaller toward the mire centre and in places with deeper peat deposits. Evapotranspiration within the mire generally proceeds at the potential rate due to the shallow groundwater table and hence unlimited water supplies.

Résumé du chapitre 7

Le modèle calibré MIKE SHE / MIKE 11 a été utilisé pour caractériser, quantifier et cartographier les flux d'eau au sein de la zone humide et de son bassin versant, et estimer les bilans hydriques totaux et mensuels sur trois ans. Les résultats confirment la validité du modèle hydrogéologique conceptuel détaillé dans le chapitre 4 sur la base d'une interprétation qualitative des données piézométriques et stratigraphiques disponibles. La tourbière correspond aux endroits où l'eau circulant dans la zone fissurée du granite suinte en surface, ce qui maintient une nappe très peu profonde et relativement stable dans la tourbe. Sur trois ans, les précipitations directes, le ruissellement de surface et les apports souterrains ont constitué 30%, 44% et 26%, respectivement, des apports à la tourbière. Le modèle suggère qu'une très grosse partie des apports par ruissellement est en fait issue de l'exfiltration d'eaux souterraines au niveau des sols minéraux en périphérie immédiate de la tourbière.

Toutefois, l'existence dans la tourbière d'une nappe à très faible profondeur ou affleurant en surface pendant la majeure partie de l'année limite l'infiltration des précipitations directes et des apports par ruissellement issus du bassin versant, et donc leur contribution au bilan hydrique du dépôt tourbeux sensu stricto. Les apports souterrains représentent donc en moyenne 92% des apports à la zone saturée de la tourbe. L'importance relative des précipitations dans ce bilan augmente en période estivale lorsque la nappe s'abaisse, permettant une infiltration plus importante, néanmoins même pendant la sécheresse de 2011 les apports souterrains ont représenté les trois quarts des apports. La tourbière est donc clairement minérotrophe, ce qui semble être en contradiction avec la présence sur une grande partie du site de végétations ayant été identifiées par d'autres auteurs comme appartenant aux tourbières ombrotrophes. Ce travail démontre donc qu'il serait nécessaire de clarifier les relations entre hydrologie, hydrochimie et végétations dans les tourbières acides sur substrat granitique dans le Massif Central et ailleurs.

Il montre également que ce type de zone humide constitue une interface quantitativement importante entre bassin versant et cours d'eau dans les têtes de bassin de moyenne montagne granitique : 96% du débit total à l'exutoire de la tourbière et de l'alvéole granitique est constitué d'eau ayant traversé à un moment ou un autre la tourbière, sous forme de ruissellement de surface ou d'écoulement souterrain ; 23% de ce débit est constitué d'eau ayant circulé dans les formations d'altération du granite puis suinté au travers du dépôt tourbeux ; et 46% des eaux souterraines quittant le bassin versant le font en suintant à travers le dépôt tourbeux. La tourbe saturée ayant une très grande capacité de séquestration des polluants, notamment des métaux

(y compris radioactifs) et des métalloïdes, il est donc possible que la tourbière ait un impact majeur sur la qualité chimique des eaux de surface en aval.

Le modèle suggère que les ruptures de pente en périphérie de la tourbière, la différence de conductivité hydraulique entre formations minérales et formations tourbeuses et la mise en charge de la nappe dans les formations minérales en résultant conduisent à une plus grande importance en volume des suintements d'eau issue des formations d'altération du granite en périphérie de la tourbière (y compris sur les sols minéraux) qu'en son centre. Le modèle prédit toutefois que les suintements existent sur l'ensemble de la tourbière, ce qui, pour quelques nids de piézomètres, ne s'accorde pas avec les gradients piézométriques verticaux observés. Il est probable que ces quelques divergences entre données simulées et observées puissent s'expliquer par une hétérogénéité locale des formations d'altération du granite non prise en compte par le modèle.

Dans la tourbière, l'évapotranspiration simulée est généralement proche de son taux de référence, du fait de la présence de la nappe à faible profondeur et donc de l'absence de stress hydrique.

Chapter 8. Impacts of catchment landuse on wetland hydrology

8.1. Introduction

As described in Section 2.2.3, major changes in landuse have occurred over the last 50-100 years in some of the Massif Central uplands. This is particularly the case in the uplands of Limousin, where heathlands, which used to cover more than 75% of the landscape, have been almost entirely replaced by woodlands. Woodlands, in particular conifer plantations, are now the dominant landuse in the catchment of most mires, including those designated under the EU 92/43/EEC Habitats Directive and those for which Ramsar status is currently being sought. As demonstrated in the following review of the international literature, the impact of such drastic landuse changes on the hydrology of mires has almost never been quantified, despite strong evidence that the replacement of open habitats by woodlands, and in particular by conifer plantations, leads to a substantial reduction in runoff and groundwater recharge. Even though in the Massif Central uplands, mires themselves have relatively rarely been directly afforested, it is likely that the afforestation of their catchment has impacted their water balance. In this chapter, the Dauges catchment is used as a case study to investigate the impacts of changes in catchment landcover on mire hydrology. The MIKE SHE model, the development, calibration and validation of which are detailed in Chapters 5 and 6, is forced using new parameters corresponding to two scenarios in which grassland and conifer plantations, respectively, are the dominant landcovers within the mire catchment. The impact of each scenario on the mire hydrology is assessed by quantifying simulated changes in overall and monthly water balances at the scale of both the mire and its catchment, as well as changes in daily stream discharge, daily groundwater table depths within selected dipwells and groundwater table depth monthly means across both the catchment and the mire.

8.2. Impacts of catchment landuse on the hydrology of mires

Even though a large body of literature conclusively suggests that both surface runoff and groundwater recharge are lower under forest cover than in open habitats, and under coniferous cover than under broadleaf cover (see review in Appendix H), few hydrological studies have investigated the impact of forest cover within catchments on the water balance of wetlands. Some studies do, however, suggest a link between catchment afforestation and mire biodiversity and hydrology. Smith and Charman (1988) showed that in Northumberland (UK) blanket bogs

surrounded by conifer plantations, the proportion of species they classified as "ombrogenous" (but in fact characteristic of relatively wet conditions in acidic mires generally speaking) was inversely proportional to the length of time elapsed since the conifers were planted. Conversely, the proportion of species characteristic of drier mire habitats was higher in mires surrounded by older conifer plantations. Furthermore, there is ample palaeo-ecological evidence that large-scale deforestation due to the development of agriculture during the Holocene has led to substantial changes in the water balance of a large number of wetlands, and has sometimes even triggered the creation of new wetlands. Woodward *et al.* (2014) carried out a global meta-analysis of 205 wetland sites, including swamps and lakes, where Holocene deforestation had been evidenced and for which it was possible to assess the presence or absence of hydrological changes through palaeo-ecological or historical methods or through direct observation. They found evidence of increased water inflow following deforestation in 28% of these wetlands, and in 55% of "swamps" (which included all non-lacustrine wetlands). Using a simple water balance model, they suggested that inflows to 9-12% of wetlands globally, and to 20-40% of Ramsar-designated wetlands, may have increased following deforestation during the Holocene. In an analysis of the timing of peat inception in the eastern Massif Central, France, Cubizolle *et al.* (2012) showed that peat inception in a large number of mires, and in particular small fens with shallow peat deposits located at relatively low altitude, could be related to the development of farming which led to both deforestation and the construction of small-scale water management structures.

If one excludes studies on the impact of urbanisation and irrigated agriculture, only a few studies have investigated the impact of catchment landuse on present wetland water balances. Using the MMS/PRMS hydrological model, Helmschrot (2006) evaluated the potential impact of catchment afforestation in a primarily grass-covered South-African catchment on several hydrogeomorphic wetland types. Forest-specific parameters were calibrated in a neighbouring afforested catchment and transposed to areas that were assumed to be planted in the wetland catchment. Runoff, interflow and groundwater discharge to wetland hydrological response units were predicted to decline substantially in nearly all cases, but with increasing magnitude depending on the hydrogeomorphic settings, from valley wetlands to slope wetlands and, most threatened, plateau wetlands located on hilltops and plateaux. In the prairie pothole region of North America, van der Kamp *et al.* (1999) reported that small runoff-fed prairie wetlands had dried out within a few years of conversion of their catchments from arable land to permanent brome grass, while no hydrological change could be evidenced in wetlands located in catchments

maintained under cultivation. Hydrological modelling confirmed the higher evapotranspiration and lower runoff rates under unmanaged grassland than under agricultural crops or managed grasslands and the associated decline in wetland inflows and water levels (Voldseth *et al.* 2007). Euliss & Mushet (1996) also showed that water level fluctuations were higher in prairie wetlands located in arable landscapes than in those located in grassland landscapes. Krause *et al.* (2007) modelled the impact of a number of complex landuse scenarios, including the development or reduction of forest cover, on the hydrology of a large floodplain wetland in Germany, using the IWAN model, which combines the WASIM-ETH-1 unsaturated zone and evapotranspiration model with the MODFLOW groundwater flow model. They found only minor effects of landuse on the floodplain water balance as alterations in vertical groundwater flow were counter-balanced by both groundwater lateral flow and the close interactions between surface water and groundwater within the floodplain.

8.3. Methods

The potential effects on the mire hydrology of large changes in landuse within the Dauges catchment were investigated by forcing the calibrated MIKE SHE / MIKE 11 model (Chapters 5 and 6) with new landuse maps, corresponding to two different catchment landuse scenarios: conifers and grassland (Figure 8-1). These scenarios were obtained by replacing all current vegetation classes but wetland and wet woodlands by either coniferous woodlands ("conifers" scenario) or pastures and meadows ("grassland" scenario). The scenarios did not include landuse change within the mire itself since mires have generally been left out of afforestation schemes in the Massif Central. On mineral soils within the mire catchment, a complete replacement of all current vegetation with either grassland or conifers was preferred to intermediate mixed scenarios in order to investigate the likely maximum range of impacts. In the Dauges catchment as in all uplands in Limousin, heathland was the dominant landuse until the second half of the 20th century, and a heathland scenario would have been more realistic. However, as explained in Section 5.4.3, very little information was found in the literature on the evapotranspiration characteristics of heathland, and therefore grassland was chosen as representative of the open habitat scenario. The model outputs for the common 01/01/2011-31/12/2013 period were compared with the baseline corresponding to the current situation, where deciduous woodlands cover most of the catchment (see Section 2.6.3 and Table 8-1). The overland flow convergence issue described in Section 6.3.5 prevented a longer run, for instance using the reconstructed precipitation and reference evapotranspiration time series detailed in Appendix E. Two water balance computations, covering the catchment and the wetland, were computed for each

landuse scenario. As for the water balance computation described in Section 7.3, the distinction between wetland and catchment was based on the presence or absence of peat soils to allow for a quantification of flow between the peat deposits and the underlying mineral substrate. Consequently, the spatial area covered by the wetland water balance does include a small proportion of vegetation classes other than open mire vegetation and wet woodlands (Table 8-1), and this small proportion was replaced by either coniferous woodlands or pastures and meadows.

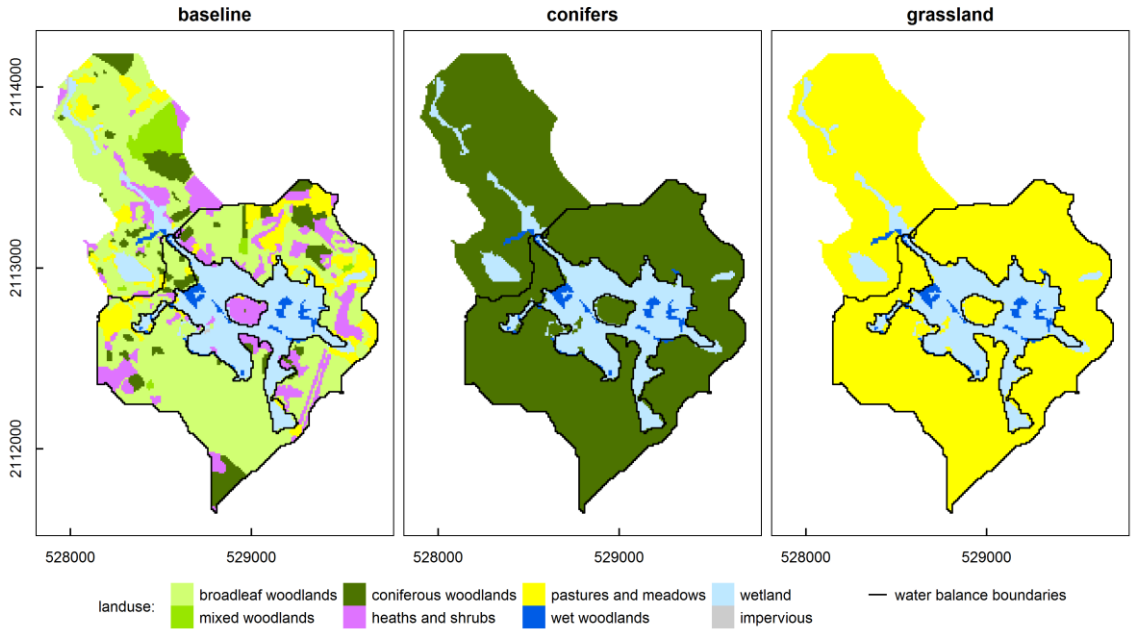

Figure 8-1. Distribution of vegetation classes in the catchment landuse scenarios.

Table 8-1. Frequency of vegetation classes within the wetland, catchment and combined water balance computation areas (baseline).

vegetation class	wetland WB (%)	catchment WB (%)	combined WB (%)
broadleaf woodlands	2.2	59.4	46.4
coniferous woodlands	0.6	8.7	6.8
heaths and shrubs	1.4	17	13.5
impervious	0.2	0	0
mixed woodlands	0	0.6	0.5
pastures and meadows	1.2	12.7	10.1
wet woodlands	8.3	0.2	2.1
wetland	86.2	1.3	20.7

The effect of landuse on discharge was investigated through the comparison of simulated time-series and flow exceedence curves at the four existing discharge monitoring stations. The effect on peat groundwater table depths was investigated using the model outputs at a selection of dipwells for which satisfactory to good model performance was achieved (see Section 6.2.1.5).

8.4. Results and discussion

Table 8-2 details the overall water balance and Figure 8-2 and Figure 8-3 the monthly water balance for the period 01/01/2011 to 31/12/2013, computed separately for the wetland and its catchment under the baseline and the two landuse scenarios. Model errors are compared in Figure 8-4, and monthly evapotranspiration rates within the catchment detailed in Figure 8-5. Since fluxes are expressed in mm, horizontal fluxes (boundary inflow or outflow, flow to or from watercourses) should not be directly compared between catchment and wetland water balances. The model predicts a substantial impact of catchment landuse on most hydrological components in both the mire and its catchment. The main impact is on the fraction of intercepted rainfall within the catchment, increased by +52% (+305mm) under the conifer scenario and reduced by -39% (-231mm) under the grassland scenario relative to the baseline, in which broadleaf woodland is the dominant landcover. In absolute terms, the difference between scenarios is lowest in winter (+1mm and -3mm under the conifer and grassland scenarios respectively in December 2011), when the evaporative demand is the smallest.

Table 8-2. Simulated impacts of catchment landuse on catchment and mire overall water balances (01/01/2011-31/12/2013).

water balance extent	**catchment**					**wetland**				
scenario	baseline	conifers		grassland		baseline	conifers		grassland	
unit	mm	mm	change (%)	mm	change (%)	mm	mm	change (%)	mm	change (%)
Precipitation	3679	3679	0.0	3679	0.0	3679	3679	0.0	3679	0.0
Evapotranspiration	1611	1746	8.4	1541	-4.3	2063	2065	0.1	2065	0.1
incl. from interception	585	890	52.2	354	-39.4	294	314	6.8	284	-3.5
incl. from ponded water	44	29	-33.2	55	25.5	1108	1080	-2.5	1123	1.3
incl. from UZ	957	800	-16.4	1109	15.9	265	267	0.9	266	0.5
incl. from SZ	25	27	5.4	23	-9.3	396	404	1.9	393	-0.9
OL boundary inflow	302	250	-17.4	304	0.4	5421	4611	-14.9	5553	2.4
OL boundary outflow	1594	1355	-15.0	1633	2.5	1063	881	-17.1	1069	0.6
OL to river	87	80	-7.9	89	3.0	8741	8445	-3.4	8594	-1.7
Infiltration from OL to UZ	2837	2571	-9.4	3041	7.2	468	477	1.8	469	0.2
Infiltration from OL to SZ	18	15	-18.5	19	3.1	25	25	0.4	25	0.9
Seepage from SZ to OL	966	880	-8.8	1016	5.2	2829	2748	-2.8	2861	1.1
Percolation from UZ to SZ	1894	1782	-5.9	1945	2.7	203	209	2.9	203	-0.3
SZ boundary inflow	275	275	-0.2	277	0.7	11	10	-4.8	11	2.0
SZ boundary outflow	1179	1154	-2.1	1188	0.8	1	1	-3.7	1	1.3
Lower to upper SZ layer	-	-	-	-	-	3127	3055	-2.3	3156	0.9
Upper to lower SZ layer	-	-	-	-	-	131	137	4.9	131	0.0
SZ to river exchange	10	9	-3.8	10	1.8	10	10	-0.5	10	0.4
River to SZ exchange	0	0	-3.0	0	-0.8	0	0	-11.4	0	0.6
Total error	247	162	-34.5	223	-9.7	-214	190	-188.7	-524	144.7
incl. overland error	218	133	-38.9	193	-11.7	-215	189	-187.8	-525	144.2
incl. UZ error	12	7	-38.8	13	4.4	0	0	92.4	0	-66.0
incl. SZ error	16	21	28.3	17	6.2	1	1	38.8	1	5.2

Percentages are percentage changes compared to the simulated water balance under the baseline (catchment mainly covered in deciduous woodlands).

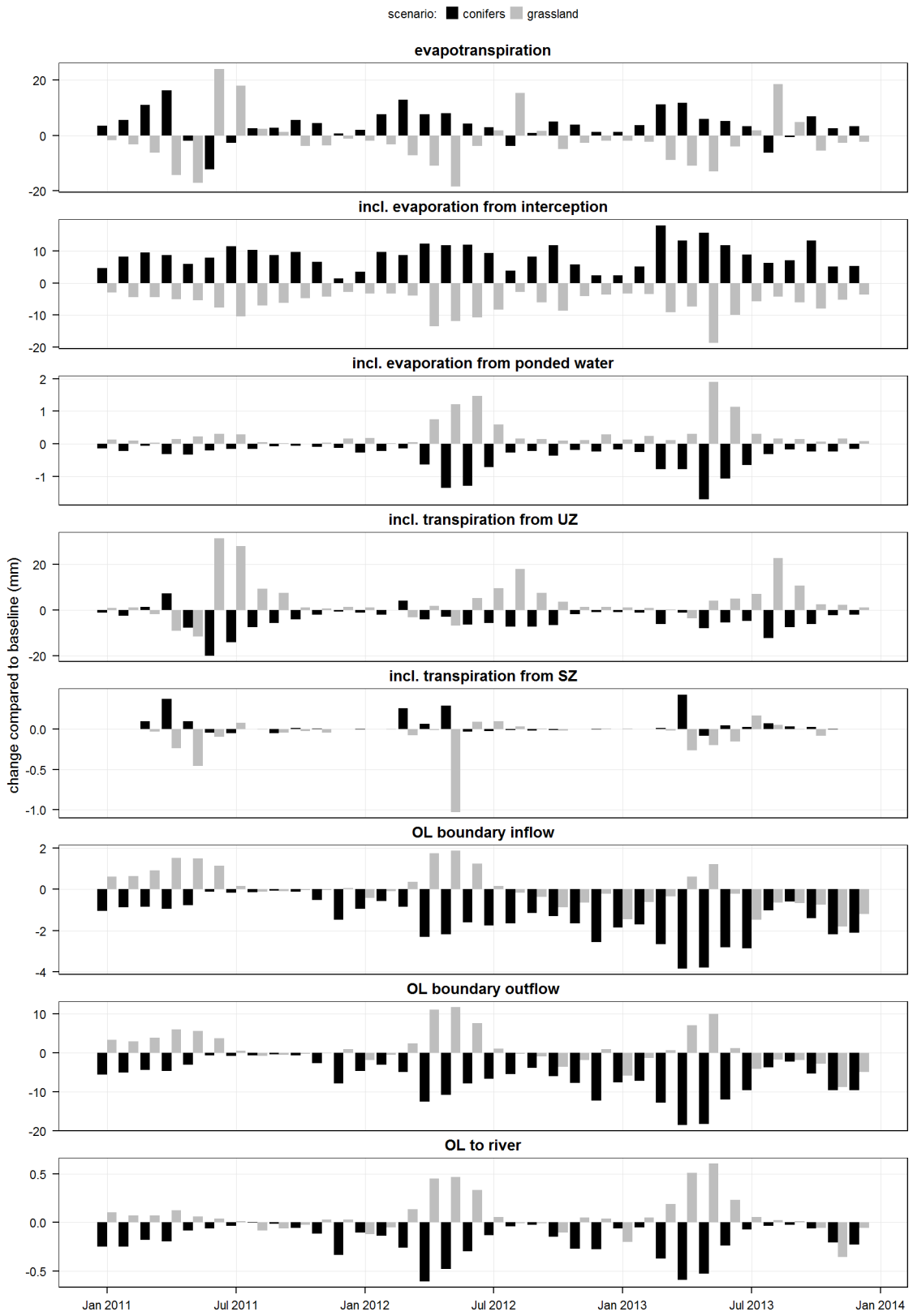

Figure 8-2. Simulated impacts of catchment landuse on the catchment monthly water balance (absolute changes relative to baseline, 01/01/2011-31/12/2013).

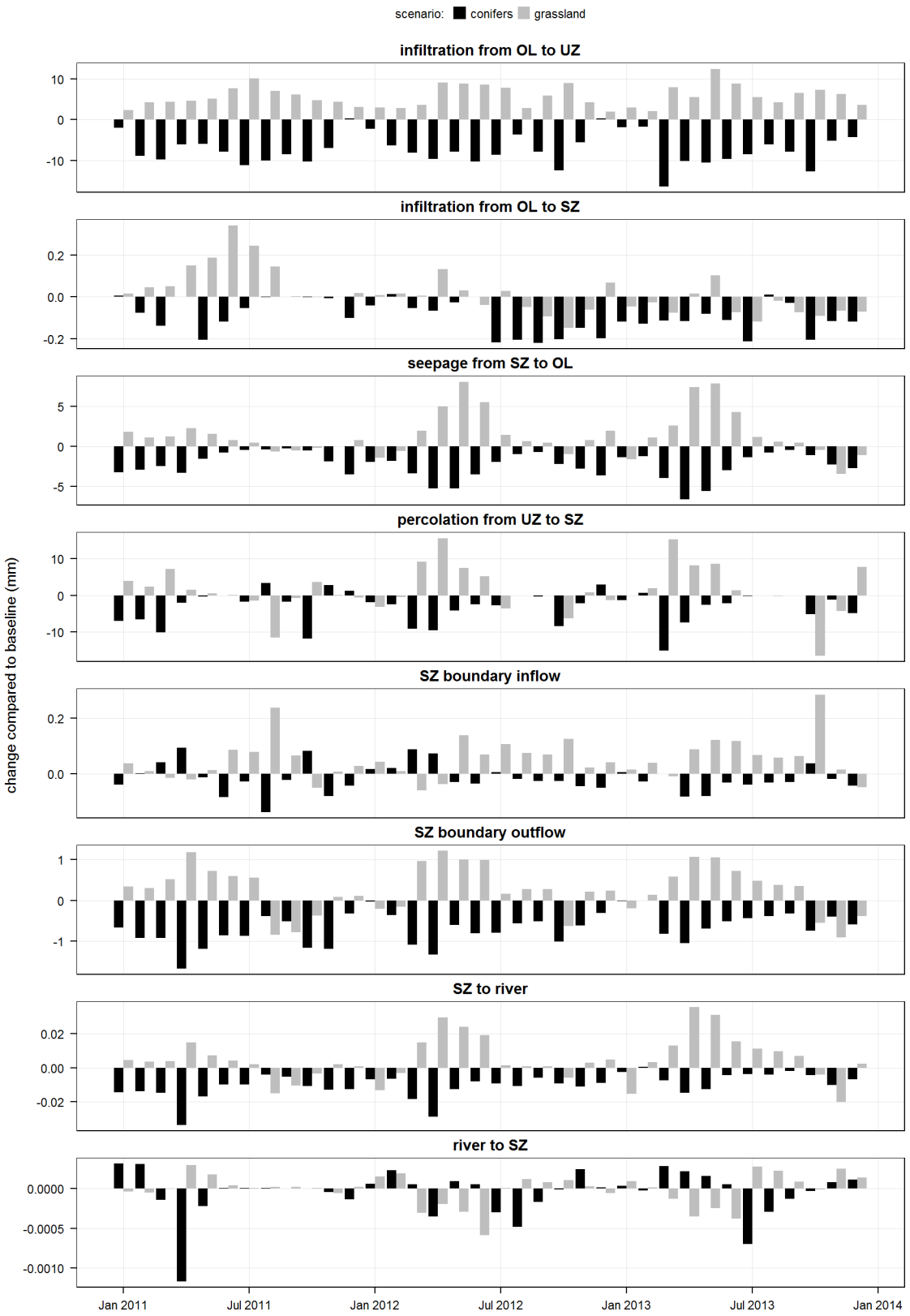

Figure 8-2 (continued). Simulated impacts of catchment landuse on the catchment monthly water balance (absolute changes relative to baseline, 01/01/2011-31/12/2013).

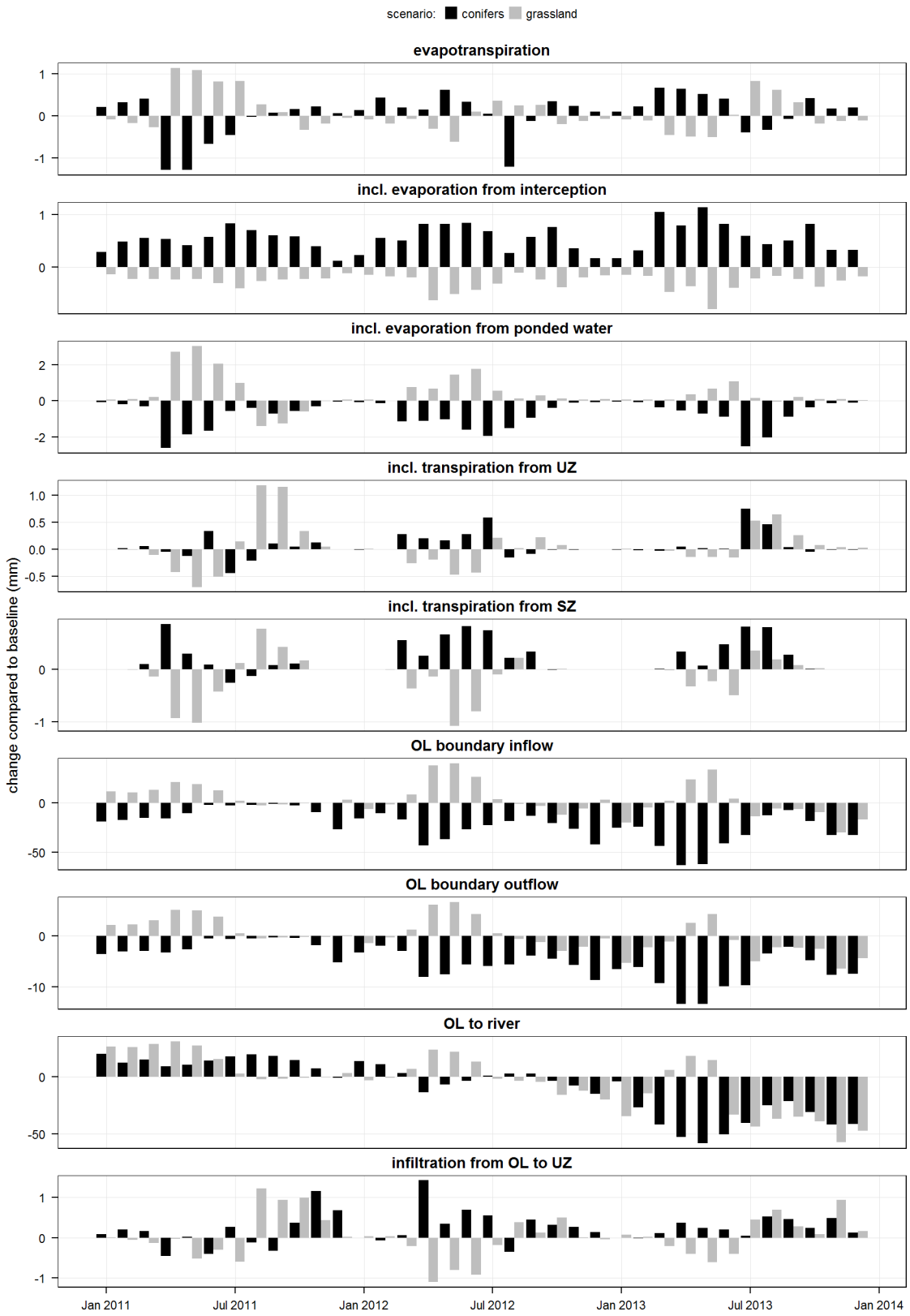

Figure 8-3. Simulated impacts of catchment landuse on the mire monthly water balance (absolute changes relative to baseline, 01/01/2011-31/12/2013).

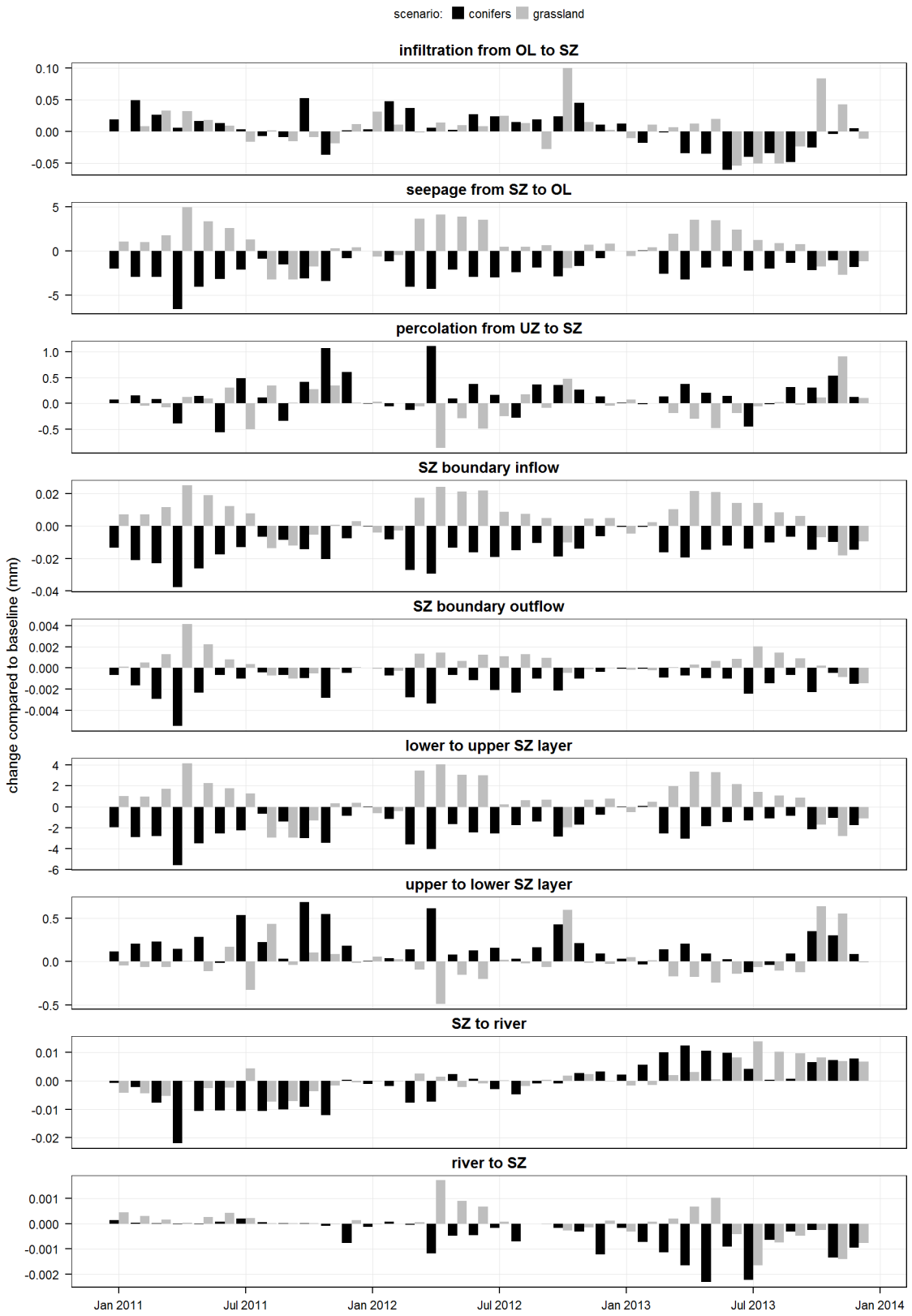

Figure 8-3 (continued). Simulated impacts of catchment landuse on the mire monthly water balance (absolute changes relative to baseline, 01/01/2011-31/12/2013).

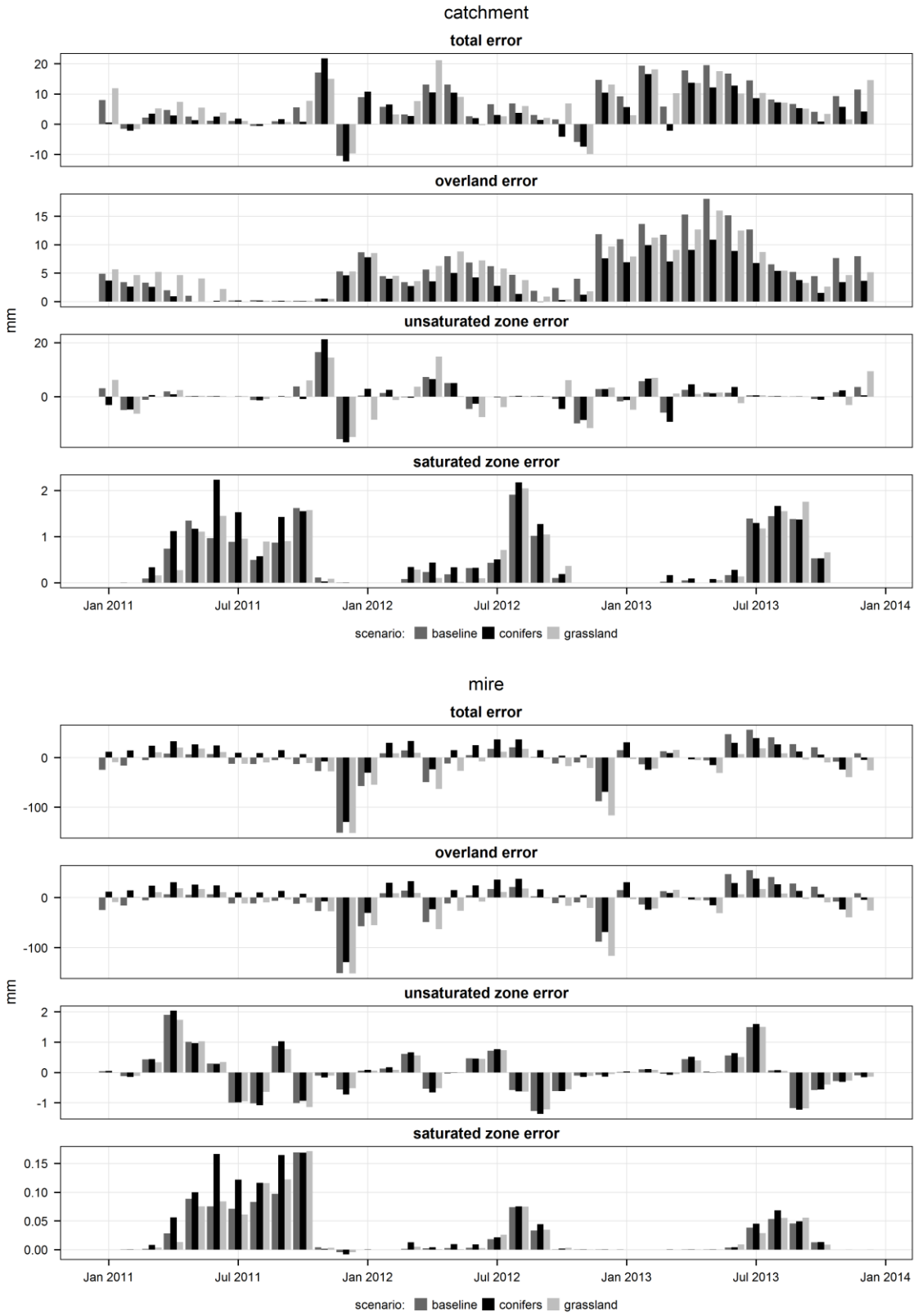

Figure 8-4. Impacts of catchment landuse on monthly water balance errors (01/01/2011-31/12/2013).

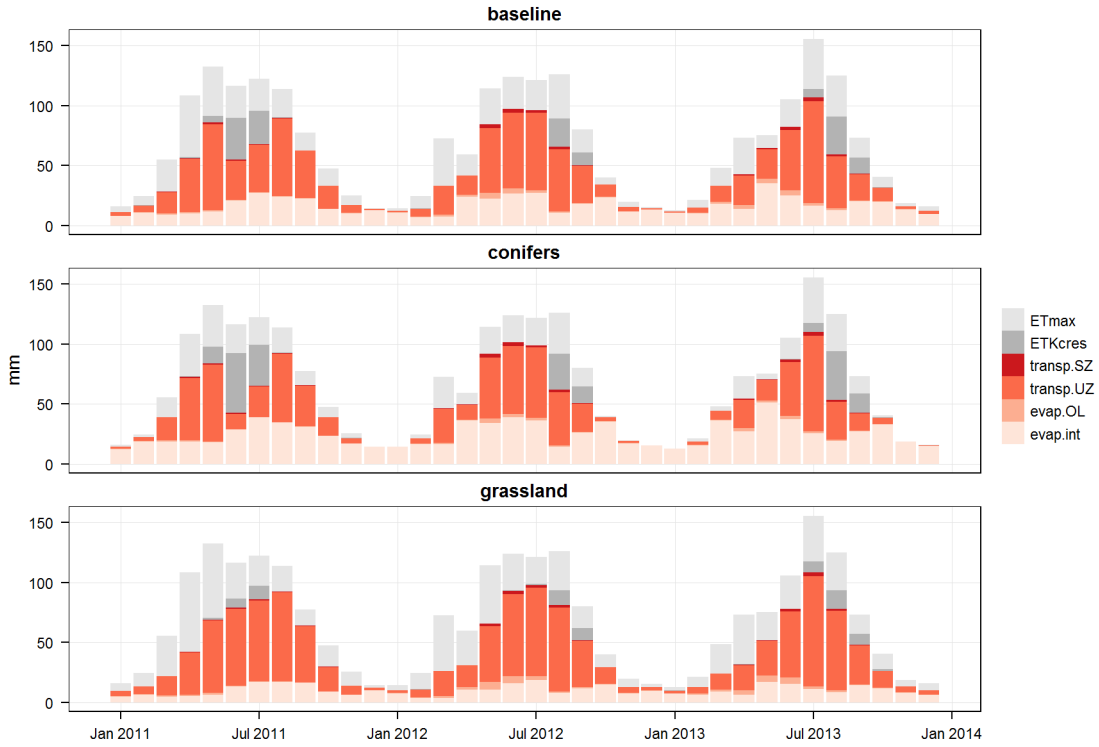

Figure 8-5. Simulated impacts of catchment landuse on evapotranspiration components within the catchment (01/01/2011-31/12/2013).

In shades of red: actual evapotranspiration, including transpiration from the saturated zone (transp.SZ), transpiration from the unsaturated zone (transp.UZ), evaporation from ponded water (evap.OL), and evaporation from interception (evap.int). The grey bars in the background give the constraints on evapotranspiration (cf. Section 5.4.2): maximum potential evapotranspiration (ETmax, equal to 1.16xETo), and crop potential evapotranspiration (ETKcres, equal to interception + ETo x Kc, capped to ETmax).

It is largest in spring and autumn (+18mm in March 2013 and -19mm in May 2013 under the conifer and grassland scenarios respectively), when interception in conifers increases due to an increased evaporative demand and relatively abundant precipitation, and interception by broadleaved trees is limited by leaf development or fall. It is intermediate in summer when precipitation are less frequent and abundant, particularly during the 2011 drought (Figure 8-2).

The model outputs (Table 8-2) suggest that part of this difference in interception is compensated by a lower evaporation from ponded water (-15mm, or -33%) and lower transpiration from the unsaturated zone (-157mm, or -16%) under the conifer scenario relative to the baseline, and a higher evaporation from ponded water (+11mm, or +26%) and higher transpiration from the unsaturated zone (+152mm, or +16%) under the grassland scenario. The lower evaporation from ponded water under conifer cover compared to the baseline, and under the baseline compared to the grassland scenario, can be explained by differences in interception, in throughfall and, therefore, in runoff, as evidenced by the lower boundary outflow under the conifer scenario than under the baseline (-182mm, or -17%). However the higher transpiration from the unsaturated zone under grassland cover is surprising given the similarity of summer crop coefficients

between conifers, broadleaf woodlands and grasslands (0.78, 0.77 and 0.80 respectively), the larger winter crop coefficient in conifers than in both broadleaf woodlands and grasslands (0.60, 0.38 and 0.35 respectively), and the larger root depth in woodlands than in grasslands (2m vs. 0.9m). One explanation could be that, since actual evapotranspiration is limited by the maximum potential evapotranspiration, a high interception for conifers restricts the residual evaporative demand for transpiration from the unsaturated zone. Figure 8-5 shows that this is indeed the case from October to February. However, Figure 8-2 shows that the difference between landcovers in transpiration from the unsaturated zone is actually largest in late summer when, surprisingly, it results in a higher actual evapotranspiration under the grassland scenario than under the baseline and conifer scenario in June and July 2011 and August 2012 and 2013. During these periods, Figure 8-5 shows that, under the grassland scenario, transpiration from the unsaturated zone constantly proceeds to almost full crop-specific potential rate (ETo x Kc), i.e. is rarely limited by soil moisture. Conversely, a large proportion of the crop-specific potential evapotranspiration is not fulfilled under the baseline and the conifer scenario, i.e., transpiration from the unsaturated zone is strongly limited by soil moisture. This is unexpected given the larger root depth of trees compared to grassland species, which in theory should allow them to draw from larger soil water reserves.

Close examination of the model gridded outputs shows that the minimum water content in the root zone, below which transpiration ceases, differs from the user-specified soil moisture content at wilting point, and differs between landuses: it is 0.6025 under coniferous, mixed and broadleaf woodlands, 0.4966 under grassland and 0.4708 under heathland & shrubs, well above the 0.01 calibrated value. The identical value under coniferous, mixed and broadleaf woodlands suggests that this issue is related to root depth since this is the only common parameter between these landuse classes. Tests with a simplified model in which landuse classes differed only by their root depth showed that this issue only occurs when root depth exceeds the depth of the saturated zone upper computational layer. When root depth is shallower than the upper computational layer, transpiration proceeds until the user-specified wilting point is reached. Using the simplified model, setting precipitation to zero and forcing evapotranspiration until the soil moisture content stabilises, it was found that the minimum soil moisture given by MIKE SHE when the root depth is larger than the depth of the upper computational depth is the average of the moisture content at wilting point and of the moisture content at saturation, weighted by the proportion of the root zone above and below the depth of the upper computational layer respectively. In other words, in unsaturated conditions, the two-layer model does not draw water

from the part of the root zone located below the bottom of the upper computational layer. Since root depths of vegetation classes found on mineral ground are always larger than the depth of the upper computational layer, this means that the model does not account for differences in root depth between vegetation classes. It therefore predicts that coniferous woodlands are more often under hydric stress than deciduous woodlands, and woodlands than grassland, simply because the higher interception leads to a lower infiltration to the unsaturated zone and therefore, since the depth from which vegetation can draw water is the same for all vegetation classes, a lower overall volume of water available for transpiration. This shows that, under the current conditions, the two-layer model may not adequately model some aspects of evapotranspiration and unsaturated flow. This methodological issue does not appear to have been described in any MIKE SHE-related publication, in particular in the software manuals (Anonymous 2009b; c).

To improve the unsaturated zone model, the depth of the upper computational layer should be increased to the maximum root depth (2m), but this would require a complete recalibration of the model. Furthermore, since the depth of the upper computational layer should be maintained to its current value within the wetland area to adequately model vertical groundwater flow, this may cause other computational issues along the wetland margins. The gravity or Richards unsaturated flow models might not be subject to the same issue and may produce more realistic results. However, as described in Section 5.3.1.1, they would require a much more detailed description of hydro-physical characteristics of both soils and fissured granite and would impose considerable computational burden.

Interestingly, the overriding of root depth in the two-layer unsaturated zone model explains why the calibrated available water capacity had to be increased beyond physically realistic values (Section 6.4.4): the very large value, in effect only applied to the first 50cm of the unsaturated zone, compensates for the reduced depth from which vegetation can draw water. In the case of woodlands, which cover most of the catchment under the baseline, the effective available water capacity is not 0.69 but 0.0975. This figure is very close to the 0.07 value used in the uncalibrated model based on data recorded by van den Bogaert (2011) on soils similar to those found within the Dauges catchment (Section 5.4.2). Consequently, the impact of the root depth issue does not undermine the validity of the baseline model, nor of the comparison between the baseline and the conifer scenario since broadleaf and evergreen woodlands have the same root depth. However, the simulated impacts of the grassland scenario on the catchment and mire hydrology

should be interpreted with caution since, in this case, differences in root depth between landuses are not properly accounted for.

As a consequence of the overestimation of transpiration under vegetation with shallower root depths, the effect of landuse on overall actual evapotranspiration is predicted to be smaller than on evaporation from interception: it increases by +8% (+135mm) under the conifer scenario and decreases by -4% (-70mm) under the grassland scenario. The increased interception under the conifer scenario leads to a reduction in overland flow. Overland outflow from the catchment is reduced by -239mm, or -15% (slightly increased by +39mm, or +3%, under the grassland scenario), and overland flow to watercourses upstream of the mire is reduced by -7mm, or -8% (increased by +2mm, or +3%, under the grassland scenario). These effects are particularly important in spring (after the end of the leafing period in deciduous trees), probably due to a combination of a relatively large potential evapotranspiration resulting in larger differences in throughflow between scenarios, a small post-winter deficit in the unsaturated zone and a high groundwater table that lead to rapid saturation and saturation-excess runoff in the lower slopes, and a rapid propagation of these differences to runoff and stream discharge volumes. Later in the year soil moisture contents are lower, more throughflow can infiltrate before runoff occurs, and therefore differences in interception between scenarios do not translate as strongly into differences in runoff and stream discharge.

Within the catchment, the increase in interception and the reduction in throughfall under conifers result in a decrease in infiltration, whereas it increases under the grassland scenario. This is the case for infiltration from overland to the unsaturated zone (-266mm, or -9% under the conifer scenario; +204 or +7% under the grassland scenario) and from overland to the saturated zone (-3mm or -19% vs. +1mm or +3%). It is also the case for percolation from unsaturated zone to the saturated zone (-112 or -6% vs. +51mm or +3%). The larger simulated impact of landcover on infiltration from overland to the unsaturated zone than on percolation from unsaturated zone to the saturated zone results from the higher transpiration from the unsaturated zone under grassland cover than under conifers, as described above. The impact of landcover on infiltration from overland to the unsaturated zone follows seasonnal patterns in reference evapotranspiration and evaporation from interception, and is therefore larger in summer, when evaporation from interception is less limited by potential evapotranspiration and the difference in interception between landcovers is larger (Figure 8-2). The larger infiltration from overland to unsaturated zone under the grassland scenario is partly compensated for by the substantially higher transpiration from the unsaturated zone under grassland than under both conifers and

baseline in late summer. As a consequence the impact of landcover on groundwater recharge is most noticeable from March to June, and is more variable in late summer. The model even suggests a substantially lower percolation from the unsaturated zone to the saturated zone under the grassland scenario than under the baseline during one or two months a year (August 2011, October 2012, October and November 2012, Figure 8-2), but the reason for this is not entirely clear.

Impacts of landcover types on infiltration have a delayed knock-on effect on groundwater outflow from the catchment: overall, it is reduced by -25mm (-2%) under the conifer scenario and increased by +9mm (+1%) under the grassland scenario. However Figure 8-2 shows that this impact varies throughout the year. On average, groundwater outflow is reduced under the conifer scenario and increased under the grassland scenario during the first 6-8 months of the year, but slightly reduced under both scenarios relative to the baseline later in the year. Groundwater seepage also follows a similar seasonal pattern: it is generally reduced under conifers (-86mm, or -9%) and increased under grassland (+50mm, or +5%), but the difference between scenarios is noticeable only in spring and early summer, and almost null later on. The model error differs substantially between landuse scenarios: it is reduced by -85mm (or -35%) under the conifer scenario and by -25mm (-10%) under the grassland scenario. This is mostly due to a reduction in error in the overland flow component. The apparent correlation between changes in monthly overland error and in monthly overland inflow and outflow under the conifer scenario (Figure 8-2 and Figure 8-4) suggests that, for this scenario, the reduction in error is linked to the reduction in overland flow. However the reason for the reduction in overland error under the grassland scenario is not clear.

Changes in catchment outflow (overland outflow, saturated zone outflow) translate into similar changes in inputs to the mire. Runoff inflows for instance are reduced by -810mm (-15%) under the conifer scenario but increased by +132mm (+2%) under the grassland scenario. Vertical groundwater upwelling is reduced by -72mm (-2%) under the conifer scenario while it increases by +29mm (+1%) under the grassland scenario. Conversely, downward saturated flow from the peat layer to the underlying mineral formations is increased by +6mm (+5%) under the conifer scenario, but is stable under the grassland scenario. Temporal patterns logically follow those described above for overland and groundwater flow out of the catchment. Seepage from the saturated zone to overland is reduced by -81mm (-3%) under the conifer scenario (+32mm or +1% under the grassland scenario). Temporal patterns in the impact of landuse on groundwater seepage within the mire follow those in groundwater outflow from the catchment, with larger

and more contrasted impacts in spring than in late summer. Seepage is reduced all year round under the conifer scenario. Under the grassland scenario, seepage is increased in spring and early summer (+5mm in April 2011) but stable or reduced in late summer and autumn, as a result of the higher transpiration from the unsaturated zone and stable or lower percolation to the saturated zone in summer within the mire catchment described above. Changes in groundwater upwelling from mineral formations to the peat layer, leading to changes in groundwater table depth as evidenced by changes in groundwater seepage from the peat layer to overland flow, also result in changes in infiltration rates as a result of a deeper and more widespread unsaturated zone. Under the conifer scenario, infiltration from overland to unsaturated peat increases by +9mm or +2% (almost unchanged under the grassland scenario), and percolation from unsaturated to saturated peat increases by +6mm or 3% (stable under the grassland scenario). However monthly patterns are complex, probably reflecting local variability and interactions between precipitation, evapotranspiration and groundwater upwelling.

Under the conifer scenario, the model predicts a reduction in overland inputs from the mire to watercourses (-296mm, or -3%). This is also the case under the grassland scenario (-147mm, or -2%), which is suprising given the simulated increases in overland and groundwater inputs to the mire, in groundwater seepage within the mire, the absence of change in evapotranspiration and the negligible change in infiltration to both unsaturated and saturated zones within the mire (Table 8-2). This counter-intuitive result is possibly a consequence of the overland flow component convergence issue, which led to an error twice as large under the grassland scenario as under other scenarios. As a whole over the simulation period, overland outflows, and therefore in all likelihood overland inputs to watercourses, which represent the bulk of overland outflows, are underestimated under the grassland scenario and the baseline, whereas they are overestimated under the conifer scenario. The total error of the mire water balance represents 4.2% of the total inputs under the grassland scenario, but only 1.7% under the baseline and conifer scenario. This calls for differences in discharge between the baseline and the grassland scenario particularly to be interpreted with care. Within the mire, slight changes in interception and evapotranspiration are caused by landuse changes imposed onto the small proportion of habitats other than open wetland habitats and wet woodland that grow on peat soils under the baseline.

Figure 8-6 and Figure 8-7 show the simulated discharge and simulated flow exceedence curves respectively at the four monitoring stations under the different landuse scenarios for the period 01/01/2011 to 31/12/2013. Table 8-3 gives changes in flow exceedence quantiles and mean

discharge relative to the baseline (note that discharge is given in $l.s^{-1}$, and not $m^3.s^{-1}$, to improve readability). The simulated effect of the conifer scenario on discharge in the small streams in the upstream part of the wetland is very clear: there is a substantial reduction of flow all year round. The effect is stronger in relative terms at low flow, with a 23% to 50% reduction in the minimum discharge and a 17% to 30% reduction of Q95, but larger in absolute terms during peak flows. The magnitude of the changes decreases in relative terms for higher flow quantiles, but the maximum discharge is still reduced by 1 to 5% under the conifer scenario. Mean discharge is reduced by 8% at both Girolles and Rocher. Change seems to be particularly large at Marzet: the model simulates a 27% reduction in mean flow under the conifer scenario.

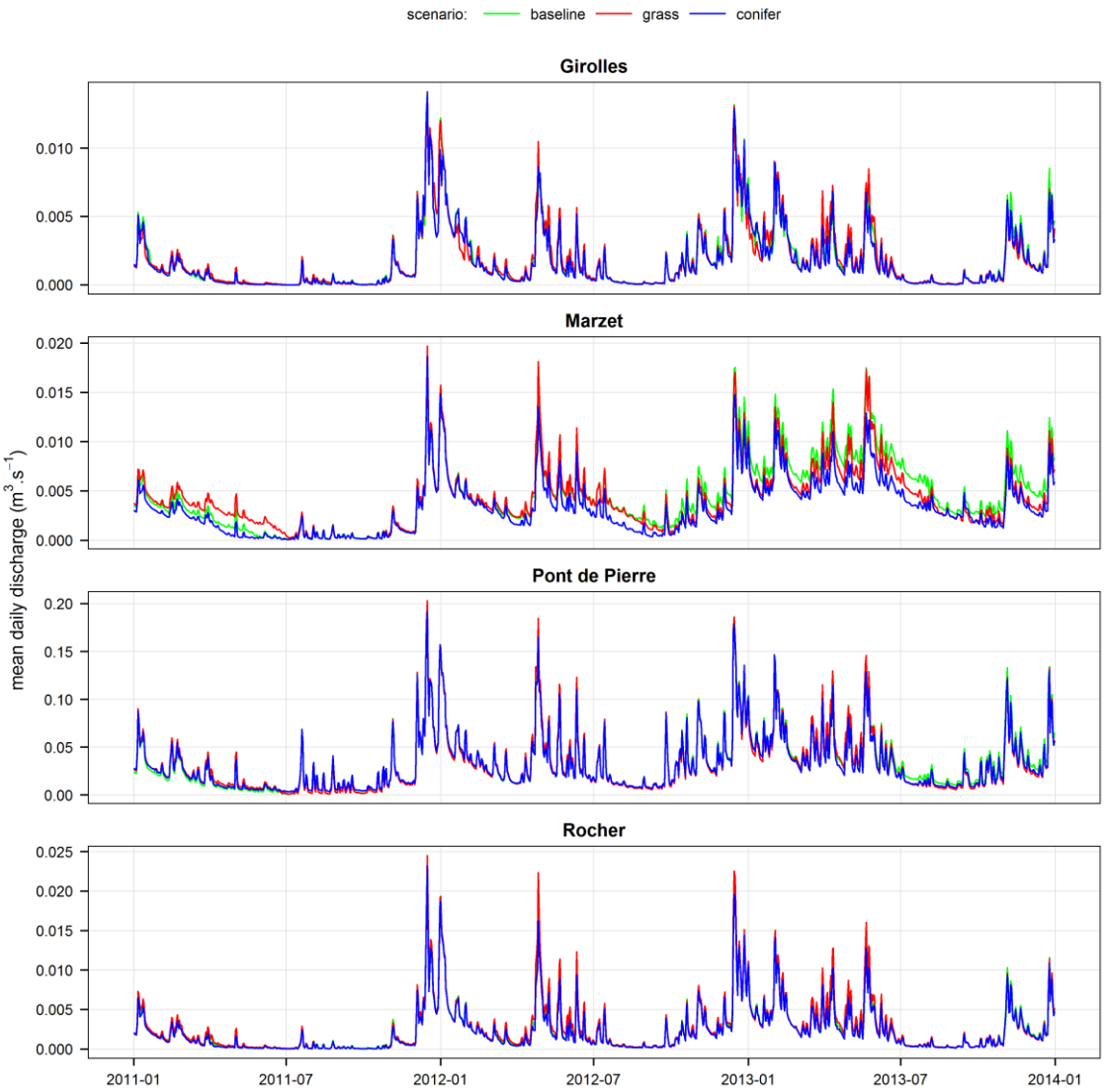

Figure 8-6. Impacts of catchment landuse on simulated daily discharge at the four discharge monitoring stations (01/01/2011-31/12/2013).

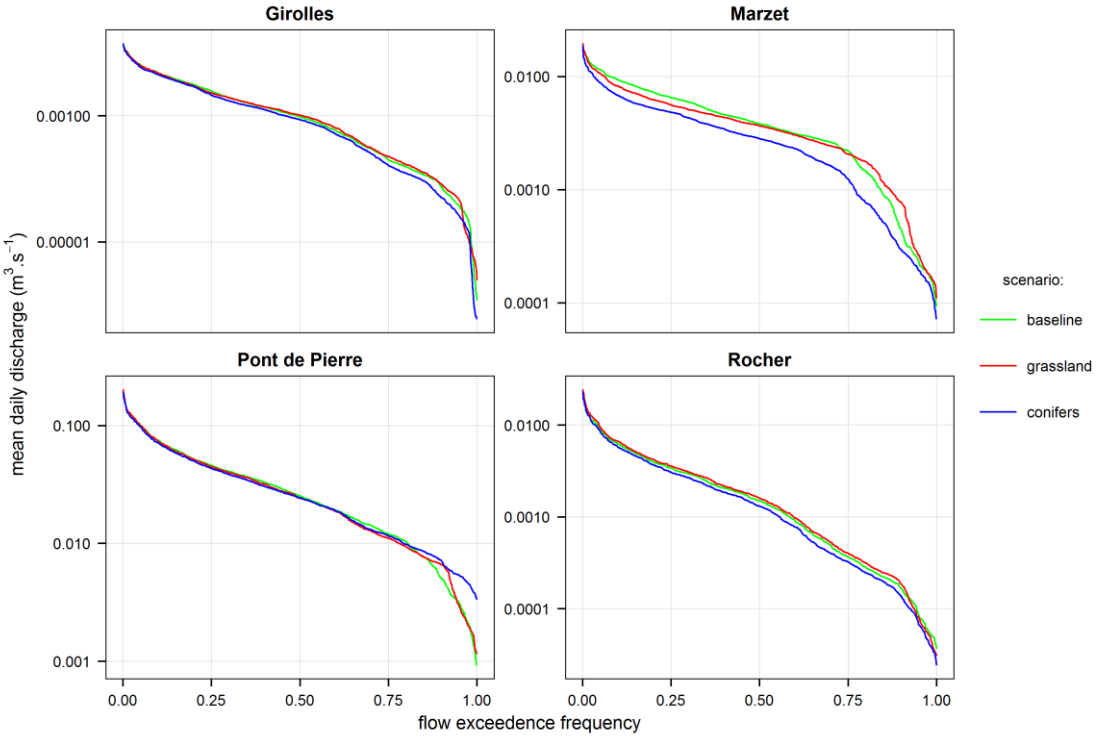

Figure 8-7. Impacts of catchment landuse on simulated flow exceedence frequency curves at the four discharge monitoring stations (01/01/2011-31/12/2013).

Table 8-3. Change (and percent change in brackets) in simulated stream flow quantiles and mean flow ($l.s^{-1}$) under conifer and grassland catchment landuse scenarios relative to the baseline (01/01/2011-31/12/2013).

	conifer				grassland			
measure	Girolles	Marzet	Rocher	Pont-de-Pierre	Girolles	Marzet	Rocher	Pont-de-Pierre
Q100 (min)	-0.00 (-49.3)	-0.02 (-23.0)	-0.01 (-33.5)	2.42 (261.2)	0.00 (108.9)	0.02 (17.8)	-0.01 (-16.3)	0.23 (24.4)
Q95	-0.01 (-30.1)	-0.04 (-16.9)	-0.02 (-22.1)	2.25 (72.2)	0.01 (23.6)	0.03 (12.7)	-0.00 (-5.7)	-0.23 (-7.3)
Q75	-0.04 (-18.6)	-0.96 (-43.6)	-0.04 (-11.5)	-0.40 (-3.4)	0.03 (13.2)	-0.15 (-6.7)	0.04 (10.0)	-0.95 (-7.9)
Q50	-0.09 (-9.3)	-1.01 (-26.3)	-0.19 (-12.4)	-0.91 (-3.6)	0.06 (5.8)	-0.16 (-4.1)	0.09 (6.3)	-1.21 (-4.8)
Q25	-0.38 (-15.0)	-1.68 (-25.8)	-0.35 (-10.1)	-2.65 (-5.8)	-0.19 (-7.5)	-0.89 (-13.7)	0.18 (5.2)	-0.96 (-2.1)
Q05	-0.56 (-8.6)	-2.69 (-23.4)	-0.85 (-9.2)	-3.40 (-3.4)	-0.23 (-3.6)	-0.85 (-7.4)	0.28 (3.1)	-1.31 (-1.3)
Q0 (max)	-0.09 (-0.7)	-0.82 (-4.2)	-1.24 (-5.1)	-9.94 (-4.9)	0.02 (0.1)	0.16 (0.8)	0.04 (0.2)	1.24 (0.6)
$\bar{Q}$	-0.14 (-7.8)	-1.23 (-27.0)	-0.21 (-8.2)	-1.22 (-3.6)	-0.01 (-0.5)	-0.35 (-7.6)	0.14 (5.6)	-0.57 (-1.7)

The simulated values at the main wetland outlet at Pont-de-Pierre are surprising: there seem to be a 3-6% decrease in most flow quantiles and a 4% decrease in total flow, a much lower change than in the upstream reaches, and a very large increase in relative terms of the lower flow quantiles: +72% for Q95 and +261% for the minimum discharge. These results are difficult to explain. The decrease in all flow quantiles and in total flow in the upstream reaches suggests that the processes involved are to be found within the wetland. A potential explanation for the lower effect of the conifer scenario at the mire outlet than in the upstream reaches could have been a compensation of the lower inflows by a lower evapotranspiration within the mire following a drop in the groundwater table depth, however the water balance computation does

not support this: evapotranspiration within the mire is almost identical under all three scenarios. Furthermore this would not explain the very large increase in Q95 and Q100. Another explanation could lie in the overland model convergence issue. The minimum and maximum flow values, in particular, would be very sensitive to model errors. Changes simulated under the grassland scenario are more difficult to interpret than those of the conifer scenario. The strength and direction of the impact is quite variable depending on the indicator and the location and no clear conclusion can be drawn from the model results. Total flow seems relatively stable at Girolles (-0.5%), to increase at Rocher (+5.6%), to slightly decrease at Pont-de-Pierre (-1.7%) and to decrease more substantially at Marzet (-7.6%). Overall, there seems to be relatively little difference between the baseline and grassland scenarios. These results are unexpected given the large number of studies demonstrating a larger water yield under grassland cover than under woodland cover (Appendix H). This is most probably a consequence of the methodological issues in soil moisture and overland flow modelling described above, that lead to an underestimation of stream discharge under the grassland scenario relative to the baseline.

Figure 8-8 and Figure 8-9 show the simulated groundwater table depth and simulated groundwater table depth exceedence frequency curves in selected dipwells installed in the peat for the different catchment landuse scenarios. Table 8-4 gives for each scenario the percentage of time during which the simulated groundwater table depth falls below specified depths below ground level. As described above, results are only shown for the locations where the model performed well. In all these dipwells, the impact of landuse within the mire catchment is clearly negligible in winter when the groundwater table depth is at ground level. At this time of the year, the impact of landuse on the water balance of the catchment, in particular on interception and on infiltration to the saturated zone, is limited by the low reference evapotranspiration, as shown in Figure 5-19 and Figure 5-21. As a consequence there is little difference between scenarios in terms of inputs to the mire, in particular with regard to groundwater upwelling (Figure 8-3). Furthermore inputs to the mire far exceed the outputs through evapotranspiration and groundwater losses to the river network (Figure 7-8), and a very large reduction in groundwater upwelling would be required to have an impact on groundwater table depth in peat.

Conversely, there is a clear effect of catchment landuse on groundwater table depths within the mire in summer, but this effect seems limited to the sloping and marginal part of the mire, as evidenced by dipwells D3 and D13 (Figure 8-8, Figure 8-9 and Table 8-4). In these dipwells, summer groundwater table depths are lower by up to 20cm under the conifer scenario than under the baseline.

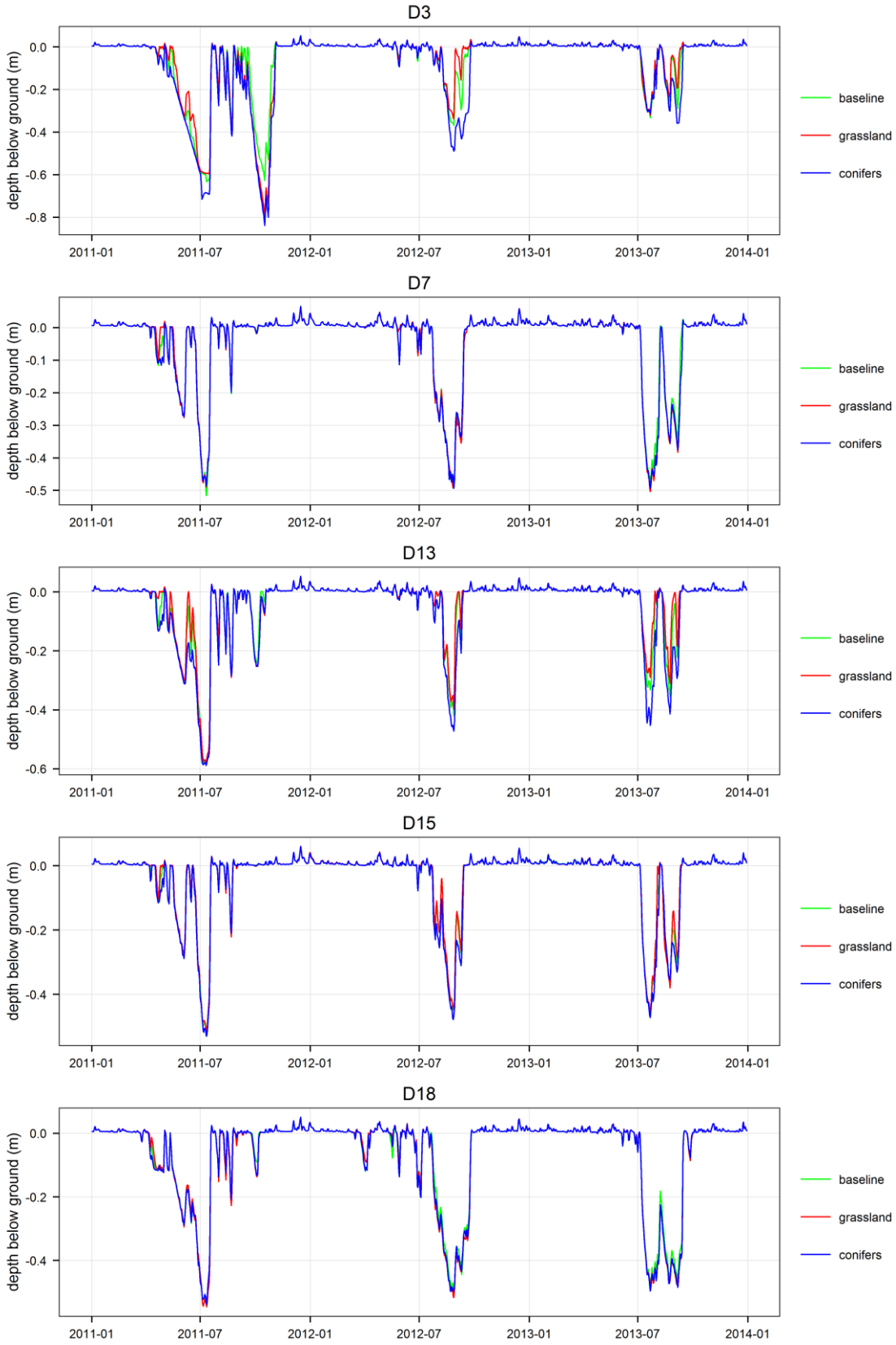

Figure 8-8. Impacts of catchment landuse on simulated groundwater table depth in a selection of dipwells within the mire (01/01/2011-31/12/2013).

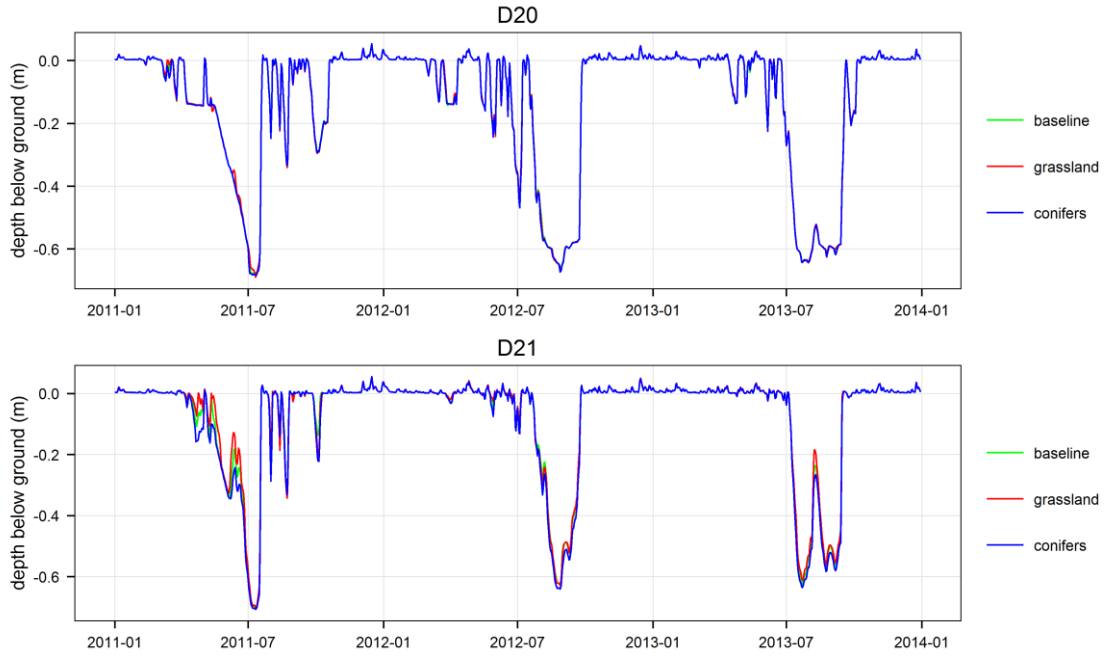

Figure 8-8 (continued). Impacts of catchment landuse on simulated groundwater table depth in a selection of dipwells within the mire (01/01/2011-31/12/2013).

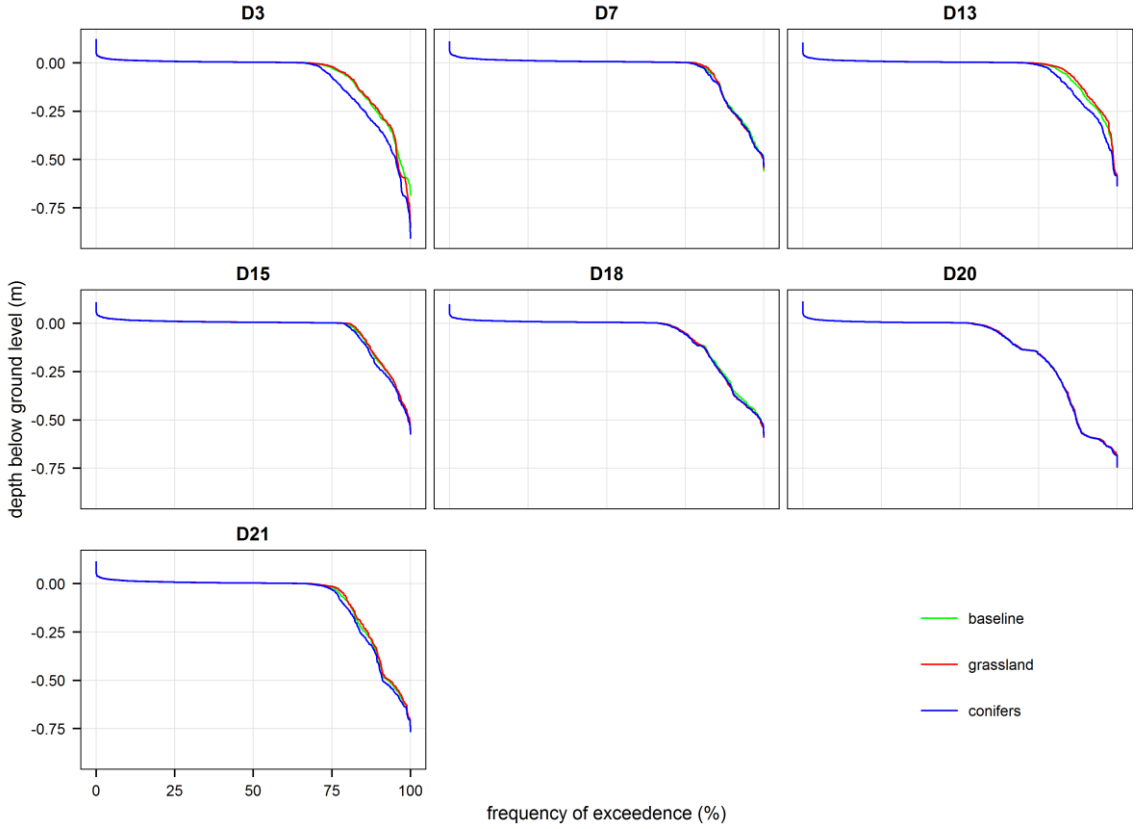

Figure 8-9. Impacts of catchment landuse on simulated groundwater table depth exceedence frequency curves in a selection of dipwells within the mire (01/01/2011-31/12/2013).

Table 8-4. Impacts of catchment landuse on the number of days per year with a simulated groundwater table depth deeper than 0, -0.1 and -0.2m below ground in a selection of dipwells within the mire (01/01/2011-31/12/2013).

GWT (m)	scenario	D3	D7	D13	D15	D18	D20	D21
0	baseline	117.7	83.7	102.7	75.3	121.0	170.3	119.0
	grassland	116.7 (-0.8%)	78.7 (-6.0%)	99.0 (-3.6%)	74.3 (-1.3%)	119.7 (-1.1%)	168.0 (-1.4%)	115.0 (-3.4%)
	conifers	125.0 (+6.2%)	87.0 (+3.9%)	107.3 (+4.5%)	78.7 (+4.5%)	122.3 (+1.1%)	170.7 (+0.2%)	121.7 (+2.3%)
-0.1	baseline	65.7	52.7	50.7	51.7	78.7	122.7	72.3
	grassland	64.3 (-2.1%)	52.7 (0.0%)	45.7 (-9.9%)	51.0 (-1.4%)	79.0 (+0.4%)	122.3 (-0.3%)	71.7 (-0.8%)
	conifers	85.0 (+29.4%)	55.3 (+4.9%)	62.7 (+23.7%)	54.0 (+4.4%)	81.7 (+3.8%)	122.3 (-0.3%)	79.0 (+9.3%)
-0.2	baseline	47.3	44.0	32.0	36.7	56.3	80.3	60.7
	grassland	46.3 (-2.1%)	43.7 (-0.7%)	28.0 (-12.5%)	35.3 (-3.8%)	58.7 (+4.3%)	81.0 (+0.9%)	57.7 (-4.9%)
	conifers	63.3 (+33.8%)	43.7 (-0.7%)	42.3 (+32.2%)	42.0 (+14.4%)	58.7 (+4.3%)	80.7 (+0.5%)	63.7 (+4.9%)

The amount of time during which the groundwater table is deeper than ground level, -0.1m and -0.2m below ground level is increased by 5-7, 12-19 and 10-16 days per year respectively (+5-6%, +24-29%, +32-34% respectively, Table 8-4).

The effect of the grassland scenario is opposite, even though smaller in absolute value. Again in dipwells D3 and D13, the summer groundwater table depth is generally reduced, except in dipwell D3 in the autumn of 2011 (Figure 8-8, Figure 8-9). The amount of time during which the groundwater table is deeper than ground level, -0.1m and -0.2m is reduced by 1-4, 1-5 and 1-4 days per year, respectively (-1% to -4%, -2% to -10% and -2% to -12% respectively, Table 8-4). The impact of catchment landcover is much smaller to negligible in the centre of the mire, where dipwells D7, D15, D18 and D21 are located. However, where a small impact exists it follows the same direction as that predicted on the mire sloping margins (see D21 in early summer 2011, D15 in summers 2012 and 2013 in Figure 8-8 for instance, and Table 8-4).

The stronger impact of catchment landcover on groundwater table depths along the mire margins than at its centre is also noticeable in Figure 8-10 and Figure 8-11. They both show change in simulated monthly mean groundwater table depth under the conifer scenario relative to the baseline for the period 01/01/2011-31/12/2013. Figure 8-10 shows the entire catchment whereas Figure 8-11 only shows the model grid cells located on peat soils upstream of the wetland outlet at Pont-de-Pierre. Figure 8-10 shows a decrease in groundwater table levels of up to about 2m under the conifer scenario. The effect is strongest on the catchment margins and in late spring and early summer, and lowest within the wetland and in autumn.

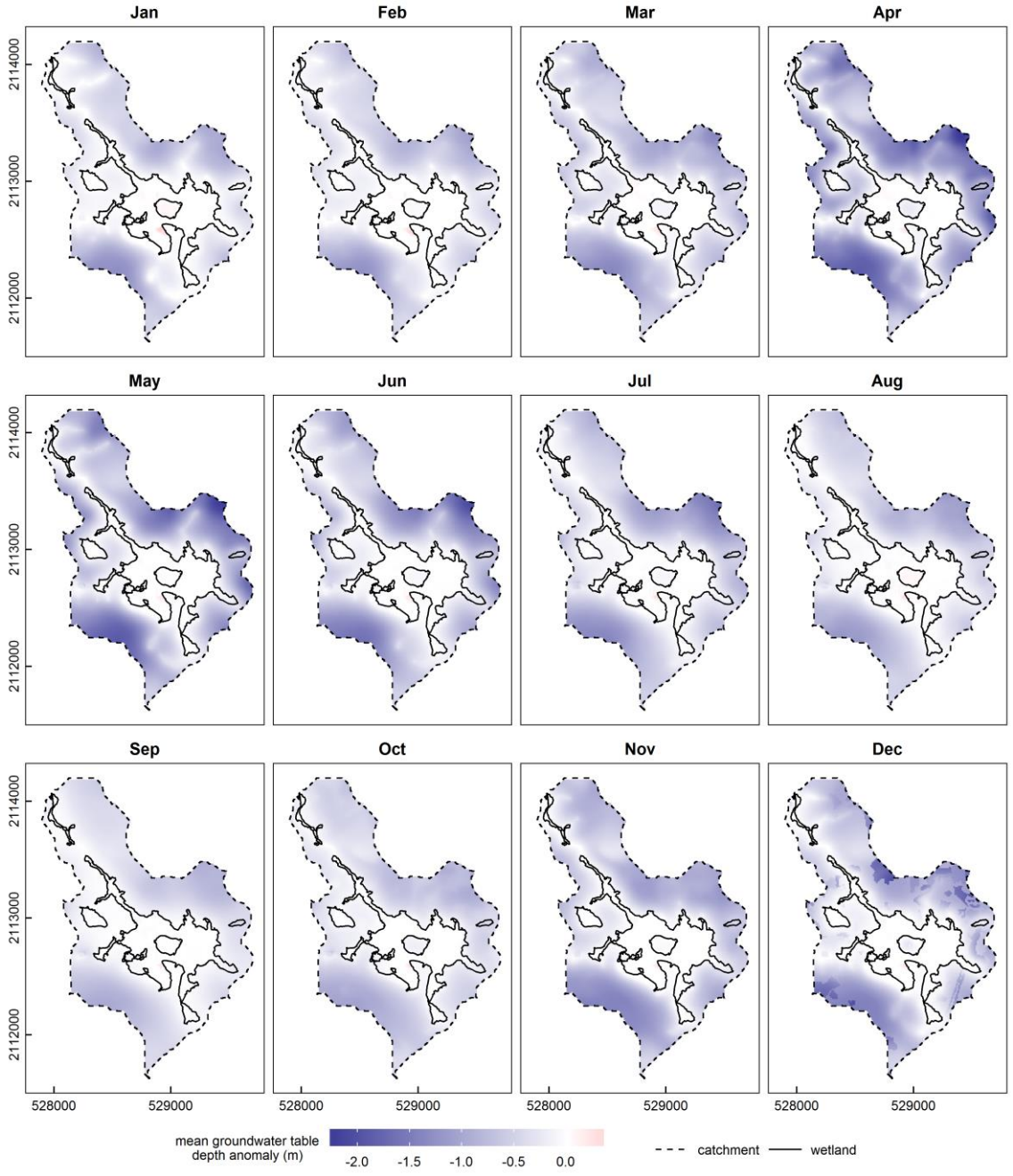

Figure 8-10. Spatial distribution of change in simulated monthly mean groundwater table depth under the conifer scenario, relative to the baseline (01/01/2011-31/12/2013).

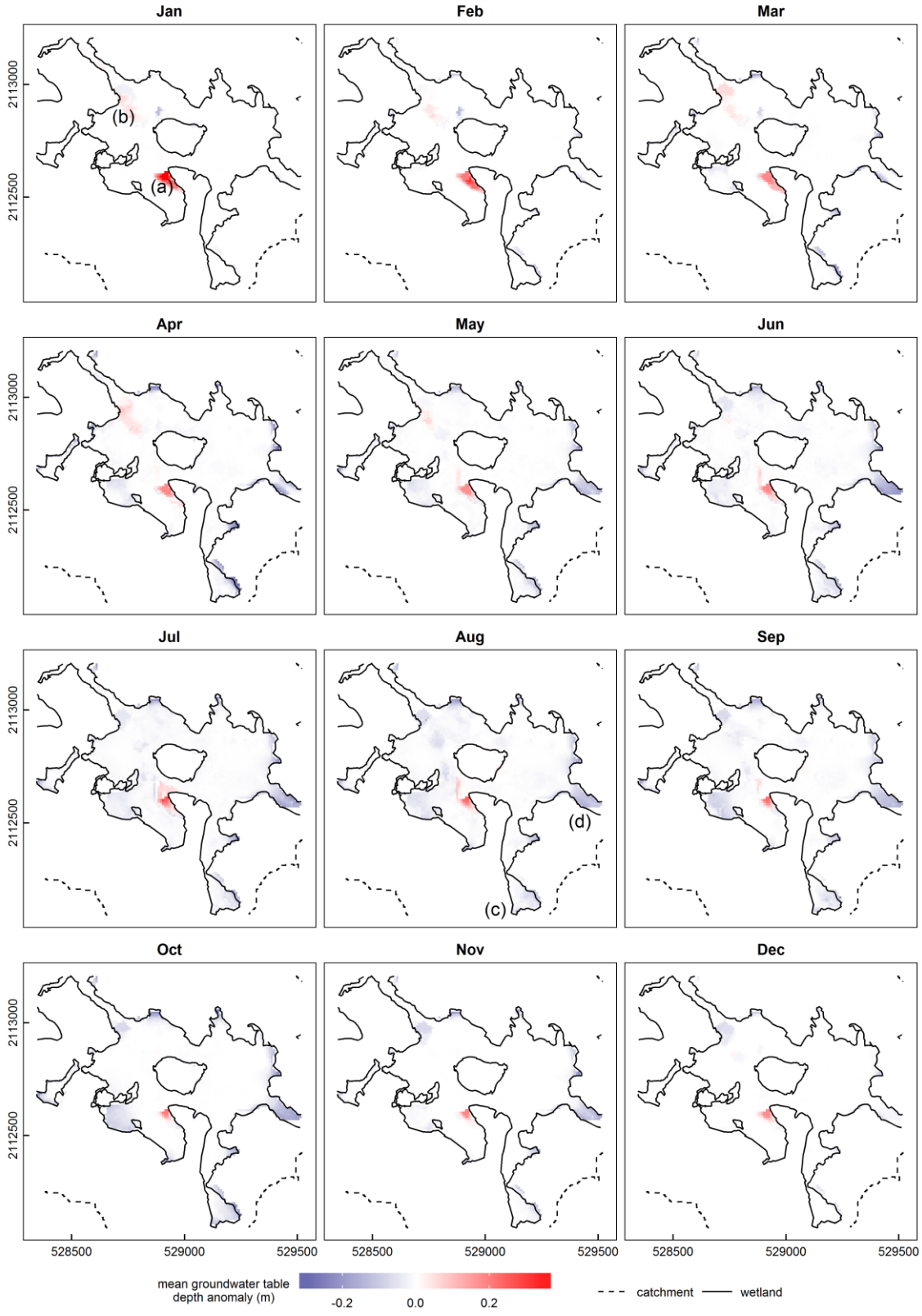

Figure 8-11. Spatial distribution of change in simulated monthly mean groundwater table depth within the mire under the conifer scenario, relative to the baseline (01/01/2011-31/12/2013).

Only grid cells corresponding to peat soils upstream of Pont-de-Pierre are shown. Grid cells on mineral soils have been masked out.

The timing is not a consequence of differences in vegetation transpiration in summer caused by the two-layer unsaturated flow model since it can be noticed across the entire catchment, including on the southern side that is entirely covered in woodlands under both the baseline and the conifer scenario and where root depths do not differ. Instead, this timing is probably a consequence of interaction between tree phenology and seasonal patterns in reference evapotranspiration. In winter, both maximum interception capacity and crop coefficients are higher in conifers than in broadleaf tree species (see Section 5.4.3), however the actual evapotranspiration from the former and therefore the difference in groundwater recharge between both landcover types are limited by the low potential evapotranspiration. This is reflected in the moderate difference in groundwater table depth between the baseline and the conifer scenario. The larger difference between both scenarios occurs in May and to a lesser extent April and June, during the leafing period and up to a month after its end, at a time when the reference evapotranspiration is already large but the evaporative demand of broadleaved tree species has not yet reached its full rate. During the leafed period, differences in interception between tree species are smaller and partly compensated by a higher transpiration under broadleaf cover, crop coefficients of evergreen and broadleaved species are similar, and transpiration from both tree species is limited by soil moisture avaibility. This is reflected in the timing of the lowest change in September.

Figure 8-11 shows that the impact of the conifer scenario on groundwater table depths in peat soils is larger around the margins of the mire, particularly in the small etch-basins perched upstream of and above the main wetland extent, upstream of the Rocher discharge monitoring station and east of the wetland (labelled (c) and (d) on the August panel). The impact is generally smaller in the middle of the mire. The timing of change in groundwater table depth in peat soils is the same as that described from dipwell time-series, and slightly different from that predicted in the wider catchment. From November to March or even May, the groundwater table depth is maintained at ground level by an excess of water from upwelling, and to a lesser extent, runoff and precipitation. The slight lowering of the simulated groundwater table within the mire catchment under the conifer scenario relative to the baseline is not large enough to negatively impact peat groundwater tables. In the summer this changes, and the largest impact is predicted to occur in July and August. This delay compared to the mire catchment probably results from the delayed phenology of the mire vegetation that reaches full development in late June or early July only; and from the time required for the water to flow through the saturated zone from the catchment to the mire. Figure 8-11 also suggests that the monthly mean groundwater table

depth is increased under the conifer scenario in some locations, particularly west of Puy Long (labelled (a) on the January panel) and to a lesser extent along the stream close to the wetland outlet at Pont-de-Pierre, downstream of Puy Rond (labelled (b) on the same panel). These two locations correspond to shallow topographic sinks where both the simulated mean depth of overland flow and the accumulated overland flow error are large, as shown in Figure 6-18 and Figure 6-19. It is therefore highly likely that the positive change predicted in these areas is a computational artefact.

Figure 8-12 show the simulated change in mean monthly groundwater table depth under the grassland scenario for the period 01/01/2011-31/12/2013 in the entire modelled area. Overall, the impact of the grassland scenario is opposite to that of the conifer scenario: groundwater table depths are generally higher by up to 2.5 metres, particularly on the catchment margins below the topographic highs and in late spring and early summer. However the model does suggests a slight lowering of the groundwater table depth by up to a few decimetres on the catchment mineral footslopes from late summer to early winter, with the largest effect occurring in October and November. This is also visible on Figure 8-13 that shows change in simulated groundwater table depth in model grids located on peat soils only. These changes are a consequence of the lower percolation from unsaturated zone to the saturated zone occurring within the mire catchment under the grassland scenario in August 2011, October 2012, October and November 2012 (Figure 8-2) and described above. As for the conifer scenario, errors caused by the lack of convergence of the overland flow model in topographic sinks probably explains the lower groundwater table depths that can be noticed west of Puy Long and upstream of the wetland outlet at Pont-de-Pierre.

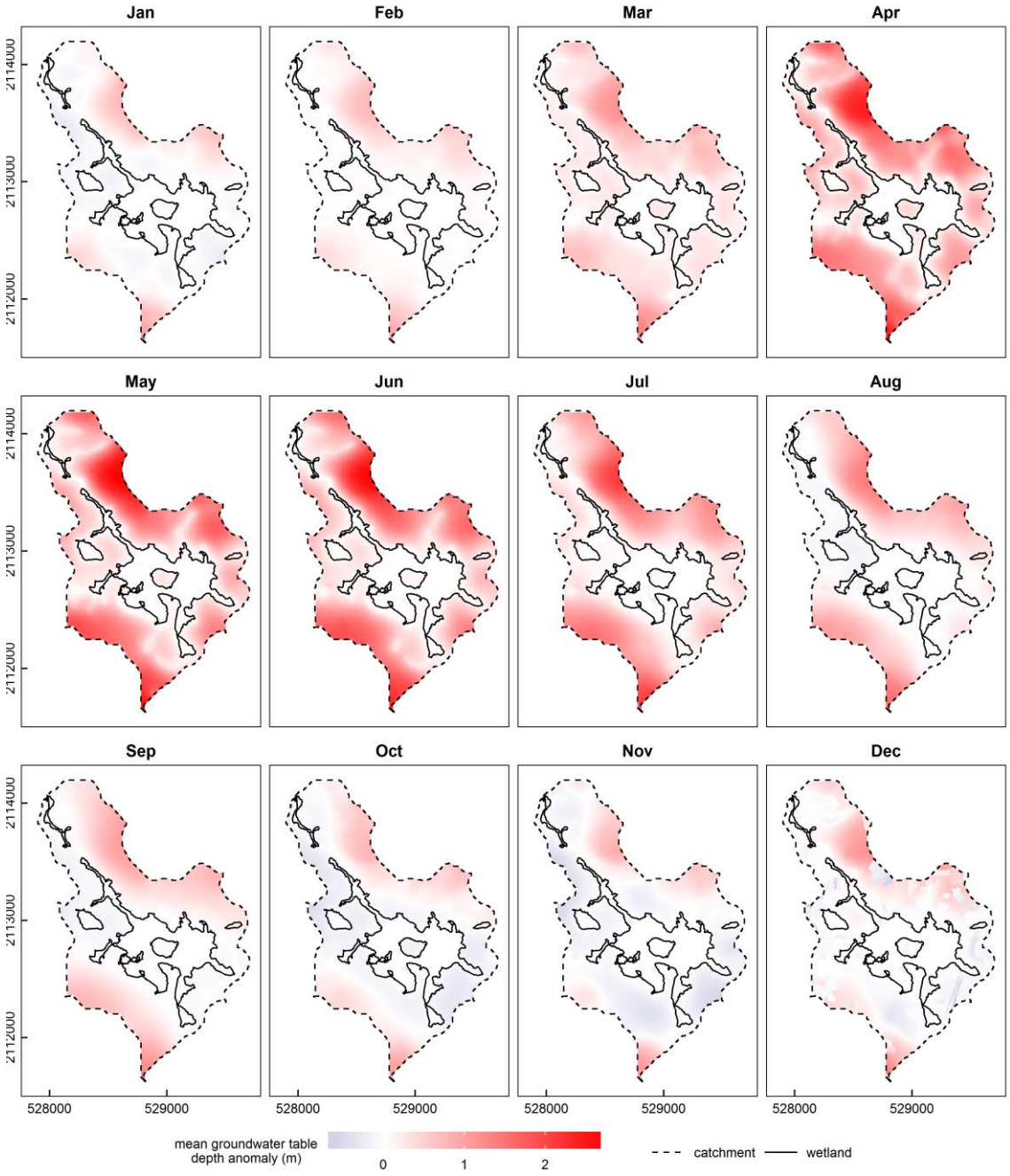

Figure 8-12. Spatial distribution of change in simulated monthly mean groundwater table depth under the grassland scenario, relative to the baseline (01/01/2011-31/12/2013).

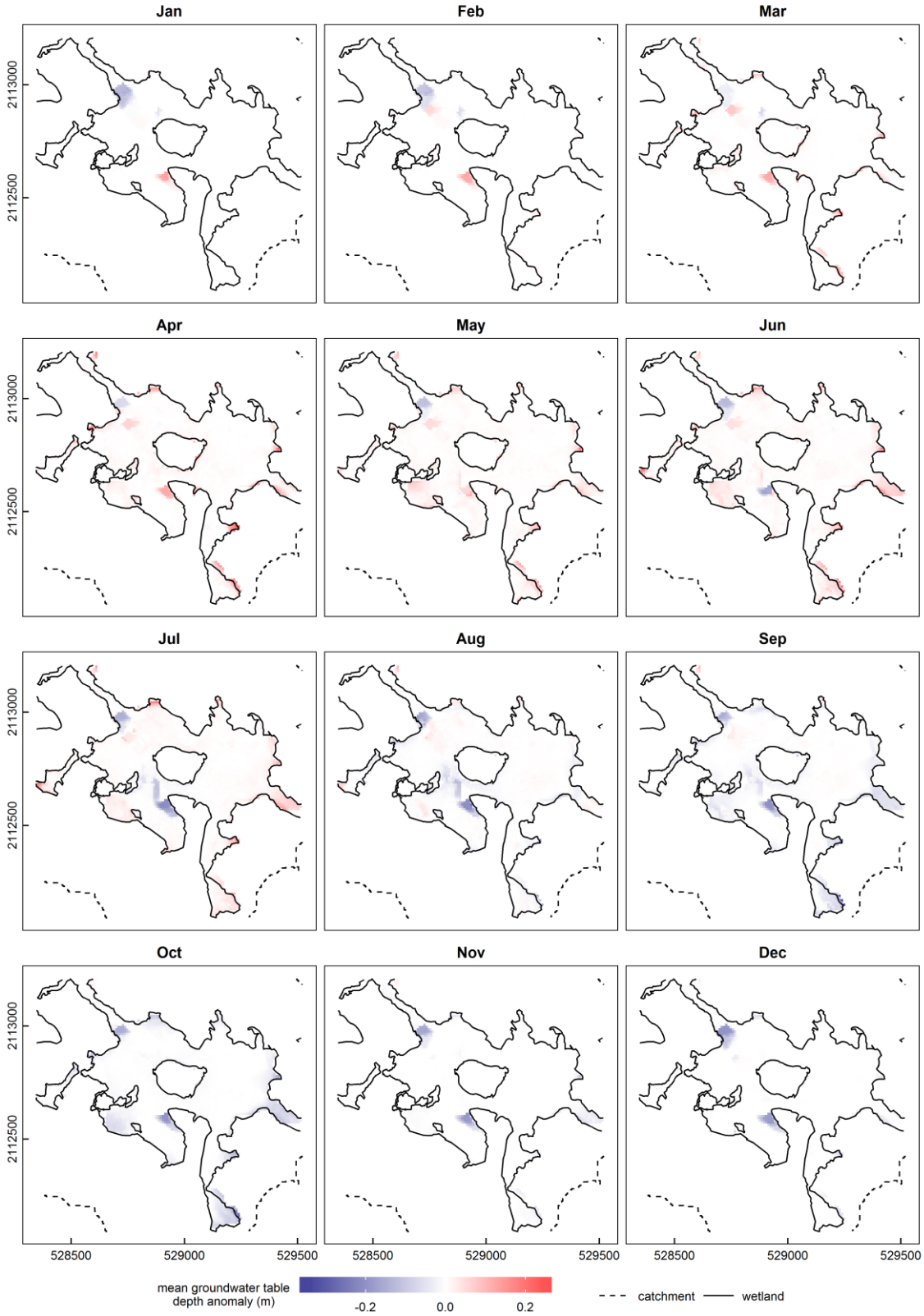

Figure 8-13. Spatial distribution of change in simulated monthly mean groundwater table depth within the mire under the grassland scenario, relative to the baseline (01/01/2011-31/12/2013).

Only grid cells corresponding to peat soils upstream of Pont-de-Pierre are shown. Grid cells on mineral soils have been masked out.

8.5. Conclusion

The impact of the grassland scenario relative to the baseline (i.e. broadleaf woodlands) scenario is surprisingly small compared to those reported in the literature (see Appendix H for a review). This may be due in part to the conservative parameter values used in this study due to the scarcity of data on grasslands and to the different methods generally used to characterise evapotranspiration and unsaturated flow in woodlands and open habitats. Interception from litter was for instance accounted for in grasslands but not in woodlands. However, this surprising result can most likely be explained by the significant limitation of the MIKE SHE two-layer unsaturated flow model that the analysis of the model outputs under different catchment landuses has highlighted. MIKE SHE overrides the user-specified root depth and replaces it with the depth of the uppermost computational layer when the latter is shallower than the former, even under unsaturated conditions when the groundwater table is well below the root depth. As a consequence, differences in root depth between landuse classes are ignored. This issue also explains why the available water capacity of mineral soils had to be increased beyond realistic values during the model calibration, since the large calibrated value matches the initial estimate when accounting for the overriden root depth of woodlands, the dominant landuse within the catchment.

This issue is particularly important when comparing the grassland scenario to the baseline, in which broadleaf woodlands are dominant. The simulated impacts of the grassland scenario should therefore be interpreted with care, and further work is required to confirm the results described here. The depth of the uppermost computational layer should be increased to 2m on mineral ground, and the model recalibrated. The gravity or the Richards unsaturated flow models might not be subject to the same limitations as the two-layer model and may generally result in a better representation of unsaturated flow. However they would impose a substantial additional computational burden. They would also require additional data on both soils (down to 2m, corresponding to the root depth of tree species) and unsaturated flow within the fissured granite.

To reduce uncertainty on evapotranspiration and unsaturated flow processes within the catchment, which have been shown to have a substantial impact on the mire water balance, the evapotranspiration and unsaturated flow model components could be calibrated and validated independently on the basis of soil moisture time-series in a number of representative locations where the groundwater table is below the evapotranspiration extinction depth. The validation of the model would also benefit from data on actual evapotranspiration. Sap flow and

interception monitoring or micrometeorological methods such as eddy covariance would provide such information in woodlands (Wilson *et al.* 2001), while lysimetry or micrometeorological methods could be used in open habitats (Drexler *et al.* 2004; Proulx-McInnis *et al.* 2012). However this would require a substantial long-term investment in hydrological monitoring within the catchment.

Issues associated with the MIKE SHE unsaturated zone simulation are of much less consequence when analysing the impact of coniferous woodlands relative to broadleaf woodlands, dominant under the baseline scenario, since both vegetation classes have the same root depth. The model results suggest that almost all investigated variables are substantially impacted by the conversion of deciduous woodlands to coniferous woodlands (here assumed to correspond to Douglas fir plantations, the most commonly planted species in Limousin's forests). Interception within the catchment would increase by +52%, even though actual evapotranspiration as a whole would increase by +9% only. Consequently, recharge of the fissured zone aquifer would be reduced by -6%, overland flow from the catchment to the mire by -15% and runoff to streams upstream of the mire by -8%. Groundwater inflow to the mire would be reduced by -2%. The model simulates a drop in groundwater table within the mire by up to 20-25cm during the dry season, but only on the mire margins. In this part of the mire, the length of time during which the groundwater table drops below surface is also increased. Changes are negligible in the mire centre which is buffered from the impacts of changes in the surrounding catchment. There is no impact of catchment landuse on groundwater table depth within the mire in winter when the water table is at or very close to the ground surface for extended periods. The model also simulates a substantial impact of conifer plantations on stream discharge, particularly in the small streams located in the upstream part of the mire, and particularly during low flow conditions. Q95 for instance would be reduced by between -22% and -30%, total flow by about -8% (if results for the Marzet gauging station are excluded). Overall, substantial reductions in stream discharge are also simulated for the Marzet and Pont-de-Pierre gauging stations, even though large overland flow errors caused by numerical convergence issues were shown to occur just upstream of these stations.

Given the sensitivity of mire vegetation to the groundwater table depth particularly in summer, this may have important consequences in terms of biodiversity conservation. The results from the current study offer a potential explanation to Smith's and Charman's (1988) findings, reported in Section 8.2, who found more species indicative of drier conditions in Northumberland (UK) mires surrounded by conifer plantations. Interestingly, these authors also

showed that species indicative of wetter conditions were more frequent in large mires with a small perimeter/area ratio, which would be supported by the stronger impact of landuse changes on groundwater table depth along the mire margins suggested by the model outputs. The predicted lowering of the groundwater table depth within the mire may also have substantial effects on the superficial peat geochemistry: lower groundwater table depths in acidic mires have been linked to increased carbon exports to the atmosphere and to downstream watercourses (Freeman *et al.* 2001; Clark *et al.* 2005, 2009; Strack *et al.* 2008; Fenner *et al.* 2013), and to the release of heavy metals, metalloids and radionuclides sequestered in the saturated peat (Owen & Otton 1995; Rothwell *et al.* 2009, 2010, 2011; Schöner *et al.* 2009). Published research on the consequences of catchment landuse changes on mire hydrology is extremely rare and should clearly be developed.

Résumé du chapitre 8

Le modèle calibré a été utilisé pour simuler l'impact de changements d'occupation des sols dans le bassin versant sur la balance hydrique de la tourbière, la profondeur de la nappe dans celle-ci et les caractéristiques des débits dans les cours d'eau en aval. Les scénarios testés correspondent à un remplacement intégral des végétations actuellement présentes sur le bassin versant par des milieux ouverts (prairies et pâturages) ou des plantations de sapin de Douglas, cette essence étant actuellement la plus fréquemment utilisée en plantation sur les hauts-plateaux limousins. En accord avec les pratiques généralement observées dans la région lors de plantation, il a été considéré que l'afforestation ne s'étend pas aux zones humides. Ces deux scénarios sont comparés à la situation actuelle, correspondant à une dominance des boisements feuillus semi-naturels.

Le modèle suggère que le remplacement des végétations actuelles, dominées par les boisements feuillus semi-naturels, par des milieux ouverts (pâtures et prairies) conduirait à une baisse de l'évapotranspiration réelle de -4% dans le bassin versant, un accroissement de +3% de la recharge de l'aquifère granitique, un accroissement de 3% des apports à la tourbière par ruissellement de surface, un accroissement des débits annuels dans les cours d'eau en amont de la tourbière de +3%, et un accroissement des apports souterrains à la tourbière de +1%. Ces impacts simulés sont étonnamment faibles si on les compare aux résultats rapportés dans la littérature internationale, dont une revue détaillée en annexe du présent document montre qu'il est maintenant clairement avéré que l'afforestation des bassins versants a un impact substantiel sur la ressource en eau, conduisant notamment à une augmentation de l'évapotranspiration réelle et à une diminution de la recharge de la nappe et des écoulements de surface. Il est montré que ce faible impact suggéré par le modèle résulte d'un problème méthodologique causé par MIKE SHE : la profondeur de la couche supérieure du modèle d'évapotranspiration et d'écoulement vadose, correspondant à la zone de prospection des racines, ne semble pas pouvoir excéder la profondeur de la couche de calcul la plus superficielle du modèle d'écoulement en zone saturée, même si celle-ci est désaturée. La partie de la zone racinaire située sous cette couche de calcul, et donc les différences de profondeur racinaire entre végétations, sont ignorées. Ce problème permet d'expliquer la très large valeur de réserve utile obtenue par calibration : elle permet de compenser la sous-estimation de la profondeur racinaire. Si on tient compte de ce phénomène, la réserve utile obtenue par calibration est de 0.0975, une valeur très proche de celles citées dans la littérature pour des sols similaires. Du fait de cette

compensation, le problème méthodologique causé par MIKE SHE ne remet pas en cause les résultats décrits aux chapitres 6 et 7, ni la comparaison de l'effet des changements d'occupation des sols sur l'hydrologie du bassin versant et de la tourbière pourvu que les végétations comparées aient des profondeurs racinaires équivalentes. Le bassin versant étant actuellement dominé par des boisements feuillus, la comparaison avec un bassin versant dominé par des conifères reste donc pertinente. Par contre, les résultats obtenus en comparant la situation actuelle avec un bassin versant dominé par des milieux ouverts sont à considérer avec circonspection.

Le modèle suggère que le remplacement des végétations actuellement présentes sur le bassin versant avec des plantations de sapin de Douglas conduirait à une augmentation de +52% de l'interception sur le bassin versant, même si l'évapotranspiration réelle ne serait augmentée que de +9%. La recharge de l'aquifère diminuerait de -6%, les apports à la tourbière par ruissellement de surface de -15%, les apports par les ruisseaux de -8% et les apports souterrains de -2%. Le modèle suggère également une baisse estivale des niveaux de nappe dans la tourbière allant jusqu'à 20 à 25cm, mais uniquement en périphérie de celle-ci. Les changements simulés au centre de la tourbière sont négligeables. L'impact hydrologique d'un changement d'occupation des sols sur les niveaux de nappe dans la tourbière serait nul en dehors de la période estivale. Le modèle suggère également un impact substantiel d'un enrésinement total du bassin versant sur les débits dans les ruisseaux, particulièrement en amont de la tourbière et pendant les périodes d'étiage. Par exemple, Q95 serait réduit de -22 à -30% selon les endroits, et les débits totaux de -8% sur les deux stations de mesure pour lesquels l'erreur associée aux simulations est la plus faible. Le modèle suggère que les débits au niveau des deux autres stations pourraient également décroître de manière substantielle, toutefois l'incertitude associée à ces deux stations est plus grande du fait d'erreurs de convergence plus importantes en amont de celles-ci.

Du fait de la sensibilité des végétations tourbeuses à la profondeur de la nappe, particulièrement en période estivale, l'abaissement de la nappe suggéré par le modèle suite à l'enrésinement du bassin versant peut avoir d'importantes conséquences en termes de conservation des milieux tourbeux. L'occupation des sols sur les bassins versants doit donc être un facteur pris en compte par les politiques de conservation des milieux tourbeux. De possibles conséquences sur la géochimie des histosols doivent également être prises en compte et étudiées de manière approfondie : la littérature suggère en effet qu'un abaissement de la nappe dans les histosols peut conduire à une augmentation des concentrations en carbone organique dissous vers les cours d'eau en aval, et à un relargage des métaux lourds et métalloïdes jusqu'alors séquestrés

dans la tourbe saturée. Les études portant sur les conséquences de l'afforestation des bassins versants sur l'hydrologie des zones humides sont très peu nombreuses, et devraient donc être multipliées.

Chapter 9. Hydrology and hydrological modelling of acidic mires in the French Massif Central: conclusion and recommendations

9.1. Concluding review

The aims of the current study were to identify, quantify and model water fluxes to, from and within an acidic valley mire representative of a large proportion of mires in the Massif Central, and in particular of the Limousin uplands. A further aim was to assess the potential impacts of catchment afforestation on the mire's hydrological conditions. These aims have been largely fulfilled. The current study constitutes a very rare example, and to the best of my knowledge, the first of its kind in France, of a successful integrated investigation of the hydrology of a minerotrophic mire and of its catchment in a basement region. In Section 2.5, the thesis aims were divided in several individual objectives. The following sections revisit these objectives and summarise and assess the results of the current study with reference to them.

9.1.1. Development of a three-dimensional geological model of the mire and its catchment

A detailed three-dimensional geological model of the Dauges catchment and mire was developed (Chapter 3). Pedological pits were dug at a number of locations to investigate the depth and nature of the mineral soils. The number of outcrops in which weathering granite formations, including peri-glacial formations, could be seen proved limited. A number of deep geological drilling logs were, however, available, but information on granite weathering formations was limited. Furthermore, all boreholes were drilled for the purpose of uranium prospection along mineralised faults located on the eastern side of the mire, and extrapolation to the wider catchment could only be considered tentative. A GIS-based analysis of the distribution of past arable land and of large boulders and granite outcrops provided some insights on the likelihood of the presence at ground level of saprolite and fissured granite respectively, although the absence of further data meant that these interpretations could not be validated. The most detailed and useful information was provided by electrical resistivity tomography (ERT). Together, these investigations showed that:

- Mineral soils are relatively homogeneous and 40-70cm deep. Their texture is loamy-sandy to sandy-gravelly, and drainage is always good.

- Peri-glacial formations are very patchy. Head is frequently missing and shallow when present. The texture is similar to that of the underlying undisturbed saprolite, and no poorly permeable fragic horizon is present.
- In-situ saprolite ranges between very shallow (less than a couple of metres deep) to absent on hilltops and hillslopes. Using ERT, no substantial saprolite layer could be evidenced at the bottom of the etch-basin beneath the western part of the mire. However, on the eastern side of the mire, geological drilling logs showed the presence of saprolite up to 37m deep. This difference may be the result of more complete erosion of saprolite downstream of Puy Rond, a residual inselberg at the centre of the mire, or may alternatively be the result of possible similarities in electrical resistivity between saturated saprolite and saturated densely fissured granite. These alternative explanations should be investigated further in order to improve the characterisation of the saprolite.
- Fissured granite is exposed on the steeper slopes, and the fissured zone extends to depths ranging from 40m to 65m. Using the available data, it proved difficult to infer the precise location of the interface between the fissured zone and the unweathered granite. Nevertheless, there were indications that the depth of the fissured zone was relatively constant, with an indicative average value of 55m below ground. The analysis of geological drilling logs and ERT data highlighted a large heterogeneity in the characteristics of the fissured zone. An accurate characterisation of the fissured zone would therefore require high-resolution data that are beyond the capacity of most research projects. However, results from the ERT survey suggested that fissure density within the fissured zone may be larger below topographic lows than below hilltops. This possible correlation between the characteristics of the fissured zone and topography could be further investigated as it may allow for the development of a much needed cost-effective method establishing the characteristics of the fissured zone from much more readily accessible topographic data.

A detailed survey of peat and alluvial deposits was carried out using manual augering, probing and slug tests (Section 3.4). It confirmed the existence of two layers with different properties within the peat column: a shallow, poorly decomposed, highly permeable peat layer (the acrotelm in the broad definition of the term) and a lower, more strongly decomposed, less permeable layer (the catotelm). However, results from the survey also showed that, in minerotrophic valley mires, peat characteristics are highly variable, and cannot be inferred from

other variables that are easier to collect such as vegetation or surface topography. This is particularly the case along the mire margins and along watercourses where colluvium and alluvium deposits are frequently found within the peat column. Deep gravel deposits were also identified beneath the peat along the main watercourse in the downstream part of the mire.

9.1.2. Hydrometeorological monitoring

A wide range of hydrometeorological data were collected to characterise the hydrology of the Dauges catchment and its mire (Chapter 4, Appendix E). Precipitation and variables required to compute the FAO Penman-Monteith reference evapotranspiration (global radiation, temperature, relative humidity and wind speed) were recorded over a period of 2.5 years, even though frequent instrument failures required a substantial amount of work to control and correct data and reconstruct missing values, a common occurrence in such monitoring programmes, especially in remote areas (Porteret 2008). It was shown that precipitation and reference evapotranspiration could be reconstructed accurately based on data recorded at the closest permanent meteorological stations, even though some were relatively far away (up to 25km) from the research site, provided data collected after 1998 are used. Before this date the error in reconstructed precipitation increases substantially due to changes in the meteorological station network. The current study also demonstrated that temperature, relative humidity and wind speed within the mire differed markedly from the upper part of its catchment. It was argued that this was due to the mire's topographic position at the bottom of a deep etch-basin and the almost constant saturation of the peat surface. However, it was shown that there was little difference in FAO Penman-Monteith reference evapotranspiration between the two locations, due to the overriding importance of solar radiation in its computation.

The monitoring of discharge proved difficult in small headwater streams, in particular due to the small number of locations suitable for the installation of V-notch weirs, frequent changes in bed sections caused by flood events and cattle trampling, and frequent equipment failures. Nevertheless, discharge was successfully monitored over approximately three years at three locations in the upper parts of the mire and at its main outlet. Discharge data collected at the catchment outlet could not be used since a reliable stage-discharge relationship could not be established due to substantial and repeated changes of the stream bed geometry. Piezometric head was also recorded in dipwells and piezometers within the mire and along its boundaries. It was shown that groundwater table depth loggers drifted substantially, and generally non-linearly, over the monitoring period, and that frequent and accurate manual measurements are required

if logger-recorded time-series are to be corrected. Overall, the scope, volume and quality of geological, geomorphological, pedological, meteorological and hydrological data collected as part of the current study are, to the best of my knowledge, unprecedented in any mire of the Massif Central and possibly of France, with the exception of those collected by Auterives (2006), Auterives *et al.* (2011) and Armandine Les Landes *et al.* (2014) in the Cotentin marshes, Normandy. This database provides firm foundations for the analysis and modelling of the hydrology of acidic valley mires in granitic regions developed in this thesis, but also for future research as detailed in Section 9.2.

9.1.3. Conceptual hydrological model

A conceptual hydrological model of the mire and its catchment was developed based on a qualitative analysis of the data collected as part of the current study and those available from previous research (Section 4.4). The model suggests that the mire is principally groundwater-fed and depends on the fissured granite aquifer. Despite the moderate permeability of the catotelm, groundwater upwelling from underlying mineral formations maintains shallow water tables in the peat except for one to three months a year. When the groundwater table within the peat is near ground level, precipitation and runoff from the mire's catchment contribute little to the water balance of the peat column as saturation excess leads to quick runoff or superficial flow through the acrotelm to water courses. In summer, the reduction in groundwater upwelling and increased evapotranspiration lead to a drop in groundwater table within the peat. Groundwater upwelling and seepage are increased along slope breaks. All these conclusions were validated by the MIKE SHE / MIKE 11 model, as detailed in Chapter 7. The qualitative analysis of observed data also suggested the existence of small-scale processes caused by the heterogeneity of the underlying mineral formations or of the peat itself, that could not be directly modelled and validated using the MIKE SHE / MIKE 11 model due to limitations in model resolution both vertically and horizontally and to the difficulty in measuring hydrogeological properties with a sufficient resolution (Chapters 3, 5 and 6). For instance, it was suggested that excess water from groundwater seepage flows rapidly through the mire and to water courses through a shallow but highly permeable poorly humified peat layer at the surface, the depth and hydrological significance of which is highly heterogeneous. Heterogeneities in the underlying substrate, in particular differences in fissure density within the weathered granite, may increase or reduce groundwater inputs locally. It was also shown that the presence of deep and highly-permeable alluvial deposits beneath or within the peat along the stream downstream of Puy Rond results

in a high degree of hydrological connectivity between the stream and the mire in this area. Water flows generally from the mire to the stream except when overbank flooding occurs and in summer when shallow groundwater levels within the mire are maintained by seepage from the stream. In the north-eastern part of the mire, artificial drainage and possibly peat fire have resulted in an alteration of peat properties and of groundwater table dynamics. There are still uncertainties in this hydrogeological conceptual model that are related to the extent, thickness and hydrological role of the saprolite layer beneath the mire. This results from the absence of geological drilling logs downstream of Puy Rond and from uncertainties on the feasibility of distinguishing between saturated saprolite and fissured granite using ERT (Sections 3.3.3.3 and 3.3.4). However, the current study has shown that groundwater table dynamics within the mire can be reproduced relatively satisfactorily with a model in which the saprolite layer is not accounted for (Chapter 6), which suggests it has a limited hydrological role.

9.1.4. Numerical hydrological model

The Dauges catchment was modelled using the MIKE SHE / MIKE 11 hydrological / hydraulic model (chapters 5 and 6). The development and performance of the model were constrained by a number of limitations, relating to the MIKE SHE / MIKE 11 modelling system and to the heterogeneity of the substrate. The modelling choices that were made responded to the necessity of limiting the model run time to a few hours, compatible with the multiple simulations required by the calibration, sensitivity analyses and exploitation of the model. It proved difficult to achieve such acceptable run times while accounting for some hydrological processes. In particular, kinematic routing had to be used instead of the 1D Saint-Venant equations to model channel flow, and as a consequence backwater effects were not adequately simulated (Section 6.2.1.5). The performance of the model with regard to stream stage was poor within the mire where backwater effects are important. As a consequence, neither rapid groundwater flow between the stream and highly permeable alluvial deposits nor overbank flooding, both shown to occur along the stream downstream of Puy Rond, could be accurately modelled.

Another constraint relates to saturated zone computational layers: they must extend across the entire modelled area which further increases the computational demand and must be at least 0.5m thick approximately to avoid numerical instabilities. This meant that the acrotelm could not be modelled as a distinct layer from the catotelm. The choice of the two-layer method to model unsaturated flow considerably reduced the computational demand and the data requirements compared to the Richards equation, but imposed other contraints. One such

constraint, potentially leading to the over-simplification of evapotranspiration processes, was avoided by modelling interception outside MIKE SHE (Sections 5.4.2 and 5.4.3). A detailed analysis of the model results for different catchment landuse scenarios (Section 8.4) also showed that MIKE SHE ignores the user-specified root-depth when it is larger than the depth of the upper computational layer and the two-layer unsaturated zone model is used. Finally, a lack of convergence of the overland flow component was noted, particularly where topographic sinks or flats occurred (Section 6.3.5).

Other limitations were related to the difficulty in characterising the properties of the geological formations with sufficient resolution and accuracy. In Section 3.4 it was shown that the properties of the peat deposit were highly variable and could not be predicted using a range of potential explanatory variables. Similarly, the results from the ERT survey suggested that the fissure density within the weathered granite was very variable (Section 3.3.3.3). As is the case in most hydrogeological modelling studies (Sections 1.4.2, C.3 in Appendix C and 5.3.2), such heterogeneity could not be incorporated within the MIKE SHE saturated zone model given the data demand that this imposes. These limitations may explain the unsatisfactory model performance with regard to groundwater in some dipwells.

However, despite these limitations, the model performance was satisfactory to good with regard to discharge and groundwater table in a large number of dipwells (Section 6.2.1.5). There was also a very good agreement between the distribution of the mean simulated groundwater table depth and the observed wetland boundaries across the entire catchment (Section 6.2.2.2).

9.1.5. Sensitivity analyses

A range of sensitivity analyses of the MIKE SHE / MIKE 11 model were undertaken (Section 6.3). A systematic sensitivity analysis showed that the parameters to which the model is most sensitive with regard to both stream discharge and groundwater table depth, including in peat, are the horizontal hydraulic conductivity and specific yield of the fissured granite. This confirms the high degree of connectivity between the mire and the fissured granite aquifer, and the importance of understanding groundwater fluxes within the catchment to improve hydrological predictions within the mire. A satisfactory model performance could not be achieved if the calibrated horizontal hydraulic conductivity of the fissured granite zone was kept to average values cited in the literature, even if the shape and depth of the fissured zone was modified substantially (Section 6.3.1). The final calibrated value was markedly lower than those cited in

the literature ($7.5x10^{-7}$ $m.s^{-1}$ vs. $1x10^{-5}$ $m.s^{-1}$ in Wyns *et al.* 2004 and Dewandel *et al.* 2006). As in other studies (Ahmed & Sreedevi 2008), it was suggested that this low calibrated bulk hydraulic conductivity results from the heterogeneity of weathering and fissure density within the fissured zone, and possibly of the presence of low permeability vertical barriers such as mineralised faults or lamprophyre veins. In a similar way, it was shown that the model performance with regard to groundwater table depth within the mire could be improved for individual dipwells by allowing for small variations in peat specific yield, peat available water capacity and crop coefficient within the mire. Given the heterogeneity of peat characteristics demonstrated in Section 3.4, and also in vegetation within the mire (Durepaire & Guerbaa 2008), it is evident that such variations exist, but they are difficult to map and therefore to account for. It was also shown that the model performance with regard to stream discharge generally improves with increasing model resolution, but the effect on performance with regard to groundwater table depth is much more variable (Section 6.3.3). Finally, the model performance with regard to stream discharge at two gauging stations was shown to be very sensitivie to the length of the simulation period. Based on the spatial distribution of overland flow errors, it was suggested that this issue is related to the lack of convergence of the overland flow component, which caused substantial water balance errors in topographic sinks and flats located upstream of these stations (Section 6.3.5).

9.1.6. Simulated water balance and hydrological fluxes

Detailed water balances of both the mire and its catchment were established on the basis of simulated water fluxes from the MIKE SHE / MIKE 11 model (Section 7.3). The spatial distribution of groundwater seepage, of groundwater flow between the peat and the underlying mineral formations and of groundwater table depth was also investigated (Section 7.2). The results confirmed the hydrogeological conceptual model detailed in Section 4.4 and based on a qualitative analysis of the data collected as part of this study. It was shown that the mire is principally fed by groundwater upwelling from the underlying mineral formations, precipitation and runoff from the catchment (a substantial part of which actually originates in edge-focused groundwater seepage just upstream of the mire boundaries). Temporal distributions of these three main sources of water differ: runoff inputs follow patterns in precipitation, modulated by interception, whereas inputs from groundwater upwelling are more regular. The latter are largest in early winter and decline gradually over time to reach their lowest value in late summer. Runoff inputs are larger than precipitation and groundwater upwelling, however both runoff and

precipitation do not contribute substantially to the water balance of the peat itself since, as discussed above, they are quickly evacuated as saturation excess runoff due to shallow water table depths. Water within the saturated peat overwhelmingly originates from groundwater upwelling from the underlying mineral formations. The water balance analysis highlighted the importance of the mire as an interface between mineral formations and watercourses, with potential repercutions in terms of stream water chemistry.

9.1.7. Hydrological response to changes in catchment landuse

The calibrated MIKE SHE / MIKE 11 model was forced with two landuse scenarios corresponding to the replacement of all current landcover classes within the mire catchment by either grassland or conifer (i.e. Douglas fir) plantations, and the model outputs compared to the baseline in which deciduous woodlands are predominant (Chapter 8). Changes were expressed in terms of overall and monthly water balances within both the mire and its catchment, discharge at the four stream gauging stations, and groundwater table depth in dipwells located in peat and for which the model performance was satisfactory to good. Changes in the spatial distribution of monthly mean groundwater table depth were also investigated. Simulated impacts of the grassland scenario were surprisingly small (Section 8.4) given the strong published evidence for substantial impacts of afforestation or deforestation on water yield and groundwater recharge (see Appendix H). Within the mire catchment and over the three-year simulation, despite a decrease by -39% of simulated interception, the model predicted a decrease in actual evapotranspiration and an increase in percolation to the saturated zone by only -4% and +3%. As a consequence, simulated changes in the mire water balance are small: +2% for runoff inflow and +1% for groundwater upwelling. The model suggested slightly shallower groundwater table depths in summer along the mire margins under the grassland scenario. The impact on stream discharge was small and variable.

It was shown that this surprisingly small impact of the grassland scenario was a consequence of MIKE SHE overriding the user-specified root depth when larger that the depth of the upper computational layer, even when the groundwater table is below the root zone. As a consequence, differences in root depth between woodland and grassland species were not accounted for, and the impacts of the grassland scenario were most probably underestimated by the model. However, this methodological issue does not compromise the validity of the model results with regard to the conifer scenario, since deciduous and coniferous woodlands were given the same root depth. Within the catchment, the model simulated an increase in actual evapotranspiration

of 9%, a reduction in percolation to the fissured granite aquifer of -6%. This led to a reduction in runoff and groundwater upwelling inputs to the mire of -15% and -2% respectively. The model also predicted a substantial reduction in stream discharge in upstream reaches, particularly at low flow. Q95 for instance would be reduced by between -22% and -30%, and total discharge by -8% on average. Simulated impacts further downstream were smaller, possibly due to overland flow model errors in topographic sinks or flats. The model predicted a drop in groundwater table depth within the mire of up to 20-25cm during the dry season, but only along the mire margins. Simulated changes were negligible in the centre of the mire.

9.2. Recommendations for further research

As discussed above, the current study has greatly improved the hydrological understanding of the Dauges mire and its catchment, and, more generally, of mires in similar hydrogeological settings within the Massif Central and beyond. It has also identified a number of potential areas where additional work is required, first, to further improve the hydrological understanding and modelling of the Dauges site as a model of minerotrophic acidic mires in the Massif Central, and beyond, of uplands of south-western Europe; second, to validate some of the findings of the current study using other approaches; and third, to broaden mire research and provide additional evidence for the future management of the NNR and of other protected mire sites.

9.2.1. Improving the hydrological understanding and modelling of the Dauges site

The MIKE SHE / MIKE 11 model developed as part of the study is a rare example of a spatially-distributed physically-based multi-objective integrated hydrological model of a groundwater-fed mire and its catchment in a basement region. It has proved useful in investigating a number of fundamental and applied research questions on the hydrology of such systems. The monitoring equipement installed as part of the study, the data collected and the MIKE SHE / MIKE 11 model could be used to investigate a number of additional questions related to hydrological processes in these environments, such as the impact of climate change on the eco-hydrology of mires, climate change mitigation management, processes affecting the export of dissolved organic carbon, metalloids or radio-nuclides, hydrological modelling of weathered granite formations, or water resource management in basement regions. Nevertheless, a number of shortcomings and additional research gaps have been identified that may need to be addressed before both the observed data and the model are used for such applications. They can be divided in three groups, related to improvements in the geological model, to improvements in the design of the MIKE

SHE / MIKE 11 model, and to the collection of new data allowing to strengthen the model calibration and validation.

9.2.1.1. Improving the geological model

Potential explanations for the discrepancies between observed groundwater table depths and those simulated by the MIKE SHE / MIKE 11 model in a number of dipwells have been identified in Section 6.2.1.5. For instance, the sensitivity analyses detailed in Sections 6.3.1 and 6.3.2 showed that the parameters to which the model performance with regard to both groundwater table depth and stream discharge is most sensitive are the depth, shape and hydraulic characteristics of the fissured granite zone. During model calibration (Chapter 6), it became apparent that observed groundwater table depths and stream discharge could not be satisfactorily reproduced if the horizontal hydraulic conductivity of the fissured zone was kept within values cited in the literature (Section 6.4.5). It was suggested that a large degree of spatial heterogeneity in fissure density and bulk hydraulic conductivity within the fissured zone could potentially explain this finding. Indeed, the electrical resistivity tomography survey and the geological borehole drilling logs indicated that neither the depth nor the fissure density of the fissured zone are homogeneous across the catchment (Section 3.3). The fissured zone was nevertheless modelled as a homogeneous layer of constant depth in the absence of more detailed informations. The poor performance of the Dauges model with regard to groundwater table depth in some dipwells on the southern side of the mire was tentatively attributed to the presence of localised outcrops of denser granite (Section 6.2.1.5). As detailed in Section 6.4.5, a number of techniques could be used to improve the accuracy of the geological model. These include geological drilling associated to borehole pumping tests, proton magnetic resonance (Wyns *et al.* 2004), ground penetrating radar (Descloîtres *et al.* 1997; Mahmoudzadeh *et al.* 2012) or electrical resistivity tomography.

Recommendation: the accuracy of the Dauges geological model should be improved using a combination of additional electrical resistivity tomography transects, geological drilling, pumping tests and any other suitable geo-physical and hydrogeological investigation methods.

However it should be recognised that these methods are time-consuming and expensive, require highly specialised equipment and skills, and therefore cannot easily be carried out at a high resolution over large areas. Furthermore, it remains unclear whether the availability of such data would substantially improve the model performance. For instance, even though Ahmed &

Sreedevi (2008) assembled a large and detailed database on the shape, depth and hydraulic characteristics of granite weathering formations within a 53km² catchment in India, they could not satisfactorily simulate piezometric heads without calibrating their model and introducing linear vertical barriers that they related to observed or assumed geological discontinuities. As stated by Singhal & Gupta (2010), the task of modelling groundwater flow in fractured rocks is hampered by the heterogeneity of such systems and the difficulties in adequately describing their hydrogeological properties. Therefore, the improvement in model performance that such techniques could provide should be tested beforehand in a theoretical study, similar to that carried out by Rochester (2010) using the Tern catchment (UK) as a case study, and in which she compared the performance of two physically-based distributed model built using either spatially-distributed or homogeneous parameters. This could be carried out in a research catchment where detailed knowledge of the granite weathering formations is available, for instance those studied by Lubczynski & Gurwin (2005) in Spain or Ahmed & Sreedevi (2008) in India, by creating several geological models based on progressively smaller subsets of data and by comparing the performance of otherwise identical hydrological models calibrated against the same observed hydrological data.

Within the Dauges catchment, the added value of collecting additional data on the shape, depth and hydraulic properties of the fissured zone could be evaluated by building a theoretical geological model with fully distributed properties based on the current understanding of the catchment as detailed in the current study. These properties could then be averaged into a homogeneous geological model, the properties of which would be determined by manual or automatic calibration based on piezometric heads and stream discharge produced by the distributed model. Finally, the potential value of further surveys could be estimated by iteratively reintroducing spatially-distributed data corresponding to these surveys within the homogeneous model, recalibrating the model and comparing its performance relative to both the homogeneous and fully distributed models. In this way the potential value of specific methods, accounting for uncertainties in interpretation for instance, or of specific survey locations could be evaluated.

Recommendation: the added value in terms of model performance of collecting additional data on the shape, depth and hydraulic properties of the fissured zone should be evaluated in a theoretical study.

Electrical resistivity tomography appeared to be a powerful, cost-effective and relatively easy-to-implement method to obtain detailed information on the depth of unsaturated saprolite, of the groundwater table depth within the fissured zone and, presumably, on fissure density within the fissured zone, at least semi-quantitatively (Section 3.3.3.3). However the comparison of the geological drilling logs, all located along the eastern part of the mire, and of the two ERT transects located further downstream highlighted potential discrepancies between the two surveys with regard to the depth of the saprolite layer underneath the mire (Section 3.3). The geological drilling logs showed the presence of a deep saprolite layer, whereas there was no evidence of it within the ERT data. This may reflect the reality: the presence of Puy Rond and of bottlenecks each side of it may have prevented the evacuation of the saprolite layer from areas upstream but not from those downstream. Alternatively, it may result from a methodological artefact if electrical resistivities of saturated saprolite and of saturated fissured granite are similar. This does not seem to be supported by the available literature (Figure 3-15) that suggests relatively clear differences between both formations, however the resistivity values suggested as characteristic of each formation are relatively inconsistent between studies.

As part of the current study, additional ERT surveys along the available geological drillings were planned to allow for the former method to be validated against the latter, however this was prevented by equipment failure. The planned additional ERT surveys could be carried out to confirm the interpretation of the available ERT transects and, if saturated saprolite and fissured granite do have different resistivities, to confirm the absence of saprolite downstream of Puy Rond. The actual depth of the saprolite layer along existing ERT transects could also be measured in a selection of representative locations using drilling or penetrometry equipment

Recommendation: in order to validate the interpretation of electrical resistivity values with regard to saprolite, additional ERT surveys should be carried out along the available deep geological drillings. Drilling or penetrometry surveys should be undertaken along existing ERT transects.

On the basis of existing geological data within the surrounding Monts d'Ambazac, of available sections through superficial geological formations and of the ERT survey, the depth of the saprolite layer (including peri-glacial formations) was deemed to be small in most places, from 0m to no more than 1.5m, except upstream of Puy Rond where geological drillings showed the presence of substantial depths of saprolite (Section 3.3.4). The potential distribution of residual saprolite was modelled at the scale of the catchment using easily available proxy variables such

as slope, large granite outcrops and boulders and historical landuse (Section 3.3.3.4). However in the absence of suitable data this approach could not be validated. On the basis of a limited number of pedological pits, mineral soils were assumed to be on average 40-70cm deep. As a consequence, saprolite and peri-glacial formations were neglected and soils were modelled as a homogeneous layer 50cm deep (Chapter 5). This is clearly a simplification, and the model performance would probably benefit from better representation of the spatial variability of superficial formations. Data collection could be carried out using drilling or penetrometry equipment using a stratified sampling scheme based on potential explanatory variables including topographic indices, elevation relative to the palaeosurface and past and present vegetation. The saprolite distribution model developed in Section 3.3 could then be validated and further refined. The factors explaining soil and saprolite depth could be investigated and a spatially-distributed empirical model developed. Similarly, in the absence of suitable field data, the unsaturated zone parameters on mineral soils were assumed to be homogeneous and estimated on the basis of literature data measured in similar environments. The representation of evapotranspiration and unsaturated flow processes might therefore be improved if a spatially-distributed model of moisture retention properties and of saturated hydraulic conductivity of soils and saprolite is developed. This should be based on the determination in the laboratory of moisture retention curves and hydraulic conductivity of a representative number of undisturbed cores and the development of a spatially-distributed empirical model of the corresponding parameters based on potential explanatory variables.

Recommendation: the 3D model of soils and saprolite should be refined by measuring and modelling the depth, soil moisture retention curve and hydraulic conductivity of soils and saprolite within the Dauges catchment using a combination of coring, drilling or penetrometry surveys and laboratory measures.

9.2.1.2. Improving the design of the MIKE SHE / MIKE 11 model

In Section 6.2.1.5 it was shown that the performance of the model with regard to discharge at Marzet during the validation period was not satisfactory. In Section 6.3.5, simulated discharge at Marzet, and to a lesser extent at Pont-de-Pierre, were shown to be very sensitive to the length of the simulation period. This was attributed to a lack of convergence of the overland flow component of the model, leading to large errors in simulated overland flow, especially in topographic sinks or flats. This should be resolved if the model is to be used for longer simulations than the three-year period used in the current study. Several potential solutions

were tested: the replacement of the topographic grid by a DEM in which topographic sinks were infilled, a higher maximum number of iterations and a shorter maximum time-step. None led to an improvement. Since diffuse runoff from the catchment makes for a substantial proportion of water inputs to the mire, overland flow must be modelled as a spatially-distributed process, and cannot easily be simplified using shallow drains routing overland flow directly to watercourses. It is possible that the error of the overland flow model could be reduced by using newer versions of MIKE SHE. Changes have been made to this component since the 2009 version used in the current study, including changes to the default threshold gradient for overland flow and the introduction of a multi-cell overland flow method that generates much more accurate water levels at a fraction of the calculation time previously required (Anonymous 2011).

Recommendation: the model should be run with a newer version of MIKE SHE to investigate whether overland flow error can be reduced.

Stream flow was modelled using kinematic routing, and stream stage calculated a posteriori using the Manning equation (Section 5.4.4). This method was preferred to the Saint-Venant equations because the latter required very long run times incompatible with the multiple runs required for the model calibration and sensitivity analyses. However kinematic routing cannot account for backwater effects, that are common in the flattest part of the mire where the stream profile slope is low. As a consequence, the model performance with regard to stream stage was poor (Section 6.2.1.5). For this reason, neither overbank flooding nor exchanges between the stream and the mire, that were shown to be particularly important downstream of Puy Rond where permeable alluvial sediments were found (Sections 3.4 and 4.3.2.3), could be accurately modelled. This explains the poor performance of the model with regard to groundwater table depth in a small number of dipwells located in this part of the mire. One solution could be to use nested models, as was done by Johansen *et al.* (2014) to model groundwater flow to and within a small fen fed by a large regional aquifer in Denmark. The model developed as part of the current study would be used to model flow at the catchment scale, while a smaller-size but higher-resolution MIKE SHE model combined to a MIKE 11 model using the Saint-Venant equations would be used to model flow within the mire. Piezometric heads, overland flow depths and stream discharge simulated by the catchment model along the mire boundaries would be used as time-varying boundary conditions for the smaller model. This solution could not be implemented with MIKE SHE version 2009 as it does not allow for time-varying boundaries to be specified for overland flow. As shown by the water balance (Section 7.3.2), overland flow

inputs to the mire make for a substantial proportion of total inflow to the mire and cannot be neglected. This restriction was lifted in later versions (Anonymous 2011).

Recommendation: the model performance with regard to stream stage, and therefore overbank flooding and stream-groundwater exchange, should be improved by using a nested model in which channel flow within the mire is modelled using the Saint-Venant equations.

The assessment of the impacts of landuse changes within the catchment on the mire water balance showed that the two-layer unsaturated zone model may not adequately simulate some aspects of evapotranspiration and unsaturated flow in mineral soils, due to MIKE SHE overriding the user-specified root depth when larger that the depth of the upper computational layer, even when the groundwater table is below the root zone (Section 8.4). This had a limited impact when comparing landcovers with similar root depths, such as broadleaf and coniferous woodlands. However this issue hindered an accurate assessment of the impact of catchment landuse conversion to grassland, and therefore it should be resolved. The depth of the upper computational layer on mineral soils could be increased to two metres, corresponding to the maximum root depth, and the model calibrated and validated again before the impact of conversion to grassland is evaluated. The replacement of the two-layer unsaturated zone model with the gravity or Richards models may allow for a more accurate representation of these processes but would require additional computing capability. To limit the number of additional parameters that require calibration, the use of these models would also require additional data on soil moisture retention and hydraulic conductivity in mineral soils, saprolite and upper fissured granite zone.

Recommendation: the representation of differences in root depth between landuse classes in the two-layer unsaturated zone model should be improved by increasing the depth of the upper computational layer on mineral soils and recalibrating the model. The ability of the gravity or Richards models to provide a better representation of unsaturated flow processes within reasonable run times should be investigated. Changes in hydrological conditions simulated under the grassland scenario should then be evaluated again.

9.2.1.3. Extending the scope of model calibration and validation

The model was calibrated against observed stream discharge, stream stage and groundwater table depth over the 01/01/2011-30/06/2012 period, and validated over the 01/07/2012-

31/12/2013 period. Similar or shorter calibration and validation periods are commonly used in published wetland studies using transient hydrological models (Thompson *et al.* 2004; Lu *et al.* 2006, 2009; Dai *et al.* 2008; Fournier 2008; Hammersmark *et al.* 2008; Singh *et al.* 2010, 2011; Singh 2010; Lewis *et al.* 2013; Johansen *et al.* 2014; Levison *et al.* 2014). Nevertheless, this may be due to practical constraints rather than evidenced-based methodological choices. Anderson & Woessner (1992a) recommended acquiring new observations long enough after the initial simulation was made to ensure that there had been adequate time for significant changes in the environmental conditions to occur and assessing the model performance against this new set of observations. This should be implemented if the Dauges model is to be used for further research, and would require that hydrometeorological monitoring is resumed and continued over the long-term. Given the scarcity of high-quality long-term hydrological datasets in French mires, such monitoring would also provide the necessary foundations for a number of other fundamental and applied scientific investigations, for instance related to the impact of climate change on the water balance of both the mire and the wider catchment

Recommendation: hydrometeorological monitoring should be resumed within the Dauges catchment and continued over the long-term.

Recommendation: once longer hydrometeorological time-series have been collected, the model calibration should be improved and the model further validated using extended stream stage, stream discharge and groundwater table depths time-series.

Due to technical and financial constraints, groundwater table depth could only be monitored in locations where it is shallow (less than three metres approximately) and in soft materials that could be augered manually (Section 4.3). These locations are not representative of the groundwater table dynamics in the fissured granite underneath hilltops and hillslopes. However, the relatively large range of elevations at which dipwells could be installed (Section 4.3) and the good agreement between the spatial distribution of the mean simulated groundwater table depth and the observed distribution of wetland vegetation (Section 6.2.2) provide some confidence in the model's ability to accurately simulate groundwater table depth across the catchment. Nevertheless, this should be verified by validating simulated groundwater table depths against data recorded in deeper observation wells located in the upper part of the catchment. The installation of these dipwells would also provide an opportunity to collect information on the properties of the fissured zone.

Recommendation: groundwater table depth should be monitored in a small number of observation wells installed within the fissured granite on hilltops and hillslopes surrounding the mire. Data from this additional monitoring should be used to improve the model calibration and validation.

In common with most hydrological modelling studies investigating mires (Sections 1.4.2 and 5.3.2) and due to technical and financial constraints, no data relating to evapotranspiration and unsaturated flow processes was available, and the two-layer unsaturated flow model was simply parameterised using literature data and calibrated in a single step with all other model components against observed stream discharge and groundwater table depth. However, as shown in Chapters 7 and 8, evapotranspiration and unsaturated flow processes within the catchment have substantial impacts on the mire water balance, and the accurate representation of these processes should be checked against additional data. These could include data on actual evapotranspiration (estimated using sap flow measurements or micrometorological methods, Wilson *et al.* 2001), interception (deduced from measures of precipitation, throughfow and stemflow, Gerrits 2010), and soil moisture time-series (estimated using Time Domain Reflectometry for instance, Ladekarl 1998, 2001). The literature review presented in Section 5.4.3 and Appendix G has highlighted a lack of published data on the evapotranspiration characteristics of dry heathland, and these should be further investigated given the past importance of this landcover class within the Massif Central (Section 2.2.3).

Recommendation: evapotranspiration and unsaturated zone processes on mineral soils should be monitored and the model calibration and validation improved using these additional data.

Recommandation: evapotranspiration processes in dry heathland should be investigated.

9.2.2. Validating research findings using other methodological approaches

Despite convicing evidence that the replacement of open habitats by woodlands, and in particular by conifer plantations, leads to a substantial reduction in runoff and groundwater recharge (see Appendix H), only a handful of studies have investigated the impact of such changes within wetland catchments on their hydrology and ecology (Section 8.2). The current study therefore provides much needed evidence on this matter. In Section 8.4, it was shown that the replacement of broadleaf woodlands with coniferous plantations within the Dauges catchment would lead to a reduction in inflows to the mire and to a lower groundwater table

depth along its margins in summer. Conversely, the model results suggested that the replacement of broadleaf woodlands with grassland would lead to an increase in inflows and to a higher groundwater table depth, even though the magnitude of these changes was probably underestimated due to methodological issues. Given the high conservation value of mires, and the substantial changes in landuse that occurred during the last century in mire catchments within the Massif Central (Section 2.2.3), these results should be confirmed by direct observation of actual changes in the hydrology, ecology and pedology of mires. Changes in mire surface wetness may have led to changes in peat properties, vegetation and other sensitive taxa such as testate amoebae (Charman 2002). The investigations carried out by Smith & Charman (1988) and Hendon & Charman (2004) to evidence such changes in mires of Northern England using direct observation in paired samples and palaeoecological techniques, respectively, should be reproduced within the Massif Central.

Recommandation: the actual impacts of changes in catchment landuse within the Massif Central on the hydrology and ecology of minerotrophic acidic mires should be investigated, for instance using methods similar to those presented by Smith & Charman (1988) and Hendon & Charman (2004) in a representative sample of mires with contrasted catchment landuses.

The current study has demonstrated that throughout most of the mire, the groundwater table is maintained at ground level or at shallow depths by groundwater upwelling from the underlying mineral formations, which makes for an overwhelming proportion of the water present within the saturated peat (Sections 4.3.2.3 and 7.3.2). The mire is clearly groundwater-fed, with the possible exception of small isolated hummocks that could not be accounted for at the model spatial resolution. Yet a large proportion of the mire vegetation has been classified and mapped by vegetation ecologists as characteristic of ombrotrophic bogs (Botineau *et al.* 1998; Durepaire & Guerbaa 2008). Plant communities similar to those mapped within the Dauges mire and occurring in similar hydrogeomorphic settings have been identified in many mires of the Limousin and Massif Central uplands and also described as belonging to “ombrotrophic mires” and/or “raised bogs” (Ghestem & Vilks 1980; Ghestem *et al.* 1988; Botineau *et al.* 1993; Vilks 1993; Cournez *et al.* 2000; Chabrol 2006; Chabrol & Reimringer 2011). Many vegetation plots described by these authors were classified as belonging to the *Erico tetralicis – Sphagnetum magellanici* (Osvald 1923) J.J. Moore 1968 phytosociological association, recently described by Thébaud & Petel (2008) and Thébaud (2011) as characteristic of raised bogs. As a consequence, many mires have been designated as Special Areas of Conservation under the EU 92/43/EEC

Habitats Directive for the conservation of “Active raised bogs” and “Degraded raised bogs still capable of natural regeneration”, listed in Annex I of the Directive. This apparent contradiction between vegetation and wetland water supply mecanisms demonstrated by the current study in the case of the Dauges site and suggested by hydrogeomorphic settings in many other mires of the Massif Central should be further investigated. In a review of environmental gradients in north-west European mires, Wheeler & Proctor (2000) showed that the limit between truly ombrotrophic and minerotrophic but acidic and oligotrophic mires is not sharp and cannot be related to consistent differences in either vegetation or water chemistry. They even suggested that this distinction should be abandoned. Unfortunately, there is very little data allowing the extension of their conclusions to mires of south-west Europe, including France. The relationship between vegetation, water chemistry and wetland water supply mecanisms in acidic mires of the Massif Central and of other French regions with crystaline bedrock should therefore be clarified, in particular by investigating the correlation between vegetation and chemical or isotopic indicators of the origin of water in the peat (Proctor *et al.* 2009) in a gradient from ombrotrophic raised bogs to minerotrophic acidic mires, including the Dauges mire.

Recommandation: the relationship between vegetation, water chemistry and wetland water mecanisms in acidic mires within the Massif Central and south-west Europe generally should be investigated.

9.2.3. Broadening research questions: the impact of climate change

Climate change is likely to be a major stress factor for mires globally (Section 1.2.6.2). Figure 9-1 and Figure 9-2 shows mean monthly anomalies in precipitation and Penman-Monteith reference evapotranspiration given for the Dauges area by the two downscaling experiments SCAMPEI and SCRATCH08 (Pagé *et al.* 2008; Lémond *et al.* 2011). These experiments downscaled the outputs of a number of global climate models to daily time-series with a resolution of 8km, covering Metropolitan France. The emission scenarios corresponded to those given by the International Panel on Climate Change Special Report on Emission Scenarios (Nakicenovic & Swart 2000).

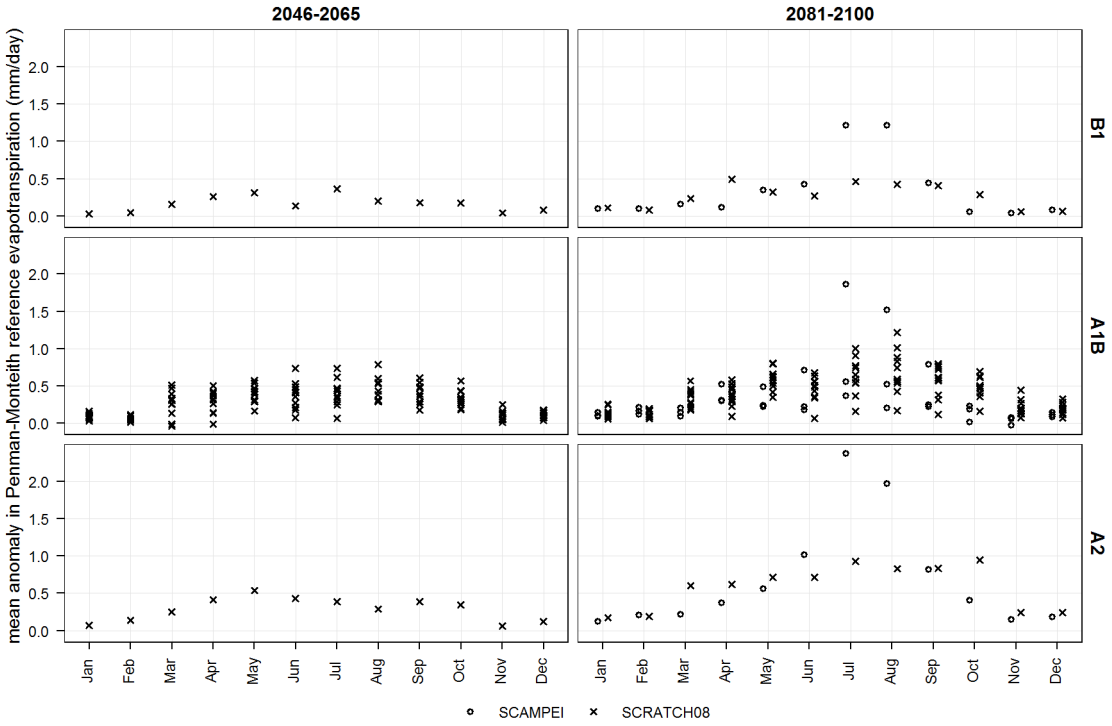

Figure 9-1. Mean anomaly in reference evapotranspiration (FAO Penman-Monteith) simulated by the SCAMPEI and SCRATCH08 GCM downscaling experiments for the Dauges area.

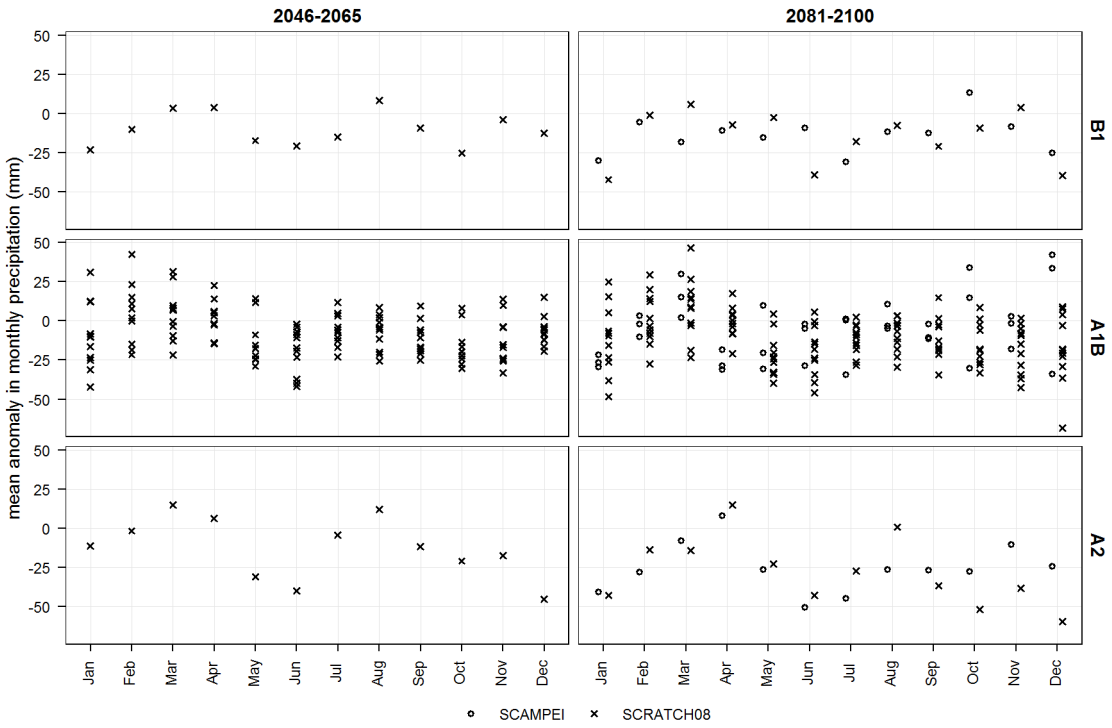

Figure 9-2. Mean anomaly in monthly precipitation simulated by the SCAMPEI and SCRATCH08 GCM downscaling experiments for the Dauges area.

Figure 9-1 shows that all downscaled GCM models consistently simulate a substantial increase in reference evapotranspiration by the end of the century for the Dauges site, particularly in summer. There is much more uncertainty on the direction, rate and seasonal patterns of changes in precipitation (Figure 9-2). The downscaling methodologies used in the SCAMPEI and SCRATCH08 experiments included GCM bias correction based on data collected by the dense network of French meteorological stations. However, Figure 9-3 shows that some bias is still present in simulated datasets particularly for precipitation, possibly due to the coarse grid size and the consequent underestimation of orographic effects.

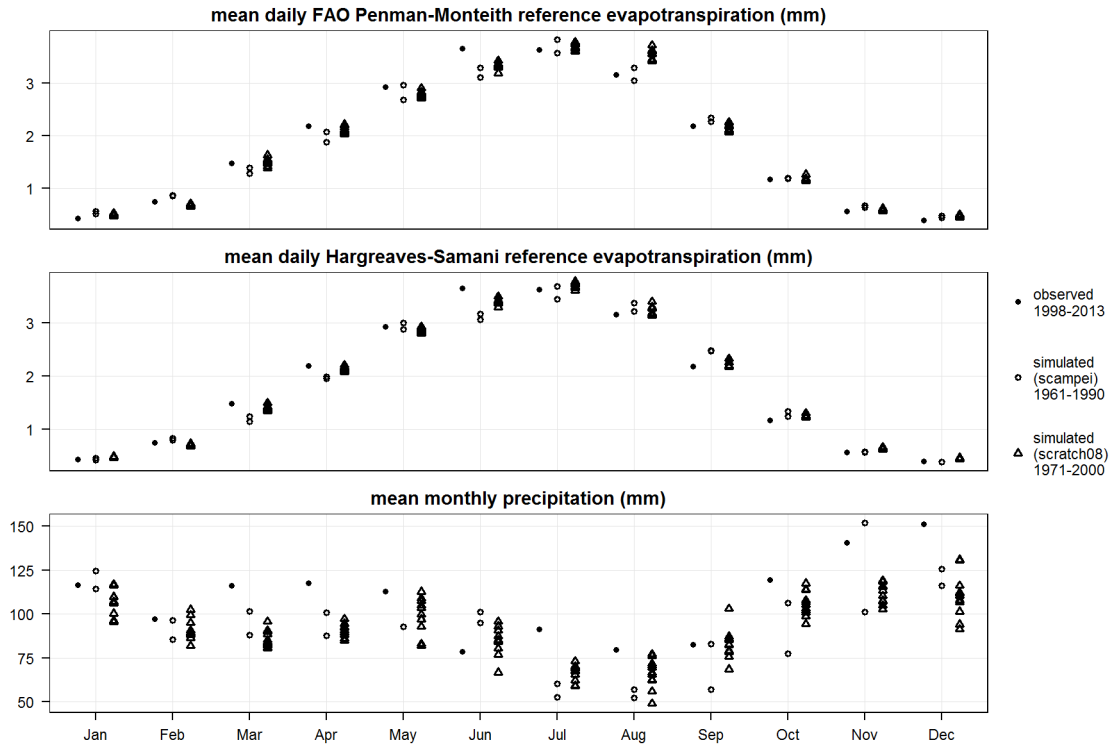

Figure 9-3. Comparison of reference evapotranspiration and precipitation observed at the Dauges site with those simulated by the SCAMPEI and SCRATCH08 downscaling experiments for the nearest grid cell.

Nevertheless, this residual bias is probably small enough for the time-series simulated for the baseline and future periods to be used to force the calibrated Dauges MIKE SHE / MIKE 11 model and to investigate expected changes in the mire water balance and groundwater table dynamics for the different emission scenarios, global climate models and downscaling methods. However, these long-term time-series cannot be used with the current Dauges model as it is sensitive to the simulation length. As discussed in Section 6.3.5, this is probably due to a lack of convergence of the overland flow model which should first be resolved. Another option would be to use a delta-factor approach, for instance by multiplying the observed precipitation and reference evapotranspiration used for the model calibration and validation and covering a period of three

years by the long-term mean monthly percentage changes provided by the downscaled climate models, a method used by Thompson *et al.* (2009) for instance. However this would not account for changes in the distribution and frequency of events. The combined impact of catchment landuse and climate change on the mire water balance and groundwater table depth, and the feasibility of managing catchment landuse to counteract climate change impacts should also be investigated.

Recommendation: the Dauges MIKE SHE / MIKE 11 model should be used to investigate the potential impact of climate change on the hydrology of the Dauges mire, as an example of groundwater-fed mires within the granitic Massif Central.

9.3. Recommendations for conservation management

9.3.1. Management of minerotrophic mires in basement regions

In Section 8.4 it was shown that changes impacting the recharge of the fissured granite aquifer within the mire catchment had a larger impact on groundwater table depth close to the mire margins compared to at its centre. Similarly, impacts on stream discharge were larger upstream of the mire than downstream of it. This shows that any experimental, monitoring or surveillance schemes aiming at detecting environmental changes within the mire as a consequence of changes occurring within the catchment, for instance water abstraction or diversion, landuse changes or climate change, should focus on or at least encompass mire margins and small headwater inlets. The current study generally shows that, for a given landuse change scenario, the magnitude of changes in groundwater table depth increases from the centre of the mire towards the catchment boundaries. Surveillance of groundwater table depth in observation wells located within the fissured zone upstream of the mire could therefore prove useful in providing an early warning system for hydrological changes within the catchment, even before such changes can be observed within the mire.

Recommendation: Mire margins should be adequately instrumented and investigated as part of experimental, monitoring or surveillance schemes aiming at detecting environmental changes in mires of similar hydrogeomorphic and hydrogeologic settings to the Dauges mire.

Recommendation: Within hydrogeomorphic and hydrogeologic settings similar to the Dauges site, hydrological monitoring schemes aiming at detecting environmental changes in mires should be extended to the fissured bedrock aquifer as far upstream of the mire as possible.

The major outcome of the current study relevant to the management of protected mire habitats within the Dauges NNR and SAC and in sites with similar hydrogeomorphic and hydrogeologic settings is the demonstration that shallow groundwater tables within the mire are principally maintained by upwelling of groundwater from the underlying mineral formations, in particular the fissured zone (Sections 3.3.3.3, 4.3.2.3, 7.2.2 and 7.3.2), and that, as a consequence, changes in aquifer recharge within the mire catchment will substantially reduce groundwater inflows to the mire and lower groundwater table depth within the mire, particularly close to its margins. The current study has indeed demonstrated that changes in catchment landuse, in particular the conversion of existing broadleaf woodlands to conifer plantations, can have such an impact (Chapter 8). Conversely, the results suggested that the replacement of woodlands by grassland would increase water inputs to the mire and reduce groundwater table depth within it, even though the simulated impact has probably been underestimated due to methodological issues (Section 8.4). As a consequence, policies aiming at the conservation of mire habitats in sites of similar hydrogeomorphic settings to the Dauges mire should encompass the whole mire catchment. Article 6 of the EU 92/43/EEC Habitats Directive states that “any plan or project […] likely to have a significant effect thereon, either individually or in combination with other plans or projects, shall be subject to appropriate assessment of its implications for the site in view of the site's conservation objectives”. The present study demonstrates that any activity likely to result in substantial changes in groundwater flow within granite weathering formations upstream of the mire, even beyond SAC boundaries, does fall within the remit of this article. This includes changes in landcover within the mire catchment, in particular the conversion of open habitats to woodland or the conversion of broadleaf forest to coniferous plantations. Policies should be implemented to avoid long-term cumulative impacts of small-scale forestry operations that may, if considered individually, not have a substantial impact or fall below area thresholds set by the regulator.

Recommendation: In policies and management documents relative to the conservation of mire sites, habitats and species in hydrogeomorphic settings similar to the Dauges site, all activities that may have an impact on groundwater recharge upstream of the mire site, including changes in landuse resulting from forestry operations, should be considered as potentially damaging to the conservation of mire habitats and species.

Recommendation: In particular, all such activities within and upstream of Special Areas of Conservation designated for the conservation of mire habitats and species in sites with similar

hydrogeomorphic settings as the Dauges site should be considered as falling within the remit of article 6 of the EU 92/43/EEC Habitats Directive.

Recommendation: In and upstream of protected mire sites in hydrogeomorphic settings similar to the Dauges site, policies and management objectives aiming at maintaining or developing open habitats rather than woodlands, and broadleaf woodlands rather than coniferous plantations, should be implemented.

9.3.2. Management of the Dauges National Nature Reserve and Special Area of Conservation

All of the recommendations made in Section 9.3.1 are obviously relevant to the Dauges NNR and SAC. In particular, all activities that may reduce groundwater recharge within the mire catchment should be considered as potentially damaging to the conservation of mire habitats and species. The conversion of open habitats to woodland and of deciduous woodland to dense plantations of coniferous species with a large interception capacity (for instance Douglas fir *Pseudotsuga menziesii*, Norway spruce *Picea abies*, Silver fir *Abies alba* or Grand fir *Abies grandis*) should be avoided, and conversely, the restoration of open habitats or deciduous woodlands from coniferous plantations should be encouraged. Forestry activities are already regulated within the NNR boundaries by the "*Décret no 98-842 du 15 septembre 1998 portant création de la réserve naturelle de la tourbière des Dauges (Haute-Vienne)".* Plantations are subject to an administrative authorisation after consultation of the NNR management committee, and the findings of the current study should be considered in this process. Future NNR management plans should promote the restoration of open habitats wherever possible.

The Dauges stream was diverted and straightened for agricultural purposes at some point in the past between Puy Rond and the wetland main outlet at Pont-de-Pierre (Durepaire & Guerbaa 2008). The date of the works is not known but pre-dates 1950, when the first aerial photograph of the area was taken. The stream now follows the boundary between two land plots, already defined in 1836 when the first cadastre was completed. The NNR management plan (Durepaire & Guerbaa 2008) recommended that the stream is restored to its pre-engineering course, on the assumption that the current straightened course increases drainage and may lead to a deeper groundwater table in the peat and a degraded eco-hydrological condition of the mire. The current study has shown that this is not the case (Section 4.3.2.3). On the contrary, in the summer, water flows from the diverted stream to the mire through highly permeable gravel deposits, and the stream contributes to the persistence of a shallow groundwater table in this part of the mire

whereas it is much deeper elsewhere. Furthermore, during overbank flooding events, flood water does not flow back to the stream immediately, but flows as diffuse overland flow along the very shallow thalweg still existing along the probable pre-engineering course of the stream. The reason for this is that the stream now flows at a higher elevation than its original course, and its slope in this area has actually been reduced by the diversion. This promotes overbank flooding. As a consequence, the stream should not be restored into its pre-engineering course if the objective is to maintain or promote a shallow groundwater table in this part of the mire. High stream stages and frequent overbank flooding are further promoted by numerous obstacles resulting from the absence of management of the stream bed and banks (Section 6.4.2). Another objective of the NNR management plan that aims at clearing these obstacles should therefore be abandonned.

Recommendation: The existing course and section profile of the stream between Puy Rond and Pont-de-Pierre should be maintained and stream restoration avoided.

In Sections 3.4, 3.5 and 4.3.2.3 it was shown that the north-eastern margin of the mire is characterised by a superficial 35-50cm deep layer of degraded granular oxidised peat associated with a deeper and more variable groundwater table than in other parts of the mire. Despite relatively deep peat deposits, the current vegetation is dominated by *Nardus stricta*, and there is no peat-forming species. In Section 6.2.1.5, the local degradation of the peat properties was suggested as the reason for the poor performance of the model in this area, where it predicted higher and more stable groundwater table depths than observed. It was suggested that the presence of numerous shallow drains in this part of the mire, possibly associated with a peat fire in the past, was responsible for the degradation of the peat physical properties, of the mire hydrological condition and of peat-forming mire vegetation that existed in the past. These findings call for the hydrological and ecological restoration of this area. They also call for a detailed analysis of the long-term impacts of shallow drains on hydrological processes, peat properties and vegetation to be carried out within the NNR and in other mires, for instance by investigating changes along transects perpendicular to long-established shallow drains.

Recommendation: The hydrology and peat-forming vegetation at the north-eastern margin of the mire should be restored by blocking existing drains.

Recommendation: The long-term impacts on peat physical properties and vegetation of existing shallow drains within the NNR should be investigated.

9.4. Conclusion

The current study is a rare example, and the first of its kind in France, of an integrated investigation of the hydrological functioning of a minerotrophic mire in a basement region. It has highlighted the high level of hydrological connectivity existing between the weathered granite aquifer and the wetland, and the importance of groundwater upwelling in the mire's water balance and groundwater table dynamics. It has also shown that there is a large amount of variability in hydrological processes within the mire, due to a high degree of heterogeneity in the properties of peat, alluvial deposits and granite weathering formations and to past human interference. It also ranges within only a handful of studies worldwide that have investigated the impact of catchment afforestation on wetland hydrological conditions, and it has demonstrated that the conversion of broadleaf woodlands to coniferous plantations upstream of a wetland can have a substantial impact on its water balance and groundwater table dynamics. It provides much needed evidence for the conservation management of these threatened habitats, and sound foundations for future research on their ecological, hydrological and biogeochemical functioning.

Résumé du chapitre 9 (conclusion)

La présente étude est un exemple rare, et le premier mené en France, d'une étude intégrée du fonctionnement hydrologique d'une tourbière minérotrophe en région de socle. Elle a mis en évidence la forte connectivité hydrologique existant entre l'aquifère des formations d'altération du granite, en particulier de la zone fissurée, et la zone humide ; ainsi que l'importance quantitative des apports souterrains dans le bilan hydrique de la tourbière. Elle a également mis en lumière la diversité des processus hydrologiques expliquant les variations de nappe dans les histosols, liée à l'hétérogénéité des caractéristiques hydro-physiques des formations d'altération du granite et des dépôts tourbeux et alluviaux, et aux perturbations anthropiques. A l'échelle internationale, elle compte parmi un nombre très restreint d'études ayant porté sur l'impact de l'afforestation des bassins versants sur l'hydrologie des zones humides. Elle a permis de démontrer que, en région de socle, l'enrésinement d'un bassin versant initialement dominé par des boisements feuillus peut avoir un impact substantiel sur le bilan hydrique de la tourbière qu'il alimente, ainsi que sur les niveaux de nappe dans celle-ci. Cette étude apporte donc des éléments nouveaux devant être pris en compte pour la conservation de ces habitats menacés, ainsi que de solides bases pour de futures recherches sur leur fonctionnement écologique, hydrologique et géochimique.

References

Abbott, M.B., Bathurst, J.C., Cunge, J.A., O'connell, P.E. & Rasmussen, J. (1986a) An introduction to the European Hydrological System—Système Hydrologique Européen, "SHE", 2: structure of a physically-based, distributed modelling system. *Journal of hydrology*, 87, 61–77.

Abbott, M.B., Bathurst, J.C., Cunge, J.A., O'Connell, P.E. & Rasmussen, J. (1986b) An introduction to the European Hydrological System—Système Hydrologique Européen, "SHE", 1: History and philosophy of a physically-based, distributed modelling system. *Journal of hydrology*, 87, 45–59.

Acreman, M.C. (2005) *Impact assessment of wetlands: focus on hydrological and hydrogeological issues*. Phase 2 report, EA W6-091 / CEH C01996, Environment Agency & Centre for Ecology and Hydrology, Bristol & Wallingford, UK.

Acreman, M.C. & Miller, F. (2006) Hydrological impact assessment of wetlands. In *The global importance of groundwater in the 21st century. Proceedings of the international symposium on groundwater sustainability (ISGWAS)* (eds S. Ragone, N. Hernández-Mora, A. de la Hera, A. Bergkamp & J. McKay), pp. 225–255. National Groundwater Association Press, Ohio, USA.

Acworth, R.I. (1987) The development of crystalline basement aquifers in a tropical environment. *Quarterly Journal of Engineering Geology and Hydrogeology*, 20, 265–272.

Adriaenssens, S., Staelens, J., Wuyts, K., Wittenberghe, S.V., Wuytack, T., Verheyen, K., Boeckx, P. & Samson, R. (2012) Canopy uptake of $^{15}NH_3$ by four temperate tree species and the interaction with leaf properties. *Water, Air, & Soil Pollution*, 223, 5643–5657.

Aerts, R. & de Caluwe, H. (1994) Effects of nitrogen supply on canopy structure and leaf nitrogen distribution in *Carex* species. *Ecology*, 1482–1490.

Ahmed, S. & Sreedevi, P.D. (2008) Simulation of flow in weathered-fractured aquifer in a semi-arid and over-exploited region. In *Groundwater dynamics in hard rock aquifers: sustainable management and optimal monitoring network design* (eds S. Ahmed, R. Jayakumar & A. Salih), pp. 219–233. Springer, Dordrecht, The Netherlands.

Al-Khudhairy, D.H.A., Thompson, J.R., Gavin, H. & Hamm, N.A.S. (1999) Hydrological modelling of a drained grazing marsh under agricultural land use and the simulation of restoration management scenarios. *Hydrological Sciences Journal*, 44, 943–971.

Allen, A. & Chapman, D. (2001) Impacts of afforestation on groundwater resources and quality. *Hydrogeology Journal*, 9, 390–400.

Allen, R.G. & Pereira, L.S. (2009) Estimating crop coefficients from fraction of ground cover and height. *Irrigation Science*, 28, 17–34.

Allen, R.G., Pereira, L.S., Raes, D. & Smith, M. (1998) *Crop evapotranspiration - Guidelines for computing crop water requirements*. FAO irrigation and drainage paper, 56, Food and Agriculture Organization, Rome, Italy.

Allen, R.G., Pruitt, W.O., Businger, J.A., Fritschen, L.J., Jensen, M.E. & Quinn, F.H. (1996) Evaporation and transpiration. In *Hydrology handbook*, 2nd ed (ed Task Committee on Hydrology Handbook of Management Group D of ASCE), pp. 125–252. American Society of Civil Engineers, Reston, USA.

Anderson, K., Bennie, J.J., Milton, E.J., Hughes, P.D.M., Lindsay, R. & Meade, R. (2010) Combining LiDAR and IKONOS data for eco-hydrological classification of an ombrotrophic peatland. *Journal of Environmental Quality*, 39, 260–73.

Anderson, D.S., Davis, R.B. & Janssens, J.A. (1995) Relationships of bryophytes and lichens to environmental gradients in Maine peatlands. *Vegetatio*, 120, 147–159.

Anderson, M.P. & Woessner, W.W. (1992a) The role of the postaudit in model validation. *Advances in Water Resources*, 15, 167–173.

Anderson, M.P. & Woessner, W.W. (1992b) *Applied groundwater modeling: simulation of flow and advective transport*. Academic Press, San Diego, California, USA.

Andréassian, V. (2004) Waters and forests: from historical controversy to scientific debate. *Journal of Hydrology*, 291, 1–27.

André, M.-F., Etlicher, B., Godard, A., Sellier, D. & Van Vliet-Lanoë, B. (2001) Cryogenic processes and ice-related restructuring of the regolith in metamorphic and igneous terrains. In *Basement regions* (eds A. Godard, J.J. Lagasquie & Y. Lageat), pp. 147–169. Springer-Verlag, Berlin, Heidelberg, Germany.

Andreu, A., Aguilar, C., Polo, M.J., Carpintero, E. & González-Dugo, M.P. (2012) Basin-scale evapotranspiration assessment based on vegetation coefficients derived from thermal remote sensing. In *Remote sensing for agriculture, ecosystems, and hydrology XIV; SPIE Proceedings* (eds C.M.U. Neale & A. Maltese), pp. 85310M1–85310M11.

Anonymous. (1995) *Déclaration d'arrêt de travaux - Gorces-Saignedresse*. COGEMA, La Crouzille, France.

Anonymous. (2009a) *AUTOCAL - Auto calibration tool user guide*. DHI, Hørsholm, Denmark.

Anonymous. (2009b) *MIKE SHE user manual. Volume 1: User guide.* DHI, Hørsholm, Denmark.

Anonymous. (2009c) *MIKE SHE user manual. Volume 2: Reference guide*. DHI, Hørsholm, Denmark.

Anonymous. (2009d) *MIKE 11 - A modelling system for rivers and channels - Reference manual*. DHI, Hørsholm, Denmark.

Anonymous. (2011) MIKE SHE release note 2011. Available at: http://releasenotes.dhigroup.com/2011/MIKESHErelinf.htm [accessed 27 May 2015]

Anonymous. (2013) Core recovery parameters. Available at: http://en.wikipedia.org/w/index.php?title=Core_recovery_parameters&oldid=527258988 [accessed 9 February 2013]

Anonymous. (2014) *Rapport d'activité 2013 du service de distribution des eaux de la ville de Limoges - Prix et qualité des services publics d'eau et d'assainissement*. Ville de Limoges, Limoges, France.

Archie, G.E. (1942) The electrical resistivity log as an aid in determining some reservoir characteristics. *Transactions of the American Institute of Mining and Metallurgical Engineers*, 146, 54–67.

Armandine Les Landes, A., Aquilina, L., De Ridder, J., Longuevergne, L., Pagé, C. & Goderniaux, P. (2014) Investigating the respective impacts of groundwater exploitation and climate change on wetland extension over 150 years. *Journal of Hydrology*, 509, 367–378.

Armstrong, A.C. (1995) Hydrological model of peat-mound form with vertically varying hydraulic conductivity. *Earth Surface Processes and Landforms*, 20, 473–477.

Armstrong, W. & Boatman, D. (1967) Some field observations relating the growth of bog plants to conditions of soil aeration. *The Journal of Ecology*, 101–110.

Armstrong, A., Holden, J., Kay, P., Francis, B., Foulger, M., Gledhill, S., McDonald, A.T. & Walker, A. (2010) The impact of peatland drain-blocking on dissolved organic carbon loss and discolouration of water; results from a national survey. *Journal of Hydrology*, 381, 112–120.

Asada, T. (2002) Vegetation gradients in relation to temporal fluctuation of environmental factors in Bekanbeushi peatland, Hokkaido, Japan. *Ecological Research*, 17, 505–518.

Asensio, H. (1998) Raw data sources for the generation of external parameter for COSMO and GME. Available at: http://cosmo-model.cscs.ch/content/model/modules/externalParams/default.htm [accessed 31 October 2013]

Asner, G.P., Scurlock, J.M. & Hicke, J.A. (2003) Global synthesis of leaf area index observations: implications for ecological and remote sensing studies. *Global Ecology and Biogeography*, 12, 191–205.

Aussenac, G. (1968) Interception des précipitations par le couvert forestier. *Annales des Sciences forestieres*, 25, 135–156.

Aussenac, G. (1970) Action du couvert forestier sur la distribution au sol des précipitations. *Annales des Sciences Forestières*, 27, 383–399.

Aussenac, G. & Boulangeat, C. (1980) Interception des précipitations et évapotranspiration réelle dans des peuplements de feuillu (*Fagus silvatica* L.) et de résineux (*Pseudotsuga menziesii* (Mirb) Franco). *Annales des Sciences Forestières*, 37, 91–107.

Auterives, C. (2006) *Influence des flux d'eau souterraine entre une zone humide superficielle et un aquifère profond sur le fonctionnement hydrochimique des tourbières : exemple des marais du Cotentin, Basse-Normandie*. Thèse de Doctorat, Université Rennes 1, Rennes, France.

Auterives, C., Aquilina, L., Bour, O., Davranche, M. & Paquereau, V. (2011) Contribution of climatic and anthropogenic effects to the hydric deficit of peatlands. *Hydrological Processes*, 25, 2890–2906.

Baird, A.J. (1997) Field estimation of macropore functioning and surface hydraulic conductivity in a fen peat. *Hydrological Processes*, 11, 287–295.

Baird, A.J. & Gaffney, S.W. (1994) Cylindrical piezometer responses in a humified fen peat. *Nordic Hydrology*, 25, 167–182.

Baird, A.J. & Gaffney, S.W. (1995) A partial explanation of the dependency of hydraulic conductivity on positive pore water pressure in peat soils. *Earth Surface Processes and Landforms*, 20, 561–566.

Baird, A.J., Morris, P.J. & Belyea, L.R. (2012) The DigiBog peatland development model 1: rationale, conceptual model, and hydrological basis. *Ecohydrology*, 5, 242–255.

Baird, A.J., Surridge, B.W.J. & Money, R.P. (2004) An assessment of the piezometer method for measuring the hydraulic conductivity of a *Cladium mariscus - Phragmites australis* root mat in a Norfolk (UK) fen. *Hydrological Processes*, 18, 275–291.

Baize, D. & Girard, M.-C. (eds). (2009) *Référentiel pédologique 2008*, Association française pour l'étude du sol. Editions Quae, Versailles, France.

Ballard, C.E., McIntyre, N., Wheater, H.S., Holden, J. & Wallage, Z.E. (2011) Hydrological modelling of drained blanket peatland. *Journal of Hydrology*, 407, 81–93.

Baltassat, J.M., Krishnamurthy, N.S., Girard, J.F., Dutta, S., Dewandel, B., Chandra, S., Descloîtres, M., Legchenko, A., Robain, H., Ananda Rao, V. & Ahmed, S. (2006) *IFCPAR project 2700-W1 - Proton magnetic resonance technique in weathered-fractured aquifers*. Detailed scientific report, RP-54538-FR, Bureau de Recherches Géologiques et Minières, Orléans, France.

Baltassat, J.M., Legchenko, A., Ambroise, B., Mathieu, F., Lachassagne, P., Wyns, R., Mercier, J.L. & Schott, J.J. (2005) Magnetic resonance sounding (MRS) and resistivity characterisation of a mountain hard rock aquifer: the Ringelbach Catchment, Vosges Massif, France. *Near Surface Geophysics*, 3, 267–274.

Banaszuk, P. & Kamocki, A. (2008) Effects of climatic fluctuations and land-use changes on the hydrology of temperate fluviogenous mire. *Ecological Engineering*, 32, 133–146.

Baron-Yellès, N. & Goeldner-Gianella, L. (2001) *Les Marais maritimes d'Europe atlantique*. Presses Universitaires de France, Paris, France.

Bartelink, H.H. (1998) Radiation interception by forest trees: a simulation study on effects of stand density and foliage clustering on absorption and transmission. *Ecological modelling*, 105, 213–225.

Bartholomeus, R.P. (2010) *Moisture matters - Climate-proof and process-based relationships between water, oxygen and vegetation*. PhD thesis, Vrije Universiteit, Amsterdam.

Bartholomeus, R.P., Witte, J.-P.M., van Bodegom, P.M., van Dam, J.C. & Aerts, R. (2008) Critical soil conditions for oxygen stress to plant roots: Substituting the Feddes-function by a process-based model. *Journal of Hydrology*, 360, 147–165.

Bartholomeus, R.P., Witte, J.-P.M., van Bodegom, P.M., van Dam, J.C., de Becker, P. & Aerts, R. (2012) Process-based proxy of oxygen stress surpasses indirect ones in predicting vegetation characteristics. *Ecohydrology*, 5, 746–758.

Batelaan, O. & Kuntohadi, T. (2002) Development and application of a groundwater model for the Upper Biebrza River basin. *Annals of Warsaw Agricultural University-SGGW, Land Reclamation*, 33, 57–69.

Bayliss, A. (1999) *Flood estimation handbook, Volume 5: Catchment descriptors*. Institute of Hydrology, Wallingford, UK.

Beauvais, A., Ritz, M., Parisot, J.C. & Bantsimba, C. (2003) Testing etching hypothesis for the shaping of granite dome structures beneath lateritic weathering landsurfaces using ERT method. *Earth Surface Processes and Landforms*, 28, 1071–1080.

Beauvais, A., Ritz, M., Parisot, J.C., Dukhan, M. & Bantsimba, C. (1999) Analysis of poorly stratified lateritic terrains overlying a granitic bedrock in West Africa, using 2-D electrical resistivity tomography. *Earth and Planetary Science Letters*, 173, 413–424.

Beckwith, C.W. & Baird, A.J. (2001) Effect of biogenic gas bubbles on water flow through poorly decomposed blanket peat. *Water Resources Research*, 37, 551–558.

Beckwith, C.W., Baird, A.J. & Heathwaite, A.L. (2003) Anisotropy and depth-related heterogeneity of hydraulic conductivity in a bog peat. II: modelling the effects on groundwater flow. *Hydrological Processes*, 17, 103–113.

Beerling, D.J. (1999) Long-term responses of boreal vegetation to global change: an experimental and modelling investigation. *Global Change Biology*, 5, 55–74.

Beier, C., Emmett, B.A., Tietema, A., Schmidt, I.K., Peñuelas, J., Láng, E.K., Duce, P., De Angelis, P., Gorissen, A., Estiarte, M., de Dato, G.D., Sowerby, A., Kröel-Dulay, G., Lellei-Kovács, E., Kull, O., Mand, P., Petersen, H., Gjelstrup, P. & Spano, D. (2009) Carbon and nitrogen balances for six shrublands across Europe. *Global Biogeochemical Cycles*, 23, 1–13.

Bertrand, L. & Durand, E. (1983) *Fracturation naturelle et fracturation provoquée - Etude de la fracturation naturelle et détermination de l'état de contrainte en massif rocheux par différentes méthodes (site de Fanay-Augères, Haute-Vienne)*. Rapport général, 83SGN653GEG, Bureau de Recherches Géologiques et Minières, Orléans, France.

Beven, K. (1989) Changing ideas in hydrology — The case of physically-based models. *Journal of Hydrology*, 105, 157–172.

Beven, K.J. & Kirkby, M.J. (1979) A physically based, variable contributing area model of basin hydrology. *Hydrological Sciences Bulletin*, 24.

Beven, K.J. & Moore, I.D. (1993) *Terrain analysis and distributed modelling in hydrology*. Wiley & Sons, Chichester, UK.

Binet, S., Gogo, S. & Laggoun-Défarge, F. (2013) A water-table dependent reservoir model to investigate the effect of drought and vascular plant invasion on peatland hydrology. *Journal of Hydrology*, 499, 132–139.

Bissardon, M., Guibal, L. & Rameau, J.-C. (2003) *CORINE biotopes: version originale, types d'habitats français*. École Nationale du Génie Rural, des Eaux et des Forêts, Nancy, France.

Blès, J.L. (1984) *Contrat n° 416-83-7-WAS-F (AD) - Fracturation profonde des massifs rocheux granitiques (2e phase) - Rapport de synthèse : études documentaire, géostructurale et géostatistique*. Rapport de synthèse, 84SGN323GEO, Bureau de Recherches Géologiques et Minières, Orléans, France.

Boelter, D.H. (1964) Water storage characteristics of several peats in situ. *Soil Science Society of America Journal*, 28, 433–435.

Boelter, D.H. (1968) Important physical properties of peat materials. In *Proceedings of the third international peat congress*, pp. 150–154. Department of Energy, Mines and Resources and National Research Council of Canada, Quebec, Canada.

Borren, W. & Bleuten, W. (2006) Simulating Holocene carbon accumulation in a western Siberian watershed mire using a three-dimensional dynamic modeling approach. *Water Resources Research*, 42, W12413.

Bortoluzzi, E., Epron, D., Siegenthaler, A., Gilbert, D. & Buttler, A. (2006) Carbon balance of a European mountain bog at contrasting stages of regeneration. *New Phytologist*, 172, 708–718.

Boswell, J.S. & Olyphant, G.A. (2007) Modeling the hydrologic response of groundwater dominated wetlands to transient boundary conditions: implications for wetland restoration. *Journal of Hydrology*, 332, 467–476.

Botineau, M., Ghestem, A. & Vilks, A. (1993) La tourbière de Pioffray (Haute-Vienne) : un site botanique remarquable. *Acta Botanica Gallica*, 140, 57–61.

Botineau, M., Ghestem, A. & Vilks, A. (1998) La végétation vasculaire de la tourbière des Dauges. *Annales Scientifiques du Limousin*, N° spécial : Tourbière des Dauges, 55–77.

Boudreau, S. & Rochefort, L. (1999) Établissement de sphaignes réintroduites sous diverses communautés végétales recolonisant les tourbières après l'exploitation. *Écologie*, 30, 53–62.

Bourgault, M.-A. (2013) *Modélisation régionale 3D des écoulements souterrains dans la région du complexe tourbeux de Lanoraie, Québec, Canada*. Mémoire de Maîtrise en sciences de la terre, Université du Québec à Montréal, Montréal, Canada.

Bourgault, M.A., Larocque, M. & Roy, M. (2014) Simulation of aquifer-peatland-river interactions under climate change. *Hydrology Research*, 45, 425.

Bradley, C. (1996) Transient modelling of water-table variation in a floodplain wetland, Narborough Bog, Leicestershire. *Journal of hydrology*, 185, 87–114.

Bradley, C. (2002) Simulation of the annual water table dynamics of a floodplain wetland, Narborough Bog, UK. *Journal of Hydrology*, 261, 150–172.

Bragazza, L. (1997) *Sphagnum* niche diversification in two oligotrophic mires in the southern Alps of Italy. *The Bryologist*, 100, 507–515.

Bragazza, L. (1999) Spatial patterns of plant species in a poor mire on the southern Alps (Italy). *Plant Biosystems*, 133, 83–92.

Bragazza, L. (2008) A climatic threshold triggers the die-off of peat mosses during an extreme heat wave. *Global Change Biology*, 14, 2688–2695.

Bragazza, L. & Gerdol, R. (1996) Response surfaces of plant species along water-table depth and pH gradients in a poor mire on the southern Alps (Italy). *Annales Botanici Fennici*, 33, 11–20.

Bragazza, L. & Gerdol, R. (1999a) Ecological gradients in some *Sphagnum* mires in the south-eastern Alps (Italy). *Applied Vegetation Science*, 2, 55–60.

Bragazza, L. & Gerdol, R. (1999b) Hydrology, groundwater chemistry and peat chemistry in relation to habitat conditions in a mire on the south – eastern Alps of Italy. *Plant Ecology*, 144, 243–256.

Bragazza, L., Rydin, H. & Gerdol, R. (2005) Multiple gradients in mire vegetation: a comparison of a Swedish and an Italian bog. *Plant Ecology*, 177, 223–236.

Bragg, O.M., Brown, J.M.B. & Ingram, H. (1991) Modelling the ecohydrological consequences of peat extraction from a Scottish raised mire. In *Hydrological basis of ecologically sound management of soil and groundwater; Proceedings of an international symposium held during the XXth general assembly of the International Union of Geodesy and Geophysics at Vienna, 11-24 August 1991* (eds H.P. Nachtnebel & K. Kovar), pp. 13–22. International Association of Hydrological Sciences Press, Wallingford, UK.

Brandyk, T., Szatylowicz, J., Oleszczuk, R. & Gnatowski, T. (2002) Water-related physical attributes of organic soils. In *Organic soils and peat materials for sustainable agriculture* (eds L.E. Parent & P. Ilnicki), pp. 33–66. CRC Press, Boca Raton, Florida, USA.

Brassard, P., Waddington, J.M., Hill, A.R. & Roulet, N.T. (2000) Modelling groundwater-surface water mixing in a headwater wetland: implications for hydrograph separation. *Hydrological Processes*, 14, 2697–2710.

Bréda, N. (1994) *Analyse du fonctionnement hydrique des chênes sessile (*Quercus petraea*) et pédonculé (*Quercus robur*) en conditions naturelles: effets des facteurs du milieu et de l'éclaircie*. Thèse de Doctorat, Université Henri Poincaré Nancy I, Nancy, France.

Bréda, N. & Granier, A. (1996) Intra- and inter-annual variations of transpiration, leaf area index and radial growth of a sessile oak stand (*Quercus petraea*). *Annales des Sciences Forestières*, 53, 521–536.

Bréda, N. & Roman-Amat, B. (2002) Impact de la conduite des peuplements forestiers sur les ressources en eau. *La Houille Blanche*, 3, 78–84.

Brenot, A., Négrel, P., Millot, R. & Bertin, C. (2014) Using ion and isotope characterization to design a frame of protection of a wetland system (Massif Central, France). *Applied Geochemistry*, 40, 104–118.

Brent, R.P. (2013) *Algorithms for minimization without derivatives*. Dover Publications, Mineola, New York, USA.

Breuer, L., Eckhardt, K. & Frede, H.-G. (2003) Plant parameter values for models in temperate climates. *Ecological Modelling*, 169, 237–293.

Breuer, L. & Frede, H.-G. (2003) PlaPaDa - an online plant parameter data drill for eco-hydrological modelling approaches. Available at: http://www.uni-giessen.de/~gh1461/plapada/plapada.html [accessed 18 July 2014]

Bridgham, S., Pastor, J., Janssens, J., Chapin, C. & Malterer, T. (1996) Multiple limiting gradients in peatlands: A call for a new paradigm. *Wetlands*, 16, 45–65.

Bridgham, S.D. & Richardson, C.J. (1993) Hydrology and nutrient gradients in North Carolina peatlands. *Wetlands*, 13, 207–218.

Bromley, J. & Robinson, M. (1995) Groundwater in raised mire systems: models, mounds and myths. In *Hydrology and Hydrochemistry of British Wetlands* (eds J.M.R. Hughes & A.L. Heathwaite), pp. 95–109. John Wiley & Sons, Chichester, UK.

Bromley, J., Robinson, M. & Barker, J.A. (2004) Scale-dependency of hydraulic conductivity: an example from Thorne Moor, a raised mire in South Yorkshire, UK. *Hydrological Processes*, 18, 973–985.

Brougham, R.K. (1960) The relationship between the critical leaf area, total chlorophyll content, and maximum growth-rate of some pasture and crop plants. *Annals of Botany*, 24, 463–474.

Brown, P.A., Gill, S.A. & Allen, S.J. (2000) Metal removal from wastewater using peat. *Water Research*, 34, 3907–3916.

Brown, J.M.B. & Ingram, H.A.P. (1988) Changing storage beneath a stationary water table - An anomaly of certain humified peats. *Quarterly Journal of Engineering Geology and Hydrogeology*, 21, 177–182.

Brunner, P. & Simmons, C.T. (2012) HydroGeoSphere: a fully integrated, physically based hydrological model. *Ground Water*, 50, 170–176.

Burt, T.P. (1995) The role of wetlands in runoff generation from headwater catchments. In *Hydrology and hydrochemistry of British wetlands* (eds J. Hughes & A.L. Heathwaite), pp. 21–38. John Wiley & Sons, Chichester, UK.

Calder, I.R. (1986) A stochastic model of rainfall interception. *Journal of Hydrology*, 89, 65–71.

Calder, I.R. (1998) Water use by forests, limits and controls. *Tree Physiology*, 18, 625–631.

Calder, I.R. (2003) Assessing the water use of short vegetation and forests: development of the Hydrological Land Use Change (HYLUC) model. *Water Resources Research*, 39, 1318.

Calder, I.R., Hall, R.L., Harding, R.J. & Wright, I.R. (1984) The use of a wet-surface weighing lysimeter system in rainfall interception studies of heather (*Calluna vulgaris*). *Journal of Climate and Applied Meteorology*, 23, 461–473.

Caldwell, P.V., Vepraskas, M.J., Skaggs, R.W. & Gregory, J.D. (2007) Simulating the water budgets of natural Carolina bay wetlands. *Wetlands*, 27, 1112–1123.

Campbell, D.I. & Williamson, J.L. (1997) Evaporation from a raised peat bog. *Journal of Hydrology*, 193, 142–160.

Camporese, M., Ferraris, S., Putti, M., Salandin, P. & Teatini, P. (2006) Hydrological modeling in swelling/shrinking peat soils. *Water Resources Research*, 42, W06420 1–15.

Canadell, J., Jackson, R.B., Ehleringer, J.B., Mooney, H.A., Sala, O.E. & Schulze, E.-D. (1996) Maximum rooting depth of vegetation types at the global scale. *Oecologia*, 108, 583–595.

Carrer, G.E., Rousseau, A.N., St-Hilaire, A. & Jutras, S. (2015) Mosaic surface storages of a small boreal catchment. *Hydrological Processes*, 29, 845–858.

Chabrol, L. (2006) *Inventaire et cartographie des zones humides du Limousin (Bilan des prospections 2002 à 2005)*. Conservatoire Botanique National du Massif Central, Limoges, France.

Chabrol, L. & Reimringer, K. (2011) *Catalogue des végétations du Parc naturel régional de Millevaches en Limousin*. Conservatoire botanique national du Massif Central, Chavaniac-Lafayette, France.

Chandra, S., Ahmed, S., Ram, A. & Dewandel, B. (2008) Estimation of hard rock aquifers hydraulic conductivity from geoelectrical measurements: A theoretical development with field application. *Journal of Hydrology*, 357, 218–227.

Charman, D.J. (2002) *Peatlands and Environmental Change*. Wiley, Chichester, UK.

Charman, D.J., Blundell, A., Chiverrell, R.C., Hendon, D. & Langdon, P.G. (2006) Compilation of non-annually resolved Holocene proxy climate records: stacked Holocene peatland palaeo-water table reconstructions from northern Britain. *Quaternary Science Reviews*, 25, 336–350.

Chason, D.B. & Siegel, D.I. (1986) Hydraulic conductivity and related physical properties of peat, Lost River Peatland, northern Minnesota. *Soil Science*, 142, 91–99.

Chen, J.M. & Black, T.A. (1991) Measuring leaf area index of plant canopies with branch architecture. *Agricultural and Forest Meteorology*, 57, 1–12.

Chesworth, W. (2008) *Encyclopedia of Soil Science*. Springer, Dordrecht, The Netherlands.

Chirino, C., Campeau, S. & Rochefort, L. (2006) *Sphagnum* establishment on bare peat: the importance of climatic variability and *Sphagnum* species richness. *Applied Vegetation Science*, 9, 285–294.

Cho, M., Choi, Y.S., Ha, K.C., Kee, W.S., Lachassagne, P. & Wyns, R. (2002) Paleoweathering covers in Korean hard rocks: A methodology for mapping their spatial distribution and the thickness of their constituting horizons. Applications to identify brittle deformation and to hard rock hydrogeology. *KIGAM Bulletin*, 6, 12–25.

Cho, M., Choi, Y., Ha, K., Kee, W., Lachassagne, P. & Wyns, R. (2003) Relationship between the permeability of hard rock aquifers and their weathering, from geological and hydrogeological observations in South Korea. In *Proceedings of the International Conference on Groundwater in Fractured Rocks, 15-19/09/2003, Prague, Czech Republic* (eds J. Krasny, Z. Hrkal & J. Bruthans), pp. 15–19. International Association of Hydrogeologists, Reading, UK.

Chormanski, J., Kardel, I., Swiatek, D., Grygoruk, M. & Okruszko, T. (2009) Management support system for wetlands protection: Red Bog and Lower Biebrza Valley case study. In *Hydroinformatics in hydrology, hydrogeology and water resources; Proceedings of the symposium JS.4 at the joint IAHS & IAH convention, Hyderabad, India, September 2009*, pp. 423–431. International Association of Hydrological Sciences Press, Wallingford, UK.

Chormański, J., Miroslaw-Świątek, D. & Michalowski, R. (2009) A hydrodynamic model coupled with GIS for flood characteristics analysis in the Biebrza riparian wetland. *Oceanological and Hydrobiological Studies*, 38, 65–73.

Christiaens, K. & Feyen, J. (2002) Use of sensitivity and uncertainty measures in distributed hydrological modeling with an application to the MIKE SHE model. *Water Resources Research*, 38, 1169.

Cienciala, E., Lindroth, A., Čermák, J., Hällgren, J.-E. & Kučera, J. (1992) Assessment of transpiration estimates for *Picea abies* trees during a growing season. *Trees*, 6, 121–127.

Clark, J.M., Ashley, D., Wagner, M., Chapman, P.J., Lane, S.N., Evans, C.D. & Heathwaite, A.L. (2009) Increased temperature sensitivity of net DOC production from ombrotrophic peat due to water table draw-down. *Global Change Biology*, 15, 794–807.

Clark, J.M., Chapman, P.J., Adamson, J.K. & Lane, S.N. (2005) Influence of drought-induced acidification on the mobility of dissolved organic carbon in peat soils. *Global Change Biology*, 11, 791–809.

Clark, J., Gallego-Sala, A., Allott, T., Chapman, S., Farewell, T., Freeman, C., House, J., Orr, H., Prentice, I. & Smith, P. (2010) Assessing the vulnerability of blanket peat to climate change using an ensemble of statistical bioclimatic envelope models. *Climate Research*, 45, 131–150.

Clymo, R. (1973) The growth of *Sphagnum*: some effects of environment. *The Journal of Ecology*, 849–869.

Clymo, R.S. (1984) The limits to peat bog growth. *Philosophical Transactions of the Royal Society of London. Series B, Biological Sciences*, 303, 605–654.

Cobbaert, D., Rochefort, L. & Price, J. (2004) Experimental restoration of a fen plant community after peat mining. *Applied Vegetation Science*, 7, 209–220.

Cognard-Plancq, A.L., Bogner, C., Vincent, M., Lavabre, J., Martin, C. & Didon-Lescot, J.F. (2004) Etude du rôle hydrologique d'une tourbière de montagne: modélisation comparée de couples "averse-crue" sur deux bassins versants du Mont-Lozère. *Etudes de géographie physique*, 31, 3–15.

Coll, J., Bourke, D., Sheehy Skeffington, M., Gormally, M. & Sweeney, J. (2014) Projected loss of active blanket bogs in Ireland. *Climate Research*, 59, 103–115.

Collective. (1975) *Flood studies report*. Natural Environment Research Council, Swindon, UK.

Congalton, R.G. (1991) A review of assessing the accuracy of classifications of remotely sensed data. *Remote Sensing of Environment*, 37, 35–46.

Conradi, T. & Friedmann, A. (2013) Plant communities and environmental gradients in mires of the Ammergauer Alps (Bavaria, Germany). *Tuexenia*, 33, 136–163.

Cook, A. (2012) *Development of an integrated surface and subsurface model of Everglades National Park*. MSc Thesis, Florida International University, Miami, Florida, USA.

Cooper, J.D. (1980) *Measurement of moisture fluxes in unsaturated soil in Thetford Forest*. Report, 66, Institute of Hydrology, Wallingford, UK.

Cooper, A., Mccann, T.P. & Hamill, B. (2001) Vegetation regeneration on blanket mire after mechanized peat-cutting. *Global Ecology and Biogeography*, 10, 275–289.

Cortizas, A.M., Biester, H., Mighall, T. & Bindler, R. (2007) Climate-driven enrichment of pollutants in peatlands. *Biogeosciences Discussions*, 4, 905–911.

Cottez, S. & Favin, S. (1980) *Etude prévisionnelle d'impact des travaux miniers sur le captage du Mogot, Saint-Sylvestre (Haute-Vienne)*. Rapport, 80 SGN 537 LIM, BRGM - COGEMA, La Crouzille.

Cournez, E., Linet, C., Hennequin, E., Bonhomme, M. & Guerbaa, K. (2000) *Les milieux tourbeux du Limousin - Synthèse des connaissances*. Rapport, Conservatoire Régional des Espaces Naturels du Limousin, St-Gence, France.

Courtois, N., Blanchin, R., Lachassagne, P., Wyns, R., Bougaïré, F.D., Somé, S. & Tapsoba, A. (2008) *Experimental GIS hydrogeological mapping of hard rock aquifers in Burkina Faso, to help groundwater management and planning*. Poster presented at the Groundwater & Climate in Africa international conference, Kampala, Uganda.

Courtois, N., Lachassagne, P., Weng, P., Théveniaut, H., Wyns, R., Joseph, B. & Laporte, P. (2003) *Détermination de secteurs potentiellement favorables pour la recherche d'eau souterraine à Cacao (Guyane)*. Rapport final, RP-52758-FR, Bureau de Recherches Géologiques et Minières, Orléans, France.

Courtois, N., Lachassagne, P., Wyns, R., Blanchin, R., Bougaïré, F.D., Somé, S. & Tapsoba, A. (2010) Large-scale mapping of hard-rock aquifer properties applied to Burkina Faso. *Ground Water*, 48, 269–283.

Couturier, D.E. & Ripley, E.A. (1973) Rainfall interception in mixed grass prairie. *Canadian Journal of Plant Science*, 53, 659–663.

Cowardin, L.M., Carter, V., Golet, F.C. & LaRoe, E.T. (1979) *Classification of wetlands and deepwater habitats of the United States*. Report, FWS/OBS-79/31, Fish and Wildlife Service, US Department of the Interior, Washington DC, USA.

Crawford, N.H. & Linsley, R.K. (1966) *Digital simulation in hydrology: Stanford watershed model IV*. Technical Report, 39, Department of Civil Engineering, Stanford Unversity, Stanford, USA.

Cris, R., Buckmaster, S., Bain, C. & Bonn, A. (2011) *UK peatland restoration: Demonstrating success*. IUCN UK National Committee Peatland Programme, Edinburgh, UK.

Cubizolle, H., Fassion, F., Argant, J., Latour-Argant, C., Galet, P. & Oberlin, C. (2012) Mire initiation, climatic change and agricultural expansion over the course of the Late-Holocene in the Massif Central mountain range (France): Causal links and implications for mire conservation. *Quaternary International*, 251, 77–96.

Cuevas, J., Calvo, M., Little, C., Pino, M. & Dassori, P. (2010) Are diurnal fluctuations in streamflow real? *Journal of Hydrology and Hydromechanics*, 58, 149–162.

Cutini, A., Matteucci, G. & Mugnozza, G.S. (1998) Estimation of leaf area index with the Li-Cor LAI 2000 in deciduous forests. *Forest Ecology and Management*, 105, 55–65.

Czerepko, J. (2008) A long-term study of successional dynamics in the forest wetlands. *Forest Ecology and Management*, 255, 630–642.

Dai, Z., Amatya, D.M., Sun, G., Li, C., Trettin, C.C. & Li, H. (2008) Modeling the effect of land use change on hydrology of a forested watershed in coastal South Carolina. In *Proceedings of the 2008 South Carolina water resources conference, 14-15 October 2008, Charleston Area, USA*.

Davie, T. (2008) *Fundamentals of hydrology*, 2nd ed. Routledge, London, UK.

Davies, F.S. & Albrigo, L.G. (1983) Water relations of small fruits. In *Water deficits and plant growth - Volume 7: Additional woody crop plants* (ed T.T. Kozlowski), pp. 89–136. Academic Press, New York, USA.

Dejean, R. & Durand, P. (1987) *Bassins versants expérimentaux du mont Lozère: recherches géomorphologiques, pédologiques et hydrodynamiques - Deuxième partie : hydrodynamique des sols*. Rapport, 85 084, Ministère de l'Environnement SRETIE, Parc National des Cévennes, France.

Dekker, S.C., Barendregt, A., Bootsma, M.C. & Schot, P.P. (2005) Modelling hydrological management for the restoration of acidified floating fens. *Hydrological processes*, 19, 3973–3984.

Descloîtres, M., Robain, H., Dabas, M., Camerlynck, C. & Albouy, Y. (1997) Apport des imageries électriques et radar à la reconnaisance des couvertures d'altération, bassin versant de Nsimi (Cameroun). In *Actes du colloque GEOFCAN - Géophysique des sols et des formations superficielles, 11-12/09/1997, Bondy, France*, pp. 33–37. BRGM, INRA, ORSTOM, UPMC.

Desire-Marchand, J. & Klein, C. (1986) Le relief du Limousin. Les avatars d'un géomorphotype. *Norois*, 129, 23–49.

Deuffic, P. (2005) La fermeture des paysages dans le Massif central: regards d'habitants sur une question d'experts. *Cahiers d'économie et sociologie rurales*, 75, 75–96.

Dewandel, B., Lachassagne, P., Wyns, R., Marechal, J.C. & Krishnamurthy, N.S. (2006) A generalized 3-D geological and hydrogeological conceptual model of granite aquifers controlled by single or multiphase weathering. *Journal of Hydrology*, 330, 260–284.

Dewandel, B., Lachassagne, P., Zaidi, F.K. & Chandra, S. (2011) A conceptual hydrodynamic model of a geological discontinuity in hard rock aquifers: Example of a quartz reef in granitic terrain in South India. *Journal of Hydrology*, 405, 474–487.

Dewandel, B., Maréchal, J.C., Bour, O., Ladouche, B., Ahmed, S., Chandra, S. & Pauwels, H. (2012) Upscaling and regionalizing hydraulic conductivity and effective porosity at watershed scale in deeply weathered crystalline aquifers. *Journal of Hydrology*, 416–417, 83–97.

Dickinson, R., Errico, R., Giorgi, F. & Bates, G. (1993) *Biosphere–Atmosphere Transfer Scheme (BATS) version 1e as coupled to the NCAR Community Climate Model*. Note NCAR/TN-387STR, National Center for Atmospheric Research, Boulder, USA.

Didon-Lescot, J.F. (1984) Les bassins versants du Mont Lozère : un laboratoire de terrain ouvert au grand public. In *Environnement, recherche et société - Actes des Journées 1994 du programme Environnement du CNRS, 29-30 mars 1984, Montpellier, France* Centre National de la Recherche Scientifique, Montpellier, France.

Dieleman, C.M., Branfireun, B.A., McLaughlin, J.W. & Lindo, Z. (2015) Climate change drives a shift in peatland ecosystem plant community: Implications for ecosystem function and stability. *Global Change Biology*, 21, 388–395.

Diggelen, R., Molenaar, W. & Kooijman, A. (1996) Vegetation succession in a floating mire in relation to management and hydrology. *Journal of Vegetation Science*, 7, 809–820.

Dimitrov, D.D., Bhatti, J.S. & Grant, R.F. (2014) The transition zones (ecotone) between boreal forests and peatlands: Modelling water table along a transition zone between upland black spruce forest and poor forested fen in central Saskatchewan. *Ecological Modelling*, 274, 57–70.

Dingman, S.L. (1994) *Physical hydrology*. Macmillan Publishing Company, New York, USA.

Dise, N.B. (2009) Peatland response to global change. *Science*, 326, 810–811.

Dodane, C. (2009) *Les nouvelles forêts du Massif Central : enjeux sociétaux et territoriaux. Ces hommes qui plantaient des résineux pour éviter la friche.* Thèse de Doctorat, Ecole normale supérieure Lettres et Sciences Humaines - ENS-LSH Lyon, Lyon, France.

Dolman, A.J. (1987) Summer and winter rainfall interception in an oak forest. Predictions with an analytical and a numerical simulation model. *Journal of Hydrology*, 90, 1–9.

Dommain, R., Couwenberg, J. & Joosten, H. (2010) Hydrological self-regulation of domed peatlands in south-east Asia and consequences for conservation and restoration. *Mires and Peat*, 6, 1–17.

Dougherty, J. (2005) *PEST - Model-independent parameter estimation. User manual*, 5th ed. Watermark Numerical Computing, Brisbane, Australia.

Drexler, J.Z., Bedford, B.L., Scognamiglio, R. & Siegel, D.I. (1999) Fine-scale characteristics of groundwater flow in a peatland. *Hydrological Processes*, 13, 1341–1359.

Drexler, J.Z., Knifong, D., Tuil, J., Flint, L.E. & Flint, A.L. (2013) Fens as whole-ecosystem gauges of groundwater recharge under climate change. *Journal of Hydrology*, 481, 22–34.

Drexler, J.Z., Snyder, R.L., Spano, D., Paw, U. & Tha, K. (2004) A review of models and micrometeorological methods used to estimate wetland evapotranspiration. *Hydrological Processes*, 18, 2071–2101.

Dupraz, C., Didon, J.F. & Lelong, F. (1984) Les bassins versants expérimentaux du Mont Lozère : premiers résultats sur le rôle hydrologique du couvert végétal. *Hydrogéologie - Géologie de l'Ingénieur*, 3, 217–226.

Dupraz, C., Lelong, F. & Didon, J.F. (1985) Bilans comparés des transferts d'eau et d'éléments minéraux dans trois petits bassins versants à végétation contrastée du Mont Lozère. *Science du Sol*, 4, 183–201.

Durand, V. (2005) *Recherche multidisciplinaire pour caractériser deux aquifères fracturés : les eaux minérales de Plancoët en contexte métamorphique, et de Quézac en milieu carbonaté*. Thèse de Doctorat, Université Pierre et Marie Curie - Paris VI, Paris, France.

Durand, V., Deffontaines, B., Leonardi, V., Guerin, R., Wyns, R., de Marsily, G. & Bonjour, J.-L. (2006) A multidisciplinary approach to determine the structural geometry of hard-rock aquifers. Application to the Plancoet migmatitic aquifer (NE Brittany, W France). *Bulletin de la Société Géologique de France*, 177, 227 –236.

Durand, P., Robson, A. & Neal, C. (1992) Modelling the hydrology of submediterranean montane catchments (Mont-Lozère, France) using TOPMODEL: initial results. *Journal of Hydrology*, 139, 1–14.

Durepaire, P. & Guerbaa, K. (2008) *Tourbière des Dauges - Plan de gestion 2008-2012*. Conservatoire Régional des Espaces Naturels du Limousin, St-Gence, France.

Durfort, J. (2007) *Les tourbières de Bretagne*. Forum Centre Bretagne Environnement, Biotope, Mèze, France.

Dutartre, P., Feybesse, J.L. & Gros, Y. (1982) *Fracturation provoquée - Etude structurale de la fracturation naturelle du site de Fanay Augères (Haute-Vienne)*. Rapport, 82 SGN 913 GEO, Bureau de Recherches Géologiques et Minières, Orléans, France.

Eeles, C.W.O., Parks, Y. & Barr, A. (1989) *HYRROM operation manual*. Institute of Hydrology, Wallingford, UK.

Eggelsmann, R., Heathwaite, A.L., Grosse-Brauckmann, G., Kuster, E., Naucke, W., Schuch, M. & Schweickle, V. (1993) Physical processes and properties of mires. In *Mires: process, exploitation, and conservation* (eds A.L. Heathwaite & K. Göttlich), pp. 171–262. Wiley, Chichester, UK.

Eggleton, R.A. (ed). (2001) *The regolith glossary*. Cooperative Centre for Landscape Evolution and Mineral Exploration, Canberra, Australia.

Epron, D., Godard, D., Cornic, G. & Genty, B. (1995) Limitation of net CO_2 assimilation rate by internal resistances to CO_2 transfer in the leaves of two tree species (*Fagus sylvatica* L. and *Castanea sativa* Mill.). *Plant, Cell & Environment*, 18, 43–51.

Etlicher, B. (1986) *Les massifs du Forez, du Pilat et du Vivarais: régionalisation et dynamique des héritages glaciaires et périglaciaires en moyenne montagne cristalline*. Centre d'Etudes Foréziennes, Presses de l'Université de Saint-Etienne, Saint-Etienne, France.

Etlicher, B. (2005) French and Belgian Uplands. In *The physical geography of Western Europe* (ed E.A. Koster), pp. 231–250. Oxford University Press, Oxford, UK.

Euliss, N.H. & Mushet, D.M. (1996) Water-level fluctuation in wetlands as a function of landscape condition in the prairie pothole region. *Wetlands*, 16, 587–593.

Evans, M.G., Burt, T.P., Holden, J. & Adamson, J.K. (1999) Runoff generation and water table fluctuations in blanket peat: evidence from UK data spanning the dry summer of 1995. *Journal of Hydrology*, 221, 141–160.

Evans, C.D., Monteith, D.T. & Cooper, D.M. (2005) Long-term increases in surface water dissolved organic carbon: observations, possible causes and environmental impacts. *Environmental Pollution*, 137, 55–71.

Fahey, B. & Jackson, R. (1997) Hydrological impacts of converting native forests and grasslands to pine plantations, South Island, New Zealand. *Agricultural and Forest Meteorology*, 84, 69–82.

Farley, K.A., Jobbágy, E.G. & Jackson, R.B. (2005) Effects of afforestation on water yield: a global synthesis with implications for policy. *Global Change Biology*, 11, 1565–1576.

Faulkner, D. (1999) *Flood estimation handbook, Volume 2: Rainfall frequency estimation*. Institute of Hydrology, Wallingford, UK.

Faure, O. (2005) *Le Massif central*. Editions Ouest-France, Rennes, France.

Fenner, N., Freeman, C. & Worrall, F. (2013) Hydrological controls on dissolved organic carbon production and release from UK peatlands. In *Carbon cycling in northern peatlands* (eds A.J. Baird, L.R. Belyea, X. Comas, A.S. Reeve & L.D. Slater), pp. 237–249. American Geophysical Union, Washington DC, USA.

Fisher, J. & Acreman, M.C. (2004) Wetland nutrient removal: a review of the evidence. *Hydrology and Earth System Sciences*, 8, 673–685.

Flageollet, J.-C. (1977) *Origine des reliefs, altérations et formations superficielles en Limousin et en Vendée du Nord-Ouest : contribution à l'étude morphologique des massifs anciens*. Thèse de Doctorat d'Etat, Université de Nancy, Nancy, France.

Fohrer, N., Haverkamp, S., Eckhardt, K. & Frede, H.-G. (2001) Hydrologic response to land use changes on the catchment scale. *Physics and Chemistry of the Earth, Part B: Hydrology, Oceans and Atmosphere*, 26, 577–582.

Forgeard, F., Gloaguen, J.C. & Touffet, J. (1980) Interception des précipitations et apport au sol d'éléments minéraux par les eaux de pluie et les pluviolessivats dans une hêtraie atlantique et dans quelques peuplements résineux en Bretagne. *Annales des Sciences Forestiéres*, 37, 53–71.

Fournier, V. (2008) *Hydrologie de la tourbière du mont Covey Hill et implications pour la conservation*. Maîtrise en sciences de la terre, Université du Québec, Montréal, Canada.

Francés, A.P., Lubczynski, M.W., Roy, J., Santos, F.A.M. & Mahmoudzadeh Ardekani, M.R. (2014) Hydrogeophysics and remote sensing for the design of hydrogeological conceptual models in hard rocks – Sardón catchment (Spain). *Journal of Applied Geophysics*, 110, 63–81.

Freeman, C., Evans, C.D., Monteith, D.T., Reynolds, B. & Fenner, N. (2001) Export of organic carbon from peat soils. *Nature*, 412, 785–785.

Freeman, C., Fenner, N., Ostle, N.J., Kang, H., Dowrick, D.J., Reynolds, B., Lock, M.A., Sleep, D., Hughes, S. & Hudson, J. (2004) Export of dissolved organic carbon from peatlands under elevated carbon dioxide levels. *Nature*, 430, 195–198.

Friend, A.D., Woodward, F.I. & Switsur, V.R. (1989) Field measurements of photosynthesis, stomatal conductance, leaf nitrogen and $\delta^{13}C$ along altitudinal gradients in Scotland. *Functional Ecology*, 3, 117–122.

Frolking, S., Roulet, N.T., Tuittila, E., Bubier, J.L., Quillet, A., Talbot, J. & Richard, P.J.H. (2010) A new model of Holocene peatland net primary production, decomposition, water balance, and peat accumulation. *Earth System Dynamics Discussions*, 1, 115–167.

Frolking, S., Talbot, J., Jones, M.C., Treat, C.C., Kauffman, J.B., Tuittila, E.-S. & Roulet, N. (2011) Peatlands in the Earth's 21st century climate system. *Environmental Reviews*, 19, 371–396.

Gallego-Sala, A.V., Clark, J.M., House, J.I., Orr, H.G., Prentice, I.C., Smith, P., Farewell, T. & Chapman, S.J. (2010) Bioclimatic envelope model of climate change impacts on blanket peatland distribution in Great Britain. *Climate Research*, 45, 152–162.

Gallego-Sala, A.V. & Prentice, I.C. (2013) Blanket peat biome endangered by climate change. *Nature Climate Change*, 3, 152–155.

Galvin, L.F. & Hanrahan, E.T. (1967) Steady state drainage flow in peat. In *Proceedings of the Symposium on Subsurface Drainage, 1966, Washington DC, USA*, pp. 77–90. Highway Research Board, Washington DC, USA.

Gash, J.H.C., Lloyd, C.R. & Lachaud, G. (1995) Estimating sparse forest rainfall interception with an analytical model. *Journal of Hydrology*, 170, 79–86.

Gassman, P.W., Reyes, M.R., Green, C.H. & Arnold, J.G. (2007) The soil and water assessment tool: historical development, applications, and future research directions. *Transactions of the American Society of Agricultural and Biological Engineers*, 50, 1211–1250.

Gaudig, G., Fengler, F., Krebs, M., Prager, A., Schulz, J., Wichmann, S. & Joosten, H. (2014) *Sphagnum* farming in Germany – a review of progress. *Mires and Peat*, 13, 1–11.

Gerdol, R., Bragazza, L. & Brancaleoni, L. (2008) Heatwave 2003: high summer temperature, rather than experimental fertilization, affects vegetation and CO_2 exchange in an alpine bog. *New Phytologist*, 179, 142–154.

Gerrits, A.M.J. (2010) *The role of interception in the hydrological cycle*. PhD thesis, Delft University of Technology, Delft, The Netherlands.

Ghestem, A., Botineau, M., Descubes-Gouilly, C. & Vilks, A. (1988) Le site du Longeroux (Corrèze) : premiers documents phytosociologiques (bas marais tourbeux, tourbière active et landes tourbeuses). *Annales Scientifiques du Limousin*, 4, 43–54.

Ghestem, A. & Vilks, A. (1980) Contribution à l'étude phytosociologique des tourbières acides du Limousin. In *Actes des VIIe Colloques Phytosociologiques - La végétation des sols tourbeux, 1978, Lille, France*, pp. 165–182.

Gignac, L.D. (1992) Niche structure, resource partitioning, and species interactions of mire bryophytes relative to climatic and ecological gradients in western Canada. *The Bryologist*, 95, 406–418.

Gignac, L.D. (1994) Peatland species preferences: an overview of our current knowledge base. *Wetlands*, 14, 216–222.

Gignac, L.D. & Vitt, D.H. (1990) Habitat limitations of *Sphagnum* along climatic, chemical, and physical gradients in mires of western Canada. *The Bryologist*, 93, 7–22.

Gignac, L.D., Vitt, D.H. & Bayley, S.E. (1991) Bryophyte response surfaces along ecological and climatic gradients. *Vegetatio*, 93, 29–45.

Giller, K. & Wheeler, B. (1988) Acidification and succession in a flood-plain mire in the Norfolk Broadland, UK. *The Journal of Ecology*, 76, 849–866.

Gilman, K. (1994) *Hydrology and wetland conservation*. Institute of Hydrology, John Wiley & Sons, Chichester, UK.

Gilman, K. (2002) *A review of evapotranspiration rates of plant communities on mires and their catchments, with particular reference to Cors y Llyn NNR*. CCW Contract Science Report, 504, Countryside Council for Wales, Bangor, UK.

Gilman, K. & Newson, M.D. (1980) *Soil pipes and pipeflow. A hydrological study in upland Wales.* GeoBooks, Cambridge, UK.

Gilmer, A., Holden, N., Ward, S., Brereton, A. & Farrell, E. (2000) A model of organic matter accumulation in a developing fen/raised bog complex. *Suo*, 51, 155–167.

Gilvear, D.J. & Bradley, C. (2009) Hydrological dynamics II: groundwater and hydrological connectivity. In *The Wetlands Handbook* (eds E. Maltby & T. Barker), pp. 169–193. Wiley-Blackwell, Chichester, UK.

Gilvear, D.J. & McInnes, R.J. (1994) Wetland hydrological vulnerability and the use of classification procedures: a Scottish case study. *Journal of Environmental Management*, 42, 403–414.

Glaser, P.H., Bennett, P.C., Siegel, D.I. & Romanowicz, E.A. (1996) Palaeo-reversals in groundwater flow and peatland development at Lost River, Minnesota, USA. *The Holocene*, 6, 413–421.

Glaser, P.H., Janssens, J.A. & Siegel, D.I. (1990) The response of vegetation to chemical and hydrological gradients in the Lost River peatland, northern Minnesota. *Journal of Ecology*, 78, 1021–1048.

Glaser, P.H., Siegel, D.I., Reeve, A.S. & Chanton, J.P. (2006) Hydrogeology of major peat basins in North America. In *Peatlands - Evolution and records of environmental and climate changes* (eds I.P. Martini, A. Martinez Cortizas & W. Chesworth), pp. 347–376. Elsevier, Amsterdam, The Netherlands.

Glaser, P.H., Siegel, D.I., Romanowicz, E.A. & Shen, Y.P. (1997) Regional linkages between raised bogs and the climate, groundwater, and landscape of north-western Minnesota. *Journal of Ecology*, 85, 3–16.

Gobat, J.M. (1990) Quelques relations entre la végétation et la qualité physico-chimique des tourbes dans le Jura. *Bulletin de la Société Neuchâteloise des Sciences Naturelles*, 113, 207–214.

Gobat, J.M., Grosvernier, P. & Matthey, Y. (1986) Les tourbières du Jura suisse: milieux naturels, modifications humaines, caractères des tourbes, potentiel de régénération. *Actes de la Société Jurassienne d'Emulation*, 213–318.

Golder Associates. (2014) *FracMan - Discrete fracture network analysis*. Golder Associates Inc., Redmond WA, USA.

González A, Z.I., Krachler, M., Cheburkin, A.K. & Shotyk, W. (2006) Spatial distribution of natural enrichments of arsenic, selenium, and uranium in a minerotrophic peatland, Gola di Lago, Canton Ticino, Switzerland. *Environmental science & technology*, 40, 6568–6574.

González, E. & Rochefort, L. (2014) Drivers of success in 53 cutover bogs restored by a moss layer transfer technique. *Ecological Engineering*, 68, 279–290.

Gorham, E. & Rochefort, L. (2003) Peatland restoration: a brief assessment with special reference to *Sphagnum* bogs. *Wetlands Ecology and Management*, 11, 109–119.

Gough, R., Holliman, P.J., Willis, N. & Freeman, C. (2014) Dissolved organic carbon and trihalomethane precursor removal at a UK upland water treatment works. *Science of The Total Environment*, 468–469, 228–239.

Gowing, D.J.G., Youngs, E.G., Gilbert, J.C. & Spoor, G. (1998) Predicting the effect of change in water regime on plant communities. In *Hydrology in a changing environment* (eds H. Wheather & C. Kirby), pp. 473–484. Wiley, Chichester, UK.

Graham, D.N. & Butts, M.B. (2005) Flexible, integrated watershed modelling with MIKE SHE. In *Watershed models* (eds V.P. Singh & D.K. Frevert), pp. 245–272. CRC Press, Boca Raton, Florida, USA.

Granier, A. (2007) Rôle des prairies dans le cycle de l'eau. Comparaison avec la forêt. *Fourrages*, 192, 399–408.

Granier, A., Biron, P. & Lemoine, D. (2000) Water balance, transpiration and canopy conductance in two beech stands. *Agricultural and Forest Meteorology*, 100, 291–308.

Granier, A., Bréda, N., Biron, P. & Villette, S. (1999) A lumped water balance model to evaluate duration and intensity of drought constraints in forest stands. *Ecological Modelling*, 116, 269–283.

Grayson, R.B., Moore, I.D. & McMahon, T.A. (1992) Physically based hydrologic modeling: 2. Is the concept realistic? *Water Resources Research*, 28, 2659–2666.

Grootjans, A., Jansen, A., Herianová, S. & Stanova, V.S. (2012) *Calcareous mires of Slovakia: landscape setting, management and restoration prospects*. Knnv Publishing, Zeist, The Netherlands.

Gros, Y., Blès, J.L., Bonijoli, D. & Martin, P. (1983) *Fracturation profonde des massifs rocheux granitiques*. Rapport d'avancement des travaux, 83-SGN-526-STO, Bureau de Recherches Géologiques et Minières, Orléans, France.

Grosvernier, P.R., Matthey, Y., Buttler, A. & Gobat, J.M. (1999) Characterization of peats from histosols disturbed by different human impacts (drainage, peat extraction, agriculture). *Ecologie*, 30, 23–31.

Grygoruk, M., Batelaan, O., Mirosław-Świątek, D., Szatyłowicz, J. & Okruszko, T. (2014) Evapotranspiration of bush encroachments on a temperate mire meadow – A nonlinear function of landscape composition and groundwater flow. *Ecological Engineering*, 73, 598–609.

Grygoruk, M., Batelaan, O., Okruszko, T., Miroslaw-Świątek, D., Chormański, J. & Rycharski, M. (2011) Groundwater modelling and hydrological system analysis of wetlands in the Middle Biebrza Basin. In *Modelling of hydrological processes in the Narew Catchment* (eds D. Miroslaw-Świątek & T. Okruszko), pp. 89–109. Springer-Verlag, Berlin, Heidelberg, Germany.

Guehl, J.-M., Fort, C. & Ferhi, A. (1995) Differential response of leaf conductance, carbon isotope discrimination and water-use efficiency to nitrogen deficiency in maritime pine and pedunculate oak plants. *New Phytologist*, 131, 149–157.

Guertin, P., Barten, P.K. & Brooks, K.N. (1987) The peatland hydrologic impact model: development and testing. *Nordic Hydrology*, 18, 79–100.

Guidi, W., Piccioni, E. & Bonari, E. (2008) Evapotranspiration and crop coefficient of poplar and willow short-rotation coppice used as vegetation filter. *Bioresource technology*, 99, 4832–4840.

Guisan, A., Weiss, S.B. & Weiss, A.D. (1999) GLM versus CCA spatial modeling of plant species distribution. *Plant Ecology*, 143, 107–122.

Gunnarsson, U. & Rydin, H. (2000) Nitrogen fertilization reduces *Sphagnum* production in bog communities. *New Phytologist*, 147, 527–537.

Haahti, K., Younis, B.A., Stenberg, L. & Koivusalo, H. (2014) Unsteady flow simulation and erosion assessment in a ditch network of a drained peatland forest catchment in eastern Finland. *Water Resources Management*, 28, 5175–5197.

Hájek, M., Horsák, M., Hájková, P. & Díte, D. (2006) Habitat diversity of central European fens in relation to environmental gradients and an effort to standardise fen terminology in ecological studies. *Perspectives in Plant Ecology, Evolution and Systematics*, 8, 97–114.

Hájková, P. & Hájek, M. (2004) Bryophyte and vascular plant responses to base-richness and water level gradients in western Carpathian *Sphagnum*-rich mires. *Folia Geobotanica*, 39, 335–351.

Hájková, P., Wolf, P. & Hájek, M. (2004) Environmental factors and Carpathian spring fen vegetation: the importance of scale and temporal variation. *Annales Botanici Fennici*, 41, 249–252.

Halldin, S., Saugier, B. & Pontailler, J.Y. (1984) Evapotranspiration of a deciduous forest: simulation using routine meteorological data. *Journal of Hydrology*, 75, 323–341.

Hammersmark, C.T., Rains, M.C. & Mount, J.F. (2008) Quantifying the hydrological effects of stream restoration in a montane meadow, northern California, USA. *River Research and Applications*, 24, 735–753.

Hammersmark, C.T., Rains, M.C., Wickland, A.C. & Mount, J.F. (2009) Vegetation and water-table relationships in a hydrologically restored riparian meadow. *Wetlands*, 29, 785–797.

Harsch, N., Brandenburg, M. & Klemm, O. (2009) Large-scale lysimeter site St. Arnold, Germany: analysis of 40 years of precipitation, leachate and evapotranspiration. *Hydrology and Earth System Sciences*, 13, 305–317.

Hasan, A., Pilesjö, P. & Persson, A. (2012) On generating digital elevation models from liDAR data – resolution versus accuracy and topographic wetness index indices in northern peatlands. *Geodesy and Cartography*, 38, 57–69.

Havnø, K., Madsen, M.N. & Dørge, J. (1995) MIKE 11 - a generalized river modelling package. In *Computer models of watershed hydrology* (ed V.P. Singh), pp. 733–782. Water Resources Publications, Colorado, USA.

Heijmans, M.M.P.D., Mauquoy, D., van Geel, B. & Berendse, F. (2008) Long-term effects of climate change on vegetation and carbon dynamics in peat bogs. *Journal of Vegetation Science*, 19, 307–320.

Helmschrot, J. (2006) *An integrated, landscape-based approach to model the formation and hydrological functioning of wetlands in semiarid headwater catchments of the Umzimvubu River, South Africa*. Dr. rer. nat. dissertation, University of Thüringen, Thüringen, Germany.

Hemond, H.F. & Goldman, J.C. (1985) On non-Darcian water flow in peat. *Journal of Ecology*, 73, 579–584.

Hendon, D. & Charman, D.J. (2004) High-resolution peatland water-table changes for the past 200 years: the influence of climate and implications for management. *The Holocene*, 14, 125–134.

Herschy, R.W. (2008) *Streamflow measurement*, 3rd ed. Taylor & Francis, Abingdon, UK.

Hettenbergerová, E., Hájek, M., Zelený, D., Jirouvsková, J. & Mikulávsková, E. (2013) Changes in species richness and species composition of vascular plants and bryophytes along a moisture gradient. *Preslia*, 85, 369–388.

Hilbert, D.W., Roulet, N. & Moore, T. (2000) Modelling and analysis of peatlands as dynamical systems. *Journal of Ecology*, 88, 230–242.

Hinshiri, H.M. (1973) *Field and experimental studies on the water relations of* Calluna vulgaris*, (L.) Hull, with special reference to the effects of wind*. PhD thesis, University of Aberdeen, Aberdeen, UK.

Hiscock, K. & Bense, V. (2014) *Hydrogeology: principles and practice*. John Wiley & Sons, Chichester, UK.

Hobbs, N.B. (1986) Mire morphology and the properties and behaviour of some British and foreign peats. *Quarterly Journal of Engineering Geology and Hydrogeology*, 19, 7–80.

Holden, J. (2006) Peatland hydrology. In *Peatlands: Evolution and records of environmental and climate changes* (eds I.P. Martini, A. Martinez Cortizas & W. Chesworth), pp. 319–346. Elsevier, Amsterdam, The Netherlands.

Holden, J. & Armstrong, A. (2007) *Monitoring the hydrological consequences of ditch blocking and related restoration activities within blanket bog in the Berwyn and South Clwyd Mountains SAC, NE Wales - Report 1 - Hydrological monitoring design*. School of Geography, University of Leeds, Leeds, UK.

Holden, J. & Burt, T.P. (2002) Piping and pipeflow in a deep peat catchment. *Catena*, 48, 163–199.

Holden, J. & Burt, T.P. (2003) Hydraulic conductivity in upland blanket peat: measurement and variability. *Hydrological Processes*, 17, 1227–1237.

Holden, J., Burt, T.P. & Cox, N.J. (2001) Macroporosity and infiltration in blanket peat: the implications of tension disc infiltrometer measurements. *Hydrological Processes*, 15, 289–303.

Höll, B.S., Fiedler, S., Jungkunst, H.F., Kalbitz, K., Freibauer, A., Drösler, M. & Stahr, K. (2009) Characteristics of dissolved organic matter following 20 years of peatland restoration. *Science of the Total Environment*, 408, 78–83.

Hörmann, G., Branding, A., Clemen, T., Herbst, M., Hinrichs, A. & Thamm, F. (1996) Calculation and simulation of wind controlled canopy interception of a beech forest in northern Germany. *Agricultural and Forest Meteorology*, 79, 131–148.

Houghton-Carr, H. (1999) *Flood estimation handbook, Volume 4: Restatement and application of the Flood Studies Report rainfall-runoff method*. Institute of Hydrology, Wallingford, UK.

House, A.R., Sorensen, J.P.R., Gooddy, D.C., Newell, A.J., Marchant, B., Mountford, J.O., Scarlett, P., Williams, P.J. & Old, G.H. (2015) Discrete wetland groundwater discharges revealed with a three-dimensional temperature model and botanical indicators (Boxford, UK). *Hydrogeology Journal*, 23, 775–787.

Hudson, J.A., Crane, S.B. & Blackie, J.R. (1999) The Plynlimon water balance 1969-1995: the impact of forest and moorland vegetation on evaporation and streamflow in upland catchments. *Hydrology and Earth System Sciences*, 1, 409–427.

Hughes, P.D.M. (2000) A reappraisal of the mechanisms leading to ombrotrophy in British raised mires. *Ecology Letters*, 3, 7–9.

Hughes, P.D.M. & Barber, K.E. (2003) Mire development across the fen–bog transition on the Teifi floodplain at Tregaron Bog, Ceredigion, Wales, and a comparison with 13 other raised bogs. *Journal of Ecology*, 91, 253–264.

Hughes, P.D.M. & Barber, K.E. (2004) Contrasting pathways to ombrotrophy in three raised bogs from Ireland and Cumbria, England. *The Holocene*, 14, 65.

Hughes, P.D.M. & Dumayne-Peaty, L. (2002) Testing theories of mire development using multiple successions at Crymlyn Bog, West Glamorgan, South Wales, UK. *Journal of Ecology*, 90, 456–471.

Hutchinson, M.F., Xu, T. & Stein, J.A. (2011) Recent progress in the ANUDEM elevation gridding procedure. In *Proceedings of the Geomorphometry 2011 conference, 7-11/09/2011, Redlands, California, USA*, pp. 19–22. International Society for Geomorphometry.

Hvorslev, M. (1951) *Time lag and soil permeability in groundwater observations*. Bulletin n°36, U.S. Army Waterways Experiment Station, Vicksburg, Mississippi, USA.

Ilnicki, P. & Zeitz, J. (2003) Irreversible loss of organic soil functions after reclamation. In *Organic soils and peat materials for sustainable agriculture* (eds L.E. Parent & P. Ilnicki), pp. 15–32. CRC Press, Boca Raton, Florida, USA.

Ingram, H.A.P. (1978) Soil layers in mires: function and terminology. *Journal of Soil Science*, 29, 224–227.

Ingram, H.A.P. (1982) Size and shape in raised mire ecosystems: a geophysical model. *Nature*, 297, 300–303.

Ingram, H.A.P. (1983) Hydrology. In *Mires: swamp, bog, fen and moor - General studies* Ecosystems of the world. (ed A.J.P. Gore), pp. 67–158. Elsevier Scientific, Amsterdam, The Netherlands.

Ingram, H.A.P., Rycroft, D.W. & Williams, D.J.A. (1974) Anomalous transmission of water through certain peats. *Journal of Hydrology*, 22, 213–218.

Ise, T., Dunn, A.L., Wofsy, S.C. & Moorcroft, P.R. (2008) High sensitivity of peat decomposition to climate change through water-table feedback. *Nature Geoscience*, 1, 763–766.

Ivanov, K.E. (1981) *Water movement in mirelands* (trans A Thomson and HAP Ingram). Academic Press, London, UK.

Jabłońska, E., Pawlikowski, P., Jarzombkowski, F., Chormański, J., Okruszko, T. & Kłosowski, S. (2011) Importance of water level dynamics for vegetation patterns in a natural percolation mire (Rospuda fen, NE Poland). *Hydrobiologia*, 674, 105–117.

Jackson, G.E., Irvine, J. & Grace, J. (1999) Xylem acoustic emissions and water relations of *Calluna vulgaris* L. at two climatological regions of Britain. *Plant Ecology*, 140, 3–14.

Jajarmizad, M., Harun, S. & Salarpour, M. (2012) A review on theoretical consideration and types of models in hydrology. *Journal of Environmental Science and Technology*, 5, 249–261.

Jarvis, P.G. (1976) The interpretation of the variations in leaf water potential and stomatal conductance found in canopies in the field. *Philosophical Transactions of the Royal Society of London B: Biological Sciences*, 273, 593–610.

Jeglum, J.K. (2011) Plant indicators of pH and water level in peatlands at Candle Lake, Saskatchewan. *Canadian Journal of Botany*, 49, 1661–1676.

Jeglum, J.K. & He, F. (1995) Pattern and vegetation–environment relationships in a boreal forested wetland in northeastern Ontario. *Canadian Journal of Botany*, 73, 629–637.

Johansen, O.M., Jensen, J.B. & Pedersen, M.L. (2014) From groundwater abstraction to vegetative response in fen ecosystems. *Hydrological Processes*, 28, 2396–2410.

Johansson, T. (1999) Biomass equations for determining fractions of pendula and pubescent birches growing on abandoned farmland and some practical implications. *Biomass and Bioenergy*, 16, 223–238.

Johnson, R. (1998) The forest cycle and low river flows: a review of UK and international studies. *Forest Ecology and Management*, 109, 1–7.

Johnson, J.D. & Ferrell, W.K. (1983) Stomatal response to vapour pressure deficit and the effect of plant water stress. *Plant, Cell & Environment*, 6, 451–456.

Johnston, C.A., Detenbeck, N.E. & Niemi, G.J. (1990) The cumulative effect of wetlands on stream water quality and quantity. A landscape approach. *Biogeochemistry*, 10, 105–141.

Jolly, W.M., Nemani, R. & Running, S.W. (2005) A generalized, bioclimatic index to predict foliar phenology in response to climate. *Global Change Biology*, 11, 619–632.

Joly, D., Brossard, T., Cardot, H., Cavailhes, J., Hilal, M. & Wavresky, P. (2010) Les types de climats en France, une construction spatiale. *Cybergeo: European Journal of Geography*, 501.

Jones, J.A.A. (2004) Implications of natural soil piping for basin management in upland Britain. *Land Degradation & Development*, 15, 325–349.

Joosten, H. (2004) The IMCG Global Peatland Database - Methods. Available at: http://www.imcg.net/pages/publications/imcg-materials.php [accessed 15 March 2015]

Joosten, H. & Clarke, D. (2002) *Wise use of mires and peatlands*. International Mire Conservation Group & International Peat Society, Jyväskylä, Finland.

Julve, P. (1996) Les tourbières de France: écologie et valeur patrimoniale. *Les Cahiers Scientifiques et Techniques du réseau "Tourbières de France"*, 1, 2–7.

Julve, P. (1998) Some proposals towards a mire classification at world scale. *International Mire Conservation Group Newsletter*, 4/5, 18–21.

Jutras, S., Rousseau, A.N. & Clerc, C. (2009) Implementation of a peatland-specific water budget algorithm in HYDROTEL. *Canadian Water Resources Journal*, 34, 349–364.

Kaffke, A. (2008) Vegetation and site conditions of a *Sphagnum* percolation bog in the Kolkheti lowlands (Georgia, Transcaucasia). *Phytocoenologia*, 38, 161–176.

Kalisz, B., Lachacz, A. & Glazewski, R. (2015) Effects of peat drainage on labile organic carbon and water repellency in NE Poland. *Turkish Journal of Agriculture and Forestry*, 39, 20–27.

Katzensteiner, K., Klimo, E., Szuckics, U. & Delaney, C.M. (2011) Impact of forest management alternatives on water budgets and runoff processes. In *Papers on impacts of forest management on environmental services* EFI Technical Report. (eds K. Raulund-Rasmussen, J. De Jong, J.W. Humphrey, M. Smith, H.P. Ravn, K. Katzensteiner, E. Klimo, U. Szuckics, C.M. Delaney, K. Hansen, I. Stupak, E. Ring, P. Gundersen & D. Lousteau), pp. 27–55. European Forest Institute, Joensuu, Finland.

Keitel, C., Adams, M.A., Holst, T., Matzarakis, A., Mayer, H., Rennenberg, H. & Geßler, A. (2003) Carbon and oxygen isotope composition of organic compounds in the phloem sap provides a short-term measure for stomatal conductance of European beech (*Fagus sylvatica* L.). *Plant, Cell & Environment*, 26, 1157–1168.

Keith, D.A., Elith, J. & Simpson, C.C. (2014) Predicting distribution changes of a mire ecosystem under future climates. *Diversity and Distributions*, 20, 440–454.

Kelliher, F.M., Leuning, R., Raupach, M.R. & Schulze, E.-D. (1995) Maximum conductances for evaporation from global vegetation types. *Agricultural and Forest Meteorology*, 73, 1–16.

Kellner, E. (2001a) *Surface energy exchange and hydrology of a poor* Sphagnum *mire*. Acta Universitatis Upsaliensis, Comprehensive summaries of Uppsala dissertations from the Faculty of Science and Technology, 657, Uppsala University, Uppsala, Sweden.

Kellner, E. (2001b) Surface energy fluxes and control of evapotranspiration from a Swedish *Sphagnum* mire. *Agricultural and Forest Meteorology*, 110, 101–123.

Kellner, E. & Halldin, S. (2002) Water budget and surface-layer water storage in a *Sphagnum* bog in central Sweden. *Hydrological Processes*, 16, 87–103.

Kerslake, J.E., Woodin, S.J. & Hartley, S.E. (1998) Effects of carbon dioxide and nitrogen enrichment on a plant–insect interaction: the quality of *Calluna vulgaris* as a host for *Operophtera brumata*. *New Phytologist*, 140, 43–53.

Kim, J. & Verma, S.B. (1996) Surface exchange of water vapour between an open *Sphagnum* fen and the atmosphere. *Boundary-Layer Meteorology*, 79, 243–264.

Kirkham, D. (1946) Proposed method for field measurement of permeability of soil below the water table. *Soil Science Society of America Journal*, 10, 58–68.

Kjeldsen, T.R. (2007) *The revitalised FSR/FEH rainfall-runoff method*. Flood estimation handbook supplementary report n°1, Centre for Ecology and Hydrology, Wallingford, UK.

Klaassen, W., Bosveld, F. & de Water, E. (1998) Water storage and evaporation as constituents of rainfall interception. *Journal of Hydrology*, 212–213, 36–50.

Klein, C. (1978) Les Monts d'Ambazac et de Saint-Goussaud. Deux points de vue sur la morphogenèse limousine. *Norois*, 97, 103–126.

Klein, C., Désiré-Marchand, J. & Giusti, C. (1990) *L'évolution géomorphologique de l'Europe hercynienne occidentale et centrale: aspects régionaux et essai de synthèse*. Centre National de la Recherche Scientifique, Paris, France.

Kleinebecker, T. (2007) *Patterns and gradients in south Patagonian ombrotrophic peatland vegetation*. PhD thesis, Westfaälischen Wilhelms-Universität Münster, Münster, Germany.

Kleinebecker, T., Hölzel, N. & Vogel, A. (2007) Gradients of continentality and moisture in south Patagonian ombrotrophic peatland vegetation. *Folia Geobotanica*, 42, 363–382.

Kleinebecker, T., HöLzel, N. & Vogel, A. (2010) Patterns and gradients of diversity in south Patagonian ombrotrophic peat bogs. *Austral Ecology*, 35, 1–12.

Klemeš, V. (1986) Operational testing of hydrological simulation models. *Hydrological Sciences Journal*, 31, 13–24.

Koenker, R. (2013) Quantreg. R package for quantile regression (version 4.98). Available at: http://cran.r-project.org/web/packages/quantreg/index.html

Koerselman, W. & Beltman, B. (1988) Evapotranspiration from fens in relation to Penman's potential free water evaporation (EO) and pan evaporation. *Aquatic Botany*, 31, 307–320.

Krause, P., Boyle, D.P. & Bäse, F. (2005) Comparison of different efficiency criteria for hydrological model assessment. *Advances in Geosciences*, 5, 89–97.

Krause, S., Jacobs, J. & Bronstert, A. (2007) Modelling the impacts of land-use and drainage density on the water balance of a lowland–floodplain landscape in northeast Germany. *Ecological Modelling*, 200, 475–492.

Kristensen, K. & Jensen, S. (1975) A model for estimating actual evapotranspiration from potential evapotranspiration. *Nordic Hydrology*, 6, 170–188.

Kumar, D., Ahmed, S., Krishnamurthy, N.S. & Dewandel, B. (2007) Reducing ambiguities in vertical electrical sounding interpretations: a geostatistical application. *Journal of Applied Geophysics*, 62, 16–32.

Kuusk, A., Lang, M. & Nilson, T. (2004) Simulation of the reflectance of ground vegetation in sub-boreal forests. *Agricultural and Forest Meteorology*, 126, 33–46.

Labadz, J., Allott, T., Evans, M., Butcher, D., Billett, M., Stainer, S., Yallop, A., Jones, P., Innerdale, M. & Harmon, N. (2010) *Peatland hydrology*. Draft scientific review, IUCN UK Peatland Programme, Edinburgh, UK.

Lachassagne, P. (2008) Overview of the hydrogeology of hard rock aquifers: applications for their survey, management, modelling and protection. In *Groundwater dynamics in hard rock aquifers: sustainable management and optimal monitoring network design* (eds S. Ahmed, R. Jayakumar & A. Salih), pp. 40–63. Springer, Dordrecht, The Netherlands.

Lachassagne, P., Ahmed, S., Dewandel, B., Courtois, N., Marechal, J., Perrin, J. & Wyns, R. (2009) Recent improvements in the conceptual model of hard rock aquifers and its application to the survey, management, modelling and protection of groundwater. In *Proceedings of the Groundwater & Climate in Africa international conference, 24-28/06/2008, Kampala, Uganda*, pp. 250–256. International Association of Hydrological Sciences Press, Wallingford, UK.

Lachassagne, P., Bérard, P., Blès, J.L., Chéry, L., Desprats, J.F., Izac, J.L., Le Strat, P. & Wyns, R. (1999) *PRD324-98. Hydrogéologie des aquifères discontinus. Ressources en eau Margeride Ouest. Synthèse des résultats de la première phase du projet. Méthodologie d'analyse multicritères pour la cartographie des potentialités en eau souterraine des aquifères de socle. Sélection de sites expérimentaux.* Rapport, R 40293, Bureau de Recherches Géologiques et Minières, Orléans, France.

Lachassagne, P., Dewandel, B., Gandolfi, J.M., Maréchal, J.C. & Wyns, R. (2006) A new geological and hydrogeological conceptual model for hard rock aquifers. Applications for their survey, management, modelling and protection. In *Proceedings of the KIGAM International Groundwater Symposium* Korea Institute of Geoscience and Mineral Resources, Korea.

Lachassagne, P., Pinault, J.-L. & Laporte, P. (2001a) Radon 222 emanometry: a relevant methodology for water well siting in hard rock aquifers. *Water Resources Research*, 37, 3131–3146.

Lachassagne, P. & Wyns, R. (2005) Aquifères de socle : nouveaux concepts - Application à la prospection et la gestion de la ressource en eau. *Geosciences*, 2, 32–37.

Lachassagne, P. & Wyns, R. (2006) Aquifères de socle. In *Aquifères et eaux souterraines en france* (ed J.C. Roux), pp. 52–58. AIH-IAH & BRGM, Orléans, France.

Lachassagne, P., Wyns, R., Bérard, P., Bruel, T., Chéry, L., Coutand, T., Desprats, J.F. & Strat, P. (2001b) Exploitation of high-yields in hard-rock aquifers: downscaling methodology combining GIS and multicriteria analysis to delineate field prospecting zones. *Ground Water*, 39, 568–581.

Lachassagne, P., Wyns, R. & Dewandel, B. (2011) The fracture permeability of hard rock aquifers is due neither to tectonics, nor to unloading, but to weathering processes. *Terra Nova*, 23, 145–161.

Ladekarl, U.L. (1998) Estimation of the components of soil water balance in a Danish oak stand from measurements of soil moisture using TDR. *Forest Ecology and Management*, 104, 227–238.

Ladekarl, U.L. (2001) *Soil moisture, evapotranspiration and groundwater recharge in forest and heathland*. PhD thesis, Aarhus University, Aarhus, Denmark.

Ladekarl, U.L., Nørnberg, P., Rasmussen, K.R., Nielsen, K.E. & Hansen, B. (2001) Effects of a heather beetle attack on soil moisture and water balance at a Danish heathland. *Plant and Soil*, 229, 147–158.

Ladekarl, U.L., Rasmussen, K.R., Christensen, S., Jensen, K.H. & Hansen, B. (2005) Groundwater recharge and evapotranspiration for two natural ecosystems covered with oak and heather. *Journal of Hydrology*, 300, 76–99.

Lafleur, P.M. (1990) Evapotranspiration from sedge-dominated wetland surfaces. *Aquatic Botany*, 37, 341–353.

Lafleur, P.M., Hember, R.A., Admiral, S.W. & Roulet, N.T. (2005) Annual and seasonal variability in evapotranspiration and water table at a shrub-covered bog in southern Ontario, Canada. *Hydrological Processes*, 19, 3533–3550.

Lafleur, P.M. & Roulet, N.T. (1992) A comparison of evaporation rates from two fens of the Hudson Bay lowland. *Aquatic Botany*, 44, 59–69.

Lageat, Y., Lagasquie, J.-J. & Simon-Coinçon, R. (2001) Structural landforms in basement terrains. In *Basement regions* (eds A. Godard, J.J. Lagasquie & Y. Lageat), pp. 65–89. Springer-Verlag, Berlin, Heidelberg, Germany.

Langner, P., Mikutta, C. & Kretzschmar, R. (2012) Arsenic sequestration by organic sulphur in peat. *Nature Geoscience*, 5, 66–73.

Lapen, D.R., Price, J.S. & Gilbert, R. (2005) Modelling two-dimensional steady-state groundwater flow and flow sensitivity to boundary conditions in blanket peat complexes. *Hydrological Processes*, 19, 371–386.

Laplace-Dolonde, A., Bory, B., Monneret, C. & Moret-Bailly, C. (2007) *Etude hydrodynamique de la tourbière des Dauges (87)*. Rapport final, Laboratoire Rhodanien de Géographie de l'Environnement, Université Lyon 2, Lyon, France.

Lappalainen, E. (1996) *Global peat resources*. International Peat Society, Jyväskylä, Finland.

Lebourgeois, F., Pierrat, J.-C., Perez, V., Piedallu, C., Cecchini, S. & Ulrich, E. (2010) Simulating phenological shifts in French temperate forests under two climatic change scenarios and four driving global circulation models. *International Journal of Biometeorology*, 54, 563–581.

Legout, A., Legout, C., Nys, C. & Dambrine, E. (2009) Preferential flow and slow convective chloride transport through the soil of a forested landscape (Fougères, France). *Geoderma*, 151, 179–190.

Lelong, F., Cosandey, C., Didon, J.F., Dupraz, C., Durand, P. & Valadas, B. (1987) Recherches programmées : les bassins versants de recherche et expérimentaux (B.V.R.E.) du Mont Lozère. In *Actes du colloque du Parc National des Cévennes, 24-27 Novembre 1987, Florac, France* Parc National des Cévennes, Florac, France.

Lémond, J., Dandin, P., Planton, S., Vautard, R., Pagé, C., Déqué, M., Franchistéguy, L., Geindre, S., Kerdoncuff, M., Li, L., Moisselin, J.M., Noël, T. & Tourre, Y.M. (2011) DRIAS: a step toward climate services in France. *Advances in Science & Research*, 6, 179–186.

Letts, M.G., Roulet, N.T., Comer, N.T., Skarupa, M.R. & Verseghy, D.L. (2000) Parametrization of peatland hydraulic properties for the Canadian Land Surface Scheme. *Atmosphere-Ocean*, 38, 141–160.

Leuschner, C. (1993) Resource availability at three presumed stages of a heathland succession on the Lüneburger Heide, Germany. *Journal of Vegetation Science*, 4, 255–262.

Leuschner, C. (2002) Forest succession and water resources: soil hydrology and ecosystem water turnover in early, mid and late stages of a 300-yr-long chronosequence on sandy soil. In *Forest development - Succession, environmental stress and forest management* (eds A. Dohrenbusch & N. Bartsch), pp. 1–68. Springer-Verlag, Berlin, Heidelberg, Germany.

Leuschner, C. & Rode, M.W. (1999) The role of plant resources in forest succession: changes in radiation, water and nutrient fluxes, and plant productivity over a 300-yr-long chronosequence in NW-Germany. *Perspectives in Plant Ecology, Evolution and Systematics*, 2, 103–147.

Levison, J., Larocque, M., Fournier, V., Gagné, S., Pellerin, S. & Ouellet, M.A. (2014) Dynamics of a headwater system and peatland under current conditions and with climate change. *Hydrological Processes*, 28, 4808–4822.

Lewis, C., Albertson, J., Zi, T., Xu, X. & Kiely, G. (2013) How does afforestation affect the hydrology of a blanket peatland? A modelling study. *Hydrological Processes*, 27, 3577–3588.

Lidman, F., Mörth, C.M. & Laudon, H. (2012) Landscape control of uranium and thorium in boreal streams – spatiotemporal variability and the role of wetlands. *Biogeosciences*, 9, 4773–4785.

Limpens, J., Berendse, F., Blodau, C., Canadell, J.G., Freeman, C., Holden, J., Roulet, N., Rydin, H. & Schaepman-Strub, G. (2008) Peatlands and the carbon cycle: from local processes to global implications – a synthesis. *Biogeosciences*, 5, 1475–1491.

Lindsay, R. (1995) *Bogs: The ecology, classification and conservation of ombrotrophic mires*. Scottish Natural Heritage, Edinburgh, UK.

Lindsay, R. (2010) *Peatbogs and carbon: a critical synthesis to inform policy development in oceanic peat bog conservation and restoration in the context of climate change.* Environmental Research Group, University of East London, London, UK.

Lindsay, R., Charman, D.J., Everingham, F., O'reilly, R.M., Palmer, M.A., Rowell, T.A. & Stroud, D.A. (1988) *The flow country: the peatlands of Caithness and Sutherland*. Nature Conservancy Council, Peterborough, UK.

Llorens, P. & Gallart, F. (2000) A simplified method for forest water storage capacity measurement. *Journal of Hydrology*, 240, 131–144.

Llorens, L., Peñuelas, J. & Emmett, B. (2002) Developmental instability and gas exchange responses of a heathland shrub to experimental drought and warming. *International Journal of Plant Sciences*, 163, 959–967.

Loke, M.H. (2000) Electrical imaging surveys for environmental and engineering studies - A practical guide to 2-D and 3-D surveys. Available at: https://pangea.stanford.edu/research/groups/sfmf/docs/DCResistivity_Notes2.pdf [accessed 13 December 2012]

Loke, M.H. (2013) RES2DINVx32/x64 - 2D RESISTIVITY & IP INVERSION software for Windows XP/Vista/7 (version 3.59.117). Available at: http://www.geotomosoft.com/

Lubczynski, M.W. & Gurwin, J. (2005) Integration of various data sources for transient groundwater modeling with spatio-temporally variable fluxes—Sardon study case, Spain. *Journal of Hydrology*, 306, 71–96.

Lucassen, E.C.H.E.T., Smolders, A.J.P. & Roelofs, J.G.M. (2002) Potential sensitivity of mires to drought, acidification and mobilisation of heavy metals: the sediment S/(Ca+Mg) ratio as diagnostic tool. *Environmental Pollution*, 120, 635–646.

Lucchese, M., Waddington, J.M., Poulin, M., Pouliot, R., Rochefort, L. & Strack, M. (2010) Organic matter accumulation in a restored peatland: evaluating restoration success. *Ecological Engineering*, 36, 482–488.

Lunt, P., Allot, T., Anderson, P., Buckler, M., Coupar, A. & Jones, P. (2010) *Peatland restoration*. Scientific review, IUCN UK Peatland Programme, Edinburgh, UK.

Lu, J., Sun, G., Amatya, D.M., Harder, S.V. & McNulty, S.G. (2006) Understanding the hydrologic response of a coastal plain watershed to forest management and climate change in South Carolina, USA. In *Proceedings of the International Conference on Hydrology and Management of Forested Wetlands* (ed T. Williams), pp. 231–239. American Society of Agricultural and Biological Engineers, St. Joseph, MI, USA.

Lu, J., Sun, G., McNulty, S.G. & Comerford, N.B. (2009) Sensitivity of pine flatwoods hydrology to climate change and forest management in Florida, USA. *Wetlands*, 29, 826–836.

Ma, L., Ashworth, P.J., Best, J.L., Elliott, L., Ingham, D.B. & Whitcombe, L.J. (2002) Computational fluid dynamics and the physical modelling of an upland urban river. *Geomorphology*, 44, 375–391.

Madsen, H. (2000) Automatic calibration of a conceptual rainfall–runoff model using multiple objectives. *Journal of Hydrology*, 235, 276–288.

Madsen, H. (2003) Parameter estimation in distributed hydrological catchment modelling using automatic calibration with multiple objectives. *Advances in Water Resources*, 26, 205–216.

Mahmoudzadeh, M.R., Francés, A.P., Lubczynski, M. & Lambot, S. (2012) Using ground penetrating radar to investigate the water table depth in weathered granites — Sardon case study, Spain. *Journal of Applied Geophysics*, 79, 17–26.

Malmer, N., Johansson, T., Olsrud, M. & Christensen, T.R. (2005) Vegetation, climatic changes and net carbon sequestration in a North-Scandinavian subarctic mire over 30 years. *Global Change Biology*, 11, 1895–1909.

Maltby, E. & Immirzi, P. (1993) Carbon dynamics in peatlands and other wetland soils regional and global perspectives. *Chemosphere*, 27, 999–1023.

Malterer, T.J., Verry, E.S. & Erjavec, J. (1992) Fiber content and degree of decomposition in peats: review of national methods. *Soil Science Society of America Journal*, 56, 1200–1211.

Manneville, O., Vergne, V. & Villepoux, O. (1999) *Le monde des tourbières et des marais: France, Suisse, Belgique, Luxembourg*. Delachaux et Niestlé, Paris, France.

Marandi, A., Karro, E., Polikarpus, M., Jõeleht, A., Kohv, M., Hang, T. & Hiiemaa, H. (2013) Simulation of the hydrogeologic effects of oil-shale mining on the neighbouring wetland water balance: case study in north-eastern Estonia. *Hydrogeology Journal*, 21, 1581–1591.

Maréchal, J.C., Dewandel, B., Ahmed, S., Galeazzi, L. & Zaidi, F.K. (2006) Combined estimation of specific yield and natural recharge in a semi-arid groundwater basin with irrigated agriculture. *Journal of Hydrology*, 329, 281–293.

Maréchal, J.C., Dewandel, B., Ahmed, S. & Lachassagne, P. (2007a) Hard rock aquifers characterization prior to modelling at catchment scale: an application to India. In *Groundwater in fractured rocks: selected papers from the Groundwater in Fractured Rocks International Conference, Prague, 2003*, p. 227.

Maréchal, J.C., Dewandel, B. & Subrahmanyam, K. (2007b) Characterization of fracture properties in hard rock aquifer system. In *Groundwater: resource evaluation, augmentation, contamination, restoration, modeling and management* (ed M. Thangarajan), pp. 156–188. Springer, Dordrecht, The Netherlands.

Maréchal, J.C., Dewandel, B., Subrahmanyam, K. & others. (2004a) Use of hydraulic tests at different scales to characterize fracture network properties in the weathered-fractured layer of a hard rock aquifer. *Water Resources Research*, 40, W11508.

Maréchal, J.C., Dewandel, B., Subrahmanyam, K. & Torri, R. (2003a) Specific methods for the evaluation of hydraulic properties in fractured hard-rock aquifers. *Current Science*, 85, 511–516.

Maréchal, J.C., Dewandel, B., Subrahmanyam, K. & Torri, R. (2008) Various pumping tests and methods for evaluation of hydraulic properties in fractured hard rock aquifers. In *Groundwater dynamics in hard rock aquifers: sustainable management and optimal monitoring network design* (eds S. Ahmed, R. Jayakumar & A. Salih), pp. 100–111. Springer, Dordrecht, The Netherlands.

Maréchal, J.C., Wyns, R., Lachassagne, P. & Subrahmanyam, K. (2004b) Vertical anisotropy of hydraulic conductivity in the fissured layer of hard-rock aquifers due to the geological structure of weathering profiles. *Journal of the Geological Society of India*, 63, 545–550.

Maréchal, J.-C., Wyns, R., Lachassagne, P., Subrahmanyam, K. & Touchard, F. (2003b) Anisotropie verticale de la perméabilité de l'horizon fissuré des aquifères de socle : concordance avec la structure géologique des profils d'altération. *Comptes Rendus Geoscience*, 335, 451–460.

Marini, L., Nascimbene, J., Scotton, M. & Klimek, S. (2008) Hydrochemistry, water table depth and related distribution patterns of vascular plants in a mixed mire. *Plant Biosystems*, 142, 79–86.

Martin, C. & Didon-Lescot, J.F. (2007) Influence d'une tourbière de moyenne montagne sur les écoulements: le cas de la tourbière des Sagnes sur le Mont-Lozère. *Études de Géographie Physique*, 34, 27–41.

Martin, C., Didon-Lescot, J.F. & Marc, V. (2002) Étude du fonctionnement hydrologique des zones humides du Mont-Lozère: l'exemple de la tourbière des Sagnes. *Etudes de géographie physique*, 29, 15–43.

Martin, C., Duguépéroux, F. & Didon-Lescot, J.F. (2008) Fonctionnement hydrologique d'une tourbière drainée: la plaine de la Sénégrière (Lozère). *Etudes de Géographie Physique*, 35, 3–23.

Maslin, M. (2014) *Climate change: A very short introduction*. Oxford University Press, Oxford, UK.

Massman, W.J. (1983) The derivation and validation of a new model for the interception of rainfall by forests. *Agricultural Meteorology*, 28, 261–286.

Massuel, S., George, B., Gaur, A. & Nune, R. (2007) Groundwater modelling for sustainable resource management in the Musi Catchment, India. In *Proceedings of the MODSIM 2007 International Congress on Modelling and Simulation* (eds L. Oxley & D. Kulasiri), pp. 1429–1435. Modelling and Simulation Society of Australia and New Zealand.

Mathys, N., Meunier, M. & Brochot, S. (1996) The forest effect on floods in small mountainous catchments: some results from the experimental catchments of Draix, France. In *Ecohydrological processes in small basins - Proceedings of the Sixth Conference of the European Network of Experimental and Representative Basins (ERB)* Technical Documents in Hydrology No. 14., pp. 124–128. IHP/UNESCO - ERB - CEREG (ULP/CNRS), Strasbourg, France.

Mauquoy, D., Engelkes, T., Groot, M.H.M., Markesteijn, F., Oudejans, M.G., Van Der Plicht, J. & Van Geel, B. (2002) High-resolution records of late-Holocene climate change and carbon accumulation in two north-west European ombrotrophic peat bogs. *Palaeogeography, Palaeoclimatology, Palaeoecology*, 186, 275–310.

Mauroux, B., Wyns, R., Martelet, G. & Lions, J. (2009) *SILURES Limousin - Module 1 SILURES "Base de données". Recueil des données, interprétations et perspectives.* Rapport final, RP-57901-FR, Bureau de Recherches Géologiques et Minières, Orléans, France.

McDonald, M.G. & Harbaugh, A.W. (2003) The history of MODFLOW. *Ground Water*, 41, 280–283.

MEDDE/CGDD/SOeS & Fédération des Conservatoires d'Espaces Naturels. (2013) Tourbières en France métropolitaine - SOeS_Tourbieres_12. Available at: http://www.statistiques.developpementdurable.gouv.fr/lessentiel/ar/265/0/tourbieres.html [accessed 13 November 2013]

Medlyn, B.E., Barton, C.V.M., Broadmeadow, M.S.J., Ceulemans, R., De Angelis, P., Forstreuter, M., Freeman, M., Jackson, S.B., Kellomäki, S., Laitat, E., Rey, A., Roberntz, P., Sigurdsson, B.D., Strassemeyer, J., Wang, K., Curtis, P.S. & Jarvis, P.G. (2001) Stomatal conductance of forest species after long-term exposure to elevated CO_2 concentration: a synthesis. *New Phytologist*, 149, 247–264.

Meiresonne, L., Sampson, D.A., Kowalski, A.S., Janssens, I.A., Nadezhdina, N., Cermák, J., Van Slycken, J. & Ceulemans, R. (2003) Water flux estimates from a Belgian Scots pine stand: a comparison of different approaches. *Journal of Hydrology*, 270, 230–252.

Merot, P., Ezzahar, B., Walter, C. & Aurousseau, P. (1995) Mapping waterlogging of soils using digital terrain models. *Hydrological Processes*, 9, 27–34.

Merot, P., Squividant, H., Aurousseau, P., Hefting, M., Burt, T., Maitre, V., Kruk, M., Butturini, A., Thenail, C. & Viaud, V. (2003) Testing a climato-topographic index for predicting wetlands distribution along an European climate gradient. *Ecological Modelling*, 163, 51–71.

Merriam, R.A. (1961) Surface water storage on annual ryegrass. *Journal of Geophysical Research*, 66, 1833–1838.

Migon, P. (2006) *Granite landscapes of the world*. Oxford University Press, Oxford, UK.

Millard, K. & Richardson, M. (2013) Wetland mapping with LiDAR derivatives, SAR polarimetric decompositions, and LiDAR–SAR fusion using a random forest classifier. *Canadian Journal of Remote Sensing*, 39, 290–307.

Miranda, A.C., Jarvis, P.G. & Grace, J. (1984) Transpiration and evaporation from heather moorland. *Boundary-Layer Meteorology*, 28, 227–243.

Miserere, L., Montacchini, F. & Buffa, G. (2003) Ecology of some mire and bog plant communities in the western Italian Alps. *Journal of Limnology*, 62, 88–96.

Moore, P.D. (1984) The classification of mires: an introduction. In *European mires* (ed P.D. Moore), pp. 1–10. Academic Press Inc., London, UK.

Moore, R.D. (2004) Introduction to salt dilution gauging for streamflow measurement: Part 1. *Streamline Watershed Management Bulletin*, 7, 20–23.

Moore, R.D.. (2005) Introduction to salt dilution gauging for streamflow measurement Part III: slug injection using salt in solution. *Streamline Watershed Management Bulletin*, 8, 1–6.

Moore, P.D. & Bellamy, D.J. (1974) *Peatlands*. Springer-Verlag, Berlin, Heidelberg, Germany.

Moore, P.A., Pypker, T.G. & Waddington, J.M. (2013) Effect of long-term water table manipulation on peatland evapotranspiration. *Agricultural and Forest Meteorology*, 178–179, 106–119.

Moriasi, D.N., Arnold, J.G., Van Liew, M.W., Bingner, R.L., Harmel, R.D. & Veith, T.L. (2007) Model evaluation guidelines for systematic quantification of accuracy in watershed simulations. *Transactions of the American Society of Agricultural and Biological Engineers*, 50, 885–900.

Móricz, N., Mátyás, C., Berki, I., Rasztovits, E., Vekerdy, Z. & Gribovszki, Z. (2012) Comparative water balance study of forest and fallow plots. *iForest*, 5, 188–196.

Morris, P.J., Baird, A.J. & Belyea, L.R. (2012) The DigiBog peatland development model 2: ecohydrological simulations in 2D. *Ecohydrology*, 5, 256–268.

Morris, P.J., Waddington, J.M., Benscoter, B.W. & Turetsky, M.R. (2011) Conceptual frameworks in peatland ecohydrology: looking beyond the two-layered (acrotelm-catotelm) model. *Ecohydrology*, 4, 1–11.

Mougin, B., Thomas, E., Wyns, R., Blanchin, R. & Mathieu, F. (2003) *Comportement hydrodynamique des roches altérées de la surface sur le bassin versant de la rade de Brest (Finistère)*. Rapport final, RP-52656-FR, Bureau de Recherches Géologiques et Minières, Orléans, France.

Muzylo, A., Llorens, P., Valente, F., Keizer, J.J., Domingo, F. & Gash, J.H.C. (2009) A review of rainfall interception modelling. *Journal of Hydrology*, 370, 191–206.

Nabighian, M.N. (ed). (1988) *Electromagnetic methods in applied geophysics: volume 1, theory*. Society of Exploration Geophysicists, Tulsa, Oklahoma, USA.

Nakicenovic, N. & Swart, R. (eds). (2000) *Special report on emissions scenarios*. Intergovernmental Panel on Climate Change, Cambridge University Press, Cambridge, UK.

Négrel, P., Millot, R., Brenot, A. & Bertin, C. (2010) Lithium isotopes as tracers of groundwater circulation in a peat land. *Chemical Geology*, 276, 119–127.

Neitsch, S.L., Arnold, J.G., Kiniry, J.R. & Williams, J.R. (2005) *Soil and water assessment tool: theoretical documentation, version 2009*. Texas, USA.

Nekola, J.C. (2004) Vascular plant compositional gradients within and between Iowa fens. *Journal of Vegetation Science*, 15, 771.

Newson, M. (1976) Soil piping in upland Wales : a call for more information. *Cambria: a Welsh Geographical Review*, 3, 33–39.

Nieveen, J.P., Jacobs, C.M.J. & Jacobs, A.F.G. (1998) Diurnal and seasonal variation of carbon dioxide exchange from a former true raised bog. *Global Change Biology*, 4, 823–833.

Nizinski, J. & Saugier, B. (1989) Dynamique de l'eau dans une chênaie (*Quercus petraea* (Matt.) Liebl.) en forêt de Fontainebleau. *Annales des Sciences Forestières*, 46, 173–186.

Nordbakken, J.-F. (1996) Plant niches along the water-table gradient on an ombrotrophic mire expanse. *Ecography*, 19, 114–121.

Nourani, V., Aminfar, M.H., Alami, M.T., Sharghi, E. & Singh, V.P. (2014) Unsteady 2-D seepage simulation using physical analog, case of Sattarkhan embankment dam. *Journal of Hydrology*, 519, 177–189.

Nourani, V., Monadjemi, P. & Singh, V.P. (2007) Liquid analog model for laboratory simulation of rainfall–runoff process. *Journal of Hydrologic Engineering*, 12, 246–255.

Økland, R.H., Økland, T. & Rydgren, K. (2001) A Scandinavian perspective on ecological gradients in north-west European mires: reply to Wheeler and Proctor. *Journal of Ecology*, 89, 481–486.

Okruszko, H. & Ilnicki, P. (2003) The moorsh horizons as quality indicators of reclaimed organic soils. In *Organic Soils and Peat Materials for Sustainable Agriculture* (eds L.E. Parent & P. Ilnicki), pp. 1–14. CRC Press, Boca Raton, Florida, USA.

Oliver, J.E. (2005) *The encyclopedia of world climatology*. Springer, Dordrecht, The Netherlands.

Olona, J., Pulgar, J.A., Fernández-Viejo, G., López-Fernández, C. & González-Cortina, J.M. (2010) Weathering variations in a granitic massif and related geotechnical properties through seismic and electrical resistivity methods. *Near Surface Geophysics*, 8, 585–599.

Owen, D.E. & Otton, J.K. (1995) Mountain wetlands: efficient uranium filters — potential impacts. *Ecological Engineering*, 5, 77–93.

Paappanen, T., Leinonen, A. & Hillebrand, K. (2006) *Fuel peat industry in EU*. Summary report, VTT -R-00545-06, Technical Research Centre of Finland, Jyväskylä, Finland.

Pagé, C., Terray, L. & Boé, J. (2008) *Projections climatiques à échelle fine sur la France pour le 21ème siècle: les scénarii SCRATCH08*. Centre Européen de Recherche et de Formation Avancée en Calcul Scientifique (CERFACS), Toulouse, France.

Päivänen, J. (1973) Hydraulic conductivity and water retention in peat soils. *Acta Forestalia Fennica*, 129, 4–68.

Parent, L.E. & Caron, J. (2008) Physical properties of organic soils and growing media: particle size and degree of decomposition. In *Soil sampling and methods of analysis* (eds M.R. Carter & E.G. Gregorich), pp. 871–883. CRC Press, Boca Raton, Florida, USA.

Parish, F., Sirin, A., Charman, D., Joosten, H., Minayeva, T., Silvius, M. & Stringer, L. (2008) *Assessment on peatlands, biodiversity and climate change*. Main report, Global Environment Centre & Wetlands International, Kuala Lumpur, Malaysia & Wageningen, The Netherlands.

Parry, L.E., Holden, J. & Chapman, P.J. (2014) Restoration of blanket peatlands. *Journal of Environmental Management*, 133, 193–205.

Pellerin, S., Lagneau, L.-A., Lavoie, M. & Larocque, M. (2009) Environmental factors explaining the vegetation patterns in a temperate peatland. *Comptes Rendus Biologies*, 332, 720–731.

Persson, G. & Lindroth, A. (1994) Simulating evaporation from short-rotation forest: variations within and between seasons. *Journal of Hydrology*, 156, 21–45.

Peterka, T., Plesková, Z., Jiroušek, M. & Hájek, M. (2014) Testing floristic and environmental differentiation of rich fens on the Bohemian Massif. *Preslia*, 86, 337–366.

Pitman, J.I. (1989) Rainfall interception by bracken in open habitats — Relations between leaf area, canopy storage and drainage rate. *Journal of Hydrology*, 105, 317–334.

Poiani, K.A., Johnson, W.C., Swanson, G.A. & Winter, T.C. (1996) Climate change and northern prairie wetlands: simulations of long-term dynamics. *Limnology and Oceanography*, 41, 871–881.

Porteret, J. (2008) *Fonctionnement hydrologique des têtes de bassin versant tourbeuses du Nord-Est du Massif Central*. Thèse de Doctorat, Université Jean Monnet, Saint-Etienne, France.

Pouliot, R., Hugron, S. & Rochefort, L. (2015) *Sphagnum* farming: a long-term study on producing peat moss biomass sustainably. *Ecological Engineering*, 74, 135–147.

Price, J.S. (1992a) Blanket bog in Newfoundland. Part 2. Hydrological processes. *Journal of Hydrology*, 135, 103–119.

Price, J.S. (1992b) Blanket bog in Newfoundland. Part 1. The occurrence and accumulation of fog-water deposits. *Journal of Hydrology*, 135, 87–101.

Price, J.S., Rochefort, L. & Campeau, S. (2002) Use of shallow basins to restore cutover peatlands: hydrology. *Restoration Ecology*, 10, 259–266.

Price, J.S. & Schlotzhauer, S.M. (1999) Importance of shrinkage and compression in determining water storage changes in peat: the case of a mined peatland. *Hydrological Processes*, 13, 2591–2601.

Proctor, M.C.F., McHaffie, H.S., Legg, C.J. & Amphlett, A. (2009) Evidence from water chemistry as a criterion of ombrotrophy in the mire complexes of Abernethy Forest, Scotland. *Journal of Vegetation Science*, 20, 160–169.

Proulx-McInnis, S., St-Hilaire, A., Rousseau, A.N., Jutras, S., Carrer, G. & Levrel, G. (2012) Automated soil lysimeter for determination of actual evapotranspiration of a bog in Quebec, Canada. *Journal of Hydrologic Engineering*, 19, 60–68.

Purseglove, J. (1988) *Taming the flood: A history and natural history of rivers and wetlands*. Oxford University Press, Oxford, UK.

Querner, E.P., Jansen, P.C., van den Akker, J.J.H. & Kwakernaak, C. (2012) Analysing water level strategies to reduce soil subsidence in Dutch peat meadows. *Journal of Hydrology*, 446–447, 59–69.

Quinn, P.F., Beven, K.J. & Lamb, R. (1995) The ln(*a*/tan*β*) index: how to calculate it and how to use it within the TOPMODEL framework. *Hydrological Processes*, 9, 161–182.

Quinty, F. & Rochefort, L. (2003) *Peatland restoration guide*, 2nd ed. Canadian Sphagnum Peat Moss Association & New Brunswick Departement of Natural Resources and Energy, St. Albert & Fredericton, Canada.

Rahim, B.E., Yusoff, I., Jafri, A.M. & Othman, Z. (2009) Simulation of integrated surface-water/groundwater flow for a freshwater wetland in Selangor State, Malaysia. *Bulletin of the Geological Society of Malaysia*, 55, 95–100.

Rahim, B.E., Yusoff, I., Jafri, A.M., Othman, Z. & Abdul Ghani, A. (2012) Application of MIKE SHE modelling system to set up a detailed water balance computation. *Water and Environment Journal*, 26, 490–503.

Rameau, J.-C., Mansion, D., Dumé, G., Timbal, J., Lecointe, A., Dupont, P. & Keller, R. (1994) *Flore forestière française. Tome 1. Plaines et collines*. Institut pour le Développement Forestier, Paris, France.

Ramsar Convention Secretariat. (2013) *The Ramsar Convention Manual: a guide to the Convention on Wetlands (Ramsar, Iran, 1971)*, 6th ed. Ramsar Convention Secretariat, Gland, Switzerland.

Rannik, Ü., Altimir, N., Raittila, J., Suni, T., Gaman, A., Hussein, T., Hölttä, T., Lassila, H., Latokartano, M., Lauri, A., Natsheh, A., Petäjä, T., Sorjamaa, R., Ylä-Mella, H., Keronen, P., Berninger, F., Vesala, T., Hari, P. & Kulmala, M. (2002) Fluxes of carbon dioxide and water vapour over Scots pine forest and clearing. *Agricultural and Forest Meteorology*, 111, 187–202.

R Core Team. (2014) *R: a language and environment for statistical computing*. R Foundation for Statistical Computing, Vienna, Austria.

Reddy, K.R. & DeLaune, R.D. (2004) *Biogeochemistry of wetlands: science and applications*. CRC Press, Boca Raton, Florida, USA.

Reeve, A.S., Evensen, R., Glaser, P.H., Siegel, D.I. & Rosenberry, D. (2006) Flow path oscillations in transient ground-water simulations of large peatland systems. *Journal of Hydrology*, 316, 313–324.

Reeve, A.S., Warzocha, J., Glaser, P.H. & Siegel, D.I. (2001) Regional ground-water flow modeling of the Glacial Lake Agassiz Peatlands, Minnesota. *Journal of Hydrology*, 243, 91–100.

Refsgaard, J.C. (1997) Parameterisation, calibration and validation of distributed hydrological models. *Journal of Hydrology*, 198, 69–97.

Refsgaard, J.C., Storm, B. & Clausen, T. (2010) Système Hydrologique Europeén (SHE): review and perspectives after 30 years development in distributed physically-based hydrological modelling. *Hydrology Research*, 41, 355.

Richards, L.A. (1931) Capillary conduction of liquids through porous mediums. *Journal of Applied Physics*, 1, 318–333.

Richardson, J.L., Arndt, J.L. & Montgomery, J.A. (2001) Hydrology of wetland and related soils. In *Wetland soils - Genesis, hydrology, landscapes, and classification* (eds J.L. Richardson & M.J. Vepraskas), pp. 35–84. CRC Press, Boca Raton, Florida, USA.

Richardson, M.C., Mitchell, C.P.J., Branfireun, B.A. & Kolka, R.K. (2010) Analysis of airborne LiDAR surveys to quantify the characteristic morphologies of northern forested wetlands. *Journal of Geophysical Research*, 115, G03005 1–16.

Rigon, R., Bertoldi, G. & Over, T.M. (2006) GEOtop: a distributed hydrological model with coupled water and energy budgets. *Journal of Hydrometeorology*, 7, 371–388.

Riley, J.L. & Michaud, L. (1994) *Ontario peatland inventory: field-work methods*. Miscellaneous paper, 155, Ontario Ministry of Northern Development and Mines, Ontario Geological Survey, Toronto, Canada.

Ringqvist, L., Holmgren, A. & Öborn, I. (2002) Poorly humified peat as an adsorbent for metals in wastewater. *Water Research*, 36, 2394–2404.

Robinson, M., Cognard-Plancq, A.-L., Cosandey, C., David, J., Durand, P., Führer, H.-W., Hall, R., Hendriques, M.O., Marc, V., McCarthy, R., McDonnell, M., Martin, C., Nisbet, T., O'Dea, P., Rodgers, M. & Zollner, A. (2003) Studies of the impact of forests on peak flows and baseflows: a European perspective. *Forest Ecology and Management*, 186, 85–97.

Robson, A. & Reed, D.W. (1999a) *Flood estimation handbook, Volume 1: Overview*. Institute of Hydrology, Wallingford, UK.

Robson, A. & Reed, D.W. (1999b) *Flood estimation handbook, Volume 3: Statistical procedures for flood freequency estimation*. Institute of Hydrology, Wallingford, UK.

Rochefort, L., Quinty, F., Campeau, S., Johnson, K. & Malterer, T. (2003) North American approach to the restoration of *Sphagnum* dominated peatlands. *Wetlands Ecology and Management*, 11, 3–20.

Rochester, R.E.. (2010) *Uncertainty in hydrological modelling: a case study in the Tern catchment, Shropshire, UK*. PhD thesis, University College London, London, UK.

Rodhe, A. & Seibert, J. (1999) Wetland occurrence in relation to topography: a test of topographic indices as moisture indicators. *Agricultural and Forest Meteorology*, 98, 325–340.

Rodwell, J.S. (ed). (1992) *British plant communities. Volume 2: mires and heaths*. Cambridge University Press, Cambridge, UK.

Rodwell, J.S. (ed). (1998) *British plant communities. Volume 4: aquatic communities, swamps and tall-herb fens*. Cambridge University Press, Cambridge, UK.

Rosenqvist, L., Hansen, K., Vesterdal, L. & van der Salm, C. (2010) Water balance in afforestation chronosequences of common oak and Norway spruce on former arable land in Denmark and southern Sweden. *Agricultural and Forest Meteorology*, 150, 196–207.

Rose, N.L., Yang, H., Turner, S.D. & Simpson, G.L. (2012) An assessment of the mechanisms for the transfer of lead and mercury from atmospherically contaminated organic soils to lake sediments with particular reference to Scotland, UK. *Geochimica et Cosmochimica Acta*, 82, 113–135.

Rossi, P.M., Ala-aho, P., Doherty, J. & Kløve, B. (2014) Impact of peatland drainage and restoration on esker groundwater resources: modeling future scenarios for management. *Hydrogeology Journal*, 22, 1131–1145.

Rossi, P.M., Ala-aho, P., Ronkanen, A.-K. & Kløve, B. (2012) Groundwater–surface water interaction between an esker aquifer and a drained fen. *Journal of Hydrology*, 432–433, 52–60.

Rothwell, J. & Evans, M. (2004) *Flux of heavy metal pollution from eroding southern Pennine peatlands*. Upland Environments Research Unit, School of Environment and Development, The University of Manchester, Manchester, UK.

Rothwell, J.J., Evans, M.G., Daniels, S.M. & Allott, T.E.H. (2008) Peat soils as a source of lead contamination to upland fluvial systems. *Environmental Pollution*, 153, 582–589.

Rothwell, J.J., Taylor, K.G., Ander, E.L., Evans, M.G., Daniels, S.M. & Allott, T.E.H. (2009) Arsenic retention and release in ombrotrophic peatlands. *Science of the Total Environment*, 407, 1405–1417.

Rothwell, J.J., Taylor, K.G., Chenery, S.R.N., Cundy, A.B., Evans, M.G. & Allott, T.E.H. (2010) Storage and behavior of As, Sb, Pb, and Cu in ombrotrophic peat bogs under contrasting water table conditions. *Environmental Science & Technology*, 44, 8497–8502.

Rothwell, J.J., Taylor, K.G., Evans, M.G. & Allott, T.E.H. (2011) Contrasting controls on arsenic and lead budgets for a degraded peatland catchment in Northern England. *Environmental Pollution*, 159, 3129–3133.

Running, S.W. (1976) Environmental control of leaf water conductance in conifers. *Canadian Journal of Forest Research*, 6, 104–112.

Rutter, A.J., Kershaw, K.A., Robins, P.C. & Morton, A.J. (1971) A predictive model of rainfall interception in forests, 1. Derivation of the model from observations in a plantation of Corsican pine. *Agricultural Meteorology*, 9, 367–384.

Rutter, A.J. & Morton, A.J. (1977) A predictive model of rainfall interception in forests. III. Sensitivity of the model to stand parameters and meteorological variables. *Journal of Applied Ecology*, 14, 567–588.

Rutter, A.J., Morton, A.J. & Robins, P.C. (1975) A predictive model of rainfall interception in forests. II. Generalization of the model and comparison with observations in some coniferous and hardwood stands. *Journal of Applied Ecology*, 12, 367–380.

Rycroft, D.W., Williams, D.J.A. & Ingram, H.A.P. (1975) The transmission of water through peat: II. Field experiments. *The Journal of Ecology*, 557–568.

Rydin, H. & Jeglum, J.K. (2006) *The biology of peatlands*. Oxford University Press, Oxford, UK.

Sahin, V. & Hall, M.J. (1996) The effects of afforestation and deforestation on water yields. *Journal of Hydrology*, 178, 293–309.

Salazar, O., Hansen, S., Abrahamsen, P., Hansen, K. & Gundersen, P. (2013) Changes in soil water balance following afforestation of former arable soils in Denmark as evaluated using the DAISY model. *Journal of Hydrology*, 484, 128–139.

Schöner, A., Noubactep, C., Büchel, G. & Sauter, M. (2009) Geochemistry of natural wetlands in former uranium milling sites (eastern Germany) and implications for uranium retention. *Chemie der Erde - Geochemistry*, 69, Supplement 2, 91–107.

Schot, P.P. & Molenaar, A. (1992) Regional changes in groundwater flow patterns and effects on groundwater composition. *Journal of Hydrology*, 130, 151–170.

Schouwenaars, J.M. (1993) Hydrological differences between bogs and bog-relicts and consequences for bog restoration. *Hydrobiologia*, 265, 217–224.

Schouwenaars, J.M. & Gosen, A.M. (2007) The sensitivity of *Sphagnum* to surface layer conditions in a re-wetted bog: a simulation study of water stress. *Mires and Peat*, 2, 1–19.

Schumann, M. & Joosten, H. (2008) *Global peatland restoration manual*. Institute of Botany and Landscape Ecology, Greifswald University, Greifswald, Germany.

Scurlock, J.M.O., Asner, G.P. & Gower, S.T. (2001) Global leaf area index from field measurements, 1932-2000. Available at: http://mercury-ops2.ornl.gov/ornldaac/send/xsltText2?fileURL=/data/Mercury_instances/ornldaac/daac/harvested/record669.xml&full_datasource=DAAC%20Datasets&full_queryString=%20Global%20Leaf%20Area%20Index%20Data%20from%20Field%20Measurements%20AND%20%28%20datasource%20:%28%20daac%20daacweb%20%20%29%20%29%20&ds_id=584 [accessed 31 October 2013]

Shaw, E.M., Beven, K.J., Chappell, N.A. & Lamb, R. (2010) *Hydrology in practice*, 4th ed. CRC Press, Boca Raton, Florida, USA.

Siegel, D.I. & Glaser, P. (2006) The hydrology of peatlands. In *Boreal peatland ecosystems* Ecological Studies. (eds R.K. Wieder & D.H. Vitt), pp. 289–311. Springer, Berlin, Heidelberg, Germany.

Sijtsma, B. & Veldhuizen, A. (1992) *Hydrology of Clara and Raheenmore bog: consolidation, evapotranspiration, storage coefficients, acrotelm transmissivity, piezometer test, groundwater dbase, retention*. Wageningen Agricultural University, Department of Water Resources, Wageningen, The Netherlands.

Silc, T. & Stanek, W. (1977) Bulk density estimation of several peats in northern Ontario using the von Post humification scale. *Canadian Journal of Soil Science*, 57, 75–75.

Silvertown, J., Dodd, M.E., Gowing, D.J.G. & Mountford, J.O. (1999) Hydrologically defined niches reveal a basis for species richness in plant communities. *Nature*, 400, 61–63.

Singh, V.P. (1988) *Hydrologic systems: rainfall-runoff modeling*. Prentice Hall, Upper Saddle River, USA.

Singh, C.R. (2010) *Hydrological and hydraulic modelling for the restoration and management of Loktak Lake, Northeast India*. PhD thesis, University College London, London, UK.

Singhal, B.B.S. & Gupta, R.P. (2010) *Applied hydrogeology of fractured rocks*, 2nd ed. Springer, Dordrecht, The Netherlands.

Singh, C.R., Thompson, J.R., French, J.R., Kingston, D.G. & Mackay, A.W. (2010) Modelling the impact of prescribed global warming on runoff from headwater catchments of the Irrawaddy River and their implications for the water level regime of Loktak Lake, northeast India. *Hydrology and Earth System Sciences*, 14, 1745–1765.

Singh, C.R., Thompson, J.R., Kingston, D.G. & French, J.R. (2011) Modelling water-level options for ecosystem services and assessment of climate change: Loktak Lake, northeast India. *Hydrological Sciences Journal*, 56, 1518–1542.

Smith, R. & Charman, D. (1988) The vegetation of upland mires within conifer plantations in Northumberland, northern England. *Journal of Applied Ecology*, 25, 579–594.

Sobolewski, A. (1999) A review of processes responsible for metal removal in wetlands treating contaminated mine drainage. *International Journal of Phytoremediation*, 1, 19–51.

Soil Classification Working Group. (1998) *The Canadian system of soil classification*, 3rd ed. NRC Research Press, Ottawa, Canada.

Sottocornola, M., Laine, A., Kiely, G., Byrne, K.A. & Tuittila, E.-S. (2008) Vegetation and environmental variation in an Atlantic blanket bog in South-western Ireland. *Plant Ecology*, 203, 69–81.

Soulsby, C., Tetzlaff, D., Rodgers, P., Dunn, S. & Waldron, S. (2006) Runoff processes, stream water residence times and controlling landscape characteristics in a mesoscale catchment: an initial evaluation. *Journal of Hydrology*, 325, 197–221.

South West Water. (2014) Peat bog restoration work holds back water, scientists say. Available at: http://www.southwestwater.co.uk/index.cfm?articleid=11311 [accessed 22 April 2014]

Spieksma, J.F.M., Dolman, A.J. & Schouwenaars, J.M. (1996) *De parametrisatie van de verdamping van natuurterreinen in hydrologische modellen*. Vakgroep Fysische Geografie, Rijksuniversiteit Groningen, Groningen, The Netherlands.

Spieksma, J., Moors, E., Dolman, A. & Schouwenaars, J. (1997) Modelling evaporation from a drained and rewetted peatland. *Journal of Hydrology*, 199, 252–271.

Staelens, J., De Schrijver, A., Verheyen, K. & Verhoest, N.E.C. (2008) Rainfall partitioning into throughfall, stemflow, and interception within a single beech (*Fagus sylvatica* L.) canopy: influence of foliation, rain event characteristics, and meteorology. *Hydrological Processes*, 22, 33–45.

Stanek, W. & Silc, T. (1977) Comparisons of four methods for determination of degree of peat humification (decomposition) with emphasis on the von Post method. *Canadian Journal of Soil Science*, 57, 109–117.

Stoner, W.A. & Miller, P.C. (1975) Water relations of plant species in the wet coastal tundra at Barrow, Alaska. *Arctic and Alpine Research*, 7, 109–124.

Strack, M. (ed). (2008) *Peatlands and climate change*. University of Calgary, Calgary, Canada.

Strack, M., Waddington, J.M., Bourbonniere, R.A., Buckton, E.L., Shaw, K., Whittington, P. & Price, J.S. (2008) Effect of water table drawdown on peatland dissolved organic carbon export and dynamics. *Hydrological Processes*, 22, 3373–3385.

Succow, M. & Lange, E. (1984) The mire types of the German Democratic Republic. In *European mires* (ed P.D. Moore), pp. 149–175. Academic Press Inc., London, UK.

Sutcliffe, J.V. (1978) *Methods of flood estimation: a guide to the flood studies report*. 49, Institute of Hydrology, Wallingford, UK.

Szajdak, L.W., Szatyłowicz, J. & Kõlli, R. (2011) Peats and peatlands: physical properties. In *Encyclopedia of agrophysics* (eds J. Gliński, J. Horabik & J. Lipiec), pp. 551–555. Springer, Dordrecht, The Netherlands.

Szkokan-Emilson, E.J., Kielstra, B., Watmough, S. & Gunn, J. (2013) Drought-induced release of metals from peatlands in watersheds recovering from historical metal and sulphur deposition. *Biogeochemistry*, 116, 131–145.

Tang, Z., Li, R., Li, X., Jiang, W. & Hirsh, A. (2014) Capturing LiDAR-derived hydrologic spatial parameters to evaluate playa wetlands. *Journal of the American Water Resources Association*, 50, 234–245.

Tarboton, D.G. (1997) A new method for the determination of flow directions and upslope areas in grid digital elevation models. *Water Resources Research*, 33, 309–319.

Tarboton, D.G. (2008) Terrain analysis using digital elevation models (TauDEM). Available at: http://hydrology.neng.usu.edu/taudem/taudem3.1/index.html#thefunctions [accessed 5 April 2010]

The ASCE task committee on definition of criteria for evaluation of watershed models of the watershed management committee, Irrigation and Drainage Division. (1993) Criteria for evaluation of watershed models. *Journal of Irrigation and Drainage Engineering*, 119, 429–442.

Thébaud, G. (2011) Contribution au prodrome des végétations de France : les *Oxycocco-Sphagnetea* Br.-Bl. & Tx 1943 (tourbières acides eurosibériennes). *Journal de Botanique de la Société Botanique de France*, 56, 69–97.

Thébaud, G. & Petel, G. (2008) A contribution to the revision of ombrotrophic and ombrominerotrophic medioeuropean mires communities. *Phytocoenologia*, 38, 287–304.

Therneau, T.M., Atkinson, B. & Ripley, B. (2014) *rpart: Recursive partitioning*.

Thiéry, D. (1990) *MARTHE software - Modelling of Aquifers with a Rectangular grid in Transient state for Hydrodynamic calculations of hEads and flows. Release 4.3*. Rapport, 32548, Bureau de Recherches Géologiques et Minières, Orléans, France.

Thompson, J.R. (2004) Simulation of wetland water-level manipulation using coupled hydrological/hydraulic modeling. *Physical Geography*, 25, 39–67.

Thompson, J.R. (2012) Modelling the impacts of climate change on upland catchments in southwest Scotland using MIKE SHE and the UKCP09 probabilistic projections. *Hydrology Research*, 43, 507.

Thompson, J., Gavin, H., Refsgaard, A., Refstrup Sørenson, H. & Gowing, D. (2009) Modelling the hydrological impacts of climate change on UK lowland wet grassland. *Wetlands Ecology and Management*, 17, 503–523.

Thompson, J.R., Green, A.J. & Kingston, D.G. (2014a) Potential evapotranspiration-related uncertainty in climate change impacts on river flow: an assessment for the Mekong River basin. *Journal of Hydrology*, 510, 259–279.

Thompson, J.R., Green, A.J., Kingston, D.G. & Gosling, S.N. (2013) Assessment of uncertainty in river flow projections for the Mekong River using multiple GCMs and hydrological models. *Journal of Hydrology*, 486, 1–30.

Thompson, J.R., Laizé, C.L.R., Green, A.J., Acreman, M.C. & Kingston, D.G. (2014b) Climate change uncertainty in environmental flows for the Mekong River. *Hydrological Sciences Journal*, 59, 935–954.

Thompson, J.R., Sørenson, H.R., Gavin, H. & Refsgaard, A. (2004) Application of the coupled MIKE SHE/MIKE 11 modelling system to a lowland wet grassland in southeast England. *Journal of Hydrology*, 293, 151–179.

Tiemeyer, B., Lennartz, B. & Vegelin, K. (2006) Hydrological modelling of a re-wetted peatland on the basis of a limited dataset for water management. *Journal of Hydrology*, 325, 376–389.

Tiktak, A. & Bouten, W. (1994) Soil water dynamics and long-term water balances of a Douglas fir stand in the Netherlands. *Journal of Hydrology*, 156, 265–283.

Tipping, E., Smith, E.J., Lawlor, A.J., Hughes, S. & Stevens, P.A. (2003) Predicting the release of metals from ombrotrophic peat due to drought-induced acidification. *Environmental Pollution*, 123, 239–253.

Tomassen, H., Smolders, A.J.P., Lamers, L.P.M. & Roelofs, J.G.M. (2003) Stimulated growth of Betula pubescens and Molinia caerulea on ombrotrophic bogs: role of high levels of atmospheric nitrogen deposition. *Journal of Ecology*, 91, 357–370.

Tomassen, H., Smolders, A.J.P., Limpens, J., Lamers, L.P.M. & Roelofs, J.G.M. (2004) Expansion of invasive species on ombrotrophic bogs: desiccation or high N deposition? *Journal of Applied Ecology*, 41, 139–150.

Ulrich, E., Lelong, N., Lanier, M. & Schneider, A. (1995) Interception des pluies en forêt: facteurs déterminants. Interprétation des mesures réalisées dans le sous-réseau CATAENAT de RENECOFOR. *Bulletin Technique de l'Office National des Forêts*, 30, 33–44.

Valadas, B. (1984) *Les hautes terres du Massif Central français: contribution à l'étude des morphodynamiques récentes sur versants cristallins et volcaniques*. Thèse de Doctorat d'Etat, Université Paris I, Paris, France.

Valadas, B. (1998) L'alvéole des Dauges : un modèle géomorphologique. *Annales Scientifiques du Limousin*, N° spécial : Tourbière des Dauges, 5–13.

van den Bogaert, R. (2011) *Typologie des sols du bassin versant de la Morcille, caractérisation de leurs propriétés hydrauliques et test de fonctions de pédotransfert*. Master Sciences et Technologies & Master Sciences et Techniques du Vivant, Université Pierre et Marie Curie & AgroParisTech, Paris, France.

van der Kamp, G., Stolte, W.J. & Clark, R.G. (1999) Drying out of small prairie wetlands after conversion of their catchments from cultivation to permanent brome grass. *Hydrological Sciences Journal*, 44, 387–397.

van der Salm, C., Denier van der Gon, H., Wieggers, R., Bleeker, A. & van den Toorn, A. (2006) The effect of afforestation on water recharge and nitrogen leaching in The Netherlands. *Forest Ecology and Management*, 221, 170–182.

van der Salm, C., Rosenqvist, L., Vesterdal, L., Hansen, K., van der Gon, H.D., Bleeker, A., Wieggers, R. & van den Toorn, A. (2007) Interception and water recharge following afforestation: experiences from oak and Norway spruce chronosequences in Denmark, Sweden and The Netherlands. In *Environmental effects of afforestation in north-western Europe* (eds G.W. Heil, B. Muys & K. Hansen), pp. 53–77. Springer, Dordrecht, The Netherlands.

van der Schaaf, S. (1999) *Analysis of the hydrology of raised bogs in the Irish Midlands. A case study of Raheenmore bog and Clara bog*. Doctoral thesis, Wageningen Agricultural University, Wageningen, The Netherlands.

van der Schaaf, S. (2002) Bog hydrology. In *Conservation and restoration of raised bogs: geological, hydrological and ecological studies* (ed M.G.C. Schouten), pp. 54–109. Stationery Office, Dublin, Ireland.

van Loon, A.H., Schot, P.P., Griffioen, J., Bierkens, M.F.P., Batelaan, O. & Wassen, M.J. (2009) Throughflow as a determining factor for habitat contiguity in a near-natural fen. *Journal of Hydrology*, 379, 30–40.

Verger, J.P. (1998) Les sols de l'alvéole de la tourbière du ruisseau des Dauges (Limousin). *Annales Scientifiques du Limousin*, N° spécial : Tourbière des Dauges, 43–54.

Verry, E.S., Boelter, D.H., Paivanen, J., Nichols, D.S., Malterer, T. & Gafni, A. (2011) Physical properties of organic soils. In *Peatland biogeochemistry and watershed hydrology at the Marcell experimental forest* (eds R.K. Kolka, S.D. Sebestyen, E.S. Verry & K.N. Brooks), pp. 135–176. CRC Press, Boca Raton, Florida, USA.

Verry, E.S., Brooks, K.N. & Barten, P.K. (1988) Streamflow response from an ombrotrophic mire. In *Proceedings of the International Symposium on the Hydrology of Wetlands in Temperate and Cold Regions, 6-8 June 1988, Joensuu, Finland*, pp. 52–59. International Peat Society & The Academy of Finland, Helsinki, Finland.

Verstraeten, W.W., Muys, B., Feyen, J., Veroustraete, F., Minnaert, M., Meiresonne, L. & De Schrijver, A. (2005) Comparative analysis of the actual evapotranspiration of Flemish forest and cropland, using the soil water balance model WAVE. *Hydrology and Earth System Sciences Discussions*, 9, 225–241.

Vet, R., Artz, R.S., Carou, S., Shaw, M., Ro, C.-U., Aas, W., Baker, A., Bowersox, V.C., Dentener, F., Galy-Lacaux, C., Hou, A., Pienaar, J.J., Gillett, R., Forti, M.C., Gromov, S., Hara, H., Khodzher, T., Mahowald, N.M., Nickovic, S., Rao, P.S.P. & Reid, N.W. (2014) A global assessment of precipitation chemistry and deposition of sulfur, nitrogen, sea salt, base cations, organic acids, acidity and pH, and phosphorus. *Atmospheric Environment*, 93, 3–100.

Vicente-Serrano, S.M., Beguería, S. & López-Moreno, J.I. (2010) A multiscalar drought index sensitive to global warming: the standardized precipitation evapotranspiration index. *Journal of Climate*, 23, 1696–1718.

Vilks, A. (1993) Un nouveau site botanique remarquable pour la Haute-Vienne : la tourbière du Petit Moulin de Veyrac. *Epops - Revue des Naturalistes du Limousin*, 2, 29–34.

Vitt, D.H. & Chee, W.-L. (1990) The relationships of vegetation to surface water chemistry and peat chemistry in fens of Alberta, Canada. *Vegetatio*, 89, 87–106.

Voldseth, R.A., Johnson, W.C., Gilmanov, T., Guntenspergen, G.R. & Millett, B.V. (2007) Model estimation of land-use effects on water levels of northern prairie wetlands. *Ecological Applications*, 17, 527–540.

von Post, L. (1922) Swedish geological peat survey with the results obtained so far. *Svenska Mosskulturföreningens tidskrift*, 36, 1–27.

Waine, J., Brown, J.M.B. & Ingram, H.A.P. (1985) Non-Darcian transmission of water in certain humified peats. *Journal of Hydrology*, 82, 327–339.

Walker, M.D., Wahren, C.H., Hollister, R.D., Henry, G.H.R., Ahlquist, L.E., Alatalo, J.M., Bret-Harte, M.S., Calef, M.P., Callaghan, T.V., Carroll, A.B., Epstein, H.E., Jónsdóttir, I.S., Klein, J.A., Magnússon, B., Molau, U., Oberbauer, S.F., Rewa, S.P., Robinson, C.H., Shaver, G.R., Suding, K.N., Thompson, C.C., Tolvanen, A., Totland, Ø., Turner, P.L., Tweedie, C.E., Webber, P.J. & Wookey, P.A. (2006) Plant community responses to experimental warming across the tundra biome. *Proceedings of the National Academy of Sciences*, 103, 1342–1346.

Wallage, Z.E., Holden, J. & McDonald, A.T. (2006) Drain blocking: an effective treatment for reducing dissolved organic carbon loss and water discolouration in a drained peatland. *Science of the Total Environment*, 367, 811–821.

Wällstedt, T., Björkvald, L. & Gustafsson, J.P. (2010) Increasing concentrations of arsenic and vanadium in (southern) Swedish streams. *Applied Geochemistry*, 25, 1162–1175.

Walsh, R.P.D. & Voigt, P.J. (1977) Vegetation litter: an underestimated variable in hydrology and geomorphology. *Journal of Biogeography*, 4, 253–274.

Walter, T. (2012) Generic parameters for modeling plant evaporation potential using the crop coefficient method. Available at: http://www.hydrology.bee.cornell.edu/Ecohydrology/Handouts/PlantParameters.pdf [accessed 4 March 2012]

Warren, C.R., Ethier, G.J., Livingston, N.J., Grant, N.J., Turpin, D.H., Harrison, D.L. & Black, T.A. (2003) Transfer conductance in second growth Douglas-fir (*Pseudotsuga menziesii* (Mirb.) Franco) canopies. *Plant, Cell & Environment*, 26, 1215–1227.

Wastiaux, C. (2000) *Facteurs hydrologiques de la dégradation des tourbières hautes à sphaignes des Hautes-Fagnes*. Thèse de Doctorat, Université de Liège, Liège, Belgique.

Weiss, R., Alm, J., Laiho, R. & Laine, J. (1998) Modeling moisture retention in peat soils. *Soil Science Society of America Journal*, 62, 305.

Weltzin, J.F., Bridgham, S.D., Pastor, J., Chen, J. & Harth, C. (2003) Potential effects of warming and drying on peatland plant community composition. *Global Change Biology*, 9, 141–151.

Weltzin, J.F., Pastor, J., Harth, C., Bridgham, S.D., Updegraff, K. & Chapin, C.T. (2000) Response of bog and fen plant communities to warming and water-table manipulations. *Ecology*, 81, 3464–3478.

Wheeler, B. & Proctor, M. (2000) Ecological gradients, subdivisions and terminology of north-west European mires. *Journal of ecology*, 88, 187–203.

Wheeler, B.D. & Shaw, S.C. (1995) A focus on fens-controls on the composition of fen vegetation in relation to restoration. In *Restoration of temperate wetlands* (eds B.D. Wheeler, S.C. Shaw, W.J. Fojt & R.A. Robertson), p. 49. John Wiley & Sons, Chichester, UK.

Wheeler, B., Shaw, S. & Cook, R. (1992) Phytometric assessment of the fertility of undrained rich-fen soils. *Journal of Applied Ecology*, 29, 466–475.

Wheeler, B.D., Shaw, S. & Tanner, K. (2009) *A wetland framework for impact assessment at statutory sites in England and Wales*. Science report, SC030232, Environment Agency, Bristol, UK.

Whitehead, D. (1998) Regulation of stomatal conductance and transpiration in forest canopies. *Tree Physiology*, 18, 633–644.

Whiteman, M., Wheeler, B., Shaw, S., Lewis, T., Grout, M. & Tanner, K. (2009) Use of WETMECs typology to aid understanding of groundwater-dependent terrestrial ecosystems in England and Wales. In *Groundwater monitoring* (eds P. Quevauviller, A.-M. Fouillac, J. Grath & R. Ward), pp. 259–272. John Wiley & Sons, Chichester, UK.

Whitfield, P.H., St-Hilaire, A. & van der Kamp, G. (2009) Improving hydrological predictions in peatlands. *Canadian Water Resources Journal*, 34, 467–478.

Whittington, P.N. & Price, J.S. (2006) The effects of water table draw-down (as a surrogate for climate change) on the hydrology of a fen peatland, Canada. *Hydrological Processes*, 20, 3589–3600.

Wierda, A., Fresco, L., Grootjans, A. & Diggelen, R. (1997) Numerical assessment of plant species as indicators of the groundwater regime. *Journal of Vegetation Science*, 8, 707–716.

Wilson, J.P. & Gallant, J.C. (eds). (2000) *Terrain analysis: principles and applications*. John Wiley & Sons, New York, USA.

Wilson, K.B., Hanson, P.J., Mulholland, P.J., Baldocchi, D.D. & Wullschleger, S.D. (2001) A comparison of methods for determining forest evapotranspiration and its components: sap-flow, soil water budget, eddy covariance and catchment water balance. *Agricultural and Forest Meteorology*, 106, 153–168.

Winter, T.C. (2000) The vulnerability of wetlands to climate change: a hydrologic landscape perspective. *Journal of the American Water Resources Association*, 36, 305–311.

Woodward, C., Shulmeister, J., Larsen, J., Jacobsen, G.E. & Zawadzki, A. (2014) The hydrological legacy of deforestation on global wetlands. *Science*, 346, 844–847.

Worrall, F., Armstrong, A. & Adamson, J.K. (2007) The effects of burning and sheep-grazing on water table depth and soil water quality in a upland peat. *Journal of Hydrology*, 339, 1–14.

Worrall, F., Chapman, P., Holden, J., Evans, C., Artz, R., Smith, P. & Grayson, R. (2010) *Peatlands and climate change*. Scientific review, IUCN UK Peatland Programme, Edinburgh, UK.

Worrall, F., Chapman, P., Holden, J., Evans, C., Artz, R., Smith, P. & Grayson, R. (2011) *A review of current evidence on carbon fluxes and greenhouse gas emissions from UK peatlands*. JNCC report, 442, Joint Nature Conservation Committee, Peterborough, UK.

Wyns, R. (1998) *PRD324. Hydrogéologie des aquifères discontinus. Ressources en eau Margeride Ouest. Modélisation de la géométrie (altitude, épaisseur) des arènes granitiques du bassin versant lozérien de la Truyère (Lozère, Massif Central)*. R 40191, Bureau de Recherches Géologiques et Minières, Orléans, France.

Wyns, R. (2002) Climat, eustatisme, tectonique: quels contrôles pour l'altération continentale? Exemple des séquences d'altération cénozoïques en France. *Bulletin d'Information des Géologues du Bassin de Paris*, 39, 5–16.

Wyns, R., Baltassat, J.-M., Lachassagne, P., Legchenko, A., Vairon, J. & Mathieu, F. (2004) Application of proton magnetic resonance soundings to groundwater reserve mapping in weathered basement rocks (Brittany, France). *Bulletin de la Société Géologique de France*, 175, 21–34.

Wyns, R., Gourry, J.C., Baltassat, J.M. & Lebert, F. (1999) Caractérisation multi-paramètres des horizons de subsurface (0-100 m) en contexte de socle altéré. In *Actes du 2ème colloque GEOFCAN, 21-22/09/1999, Orléans, France* Bureau de Recherches Géologiques et Minières, Orléans, France.

Wyns, R., Quesnel, F., Lacquement, F., Bourgine, B., Mathieu, F., Lebert, F., Baltassat, J.M., Bitri, A. & Mathon, D. (2005) *Contrat de plan Etat-Région : cartographie quantitative des propriétés du sol et du sous-sol dans la région des Pays-de-la-Loire*. Rapport final, RP-53676-FR, Bureau de Recherches Géologiques et Minières, Orléans, France.

Wyns, R., Quesnel, F., Simon-Coinçon, R., Guillocheau, F. & Lacquement, F. (2003) Major weathering in France related to lithospheric deformation. *Géologie de la France*, 1, 79–87.

Wyns, R. & Tegyey, M. (2012) *Etude géologique du cadre structural et des forages du bassin versant de recherche du Ringelbach (Soultzeren, Haut-Rhin)*. Rapport final, RP-56540-FR, Bureau de Recherches Géologiques et Minières, Orléans, France.

Yan, J. & Smith, K.R. (1994) Simulation of integrated surface water and ground water systems-model formulation. *Journal of the American Water Resources Association*, 30, 879–890.

Yazaki, T., Urano, S. & Yabe, K. (2006) Water balance and water movement in unsaturated zones of *Sphagnum* hummocks in Fuhrengawa Mire, Hokkaido, Japan. *Journal of Hydrology*, 319, 312–327.

Yu, Z., Beilman, D.W., Frolking, S., MacDonald, G.M., Roulet, N.T., Camill, P. & Charman, D.J. (2011) Peatlands and their role in the global carbon cycle. *Eos, Transactions of the American Geophysical Union*, 92, 97–98.

Yu, Z., Campbell, I.D., Campbell, C., Vitt, D.H., Bond, G.C. & Apps, M.J. (2003) Carbon sequestration in western Canadian peat highly sensitive to Holocene wet-dry climate cycles at millennial timescales. *The Holocene*, 13, 801–808.

Yu, Z., Loisel, J., Brosseau, D.P., Beilman, D.W. & Hunt, S.J. (2010) Global peatland dynamics since the Last Glacial Maximum. *Geophysical Research Letters*, 37, L13402 1–5.

Zeitz, J. & Velty, S. (2002) Soil properties of drained and rewetted fen soils. *Journal of Plant Nutrition and Soil Science*, 165, 618–626.

Zhang, H. & Hiscock, K.M. (2010) Modelling the impact of forest cover on groundwater resources: A case study of the Sherwood sandstone aquifer in the East Midlands, UK. *Journal of Hydrology*, 392, 136–149.

Zhang, J., Marshall, J.D. & Jaquish, B.C. (1993) Genetic differentiation in carbon isotope discrimination and gas exchange in *Pseudotsuga menziesii*. *Oecologia*, 93, 80–87.

Zhaojun, B., Joosten, H., Hongkai, L., Gaolin, Z., Xingxing, Z., Jinze, M. & Jing, Z. (2011) The response of peatlands to climate warming: a review. *Acta Ecologica Sinica*, 31, 157–162.

Appendix A. Mire classification

This appendix reviews a number of mire classifications currently in use since, taken together, they provide a good overview of the diversity of mire types, of the varying hydrogeomorphic settings that explain them and of their hydrological functioning.

A.1. Hydrogeomorphic classification

In most classifications of peatland types, the definition of the higher-order groups is based on the site hydrogeomorphology: the overall shape of the peat deposit and its topographic position within the landscape are used to infer the main water source, which itself determines the mire water chemistry and vegetation (Charman 2002). Figure A-1 shows the main peatland hydrogeomorphic types.

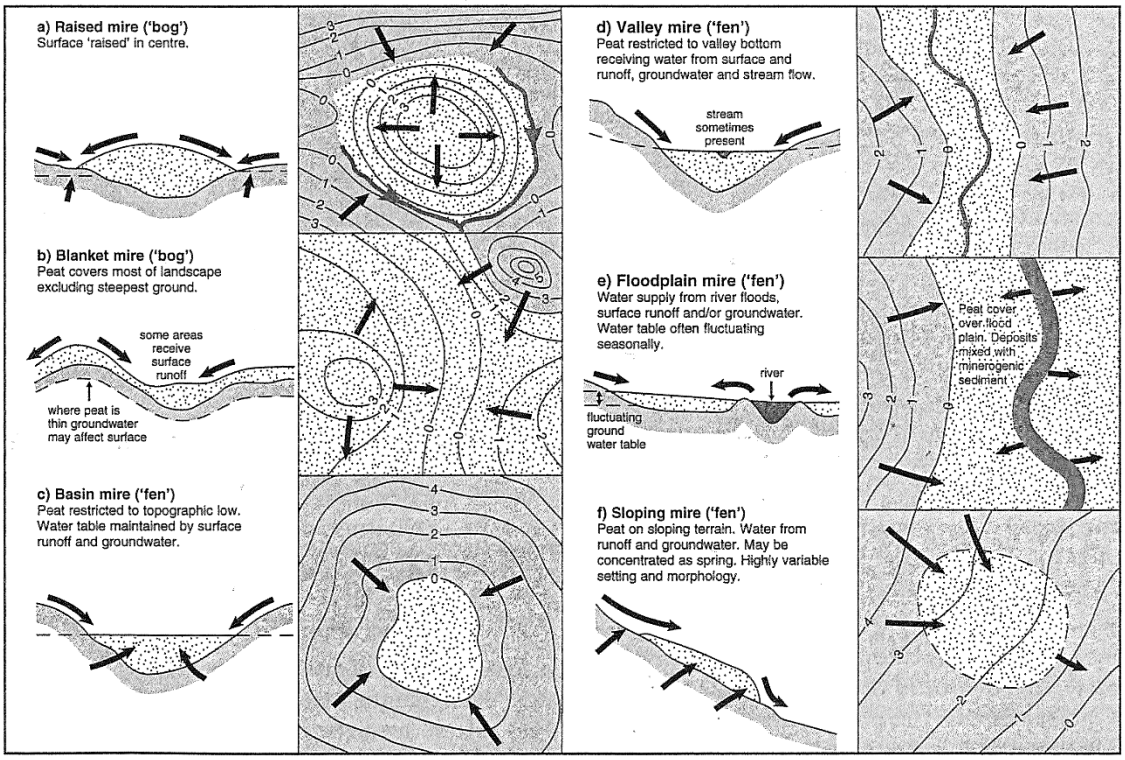

Figure A-1. Cross-sections and plan views of key hydrogeomorphic mire types (from Charman 2002).

Raised bogs have a distinct convex shape, and as a result they are hydrologically disconnected from the surrounding landscape and receive all their water input from precipitation. As a consequence they are among the most acidic and nutrient-poor wetland systems. Because of their dependence on precipitation, they can only form where precipitation is substantially higher than evapotranspiration for most of the year (Lindsay 1995). In Europe, for instance, raised bogs

occur at low altitude in an area covering part of Russia, the Baltic states, Poland, northern Germany, southern Scandinavia, the Netherlands and the British Isles (Moore & Bellamy 1974). They also occur in more southern countries in mountainous areas. In France for instance, raised bogs are found in almost all massifs: the Vosges, the Jura, the Alps, the Massif Central and the Pyrenees (Manneville *et al.* 1999). They are also found at lower elevation under oceanic climate in Brittany (Durfort 2007).

Blanket bogs are ombrotrophic wetlands covering the entire landscape but the steepest slopes. They occur under hyper-oceanic climates (in Europe: western Norway, western Ireland, western England, Wales, Scotland, western Iceland, Lindsay 1995) where constantly wet and cold conditions allow for peat to form on sloping terrain. Lindsay *et al.* (1988) suggested that the formation of blanket bogs requires at least 1000mm annual rainfall, a minimum of 160 wet days, a mean temperature lower than 15°C for the warmest month and with only minor seasonal temperature fluctuations. By definition, blanket bogs occur in a variety of hydrogeomorphic conditions, and as such are more a complex of mire types. Depending on their position within the landscape, elements of blanket bogs have been divided into watershed, saddle, spur and valleyside blanket bogs (Lindsay *et al.* 1988; Lindsay 1995; Charman 2002). They can also include some minor minerotrophic elements around springs or seepages (Lindsay 1995).

Basin mires form in closed topographic depressions, often through the progressive filling of open water bodies by floating vegetation mats (Diggelen *et al.* 1996; Rydin & Jeglum 2006). Sloping mires occur on slopes below groundwater resurgence points. Classic examples are calcareous mires formed at the interface between a lower impermeable geological layer (clay for instance) and an upper water-bearing limestone layer (Acreman 2005; Wheeler *et al.* 2009; Grootjans *et al.* 2012). Valley mires form along the bottom and lower slopes of valleys due to the shallowness of the groundwater table, but with limited input from the stream that frequently flows in the middle. Groundwater inflow may be diffuse or localised as springs along the mire margins (Charman 2002). Floodplain mires, as their name suggests, form within river floodplain of rivers, and receive a substantial part of their water input from over-bank flooding. In these mires peat is often intermixed with mineral layers deposited by floods (Joosten & Clarke 2002).

A.1. Hydrogenetic classification

Joosten & Clarke (2002) and Schumann & Joosten (2008) proposed a hydrogenetic classification of mires, based on work carried out by Succow and collaborators in Eastern Germany (Succow &

Lange 1984; Succow 1981, 1983, 1999 in Joosten & Clarke 2002). Hydrogenetic types are defined by the gradient of the water table in the peat (non-null or null, implying the existence or absence of significant lateral flow), the conditions of peat formation and the main source of water to the mire. The gradient of the water table in the peat distinguishes between two main groups. In horizontal mires, the water table forms a horizontal plane in a closed basin. The water level may fluctuates vertically but there is no or insignificant lateral flow. In sloping mires, the water table in the peat is inclined and a lateral water flow exists. These two groups are further divided according to the way peat accumulates. In horizontal mires (Figure A-2), peat can accumulate through the formation of floating mats on open water bodies (*schwingmoor* mires); at the bottom of a shallow water body, for instance in many flooded reedbeds (immersion mires); through the progressive rise of the regional water table, for instance through sea level rise (water rise mires); or following the periodic flooding of a depression, for instance in a floodplain (flood mires). Flood mires of substantial peat depth can only occur when the source of flood water and the water table in peat progressively rise, and as such they are in practice related to water rise mires. According to Joosten & Clarke (2002) and Schumann & Joosten (2008), the difference lies in the frequent input of allogenic sediments to flood mires.

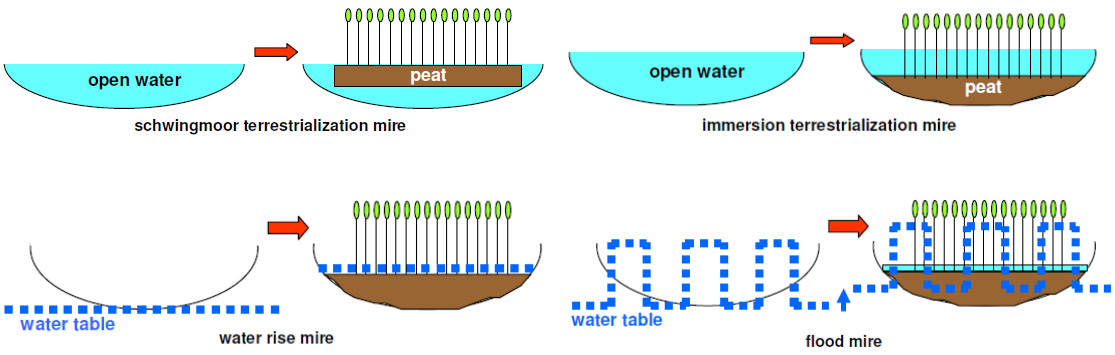

Figure A-2. Sub-types of horizontal mires (from Schumann & Joosten 2008)

Sloping mires are divided into three groups depending on the hydraulic characteristics of the peat body. In percolation mires, a large and constant water supply results in a weakly decomposed and highly permeable peat deposit. Flow exists through the entire peat column (Figure A-3). These mires are generally groundwater-fed since only groundwater can provide large and constant inflow throughout the year, except in highly and constantly humid climates such as south-east Asia (Schumann & Joosten 2008).

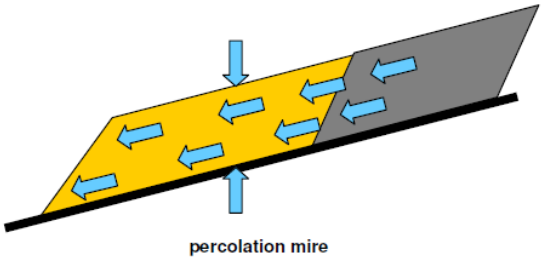

Figure A-3. Percolation mire (from Schumann & Joosten 2008).

Surface flow mires occur where water inflow is large and regular but exceeded by evapotranspiration and runoff during at least part of the year. This results in a greater peat humification than in percolation mires, making it less permeable and reducing water flow through the peat body. Depending on the source of water three types of surface flow mires have been distinguished (Figure A-4). Blanket bogs are fed by precipitation under hyper-oceanic climates, and cover almost all the landscape. Hill slope mires are additionally fed by surface or near-surface flow from upstream mineral ground. Spring mires are linked to the resurgence of groundwater.

Finally, acrotelm mires are defined by the existence of an acrotelm (see Section 1.3.1.4) at the surface of the peat column (Figure A-5). The acrotelm is characterised by a large specific yield and a rapidly decreasing horizontal hydraulic conductivity with depth, which leads to self-regulation of the groundwater table since lateral runoff is inversely proportional to the depth of the groundwater table. In times of water excess, water is rapidly evacuated through the uppermost part of the acrotelm. In the absence of water inflow, runoff decreases to negligible quantities as the water table drops into less permeable peat. The large specific yield reduces the impact of evapotranspiration and further stabilises the groundwater table. According to Joosten & Clarke (2002), raised bogs are the only acrotelm mires so far identified worldwide. Their acrotelm properties derive from the limited ability to decay of a few peat-building *Sphagnum* species. Domed tropical forested swamps of south-east Asia show similar groundwater table regulation properties, but in these the water table is regulated by the topography of the forest floor (Dommain *et al.* 2010).

Mires can further be divided according to the main water source: precipitation (ombrogenous), rapid surface and sub-surface flow (soligenous), deep groundwater flow (lithogenous) or seawater (thallassogenous), giving the hydrogenetic classification shown in Table A-1.

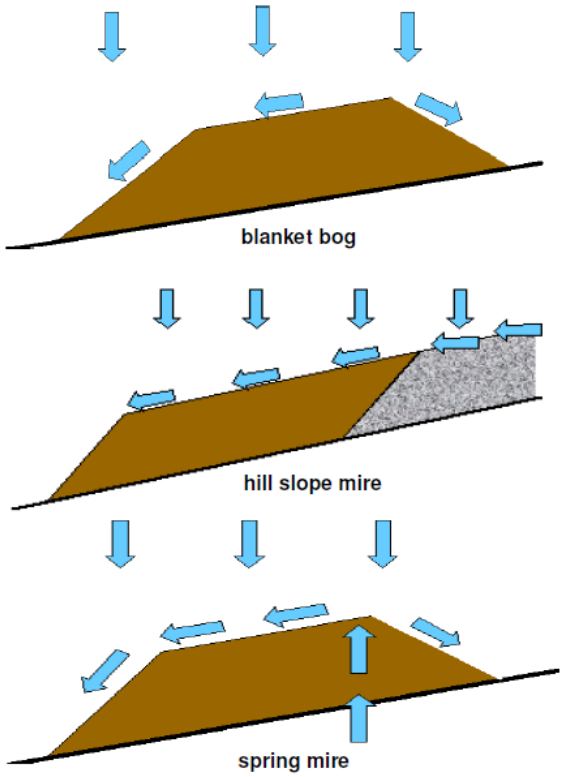

Figure A-4. Surface flow mires (from Schumann & Joosten 2008).

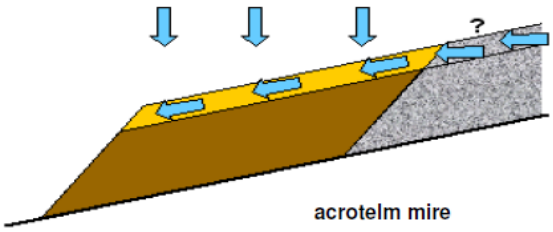

Figure A-5. Acrotelm mire (from Schumann & Joosten 2008).

Table A-1. Hydrogenetic mire types (modified from Joosten & Clarke 2002).

Groundwater table gradient			Horizontal mires				Sloping mires		
Peat formation strategy			Schwingmoor mires	Immersion mires	Water rise mires	Flood mires	Surface flow mires	Acrotelm mires	Percolation mires
Origin of water	ombrogenous		ombrogenous schwingmoor mire *floating mat in bog pool*	ombrogenous immersion mire *terrestrialisation in bog pool*	ombrogenous water rise mire *water rise in bog complex*	ombrogenous flood mire *flood mire in bog complex*	ombrogenous surface flow mire *blanket bog*	ombrogenous acrotelm mire *raised bog*	ombrogenous percolation mire *percolation raised bog (Kaffke 2008)*
	geogenous	soligenous	soligenous shwingmoor mire *floating mat in moorpool*	soligenous immersion mire *terrestrialisation in moorpool*	soligenous water rise mire *kettle bog / kessel-moor*	soligenous flood mire *kessel-standmoor*	soligenous surface flow mire *hangmoor*	soligenous acrotelm mire ?	soligenous percolation mire *some sloping fens*
		lithogenous	lithogenous schwingmoor mire *floating mat on lake*	lithogenous immersion mire *lake terrestrialisation mire*	lithogenous water rise mire *groundwater rise mire*	lithogenous flood mire *river floodplain mire*	lithogenous surface flow mire *most spring mires*	lithogenous acrotelm mire ?	lithogenous percolation mire *typical percolation mires*
		thallasogenous	thallassogenous shwingmoor mire ?	thallassogenous immersion mire *coastal terrestrialisation mire, mangrove*	thallassogenous water rise mire *coastal transgression mire*	thallassogenous flood mire *mangrove*	thallassogenous surface flow mire ?	thallassogenous acrotelm mire ?	thallassogenous percolation mire ?

Known examples of hydrogenetic mire types are given in italics. Interrogation points show hydrogenetic types for which no example has been identified yet.

A.2. Ontogenetic classification

Julve (1998) proposed an ontogenetic classification based on both the source of water at peat inception (described using the suffix – *genous*) and the present source of water. It is detailed here since, with vegetation-based classifications, it is the only classification that has been more or less adopted by mire managers and scientists in France, even though not always rigorously. Julve (1998) defined seven ontogenetic types:

- topogenous mires, formed by a shallow groundwater table in topographic depressions (swamp mires sensu Succow & Lange 1984, palsa mires, polygonous mires);
- soligenous mires, formed by the resurgence of groundwater (sloping mires, spring mires, percolating mires, aapa mires);
- limnogenous mires, formed through the influence of open water (floating mats);
- fluviogenous mires, formed under the influence of river flooding (alluvial valley mires);
- thalassogenous mires, formed along the coast where the groundwater table is shallow due to the proximity to the sea (dune slack mires);
- condensarogenous mires, formed by the condensation of water at the base of stone runs or scree slopes.

These groups can be divided further according to the developmental stage of the mire, which dictates the present source of water and its mineral content. The geotrophic stage corresponds to mires fed by surface runoff and groundwater flow from a mineral catchment. The ombrotrophic stage corresponds to the disconnection from these sources of water: precipitation becomes the sole water input. Finally, allogenous changes (climatic change, drainage, etc.) can lead to a mineralised stage, in which peat mineralisation leads to higher nutrient content at the mire surface even though it is still fed solely by precipitation. A raised bog for instance can be classified as limnogenous, topogenous, etc., depending on the conditions in which peat started to accumulate, and as either ombrotrophic or mineralised depending on its developmental stage.

A.3. Classification based on wetland mechanisms

In the last two decades, British researchers have devised a number of classification schemes focussing on the mechanisms that supply water to wetlands, with the aim of facilitating hydrological vulnerability and impact assessments in wetlands. Gilvear & McInnes (1994) proposed a 12-fold hydrological classification based on the relative importance of precipitation, surface water and groundwater in the wetland water balance (Figure A-6). They used the terms

ombrotrophic to designate rainwater-fed wetlands, minerotrophic for groundwater-fed wetlands, rheotrophic for surface water fed wetlands and omnitrophic when all water sources are present.

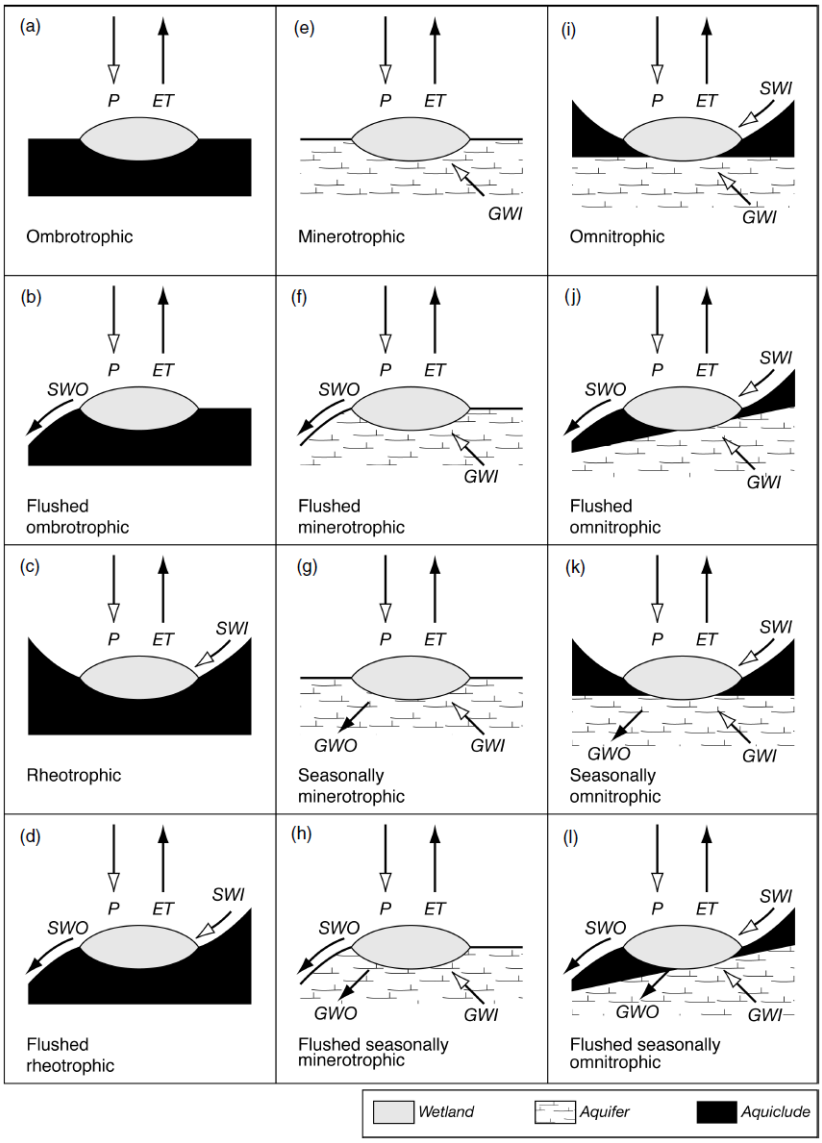

Figure A-6. Gilvear's & McInnes' (1994) wetland classification scheme (from Gilvear & Bradley 2009).

P: precipitation; ET: evapotranspiration; SWI/SWO: surface water inflow / outflow; GWI/GWO: groundwater inflow / outflow.

Acreman & Miller (2006) recognised 14 different wetland water transfer mechanisms (precipitation, evapotranspiration, runoff, lateral inflow, drainage, over-bank flow, out flow, pumping, tidal inflow, tidal outflow, spring, groundwater discharge, groundwater recharge and groundwater seepage). In combination with seven recognised landscape positions (hilltop or flat upland, slope, valley bottom, underground, depression, flat lowland, coastal), the identification of the main water transfer mechanisms allows for the classification, conceptual hydrological modelling and preliminary hydrological impact assessment of wetlands. Both Gilvear's &

McInnes' (1994) and Acreman's & Miller's (2006) classification schemes were devised for wetland as a whole, not just mires. However all categories are perfectly applicable to mires, except for the underground wetlands identified by Acreman & Miller (2006).

Wheeler *et al.* (2009) devised a Wetland Framework, a series of generic descriptors that can be used in combination to categorise wetland sites or parts of sites. They provide detailed definitions and examples of the descriptors. Similarly to Gilvear & McInnes (1994) and Acreman & Miller (2006), the focus is on identifying the wetland water supply mechanisms (or WETMECs) that, in combination with the position in the landscape, management and water chemistry, explain the presence of a specific vegetation patch (Table A-2, Table A-3). Unlike the classification systems detailed above, the Wetland Framework follows a bottom-up approach, in that units and their limits are explicitly based on homogeneous vegetation patches, not on entire wetland sites. Over 1500 stands from over 200 wetland sites were analysed to identify the main water supply mechanisms (Whiteman *et al.* 2009). The geographical scope of the Wetland Framework is England and Wales, but it is applicable to most of temperate Europe even though a number of mire types such as blanket bogs might not be well accounted for yet.

Table A-2. Descriptors of the wetland framework (Wheeler et al. *2009).*

Landscape type	Hillslope	Valleyhead	Valleyhead trough/basin	Basin	Lakeside	Trough (valley-bottom)	Floodplain	Coastal plain	Plateau-plain

WETMEC	1	2	3	4	5	6	7	8	9	10
	11	12	13	14	15	16	17	18	19	20

pH & base richness	Highly acidic (<4.0)	Acidic (4.0-5.5)	Sub-neutral (5.5-6.5)	Base rich (>6.5)

Fertility	Oligotrophic	Mesotrophic	Eutrophic	Hypertrophic

Management	Unmanaged	Winter grazed	Winter mown	Summer grazed	Summer mown	Burnt

Table A-3. Wetland Water Supply Mechanisms (WETMECs, Wheeler et al. *2009; Whiteman* et al. *2009).*

WETMECs	
1: Domed Ombrogenous Surfaces ('Raised Bogs')	11: Intermittent & Part-Drained Seepages
2: Buoyant Ombrogenous Surfaces ('Quag Bogs')	12: Fluctuating Seepage Basins
3: Buoyant Weakly Minerotrophic Surfaces ('Transition Bogs')	13: Seepage Percolation Basins
4: Drained Ombrotrophic Surfaces in Bogs and Fens	14: Seepage Percolation Troughs
5: Summer 'Dry' Floodplains	15: Seepage Flow Tracks
6: Surface Water Percolation Floodplains	16: Groundwater-flushed Bottoms
7: Groundwater Floodplains	17: Groundwater-flushed Slopes
8: Groundwater-fed Bottoms with Aquitard	18: Percolation Troughs
9: Groundwater-fed Bottoms	19: Flow Tracks
10: Permanent Seepage Slopes	20: Percolation Basins

A.4. The issue of scale

Except possibly for the Wetland Framework devised by Wheeler *et al.* (2009), the classifications presented above are applicable to a single spatial scale, taken as that of the mire site. Yet different peatland hydrogeomorphic, hydrogenetic or ontogenetic types are often part of larger peatland complexes, particularly in boreal regions were favourable climatic conditions have led to the development of peat over very large areas and coalescence of different mire types (Rydin & Jeglum 2006). This issue of scale was central to the analysis and classification of peat landforms by Soviet peatland scientists, in particular Galkina and Ivanov (Ivanov 1981). They introduced the concepts of micro-, meso- and macro-topes. A microtope was defined as the "part of the mire where the plant cover and all other physical components of the environment connected with it are uniform" (Ivanov 1981). Ivanov's definition refers to homogeneous vegetation over areas in the order of 100m² to one hectare, which themselves contain intricate mosaics of smaller features such as hummocks, pools, hollows and ridges, often referred to as microforms. A mesotope was defined as "isolated mire massifs formed from one original centre, and possessing at each stage of their development a pattern of microtope distribution that conforms to clearly defined principles". The simplest example would be an isolated raised mire. Finally, a macrotope was defined as "formed by the fusion of isolated mire mesotope", and corresponds to a mire complex. Examples include peatlands formed by the coalescence of several adjacent raised bogs, or complexes of raised bogs separated by minerotrophic mires. In the Soviet school, micro-, meso- and macro-topes were generally delineated using aerial photographs to infer vegetation communities and surface flow rate and direction. Ivanov (1981) acknowledged that it may not always be possible to delineate mesotopes precisely within complex macrotopes unless detailed stratigraphic data are also available. Both Galkina and Ivanov (Ivanov 1981) recognised the mesotope as the fundamental unit in mire type classification.

Appendix B. Von Post humification index

Table B-1. Von Post humification index (adapted from Soil Classification Working Group 1998; Quinty & Rochefort 2003; Parent & Caron 2008)

H	Interpretation	Plant residues	Extruded matter	Residue after pressing
1	Undecomposed	Unaltered	Clear, colourless water; no peat substance passes between the fingers	Very spongy, not mushy, springs back after pressure, holds no shape
2	Almost undecomposed	Almost unaltered, entire structure distinct	Almost clear yellow-brown water; no peat substance passes between the fingers	Spongy, not mushy, springs back after pressure, holds almost no shape
3	Very weakly decomposed	Most remains easily identifiable but breaking into piece	Slightly turbid, brown-yellow water; no peat substance passes between the fingers	Slightly spongy, not mushy, holds a fairly definite form of handprint with rounded edge
4	Weakly decomposed	Most remains identifiable	Turbid brown water; no peat substance escapes between the fingers	Rather mushy, not spongy, forms a distinct replica of handprint
5	Moderately decomposed	Clear but becoming indistinct, some amorphous material present	Strongly turbid brown water; some peat escapes between the fingers	Very mushy, slightly soapy
6	Well decomposed	About half sample in amorphous state, bulk of remains unidentifiable but clearer in the squeezed residue than in the undisturbed peat	Some free water but muddy and with much peat in suspension; about one-third of the peat escapes between the fingers	Strongly mushy, soapy
7	Strongly decomposed	Relatively few remains identifiable	Little free water, strongly muddy; about half the peat escapes between the fingers	Somewhat pasty
8	Very strongly decomposed	Very indistinct; only resistant roots, fibres and bark are identifiable	Almost no free water; about two-thirds of the peat escapes between the fingers	Pasty
9	Almost completely decomposed	Almost unrecognizable	No free water; nearly all the peat escapes between the fingers	A few fibres
10	Completely decomposed	Unrecognizable	All the peat escapes between the fingers	None

Appendix C. Recent advances in hydrogeology of hard-rock regions

C.1. The stratiform conceptual model of hard-rock aquifers

Unweathered hard rocks, including granite, have a very low matrix hydraulic conductivity, below 10^{-8} m.s^{-1}. Their overall hydraulic conductivity is therefore dependant on secondary fissure or fracture permeability (Lachassagne *et al.* 2011). Until recently, hard-rock aquifers were therefore considered as discontinuous, isolated in more or less vertical, highly fractured corridors of tectonic origin, that are fed from the surface through a shallow layer of alterites (i.e. the weathered rock in which the fabric of the parent bedrock is retained, Eggleton 2001), the thickness of which is in the order of two to three metres (Figure C-1).

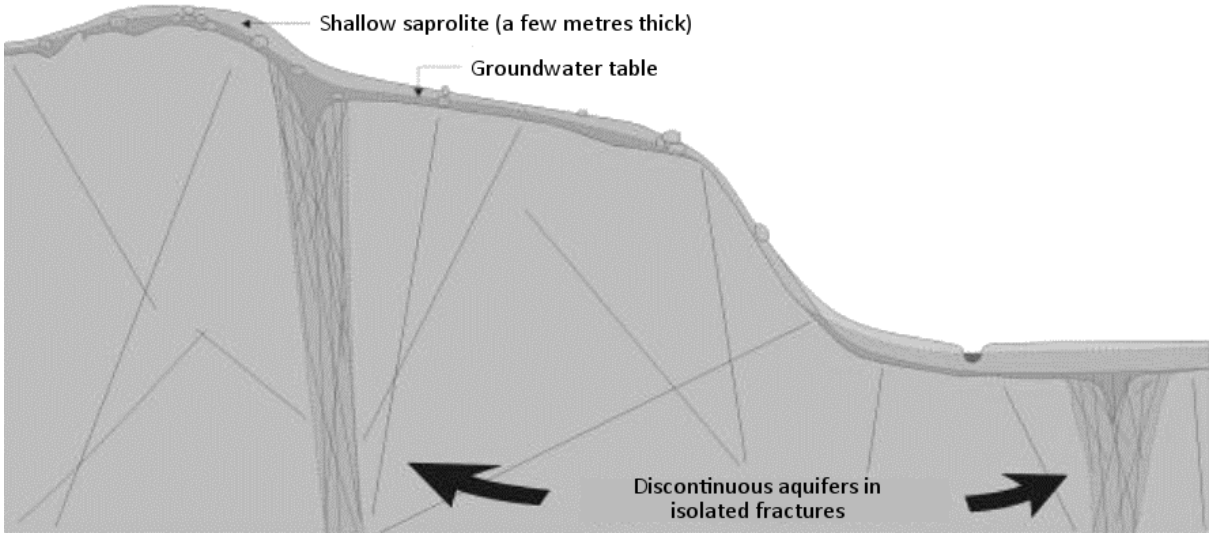

Figure C-1. Classical conceptual hydrogeological model of hard-rock aquifers (translated from Lachassagne et al. *2009).*

The prospection and exploitation of these aquifers has generally been limited to the superficial saprolite layer, particularly along sub-vertical, tectonic open fractures where it is deeper (Lachassagne *et al.* 2009). Following advances in hard rock geomorphology in the 1970s and 1980s, and the development of new drilling techniques, several authors recognised that the upper part of the bedrock shows sub-horizontal joints, the density of which decreases with depth (Lachassagne & Wyns 2006). Several origins were hypothesised to explain these joints, namely cooling stresses in the magma, tectonics and unloading processes (Migon 2006; Lachassagne *et al.* 2009). The decrease in fissure density with depth was attributed to an increase in the

lithostatic pressure resulting in a closure of the voids. It was also recognised that this fissured part of the bedrock had a relatively higher hydraulic conductivity but a lower porosity than superficial saprolites (Acworth 1987), and that it could be exploited for water production. In the last 15 years, the hard-rock aquifers team at the French *Bureau de Recherches Géologiques et Minières* and their collaborators published a number of studies mostly conducted in granitic areas in France, South Korea, French Guyana, India and Burkina Faso among others, which has led to a better understanding of the origin and characteristics of this fissured layer and to a complete revision of the classical model of hard-rock aquifers (Wyns 1998; Lachassagne *et al.* 1999, 2001a; b, 2006, 2009, 2011; Wyns *et al.* 1999, 2005; Cho *et al.* 2002, 2003; Courtois *et al.* 2003, 2010; Maréchal *et al.* 2003a; b, 2004a; b, 2006, 2007a; b, 2008; Mougin *et al.* 2003; Lachassagne & Wyns 2005, 2006; Baltassat *et al.* 2005; Durand 2005; Durand *et al.* 2006; Dewandel *et al.* 2006, 2011, 2012; Kumar *et al.* 2007; Lachassagne 2008; Chandra *et al.* 2008). In particular, Lachassagne *et al.* (2011) questioned the generally accepted but never demonstrated genetic hypotheses for the systematic presence of sub-horizontal joints in hard rocks. They noted that tectonic fractures are complex objects that do not always translate into a higher hydraulic conductivity, and in a substantial number of cases can even act as barriers to groundwater flow, that they are unevenly distributed in the landscape, that they are usually sealed by mineral precipitations very quickly in geological terms after their opening, and, therefore, that tectonics cannot be invoked to explain the ubiquity of fissures in the superficial bedrock. They suggested that the sub-horizontal joints actually result from a weathering process and are a consequence of the stress caused by the swelling of phyllitic minerals during hydrolysis. The volume of biotite in particular increases by up to 30%. In isotropic rocks such as granite in which minerals are oriented at random, the resulting stresses lead to the formation of sub-horizontal fissures parallel to the palaeosurface in place during the weathering process. Several tens of these fissures cross any vertical profile, however sealing by mineral deposition or formation of clay during the weathering process results in only zero to five of them being permeable enough to be detected and exploited in any narrow-diameter well. This explains the variability of well discharges frequently observed in hard-rock aquifers, and why these aquifers have long been regarded as discontinuous. Using pumping tests in a granitic watershed in India, Maréchal *et al.* (2003b, 2004b) showed that these sub-horizontal fissures have a radius in the order of 3-30 metres, and that the hydraulic conductivity of the fissured layer is strongly and systematically anisotropic, the horizontal conductivity being 2-30 times larger than the vertical conductivity. This anisotropy results from the much higher frequency of sub-horizontal fissures.

The fissured layer is actually the lower part of a stratiform lateritic weathering profile, a typical example of which includes the following layers from top to bottom (Wyns 1998; Wyns *et al.* 1999; Lachassagne *et al.* 2006) - typical thicknesses are those cited by Wyns *et al.* (1999) for French examples, mainly in Britany and the Massif Central - :

- the laterite crust (or iron or bauxitic crust), is zero to a few metres thick. It is often missing due to erosion or evolution towards a latosol.
- the saprolite is 20-30m thick on average, and may be sub-divided in two parts:
    - the alloterite, from a few metres to a few tens of metres thick, where the structure of the original rock is lost due to volume reduction. The content of clay is important, and the hydraulic conductivity and specific yield are relatively low.
    - the isalterite, several tens of metres thick, where there has been limited or no reduction in volume and the original rock structure has been preserved. Dissolved and leached minerals are replaced by voids, resulting in a quite large specific yield. On granitic bedrock the texture is clayey-sandy. Also on granitic bedrock, the base of the isalterite is often laminated and is therefore called the laminated layer. It results from the intensification of horizontal fissuring at the top of the fissured layer.
- the fissured layer, described above, also called weathered-fractured layer or saprock, has a total thickness of 40-50 metres on average. The top of this layer is highly fissured, with a conductive fissure density of 0.5-0.7 m^{-1} (Dewandel *et al.* 2006), and is called the transition zone. Its depth is in the order of 2-12 metres. Fissure density and therefore the probability of fissure inter-connexion decrease with depth.
- the fresh bedrock.

Together, and where saturated, the saprolite and fissured layers form a continuous stratiform composite aquifer (Lachassagne & Wyns 2006) (Figure C-2). Due to its clayey-sandy texture, the bulk porosity of the saprolite layer can be quite high, generally between 5 to 30%, and its hydraulic conductivity is generally low, about $10^{-6}m.s^{-1}$ (Dewandel *et al.* 2006). Where it has not been eroded away and is saturated, the saprolite is responsible for the capacitive function of the composite aquifer. Using injection tests on a granitic site in India, Maréchal *et al.* (2004a) characterised the hydrodynamic properties of the fissured layer. The rock matrix had a hydraulic conductivity of 10^{-9} to 10^{-14} $m.s^{-1}$. Two sets of fissures could be identified.

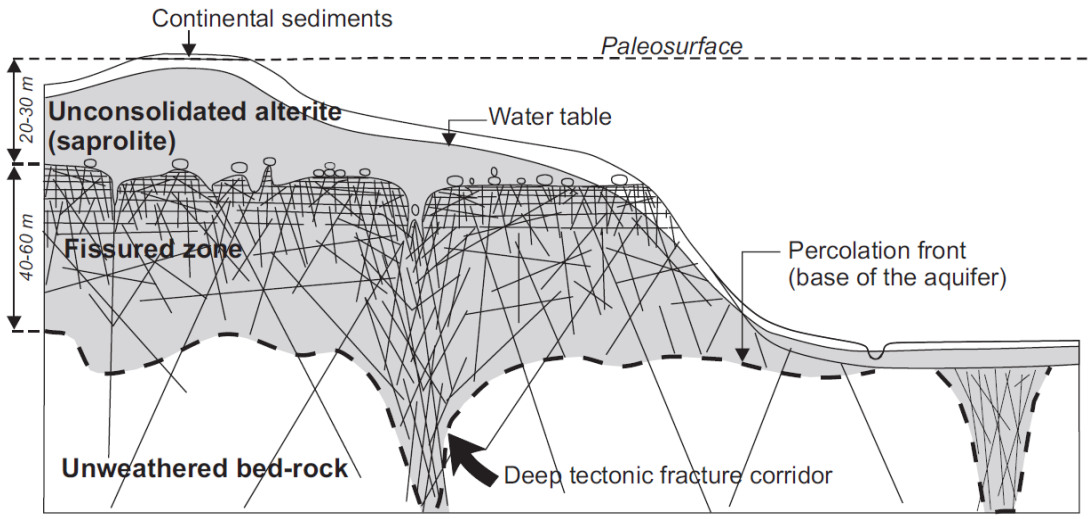

Figure C-2. Conceptual hydrogeological model of stratiform hard-rock aquifers (from Wyns et al. *2004).*

A primary fissure network, with a decimetre scale, resulted in an increase in the bulk hydraulic conductivity and storage coefficient of granite blocks to 5×10^{-8} m.s^{-1} and 5.7×10^{-3}, respectively. The primary fissure networks accounted for 91% of the bulk storage capacity of the fissured layer. Much larger fissures formed a secondary fissure network, accounting for only 9% of the bulk storage coefficient, but allowing for a large increase in the bulk hydraulic conductivity to about 10^{-5} m.s^{-1} horizontally and 10^{-6} m.s^{-1} vertically. Dewandel *et al.* (2006) found similar values for the overall hydraulic conductivity when reviewing the literature, even though none of the eight reviewed studies, conducted mainly in India and Africa, distinguished between vertical and horizontal hydraulic conductivities. They also showed that the hydraulic conductivity anisotropy was due to the higher density of conductive horizontal fissures (vertical density of 0.15 to 0.24 m^{-1}). In the study conducted by Maréchal *et al.* (2004a), the length of the large horizontal fissures was in the order of a few tens of metres. The total storage coefficient of the fissured layer was $6\text{x}10^{-3}$. Using Proton Magnetic Resonance, Mougin *et al.* (2003) and Wyns *et al.* (2004) found similar values in the order of 0.2-5% in several granitic sites in France. Measurements in different granitic sites around the world have shown that the hydraulic conductivity of the secondary fissure network in the fissured layer is relatively constant from one site to the other and with depth (Lachassagne *et al.* 2006). It is the density and the anisotropy of the fissures that dictates the overall hydrodynamic properties of this layer and the top of the fissured layer (the transition layer) is therefore the most permeable layer of the weathering profile. Given its hydrodynamics characteristics, the fissured layer is responsible for the transmissive function of the combined aquifer (Lachassagne *et al.* 2006). The fresh bedrock, with a matrix hydraulic conductivity of 10^{-14} to 10^{-9} m.s^{-1}, is only permeable locally where tectonic fractures are present and have not been

sealed (Lachassagne & Wyns 2005). For instance, in the Auriat granitic massif in Limousin, France, close to the Dauges catchment investigated in the current study, nearly all tectonic fractures observed at depth in the bedrock were sealed by quartz or calcite precipitations or by weathering clays. The bulk hydraulic conductivity of the unweathered bedrock was therefore very small: 10^{-9} m.s^{-1} near the surface, gradually declining to about 10^{-12} m.s^{-1} between 500 and 1000m below ground level (Blès 1984). Just a few kilometres west of the Dauges catchment, Bertrand & Durand (1983) measured the hydraulic conductivity in a 90m deep borehole, in a two-mica alkaline leucogranite (Table C-1). The drop in hydraulic conductivity at around 30-40m deep most probably corresponds to the interface between the fissured layer and the unweathered bedrock. As a general rule, fracture density in the unweathered bedrock is much lower than in the overlying fissured layer, and for most purposes the former can therefore be considered as impermeable and of very low storativity.

Table C-1. Variation of hydraulic conductivity with depth in a leucogranite in St-Sylvestre (Bertrand & Durand 1983).

Depth (m)	Hydraulic conductivity (m.s^{-1})
11.7 – 17.3	5.0×10^{-6}
17.8 – 23.4	3.0×10^{-6}
23.4 – 29.0	1.8×10^{-6}
29.0 – 34.6	2.5×10^{-7}
34.5 – 40.1	5.8×10^{-8}
40.2 – 45.8	3.5×10^{-9}
45.8 – 51.4	3.7×10^{-9}
51.4 – 57.0	3.0×10^{-10}
57.0 – 62.6	$< 3.0 \times 10^{-10}$
62.6 – 68.2	$< 3.0 \times 10^{-10}$
68.2 – 73.8	6.5×10^{-9}
73.8 – 79.4	2.5×10^{-9}
79.4 – 85.0	1.0×10^{-9}
85.0 – 90.6	9.0×10^{-9}

The formation of lateritic weathering profiles thick enough (several tens of metres) to have a substantial role in groundwater movement requires a number of conditions (Wyns 2002; Wyns *et al.* 2003; Lachassagne *et al.* 2011):

- Sufficient rainfall to allow for substantial mineral hydrolysis. Thick weathering profiles cannot form in very arid or permanently glaciated areas where water is either lacking or sequestrated as ice. Temperature only marginally affects the weathering process, which is only slightly quicker under tropical environments than under temperate ones.
- An erosion rate that does not exceed the weathering rate.
- A relatively flat gently sloping topography that reduces erosion and facilitates water infiltration.

- A raised topographic position that allows for infiltrated water to evacuate leached minerals and for the progressive lowering of the weathering front to substantial depths.
- The stability of these conditions, and therefore a stable tectonic regime, over periods of a few million to a few tens of million years.

These conditions are a consequence of regional tectonic uplift with a large wavelength, followed by a period of tectonic stability long enough to allow for the formation of planation surfaces (Wyns 2002). In Europe, substantial (70-100m deep) weathering profiles are Carboniferous, Infra-Permian, Infra-Triassic, Early Cretaceous, and Early and Middle Eocene (Wyns 2002; Lachassagne *et al.* 2011). Compression phases between these periods (in particular during the Pyrenean and Alpine orogeneses) led to the uplift of the older palaeosurfaces and the subsequent formation of newer and lower planation surfaces on their margins. An erosion scarp generally marks the boundary between the two palaeosurfaces (Klein *et al.* 1990). This is the case in Limousin, on the north-eastern side of the Massif Central, where the Millevaches plateau, which constitutes the infra-Cretaceous planation surface according to Mauroux *et al.* (2009), lies 300m above the surrounding Eocene plateaux (Figure C-3). The age of the weathering profile is relevant in terms of hydrogeology for two reasons. Firstly, older weathering profiles that have been buried under sediment at some point in their history may show a lower porosity and hydraulic conductivity due to the precipitation of illuvial minerals in the fissures (Wyns & Tegyey 2012). In Limousin, pre-Liassic weathering profiles fall in this category (Mauroux *et al.* 2009) but are very restricted in extent. Secondly, older uplifted palaeosurfaces have been subject to erosion processes for a longer time, and are more likely to have lost part of their original weathering profile to erosion. This is the case in Limousin, where results from airborne spectral radiometry suggest that the infra-Cretaceous planation surface (*Millevaches plateau, Monts de Blond, Mont d'Ambazac, Monts de St-Goussaud, etc.*) has lost most of its saprolite cover, whereas thick saprolite covers have been preserved on the lower Eocene planation surface (Mauroux *et al.* 2009).

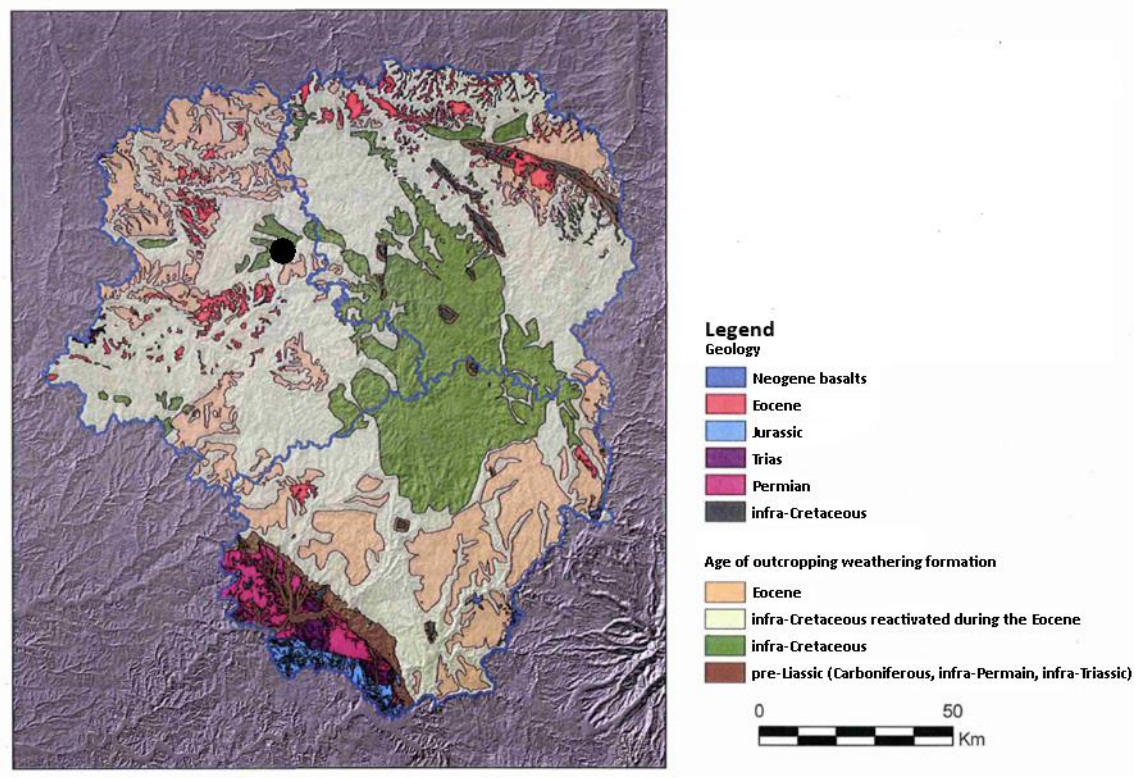

Figure C-3. Age of weathering formations in Limousin (translated from Mauroux et al. *2009).*

The black dot shows the location of the Dauges catchment investigated in the current study.

C.2. Mapping the depth of weathering profiles

An important consequence of the conditions required for the formation of thick weathering profiles is that, at large scales, the constitutive layers were approximately parallel to the palaeosurface in place at the time of the weathering process, and were therefore sub-horizontal. Even though subsequent tectonic activity may complicate the arrangement of the different layers across the landscape (Figure C-4), it has been suggested that it could be possible to map the altitude of the interfaces between the saprolite and the fissured layer on one hand and between the fissured layer and the bedrock on the other hand from punctual observation of these interfaces in field outcrops, drilling logs or geophysical surveys (Wyns 1998; Durand 2005; Durand *et al.* 2006; Lachassagne *et al.* 2006). In particular, in the uplands of the Hercynian platform of western Europe, the saprolite – fissured layer interface is frequently intersected by valleys created by fluvial erosion. As the fissured layer – bedrock interface is much deeper and the fissured layer less easily eroded, it is generally less readily mapable from field observations alone. Because these interfaces were originally sub-horizontal, it has been suggested that their current altitude could be reliably estimated at any location by interpolating relatively sparse punctual field observations using geostatistics, once post-weathering tectonic deformations

have been accounted for (Figure C-5). The residual depth of the weathering layers can then be mapped by subtracting the altitude of these interfaces from a Digital Elevation Model (Lachassagne *et al.* 2001b).

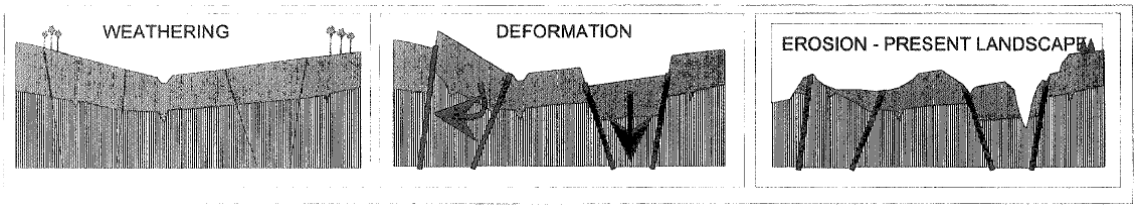

Figure C-4. Formation of the present-day landscape from the infra-Cretaceous planation surface (from Lachassagne et al. *2001b).*

The upper layer is the saprolite, the lower the fissured layer. Thick black lines show post-weathering faults.

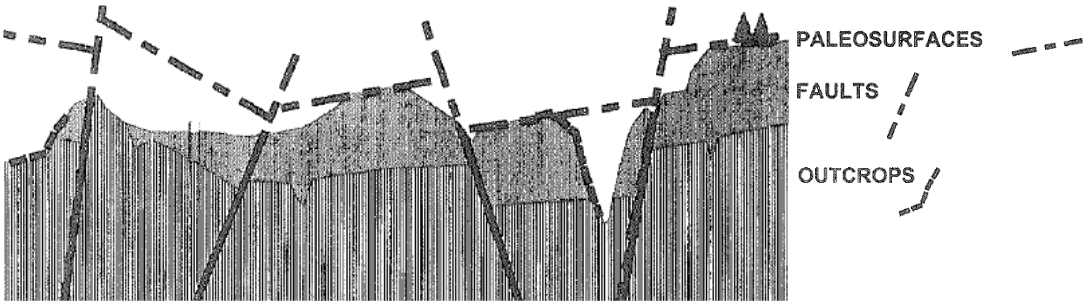

Figure C-5. Reconstitution of palaeosurfaces (from Lachassagne et al. *2001b).*

The upper layer is the saprolite, the lower the fissured layer.

The physical characteristics of the different layers of the weathering profile have geomorphological consequences that can also be used to help map their distribution at the local scale (Courtois *et al.* 2003) where their interfaces cannot be observed directly in the field due to the paucity of fresh outcrops and drilling logs. For instance, saprolites are not mechanically resistant and are easily mobilised, leading to gentle slopes. On the contrary, the fissured layer and the fresh basement are more resistant and can form steeper slopes. These concepts have been applied to map the distribution and thickness of the different layers of the weathering profile at several spatial scales, from a country (e.g. as French Guyana and Burkina Faso, Courtois *et al.* 2008, 2010), to the regional or catchment scale (Wyns 1998; Lachassagne *et al.* 1999, 2001b; Cho *et al.* 2002; Wyns *et al.* 2005; Dewandel *et al.* 2006, 2012; Maréchal *et al.* 2007a; Mauroux *et al.* 2009) and to the local scale (Courtois *et al.* 2003). However several factors often complicate this approach. Tectonic uplifting of an existing planation surface can lead to polyphased weathering profiles that are frequently observed around the world, whereby the formation of a secondary planation surface at a slightly lower altitude than the pre-existing one leads to the

incomplete truncation of the older weathering profile and its subsequent reworking by weathering processes (Cho *et al.* 2002; Dewandel *et al.* 2006). At the local scale (100-1000m), local differences in lithology and tectonic fracturation lead to differential weathering with local variations in the depth of the weathering profile. For instance, leucogranite intrusions, which are more resistant to weathering, produce shallower weathering profiles than porphyroid granites (Wyns 1998). Following rejuvenation of the planation surface, differential erosion can lead to the development of positive topographic anomalies such as inselbergs protruding above the newer planation surface (Lachassagne *et al.* 2006; Migon 2006). Inversely, negative topographic anomalies are produced where petrographic and structural weaknesses have facilitated the penetration of water at depth, the deepening of the weathering front and, following a lowering of the base level, the subsequent differential erosion. The alveolate relief typical of the Hercynian platform of western Europe, and particularly of Limousin, derives from this etching process (Valadas 1984; Lageat *et al.* 2001). Differences between the hilltops and the etch basin bottom can reach several tens of metres, and in some cases approach or exceed a hundred metres. Depending on the local topography, small-scale saprolite formations can develop even in an actively eroding landscape and therefore below the lower level of the deep saprolite formations inherited from the anterior peneplain or pediplain. At an even more local scale, pre-existing discontinuities in the bedrock such as tectonic fractures, veins of quartz, pegmatite or aplite, and contacts with other geological formations can facilitate the penetration of water to depth and increase the weathering rate, leading to an abrupt and localised deepening of the weathering profile (Dewandel *et al.* 2011) that can in some situations reach depths of up to several hundred metres. Saprolite has for instance been found at depths of up to 300m along faults in the French Cévennes (Wyns, pers. comm.). Cottez & Favin (1980) stated that the numerous boreholes drilled by the uranium mining company COGEMA in the Saint-Sylvestre granitic massif in Limousin have shown that saprolites thicken considerably along tectonic fractures. They describe a north-west/south-east fracture from Saint-Léger-la-Montagne to Le Mazeaud and Chanteloube, just a few kilometres north-west of the Dauges catchment investigated in the current study, along which saprolite can reach depths of 20m, and weathered granite (actually probably the upper part of the fissured zone only) 45m below ground level. This widespread small-scale variability of the interface between fissured zone and saprolite raises questions about the density of field observations that is required to achieve a reasonable accuracy when mapping the altitude of the interface between fissured zone and saprolite, and therefore the saprolite thickness as proposed by Lachassagne et al. (2001b) and Wyns (1998).

C.3. Modelling groundwater flow in weathered hardrocks

Fractured/fissured aquifers can be considered to consist of impermeable rock blocks separated by discrete discontinuities such as fractures, fissures, joints and shear zones that may be open or mineral-filled. Groundwater flow only occurs in open discontinuities. Several conceptual models can be used to describe flows in such aquifers (Table C-2).

Table C-2. Conceptual models of flow in fractured/fissured media (modified from Singhal & Gupta 2010).

Conceptual model	Assumptions	Applications	Limitations
Equivalent Porous Medium Model	The material behaves as a continuous porous medium at larger spatial scales.	High density of interconnected fractures or fissures in various directions, such that a representative elementary volume of material with effective hydraulic conductivity, porosity and specific storage can be defined.	May reproduce regional flow system satisfactorily, but generally not local flow.
Discrete Fracture Network Model	Flow is confined to an inter-connected network of discrete fractures.	Typical fractured crystalline hard-rock aquifers.	The statistical distribution of fracture geometries (orientation, frequency, aperture) must be estimated. Applicability limited in terms of volume simulated, must be used in combination with stochastic continuum models.
Channel Network Model	Flow is confined to discrete, one-dimensional pathways due to intersection of fractures at various intervals (simplification of Discrete Fracture Network Model).		
Dual Porosity Medium Model	Flow occur in both the fracture network and the rock matrix.	Sandstone aquifers.	
Triple Porosity Medium Model	Three levels of water-bearing porosities occur: inter-granular, within fractures, in cavities of larger dimensions.	Karst aquifers.	
Stochastic Continuum Model	Hydraulic conductivity, specific storage and porosity vary in space according to spatially varying random functions. The material can be represented by spatially varying blocks of an equivalent homogeneous porous medium.		

At present, computer software based on other conceptual models than the Equivalent Porous Medium approach are still scarce: examples include HydroGeoSphere (Brunner & Simmons 2012) and FracMan (Golder Associates 2014). Only the former can model all components of the water cycle, while the latter can only model saturated flow. Consequently, most researchers who modelled groundwater flow in weathered hard-rock aquifers have used the equivalent porous medium approach. For instance, Lubczynski & Gurwin (2005) used MODFLOW to model groundwater flow in a 80km² granitic catchment in Spain. They conceptualised and modelled the aquifer using a two-layer representation, the superficial one corresponding to the saprolite and the deeper one to the fissured zone. The geometry of each layer was determined based on

surface geological and tectonic observations, a small number of deep geological drilling logs, shallow percussion drillings, electrical resistivity sounding and profiling and proton magnetic resonance sounding. Spatially-varying hydraulic characteristics of both the saprolite and fissured zone layers were mapped based on measured data and a complex interpolation procedure. The model was then automatically calibrated based on observed piezometric heads in 12 locations while preserving the relative spatial distribution of hydraulic characteristics. The calibrated model was able to reproduce observed groundwater table depths satisfactorily in most observation points. Ahmed & Sreedevi (2008) used an equivalent porous medium approach to model groundwater flow in a 53 km² granitic catchment in India using MARTHE, a transient hydrodynamic model using finite differences with a rectangular grid. They conceptualised the aquifer in a two-layer system, the superficial one corresponding to the saprolite and the deeper one to the fissured zone. The geometry of both layers was interpolated based on 25 drilling logs and vertical electric sounding surveys and the depth of 900 wells within the watershed, assuming that the well depth corresponded to the maximum depth of the fissured zone. The hydraulic conductivity was estimated from 34 and 25 pumping and slug tests in the saprolite and fissured layer respectively. They found that they could not reproduce the observed piezometric data without introducing linear vertical barriers that they related to observed or assumed dykes and quartz reefs. The calibrated hydraulic conductivities in the fissured zone were very variable (from $1x10^{-7}$ to $3x10^{-5}$ $m.s^{-1}$), due to the heterogeneity in rock weathering. Other examples of the use of the Equivalent Porous Medium approach to model groundwater flow in weathered granite aquifers include Massuel *et al.* (2007) and Prasad (1999, in Singhal & Gupta 2010). Both studies also used MODFLOW and modelled the aquifer using a two-layer representation, the superficial one corresponding to the saprolite and the deeper one to the fissured zone.

Appendix D. Description of pedological pits

The following pages reproduce an unpublished report written by Bruno GRATIA based on field notes taken by A. DURANEL during a survey carried out by B. GRATIA and A. DURANEL within the Dauges NNR in August 2012.

The figures on the top left of each page relate to the code of pedological pits, the position of which is given on Figure 3-41. Table D-1 gives the position of each pit, surveyed using a portable DGPS with decimetric precision, except for pit 4 that was positioned with ±2-3m precision using the IGN BD Ortho ortho-rectified photograph and the known position of dipwell D26.

Table D-1. Position of pedological pits

Code	Positionning method	Easting (L2E)	Northing (L2E)
1	DGPS Trimble GeoXT with post-treatment	529580.4	2113161.4
2	DGPS Trimble GeoXT with post-treatment	529628.2	2113065.5
3	DGPS Trimble GeoXT with post-treatment	529298.9	2112424.3
4	ortho-rectified aerial photograph and known position of dipwell D26	529412.4	2112895.9
5	DGPS Trimble GeoXT with post-treatment	529525.3	2112945.4

Présentation des profils pédologiques sur la séquence topographique de la tourbière des Dauges …

① En situation de **haut** de **versant** : profil en **situation éluviale**, sous **couvert forestier** :

Situation favorable pour le drainage, pas d'excédent d'eau, les profils sont toujours sains. Sols en situation éluviale, il y a toujours davantage de **pertes** d'**eau** et d'**éléments nutritifs** par **colluvionnement**. En l'absence d'analyses chimiques des horizons, il est difficile de rattacher ce solum à un Grand Ensemble de Référence, tels qu'ils sont définis dans le Référentiel Pédologique (AFES, INRA, 2009). En termes de **processus pédogénétiques**, ce sol est certainement **polyphasé**, siège d'une brunification acide (ALOCRISOLs) à évolution ocre podzolique (PODZOSOLs Ocriques) avec la fermeture de couvert forestier dans l'horizon H_3.

Figure N°1 : profil pédologique sous couvert forestier en situation de haut de versant :

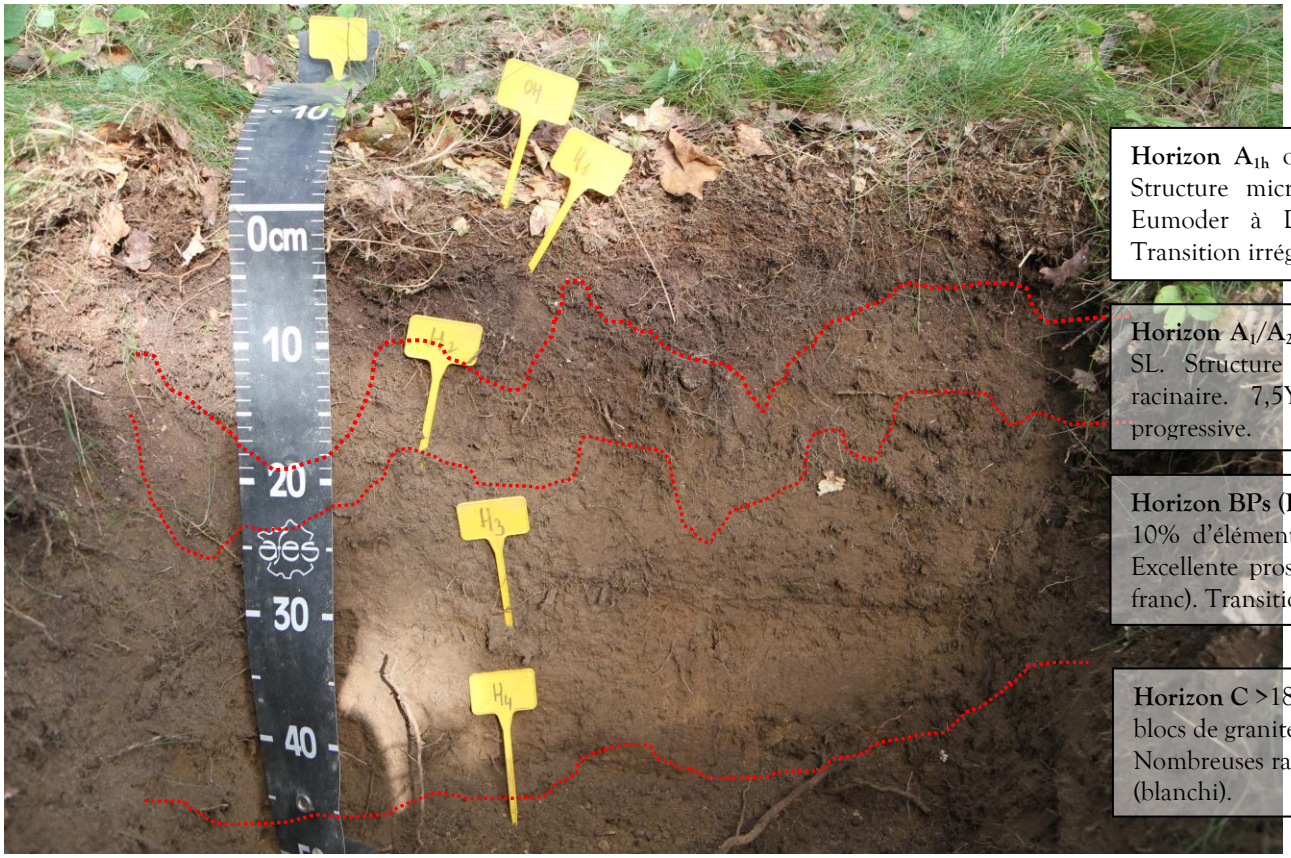

Horizon A_{1h} ou **A_h** de 12 à 16 cm d'épaisseur. Texture LS. Structure microgrumeleuse à particulaire. Humus de forme Eumoder à Dysmoder. 7,5YR2,5/1 (brun foncé à noir). Transition irrégulière et diffuse.

Horizon A_1/A_2 ou **A/E** de 8 à 13 cm d'épaisseur. Texture LS à SL. Structure particulaire apédique. Excellente prospection racinaire. 7,5YR4/1 (gris sombre).Transition irrégulière et progressive.

Horizon BPs (Bs) ou Sal de 21 à 28 cm d'épaisseur, à texture SL. 10% d'éléments grossiers. Structure particulaire mais massive. Excellente prospection racinaire >10 :Dm^2 ; 7,5YR5/8 (marron franc). Transition irrégulière et progressive.

Horizon C >18 cm, texture S avec %EG >20%, sous la forme de blocs de granite, peu stables cependant. Structure particulaire. Nombreuses racines localisées dans les zones meubles. 7,5YR8/1 (blanchi).

② En situation de **haut** de **versant** : profil en **situation éluviale**, sous **couvert agricole** :

Situation favorable pour le drainage, pas d'excédent d'eau, les profils sont toujours sains. Sols en situation éluviale, il y a toujours davantage de **pertes** d'**eau** et d'**éléments nutritifs** par **colluvionnement**. En l'absence d'analyses chimiques des horizons, il est difficile de rattacher ce solum à un Grand Ensemble de Référence, tels qu'ils sont définis dans le Référentiel Pédologique (AFES, INRA, 2009). Le travail du sol associé à la pratique récurrente à la remédiation chimique, favorise la dynamique biologique dans l'horizon H1 de surface, dont la structure l'apparente à une forme MULL. Le taux de saturation est certainement relevé par les apports exogènes. La dynamique pédologique est maintenue au stade de la brunification (BRUNISOLs ressaturés ou ALOCRISOLs typiques).

Figure N°2 : profil pédologique sous couvert agricole en situation de haut de versant :

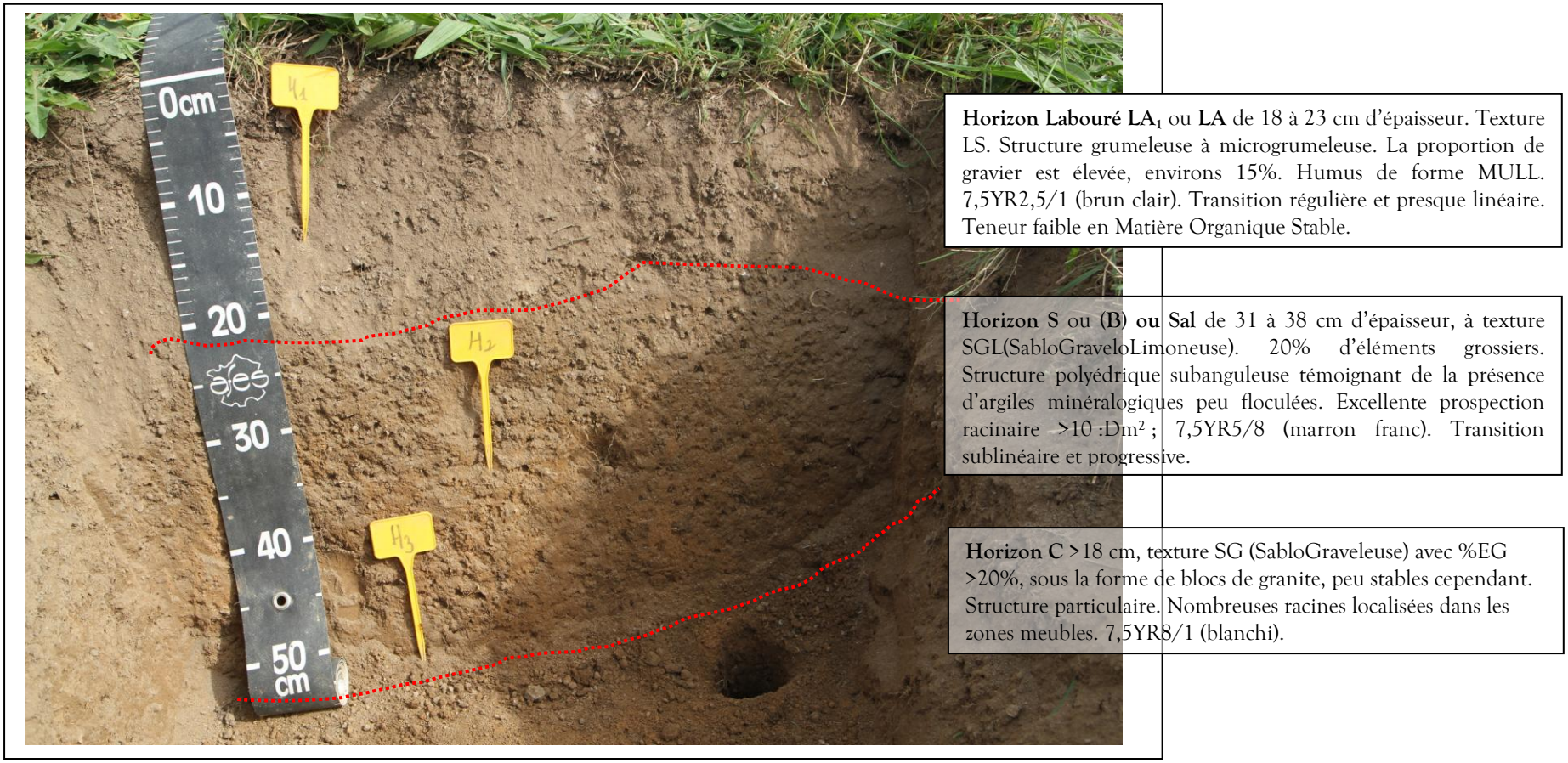

③ En situation de **haut** de **versant** : profil en **situation éluviale**, sous **couvert** de **landes** à ***Ericacées*** à **vocation pastorales** :

Situation favorable pour le drainage, pas d'excédent d'eau, les profils sont toujours sains. Sols en situation éluviale, il y a toujours davantage de **pertes** d'**eau** et d'**éléments nutritifs** par **colluvionnement**. En l'absence d'analyses chimiques des horizons, il est difficile de rattacher ce solum à un Grand Ensemble de Référence, tels qu'ils sont définis dans le Référentiel Pédologique (AFES, INRA, 2009). En termes de **processus pédogénétiques**, ce sol est certainement **polyphasé**, siège d'une brunification acide (ALOCRISOLs) à évolution ocre podzolique (PODZOSOLs Ocriques) avec la fermeture de couvert forestier dans l'horizon H_3.

Figure N°3 : profil pédologique sous landes à *Ericacées* en situation de haut de versant :

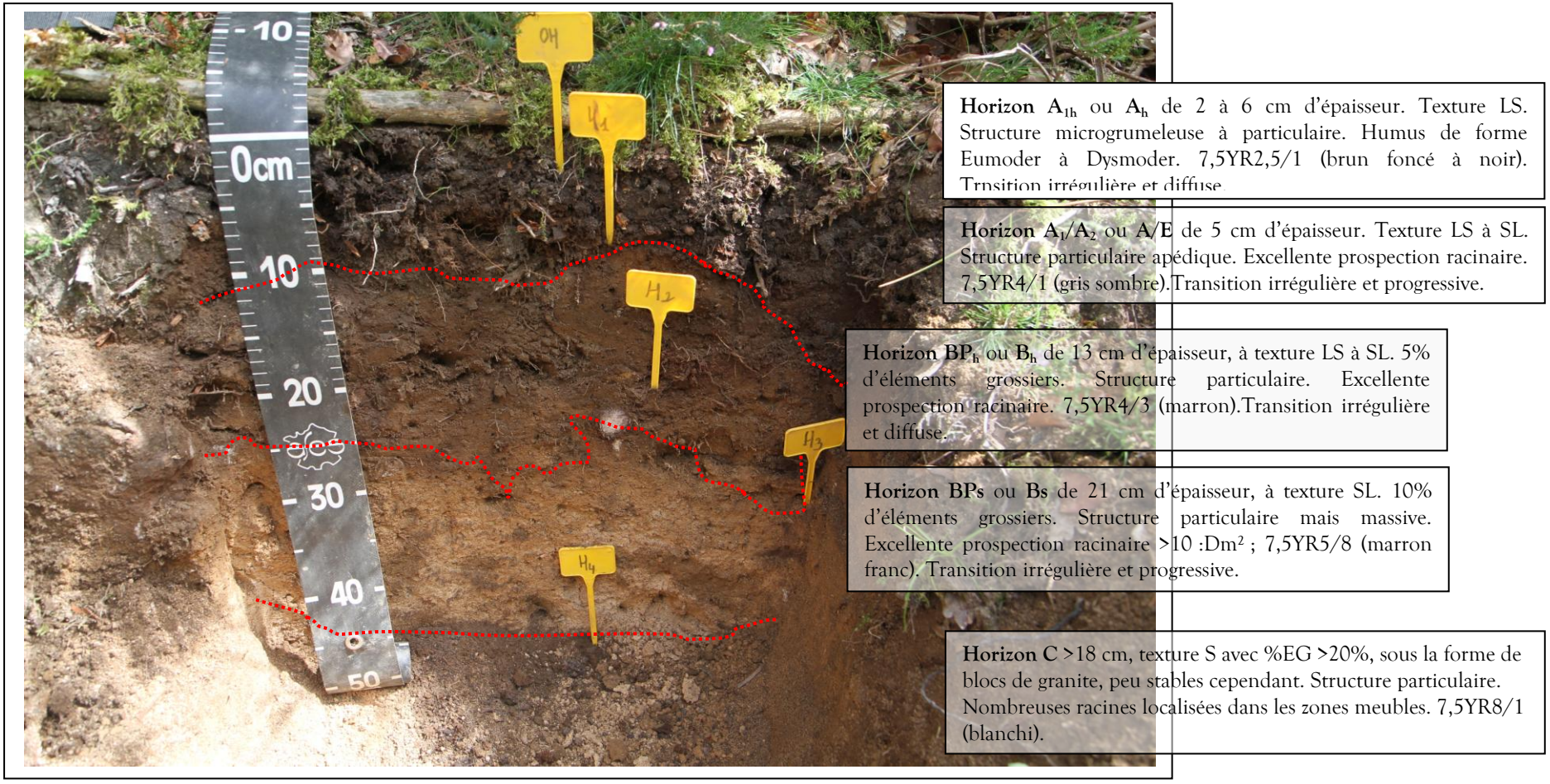

④ En situation de **milieu** de **versant** (rupture de pente) : profil en **situation illuviale**, sous **couvert pastoral** :

Situation favorable pour le drainage, pas d'excédent d'eau, les profils sont toujours sains. Sols en situation **illuviale**, il y a davantage d'**apports** d'**eau** et d'**éléments nutritifs** par **colluvionnement**. En l'absence d'analyses chimiques des horizons, il est difficile de rattacher ce solum à un Grand Ensemble de Référence, tels qu'ils sont définis dans le Référentiel Pédologique (AFES, INRA, 2009). La dynamique pédologique *in situ* (**Brunification acide**, vraisemblablement GER des ALOCISOLs) est masquée par les **apports** par **colluvionnement** : le **profil** est **peu différencié** par la couleur. La teneur en argiles est supérieure dans l'horizon structural S, son épaisseur est d'ailleurs plus importante que sur les profils précédents.

Figure N°4 : profil pédologique sous couvert agricole en situation de haut de versant :

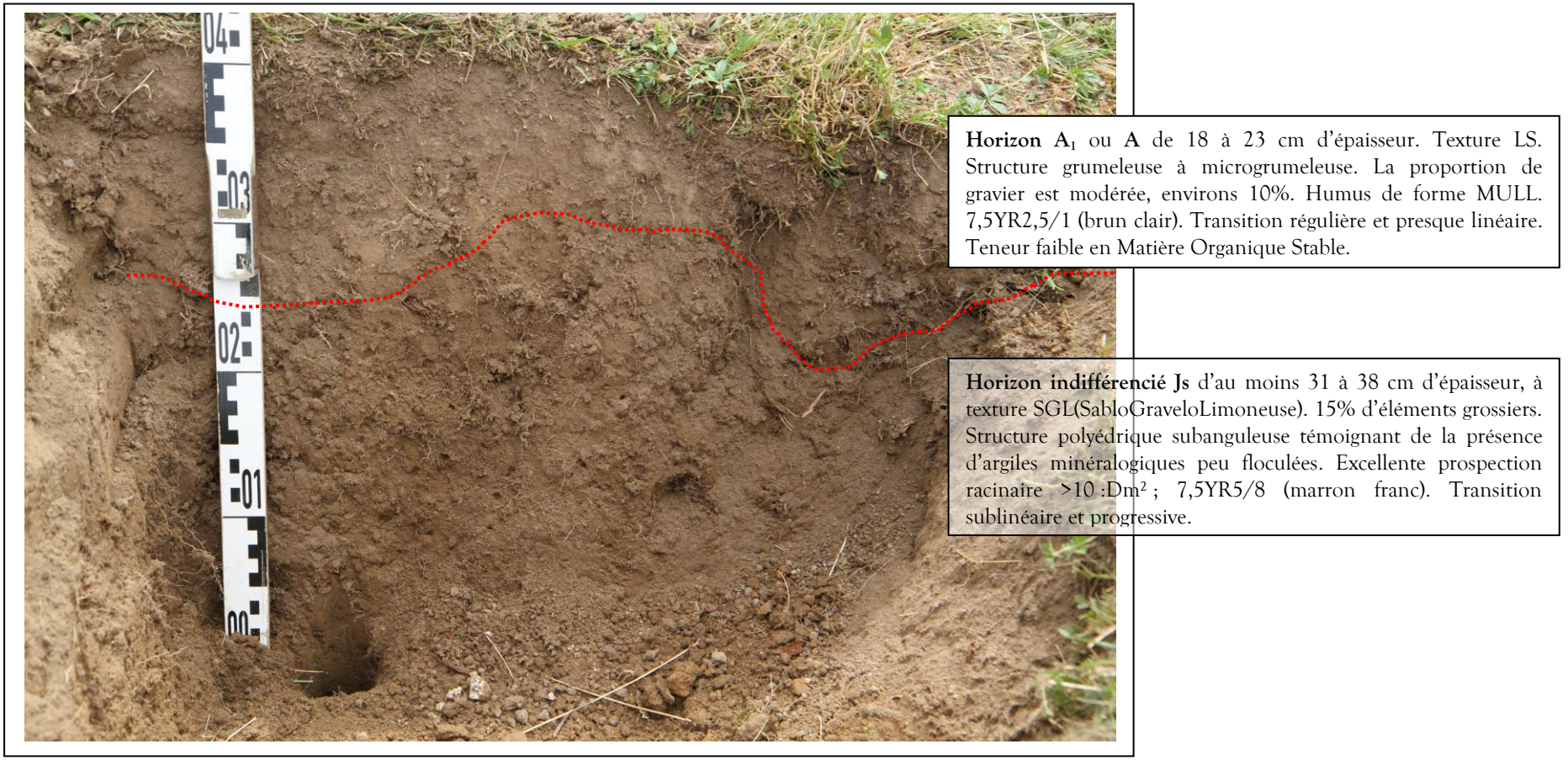

⑤ En situation de bas de **versant** (versant concave, zone de thalweg) : profil en **situation illuviale**, sous **couvert pastoral (lande humide)** :

Situation défavorable pour le drainage, présence plus ou moins ponctuelle d'excédent d'eau, les profils sont hypoxiques à anoxiques, rédoxiques en surface et réductiques au-delà de 40 à 50 centimètres de profondeur. Sols en situation **illuviale**, il y a davantage d'**apports** d'**eau** et d'**éléments nutritifs** par **colluvionnement**. En l'absence d'analyses chimiques des horizons, il est difficile de rattacher ce solum à un Grand Ensemble de Référence, tels qu'ils sont définis dans le Référentiel Pédologique (AFES, INRA, 2009). Le profil se caractérise i) d'une part par le **blocage** de la **minéralisation** de la **matière organique** après **humification**, ii) d'autre part par les **réactions** d'**oxydoréduction** du **fer** qui n'ont de contribuer davantage à l'**acidification** des solutions du sol. Ces profils se rattacheraient vraisemblablement aux **REDOXISOLs** et/ou **REDUCTISOLs humifères**.

Figure N°5 : profil pédologique sous lande humide pastorale, en situation de thalweg :

A_1 ou **A** de 4 à 6 cm. Texture LS, structure particulaire à microgrumeleuse. Eléments grossiers négligeables. Couleur 7,5YR3/1 (brun foncé à noir). Forte teneur en Matière Organique Stable (MOS> à 14%) ; Humus de forme HYDROMODER à ANMOOR.

A_1h ou **A_h** de 10 cm. Texture LS, structure particulaire à microgrumeleuse. Eléments grossiers négligeables. Couleur 7,5YR2,5/1 (brun foncé à noir). Prospection racinaire moyenne. Transition lobée et diffuse.

Go de 8 à 11 cm. Texture SL, structure massive. Eléments grossiers négligeables. Couleur 7,5YR4/1. Faible prospection racinaire (<à 1/dm²). Transition irrégulière et diffuse.

Gr de 33cm. Texture SLA, structure massive apédique. 10% d'éléments grossiers. Couleur Gley 2/5/5B. 5% de tâches de réoxydation brun franc (7,5YR4/3). Présence de racines nécrosées et de racines gainées de rouille.

Appendix E. Meteorology: data acquisition and reconstruction of missing and historical time-series

E.1. Introduction

This appendix describes the development of precipitation and reference evapotranspiration time-series required as inputs to the MIKE SHE hydrological model. Precipitation and meteorological variables required for the computation of the reference evapotranspiration (ETo) according to the FAO Penman-Monteith method (Allen *et al.* 1998) were monitored for a period of three years. In order to replace missing values and to reconstruct and characterise the local climate over a longer time span than the three-year observation period, these variables were modelled using regression techniques on the basis of records obtained from nearby permanent weather stations.

E.2. Methods

E.2.1. Météo-France permanent meteorological stations

Relatively long meteorological series are available from nearby meteorological stations deployed by Météo-France, the French meteorological institute (Table E-1, Table E-2, Table E-3 and Table E-4).

Table E-1. Météo-France permanent meteorological stations close to the Dauges site.

Name	ID	Location	Opening date	Closing date	Type	Altitude	Latitude	Longitude	Distance from the site
ST LEGER – MAN	87159001	Leycuras	01/10/1950	29/02/1972	Manual	610	46°01'42" N	01°25'12" E	1.8km
			01/03/1972	-	Manual	629	46°02'00" N	01°26'18" E	3.0km
ST LEGER LA MON	87159002	Le Pétalus	01/08/1998	-	Automatic	664	46°02'06" N	01°27'30" E	4.2km
LIMOGES	87085006	Bellegarde	01/01/1973	-	Automatic	402	45°51'36" N	01°10'30" E	25km
BOURGANEUF	23030004	Les Vignes	01/07/1994		Automatic	513	45°56'30" N	01°43'30" E	25km
BENEVENT	23021001	La Tannerie	01/09/1947	30/04/1996	Manual	530	46°07'06" N	01°37'48" E	20km
			01/05/1996	-	Automatic	480	46°06'42" N	01°37'48" E	20km
LA SOUTERRAINE	23176001	Les Ribières	01/10/1965	13/06/1996	Manual	370	46°14'36" N	01°29'48" E	27km
			14/06/1996	08/06/2011	Automatic	403	46°14'30" N	01°28'00" E	26km
			09/06/2011	-	Automatic	370	46°14'30" N	01°27'06" E	26km

Table E-2. Availability of meteorological data at Météo-France stations close to the Dauges site.

Name	ID	Air temperature at 2m	Precipitation	Relative humidity	Wind speed at 2m	Global radiation	Data availability
ST LEGER - MAN	87159001		✓				Since 01/10/1950
ST LEGER LA MON	87159002	✓	✓				Since 01/08/1998
LIMOGES	87085006	✓	✓	✓	✓	✓	Since 01/01/1973
BOURGANEUF	23030004	✓	✓	✓	✓		Since 01/07/1994
BOURGANEUF	23030004					✓	Since 18/01/1995
BENEVENT	23021001		✓				Since 01/10/1947
BENEVENT	23021001	✓					Since 01/05/1996
LA SOUTERRAINE	23176001		✓				Since 01/11/1965
LA SOUTERRAINE	23176001	✓					Since 01/01/1966
LA SOUTERRAINE	23176001				✓		Since 01/06/1996
LA SOUTERRAINE	23176001			✓			Since 15/06/1996

Table E-3. Definition of meteorological variables provided by Météo-France.

Variable	Definition
Mean wind speed	Mean wind speed at 10m over the 10-min period preceding hour h
Cumulated precipitation	Cumulated rainfall or melted snow height in the hour preceding hour h
Temperature	Temperature measured in a 2m-high shed at hour h
Minimum/maximum temperatures	Minimum/maximum temperatures measured during the hour preceding hour h
Relative humidity	Relative humidity measured in a 2m-high shed at hour h
Global radiation	Cumulated global radiation in the hour preceding hour h

Table E-4. 24-hour periods used by Meteo-France to aggregate meteorological variables.

Variable	Start of aggregation period	End of aggregation period
Cumulated rainfall	06:00 UTC on day d (not included)	06:00 UTC on day d+1
Mean wind speed	01:00 UTC on day d	00:00 UTC on day d+1
Minimum temperature	18:00 UTC on day d-1 (not included)	18:00 UTC on day d
Maximum temperature	06:00 UTC on day d (not included)	06:00 UTC on day d+1
Mean temperature	01:00 UTC on day d	00:00 UTC on day d+1
Global radiation	00:00 UTC on day d	23:59 UTC on day d
Minimum/maximum relative humidity	00:00 UTC on day d (not included)	00:00 UTC on day d+1

E.2.2. On site

A number of instruments (Table E-5) were installed at the centre of the wetland (latitude 1°25'6"E, longitude 46°0'42"N, altitude 552m NGF69) to measure global and reflected radiation, air temperature, relative humidity, wind speed and rainfall. Most of the data were collected using an Enerco 404 met station from 02/06/2010 to 03/03/2013 and a CMA7 albedometer from 03/07/2010 to 11/11/2012. As early observations showed that the Enerco 404 station was not fully reliable due to a severely drifting hygrometer and issues with the device memory, an additional thermo-hygrometer and rain gauge were installed at the same location to provide a back-up and to allow for better quality control.

Table E-5. Definition of variables measured at the Dauges site.

Equipment	Variable & sensor name	Definition	Resolution, precision & accuracy according to manufacturer	Sampling frequency
CE188-5 rain gauge (Enerco 404 weather station, Cimel)	Cumulated rainfall	Cumulated rainfall or melted snow height in the hour following hour h	Resolution 0.5mm	hourly
CE155 anemometer (Enerco 404 weather station, Cimel)	Mean wind speed at 2m	Integer value of cumulated wind distance in the hour following hour h. Fractions are carried forward to the next hour.	Resolution 1km/h	hourly
CE185A thermometer (Enerco 404 weather station, Cimel)	Temperature at 2m	Temperature at h+1	Resolution 0.1°C Precision ±0.1°C	hourly
CE191 hygrometer (Enerco 404 weather station, Cimel)	Relative humidity at 2m	Relative humidity at h+1	Resolution 0.5% Precision ±1.5%	hourly
CMA7 albedometer with Geobox logger (Précis Mécanique)	Global and reflected radiations	Total global and reflected shortwave radiations in the hour preceding hour h	Resolution 0.1 W/m²	15min
Hobo U12-011 logger (Onset)	Temperature at 2m	Temperature at time t	Measurement range: -20°C to 70°C Accuracy: ± 0.35°C from 0° to 50°C Resolution: 0.03°C at 25°C Drift: 0.1°C/year	15min
Hobo U12-011 logger (Onset)	Relative humidity at 2m	Relative humidity at time t	Mesurement range: 5% to 95% Accuracy: +/- 2.5% from 10% to 90% RH (typical), to a maximum of +/- 3.5% Resolution: 0.03% Drift:<1%/year typical	15min
PM3030 rain gauge with DANAE R62LC logger (Précis Mécanique)	Cumulated rainfall	Actual time of tipping bucket movement	Resolution 0.2mm	actual time

A second Hobo U12-011 thermo-hygrometer was also installed from 23/06/2012 to 04/11/2012 at Les Ribières, in a pasture located at higher altitude (601m), on the hill slope just below a soft ridge marking the catchment boundary. The objective of this instrument was to investigate whether temperature and relative humidity data recorded in the wetland at the bottom of the etch-basin were representative of the wider catchment. The Food and Agriculture Organisation's guidelines for the estimation of reference evapotranspiration (ETo) using the Penman-Monteith method (Allen *et al.* 1998) requires meteorological values, such as minimum and maximum temperature, aggregated over a 24-hour period starting at midnight. However, in line with the World Meteorological Organisation's guidelines, daily values provided by Météo-France are aggregated on 24-hour periods that vary according to the variable measured (Table E-4).

To allow for the comparison of data recorded on site and at nearby Météo-France stations, it was decided to follow WMO guidelines. Unfortunately, absolute daily temperature and relative humidity extremes recorded by the Enerco met station are given for 24-hour periods starting and finishing 2 hours before the aggregation periods used by Météo-France, and this could not be changed a posteriori. Temperature and relative humidity records from the Hobo logger,

available from 25/11/2011 to 28/02/2013, were therefore used to investigate the impact that this issue could have on the quality of daily minimum and maximum temperature and relative humidity records, and whether or not daily extremes should be estimated from hourly data instead. Daily extremes computed from the full 15min resolution dataset were used as a reference, and compared to daily extremes computed from either a 1min-resolution time-series reconstructed from hourly records using spline interpolation, the hourly time-series using 25 or 24 records, or the original 15min-resolution time-series lagged by 2 hours. Figure E-1 shows that the best method to estimate actual daily extremes for the Dauges site from the Enerco data varies according to the variable of interest. Using the daily extremes recorded by the Enerco station, even with a 2 hour lag, is the best way to estimate maximum temperature and minimum relative humidity, probably because few of these extreme values are recorded during the two hours preceding the start and end of aggregation periods (06:00 for maximum temperature and 00:00 for minimum relative humidity). However, when this happens, there can be large outliers that are particularly noticeable, particularly in the minimum relative humidity time-series. This dataset could therefore be further improved by replacing large outliers - and only those - by estimates obtained by spline interpolation of hourly records. Further tests showed that replacing large outliers identified by a difference with spline-interpolated data larger than 8% by the corresponding spline-interpolated data resulted in halving the RMSE, from 1.319 to 0.657. Maximum relative humidity is generally reached during the night and is therefore more likely than minimum relative humidity to occur between 22:00 and 00:00. As a consequence, using the Enerco daily maximum humidity records would result in more error than any other estimation method. The best way to estimate actual maximum relative humidity is to calculate it from hourly records, using 25 records per day (i.e. from 00:00 included to 24:00 included), even though this results in a slight but frequent underestimation of the maxima. Finally, the best way to estimate daily minimum temperature appears to be by reconstructing a high-resolution time-series using spline interpolation of hourly records, and to compute daily minima from this. This might be because spline interpolation can predict values that are beyond the range of observed values and is therefore quite efficient at estimating extremes when the observed data vary relatively smoothly as is the case with temperatures at night. Daily temperature and relative humidity extremes were therefore estimated from the Enerco hourly and daily records using the best method available for each variable. Precipitation and wind speed were not affected by this issue as daily values could be exactly calculated from hourly data.

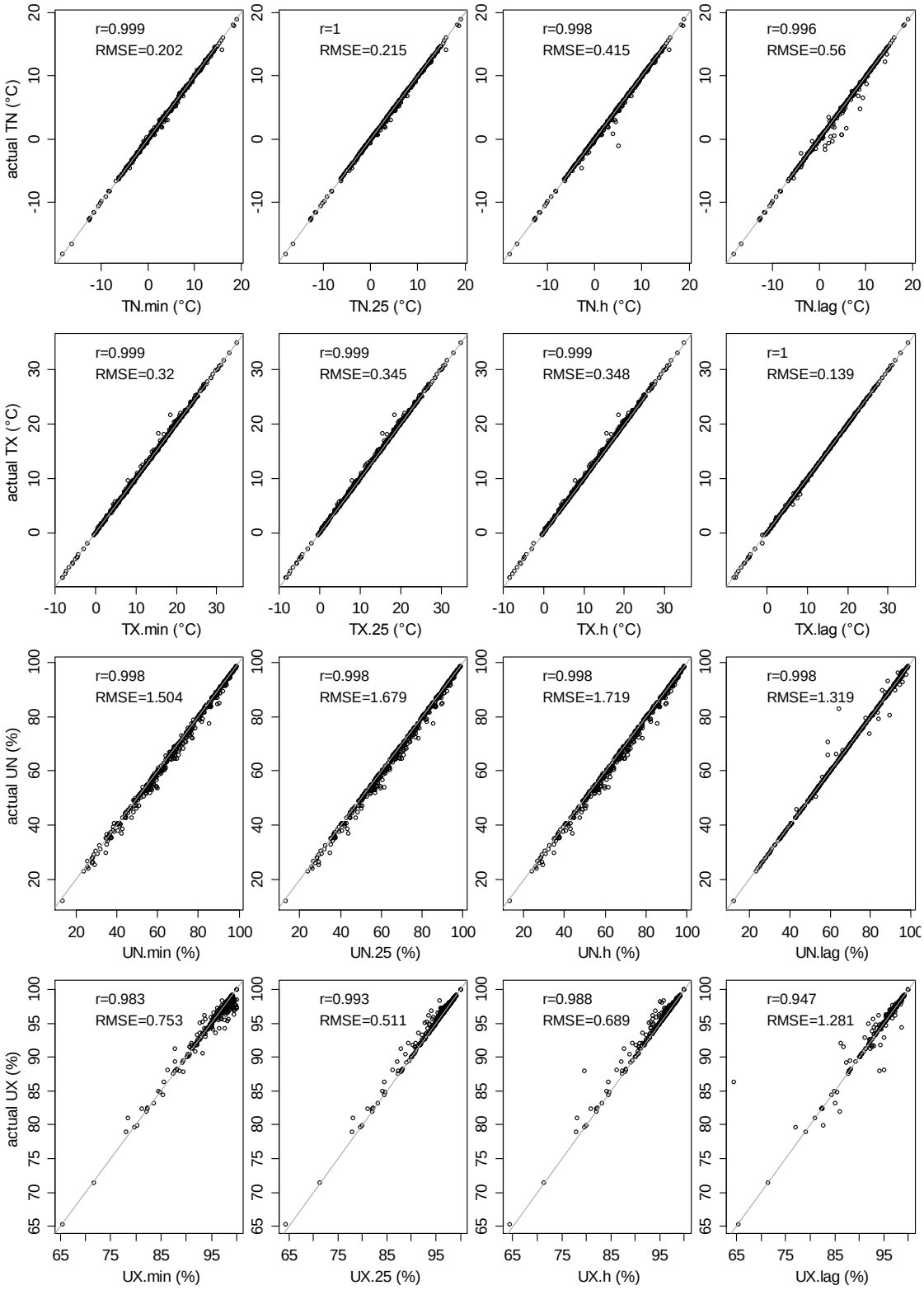

Figure E-1. Influence of computation method on daily temperature and relative humidity extremes.

From top to bottom: minimum and maximum temperature (TN and TX), minimum and maximum relative humidity (UN and UX). _.min: aggregation of 1min-resolution spline-interpolated dataset; _.25: aggregation of 25 hourly records; _.h: aggregation of 24 hourly records; _.lag: aggregation of original dataset lagged by 2 hours. The grey line is the identity line.

A number of checks were carried out on all meteorological records, in particular by checking them against each other and against records from the nearby Météo-France stations, and corrected when necessary. Daily reference evapotranspiration was calculated from the corrected time-series using the FAO-recommended Penman-Monteith method, with the actual vapour pressure calculated from both minimum and maximum relative humidity (Allen *et al.* 1998). Results were compared with other Penman-Monteith variants (using the maximum relative humidity only or the mean relative humidity to compute the actual vapour pressure) and with the Hargreaves-Samani method.

E.2.3. Time-series reconstruction

Meteorological time-series at the Dauges site were modelled and reconstructed using regression techniques with meteorological time-series at nearby Météo-France weather stations used as explanatory variables. This had two objectives: to replace missing data and to reconstruct historical data to allow for the hydrological model to be run over a longer period than that for which meteorological records are available.

A preliminary exploratory analysis was carried out using tools such as scatterplots, regression trees with the rpart package for R and best subset regression with the regsubsets() function of the leaps package for R. Time-series were modelled using ordinary least square regression with the lm() function of base R. Variables included in the full model were selected on the basis of the preliminary analysis results and of the conceptual understanding of the causal relationship and potential interactions between variables. Collinearity was checked using scatterplots and correlation matrices, and highly collinear variables removed. Model selection was carried out backwards from the full model using AIC comparison and t-tests. Residuals from the minimal adequate model were checked against the assumptions of ordinary least square regression using scatterplots and formal tests, but these assumptions were rarely met. Several solutions were tested. First, squared and cubic terms were introduced to model non-linear relationships when inspection of the residuals proved that this was necessary. Second, when an auto-correlogram of the residuals proved that they were significantly auto-correlated, the minimal model was refitted using generalised least square regression with the correlation between errors modelled as a function of time with an auto-regressive model of order 1. The final model was used to predict meteorological time-series at the Dauges site from 01/08/1998 to 31/12/2013 on the basis of records from nearby Météo-France stations. Missing data were infilled using predicted values, and this infilled time-series was used as input to the MIKE SHE model.

E.3. Results

E.3.1. Solar radiation

Global and reflected radiations were measured at the Dauges site from 02/07/2010 to 17/01/2013. There were some gaps in the time-series in January 2011 and March-May 2011 caused by a malfunctioning of the solar panel providing electricity to the data logger. The upper enveloppe of observed daily global radiation agreed very well with the theoretical clear-sky radiation for the site (Figure E-2).

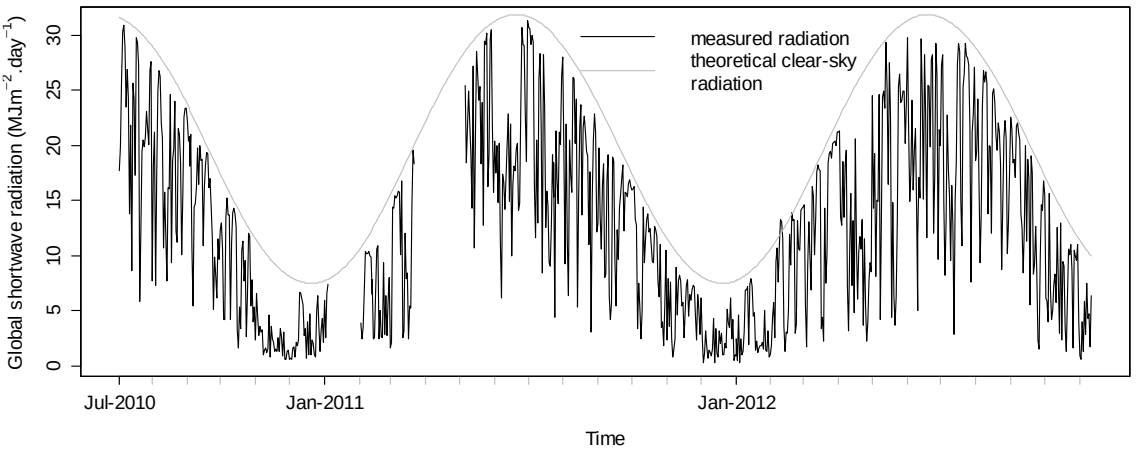

Figure E-2. Theoretical clear-sky and measured daily global radiations at the Dauges site.

The former only exceeded the latter once during the study, in February 2012 at a time when there was snow on the ground and the vegetation. As the logger is in the wetland at the bottom of a deep granitic etch-basin, the global radiation pyranometer also records radiation reflected by higher ground which may be substantial when the latter is covered by snow and highly reflective. Figure E-3 shows measured daily global and reflected radiations and their ratio. Punctual field observations suggest that winter peaks in reflected radiation and in the global/reflected radiation ratio (higher than 0.2-0.3) also correspond to times when there was snow on the ground. Ratios higher than 1 can be explained by the presence of snow on the upper pyranometer, resulting in a substantial under-estimation of global radiation.

Figure E-3 shows that, if periods with snow on the ground are discounted, the reflected/global radiation ratio reaches a fairly constant maxima at about 0.18, which was taken as representative of the albedo of the underlying wetland vegetation. This value is close to those measured in other similar wetlands (0.11-0.14 in a Swedish boreal bog, Kellner 2001b; 0.18-0.195 in acidic mires of the eastern Massif Central, France, Porteret 2008).

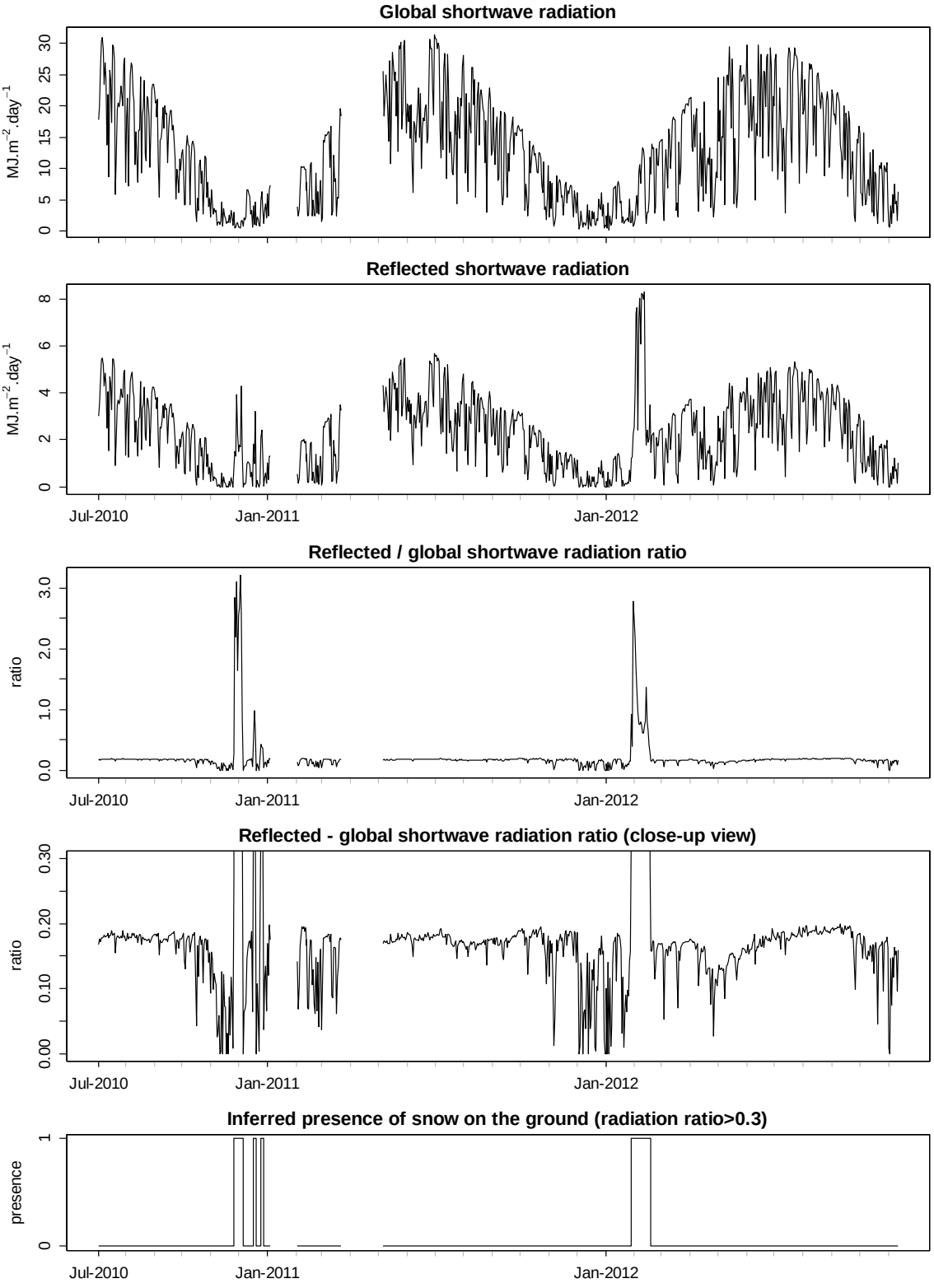

Figure E-3. Daily global and reflected radiations and their ratio at the Dauges site, inferred presence of snow on the ground.

The ratio probably decreases below this value when the ground surface becomes saturated or flooded. However without a record of the water table underneath the albedometer it is not possible to clarify whether small albedo changes are due to changes in vegetation or in the depth and extent of flooding water.

The double mass curve of daily global radiations at the Dauges site and at the two closest weather stations operated by Météo-France show no sign of instrumental issue at the Dauges site (Figure E-4). Daily global solar radiation at the Dauges site is slightly lower than at the two Météo-France sites, one of which is at approximately the same latitude, when one would expect it to be higher due to a higher altitude. A possible explanation is a difference in nebulosity caused by altitude.

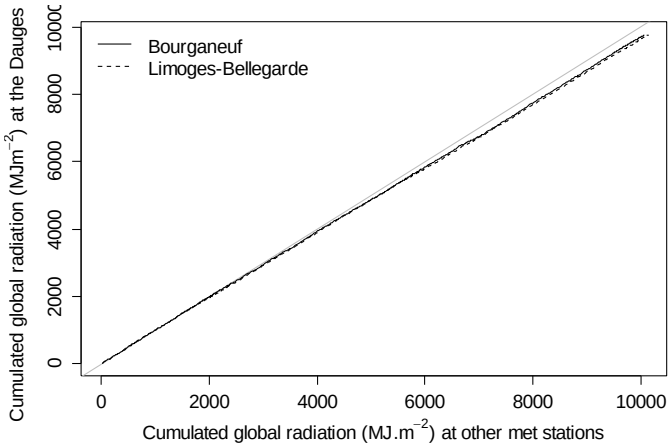

Figure E-4. Double mass curve of global shortwave radiation at the Dauges site and at the two nearest Météo-France stations.

The grey line is the identity line.

Figure E-5 shows scatterplots between daily global radiation at the Dauges site and at the two Météo-France stations. The correlation is high and the relationship linear. In order to reconstruct time-series at the Dauges site based on long-term records at the Météo-France site, global radiation at the Dauges site was modelled as a linear function of radiation at Limoges-Bellegarde, as the best correlation was obtained with this station. As there was residual autocorrelation in a linear model, this was achieved using Generalised Least Square with an AR-1 auto-correlation structure (Table E-6, n=753, df=751, $p<0.001$). A coefficient of determination as computed in Ordinary Least Square regression is meaningless in Generalised Least Square regression, so no r^2 will be given here. Pearson's correlation coefficient and RMSE between observed and modelled radiation were 0.985 and 1.411 respectively. Figure E-6 shows predicted vs. measured time-series.

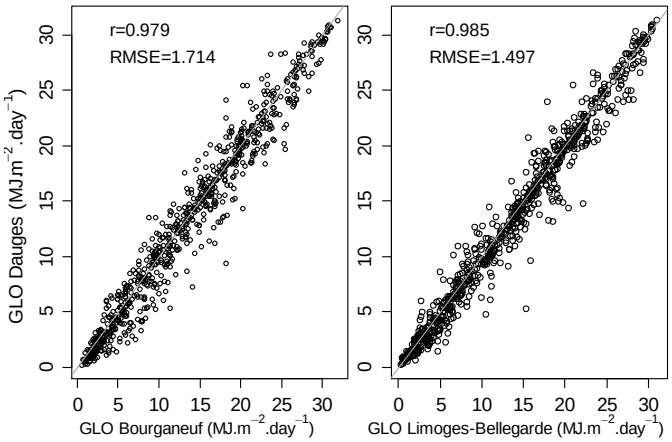

Figure E-5. Scatterplots of global shortwave radiation at the Dauges site and at the two nearest Météo-France stations.

The grey line is the identity line.

Table E-6. Coefficients of the minimal model for global radiation at the Dauges site.

	Value	Std. error	t-value	p-value
Intercept	-0.3100884	0.10958855	-2.82957	0.0048
lmgb	0.9863143	0.00685896	143.79931	0.0000

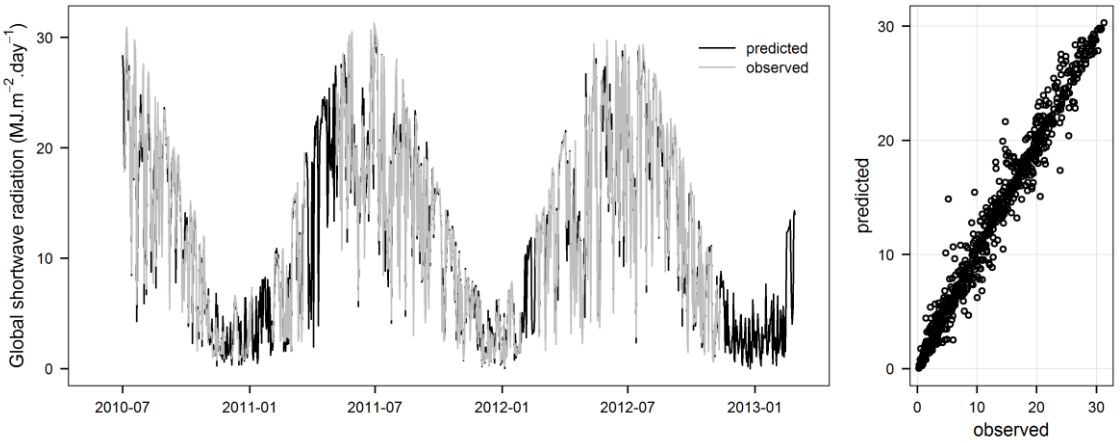

Figure E-6. Observed vs. predicted daily global shortwave radiation at the Dauges site.

Over the 1998-2013 period, the model predicted slightly negative global radiation values in two cases, which were corrected to 0 (the minimum value measured at Limoges-Bellegarde was 0.29 MJ.m^{-2}.day^{-1}).

E.3.2. Temperature

The quality of the Enerco temperature dataset was checked by comparing it to data collected using the Hobo U12-011 logger installed at the same location from 25/11/2011 onwards. Hourly

records from both loggers were very close to each other, with a correlation of 0.999 and a RMSE of 0.365. Figure E-7 suggests that temperatures measured by the Enerco logger were slightly higher than those measured by the Hobo logger towards the upper end of the temperature range.

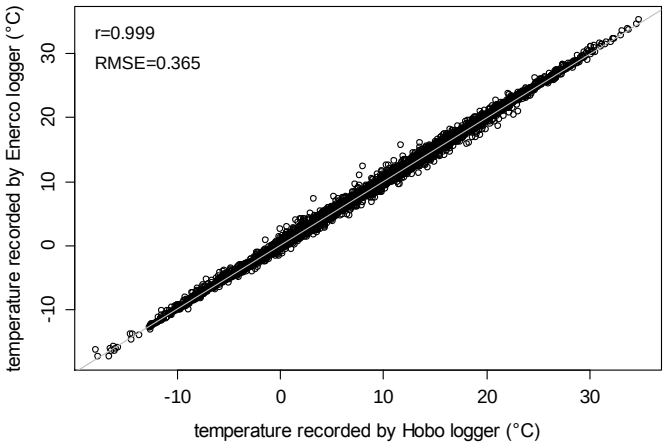

Figure E-7. Scatterplot of air temperatures measured with the Hobo and Enerco loggers at the Dauges site.

The grey line is the identity line.

This was confirmed by linear modelling (*enerco = 1.002*hobo-0.077*, with both coefficient and intercept significantly - $p<0.001$ - different from 1 and 0 respectively, n=10585, df=10583). Daily minimum temperatures recorded by both loggers were nearly equivalent while maximum temperatures recorded by the Enerco logger were slightly higher than those recorded by the Hobo logger (Figure E-8). This may be caused in part by larger differences in sensor errors towards the upper end of the temperature range. However this cannot be the only explanation as the difference between temperature extremes recorded by both loggers is similar whatever their values, and is noticeable in temperature maxima whereas it is not in temperature minima. This is therefore most likely also due to the different way daily extremes were computed for both loggers: temperature extremes given by the Hobo logger were calculated from 15min-resolution data whereas those given by the Enerco logger are the absolute maxima (albeit with a recording period starting two hours before the Hobo one), and minima calculated from spline-interpolated hourly records. The difference between daily temperature extremes given by both loggers was considered small enough to be ignored, and the Enerco time-series was used in subsequent analyses as it spans a longer period. Figure E-9 shows the latter dataset.

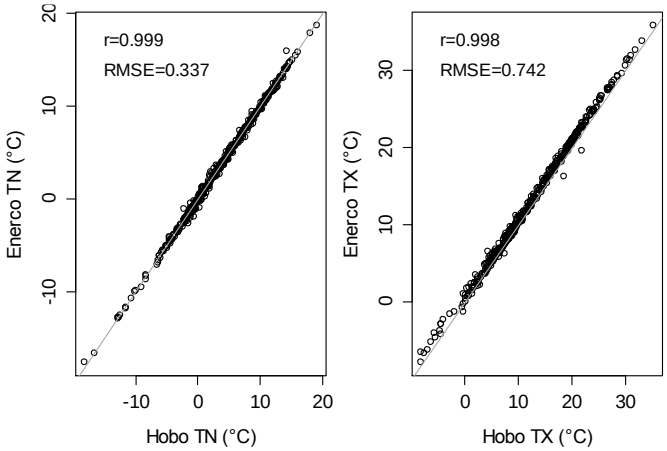

Figure E-8. Scatterplots of temperature extremes recorded by the Enerco and Hobo loggers at the Dauges site.

The grey line is the identity line.

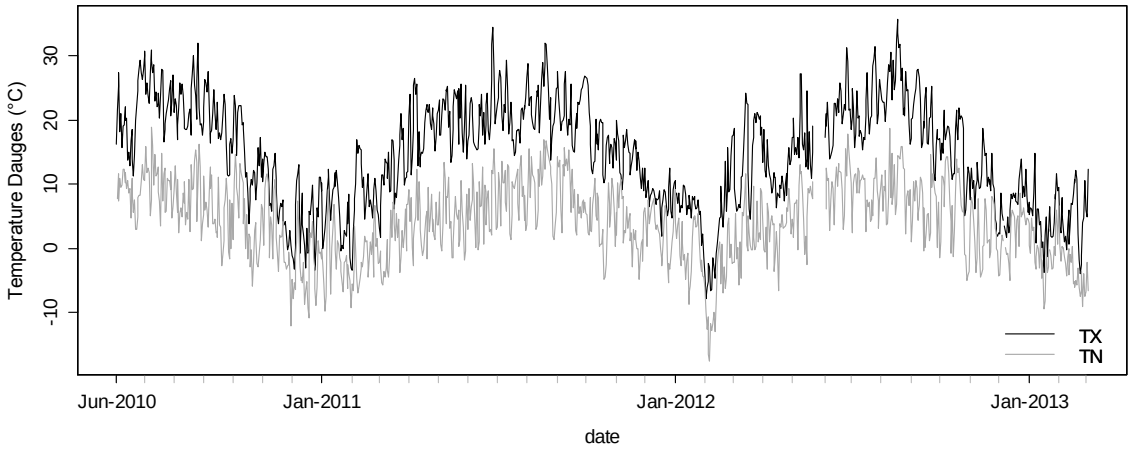

Figure E-9. Daily temperature extremes at the Dauges site.

Figure E-10 shows scatterplots of daily maximum temperatures at the Dauges site (as recorded by the Enerco logger) against records at nearby Météo-France stations. The correlation is excellent for all time-series. The closest fit is for Saint-Léger-la Montagne, the nearest station, for which data are available since 1998 and can therefore be used to reconstruct time-series at the Dauges site. Before that date, data from the Limoges-Bellegarde station, available since 1973, could be used. Maximum temperatures at the Dauges site are nearly always slightly higher than at the Saint-Léger-la-Montagne station: the mean difference is 0.95°C (sd=0.76, n=982), which is broadly equal to the expected temperature differential caused by the 110m-difference in altitude between both sites (Oliver 2005). Pearson's correlation coefficients are much lower for daily minimum temperatures (Figure E-11).

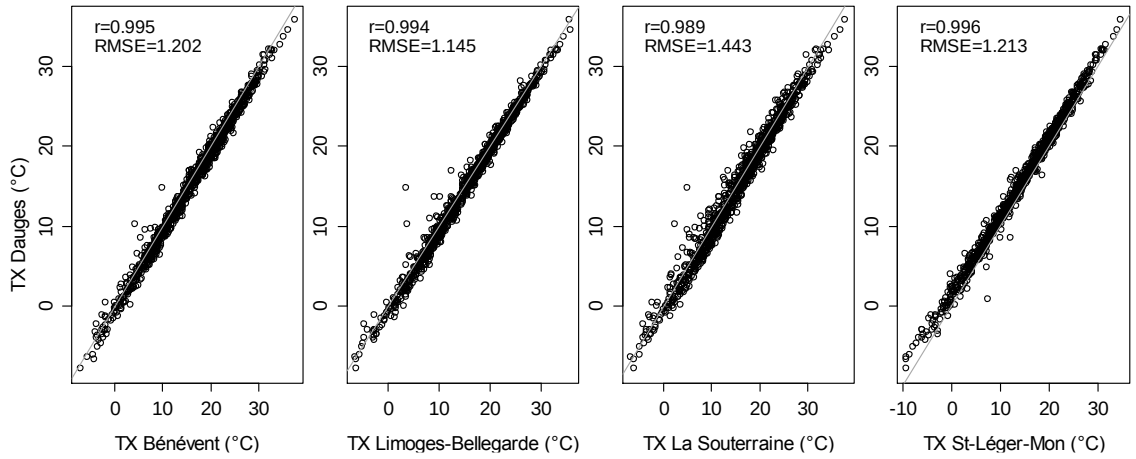

Figure E-10. Scatterplots of daily maximum temperatures at the Dauges site against records at nearby Météo-France stations.

The grey line is the identity line.

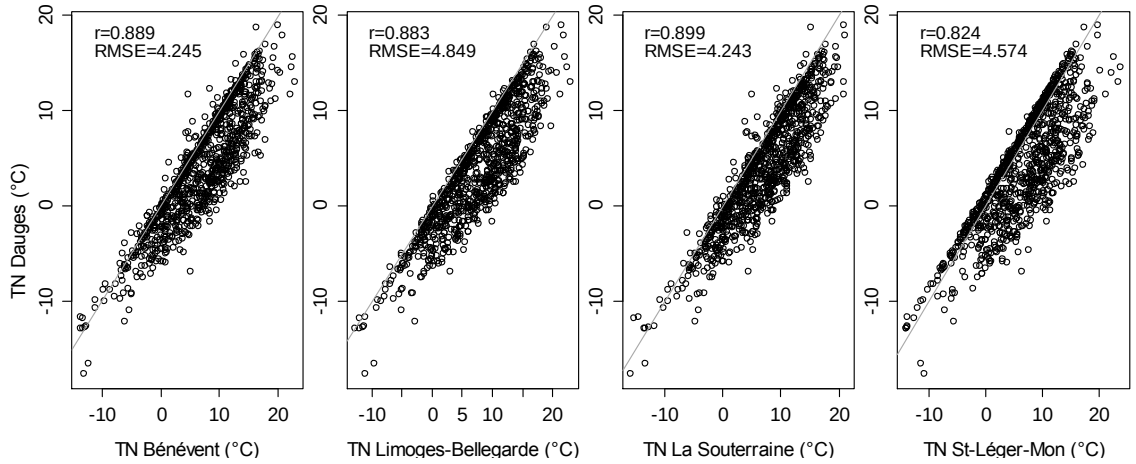

Figure E-11. Scatterplots of daily minimum temperatures at the Dauges site against records at nearby Météo-France stations.

The grey line is the identity line.

Daily minimum temperatures at the Dauges site plotted against those at the nearby Saint-Léger-la-Montagne station show an interesting pattern, with a point scatter that seems to be composed of two groups. The first one includes records that are closely and linearly related to each other, with minimum temperatures at the Dauges site slightly higher than those at Saint-Léger-la-Montagne, a pattern already found in daily maximum temperatures. The second group includes temperature records from the Dauges site that do not follow this relation and are systematically lower than predicted by it, with minimum temperatures at the Dauges site being up to 13.2°C lower than at the Saint-Léger-la-Montagne station.

A similar pattern was observed when comparing daily minimum temperature measured at the bottom of the wetland and at the catchment mid-slope at *Les Ribières* from late June to early November 2012 (Figure E-12). The maximum difference between daily maximum temperatures between both locations was 1.4°C, whereas it was 10.4°C for minimum temperatures. Figure E-13 shows part of the 15min-resolution temperature datasets obtained from both locations using identical Hobo U12-011 loggers. Day time temperatures are very similar whereas night temperatures are much lower in the wetland. A scatterplot of daily extremes at *Les Ribières* and at Saint-Léger-la-Montagne shows a much more linear relationship (Figure E-14).

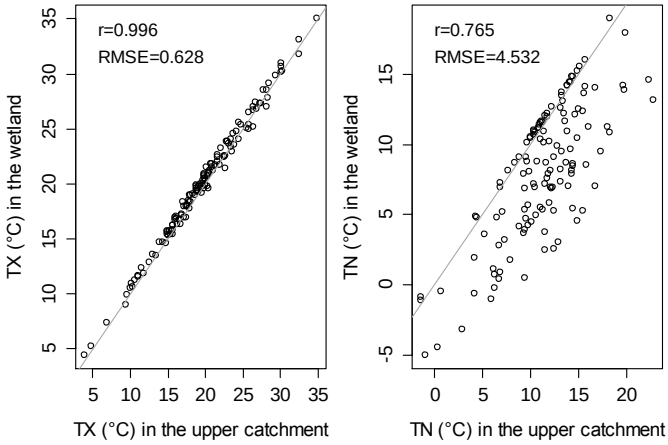

Figure E-12. Scatterplots of daily temperature extremes at the bottom of the wetland and at mid-slope (Les Ribières) at the Dauges site.

Data were obtained from identical Hobo U12-011 thermo-hygrometers at both locations. The grey line is the identity line.

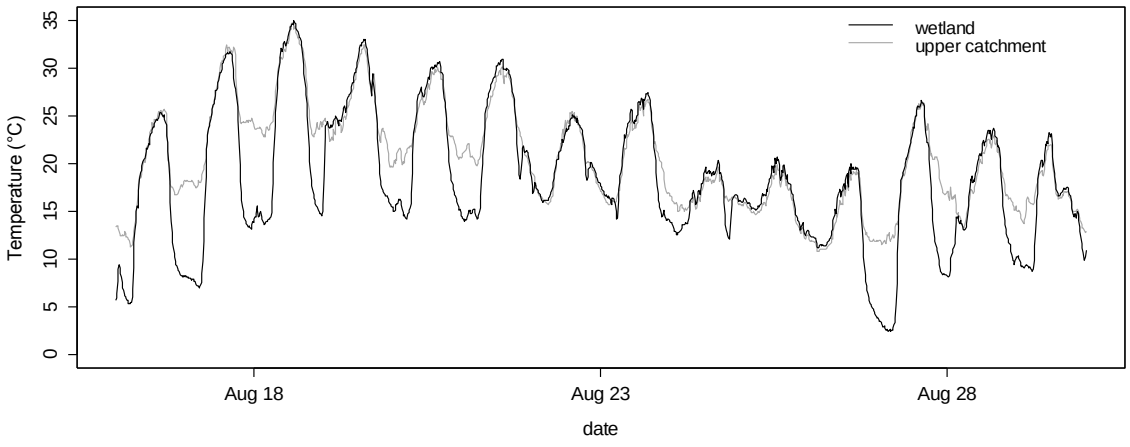

Figure E-13. Temperatures measured at the bottom of the wetland and in the upper part of the catchment (Les Ribières) at the Dauges site.

Data were obtained from identical Hobo U12-011 thermo-hygrometers at both locations.

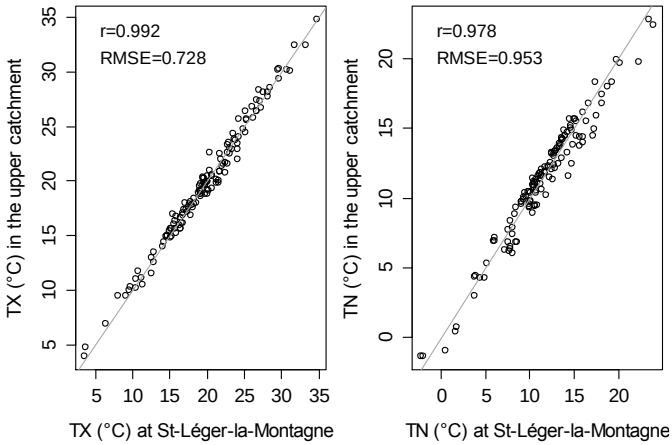

Figure E-14. Scatterplots of daily temperature extremes at mid-slope (Les Ribières) and at St-Léger-Mon.

The grey line is the identity line.

This suggests that a strong temperature inversion phenomenon takes place at night in the wetland, with cold air flowing from the upper part of the catchment into the bottom of the etch-basin where it is trapped due to the bowl-shaped topography. As this phenomenon considerably reduces the correlation between daily minimum temperatures at the Dauges site and nearby Météo-France stations and would increase the error when reconstructing the former based on the latters, the anomaly in daily minimum temperature at the Dauges site compared to records at Saint-Léger-la-Montagne was investigated in more detail and potential explanatory variables were sought, with the aim of informing models of minimum temperature. The anomaly was defined as the difference between daily minimum temperatures in the wetland and at the Saint-Léger station.

Figure E-15 shows a series of scatterplots of this anomaly against a number of meteorological variables recorded in the wetland and at selected Météo-France stations. The radiation ratio was defined as the ratio of observed global radiation and of the theoretical clear-sky radiation, and was used as a proxy for nebulosity. Figure E-15 suggests that the anomaly increases (in absolute value) when rainfall is zero or low, wind speed decreases, the radiation ratio increases, maximum temperature in the wetland and both maximum and minimum temperatures at Saint-Léger increase, and minimum relative humidity decreases in the wetland and at Limoges-Bellegarde. This is in line with the inversion phenomenon being more pronounced during clear-sky nights when radiation losses are higher, that are themselves associated with dry warm days, and during windless periods when air stratification is not perturbed.

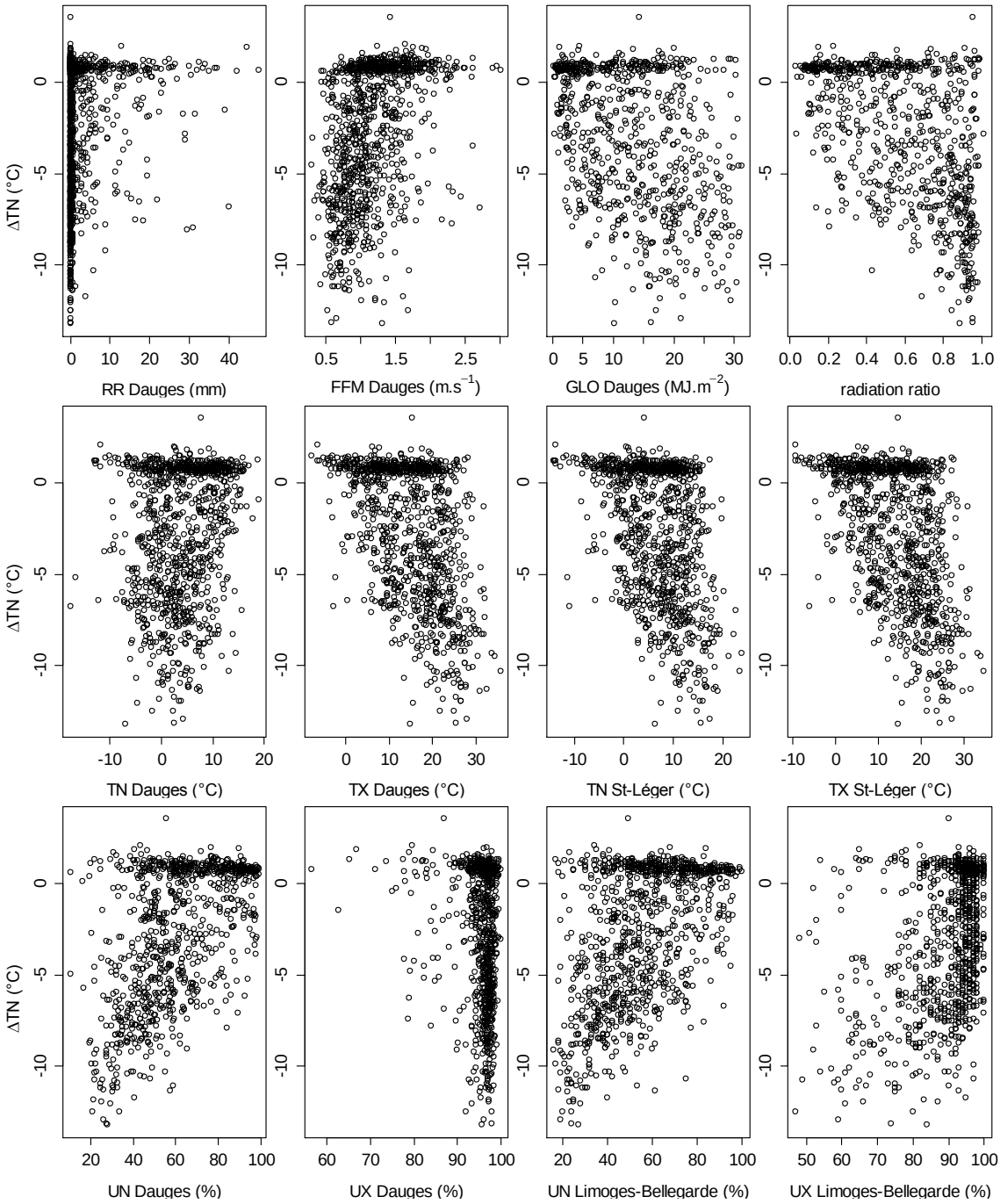

Figure E-15. Scatterplots of the anomaly in daily minimum temperature at the Dauges site against other meteorological variables.

TN, TX: daily minimum and maximum temperature; UN, UX: daily minimum and maximum relative humidity; RR: daily precipitation; FFM: daily mean wind speed; GLO: daily global shortwave radiation.

To model daily minimum temperatures in the wetland based on time-series obtained from nearby Météo-France stations, it was therefore necessary to account for some of these parameters. For each of the potential parameters to be included in the model, data were obtained from the nearest station, those with best correlations with records at the Dauges site

or those with the longest time-series, namely Saint-Léger-la-Montagne for temperatures and precipitation and Limoges-Bellegarde for global radiation, wind speed and relative humidity. Figure E-16 shows a correlation matrix of these variables and highlights possible colinearity issues. It suggests that the model should not include maximum temperature at Saint-Léger-la-Montagne since it is strongly correlated to minimum temperature. Similarly, minimum temperature, global radiation and radiation ratio at Limoges-Bellegarde are correlated to each other and should not be included in the same model. The radiation ratio was chosen as, at the Dauges site, this variable is better correlated to the minimum temperature anomaly, and can be more accurately predicted at the Dauges site using the data from Limodes-Bellegarde than minimum relative humidity.

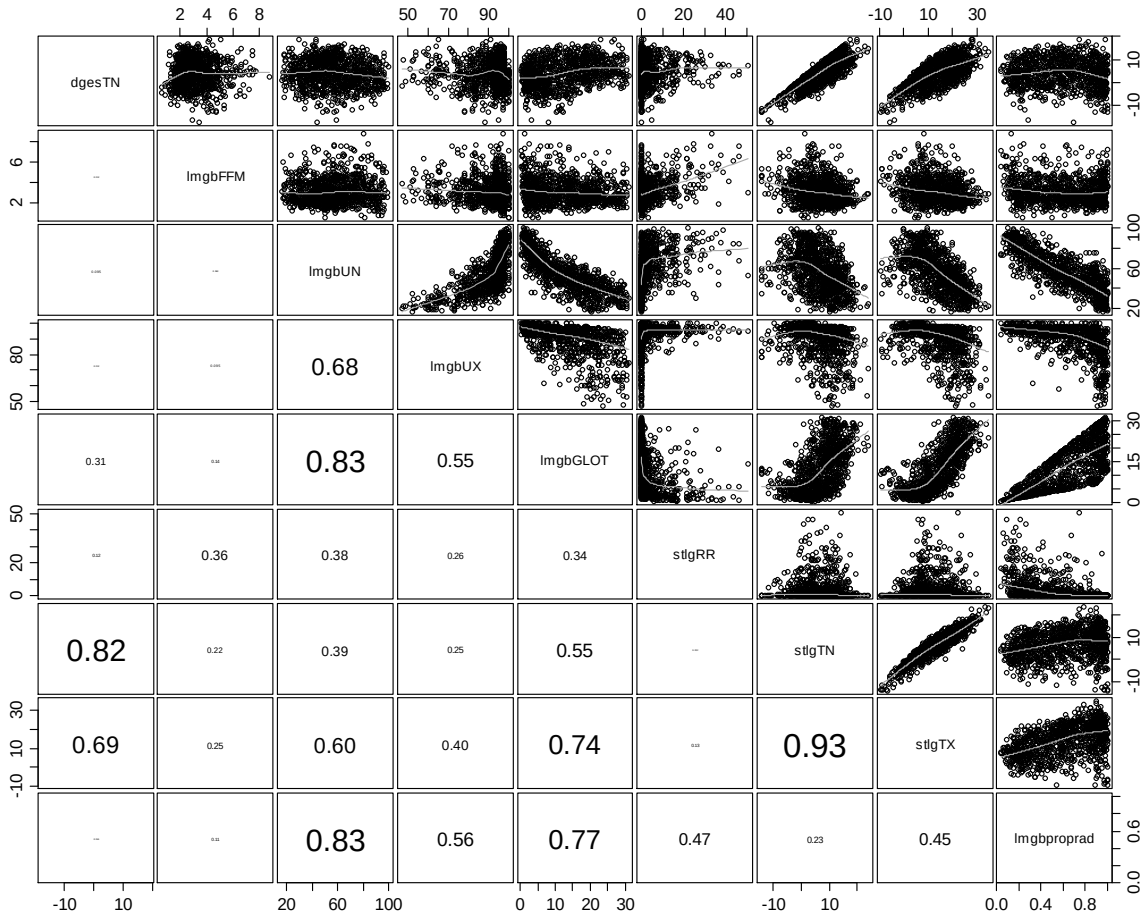

Figure E-16. Correlation matrix of potential variables to be included in a model of daily minimum temperatures at the Dauges site.

The matrix diagonal gives the variable names (dges: Dauges, lmgb: Limoges-Bellegarde, stlg: Saint-Léger-la-Montagne; TN & TX: daily minimum and maximum temperatures, UN & UX: daily minimum and maximum relative humidities, FFM: mean wind speed, GLOT: global radiation, RR: precipitation). The below-diagonal panels give the Pearson's correlation coefficient of the two corresponding variables, with a font size proportional to it. The above-diagonal panels show a scatterplot of the two corresponding variables, with a LOESS smoother superimposed in grey to help visualise the shape of the relationship between variables.

Daily minimum temperature in the wetland was therefore modelled as a linear function of wind speed, maximum relative humidity and radiation ratio at Limoges-Bellegarde, minimum temperature and precipitation at Saint-Léger-la-Montagne, and their interactions. A preliminary model selection using the regsubsets() function of the leaps package for R indicated that no interaction with terms higher than 2 was important. Model selection was therefore carried backwards from the full model with all two-way interactions, using AIC and F-tests to compare nested models and remove non-significant terms one by one. The minimal model was tested against the linear model assumptions by looking at residuals plotted against the predictors. There were some minor departures from these assumptions that were partly improved by introducing the squared term for the radiation ratio but could not be entirely resolved. As there was some minor residual autocorrelation, the model was refitted using generalised least squares with an autocorrelation structure of order 1, but an F-test showed no significant improvement compared to the model without auto-correlated errors. It was therefore decided to use the linear model (Table E-7, n=954, df=946, adj. r^2=0.816, p<0.001).

Table E-7. Coefficients of the minimal model for daily minimum temperature at the Dauges site.

	Estimate	Std. Error	t value	Pr(>|t|)	
(Intercept)	-8.8612	1.2238	-7.241	9.24E-13	***
lmgbFFM	0.08737	0.14563	0.6	0.548699	
lmgbUX	0.07933	0.01122	7.069	3.02E-12	***
stlgTN	1.01524	0.03647	27.837	< 2e-16	***
lmgbproprad	-2.20819	1.88143	-1.174	0.240821	
I(lmgbproprad^2)	-5.72073	1.4016	-4.082	4.85E-05	***
lmgbFFM:lmgbproprad	1.76511	0.23404	7.542	1.09E-13	***
stlgTN:lmgbproprad	-0.17873	0.05228	-3.419	0.000656	***

The model suggests that daily minimum temperature is related to minimum temperature at Saint-Léger-la-Montagne but that other variables modulate this relationship. Minimum temperature increases with maximum relative humidity. The radiation ratio has, overall, a non-linear negative effect on minimum temperature in the wetland, but this effect is much more pronounced when wind speed is low and minimum temperature at Saint-Léger-la-Montagne is high. All of this is consistent with an inversion phenomenon occurring at the bottom of the etch-basin and being more pronounced during clear-sky windless nights following dry warm days. Figure E-17 shows a scatterplot of predicted vs. observed values. The model had an adjusted determination coefficient of 0.816 (F-statistic: 603.4 on 7 and 946 DF, p-value: < 2.2e-16), and the RMSE of the predicted values against observed values in the wetland was 2.57.

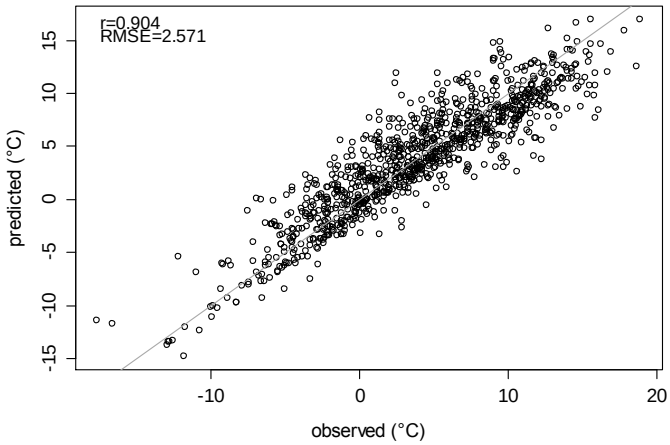

Figure E-17. Observed vs. predicted daily minimum temperatures at the Dauges site.

The grey line is the identity line.

This is to compare to a simple linear model of daily minimum temperature in the wetland based on minimum temperature at Saint-Léger-la-Montagne that achieved an r^2 of just 0.680 and a RMSE of 3.39.

An exploratory analysis using scatterplots suggested that the relationship between daily maximum temperatures in the wetland and at Saint-Léger-la-Montagne was actually not strictly linear, and that there might be an effect of wind speed and radiation ratio. Daily maximum temperature in the wetland was therefore modelled as a linear function of these variables, their two-way interactions and the square of the maximum temperature at Saint-Léger. Model selection was carried backwards from the full model with all two-way interactions, using AIC comparison and F-tests. Residuals from the minimal adequate model showed some temporal auto-correlation, and the model was therefore refitted using generalised least squares with a with an autocorrelation structure of order 1. The correlation structure did improve the model (AIC 2041.296 vs. 2028.895, L ratio 14.40, p= 1e-04), even though there was still some minor residual auto-correlation. Plots of residuals vs. individual predictors did not show any obvious pattern. The model coefficients are given in Table E-8 (n=957, df=951).

Table E-8. Coefficients of the minimal model for daily maximum temperature at the Dauges site.

	Value	Std.Error	t-value	p-value
(Intercept)	0.4146966	0.11859541	3.49673	5.00E-04
stlgTX	0.9695388	0.0099586	97.35694	<.0001
lmgbFFM	0.1038723	0.01911962	5.43276	<.0001
lmgbproprad	1.2091722	0.15897445	7.60608	<.0001
stlgTX^2	0.0015307	0.00032034	4.77833	<.0001
stlgTX:lmgbproprad	-0.0537116	0.01201687	-4.46968	<.0001

The squared term suggests that daily maximum temperatures in the wetland are very slightly higher than expected by a strictly linear relationship when temperature is at the lower or upper end of its range. The interaction term suggests that the slope of the relationship between temperatures in the wetland and at Saint-Léger varies very slightly according to the radiation ratio, with low temperatures being slightly higher in the wetland when the radiation ratio is high. Finally it seems that maximum temperatures in the wetland are slightly higher when wind speed at Limoges-Bellegarde is high. The effect of variables other than maximum temperature at Saint-Léger-la-Montagne is significant but very small and may reflects differences in the topography and wind conditions around both stations, the station in the wetland being more sheltered than at Saint-Léger-la-Montagne. A determination coefficient does not make sense when fitting a model with Generalised Least Square. The Pearson's correlation coefficient between observed and fitted daily maximum temperatures in the wetland was 0.997, and the RMSE 0.681. Figure E-18 show the predicted vs. observed values.

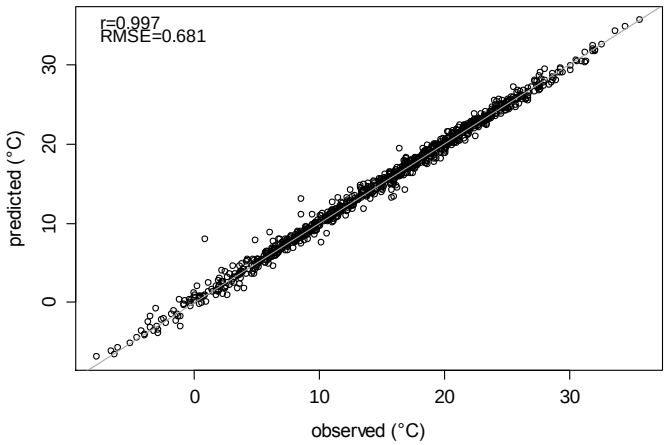

Figure E-18. Observed vs. predicted daily maximum temperatures at the Dauges site.

The grey line is the identity line.

E.3.3. Relative humidity

The CE191 (Enerco 404, Cimel) relative humidity sensor installed in June 2010 soon proved to be subject to a substantial drift over time, recording values of up to 110% towards the end of the recording period (Figure E-19). As the sensor itself could not be replaced for financial reasons, a second thermo-hygrometer (Hobo U12-011, Onset) was installed at the same location from 25/11/2011 onwards. The Hobo series did not show such a drift, but is available for less than half the study duration. Moreover the Hobo sensor specifications make it accurate for relative humidity below 95% only.

It was therefore necessary to correct the Enerco data to obtain relative humidity records spanning most of the study duration. Two different correction methods were attempted. First, the maximum relative humidity potentially measured by the sensor (Umax) was modelled as a linear function of time using quantile regression with a tau set to one, using the rq() function of the Quantreg package for R (Koenker 2013).

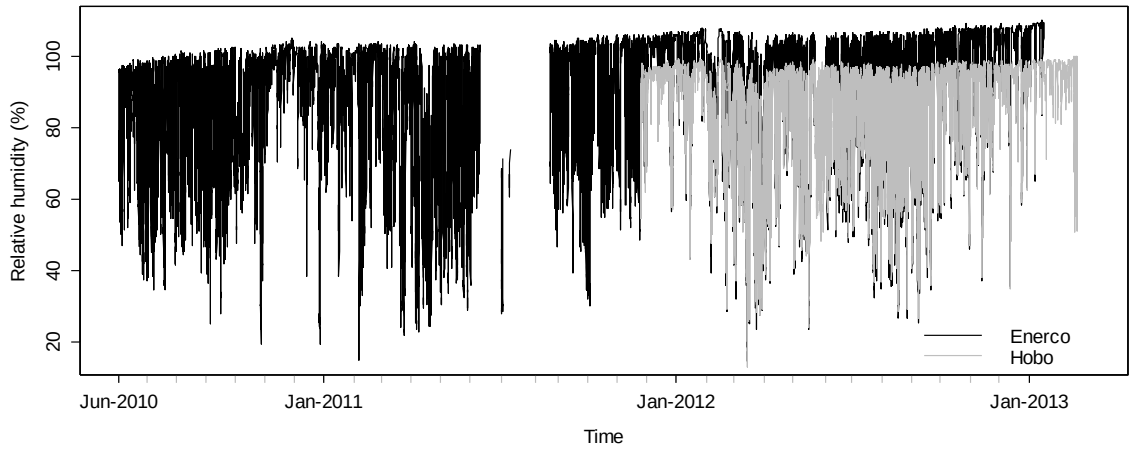

Figure E-19. Uncorrected hourly relative humidity measured by the Enerco and Hobo loggers at the Dauges site.

This gave the following equation for Umax:

$$Umax=8.180e^{-08}*time-6.070e^{-01} \quad \text{Equation E-1}$$

The equation predicted a maximum relative humidity of 100.23% for 23/01/2009, the date when the sensor was calibrated by the manufacturer. The entire dataset was then scaled back from a maximum range of 0 to Umax to a maximum range of 0-100% by multiplying it by 100/Umax, with Umax calculated as a function of time from Equation E-1. The second correction method that was tested aimed at finding the best drift parameters, modelled as a linear function of time, that minimised the difference between data recorded by the Enerco logger after correction and data recorded by the Hobo logger, while setting Umax equal to 100% (i.e. drift=1) at the date of the sensor calibration. This followed the following mathematical reasoning. Let drift(t) be the factor by which the uncorrected Enerco data is multiplied to obtain the corrected data (or Umax to obtain 100%) at time t:

$$enerco.cor = drift(t)*enerco \quad \text{Equation E-2}$$

where enerco.cor and enerco are the corrected and uncorrected Enerco time-series respectively. Drift is a linear function of time:

$$drift(t)=a*t+b \quad \text{Equation E-3}$$

where t is time and a and b are constants.

Combining Equation E-2 and Equation E-3 gives:

$$enerco.cor = a*t*enerco + b*enerco \quad \text{Equation E-4}$$

Drift is equal to 1 at t_0 = 23/01/2009, when the sensor was factory-calibrated, hence:

$$a*t_0 + b = 1 \quad \text{Equation E-5}$$

Combining Equation E-4 and Equation E-5 gives:

$$enerco.cor = a*t*enerco + enerco - a*t_0*enerco \quad \text{Equation E-6}$$

To find the best drift slope *a* that minimised the difference between the corrected Enerco data and the Hobo data, the latter were substituted to the former in Equation E-6 which was then fitted by least-square estimation using the nls() function in R. As the Hobo logger is not accurate beyond 95%, only data points where the Hobo value was less than or equal to this value were used. The estimated *a* was -5.841×10^{-10}. Equation E-6 was then used to predict the corrected Enerco data. Corrected data were caped to 100%.

Figure E-20 shows the corrected data using both methods. To help decide which method should be used, data corrected using both were compared to relative humidity time-series obtained from the Hobo logger and from the three closest Météo-France weather stations, in terms of their Pearson's correlation and RMSE (Table E-9 and Table E-10). The comparison period was taken as 25/11/2011 to 30/06/2012. Correlations are very similar if not identical between both methods. RMSE, on the other hand, is slightly lower when the Enerco data are corrected using quantile regression when comparing to Météo-France datasets. However differences are very small and both methods give essentially the same results.

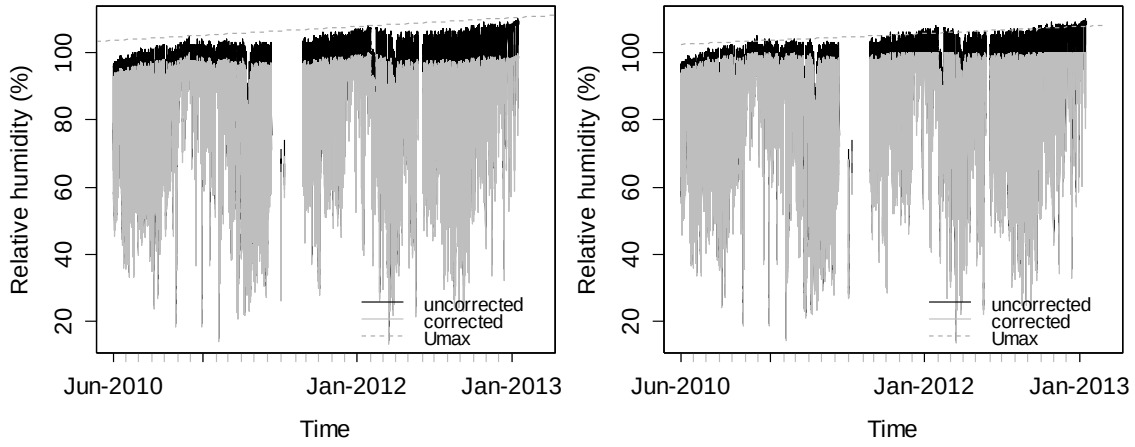

Figure E-20. Uncorrected and corrected relative humidity data from the Enerco logger using two different methods.

Left: data corrected using quantile regression. Right: data corrected to minimise differences with Hobo data. The dotted line shows the maximum relative humidity predicted by each method as a function of time.

Table E-9. Correlation of corrected humidity data at the Dauges site with control datasets.

	qr	min diff	hobo <=95%	hobo	bgnf	lmgb	lstr
qr	1	1	0.984	0.987	0.853	0.859	0.857
min diff	1	1	0.984	0.988	0.853	0.859	0.857

qr: Enerco-recorded data corrected using quantile regression, min diff: Enerco-recorded data corrected by minimising the difference with Hobo-recorded data, hobo<=95%: Hobo-recorded data at the Dauges site (<=95%), Hobo: Hobo-recorded data at the Dauges site (full dataset), bgnf: data recorded by Météo-France in Bourganeuf, lmgb: data recorded by Météo-France in Limoges-Bellegarde, lstr: data recorded by Météo-France in La Souterraine.

Table E-10. RMSE of corrected relative humidity data at the Dauges site with control datasets.

	qr	min diff	hobo <=95%	hobo	bgnf	lmgb	lstr
qr	0	1.615	4.28	3.778	10.588	11.885	9.599
min diff	1.615	0	3.979	3.765	11.476	12.974	10.164

qr: Enerco-recorded data corrected using quantile regression, min diff: Enerco-recorded data corrected by minimising the difference with Hobo-recorded data, hobo<=95%: Hobo-recorded data at the Dauges site (<=95%), Hobo: Hobo-recorded data at the Dauges site (full dataset), bgnf: data recorded by Météo-France in Bourganeuf, lmgb: data recorded by Météo-France in Limoges-Bellegarde, lstr: data recorded by Météo-France in La Souterraine.

The method based on quantile regression was selected to correct the Enerco relative humidity dataset at both hourly and daily time steps. Figure E-21 shows a scatterplot of the corrected Enerco hourly dataset against the Hobo dataset. The relationship is non-linear: the scatterplot approximately follows the 1:1 line for low (<25%) and high relative humidity values, but the Hobo logger records slightly higher values between 25 and 90%. Consequently, the same relationship is found in relative humidity daily extremes (Figure E-22). In the absence of another logger in the wetland that could point towards the most accurate logger, the Enerco dataset was used as it spans a longer period. Figure E-23 shows the latter dataset. Figure E-24 shows scatterplots of daily maximum relative humidity in the wetland and at nearby Météo-France stations (there is no Météo-France station located less than 25km away from the site that records relative humidity).

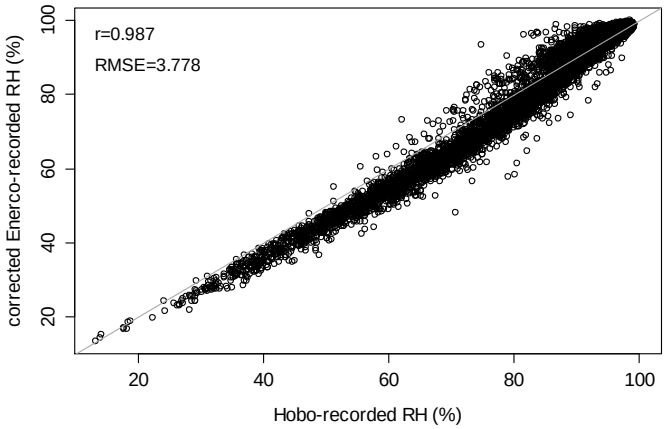

Figure E-21. Scatterplot of corrected Enerco-recorded vs. Hobo-recorded hourly relative humidity at the Dauges site.

The grey line is the identity line.

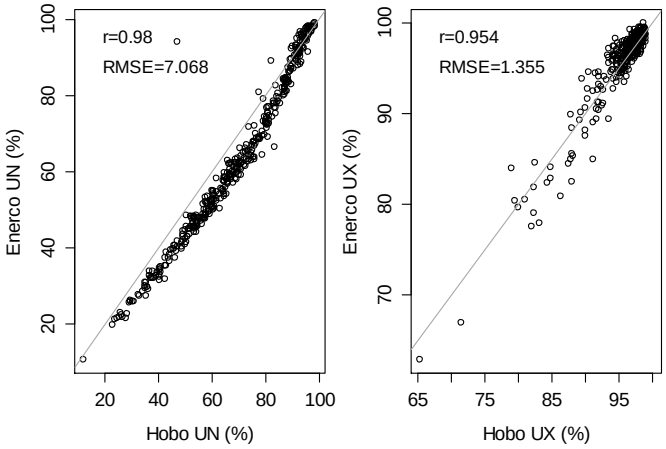

Figure E-22. Scatterplots of relative humidity daily extremes recorded by the Enerco and Hobo loggers at the Dauges site.

The grey line is the identity line.

Pearson's correlation coefficients are high for all the stations, and the largest for Limoges-Bellegarde. The scatterplots do not show a curved relationship like the one found when comparing data from the Enerco and Hobo loggers, which suggests that this issue might have been caused by the Hobo logger. Daily minimum relative humidity measured in the wetland is generally higher than at other stations, especially towards the upper range of the measurements. Correlations are much lower in the case of maximum relative humidity (Figure E-25). Measurements in the wetland are nearly always higher than those measured at the Météo-France stations, and large values higher than 90% are much more frequent at the former than at the latters. The most likely explanation is that, for a fixed mass of water vapour in the air, relative humidity is a function of temperature, increasing as air temperature decreases.

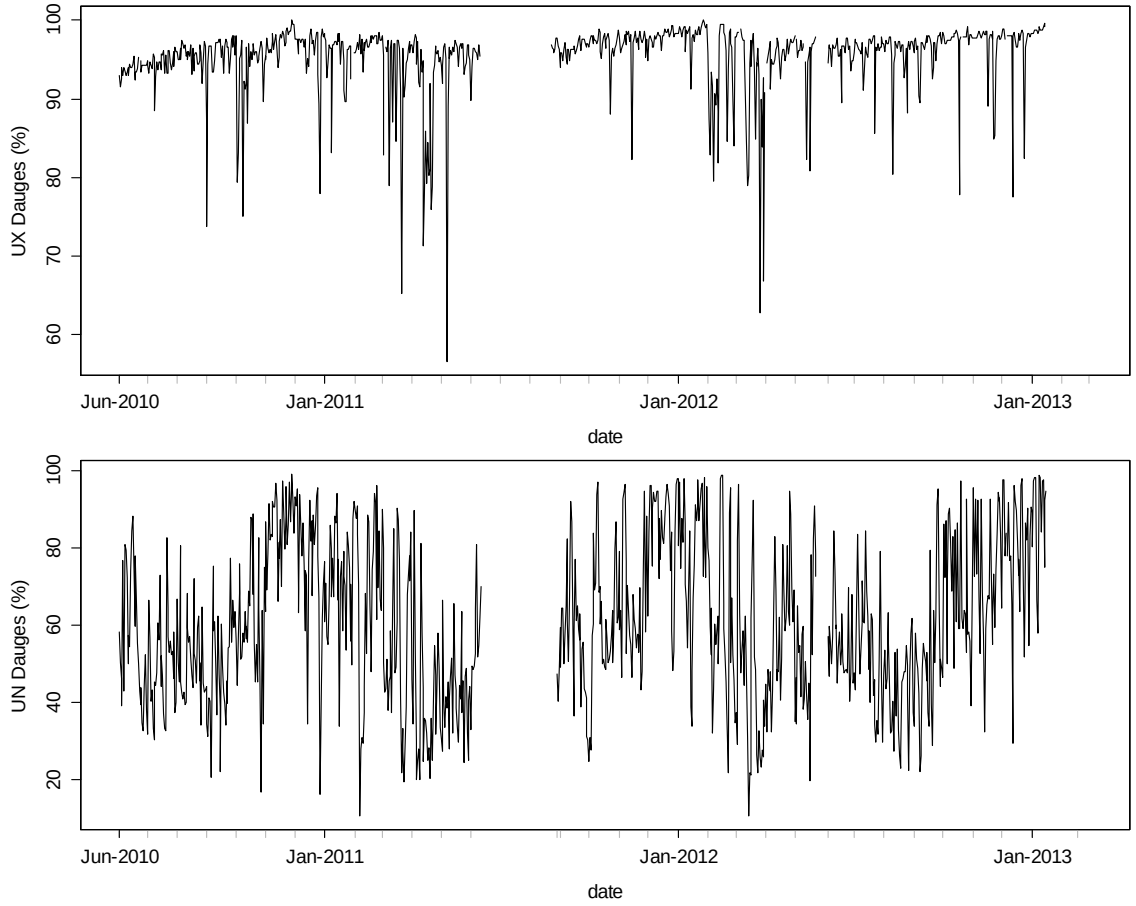

Figure E-23. Daily minimum and maximum relative humidity at the Dauges site.

Top: daily maximum relative humidity, bottom: daily minimum relative humidity. Data recorded by the Enerco logger, after adjustment.

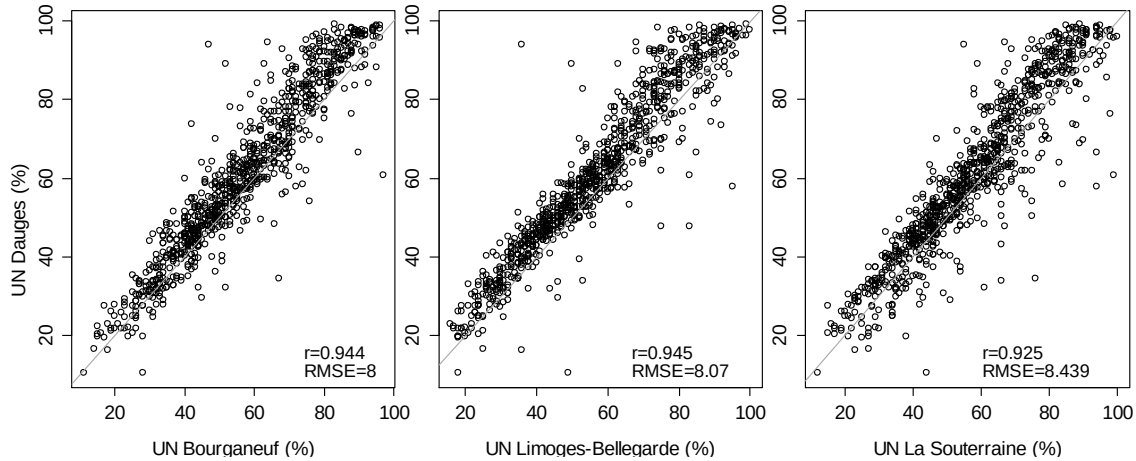

Figure E-24. Scatterplots of daily minimum relative humidity at the Dauges site and at nearby Météo-France stations.

The grey line is the identity line.

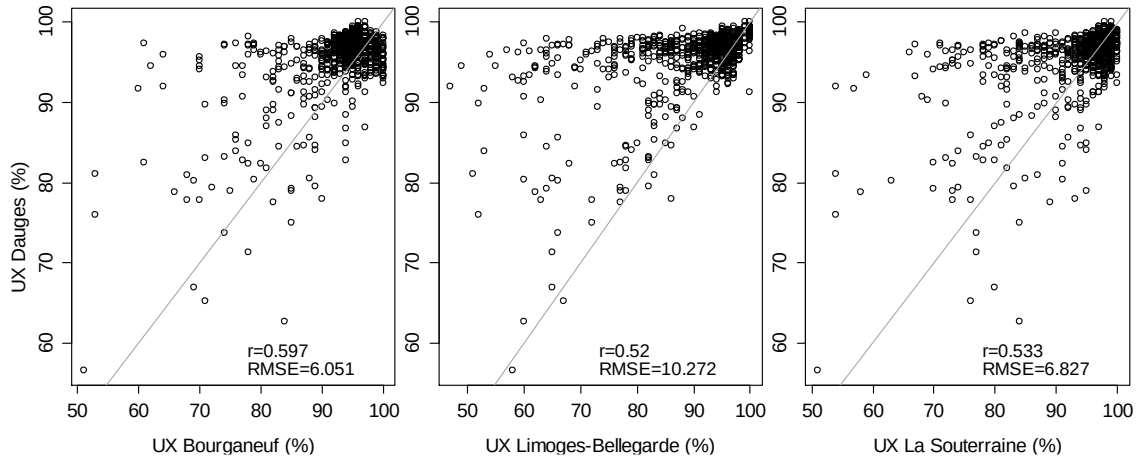

Figure E-25. Scatterplots of daily maximum relative humidity at the Dauges site and at nearby Météo-France stations.

The grey line is the identity line.

As temperatures are lower in the wetland than at nearby stations, relative humidity is consequently higher, especially at night when the difference in temperature is much more important due to temperature inversion occurring in the Dauges basin. Similarly, as correlations between minimum temperatures between stations are not good, this reflects on correlations between maximum relative humidity records. Other explanations could be, first, that the wetland is located at the bottom of a deep etch-basin in which wind speed is generally lower, which reduces the redistribution of saturated air towards the upper atmosphere, and second, that actual evapotranspiration is very rarely limited in the wetland due to a shallow groundwater table, increasing the amount of water vapour in the air above. However the latter two explanations would have an impact on relative humidity minima as well, and are therefore probably less important factors. A similar pattern is observed when comparing daily relative humidity extremes recorded in the wetland and in the upper part of the catchment at *Les Ribières* (Figure E-26).

A comparison of daily extremes at *Les Ribières* in the upper part of the catchment and at nearby Météo-France stations, especially the Limoges-Bellegarde station, shows a slightly better correlation of maximum relative humidity records (Figure E-27). Again this suggests that the weak correlation between maximum relative humidity records in the wetland and at other locations is a relatively local phenomenon restricted to the bottom of the etch-basin and caused by the topography and temperature inversion at night.

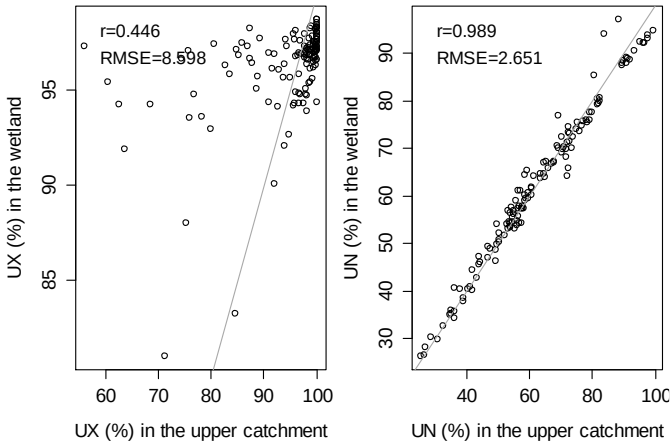

Figure E-26. Scatterplots of daily temperature extremes at the bottom of the wetland and at mid-slope (Les Ribières) at the Dauges site.

Data were obtained from identical Hobo U12-011 thermo-hygrometers at both locations. The grey line is the identity line.

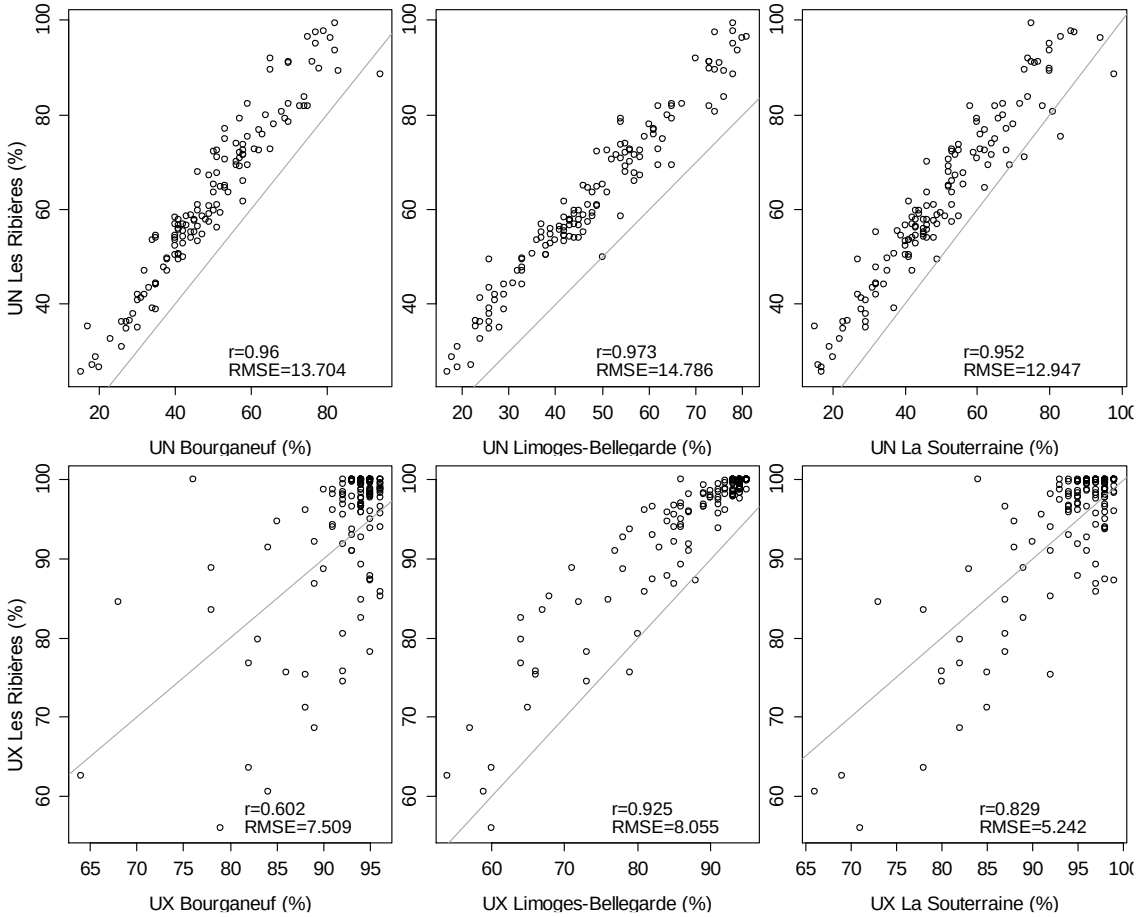

Figure E-27. Scatterplots of daily relative humidity extremes at les Ribières and at nearby Météo-France stations.

The grey line is the identity line.

As for temperature, daily minimum relative humidity in the wetland was modelled as a linear function of selected meteorological records from nearby Météo-France stations (Limoges-Bellegarde for wind speed, relative humidity and radiation ratio, and Saint-Léger-la-Montagne for temperature and precipitation).

Preliminary exploratory analyses using regression trees and best subset regression suggested that the main predictor was daily minimum relative humidity, with possible interactions with minimum and maximum temperatures. As the two latter variables are highly correlated, only maximum temperature was included in the full model, together with minimum relative humidity and their interactions. All terms were significant. An auto-correlogram showed high levels of auto-correlation, and the model was therefore refitted using Generalised Least Square with an AR-1 auto-correlation structure. This greatly improved the model (AIC: 5539.3 vs. 5607.8 for the model without auto-correlation structure, L-ratio: 72.2, p-value <0.0001). The amount of auto-correlation in the residuals was considerably reduced but not totally eliminated. Table E-11 shows the coefficients of the minimal model (n=840, df=836).

Table E-11. Coefficients of the minimal model for daily minimum relative humidity at the Dauges site.

	Value	Std.Error	t-value	p-value
(Intercept)	12.11688	1.9398001	6.24646	0
lmgbUN	0.950615	0.0280505	33.8894	0
stlgTX	-0.140123	0.1043601	-1.34269	0.1797
lmgbUN:stlgTX	-0.004316	0.0018161	-2.37629	0.0177

This suggests that daily minimum relative humidity in the wetland decreases more strongly with decreasing humidity at Limoges-Bellegarde when temperatures at Saint-Léger-la-Montagne are high. Over the 1998-2013 period, the model predicted a daily minimum relative humidity higher than 100% in 59 cases. These were corrected back to 100%. Pearson's correlation coefficient and the RMSE between predicted (after correction) and observed time-series were 0.948 and 6.535 respectively (Figure E-28).

Preliminary exploratory analyses of daily maximum relative humidity at the Dauges site using regression trees and best subset regression suggested that, on top of maximum relative humidity at Limoges-Bellegarde, a predictive model should include wind speed at Limoges Bellegarde and maximum temperature at Saint-Léger-la-Montagne. Backward selection was therefore carried out from a full linear model including these parameters and their first-order interactions using AIC comparison and F-tests.

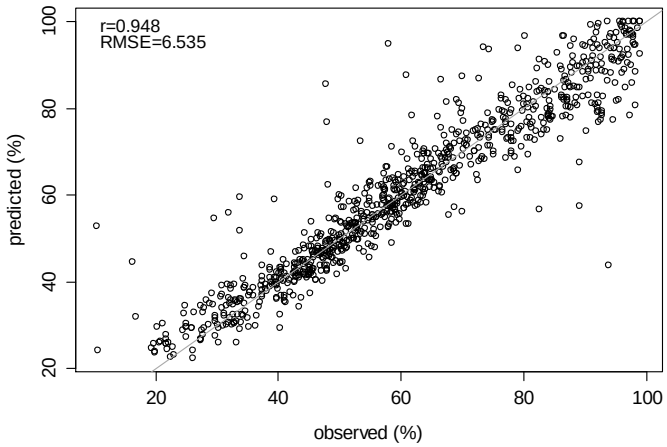

Figure E-28. Predicted vs. observed daily minimum relative humidity at the Dauges site.

The grey line is the identity line.

Residuals from the minimal model were auto-correlated and the model was therefore refitted using generalised least square with an AR-1 auto-correlation structure. The improvement was significant (AIC 6913.0 vs. 7257.7 for the model without auto-correlation structure, F: 41.186, p-value: 2.33e-10), even though there was some minor auto-correlation left in the residuals. Table E-12 shows the terms included in the minimal model (n=832, df=836) and the corresponding coefficients.

Table E-12. Coefficients of the minimal model for daily maximum relative humidity at the Dauges site.

	Value	Std.Error	t-value	p-value
(Intercept)	112.52992	4.328345	25.998371	0
lmgbUX	-0.15261	0.046291	-3.296796	0.001
lmgbFFM	-15.70985	0.808027	-19.442226	0
stlgTX	0.81964	0.140675	5.826479	0
lmgbUX:lmgbFFM	0.16306	0.008856	18.413135	0
lmgbUX:stlgTX	-0.00914	0.001537	-5.95062	0

The interaction terms suggest that maximum relative humidity at the Dauges site and at Limoges-Bellegarde are positively correlated but the strength of that correlation decreases with increasing temperature at Saint-Léger-la-Montagne, and decreasing wind speed at Limoges-Bellegarde. One likely explanation is that higher temperatures promote evapotranspiration in the wetland, where it is not limited by falling soil water content in the summer unlike at Limoges-Bellegarde; while high wind speed increases the mixing of saturated air above the wetland with drier air masses, reducing the local impact of the wetland on relative humidity. Over the 1998-2013 period, the model predicted values higher than 100% in 15 cases, which were corrected back to 100%. The Pearson's correlation coefficient and RMSE of the predicted (after correction) vs. observed values were 0.769 and 2.878 respectively (Figure E-29).

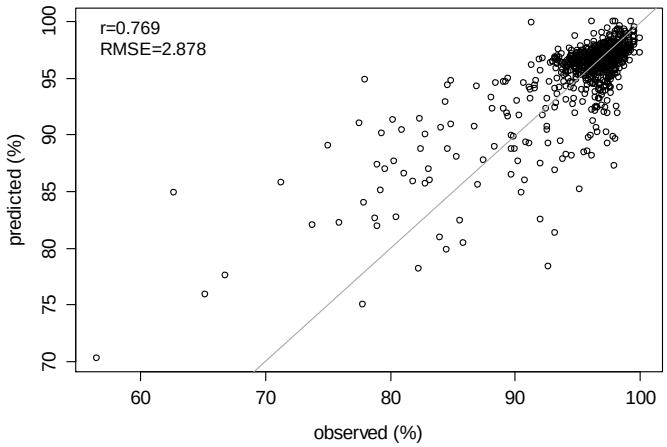

Figure E-29. Predicted vs. observed daily maximum relative humidity at the Dauges site.

The grey line is the identity line.

The correlation is not very good, but, as most of the observed and predicted values are within a relatively small range, the RMSE achieved by the maximum relative humidity model is actually much better than the RMSE of the minimum relative humidity model. The impact on evapotranspiration estimation will therefore be limited.

E.3.4. Precipitation

The quality of the Enerco precipitation dataset was checked by comparing it to data collected using the PM3030 rain gauge installed at the same location between 03/02/2011 and 19/07/2012 as well as daily precipitation recorded by Météo-France at the nearby Saint-Léger-la-Montagne station. This showed that the Enerco rain gauge briefly malfunctioned between 28/04/2012 and 22/05/2012, over- or under-recording rainfall events by as much as 35mm before ceasing measurements completely. Recording then resumed normally. This issue remains unexplained but never recurred. Erroneous data were deleted and replaced with the PM3030 data. Figure E-30 shows that once this issue had been addressed, both time-series were reassuringly similar, including during large rainfall events.

Pearson's correlation coefficient between hourly datasets is slightly lower than between daily datasets, probably due to the fact that the tipping bucket volumes are different. However differences at the 1-hour resolution are averaged out when data are aggregated to daily resolution. The Enerco dataset was used in subsequent analyses as it spans a longer period, and small gaps were in-filled with data from the PM3030 time-series when available.

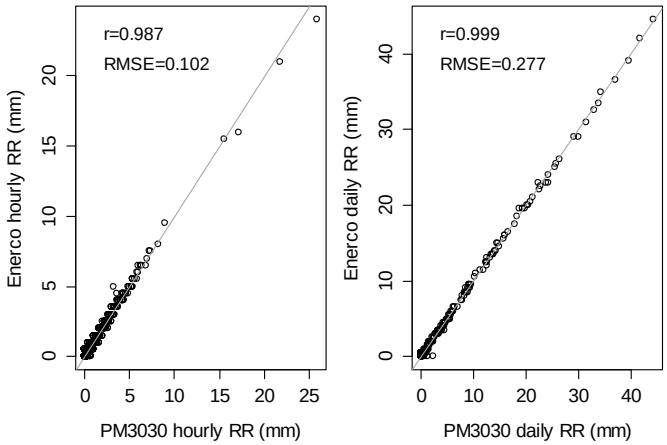

Figure E-30. Scatterplots of hourly and daily precipitation recorded by the Enerco and PM3030 raing gauges at the Dauges site.

The grey line is the identity line.

Rainfall records at the Dauges site were further quality-controlled by comparing them to records obtained from four Météo-France precipitation gauges, one of which (Saint-Léger-la-Montagne) is only 4.2km away from the site. Figure E-31 shows that precipitation records at the Dauges site are very similar to those at the Saint-Léger-la-Montagne station, but there are a few large events when the records at both station differed, in late 2011, early 2012 and possibly early 2013.

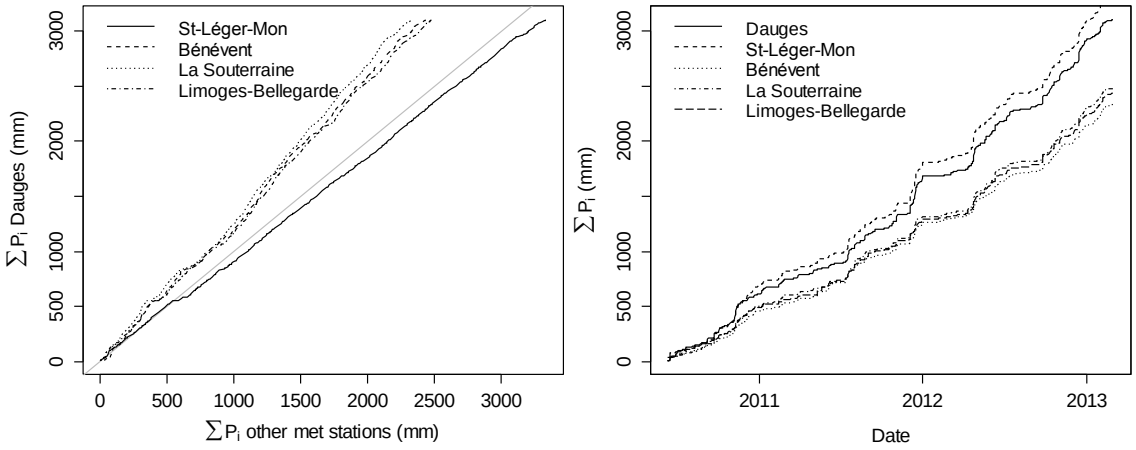

Figure E-31. Double mass curves (left) and cumulative curves (right) of precipitation records at the Dauges site and at nearby Météo-France stations.

Figure E-32 shows that at least some of the discrepancies are due to large snowfall events, for instance in late 2011 and early 2012, as evidenced by an albedo larger than 0.3 being recorded at the Dauges site simultaneously. The rain gauges that were used at the Dauges site were not heated, and as a consequence did not accurately record precipitation in the form of snow.

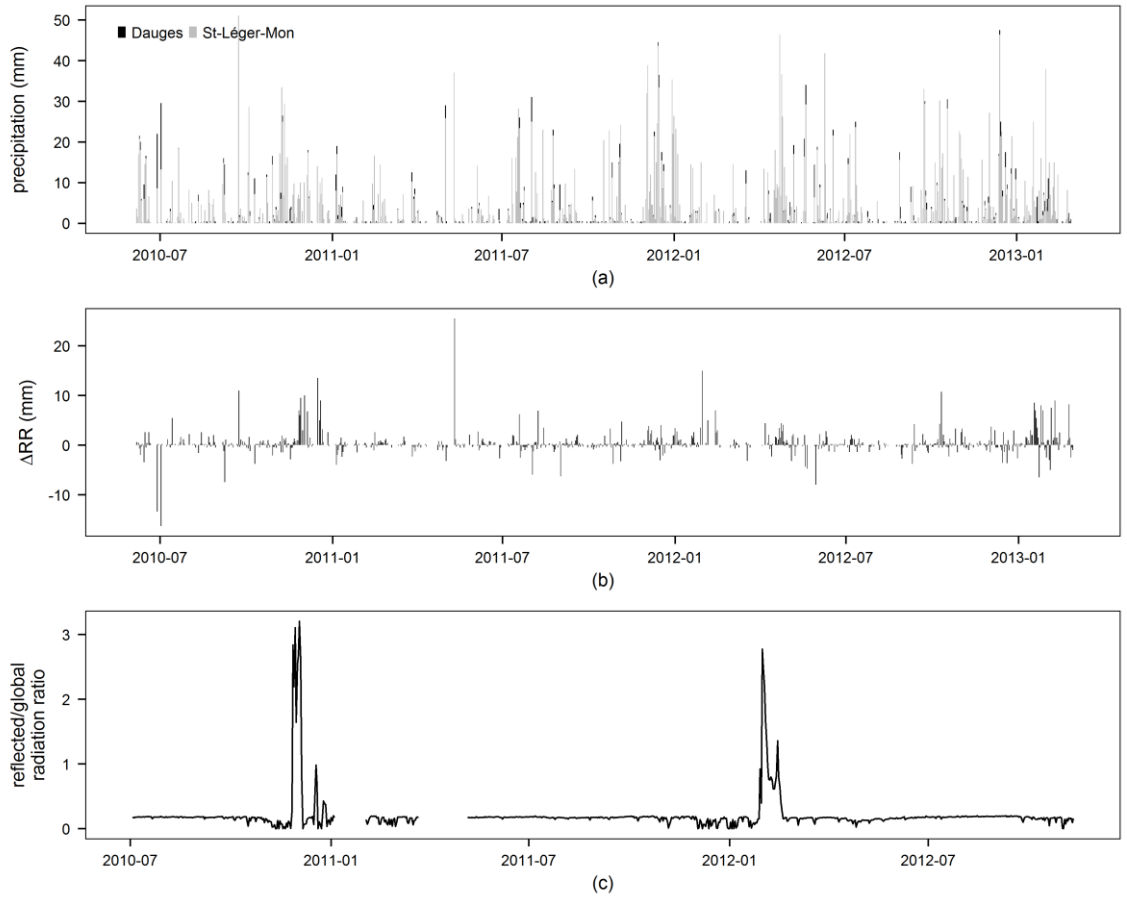

Figure E-32. Impact of snow fall events on the difference between precipitation records at the Dauges site and at the Saint-Léger-la-Montagne station.

(a): precipitation records at the Dauges site and at Saint-Léger-la-Montagne, (b) difference between both time-series, (c) albedo at the Dauges site.

The albedometer at the Dauges site was not operational between 11/11/2012 and 28/02/2013, and it is therefore not possible to attribute large differences observed in early 2013 to snow fall events with absolute certainty, but this is very likely. Precipitation records at the Dauges site that showed large discrepancies with those at Saint-Léger-la-Montagne at times when the albedo records indicated the presence of snow on the ground were therefore deleted (precipitation at the Dauges site was modelled in a second time as a function of precipitation at Saint-Léger-la-Montagne and missing values replaced by values predicted by the model, see Section E.3.7). Figure E-33 shows the corrected Enerco dataset (with missing values). Figure E-34 shows that, expectedly, precipitation at the Dauges site is best correlated with records from the nearest two Météo-France stations, one automatic and the other manual, both located in Saint-Léger-la-Montagne, just 4.2 and 3 km away from the wetland, respectively.

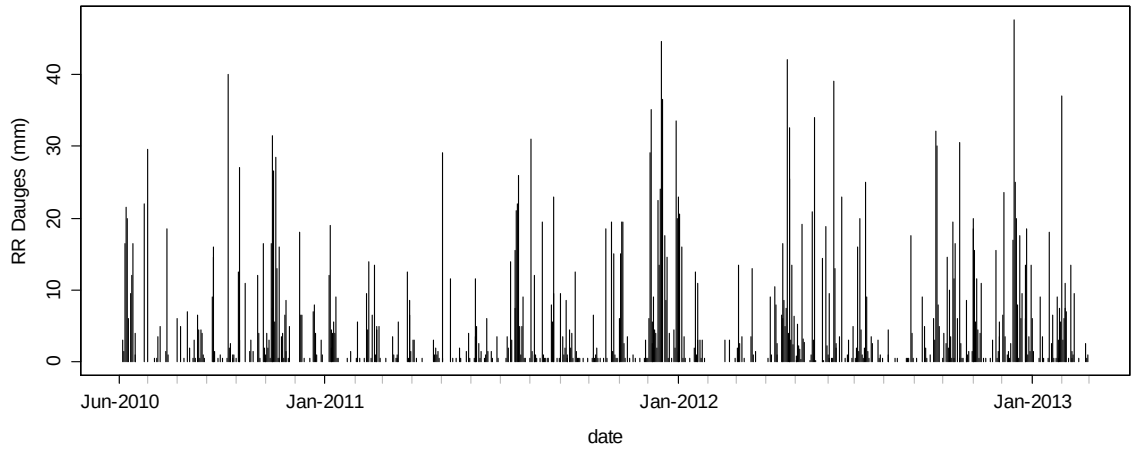

Figure E-33. Daily precipitation at the Dauges site.

Data recorded by the Enerco logger after correction, with missing values.

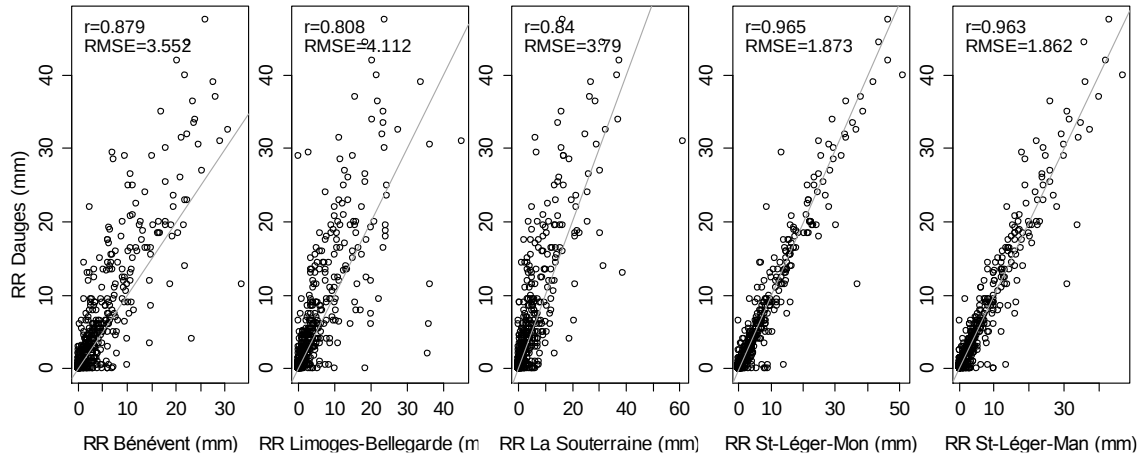

Figure E-34. Scatterplots of precipitation records at the Dauges site against records at nearby Météo-France stations.

The grey line is the identity line.

The correlation is high with both datasets (Pearson's correlation coefficient is 0.965 and 0.963 respectively) and linear, but there is still a fair amount of scatter that might seem surprising for gauges so close to each other. This is unlikely to be due to a fault in the Enerco rain gauge, as demonstrated by the excellent correlation with data from the PM3030 rain gauge at the same location. Instead these differences reflect the relatively high variability of precipitation even at a very local scale, further evidenced by the similar correlation and RMSE found between time-series from the two Météo-France rain gauges at Saint-Léger-la-Montagne, located just 1.6km apart (Figure E-35). However, the slight departure from the identity line during very small precipitation events, already visible when comparing to the PM3030 data, suggests that the Enerco rain gauge may under-record a number of very small rainfall events, possibly due to its larger tipping bucket.

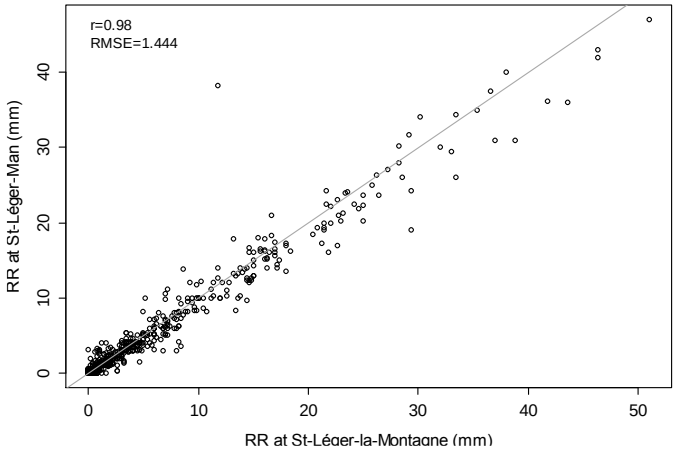

Figure E-35. Scatterplot of precipitation at the two Météo-France rain gauges in Saint-Léger-la-Montagne.

The grey line is the identity line.

The correlation with other Météo-France rain gauges located further away is much poorer, and suggests that the reconstruction of precipitation time-series at the Dauges site should only be based on data from one or another gauge at Saint-Léger-la-Montagne. Data are available for the automatic station since 1998, and for the manual station since 1972 (records are actually available for the later since 1950 but the station was moved in 1972). A preliminary exploratory analysis using regression trees and best subset regression showed that no other predictor could potentially be useful to improve the model. Precipitation in the wetland was therefore modelled as a linear function of precipitation at the Saint-Léger-la-Montagne automatic station. Minor but significant auto-correlation was found in the model residuals, and the model was therefore refitted using Generalised Least Square with an autocorrelation structure of order 1. The improvement was significant (AIC: 3748.41 vs. 3750.54 for the model without auto-correlation structure, L-ratio 4.13077, p-value 0.0421). Table E-13 gives the coefficients of the final model (n=950, df=948). The model suggests that precipitation in the wetland is generally lower than at Saint-Léger-la-Montagne and that this difference increases with the event depth.

Table E-13. Coefficients of the minimal model for daily precipitation at the Dauges site.

	Value	Std.Error	t-value	p-value
(Intercept)	0.0520287	0.06586731	0.7899	0.4298
stlgRR	0.9272792	0.00796819	116.3727	0

This is unlikely to result from an instrumental error caused by the Enerco rain gauge as comparison with the additional PM3030 rain-gauge at the same location showed an excellent agreement of both instruments at daily resolution, including during large events. It is therefore

likely that this difference originates in different topography settings and altitudes, the station at Saint-Léger-la-Montagne being located on a ridge and 110m higher in elevation than the Dauges station. Figure E-36 shows predicted vs. observed values. The Pearson's correlation coefficient and the RMSE were 0.966 and 1.778 respectively.

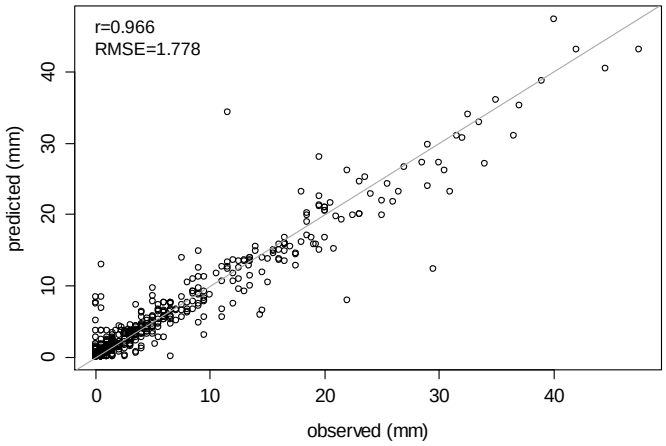

Figure E-36. Observed vs. predicted daily precipitation at the Dauges site.

The grey line is the identity line.

E.3.5. Wind speed

Figure E-37 shows daily mean wind speeds recorded in the wetland. There was no other anemometer within the wetland that could be used to check the accuracy of the dataset. Figure E-38 shows scatterplots of daily mean wind speed recorded in the wetland against those recorded at three nearby Météo-France stations. At the Dauges site, the anemometer was located at 2m above ground in agreement with FAO guidelines for the computation of potential evapotranspiration, whereas it was located at 10m above ground at Météo-France stations, in agreement with WMO guidelines of wind speed measurement alone. As a consequence, no 1:1 relationship was expected. It is possible to make an estimate of the wind speed that would have been measured at 2m at the Météo-France stations based on records at 10m, using the formula given in Allen *et al.* (1998):

$$U_2 = U_z \frac{4.87}{ln(67.8z - 5.42)} \qquad \text{Equation E-7}$$

where U_2 is the wind speed at 2m above ground and U_z the wind speed at z m above ground (here, 10m).

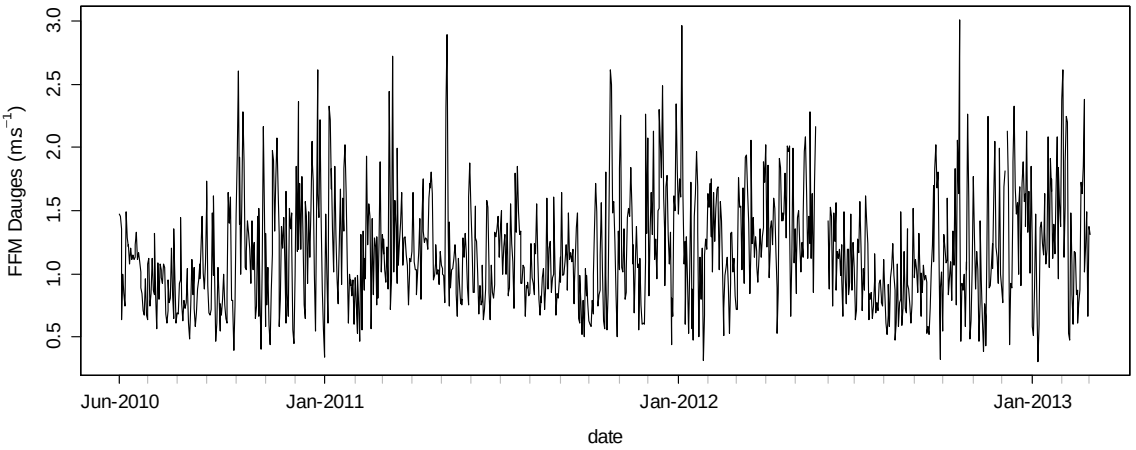

Figure E-37. Daily mean wind speed at the Dauges site.

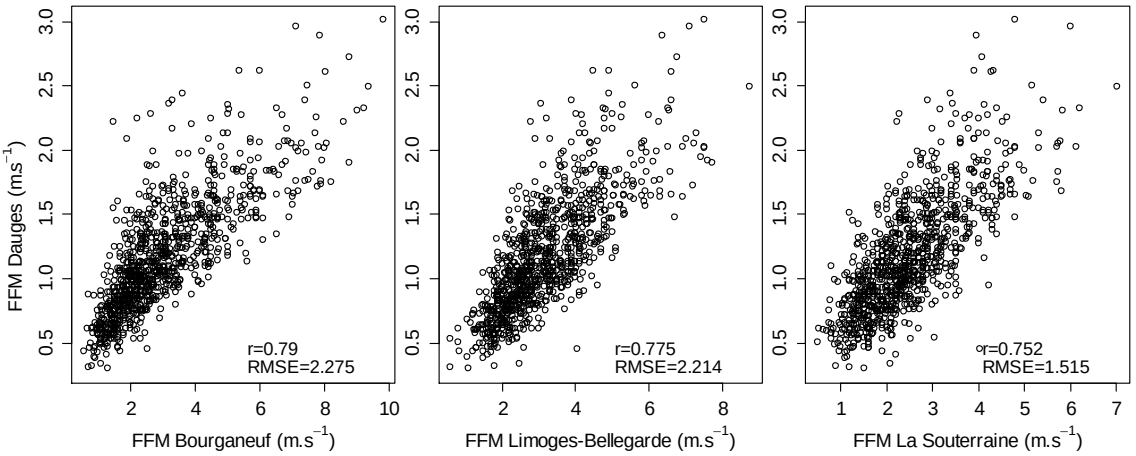

Figure E-38. Scatterplots of daily mean wind speed records at the Dauges site against those at nearby Météo-France stations.

No identity line is drawn as the measuring heights differed between site and no 1:1 relationship is expected.

However, as the aim of the meteorological monitoring is to reconstruct time-series at the Dauges site using longer records from nearby Météo-France stations, that correction was directly accounted for in the model, and was not made on the raw data. Wind speed at the Dauges site was modelled as a function of selected meteorological variables recorded at nearby stations. Preliminary exploratory analysis suggested that, on top of wind speed at Limoges-Bellegarde, the radiation ratio at Limoges-Bellegarde might be a potential predictor. Backwards selection was therefore carried out from a model including these two parameters, their interaction and squared and cubic terms for wind speed as residuals showed that a non-linear relationship might exist. Residuals of the minimal model were significantly auto-correlated, and the model was therefore refitted using Generalised Least Square with an AR-1 auto-correlation structure. The improvement was significant (AIC 213.31 vs. 283.42 for the model without auto-correlation structure, F: 72.11, p-value <0.0001), even though there was some minor auto-correlation left in

the residuals. Table E-14 shows the terms included in the minimal model (n=954, df=950) and the corresponding coefficients.

Table E-14. Coefficients of the minimal model for daily mean wind speed at the Dauges site.

	Value	Std.Error	t-value	p-value
(Intercept)	0.2420137	0.05835021	4.147606	0.00E+00
lmgbFFM	0.3857244	0.02942375	13.109288	0.00E+00
lmgbproprad	-0.189921	0.03387408	-5.606676	0.00E+00
I(lmgbFFM^2)	-0.0150906	0.00373833	-4.036738	1.00E-04

This suggests that, expectedly, wind speed in the wetland increases with wind speed at Limoges-Bellegarde, but less rapidly so at high wind speeds. Wind speed also increases with decreasing radiation ratio. The Pearson's correlation coefficient and RMSE of the predicted vs. observed values were 0.785 and 0.277 respectively (Figure E-39). The model seem to slightly under-predict the largest values but no better model could be found.

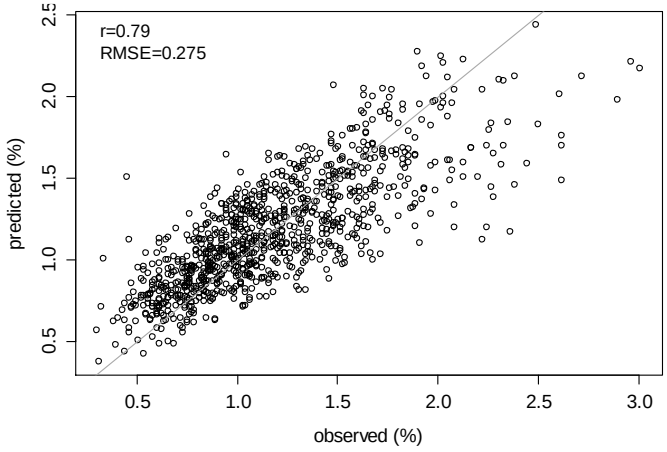

Figure E-39. Predicted vs. observed daily mean wind speed at the Dauges site.

The grey line is the identity line.

E.3.6. Reference evapotranspiration

Reference evapotranspiration time-series computed with different methods are shown in Figure E-40. The computation of ETo using Penman-Monteith methods is constrained by some gaps in radiation and relative humidity time-series at the Dauges site, whereas the Hargreaves-Samani method only uses temperatures and could therefore be computed for most of the study duration. Figure E-41 compares the different time-series using scatterplots, Pearson's correlation coefficient and RMSE. It shows that results obtained from the different Penman-Monteith methods are close to each other, whereas the Hargreaves-Samani method overestimates large values when compared to Penman-Monteith methods.

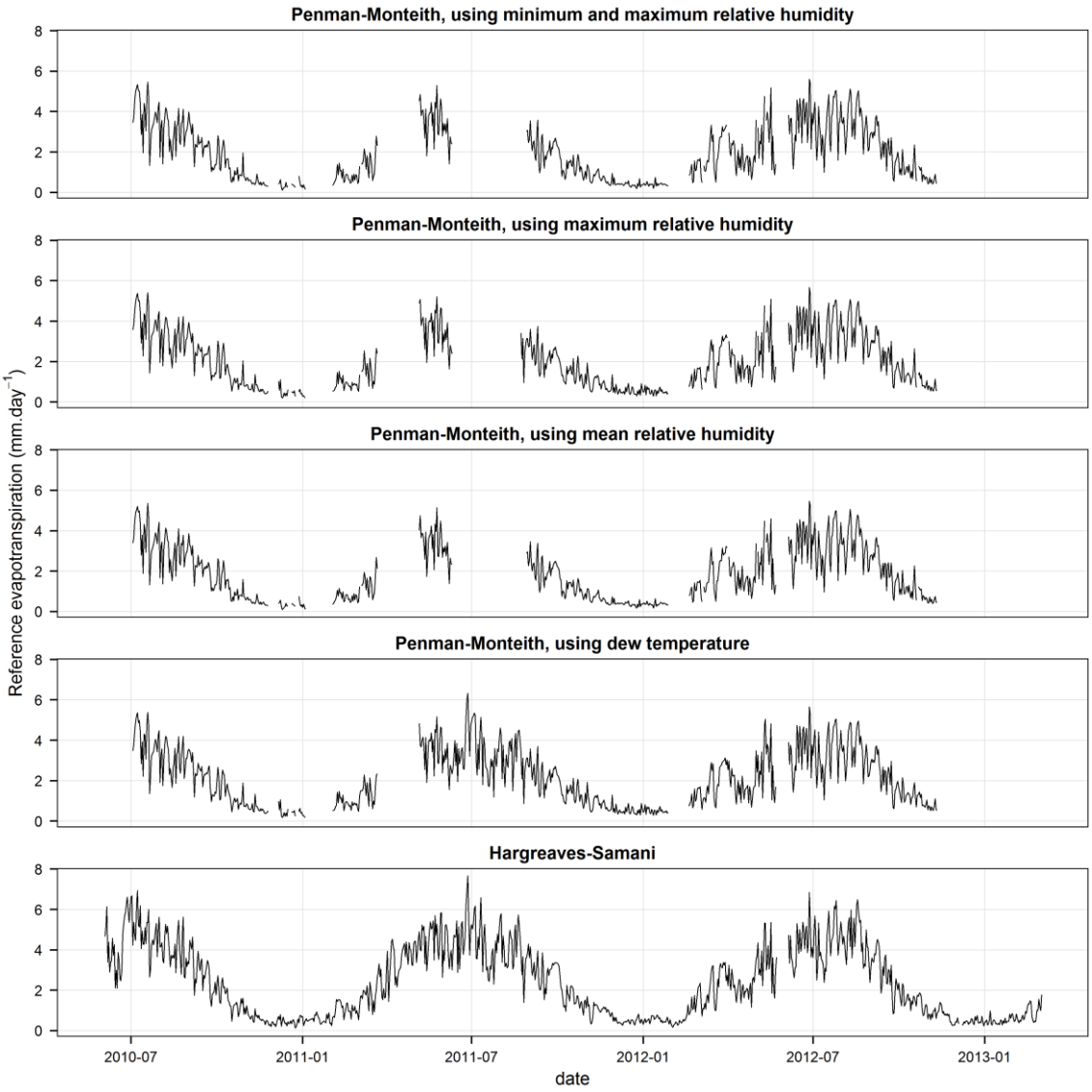

Figure E-40. Reference evapotranspiration at the Dauges site computed using different methods.

One important question concerns the validity of the reference evapotranspiration over the entire catchment, as analysis of the meteorological data has shown that the bottom of the basin is subject to a specific micro-climate caused, it is suggested, mainly by its topographic situation but also by the presence of a permanently shallow groundwater table, minimum temperature and maximum relative humidity records being particularly altered. This issue was therefore investigated by comparing reference evapotranspiration computed using temperature datasets recorded at two different locations: within the wetland and at the nearby Saint-Léger-la-Montagne (Figure E-42).

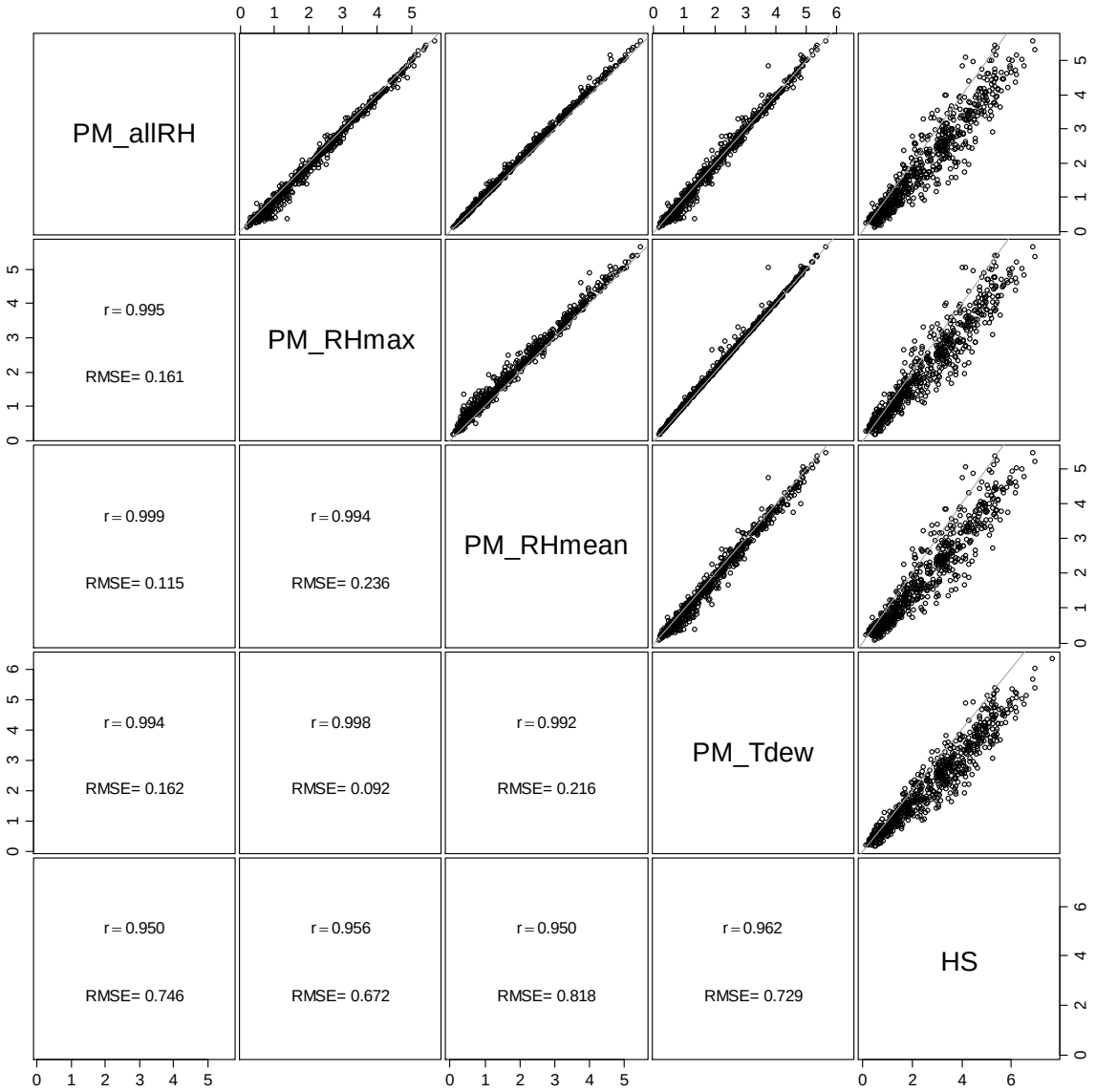

Figure E-41. Scatterplot matrix of reference evapotranspiration at the Dauges site computed using different methods.

PM: FAO Penman-Monteith, with estimation of the actual vapour pressure using: allRH: minimum and maximum relative humidity, RHmax: maximum relative humidity only, RHmean: mean relative humidity, Tdew: temperature records only. HS: Hargreaves-Samani. The grey line is the identity line.

These records were therefore assumed to better reflect conditions in the upper part of the catchment, a very reasonable assumption considering the good fit with data recorded at Les Ribières (Figure E-14). Figure E-42 shows that the use of temperature data from St-Léger does not result in a large difference to reference evapotranspiration estimations for any of the methods.

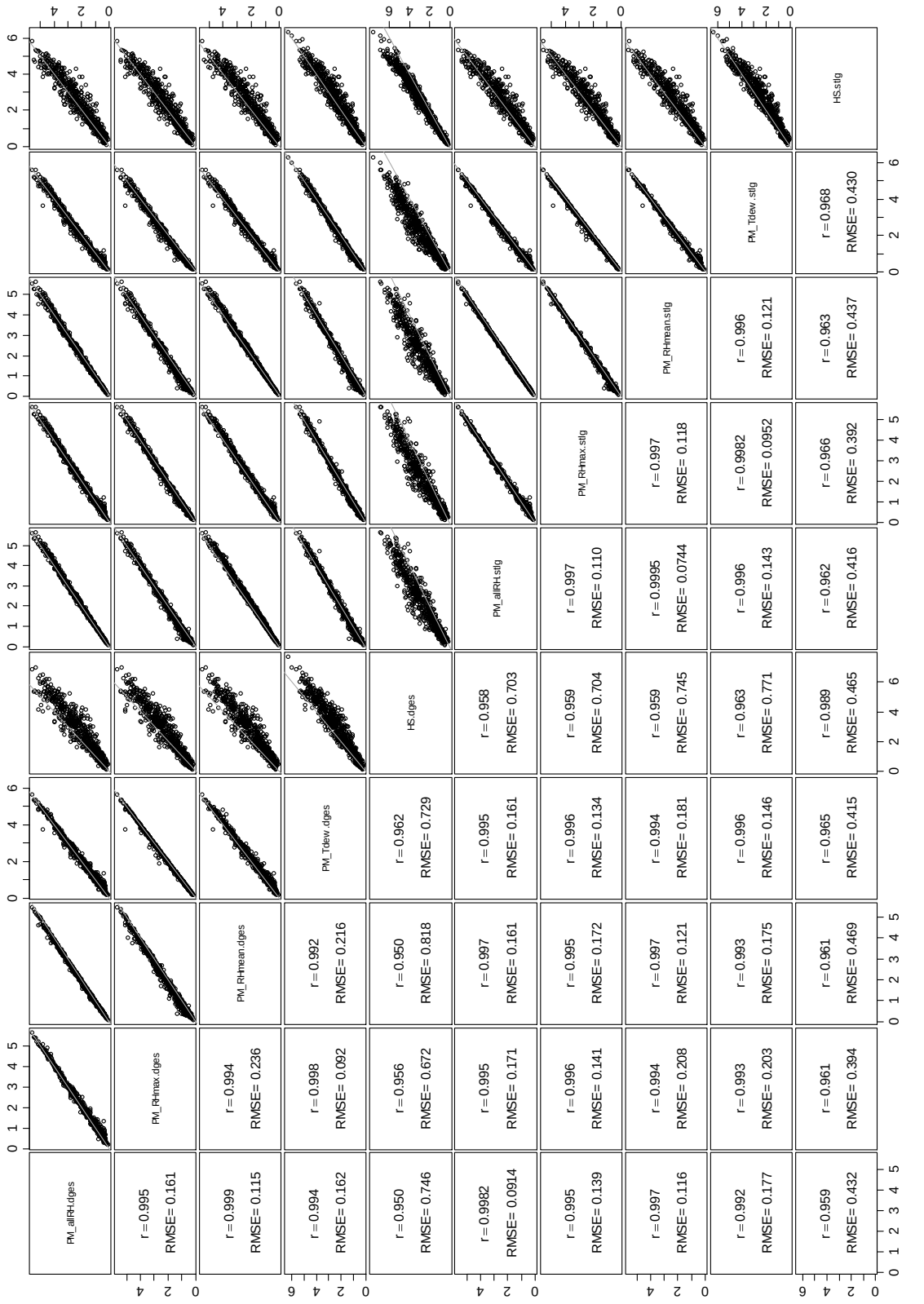

Figure E-42. Scatterplot matrix of different potential evapotranspiration estimations using temperature records from the wetland and from the nearby Météo-France station at Saint-Léger-la-Montagne.

PM: FAO Penman-Monteith, with estimation of the actual vapour pressure using: allRH: minimum and maximum relative humidity, RHmax: maximum relative humidity only, RHmean: mean relative humidity, Tdew: temperature records only. HS: Hargreaves-Samani. The grey line is the identity line.

The smallest differences are when ETo are computed using the Penman-Monteith method with the actual vapour pressure derived from both minimum and maximum relative humidity (r=0.998, RMSE=0.091) and the largest when using the Hargreaves-Samani (r=0.989, RMSE=0.465), due the reliance of the method on temperature records only and its consequent sensitivity to the temperature differential between the wetland and Saint-Léger-la-Montagne station.

Interestingly, ETo computed using the Hargreaves-Samani method is closer to Penman-Monteith ETo at the Dauges site when using temperatures recorded at the St-Léger station (r=0.959, RMSE=0.432) instead of temperatures recorded at the Dauges site itself (r=0.950, RMSE=0.746), probably due to the sensitivity of the method to minimum temperatures. This suggests that, provided the Penman-Monteith method is used, the reference evapotranspiration derived from meteorological data recorded in the wetland can be used for the entire catchment without major errors. This is due to the overriding importance of global radiation in this method.

Another important requirement to be able to run a hydrological model of the Dauges site over long periods concerns the method to use to estimate ETo in the absence of any meteorological data recorded on site. Figure E-43 shows scatterplots of ETo computed using observed data and the Penman-Monteith equation (with actual vapour pressure calculated from minimum and maximum relative humidity) against ETo computed using meteorological data predicted by the models described in the preceding chapters. Figure E-44 shows scatterplots of ETo at the Dauges site computed using observed data and the Penman-Monteith equation (with actual vapour pressure calculated from minimum and maximum relative humidity) against ETo computed using data recorded at Limoges-Bellegarde. The two figures show that the best way to estimate ETo at the Dauges site in the absence of data recorded on site is to use the full Penman-Monteith equation (with actual vapour pressure calculated from minimum and maximum relative humidity) with individual meteorological variables predicted by the models presented in the preceding chapters (r=0.992, RMSE=0.172). Using the Hargreaves-Samani method with reconstructed temperatures overestimates high ETo values and results in a poorer fit than when using the same method with temperatures recorded at Saint-Léger-la-Montagne, due to the sensitivity of the method to lower minimum temperatures at the Dauges site. Calculating ETo at another site and using it to predict ETo at the Dauges site using a linear model for instance would result in a poorer fit as shown by the lower Pearson's correlation coefficient.

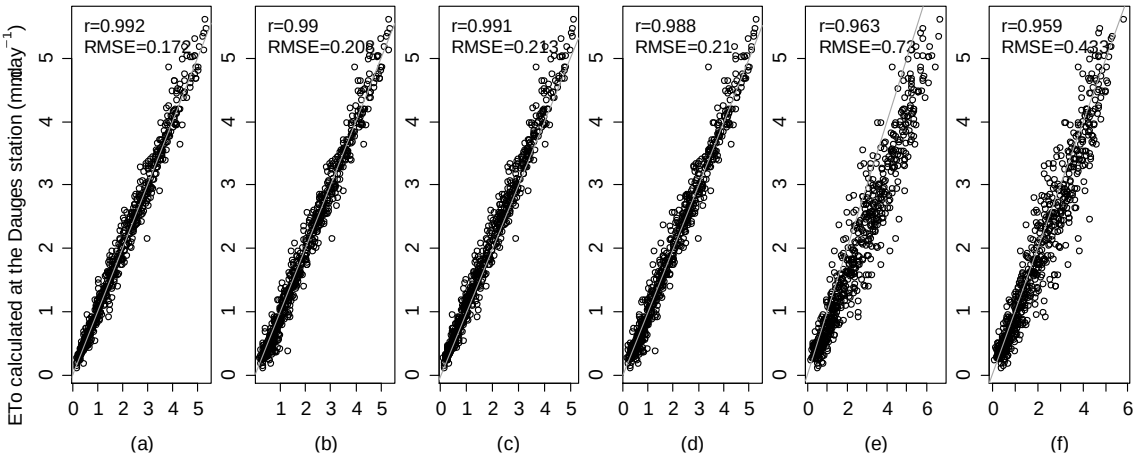

Figure E-43. Scatterplots of reference evapotranspiration derived from observed vs. modelled meteorological time-series at the Dauges site.

(a) : predicted Penman-Monteith ETo (UN & UX), (b): predicted Penman-Monteith ETo (UX), (c): predicted Penman-Monteith ETo ((UN+UX)/2), (d): predicted Penman-Monteith ETo (Tdew), (e): Hargreaves-Samani ETo using predicted temperatures, (f): Hargreaves-Samani ETo using observed temperatures at St-Léger-la-Montagne. The grey line is the identity line.

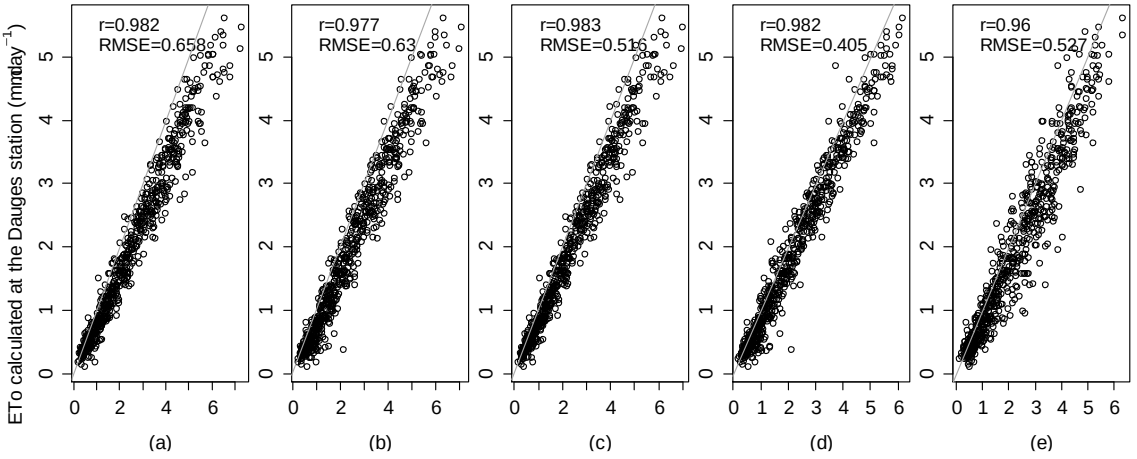

Figure E-44. Scatterplots of reference evapotranspiration derived from observed meteorological data at the Dauges site vs. at Limoges-Bellegarde.

(a) : Penman-Monteith ETo (UN & UX), (b): Penman-Monteith ETo (UX), (c): Penman-Monteith ETo ((UN+UX)/2), (d Penman-Monteith ETo (Tdew), (e): Hargreaves-Samani ETo. ETo at the Dauges site was calculated using the Penman-Monteith equation with actual vapour pressure derived from minimum and maximum relative humidity The grey line is the identity line.

E.3.7. In-filled meteorological data

Meteorological time-series (global shortwave radiation, maximum and minimum temperature, maximum and minimum relative humidity, precipitation, wind speed and FAO Penman-Monteith reference evapotranspiration) were reconstructed at a daily resolution for the period 01/08/1998-31/12/2013 using the best performing models described in the preceding sections. The start of this period corresponds to the opening date of the automatic meteorological station at Saint-Léger-la-Montagne and the earliest availability of local air temperature records.

Precipitation could potentially be reconstructed from as early as 01/10/1950 based on records from the manual station at Saint-Léger-la-Montagne; however the earliest dates at which air temperature records are available is 01/01/1966 (at La Souterraine), while the earliest date at which global radiation, wind speed and relative humidity are available is 01/01/1973 (at Limoges Bellegarde).

In order to run the hydrological model over the duration of the calibration and validation period, missing data in the meteorological records observed at the site from 01/07/2010 to 31/12/2013 were in-filled using values predicted by the statistical models. Figure E-45 shows the observed and in-filled time-series for all meteorological parameters for this period.

E.3.8. Representativeness of the model calibration and validation period in terms of climate

The mean annual precipitation at the Dauges site computed using infilled data over the period 01/07/2010-31/12/2013 and reconstructed data over the period 01/01/1999-30/06/2010 was found to be 1299.2 +/-160.3, slightly below the 1367.1mm mean annual precipitation recorded over the period 1998-2010 at the St-Léger-Mon met station, located at an altitude 112m higher than the Dauges met station. The mean annual FAO Penman-Monteith ETo was 687.6 +/-32.2 mm. The figures were 1226.5mm for mean annual rainfall and 696.2mm for mean annual ETo from 01/01/2011 to 31/12/2013, showing that the model was calibrated and validated in slightly drier conditions than usual. This was particularly the case in 2011 (Table E-15).

Table E-15. Mean annual precipitation and reference evapotranspiration at the Dauges site.

period	1999-2013	2011	2012	2013	2011-2013
mean annual precipitation (mm)	1299.2	1077.0	1368.2	1234.2	1226.5
mean annual reference evapotranspiration (mm)	687.6	734.1	697.3	657.1	696.2

Figure E-46 shows the standardised precipitation-evapotranspiration index (SPEI) at the Dauges site calculated for the 1998-2013 period using the in-filled meteorological data. The SPEI is a simplified water balance based on the difference between monthly precipitation and monthly reference evapotranspiration, aggregated over a user-specified period and standardised (Vicente-Serrano *et al.* 2010). Contrary to the widely used Palmer drought index, it has no fixed time-scale and can be calculated over any aggregation period to characterise drought at different temporal scales. Contrary to the standardised precipitation index, another commonly used drought index, it accounts for both precipitation and potential evapotranspiration.

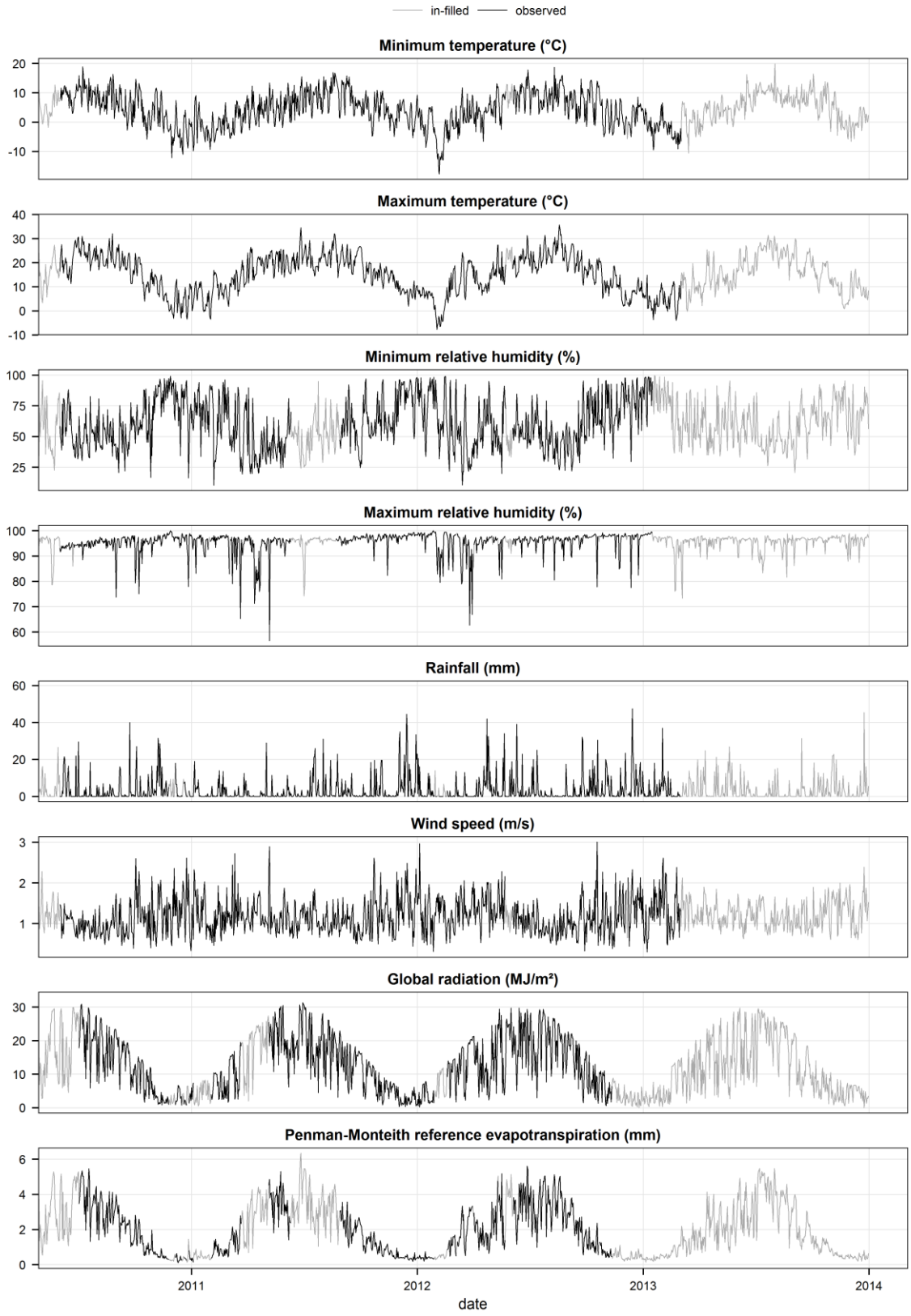

Figure E-45. Observed and in-filled meteorological time-series at the Dauges site.

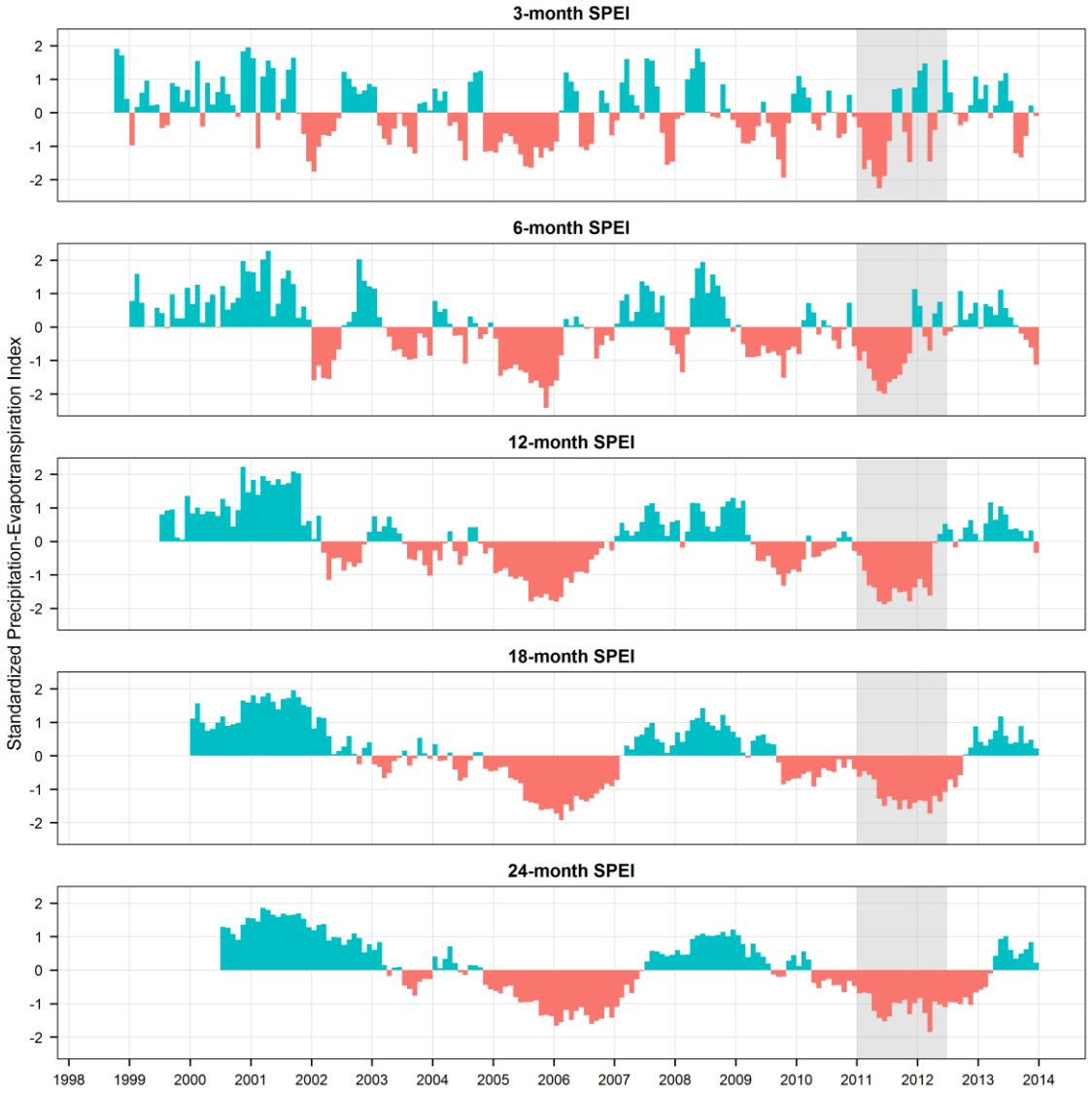

Figure E-46. Standardised Precipitation-Evapotranspiration Index (1998-2013).

The grey band indicates the calibration period of the MIKE SHE model (01/01/2011-30/06/2012). The validation period immediately follows and extends to the end of the meteorological records (01/07/2012-31/12/2013).

The SPEI plot shows that the period during which the meteorological and hydrological datasets were acquired (01/07/2010-31/12/2012) was relatively drier than average: the SPEI (at all temporal scales) is more frequently negative than positive during this period. The MIKE SHE model calibration period (01/07/2010-30/06/2012) coincides with a drought which, relative to the entire 1998-2013 period, was quite severe when the water balance is assessed over a short period (3 months), but not exceptional when it is assessed over a longer aggregation period. In other words it was a pronounced but short drought following a relatively wet period. The validation period (01/07/2012-31/12/2013) coincides with average to slightly wet conditions.

E.4. Conclusion

Meteorological data required to produce daily time-series of precipitation and FAO Penman-Monteith reference evapotranspiration were recorded at the centre of the research site for 2.5 years. Frequent instrument failures required a substantial amount of work to correct or replace erroneous or missing data. It was shown that daily precipitation can be accurately predicted based on data recorded at the closest permanent automatic meteorological station St-Léger-Mon, which opened in August 1998. Despite relatively poor correlations between minimum temperature, maximum relative humidity and wind speed recorded within the research site and those recorded at the closest permanent meteorological stations, it was shown that the later data could be used to accurately predict reference evapotranspiration within the site. This is due to overriding importance of global radiation in the FAO Penman-Monteith formula and the very good correlation between global radiation records within the Dauges site and at the nearest permanent meteorological station recording this parameter.

The climate within the mire is strongly influenced by both the location of the mire at the bottom of a relatively deep etch-basin and the presence of water at ground level for most of the year. Temperature records show minimum temperatures up to 10°C lower in the wetland than on the hill slopes, particularly during clear-sky nights in the absence of wind. This is due to the topographic position of the wetland causing temperature inversions. Wind speeds are considerably lower in the wetland due to its sheltered location. Finally, maximum relative humidity records are often close to saturation, principally due to lower minimum temperatures, but also to the constant availability of water for evapotranspiration and to low wind speeds preventing the redistribution of water towards the upper atmosphere.

The standardised precipitation-evapotranspiration index and the comparison of mean annual precipitation and evapotranspiration recorded during the model calibration and validation period with long-term means show that the model calibration period was relatively dry compared to long-term records. The validation period coincides with average to slightly wet conditions. The acquisition of meteorological records and model calibration and validation over longer periods would therefore improve the confidence in the model predictions.

Appendix F. Characteristics of dipwells and piezometers installed at the Dauges site

Table F-1. Characteristics of dipwells and piezometers installed at the Dauges site.

cluster	ID	type	depth below surface (cm)	total length (cm)	depth below surface of intake top (cm)	depth below surface of intake bottom (cm)	depth below surface of bottom of bentonite seal (cm)	intake in
3	D3-100	dipwell	100	133	0	100	-	peat
3	P3-40	piezometer	40	73	10	40	-	peat
3	P3-190	piezometer	190	223	130	190	-	saprolite
4	D4-70	dipwell	70	103	0	70	-	peat
4	P4-35	piezometer	35	68	10	35	-	peat
4	P4-60	piezometer	60	93	50	60	-	peat
4	P4-85	piezometer	85	118	75	85	-	saprolite
5	D5-30	dipwell	30	63	0	30	-	peat
5	P5-85	piezometer	85	118	40	85	-	saprolite
6	D6-70	dipwell	70	103	0	70	-	peat
7	D7-70	dipwell	70	103	0	70	-	peat
7	D7-130	dipwell	130	163	0	130	-	peat
7	P7-30	piezometer	30	63	5	30	-	peat
7	P7-120	piezometer	120	153	50	120	-	peat
7	P7-190	piezometer	190	223	150	190	-	saprolite
8	D8-100	dipwell	100	133	0	100	-	peat
8	P8-170	piezometer	170	203	150	170	-	gravel
8	P8-237	piezometer	237	270	210	237	-	saprolite
9	D9-130	dipwell	130	153	5	130	5	soil & saprolite
10	D10-120	dipwell	120	143	5	120	5	soil & saprolite
11	D11-120	dipwell	120	143	5	120	-	peat & saprolite
11	P11-30	piezometer	30	53	0	30	-	peat
11	P11-120	piezometer	120	143	70	120	45	saprolite
12	D12-100	dipwell	100	123	0	100	-	peat & saprolite
12	P12-30	piezometer	30	53	5	30	-	peat
12	P12-180	piezometer	180	203	70	180	70	saprolite
13	D13-100	dipwell	100	123	0	100	-	peat & saprolite
13	P13-40	piezometer	40	63	5	40	-	peat
13	P13-80	piezometer	80	103	50	80	-	peat
13	P13-180	piezometer	180	203	100	180	100	saprolite
14	D14-100	dipwell	100	123	0	100	-	peat & saprolite
14	P14-25	piezometer	25	48	5	25	-	peat
14	P14-120	piezometer	120	143	40	120	35	saprolite
15	D15-100	dipwell	100	123	0	100	-	peat
15	P15-100	piezometer	100	123	70	100	-	peat
15	P15-200	piezometer	200	223	130	200	125	saprolite
16	D16-120	dipwell	120	143	0	120	-	peat
16	P16-150	piezometer	150	173	120	150	-	peat
16	P16-325	piezometer	325	348	310	325	305	saprolite
17	D17-120	dipwell	120	143	0	120	-	peat & gravel
18	D18-100	dipwell	100	123	0	100	-	peat
18	P18-270	piezometer	270	293	150	270	150	saprolite
19	D19-50	dipwell	50	73	5	50	-	peat
19	D19-110	dipwell	110	133	0	110	-	peat
19	P19-110	piezometer	110	133	60	110	-	peat
19	P19-220	piezometer	220	243	150	220	145	saprolite
20	D20-30	dipwell	30	53	5	30	-	peat
20	D20-100	dipwell	100	123	0	100	-	peat
20	P20-190	piezometer	190	213	135	190	135	saprolite
21	D21-140	dipwell	140	163	0	140	-	peat
21	P21-310	piezometer	310	333	260	310	250	saprolite
22	D22-130	dipwell	130	153	0	130	-	peat
22	P22-230	piezometer	230	253	190	230	190	saprolite

Table F-1 (continued). Characteristics of dipwells and piezometers installed at the Dauges site.

cluster	ID	type	depth below surface (cm)	total length (cm)	depth below surface of intake top (cm)	depth below surface of intake bottom (cm)	depth below surface of bottom of bentonite seal (cm)	intake in
23	D23-130	dipwell	130	153	0	130	-	peat
23	P23-250	piezometer	250	273	170	250	155	saprolite
24	D24-280	dipwell	280	303	0	280	10	soil & gravel
25	D25-185	dipwell	185	208	0	185	10	soil & gravel
26	D26-90	dipwell	90	113	0	90	10	soil & gravel
PZ1	DZ1	dipwell	80	103	0	80	-	peat
PZ2	DZ2	dipwell	80	103	0	80	-	peat
PZ3	DZ3	dipwell	80	103	0	80	-	peat
PZ4	DZ4	dipwell	80	103	0	80	-	peat
PZ5	DZ5	dipwell	80	103	0	80	-	peat
PZ6	DZ6	dipwell	80	103	0	80	-	peat
PZ1	PZ1	dipwell	95	115	0	95	-	peat and saprolite
PZ2	PZ2	dipwell	245	256	0	245	-	peat and saprolite
PZ3	PZ3	dipwell	170	185	0	170	-	peat
PZ4	PZ4	dipwell	190	200	0	190	-	peat & gravel
PZ5	PZ5	dipwell	150	165	0	150	-	peat & gravel
PZ6	PZ6	dipwell	185	193	0	185	-	peat & gravel

Note: saprolite is here taken in the broad sense, including all compact mineral formations with a texture similar to in-situ saprolite (i.e. with a relatively high silt and clay content). Gravel include all washed sands and gravels of alluvial or colluvial origin.

Appendix G. Published values of evapotranspiration and unsaturated flow parameters

Table G-1. Literature review of crop coefficients relevant to the Dauges site.

vegetation	stand characteristics	Kc ini (or Kc min / Kc winter)	Kc mid (or Kc max / Kc summer)	Kc end	type of data	location	source
Evergreen needle-leaved woodland							
conifer trees	max 10m high, well watered large forests	1	1	1	FAO reference value	subhumid climate	(Allen *et al.* 1998)
conifer forest		1.15	1.15	1.15	proposed model value	UK	(Zhang & Hiscock 2010)
conifer forest		1.01-1.34	1.29-1.38		ET (remote-sensing)/ETref (FAO Penman-Monteith)	southern Spain	(Andreu *et al.* 2012)
Pinus sylvestris		0.71	0.97		calibrated value from soil water balance model (ETref FAO Penman-Monteith)	Belgium	(Verstraeten *et al.* 2005)
Pinus sylvestris		1.07-1.17	1.13-1.18		ET Penman-Monteith/ETref (FAO Penman-Monteith)	Belgium	(Meiresonne *et al.* 2003)
Picea abies plantation		0.7	1.1		calibrated value from soil water balance model (ETref FAO Penman-Monteith)	Denmark	(Salazar *et al.* 2013)
Pseudotsuga menziesii plantation		0.85	0.95		calibrated value from soil water balance model (ETref Makkink)	Belgium	(Tiktak & Bouten 1994)
Pseudotsuga menziesii plantation			0.92		ET (water balance)/Etref (Penman)		(Aussenac & Boulangeat 1980)
Deciduous broad-leaved woodland							
broadleaf forest		0.6	1.15	0.8	proposed model value	UK	(Zhang & Hiscock 2010)
Fagus sylvatica		0.78	0.9		calibrated value from soil water balance model (ETref FAO Penman-Monteith)	Belgium	(Verstraeten *et al.* 2005)
Fagus sylvatica	23 year old		0.91		ET (water balance)/Etref (Penman)		(Aussenac & Boulangeat 1980)
Fagus sylvatica & Quercus robur		0.45	0.95		calibrated value from soil water balance model (ETref FAO Penman-Monteith)	Belgium	(Verstraeten *et al.* 2005)
Fagus sylvatica & Quercus robur			0.61 (annual)		long-term ET (lysimetry)/Etref (FAO Penman-Monteith)	Germany	(Harsch *et al.* 2009)
Quercus petraea	120 year old, LAI=4.38		0.83		ET (water balance)/Etref (Penman-Van Bavel) in the absence of water stress	Fontainebleau, France	(Nizinski & Saugier 1989)
Quercus petraea			0.8		T (sap flow)/Etref (Penman) in the absence of water stress	France	(Bréda & Granier 1996)
Quercus robur		0.75	0.86		calibrated value from soil water balance model (ETref FAO Penman-Monteith)	Belgium	(Verstraeten *et al.* 2005)
Quercus robur plantation		0.4	1		calibrated value from soil water balance model (ETref FAO Penman-Monteith)	Denmark	(Salazar *et al.* 2013)
Quercus robur old forest			0.89 (0.75-0.95)		calibrated value from soil water balance model (Etref modified Penman)	Denmark	(Ladekarl 1998)
Wet woodlands							
Wet woodland (*Salix*)		0.65	2.35		proposed model value	Germany	(Tiemeyer *et al.* 2006)
Salix alba	2-3 year old, unfertilised	0.19	1.25-1.97	0.4	ET (lysimetry)/Etref (FAO Penman-Monteith)	Italy	(Guidi *et al.* 2008)
Salix viminalis	2-5 year-old, 1.9-3.9m, LAI 4-7	0.7-1.0	1.2-1.6	2	ET (Bowen ratio) / Etref (Penman)	Sweden	(Persson & Lindroth 1994)

Table G-1 (continued). Literature review of crop coefficients relevant to the Dauges site.

vegetation	stand characteristics	Kc ini (or Kc min / Kc winter)	Kc mid (or Kc max / Kc summer)	Kc end	type of data	location	source
Pastures and meadows							
grazing pasture	extensive grazing, max 0.1m high	0.3	0.75	0.75	FAO reference value	subhumid climate	(Allen *et al.* 1998)
rye grass hay	averaging cutting effects, max 0.3m high	0.95	1.05	1	FAO reference value	subhumid climate	(Allen *et al.* 1998)
grassland		0.8	0.9	0.85	proposed model value	UK	(Zhang & Hiscock 2010)
grassland			0.5 (annual)		long-term ET (lysimetry)/Etref (FAO Penman-Monteith)	Germany	(Harsch *et al.* 2009)
grassland			1		ET (lysimeter)/Etref (Penman)	UK	(Calder 2003)
oligotrophic grassland	water table maintained at ground level	0.6 (April)	0.9-1.0		ET (lysimeter) /Etref (Penman)	The Netherlands	Janssen, 1994, in (Spieksma *et al.* 1996)
oligotrophic grassland	water table maintained 30cm below ground level	0.5 (April)	0.8-0.9		ET (lysimeter) /Etref (Penman)	The Netherlands	Janssen, 1994, in (Spieksma *et al.* 1996)
Molinia grassland on mineral soil	water table maintained at ground level	0.7 (April)	1.0-1.2		ET (lysimeter) /Etref (Penman)	The Netherlands	Janssen, 1994, in (Spieksma *et al.* 1996)
Molinia grassland on mineral soil	water table maintained 30cm below ground level	0.6 (April)	0.9-1.1		ET (lysimeter) /Etref (Penman)	The Netherlands	Janssen, 1994, in (Spieksma *et al.* 1996)
Heathlands							
dry heathland			0.25-0.5		ET (lysimeter)/Etref (Penman)	UK	(Calder 2003)
Calluna-Deschampsia heathland			1.13 (annual)		calibrated value from soil water balance model (ETref FAO Penman-Monteith)	UK	(Beier *et al.* 2009)
Calluna-Deschampsia heathland			0.63 (annual)		calibrated value from soil water balance model (ETref FAO Penman-Monteith)	DK	(Beier *et al.* 2009)
Calluna-Molinia heathland			0.69 (annual)		calibrated value from soil water balance model (ETref FAO Penman-Monteith)	NL	(Beier *et al.* 2009)
wet heathland		0.6-0.7 (April)	0.8-0.9		ET (lysimetry) / Etref (Penman)	The Netherlands	Eggink & Vink, 1989, in (Spieksma *et al.* 1996)
wet heathland	water table maintained 30cm below ground level	0.5 (April)	0.6		ET (lysimetry) / Etref (Penman)	The Netherlands	Janssen, 1994, in (Spieksma *et al.* 1996)
wet heathland	water table maintained at ground level	0.6 (April)	0.7-0.75		ET (lysimetry) / Etref (Penman)	The Netherlands	Janssen, 1994, in (Spieksma *et al.* 1996)
wet heathland			0.75		ET (lysimetry) / Etref (Penman)	The Netherlands	Bakker, 1984, in (Spieksma *et al.* 1996)
Bogs and acidic fens							
wetland	short vegetation (max 0.3m high), no frost	1.05	1.1	1.1	FAO reference value	subhumid climate	(Allen *et al.* 1998)
open water, <2m deep		NA	1.05	1.05	FAO reference value	subhumid climate	(Allen *et al.* 1998)
C. acutiformis / Sphagnum fen			0.74		ET (lysimetry)/Etref (Penman)	The Netherlands	(Koerselman & Beltman 1988)
Sphagnum-dominated acidic fen			0.2		calibrated value from soil water balance model (ETref Penman)	France	(Binet *et al.* 2013)

Table G-1 (continued). Literature review of crop coefficients relevant to the Dauges site.

vegetation	stand characteristics	Kc ini (or Kc min / Kc winter)	Kc mid (or Kc max / Kc summer)	Kc end	type of data	location	source
Molinia & Betula dominated acidic fen			0.28		calibrated value from soil water balance model (ETref Penman)	France	(Binet *et al.* 2013)
raised bog			0.23		ET (Bowen ratio)/Etref (Penman)	New Zealand	(Campbell & Williamson 1997)
shrub-dominated raised bog			0.52 (0.44-0.59)		ET (eddy covariance)/Etref ratio (Penman-Monteith)	Canada	(Lafleur *et al.* 2005)
moorland			0.25-0.5		ET (lysimeter)/Etref (Penman)	UK	(Calder 2003)
Sphagnum-dominated raised bog			0.74		ET (Bowen ratio)/Etref (Penman)	Sweden	(Kellner 2001a)
Sphagnum dominated acidic fen			1		ET/Etref (Penman)	Minnesota	(Kim & Verma 1996)
Molinia-dominated raised bog			1		ET (lysimetry)/Etref (Makkink)	The Netherlands	(Schouwenaars 1993)
grassland & small-sedge communities		1	1.1		proposed model value	Germany	(Tiemeyer *et al.* 2006)
Sphagnum-dominated raised bog			0.72		ET (Bowen ratio)/ Etref (Penman)	Belgium	(Wastiaux 2000)
Molinia-dominated raised bog			0.98		ET (Bowen ratio)/ Etref (Penman)	Belgium	(Wastiaux 2000)
graminoïd-dominated peatland			0.9		model value, chosen from literature		(Heijmans *et al.* 2008)
ericoïd-dominated peatland			0.7		model value, chosen from literature		(Heijmans *et al.* 2008)
hummock *Sphagna*			1.4		model value, chosen from literature		(Heijmans *et al.* 2008)
lawn *Sphagna*			1.3		model value, chosen from literature		(Heijmans *et al.* 2008)
hollow *Sphagna*			1.2		model value, chosen from literature		(Heijmans *et al.* 2008)
short fen vegetation			0.8		recommended value based on literature survey		(Spieksma *et al.* 1996)
sedge-dominated fen	average of vegetated and non-vegetated periods		0.9		ET (Bowen ratio) / Etref (Penman)	Ontario, Canada	(Lafleur 1990)
sedge-dominated fen	non-vegetated period	0.85	1.02		ET (Bowen ratio) / Etref (Penman)	Ontario, Canada	(Lafleur 1990)
Shagnum-dominated poor fen			0.73		ET (Bowen ratio) / Etref (Penman)	Ontario, Canada	(Lafleur & Roulet 1992)
Sphagnum sp.			0.67		ET (lysimeter)/Etref (Penman)	The Netherlands	Wirdum (1991), in (Spieksma *et al.* 1996)
Polytrichum sp.			0.45		ET (lysimeter)/Etref (Penman)	The Netherlands	Wirdum (1991), in (Spieksma *et al.* 1996)
Molinia-dominated bog		0.40-0.45	0.75-0.85		ET (lysimeter) /Etref (Penman)	The Netherlands	Schouwenaars, 1990, 1993, in (Spieksma *et al.* 1996)
Sphagnum-dominated bog			1.2		ET (lysimeter) /Etref (Penman)	Ireland	Sijtsma and Veldhuizen, 1992, in (Spieksma *et al.* 1996)
Eriophorum vaginatum-dominated bog			1		ET (lysimeter) /Etref (Penman)	Ireland	Sijtsma and Veldhuizen, 1992, in (Spieksma *et al.* 1996)
Erica tetralix-dominated bog			1		ET (lysimeter) /Etref (Penman)	Ireland	Sijtsma and Veldhuizen, 1992, in (Spieksma *et al.* 1996)

Table G-1 (continued). Literature review of crop coefficients relevant to the Dauges site.

vegetation	stand characteristics	Kc ini (or Kc min / Kc winter)	Kc mid (or Kc max / Kc summer)	Kc end	type of data	location	source
Narthecium-dominated bog			0.9		ET (lysimeter) /Etref (Penman)	Ireland	Sijtsma and Veldhuizen, 1992, in (Spieksma *et al.* 1996)

Table G-2. Literature review of leaf area index (LAI) values used in hydrological modelling or measured in contexts similar to the Dauges site.

vegetation class	max LAI	min LAI (winter)	nb of studies reviewed	location	type of data	source
Evergreen needle-leaved woodland						
-	5		NA	global	proposed model parameter	(Asensio 1998)
-	6	0.5	NA	global	proposed model parameter	(Dickinson *et al.* 1993)
-	5.3		1	Germany	measured	(Leuschner 2002)
-	5.5		215	temperate zone	measured	(Scurlock *et al.* 2001; Asner *et al.* 2003)
-	2.65	2.65	NA	United Kingdom	proposed model parameter	(Rochester 2010)
Pseudotsuga menziesii	8.1		16	temperate zone	measured	(Scurlock *et al.* 2001; Asner *et al.* 2003)
Pseudotsuga menziesii	9.65 (min: 5.1, max: 15.5)		8	temperate zone	measured	(Breuer *et al.* 2003)
Pseudotsuga menziesii	6		NA	France	measured	(Bréda & Roman-Amat 2002)
Pseudotsuga menziesii (25 year-old)	7.6		1	The Netherlands	measured	(Bartelink 1998)
Pseudotsuga menziesii (74 year-old)	5.1		1	The Netherlands	measured	(Bartelink 1998)
Pseudotsuga menziesii (26 year-old)	7.8		1	Canada	measured	(Chen & Black 1991)
Pseudotsuga menziesii plantation	13	9	1	The Netherlands	measured	(Klaassen *et al.* 1998)
Pseudotsuga menziesii plantation	11		1	The Netherlands	measured	(Tiktak & Bouten 1994)
Pinus sylvestris	8.7		12	Europe	measured	(Scurlock *et al.* 2001; Asner *et al.* 2003)
Pinus sylvestris	3.8 (min: 1.1, max: 7.2)		14	temperate zone	measured	(Breuer *et al.* 2003)
Pinus spp.	4		NA	France	measured	(Bréda & Roman-Amat 2002)
young birch-pine forest	4		1	Germany	measured	(Leuschner 1993)
Deciduous broad-leaved woodland						
-	4	0	NA	United Kingdom	proposed model parameter	(Rochester 2010)
-	6	1	NA	global	proposed model parameter	(Dickinson *et al.* 1993)
-	5.1		187	temperate zone	measured	(Scurlock *et al.* 2001; Asner *et al.* 2003)
closed canopy	6		NA	global	proposed model parameter	(Asensio 1998)
open canopy	4		NA	global	proposed model parameter	(Asensio 1998)
Quercus & *Fagus* mature forest	5.3		1	Germany	measured	(Leuschner 2002)
Quercus & *Fagus* forest	5.3		1	Germany	measured	(Leuschner & Rode 1999)
Quercus & *Fagus* forest	4.5		1	Germany	measured	(Leuschner 1993)
Quercus robur	5.2		4	Europe	measured	(Scurlock *et al.* 2001; Asner *et al.* 2003)
Quercus robur	4.6		1	temperate zone	measured	(Breuer *et al.* 2003)
Quercus robur forest	3.9	1.5	1	Hungary	measured	(Móricz *et al.* 2012)
Quercus robur forest	4.7		1	Denmark	measured	(Rosenqvist *et al.* 2010)
Quercus spp.	4.5		NA	France	measured	(Bréda & Roman-Amat 2002)
Quercus robur & *petraea* old forest	4		1	Denmark	measured	(Ladekarl *et al.* 2005)
Quercus robur/petraea (mature)	5.5		1	France	measured	Le Dantec et al., 2000, in (Breuer & Frede 2003)
Quercus petrea (35 year-old, thinned)	3.3		1	France	measured	(Bréda & Granier 1996)

Table G-2 (continued). Literature review of leaf area index (LAI) values used in hydrological modelling or measured in contexts similar to the Dauges site.

vegetation class	max LAI	min LAI (winter)	nb of studies reviewed	location	type of data	source
Quercus petrea (35 year-old, unthinned)	6		1	France	measured	(Bréda & Granier 1996)
Fagus sylvatica forest		1.1	NA	temperate zone	measured	(Breuer *et al.* 2003)
Fagus sylvatica	5.4		11	temperate zone	measured	(Scurlock *et al.* 2001; Asner *et al.* 2003)
Fagus sylvatica	6.4 (min: 4, max: 10)		16	temperate zone	measured	(Breuer *et al.* 2003)
Fagus sylvatica	5.5-6		NA	France	measured	(Bréda & Roman-Amat 2002)
Fagus sylvatica (62 year-old)	7.4		1	The Netherlands	measured	(Bartelink 1998)
Fagus sylvatica (47 year-old)	6.8		1	Italy	measured	(Cutini *et al.* 1998)
Fagus sylvatica (47 year-old, thinned)	5.9		1	Italy	measured	(Cutini *et al.* 1998)
Fagus sylvatica (90 year-old)	4.9		1	Italy	measured	(Cutini *et al.* 1998)
Fagus sylvatica (30 year-old)	6.0		1	Alsace, France	measured	(Granier *et al.* 2000)
Castanea sativa	5.6		1	temperate zone	measured	(Scurlock *et al.* 2001; Asner *et al.* 2003)
Castanea sativa	5		NA	France	measured	(Bréda & Roman-Amat 2002)
Castanea sativa (40yr, thinned)	4.1		1	temperate zone	measured	(Breuer *et al.* 2003)
Mixed woodland						
-	5		NA	global	proposed model parameter	(Asensio 1998)
-	6	0.5	NA	global	proposed model parameter	(Dickinson *et al.* 1993)
Wet woodland						
Betula pubescens	1.57		1	Greenland	measured	(Scurlock *et al.* 2001; Asner *et al.* 2003)
Betula pubescens	3.0		1	Sweden	measured	(Johansson 1999)
Betula pendula (18 year-old)	5.3		1	Russia	measured	Rauner, 1976, in (Breuer & Frede 2003)
Betula pendula	2.9		1	Sweden	measured	(Johansson 1999)
Pastures and meadows						
-	1.1	1.1	NA	United Kingdom	proposed model parameter	(Rochester 2010)
-		0.3-2	NA	temperate zone	measured	(Breuer *et al.* 2003)
Tall grass	6	0.5	NA	global	proposed model parameter	(Dickinson *et al.* 1993)
Short grass	2	0.5	NA	global	proposed model parameter	(Dickinson *et al.* 1993)
Dactylis glomerata	6.4		1	New Zealand	measured	(Brougham 1960)
Lolium perenne	6		1	New Zealand	measured	(Brougham 1960)
Festuca rubra, Alopecurus pratensis, Poa pratensis (fertilised)	3		1	Germany	measured	Geyger, 1977, in (Breuer & Frede 2003)
Festuca rubra, Alopecurus pratensis, Poa pratensis (fertilised)	6		1	Germany	measured	Geyger, 1977, in (Breuer & Frede 2003)
Nardus-dominated grassland	3.7		1	Italy	measured	Wohlfahrt et al., 2001, in (Breuer & Frede 2003)
Heathlands						
-	1	1	NA	United Kingdom	proposed model parameter	(Rochester 2010)
-	2		NA	Europe	proposed model parameter	MIKE SHE default
-	2.5		1	Denmark	measured	(Ladekarl *et al.* 2001)
-	1.7		1	Germany	measured	(Leuschner 2002)
-	1.3		1	Germany	measured	(Leuschner 1993)
-	2.5		1	Denmark	measured	(Ladekarl *et al.* 2005)
Calluna-dominated heathland	1.7		1	Germany	measured	(Leuschner & Rode 1999)
Calluna vulgaris	2.6		1	Austria	measured	(Scurlock *et al.* 2001; Asner *et al.* 2003)
Calluna vulgaris	1.6-1.7 (+dead leaves 0.3-0.4)		1	United Kingdom	measured	(Calder *et al.* 1984)

Table G-2 (continued). Literature review of leaf area index (LAI) values used in hydrological modelling or measured in contexts similar to the Dauges site.

vegetation class	max LAI	min LAI (winter)	nb of studies reviewed	location	type of data	source
Calluna & *Vaccinium* dominated clear-cut in sub-boreal forest, with 2 year old pine-birch growth	1.3-1.6		1	Estonia & Sweden	measured	(Kuusk *et al.* 2004)
Vaccinium myrtillus	2		1	Austria	measured	Vareschi, 1951, in (Breuer & Frede 2003)
Pteridium aquilinum	1.63		1	United Kingdom	measured	Leyton et al., 1967, in (Breuer & Frede 2003)
Bogs and acidic fens						
Carex rostrata (fertilised, 33 kg N/ha)	2.1		1	The Netherlands	measured	(Aerts & de Caluwe 1994)
Narthecium-dominated bog	1.4	0	4	Ireland	measured	(Sijtsma & Veldhuizen 1992)
Sphagnum	1.02		1	Estonia & Sweden	measured	(Kuusk *et al.* 2004)
Sphagnum-dominated bog	0.25-0.4	0.05-0.15	1	France	measured (read from graph)	(Bortoluzzi *et al.* 2006)
Sphagnum-dominated open fen	0.4-0.7		NA	Minnesota	measured	(Kim & Verma 1996)
bog hollows (*Sphagnum* + sedges)	1.3-2		1	Michigan	measured	(Moore *et al.* 2013)
bog hummocks (*Sphagnum* + chamaephytes)	1.5-2.7		1	Michigan	measured	(Moore *et al.* 2013)
Sphagnum-Eriophorum bog	1.2	0.7	4	Ireland	measured	(Sijtsma & Veldhuizen 1992)
Sphagnum, E. vaginatum & *C. vulgaris* raised bog	0.3		1	Sweden	measured	(Kellner 2001a)
E. vaginatum-dominated bog	0.6-0.9	0	1	France	measured (read from graph)	(Bortoluzzi *et al.* 2006)
Eriophorum vaginatum	2.7		1	Japan	measured	Kimura et al., 1999, in (Breuer & Frede 2003)
Tussocky, *Molinia*-dominated peat bog	1.7	0	1	The Netherlands	measured	(Nieveen *et al.* 1998)
Molinia coerulea	2.4		1	United Kingdom	measured	Leyton et al., 1967, in (Breuer & Frede 2003)
Molinia-dominated raised bog	3	0	1	The Netherlands	measured	(Spieksma *et al.* 1997)
Molinia-dominated raised bog	5	0	1	Belgium	measured	(Wastiaux 2000)

Table G-3. Literature review of rooting depth values used in hydrological modelling or measured in contexts similar to the Dauges site.

vegetation class	root depth	nb of studies reviewed	location	type of data	source
Evergreen needle-leaved woodland					
-	2	NA	United Kingdom	proposed model parameter	(Zhang & Hiscock 2010)
-	1.5	NA	global	proposed model parameter	(Dickinson *et al.* 1993)
-	1.5	NA	global	proposed model parameter	(Walter 2012)
-	0.6	NA	global	proposed model parameter	(Asensio 1998)
-	2	NA	United Kingdom	proposed model parameter	(Zhang & Hiscock 2010)
-	1	NA	United Kingdom	proposed model parameter	(Rochester 2010)
-	3.9 +/- 0.4 m	NA	temperate zone	measured	(Canadell *et al.* 1996)
-	2.1 ± 1.3	NA	temperate zone	measured	(Breuer *et al.* 2003)
Pinus sylvestris	1.74 (min: 1.4, max: 2.5)	5	temperate zone	measured	(Breuer *et al.* 2003)
Pinus sylvestris	2.7	1	United Kingdom	measured	(Canadell *et al.* 1996)
Deciduous broad-leaved woodland					
-	2	NA	United Kingdom	proposed model parameter	(Zhang & Hiscock 2010)
-	2	NA	global	proposed model parameter	(Dickinson *et al.* 1993)
-	1.5	NA	global	proposed model parameter	(Walter 2012)
-	1	NA	United Kingdom	proposed model parameter	(Rochester 2010)
-	2.9 +/- 0.2 m	NA	temperate zone	measured	(Canadell *et al.* 1996)
-	1.9±1.8	NA	temperate zone	measured	(Breuer *et al.* 2003)
closed canopy	1	NA	global	proposed model parameter	(Asensio 1998)
open canopy	2	NA	global	proposed model parameter	(Asensio 1998)

Table G-3 (continued). Literature review of rooting depth values used in hydrological modelling or measured in contexts similar to the Dauges site.

vegetation class	root depth	nb of studies reviewed	location	type of data	source
Fagus sylvatica	1.75 (min: 0.6, max: 3.4)	6	temperate zone	measured	(Breuer *et al.* 2003)
Quercus robur	1.4 (min: 1.3, max: 1.6)	3	temperate zone	measured	(Breuer *et al.* 2003)
Mixed woodland					
-	2	NA	global	proposed model parameter	(Dickinson *et al.* 1993)
-	1.5	NA	global	proposed model parameter	(Walter 2012)
-	0.8	NA	global	proposed model parameter	(Asensio 1998)
Wet woodland					
Betula verrucosa	1.8 (min: 0.5, max: 4)	14	temperate zone	measured	(Breuer *et al.* 2003)
Pastures and meadows					
-	1	NA	United Kingdom	proposed model parameter	(Zhang & Hiscock 2010)
-	0.6	NA	global	proposed model parameter	(Walter 2012)
-	0.1	NA	United Kingdom	proposed model parameter	(Rochester 2010)
-	0.9 ± 0.6	NA	temperate zone	measured	(Breuer *et al.* 2003)
-	2.6 +/- 0.2m	NA	temperate zone	measured	(Canadell *et al.* 1996)
Heathlands					
-	0.2	NA	United Kingdom	proposed model parameter	(Rochester 2010)
-	0.4	NA	Europe	proposed model parameter	MIKE SHE default
-	0.6	1	Denmark	measured	(Ladekarl *et al.* 2001)
Bogs and acidic fens					
Eriophorum vaginatum	0.6	1	Alaska	measured	(Canadell *et al.* 1996)
Eriophorum vaginatum	0.6	1	-	measured	Boggie et al., 1958, in (Wastiaux 2000)
Eriophorum vaginatum	0.3-0.4	1	-	measured	Metsävaino, 1931, in (Wastiaux 2000)
Calluna vulgaris & Erica tetralix	0.1-0.2	1	-	measured	Boggie et al., 1958, in (Wastiaux 2000)
Andromeda polifolia	0.1-0.15	1	-	measured	Metsävaino, 1931, in (Wastiaux 2000)

Table G-4. Literature review of mean leaf resistance (r_l) values used in hydrological modelling or measured in contexts similar to the Dauges site.

Vegetation class	mean leaf resistance ($s.m^{-1}$)*	minimum leaf resistance ($s.m^{-1}$)*	location	type of data	source
Evergreen needle-leaved woodland					
-		200		proposed model parameter	(Dickinson *et al.* 1993)
Pseudotsuga menziesii		120-300		tabulated	(Allen *et al.* 1996)
Pseudotsuga menziesii		300	USA	Measured	(Running 1976)
Pseudotsuga menziesii		330		measured	(Jarvis 1976)
Pseudotsuga menziesii	588		USA	measured	Körner et al., 1979, in (Breuer & Frede 2003)
Pseudotsuga menziesii (seedlings)	303			measured	Körner et al., 1979, in (Breuer & Frede 2003)
Pseudotsuga menziesii	434		USA	measured	(Zhang *et al.* 1993)
Pseudotsuga menziesii	374		Canada	measured	(Warren *et al.* 2003)
Pseudotsuga menziesii		59	Canada	measured	McNaughton & Black, 1973, in (Kelliher *et al.* 1995)
Pseudotsuga menziesii		63	Canada	measured	Price & Black, 1990, in (Kelliher *et al.* 1995)
Pseudotsuga menziesii (seedlings)		417		measured	(Johnson & Ferrell 1983)
Pinus sylvestris (1 yr old needles)	667		Austria	measured	Körner et al., 1979, in (Breuer & Frede 2003)
Pinus sylvestris (current needles)	625		Austria	measured	Körner et al., 1979, in (Breuer & Frede 2003)
Pinus sylvestris (1 yr old needles)	588		Austria	measured	Körner et al., 1979, in (Breuer & Frede 2003)
Pinus sylvestris	194			measured	Sandford and Jarvis, 1986, in (Breuer & Frede 2003)
Pinus sylvestris	135			measured	Sandford and Jarvis, 1986, in (Breuer & Frede 2003)

Table G-4 (continued). Literature review of mean leaf resistance (r_l) values used in hydrological modelling or measured in contexts similar to the Dauges site.

Vegetation class	mean leaf resistance (s.m^{-1})*	minimum leaf resistance (s.m^{-1})*	location	type of data	source
Pinus sylvestris		43	Sweden	measured	(Cienciala *et al.* 1992)
Pinus sylvestris		330	Finland	calibrated model parameter	(Rannik *et al.* 2002)
Pinus sylvestris	283		Finland	measured	(Medlyn *et al.* 2001)
Pinus sylvestris		20	France	measured	(Adriaenssens *et al.* 2012)
Pinus sylvestris	513		Norway	measured	(Beerling 1999)
Deciduous broad-leaved woodland					
-		150		tabulated	(Allen *et al.* 1996)
-		200		proposed model parameter	(Dickinson *et al.* 1993)
Fagus sylvatica	500		Germany	measured	Körner et al., 1979, in (Breuer & Frede 2003)
Fagus sylvatica	357		Austria	measured	Körner et al., 1979, in (Breuer & Frede 2003)
Fagus sylvatica		36	France	measured	(Adriaenssens *et al.* 2012)
Fagus sylvatica (mature)	482		Germany	measured	(Keitel *et al.* 2003)
Fagus sylvatica (seedling)	342		France	measured	(Epron *et al.* 1995)
Fagus sylvatica	502		Germany	measured	(Medlyn *et al.* 2001)
Fagus sylvatica	229		Denmark	measured	(Medlyn *et al.* 2001)
Quercus petraea (no hydric stress)	192		UK	measured	(Medlyn *et al.* 2001)
Quercus petraea (hydric stress)	270		UK	measured	(Medlyn *et al.* 2001)
Quercus petraea	234		UK	measured	(Medlyn *et al.* 2001)
Quercus robur		35	France	measured	(Adriaenssens *et al.* 2012)
Quercus robur	228		UK	measured	(Medlyn *et al.* 2001)
Quercus robur	376		Germany	measured	(Medlyn *et al.* 2001)
Quercus robur	1111			measured	Holmgren et al., 1965, in (Breuer & Frede 2003)
Quercus robur	345		Austria	measured	Körner et al., 1979, in (Breuer & Frede 2003)
Quercus robur	707		France	measured	(Guehl *et al.* 1995)
Castanea sativa	625		Italy	measured	Körner et al., 1979, in (Breuer & Frede 2003)
Castanea sativa (seedling)	446		France	measured	(Epron *et al.* 1995)
Wet woodland					
Betula pendula	170		UK	measured	(Medlyn *et al.* 2001)
Betula pendula	123			measured	Holmgren et al., 1965, in (Breuer & Frede 2003)
Betula pendula (seedling)	238			measured	Körner et al., 1979, in (Breuer & Frede 2003)
Betula pendula		29	France	measured	(Adriaenssens *et al.* 2012)
Betula pubescens	315		Norway	measured	(Beerling 1999)
Salix pulchra		200	Alaska, USA	measured	(Stoner & Miller 1975)
Pastures and meadows					
grass (clipped, 0.15m)	100-150			tabularised	(Allen *et al.* 1996)
grass (irrigated, clipped, 0.10-0.12m)	75	40		tabularised	(Allen *et al.* 1996)
short grass		200		proposed model parameter	(Dickinson *et al.* 1993)
tall grass		200		proposed model parameter	(Dickinson *et al.* 1993)
Alopecurus pratensis	179		Czechoslovakia	measured	Körner et al., 1979, in (Breuer & Frede 2003)
Alopecurus pratensis	149		Czechoslovakia	measured	Körner et al., 1979, in (Breuer & Frede 2003)
Arrhenatherum elatius	130		Austria	measured	Körner et al., 1979, in (Breuer & Frede 2003)
Carex flacca	315		Germany	measured	Wedler et al., 1996, in (Breuer & Frede 2003)
Dactylis glomerata	400			measured	Körner et al., 1979, in (Breuer & Frede 2003)
Dactylis glomerata	149		Austria	measured	Körner et al., 1979, in (Breuer & Frede 2003)
Deschampsia cespitosa	250			measured	Körner et al., 1979, in (Breuer & Frede 2003)
Holcus lanatus	159		Austria	measured	Körner et al., 1979, in (Breuer & Frede 2003)

Table G-4 (continued). Literature review of mean leaf resistance (r_l) values used in hydrological modelling or measured in contexts similar to the Dauges site.

Vegetation class	mean leaf resistance (s.m^{-1})*	minimum leaf resistance (s.m^{-1})*	location	type of data	source
Lolium perenne	400			measured	Körner et al., 1979, in (Breuer & Frede 2003)
Nardus stricta	628		UK	measured	(Friend *et al.* 1989)
Heathlands					
Calluna vulgaris		40-70	UK	measured	(Jackson *et al.* 1999)
Calluna vulgaris	82		UK	measured	(Kerslake *et al.* 1998)
Calluna vulgaris (wind speed 1m.s^{-1})	248		UK	measured	(Hinshiri 1973)
Calluna vulgaris (wind speed 2.5m.s^{-1})	345		UK	measured	(Hinshiri 1973)
Calluna vulgaris	110 (50-290)	50	UK	measured	(Miranda *et al.* 1984)
Vaccinium myrtillus	526		Austria	measured	Körner et al., 1979, in (Breuer & Frede 2003)
Vaccinum myrtillus (shade leaves)	769		USA	measured	Körner et al., 1979, in (Breuer & Frede 2003)
Vaccinum myrtillus (sun leaves)	435		USA	measured	Körner et al., 1979, in (Breuer & Frede 2003)
Vaccinum myrtillus (timberline, exposed)	385		Austria	measured	Körner et al., 1979, in (Breuer & Frede 2003)
Vaccinium myrtillus	456		Norway	measured	(Beerling 1999)
Vaccinium myrtillus	553		UK	measured	(Friend *et al.* 1989)
Vaccinium myrtillus	165-375		UK	measured	(Llorens *et al.* 2002)
Vaccinium myrtillus		100 (unfolding leaves), 300 (mature leaves)		measured	(Davies & Albrigo 1983)
Bogs and acidic fens					
Eriophorum angustifolium		200	Alaska, USA	measured	(Stoner & Miller 1975)
Carex aquatilis		300	Alaska, USA	measured	(Stoner & Miller 1975)

*Leaf resistance and conductance were assumed to equal stomatal resistance and conductance respectively. Leaf and stomatal conductances expressed in mol.m-2.s-1 were converted to m.s-1 by dividing them by 41, assuming a temperature of 20°C and mean sea level pressure.

Table G-5. Literature review of bulk interception ratios measured in contexts similar to the Dauges site.

vegetation	stand characteristics	bulk interception ratio			understorey & litter included ?	location	source
		annual	winter	summer			
Evergreen needle-leaved woodland							
Picea abies		0.3			yes (lysimeter)	UK	(Calder 2003)
Picea abies	24 year-old, 13m, 2160 stems/ha	0.36	0.38	0.31	no	Lorraine, France	(Aussenac 1970)
Picea abies	30 year-old, 13m, 2160 stems/ha	0.34			?	Lorraine, France	(Aussenac 1968)
Picea abies	50 year-old	0.28			?		Johnson, 1980, in (Ulrich *et al.* 1995)
Picea abies		0.23-0.38			?	Belgium	Noirfalise, 1959, in (Forgeard *et al.* 1980)
Picea abies		0.38-0.40			?	Sweden	Nihlgard, 1970, in (Forgeard *et al.* 1980)
Picea abies		0.59			?	?	Horton, 1919, in (Forgeard *et al.* 1980)
Picea abies		0.48			?	?	Ovington, 1954, in (Forgeard *et al.* 1980)
Abies grandis	33 year-old, 23m, 620 stems/ha	0.42	0.47	0.36	no	Lorraine, France	(Aussenac 1970)
Pseudotsuga menziesii		0.38			no	The Netherlands	(Tiktak & Bouten 1994)
Pseudotsuga menziesii	23 year-old, 16m, 535 stems/ha	0.35 (Oct-Jul)	0.32	0.36	no	Lorraine, France	(Aussenac & Boulangeat 1980)
Pseudotsuga menziesii	23 year-old, 18m, 1030 stems/ha	0.36 (Oct-Jul)	0.35	0.36	no	Lorraine, France	(Aussenac & Boulangeat 1980)
Pseudotsuga menziesii	23 year-old, 17m, 2229 stems/ha	0.37 (Oct-Jul)	0.36	0.37	no	Lorraine, France	(Aussenac & Boulangeat 1980)
Pseudotsuga menziesii		0.39			no	United Kingdom	(Rutter *et al.* 1975)
Pseudotsuga menziesii		0.35			no	United Kingdom	(Rutter *et al.* 1975)
Pinus sylvestris	29 year-old, 13m, 1520 stems/ha	0.32	0.33	0.31	no	Lorraine, France	(Aussenac 1970)

Table G-5 (continued). Literature review of bulk interception ratios measured in contexts similar to the Dauges site.

vegetation	stand characteristics	bulk interception ratio			understorey & litter included ?	location	source
		annual	winter	summer			
Pinus sylvestris	28 year-old, 13m, 1520 stems/ha	0.31			?	Lorraine, France	(Aussenac 1968)
Deciduous broad-leaved woodland							
Quercus petraea	120 year-old, 30m, 182 stems/ha, LAI 4.38	0.29	0.22	0.34	no	Fontainebleau, France	(Nizinski & Saugier 1989)
Quercus petraea	65 year-old	0.23			?		Szabo, 1975, in (Ulrich *et al.* 1995)
Quercus petraea	LAI 3.3-5.6	0.17-0.23			no	Lorraine, France	(Bréda 1994)
Quercus robur		0.18			no	United Kingdom	(Rutter *et al.* 1975)
Q. robur & F. sylvatica	85 year-old, 27m, 345 stems/ha	0.21	0.1	0.31	no	Belgium	(Staelens *et al.* 2008)
F. sylvatica & Q. petraea			0.25	0.32	no	Germany	(Leuschner & Rode 1999)
Fagus sylvatica	80 year-old, 25m, 743 stems/ha	0.15 (Oct-Jul)	0.06	0.21	no	Lorraine, France	(Aussenac & Boulangeat 1980)
F. sylvatica & Carpinus betulus	24 year-old, 13m, 1300 stems/ha	0.24	0.23	0.36	no	Lorraine, France	(Aussenac 1970)
F. sylvatica & Carpinus betulus	30 year-old, 13m, 1300 stems/ha	0.17			?	Lorraine, France	(Aussenac 1968)
Fagus sylvatica	50 year-old	0.17			?		Cepel, 1967, in (Ulrich *et al.* 1995)
Fagus sylvatica	50 year-old, 26m	0.34			no	Pyrenees, France	(Ulrich *et al.* 1995)
Fagus sylvatica	90 year-old	0.21			no	Lorraine, France	(Ulrich *et al.* 1995)
Fagus sylvatica	80-100 year-old	0.10			no	Gard, France	(Ulrich *et al.* 1995)
Fagus sylvatica	30 year-old, LAI=6			0.26 on average (0.30, 0.27, 0.25 for events of 5, 10 and 15mm respectively)	no	Alsace, France	(Granier *et al.* 2000)
Fagus sylvatica		0.24-0.28			?	Lorraine, France	Aussenac, 1975, in (Forgeard *et al.* 1980)
Fagus sylvatica		0.25			?	Belgium	Noirfalise, 1959, in (Forgeard *et al.* 1980)
Fagus sylvatica		0.18-0.20			?	Sweden	Nihlgard, 1970, in (Forgeard *et al.* 1980)
Fagus sylvatica		0.22			?	?	Horton, 1919, in (Forgeard *et al.* 1980)
Fagus sylvatica	120 year-old, 15m, 168 stems/ha		0.07	0.15	no	Luxembourg	(Gerrits 2010)
Fagus sylvatica forest floor			0.22	0.22	-	Luxembourg	(Gerrits 2010)
Pastures and meadows							
grassland	ungrazed (year 1)			0.14	yes	Canada	(Couturier & Ripley 1973)
grassland	ungrazed (year 2)			0.22	yes	Canada	(Couturier & Ripley 1973)
grassland	grazed (year 2)			0.16	yes	Canada	(Couturier & Ripley 1973)
Heathlands							
Calluna heathland		0.16			yes (lysimeter)	United Kingdom	(Calder 2003)
Calluna heathland			0.2	0.23	no (stemflow not included)	Germany	(Leuschner & Rode 1999)
Calluna heathland		0.11			yes (calibrated soil moisture model)	Denmark	(Ladekarl *et al.* 2001)
moorland		0.19			yes (lysimeter)	United Kingdom	(Calder 2003)

Table G-6. Literature review of maximum and specific storage capacities measured in contexts similar to the Dauges site.

vegetation	stand characteristics	maximum storage capacity (mm)	specific storage capacity (mm per LAI unit)	understorey & litter included ?	location	source
Evergreen needle-leaved woodland						
Abies alba			0.37	no	Denmark	(Rosenqvist *et al.* 2010)
Abies grandis		3.8 (summer)		no	Lorraine, France	(Aussenac 1968)
Picea abies		3.1 (summer)		no	Lorraine, France	(Aussenac 1968)
Pseudotsuga menziesii		2.4	0.22	no	The Netherlands	(Klaassen *et al.* 1998)
Pseudotsuga menziesii		3.6-3.9 (summer)		no	Lorraine, France	(Aussenac & Boulangeat 1980)
Pseudotsuga menziesii	LAI 19.2	1.5	0.08	no	USA	(Massman 1983)
Pseudotsuga menziesii	35 year-old, thinned heavily	1.6		?	Germany	Mischerlich & Moll, 1970, in (Breuer & Frede 2003)
Pseudotsuga menziesii		2.1		?	Hampshire, UK	Robins, 1969, 1974, in (Rutter *et al.* 1975)
Pseudotsuga menziesii	35 year-old, thinned weakly	2.4		?	Germany	Mischerlich & Moll, 1970, in (Breuer & Frede 2003)
Pseudotsuga menziesii	35 year-old, thinned moderately	3.1		?	Germany	Mischerlich & Moll, 1970, in (Breuer & Frede 2003)
Pinus sylvestris		3 (summer)		no	Lorraine, France	(Aussenac 1968)
Pinus sylvestris	23 year-old, 2900 stems/ha	0.3		?	Sweden	(Llorens & Gallart 2000)
Pinus sylvestris	LAI 1.46	2.47-2.65		no	Spain	(Llorens & Gallart 2000)
Pinus sylvestris	LAI 0.84	1.42-1.52		no	Spain	(Llorens & Gallart 2000)
Pinus sylvestris	LAI 1.12	1.90-2.03		no	Spain	(Llorens & Gallart 2000)
Pinus sylvestris	LAI 0.68	1.16-1.24		no	Spain	(Llorens & Gallart 2000)
Pinus sylvestris	LAI 1.29	2.18-2.34		no	Spain	(Llorens & Gallart 2000)
Pinus sylvestris	1870 stems/ha	1		?		Gash et a., 1980, in (Llorens & Gallart 2000)
Pinus sylvestris	800 stems/ha	0.8		?		Gash & Morton, 1978, in (Llorens & Gallart 2000)
Pinus sylvestris	2400 stems/ha	1.3		?		Llorens et al., 1997, in (Llorens & Gallart 2000)
Pinus sylvestris	3600	1.6		?		Rutter 1963, 1975, in (Llorens & Gallart 2000)
Pinus sylvestris			1.83-2.00	no		(Llorens & Gallart 2000)
Pine litter		0.6-1.7		-	United kingdom	(Walsh & Voigt 1977)
Deciduous broad-leaved woodland						
Quercus petraea	120 year-old, LAI 5.3	2.29 (summer), 1.48 (winter)	0.43 (summer)	no	Fontainebleau, France	(Halldin *et al.* 1984)
Quercus robur	60 year-old	1		?	United kingdom	(Breuer & Frede 2003)
Quercus robur			0.25	no	Denmark	(Rosenqvist *et al.* 2010)
Quercus robur		0.8 (summer), 0.3 (winter)		no		(Dolman 1987)
Quercus robur		1 (summer), 0.3-0.4 (winter)		no	Oxfordshire, UK	Thompson, 1972, in (Rutter *et al.* 1975)
F. sylvatica & Q. robur		0.6 (summer)		no		Schröder, 1984, 1985, in (Hörmann *et al.* 1996)
F. sylvatica & C. betulus		1.9 (summer)		no	Lorraine, France	(Aussenac 1968)
Fagus sylvatica		0.6 (summer)		?		Weihe (1968), in (Breuer & Frede 2003)
Fagus sylvatica	120 year-old	2.6		?	Germany	(Breuer & Frede 2003)
Fagus sylvatica		1.7 (summer)		no	Lorraine, France	(Aussenac & Boulangeat 1980)
Fagus sylvatica	120 year-old, 15m, 168 stems/ha	0.4 mm (winter) 0.9 mm (summer)		no	Luxembourg	(Gerrits 2010)
Fagus sylvatica		1.2 (summer), 0.5 (winter)		no		Kändler, 1986, in (Hörmann *et al.* 1996)
Fagus sylvatica		2.6 (summer)		no		Elling et al., 1990, in (Hörmann *et al.* 1996)
Bracken litter		1.67		-	United kingdom	(Walsh & Voigt 1977)
Bracken litter			minimum 0.16, maximum 0.47	-	United kingdom	(Pitman 1989)
Beech litter		0.9-2.8		-	United kingdom	(Walsh & Voigt 1977)
Beech litter		1.8mm (both in summer and winter)		-	Luxembourg	(Gerrits 2010)

Table G-6 (continued). Literature review of maximum and specific storage capacities measured in contexts similar to the Dauges site.

vegetation	stand characteristics	maximum storage capacity (mm)	specific storage capacity (mm per LAI unit)	understorey & litter included ?	location	source
Pastures and meadows						
grassland		1.23 (of which 1.19 is due to dead vegetation)		yes	Canada	(Couturier & Ripley 1973)
Lolium perenne		0.43-2.82		?	USA	(Merriam 1961)
Heathlands						
Calluna heathland		1.5	0.75	yes	United kingdom	(Calder *et al.* 1984)
Erica spp.		2		?	United kingdom	Leyton et al. (1967), in (Breuer & Frede 2003)
Pteridium aquilinum		0.9		?	United kingdom	Leyton et al. (1967), in (Breuer & Frede 2003)
Pteridium aquilinum		1.27		?		Brookes (1950), in (Breuer & Frede 2003)
Bogs and acidic fens						
Molinia caerulea		0.66		?	United kingdom	Leyton et al. (1967), in (Breuer & Frede 2003)

Appendix H. Differential impacts of open habitats, broadleaf forests and coniferous forests on water yield

The impact of forests on the water cycle was recognised as early as the first century AD, when Pliny the Elder wrote his Natural History and observed that "Often, after woods have been cut down, springs on which trees used to feed emerge […]. Often, disastrous torrents are formed after the felling of mountain woods, which used to hold back clouds and feed on them". The first attempts at quantifying this impact using discharge and precipitation measurements in catchments with contrasted land covers were carried out as early as the second half of the 19th century in France (Andréassian 2004). Since then, a very large amount of research has been carried out on this issue, particularly through the use of paired experimental catchments, whereby at least two small geographically close and environmentally similar catchments are monitored for a number of years before land cover is altered in one of them and changes in water fluxes compared to those recorded in the control catchment (Andréassian 2004). Paired catchment experiments investigating the effect of afforestation and deforestation have conclusively shown a lower total annual flow in forested catchments than in unforested ones (Figure H-1), even though the magnitude of this impact is highly variable depending on the catchment environmental characteristics. Numerous paired-catchment experiments have also highlighted differences in water yield between evergreen coniferous forests and deciduous broadleaf forests.

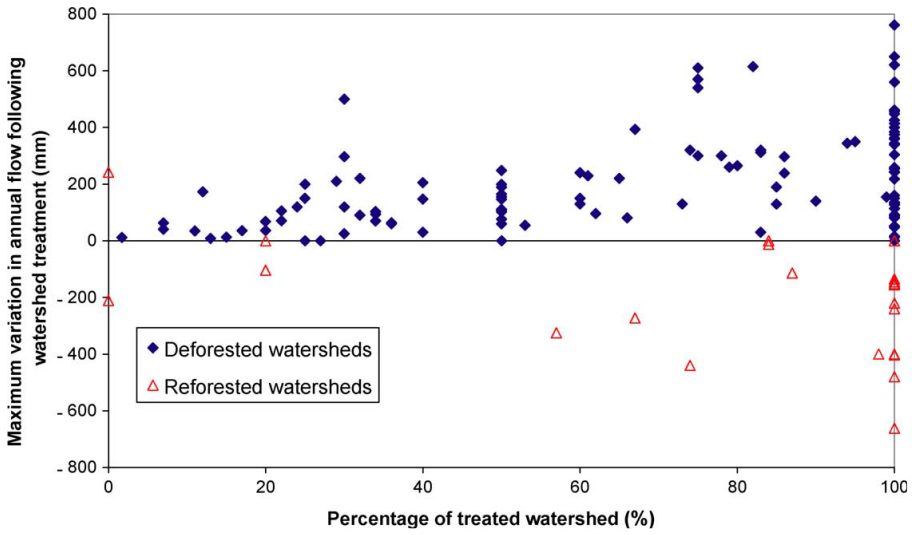

Figure H-1. Maximum change in annual flow following deforestation or afforestation in 137 paired-catchment experiments (from Andréassian 2004).

Sahin & Hall (1996) applied fuzzy linear regression to the results of 145 deforestation experiments carried out across the world. They showed that 100% clear-felling of forests would result in an average increase in water yield of 330mm.yr^{-1} in conifer forests, 201 mm.yr^{-1} in mixed forests, 201 mm.yr^{-1} in deciduous forests when annual precipitation is lower than 1500mm (169 mm.yr^{-1} when higher) and 92 mm.yr^{-1} in scrub stands. Katzensteiner *et al.* (2011) also carried out a meta-analysis of the response of runoff to changes in forest cover from deforestation experiments, and showed that the increase in water yield after clear-felling is higher in conifers than in broadleaf woodlands, that this increase is larger under wetter climates, and that the difference between conifers and broadleaf woodlands is also larger under wetter climates. These findings point toward interception as the main mechanism behind the difference in water yield between conifer and broadleaf species. One drawback of deforestation studies is that part of the increased runoff in clear-fell catchments may be a consequence of forestry operations rather than of the removal of forest itself, for instance through soil compaction (Katzensteiner *et al.* 2011). Afforestation experiments are much less common than deforestation studies given the time required to reach forest maturity. In a review of 26 such paired catchment experiments, Farley *et al.* (2005) found that annual runoff was reduced on average by 44% (+/-3%) and 31% (+/-2%) when grasslands and shrublands, respectively, were afforested. Eucalypts had a larger impact than other tree species; but even the replacement of grassland with pine trees led to a 40% (+/-3%) decrease in runoff. Absolute reductions were larger on wetter sites, but proportional reductions were larger on drier sites.

The effect of forest on low flows were reviewed by Johnson (1998), who concluded that most clear-felling experiments recorded substantial increases (15-350%) in low flows. In general a reduction in forest cover of at least 25% is required before any changes are observed. In very dry summers low flows are generally sustained by deep groundwater sources and are only affected if the forests prevent sufficient groundwater recharge.

Some paired-catchment experiments have suggested a reduction of floods in forested catchments relative to those covered in grasslands. Fahey & Jackson (1997), for instance, described the results from two paired tussock grassland catchments in New-Zealand, where one of the catchments was planted in pines over two-third of its area. After ten years of tree growth, the annual water yield had fallen by 27% in the forested catchment compared to the grassland control. Mean flood peaks had fallen by 55% to 65% and quick flows decreased by 50%. However, Andréassian (2004), who reviewed a number of studies assessing the impact of deforestation on

peak flow, concluded that it may, in some cases, increase both flood volumes and flood peaks, but that this effect was much more variable than that observed for total flow and may even be inverted in some years or seasons. Afforestation studies showed very limited effect on floods and no effect at all on larger flood events. He concluded that the increase in floods observed in some deforestation studies was caused by the exploitation itself rather than by the removal of forest cover.

The effect of forests on peak flows in Europe specifically were reviewed by Robinson *et al.* (2003). They also found that, at the local scale, there were specific situations where forests had a substantial impact on peak flows; however, in general, the impact was relatively small on extreme flows. In conifer plantations on peaty soils in north-west Europe, peak flows from mature forest and unforested land were little different. Forest cutting, however, led to short-term increases in peak flow at the local scale, although this was generally not detectable at the larger catchment scales. In fact, the largest effect was caused by drainage that often accompanies afforestation in these regions, causing a substantial increase in peak flows during the early stage of the forest cycle. In central European broadleaved forests, the effects of partial harvesting was relatively small. The largest impact was found in eucalypt plantations in Mediterranean regions, where clear-felling led to an immediate increase in peak flows that was however short-lived due to rapid regrowth. The impact of forests on floods may require longer time-scales to be noticeable than those generally used in afforestation/deforestation experiments. Mathys *et al.* (1996) reported on the flood regime of two small mountainous catchments in the southern French Alps, one of which had been afforested at the end of the 19th century and the other being bare with almost no vegetation cover at all. In the forested catchment, peak floods were between five and ten times lower than in the bare catchment, flood runoff volume more than two times lower and flood peaks substantially delayed. Despite similar topographic and geological settings, the specific sediment yield was 200 times lower in the forested than in the bare catchment. This shows that, on erosive soils, forests may contribute to the creation or preservation of soils and, indirectly, considerably modify catchment hydrological behaviour.

A number of studies have also highlighted smaller groundwater recharge under coniferous forests than broadleaf forests, and under forests than open habitats. Kantor (1995, cited by Katzensteiner *et al.* 2011) compared water balances in mature spruce and beech stands in the Czech Republic and found that the annual recharge / precipitation ratio was 60% under spruce

stands compared to 70% under beech. Rosenqvist *et al.* (2010) monitored and modelled the water fluxes in stands of Norway spruce and common oak in Denmark and Sweden. Water fluxes were similar in both species up to 20 years after planting, but in stands older than 20-25 years, there was a difference in annual recharge in the range of 60-110mm.yr^{-1} (annual rainfall ranged from 780 to 1280mm depending on the site), spruce using more water than oak. This was mainly caused by higher evaporation of intercepted water in spruce stands (26-44% of annual rainfall) than in oak stands of comparable age (18-30%). Soil water content was higher under oak stands than under spruce stands. From experiments in Sweden, Norway and the Netherlands, van der Salm *et al.* (2007) reported a decline in groundwater recharge under oak stands from 35% of precipitation four years after planting to 19% 30 years after planting. In spruce stands, recharge made for 5% to 30% of precipitation. The decline in recharge with stand age was very variable but was approximately 10-20% over the experiment duration. These differences were mainly due to an increase of evaporation from interception, from 9% of precipitation in four-year old oak stands to 20% in 30-year old stands, and from 16 to 52% in spruce stands. Van der Salm *et al.* (2006) reported declines in groundwater recharge from approximately 485mm.yr^{-1} on arable land to 172mm in an oak stand 18-year after planting and to 100mm in a spruce stand 13-14 years after planting. Cooper (1980) measured evapotranspiration and groundwater recharge using the zero-flux plane method in a Scots pine plantation and in a nearby grassed clearing on sandy soils in eastern England. He found that evaporation from the forest was 49% greater than that of grass, and groundwater recharge 44% less. Finally, Moss and Edmunds (1989, cited by Allen & Chapman 2001) found that rates of recharge were at least three times lower under forest than under heathland in the British West Midlands.

As described above, the reason for the lower water yield under conifer trees compared to broadleaf trees, and under forest compared to open habitats, lies in different evapotranspiration rates. For instance, Granier (2007) found that in summer, the actual evapotranspiration in a pasture was on average 50% of that in a beech stand. Harsch *et al.* (2009) analysed the results of large-scale 40-year long lysimeter experiment in Germany, and concluded that, on average, grassland evapotranspiration is 36% of total precipitation, oak-beech forest 56% and pine forest 65%. Using data from the paired catchment Plynlimon experiment in Wales, Hudson *et al.* (1999) found that evapotranspiration from coniferous forests was always higher than that from moorland, but that the difference declined with the ageing of the plantation from 61% at the start of the experiment to 18% before clear-felling 13 years later. Fohrer *et al.* (2001) calibrated and validated SWAT models of four catchment with contrasting land covers, then forced the

model with a unique landuse, including pasture and forest (a mixture of pine, beech and oak trees). Evapotranspiration was 24% higher under forest than under pasture. Total stream flow was 20% lower under forest than under pasture.

Differences in transpiration rates under non-limiting water supply conditions do not seem to explain the reported differences in evapotranspiration between vegetation types. Aussenac & Boulangeat (1980) and Verstraeten *et al.* (2005) found almost no difference in summer between transpiration rates of Douglas fir and of beech in Lorraine (France) and in Belgium respectively. Based on their own data and a literature review, Granier *et al.* (1999) found that, under non-limiting soil water content, the T/ETo ratio in both broadleaf and conifer trees was linearly related to the LAI when LAI was less than 6, but constant above this threshold. Stands with a LAI ≥ 6 had relatively similar T/ETo ratios independent of the species (0.65-0.72 for Douglas fir *Pseudotsuga menziesii*, 0.75 for beech *Fagus sylvatica*, 0.70-0.80 for sessile oak *Quercus petraea*, 0.70-0.80 for Norway spruce *Picea abies*). Kantor (1995, cited by Katzensteiner *et al.* 2011) also came to similar conclusions after studying transpiration in spruce and beech stands from planting to maturity. Forests and open habitats differ in their rooting depth, which influences the ability to draw water from the soil and therefore transpiration rates, particularly under water supply limitation in drier climates and in places where the groundwater table is inaccessible to roots. A literature review of rooting depths for species relevant to the Dauges research site is given in Section 5.4.3 and Appendix G as this is an important model parameter. Relatively few values were found for tree species and these were quite variable, probably due to the technical difficulties of measuring root depth in trees. Overall, conifer and broadleaf species appeared to have similar root depths, around 2m, much larger than grassland species (0.9m on average in a global review by Breuer *et al.* 2003) and heathland species (0.6m in Ladekarl *et al.* 2001).

However, the main reason for the differences observed in evapotranspiration between vegetation types lie in their interception capacity. The bulk interception ratio, i.e. the proportion of precipitation reaching the soil surface, has been the focus of a large number of studies. Some values measured for species and vegetation types relevant to the Dauges research site are given in Section 5.4.3 and Appendix G since they are an important parameter for hydrological modelling. Except for a few high values recorded under Norway spruce *Picea abies* and grand fir *Abies grandis*, annual interception ratios are noticeably similar in measurements carried out on conifers. There seems to be no difference between winter and summer, however it should be noted that studies that differentiated between winter and summer interception were all

conducted in Lorraine, France, so this may not apply to other climates. The mean annual ratio for Douglas fir was found to be 0.37. Data on annual interception for beech and oak forests are much more variable, ranging from 0.10 to 0.34. The mean value is 0.21. Interception is higher in summer (0.15-0.36, mean: 0.28) than during the leafless season (0.06-0.25, mean: 0.16). The overwhelming majority of researchers that measured interception in forests did not include interception by the forest understorey and litter. Yet, as shown by Gerrits (2010), this can account for a very large proportion of total rainfall intercepted by forests, sometimes more than that intercepted by the canopy. This may be an issue when comparing interception fraction between forests and open habitats, in which other methods have been used that do include the effect of dead vegetation. As noted by Breuer *et al.* (2003), surprisingly little information is available on bulk interception ratios in grasslands, probably due to methodological limitations. The only relevant publication that could be found as part of the current study seems to suggest it is of the same order as that observed in heathlands, in the order of 0.11-0.23 (mean: 0.17).

Interception capacity is directly correlated to leaf area index. It therefore varies with plant density, age, and forestry or agricultural practices. This in part explains the larger variation in interception values measured by studies carried out under broadleaf forests than under conifer forests since the former were generally carried out in semi-natural woodlands with variable forestry practices and stand characteristics whereas the latter were carried out in homogeneous plantations, at least for studies retained as part of this work for their similarity with the Massif Central context. Nevertheless, LAI is generally higher in coniferous than deciduous tree species under similar stand density and age conditions, and much higher in tree species than in grassland species. A review of LAI values found in the literature for species relevant to the research site investigated during the current study is given in Section 5.4.3 and Appendix G. In the case of plantations, only values measured from stands aged at least 25-30 years were retained. The mean LAI values during the vegetation season obtained from this review were 8.5 for Douglas fir, 6 for beech, 4.9 for chestnut tree and 4.8 for common oak, but a large variation was found. LAI is relatively stable throughout the year in evergreen conifers, but obviously decreases with leaf fall in deciduous species, even though branches do intercept some precipitation. LAI in heathlands ranged from 1.3 to 2.6.

Even though forests have a higher ability to supply water to the atmosphere than open habitats because of their higher interception storage capacity and deeper roots, and conifer forests a higher ability than broadleaf forests, evapotranspiration is limited by the evaporative demand of

the atmosphere. Therefore, the higher evapotranspiration recorded in forests than in open habitats is also a consequence of higher radiative and advective energy inputs, leading to a larger evaporative demand. Forests have a high aerodynamic roughness that allows the transport of heat from the air to the forest surface and of water vapour from the surface to the atmosphere to occur at rates up to ten times those possible from shorter vegetation. The much higher utilisation of advected energy combined with a higher interception capacity is the principal reason for higher evaporative losses from forests compared to shorter vegetation (Calder 1998). Conifer forests also have generally smaller albedos than broadleaf forests and open habitats, leading to larger radiative inputs. For instance, Rost & Mayer (2006, in Granier 2007) recorded albedo values of 0.23 in pasture and 0.11 in a pine stand. Breuer *et al.* (2003) found similar values in crops, pasture and deciduous forests ranging from 0.20 to 0.27 in a literature review covering temperate vegetation. Conifers had values ranging from 0.11 to 0.14.